

**TARGETED DELIVERY OF HISTONE DEACETYLASE
INHIBITORS FOR USE IN CANCER THERAPY**

A Dissertation
Presented to
The Academic Faculty

by

Shaghayegh Fathi

In Partial Fulfillment
of the Requirements for the Degree
Doctor of Philosophy in the
School of Chemistry and Biochemistry

Georgia Institute of Technology
December 2016

COPYRIGHT 2016 BY SHAGHAYEGH FATHI

TARGETED DELIVERY OF HISTONE DEACETYLASE INHIBITORS FOR USE IN CANCER THERAPY

Approved by:

Dr. Adegboyega Oyelere, Advisor
School of Chemistry and Biochemistry
Georgia Institute of Technology

Dr. M. G. Finn
School of Chemistry and Biochemistry
Georgia Institute of Technology

Dr. Stefan France
School of Chemistry and Biochemistry
Georgia Institute of Technology

Dr. Julia Kubanek
School of Biology
Georgia Institute of Technology

Dr. Manu Platt
School of Biomedical Engineering
Georgia Institute of Technology

Date Approved: July 25th, 2016

To my parents Mohammad Fathi and Susan Hosseinkhanli

ACKNOWLEDGEMENTS

First of all, I would like to thank God, the merciful the compassionate, for never leaving me alone in my hard moments, helping me in my time of need, and guiding me to take the best and right decisions. I would like to thank God for paving the road for me to achieve my goals, and giving me the courage and strength to come to another country and peruse my dreams.

I am deeply indebted to my advisor, Dr. Oyelere, who guided me through five years of my PhD and never lost faith in me. He was always understanding and supportive through ups and downs of research. He not only thought me how to think and approach obstacles in research, but he was also there for me when I needed assistance and advice on life hurdles. His passion toward science and research encouraged me to work harder and be eager to learn more and more every day.

My special gratitude goes to my thesis committee members, Dr. M.G Finn, Dr. Stefan France, Dr. Julia Kubanek, and Dr. Manu Platt for their invaluable assistance and guidance. Their patronage helped me with my research through my PhD journey, and their commitment assisted me with accomplishing my PhD studies.

I would also like to thank our collaborators, James Kornaki, Lindsey Szymczak, and Dr. Milan Mrksich at Northwestern University, Dr. Muthusamy Thangaraju at Augusta University, and Dr Li at Georgia State University.

I would like to thank Dr. Oyelere research group for their training and support. I would like to send my deep gratitude to Dr. Subhasish Tapadar for his training and mentoring in organic synthesis, and former labmate Dr. Quaovi Sodji for mentoring me on the cell work. I would like to extend my appreciation to my other former and current labmates, Dr. Berkeley Gryder, Idris Raji, Arren Washington, Nathaneal Levinson, Eric Raftary, Michelle Akbashev, Bocheng Wu, Henry Goh, Fatimah Yadudu, Verjine

Khodaverdian and Leslie Dionne White. I would also like to thank Teresa Jonsson for being very supportive and helpful. She was always there for me when I needed someone to listen to me.

I would also like to thank Dr. Amit Reddi for letting me use his lab for performing cell work studies.

I would like to express my gratitude to Dr. Baron, for whom I was a teaching assistant for almost four years. He is a role model to me in teaching. He is patient, understanding and really kind to both his students and teaching assistants.

I would like to express my deep indebtedness to my parents Mohammad Fathi and Susan Hosseinkhanli Khaneghah. I can never express in words how thankful I am to have them, but I will try my best to always make them proud of me. They always have been very understanding, helpful and supportive of my decisions. Even being thousands of miles away never stopped me from feeling their love.

I would like to extend my gratitude to my amazing brother, Alireza Fathi. I would not be where I am without his help in my life.

I am greatly indebted to my best friend, Amir Darabi, for his support over the past two years. He never lost faith in me or deprived me from his support when I needed help the most.

I would also like to thank Chitta Ranjan, for his help in improving my writing skills and assisting me with editing my documents.

I would also like to send my gratitude to ones who always believed in me and never lost faith in me. All friends and family who were there for me when I was feeling down. They helped and encouraged me to stand tall and motivated to defeat all the challenges and problems in the world.

TABLE OF CONTENTS

	Page
ACKNOWLEDGEMENTS	i
LIST OF TABLES	ix
LIST OF FIGURES	x
LIST OF SYMBOLS AND ABBREVIATIONS	xiii
SUMMARY	xix
<u>CHAPTER</u>	
1 INTRODUCTION	1
1.1. Background	1
1.2. Epigenetics	2
1.3. Histone acetylation	3
1.4. Histone deacetylation	5
1.4.1. Histone deacetylase isoforms	8
1.4.1.1. Class I isoforms	8
1.4.1.2. Class II isoforms	10
1.4.1.3. Class IV isoforms	11
1.5. Histone deacetylase inhibition	11
1.6. Pharmacophoric model of HDACi	12
1.6.1. Recognition cap group	14
1.6.2. Linker group	15
1.6.3. Zinc binding group	15
1.6.3.1. Zinc dependent mechanism of lysine deacetylation	17
1.6.3.2. Hydroxamic acid derived HDACi	19

1.6.3.3. Depsipeptide-derived HDACi	20
1.6.3.4. Benzamide-derived HDACi	20
1.6.3.5. Epoxide-derived HDACi	21
1.6.3.6. Carboxylic acid (short fatty acid) HDACi	21
1.7. US FDA approved HDACi	22
1.7.1. Suberoylanilide hydroxamic acid (SAHA)	23
1.7.2. Romidepsin (FK228)	24
1.7.3. Belinostat (PXD101)	25
1.7.4. Panobinostat (LBH589)	25
1.8. Mechanism of HDACi-induced cell death	26
1.9. FDA approved HDACi in combination therapy	27
1.10. HDACi in clinical trials	28
1.10.1. Abexinostat (PCI-24781)	29
1.10.2. Givinostat (ITF2357)	30
1.10.3. Reminostat (4SCAG)	30
1.10.4. Pracinostat (SB939)	30
1.10.5. CUDC-101	31
1.10.6. Mocetinostat (MGCD0103)	31
1.10.7. Entinostat (MS-275)	31
1.10.8. Valproic acid (VPA)	32
1.11. HDACi deficiencies	32
1.11.1. Lack of accumulation in solid tumors	32
1.11.2. Cardiotoxicity	33
1.12. Mechanism of resistance to HDACi	35
1.12.1. Efflux pump	35

1.12.2. Epigenetic changes	35
1.12.3. Anti-apoptotic and pro-survival mechanisms	36
1.12.4. Autophagy	36
1.13. Improving HDACi efficacy in clinic	37
1.13.1. Localized administration	37
1.13.2. Reduction of hERG binding	39
1.13.3. Isoform-selective HDACi	39
1.13.3.1. Isoform selectivity through cap group modification	40
1.13.3.2. Isoform-selectivity through ZBG modification	40
1.13.4. Targeted delivery	41
1.13.4.1. Tissue selective FDA approved drug as the ‘cap group’	41
1.13.4.2. Tumor receptor antagonist as the ‘cap group’	42
1.14. Conclusion	43
1.15. References	44
2 Structure activity relationship of azithromycin derived HDACi with hydroxamic acid as zinc binding group	60
2.1. Introduction	60
2.2. Azithromycin derived HDACi design	63
2.3. Chemistry and synthesis	64
2.4. Docking study	66
2.5. HDAC inhibitory activity	69
2.6. Anti-proliferative activity	70
2.7. Anti-inflammatory activity	72
2.8. Conclusion	73
2.9. Experimental	74
2.9.1. Materials and methods	74

2.9.2. Cell viability assay	74
2.9.3. SAMDI assay	75
2.9.4. Anti-inflammatory assay	76
2.9.5. Synthesis	76
2.10. References	95
2.11. Supplementary data	99
3 Isoform selective azithromycin HDACi conjugates	123
3.1. Introduction	123
3.2. Isoform selective HDACi	124
3.3. Isoform selective HDACi design	127
3.4. Chemistry	129
3.5. HDAC inhibitory activity	131
3.6. Docking study	133
3.7. Anti-proliferative activity	134
3.8. <i>In vivo</i> study	136
3.8. Conclusion	137
3.10. Experimental	138
3.10.1. Materials and methods	138
3.10.2. Cell viability assay	147
3.10.3. SAMDI assay	147
3.10.3. <i>In vitro</i> HDAC inhibiton	148
3.11. References	149
3.12. Supplementary data	153
4 Histone deacetylase inhibitors equipped with estrogen receptor modulators for selectively targeting breast cancer	170
4.1. Introduction	170

4.2. Synthesis of tamoxifen-derived dual-acting SERM-HDACi	172
4.3. Chemistry and synthesis	174
4.4. HDAC inhibitory potency	176
4.5. Anti-proliferative activity and therapeutic index	177
4.6. Conclusion	179
4.7. Experimental	179
4.7.1. Materials and methods	179
4.7.2. Cell viability	187
4.7.3. SAMDI assay	188
4.8. References	189
4.9. Supplementary data	193
5 Bifunctional STAT3/Histone deacetylase inhibitors for treating STAT3 dependent tumors	208
5.1. Introduction	208
5.2. Design of pyrimethamine-HDACi conjugates	212
5.3. Chemistry and synthesis	213
5.4. HDAC inhibitory potency	215
5.5. Docking studies	215
5.6. Antiproliferative activity	220
5.7. Conclusion	221
5.8. Experimental	222
5.8.1. Materials and methods	222
5.8.2. Cell viability assay	229
5.8.3. <i>In vitro</i> HDAC inhibition	229
5.9. References	230
5.10. Supplementary data	235

6 Conclusion and HDACi therapeutic future	257
6.1. Conclusion	257
6.2. References	260
APPENDIX A: Liposomal drug delivery systems for targeted cancer therapy	263
APPENDIX B: Azithromycin functionalized liposomes	317
VITA	340

LIST OF TABLES

Table 1.1: HDAC isoforms with their size, function, localization, and selected examples of their target proteins	8
Table 1.2: Selected examples of HDACi with various zinc binding groups	17
Table 2.1: HDAC 1, HDAC6, and HDAC8 inhibition activities of azithromycin derived hydroxamic acid compounds	69
Table 2.2. Anti-proliferative activity of selected azithromycin conjugated HDACi	71
Table 2.3. Anti-inflammatory activity (NF- κ B inhibition) of selected HDACis	73
Table 3.1. HDAC 1, 2, 3, 6, and 8 inhibition activities of azithromycin conjugated N-(2-amino-5-(thiophen-2-yl)phenyl)acylamide derived HDACi (IC ₅₀ in nM) obtained using label-free mass spectrometry-based SAMDI assay, and their comparison with azithromycin derived hydroxamate and FDA approved pan-HDACi SAHA	132
Table 3.2. HDAC inhibition potency against all Zn-dependent HDAC isoforms using the Fluor de Lys assay available through BPS Bioscience	133
Table 3.3. Anti-proliferative activity of azithromycin conjugated N-(2-amino-5-(thiophen-2-yl)phenyl)acylamide HDACi	135
Table 4.1. HDAC 1, 2, 3, 6, and 8 inhibition activities of three different classes of tamoxifen conjugated HDACi	177
Table 4.2. Anti-proliferative activity of selected tamoxifen conjugated HDACi	178
Table 5.1. HDAC inhibition activities of pyrimethamine-HDACi conjugates	215
Table 5.2. Anti-proliferative activity of pyrimethamine-HDACi conjugates	221
Table A.1: FDA approved liposomal and lipid based formulations	267
Table A.2: Different head groups and their effect on the liposome overall charge	271

LIST OF FIGURES

	Page
Figure 1.1: Nucleosome consists of 4 core histones, H2A, H2B, H3, H4, and the linker histone H1	5
Figure 1.2: HDAC activation regulates expression of genes that are involved in tumorigenesis	6
Figure 1.3: HDAC enzymes are functionally opposite to the HAT enzymes	7
Figure 1.4. Pharmacophoric model of HDACi with selected examples of each group	13
Figure 1.5. Selected examples of HDACi	13
Figure 1.6. Chemical structure of trapoxin A, a naturally occurring class I isoform selective HDACi	14
Figure 1.7. Zinc atom in the catalytic pocket of HDAC 1, a class I HDAC isoform. Green sphere represents zinc atom	16
Figure 1.8. Proposed mechanism for lysine residue deacetylation by zinc-dependent HDAC enzymes	19
Figure 1.9. Chemical structure of trichostatin A (TSA), a naturally occurring non-selective HDACi	20
Figure 1.10. Chemical structures of valproic acid and phenylbutyrate, two well established short fatty acid HDACi have been tested in clinical trials for treating various types of cancer	23
Figure 1.11. FDA approved HDACi and their clinical indications	23
Figure 1.12. Reduction of romidepsin to its active form. Romidepsin is a prodrug, and its disulfide bond is reduced to alkyl thiol by glutathione <i>in vivo</i>	25
Figure 1.13. HDACi in clinical trials	30
Figure 2.1. Naturally occurring HDACi trichostatin A and FDA approved HDACi SAHA.	62
Figure 2.2. Structure activity relationship of azithromycin conjugated HDACi by modifying desosamine and cladinose sugar rings	63
Figure 2.3. Docking studies of example cladinose modified azithromycin HDACi with six methylene linker group against HDAC1 and HDAC6	68

Figure 3.1. US FDA approved pan-HDACi	124
Figure 3.2. Docking study of our proposed design of azithromycin conjugated N-(2-amino-5-(thiophen-2-yl)phenyl)acylamide derived HDACi against HDAC2	125
Figure 3.3. Mocetinostat entinostat, and chidamide, three benzamide derived HDACi in clinical trials for treating various types of cancers	126
Figure 3.4. Three-motif pharmacophoric model of SAHA as well as selected examples of designed and published class I selective N-(2-amino-5-(thiophen-2-yl)phenyl)acylamide derived HDACi, which led to the design of azithromycin conjugated N-(2-amino-5-(thiophen-2-yl)phenyl)acylamide derived HDACi	128
Figure 3.5. Docked structure of azithromycin HDACi conjugate with six methylene linker group against HDAC2	134
Figure 3.6. Tumor regression and number of nodules in MMTV-PyMT-Tg mice with metastatic lung cancer	136
Figure 4.1. Three classes of tamoxifen conjugated HDACi with different ZBG and linker length	173
Figure 5.1. Structure of pyrimethamine, an antifolate drug with antimalarial activity	208
Figure 5.2. US FDA approved HDACi	211
Figure 5.3. Pharmacophoric model of HDACi, and the two classes of pyrimethamine HDACi-conjugates	213
Figure 5.4. Docking structures of various pyrimethamine conjugated HDACi	220
Figure A.1. Liposomes as carriers in drug delivery systems	265
Figure A.2. General structure of phospholipid constituent of liposomes with the head and fatty acid tail groups	270
Figure A.3. Passive liposomal delivery	281
Figure A.4. Ligand targeted liposome	282
Figure A.5. Liposomal active targeting	284
Figure A.6. Folic acid structure	287
Figure A.7. Structure of EC17, the first folate ligand mediated targeting liposome in clinical trial	289

Figure A.8. TPP and STPP structures	292
Figure A.9. Antibody Y-shaped structure	298
Figure B.1. Liposomal drug delivery system	319
Figure B.2. Three different design of functionalized liposome	320
Figure B.3. Three different designs of azithromycin functionalized phospholipid	321
Figure B.4. Azithromycin structure, a FDA approved antibiotic for treating bacterial infection	322

LIST OF SYMBOLS AND ABBREVIATIONS

°C	Degree Celsius
μM	Micromolar
Å	Angstrom
A549	A Non-small cell lung cancer cell line
Ab	Antibody
Ac	Acetyl group
Acetyl CoA	Acetyl coenzyme A
ACS	American Chemical Society
ACUPA	<i>S,S</i> -2-[3-[5- <u>a</u> mino-1- <u>c</u> arboxypentyl]- <u>u</u> reido]- <u>p</u> entanedioic <u>a</u> cid
AML	Acute myeloid leukemia
Bak	Bcl-2 antagonist killer (pro-apoptotic)
Bax	Bcl-2 associated X protein (pro-apoptotic)
Bcl-2	B-cell lymphoma 2 protein (anti-apoptotic)
Boc	Tert-butoxycarbonyl
C	Carbon
CD ₃ OD	Deuterated Methanol
CDCl ₃	Deuterated chloroform
CHEMS	Cholestrol hemisuccinate
CKII	Casein kinase II
CLL	Chronic lymphocytic leukemia
CNS	Central nervous system tumors
CS055	Chidamide
CTCL	Cutaneous T-cell lymphoma

d	Doublet
DARPin	(Designed) Ankyrin Repeat Proteins
DCM	Dichloromethane
DHFR	Dihydrofolate reductase
DISC	Dead-induced signaling complex
DLBCL	Diffuse large B-cell lymphoma
DMEM	Dulbecco's Modified Eagle Medium
DMSO	Dimethyl sulfoxide
DNA	Deoxyribonucleic acid
DOPE	Dioleoylphosphatidylethanolamine
DSPE	1,2-Distearoyl- <i>sn</i> -glycero-3-phosphoethanolamine
EDCI	1-Ethyl-3-(3-dimethylaminopropyl)carbodiimide
EGFR	Epidermal growth factor
EMEM	Eagles's Minimum Essential Medium
EpCAM	Epithelial cell adhesion molecule
EPR effect	Enhanced permeability and retention effect
ER	Endoplasmic reticulum
ER	Estrogen receptor
ERK	Extracellular regulated kinase
ER α	Estrogen receptor alpha
ESI	Electron spray ionization
Et ₂ O	Ethyl ether
EtOAc	Ethyl acetate
EtOH	Ethanol
FBS	Fetal bovine serum
FDA	Food and drug administration
FK228	Romidepsin

FR	Folate receptor
H	Hydrogen
H ₂ O	Water
HAT	Histone acetyl transferase
HDAC	Histone deacetylase
HDACi	Histone deacetylase inhibitor
HER2	Human epidermal growth factor receptor 2
hERGK ⁺	Human ether-a-go-go-related gene potassium ion channels
HIF1 α	Hypoxia-inducible factor 1alpha
HOBT	Hydroxybenzotriazole
HPLC	High performance liquid chromatography
HSP90	Heat shock protein 90
HVR	Hypervariable region
Hz	Hertz
IC ₅₀	Half-maximal inhibitory concentration
IG	Immunoglobulin
IP	Intraperitoneal
IV	Intravenous
IVTI	<i>In Vitro</i> Therapeutic index
J	Coupling constant
JAK	Janus kinase
K ⁺	Potassium ion
LTL	Ligand targeting liposome
LYS	K, Lysine
m	Multiplet
m/z	Mass to charge ratio
MAPK	Mitogen-activated protein kinase

MCF-7	An ER positive breast cancer cell line
MDA-MB231	An ER negative breast cancer cell line
MDS	Myelodysplastic syndromes
MeOH	Methanol
MF	Myelofibrosis
MiRP1	Mink-related peptide
mL	Milliliter
MPN	Myeloproliferative neoplasms
MPS	Mono phagocyte system
MS	Mass spectroscopy
MTS	3-(4,5-dimethylthiazol-2-yl)-5-(3-carboxymethoxyphenyl)-2-(4-sulfophenyl)-2H- tetrazolium
NAD ⁺	Nicotinamide adenine dinucleotide
ND	Not determined
NF-κB	Nuclear factor-κB
NGR	Asparagine(N) –Glycine(G) –Arginine(R)
NI	No inhibition
nM	Nanomolar
NMR	Nuclear magnetic resonance
NP	Nanoparticle
NPC	Keratinizing nasopharyngeal carcinoma
NSCLC	Non-small cell lung cancer
NT	Not tested
O-trityl	<i>O</i> -Triphenylmethyl
p21	Cyclin dependent kinase inhibitor
p53	Tumor suppressor protein
PE	Phosphatidylethanolamine

PEG	Polyethylene glycol
PKA	Protein kinase A
PPh ₃	Triphenyl phosphine
ppm	Parts per million
Prep TLC	Preparative TLC
PTCL	Peripheral T-cell lymphoma
PXD101	Belinostat
q	Quartet
QT interval	Time between the beginning of the Q wave and the end of T wave in the cardiac electrical cycle
RES	ReticuloEndothelial system
RGD	Arginine(R) -Glycine(G) –Aspartic acid(D)
RNA	Ribonucleic acid
ROS	Reactive oxygen species
rt	Room temperature
s	Singlet
SAHA	Suberoylanilide hydroxamic acid
SAMDI	Self-assembled monolayers for matrix-assisted laser Desorption ionization
SAR	Structure activity relationship
SB939	Panobinostat
SC	Subcutaneous
SERM	Selective estrogen receptor modulators
SiRNA	Small interfering RNA
SLL	Small lymphatic lymphoma
STAT	Signal transducer and activator of transcription
STPP	Stearyl TPP
t	Triplet

Tam	Tamoxifen
TdP	Torsades de pointes
<i>tert</i>	Tertiary
TF	Transferrin
TFA	Trifluoroacetic acid
TfN ₃	Trifluoromethanesulfonyl azide
TFR	Transferrin receptor
THF	Tetrahydrofuran
TIPS	Triisopropylsilane
TLC	Thin layer chromatography
TPP	Triphenyl phosphonium
TPX	Trapoxin A
TRAIL	Tumor necrosis factor-related apoptosis-induced ligand
TSA	Trichostatin A
TSL	Thermosensitive liposome
VEGF	Vascular endothelial growth factor
VERO	Monkey kidney epithelial cell line
VPA	Valporic acid
WHO	World health organization
ZBG	Zinc binding group
Zn ²⁺	Zinc ion

SUMMARY

Cancer is one of the leading causes of death around the world, with lung, breast and prostate cancer being the most common cancers. Most of current cancer treatments are associated with various side effects such as depression, fatigue, hair loss, nausea, infection, fertility problems, anemia, and myelosuppression. Therefore, there is an unmet need to develop new and more potent anticancer therapeutic agents with less off-target toxicities. This thesis documents efforts at the design and synthesis of different classes of HDAC inhibitors (HDACi) as promising therapeutic agents in cancer therapy. These HDACi are anticipated to accumulate at the site of tumor due to selective tissue/cell distribution conferred on them by ligands, known to accumulate in certain tissues or target receptors that are overexpressed on tumor cells, incorporated into their the cap group.

FDA approved macrolide, azithromycin, is known to accumulate in macrophage cells. Macrophage cells are known to have a high concentration in lung, hence, azithromycin has the potential to target and accumulate in lung tissue. An unpublished *in vivo* data in our lab, showed that azithromycin maintains its lung accumulation after being modified and attached to HDACi moiety. Thus, we hypothesized conjugating the HDACi to azithromycin can lead to their delivery to lung tissues. To this end, in the second chapter, we designed and synthesized three different classes of azithromycin conjugated hydroxamic acid derived HDACi and evaluated their HDAC inhibitory potency and anti-proliferative activity in lung (A549) and breast (MCF-7) cancer cell lines.

It is believed that isoform selective HDACi may be endowed with less off-target toxicities and better therapeutic outcome and efficacy compared to pan HDACi which have no selectivity toward different HDAC isoforms. To evaluate this hypothesis, in the third chapter, we designed and synthesized isoform selective azithromycin conjugated

HDACi, by replacing the hydroxamic acid zinc binding group with the N-(2-amino-5-(thiophen-2-yl)phenyl)acylamide zinc binding group which is a HDAC1 and HDAC2 selective. Additionally to determine these compounds ability to target lung tissue and protect it from metastasis, we tested the lead compound in a model of lung metastasis of breast cancer using spontaneous mouse mammary tumor model MMTV-PyMT-Tg. The *in vivo* study results showed that there was a greater tumor regression in mice that were treated with N-(2-amino-5-(thiophen-2-yl)phenyl)acylamide derived HDACi compared to hydroxamic acid derived HDACi. Additionally this class of HDACi was able to protect the lung tissue from metastasis better than its hydroxamic acid analogue.

The fourth chapter focuses on continuation of prior SAR study on design multiple ligand compounds with selective estrogen receptor modular (SERM) and HDACi activities. In this study tamoxifen, an estrogen receptor (ER) antagonist, with a high binding affinity for ER, was used as the HDACi cap group. These antiestrogen equipped HDACi are expected to be better uptaken by ER positive breast cancer cells possibly due to tamoxifen affinity for binding to ER. This selective uptake is anticipated to eventually lead to an improved antiproliferative activity. MTT assay results confirmed the hypothesis. Hydroxamic acid derived HDACi showed about 4 fold more cytotoxicity toward ER α positive breast cancer cells compared to ER α negative breast cancer cells. Two of these SERM HDACi conjugates are currently being studied in animal models.

The fifth chapter illustrates bifunctional STAT3/HDAC inhibitors for treating STAT3 activated cancers, such as acute myeloid leukemia. In this study, pyrimethamine, a selective STAT3 inhibitor was used as the HDACi cap group. We hypothesized that design multiple ligand compounds comprising STAT3 inhibitor and HADCi will integrate direct STAT3 and HDAC inhibition, and downregulation of Mcl-1 within a single molecular template. These bifunctional compounds can be potential inhibitors of proliferation of CLL, DLBCL and probably other tumors that are dependent on STAT3 signaling pathway.

CHAPTER 1

INTRODUCTION

1.1. Background

Cancer is one of the leading causes of death worldwide and is the second cause of death after cardiovascular diseases in the United States [1], [2]. According to National Cancer Institute there will be approximately 1,685,210 new cases of cancer, and 595,690 cancer deaths which is equal to 1600 deaths per day only in United States in 2016 [3].

Cancer develops when there is an environmental or inherited mutation or damage in the genetic materials of cells such as proto-oncogenes that are responsible for coding for proteins involved in cell proliferation and differentiation or tumor suppressor genes inhibit cancer cell growth or induce apoptosis. Normal cells grow, divide, die, and eventually are replaced by new cells. However, cancer is an uncontrollable cell growth, division and proliferation that is resistant to normal cell death, consequently leading to the formation of an abnormal cell mass or tumor [4]. Cancerous cells can become metastatic with time and migrate to other parts of body as well [5]. In fact tumor cells ability to sustain proliferating signaling and replicative immortality helps them to evade tumor growth suppressors, activate invasion and metastasis, induce angiogenesis and finally resist cell death, which is why it is difficult to eradicate tumor growth and cure cancer [6].

The most common cancers in US are that of the lung, bronchus, colorectal and prostate (in men), and breast (in women). Together, these cancers account for about 46% of cancer prevalence with the lung cancer being the most prevalent with 27% occurrence [1]. Moreover, cancer mortality is higher for men rather than women and it has its highest rate for African American men and lowest rate for Asian/Pacific Islander women [7].

Surgery, chemotherapy, and radiation are the most common cancer treatments [8], with hormone therapy, immunotherapy or targeted therapy serving as other choices of treatment. Surgery is used to remove the tumor as well as other cells or parts of the body that were affected by tumor cells. For example, a common surgical procedure is the removal of part or all of breast or prostate gland in the case of breast and prostate cancers. Chemotherapy on the other hand is the administration of drugs orally or intravenously to kill tumor cells or to slow their growth [9]. Additionally, radiation is another choice of treatment used in combination with other treatments or as a standalone therapy to treat cancer. Surgery and radiotherapy are the most effective therapy for non-metastatic cancers that are limited to certain areas of the body and has not yet spread to other tissues, whereas, chemotherapy and hormone therapy are the only treatments for metastatic cancers since they can reach all the organs in the body through blood circulation [10]. Unfortunately, these treatments are accompanied with side effects such as nausea, vomiting, fatigue, anemia, and lymphedema due to their off-target toxicities to healthy cells. Furthermore, emergence of multi-drug resistance in addition to cytotoxicity of current anticancer agents brings up the critical need for developing targeted cancer drugs.

1.2. Epigenetics

Epigenetics is mitotically and meiotically heritable changes in DNA expression and histone modification without alteration to gene sequences that regulate cell function. Epigenetic silencing is caused by RNA- associated silencing, chromatin remodeling and most importantly DNA methylation, and histone modifications such as methylation, acetylation, phosphorylation, ubiquitination and sumoylation. These processes are associated with dysfunctions in transcriptional activation. Aberrant regulation of the epigenome results in dysfunction in the control of gene expression which can present in

various physiological conditions. Disruption of these regulating systems can lead to various diseases including cancer [11].

Nucleosomes are the basal units of chromatin, and are made of five histone proteins. Nucleosome core consists of the core histone octamers H2A, H2B, H3 and H4. Core histones are involved in both histone-histone interactions as well as histone-DNA's. H1 on the other hand, is a linker histone and is responsible for chromatin compaction and maintaining chromosome structure. The state of chromatin is very important for many cellular mechanisms such as transcription, translation and repair. Chromatin state is determined by changes in amino terminal tails of the histones. Around 30-40% of core histone amino acids are positively charged lysine and arginine. The high density of positive charge, along with the undetectable secondary structure of free histones, led to the presumption that *N*-termini of histones operate by binding as unstructured coils to DNA components in nucleosome [12].

The histone amino tail groups are believed to interact with negatively charged DNA backbone or other chromatin related proteins. The DNA interaction with chromatin can facilitate or hinder cellular processes like transcription, translation and apoptosis [13]. Histone tail post-translation modifications such as methylation, acetylation, phosphorylation, and ubiquitination have been the subject of many studies [14].

The focus of this thesis is on histone deacetylation, the link between aberrant histone deacetylation tumorigenesis and design of small molecules which promote histone acetylation through inhibition of the deacetylase activities of various histone deacetylase isoforms. The sections below are focused on histone deacetylation and its inhibition in efforts aimed at identifying tumor selective histone deacetylase inhibitors. Additionally, it focuses on different methods for HDACi specific tissue delivery to enhance their potency and lower their off-target toxicities.

1.3. Histone acetylation

Nucleosome consists of 146 base pairs of DNA wrapped around core histone octamer [15]. Nucleosome has two copies of each core histone. All four core histones in nucleosome are subject to post acetylation of their terminus amino groups of specific lysine residues (Figure 1.1) [16]. Core histones H2B, H3 and H4 each has 16 possible isoforms including 1 non-acetylated, 4 mono-acetylated, 6 di-acetylated, 2 tri-acetylated and 1 tetra-acetylated. H2A only has 2 isoforms: 1 non-acetylated and 1 mono-acetylated. Thus altogether there are $16 \times 16 \times 16 \times 2 = 8192$ possible combinations within every single nucleosome [14]. Furthermore, H1 histone protein is associated with each nucleosome and plays an important role in DNA level of condensation [17].

The idea of histone acetylation and its relation with gene transcription was suggested about five decades ago [18]. Histones are acetylated by histone acetyl transferase enzyme (HAT) which transfers the acetyl group from acetyl coenzyme (acetyl CoA) to the terminal amine group of histone lysine residues. Histone acetylation revamps the structure of chromatin and therefore influences transcription as well as DNA replication. Acetylation affects initiation and elongation of transcription by diminishing the interactions between DNA and histone leading to an open chromatin and more accessible transcription factors [19]. *In vitro* studies have revealed that acetylation of lysine residues of histone promotes binding of particular transcription factors to DNA and therefore stimulate gene expression [19].

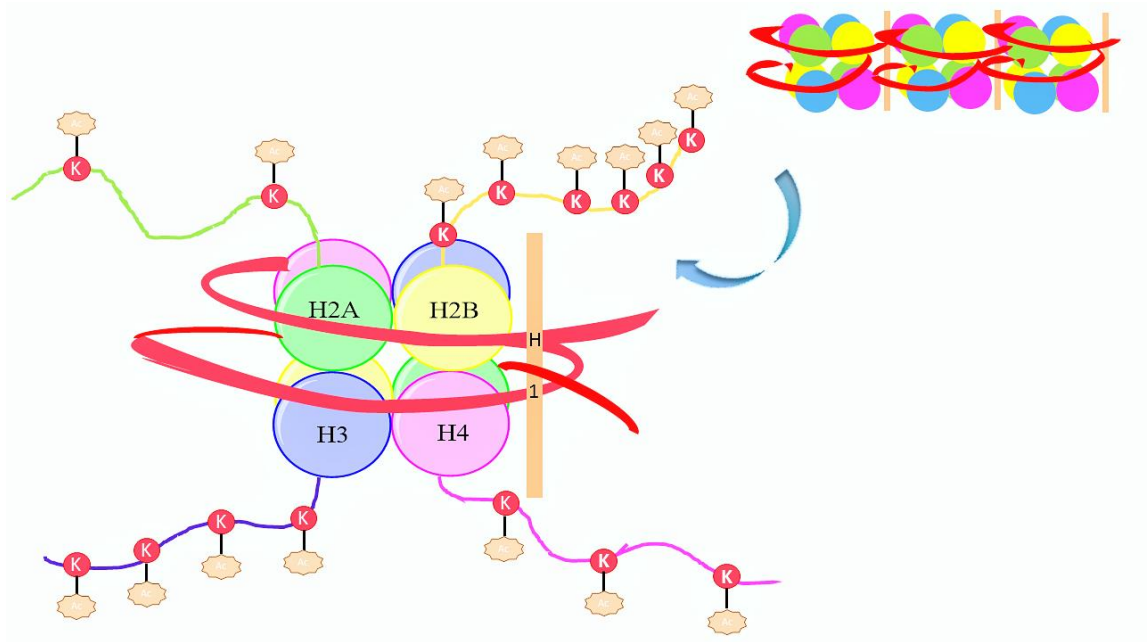


Figure 1.1. Nucleosome consists of 4 core histones, H2A, H2B, H3, H4, and the linker histone H1. Histones are the main proteins of chromatin which DNA winds around. These core histones are subject to post-translation modifications, one of which is acetylation of the amine group of specific terminal lysine residues by histone acetyl transferase enzyme. Adding acetyl group on positively charged lysine residues results in less electrostatic interactions between histone and negatively charged DNA leading to an open chromatin which is accessible transcription factors.

1.4. Histone deacetylation

Dynamic acetylation and deacetylation of histones is one of the mechanisms of regulation of gene expression. Histone acetylation status is controlled by the activities of histone acetyl transferases (HAT) and histone deacetylase (HDAC) enzymes. HDACs are functionally opposing to HATs as they hydrolyze the acetyl groups of acetylated lysine residues on the tail of histones [20]. HDAC isoforms not only remove the acetyl group from the tail of histones, they also bind to and deacetylate other non-histone proteins that

are responsible for regulating cell growth, differentiation, transcription, apoptosis and tumorigenesis inhibition: such as p53, p21, p65, E2F, STAT3 and NF- κ B [21]. Histone deacetylation has a vital role in cancer development by regulating expression of proteins that are involved in initiation and progression of cancer (Figure 1.2).

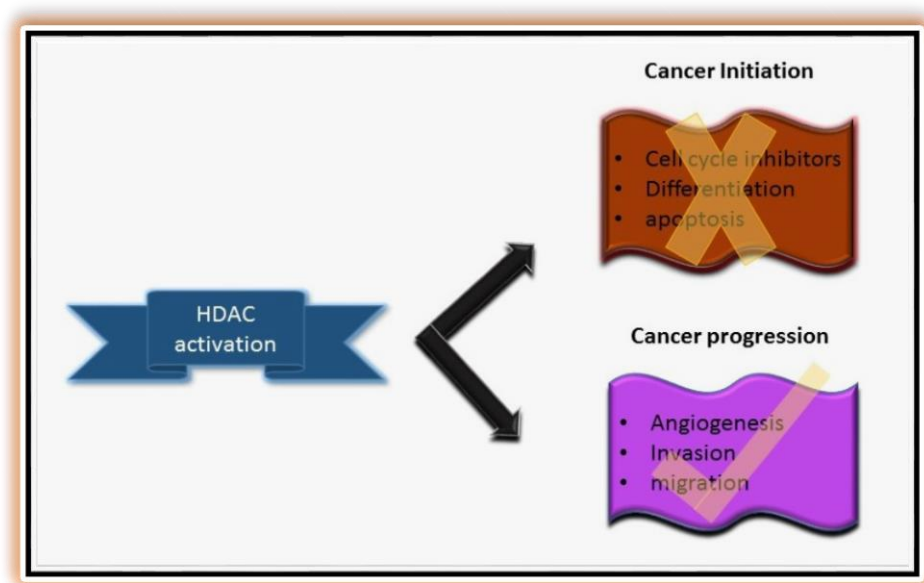


Figure 1.2. HDAC activation regulates expression of genes that are involved in tumorigenesis [21].

The hydrolysis of the acetyl group increases the net positive charge on histones, resulting in enhanced electrostatic interactions with the negative charge of DNA backbone and ultimately compacting chromatin (Figure 1.3).

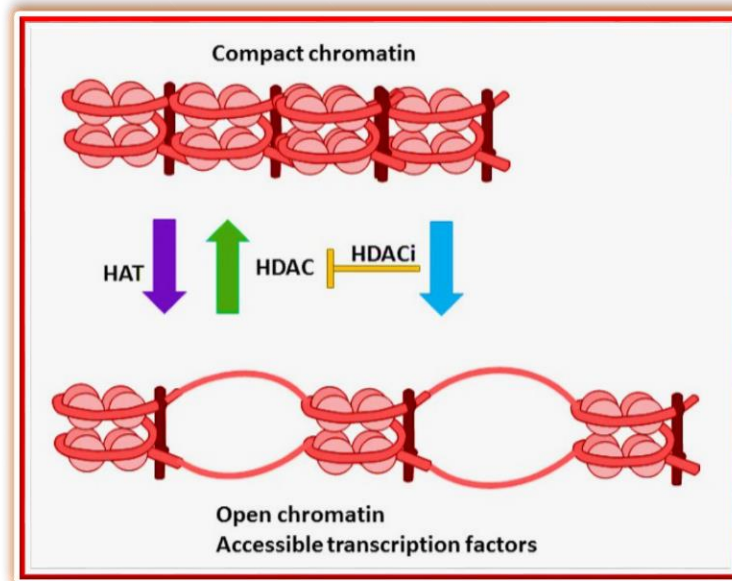


Figure 1.3. HDAC enzymes are functionally opposite to the HAT enzymes. They hydrolyze the acetyl groups from the amine moiety of terminal lysine residues of histones. This leaves a positive charge on histone and induces electrostatic interactions with negatively charged DNA, resulting in condensed chromatin less accessible to transcription factors. HDACi impede HDAC isoforms functions and shift the equilibrium towards an open and accessible chromatin.

Apart from cancer, HDAC activities have also been implicated in survival of *Plasmodium* spp., the causative organisms of malaria, neurodegenerative diseases, embryogenesis, immunological responses and cell differentiation. Impeding the activity of HDAC enzymes by using HDACi shifts the equilibrium toward more open and accessible chromatin which leads to gene transcription [22].

1.4.1. Histone deacetylase isoforms

There are 18 isoforms of HDAC. These isoforms are divided into four classes depending on their sequence homology to their yeast homologs as well as their cellular location. Classes I, II, IV are zinc atom (Zn^{2+}) dependent while class III is nicotinamide adenine dinucleotide (NAD^+) dependent, and is not the focus of this dissertation. Class I isoforms (HDAC1 - 483 AA, HDAC2 - 488 AA, HDAC3 - 423 AA, HDAC8 - 377 AA) are located in nucleus and are homologous to yeast Rpd3 protein. Class II isoforms are divided into two subclasses. Class IIa isoforms (HDAC4 - 1084 AA, HDAC5 - 1122 AA, HDAC7 - 855 AA, HDAC9 - 1011 AA) have both nucleus and cytoplasmic localizations while class IIb isoforms (HDAC6 - 1215 AA, HDAC10 - 699 AA) are mainly localized in cytoplasm. Class IIb isoforms are the only isoforms with two catalytic active sites [21]. The only isoform of class IV is HDAC11 (with 347 AA) can be found both in nucleus and cytoplasm (Table 1.1) [24].

Table 1.1. HDAC isoforms with their size, function, localization, and selected examples of their target proteins [25], [26], [27].

Class	HDAC isoform	Size (AA)	Physiological function	Expression	Selected target proteins
Class I	HDAC1	483	Cell survival and proliferation	Nucleus	p53, NF- κ B, E2F1, Stat3, AR
	HDAC2	488	Cell proliferation/ Insulin resistance		Bcl-6, NF- κ B, Stat3

Table 1.2. HDAC isoforms with their size, function, localization, and selected examples of their target proteins (continued)

	HDAC3	423	Cell survival and proliferation		Stat3, SHP
	HDAC8	377	Cell proliferation		–
Class IIa	HDAC4	1084	Regulation of skeletogenesis and gluconeogenesis	Nucleus/ Cytoplasm	GATA-1, HP-1
	HDAC5	1122	Cardiovascular growth and function/ Gluconeogenesis/ Cardiac myocytes and endothelial cell function		Smad7, HP-1
	HDAC7	855	Thymocyte differentiation/ Endothelial function/ Gluconeogenesis		Plag1/ Plag2
	HDAC9	1011	Homologous recombination/ Thymocyte differentiation/ Cardiovascular growth and function		–
Class IIb	HDAC6	1215	Cell motility/ Control of cytoskeletal dynamics	Cytoplasm	Tubulin, Hsp90, Smad7
	HDAC10	669	Homologous recombination/ Autophagy mediated cell survival		–
Class IV	HDAC11	347	Immunomodulators- DNA replication	Nucleus/ Cytoplasm	–

1.4.1.1. Class I isoforms

Class I HDAC isoforms are located in the nucleus. They are found in many human tissues and cell lines [28]. Class I isoforms can be divided into three subclasses, class Ia (HDAC1 and HDAC2), class Ib (HDAC3) and class Ic (HDAC8) [26], [27]. HDAC1 and HDAC2 interact with each other, and form the catalytic core of multiprotein complexes, while HDAC3 is in complex with nuclear receptor corepressors [29]. HDAC8, with less tissue expression compared to other class I HDAC isoforms, is an unusual member of class I family. According to its sequence homology it should be classified as a class I member, but based on phylogenetic analysis it is on the border line of class I and class II. The main difference between HDAC8 and other class I isoforms is that HDAC8 lack the 50-111 amino acid terminal domain which is necessary for other class I isoforms to modulate their enzyme activity and localization [30]. Furthermore, unlike other class I members it is not phosphorylated by Casein kinase II (CKII) but by protein kinase A (PKA) which is involved in regulation of catalytic activity of HDAC8 [31].

Class I HDAC isoforms are activated by other mechanisms including inositol phosphate which are derived from membrane phospholipids. Class I HDAC isoforms regulation by inositol phosphate was first reported by the discovery of inositol 1,4,5,6-tetrakisphosphate (Ins(1,4,5,6)P₄) in the crystal structure of HDAC3:SMRT [32]. Inositol phosphates locate in a binding pocket between HDACs and co-repressor proteins and mediate their interactions [32].

1.4.1.2. Class II isoforms

Class II isoforms are homologues to Hda1 yeast protein. This class of HDAC isoforms shuttle between nucleus and cytoplasm and their expression level varies between different tissues. Class IIa HDAC isoforms are involved in differentiation

process, and is believed their deacetylation activity is due to their interaction with HDAC3 [33].

The unique property of class IIb isoforms is the presence of two catalytic active sites [22]. HDAC6 has a C-terminal zinc finger domain with cysteine and histidine rich regions that binds to proteins. However, since HDAC6 is mainly located in cytosol it is not counted strictly as an epigenetic enzyme. HDAC6 does not deacetylate histones. The anti-cancer activity of HDAC6 inhibitors, such as tubacin and Tubastatin A, is not due to the perturbation of epigenomes which leads to re-expression of tumor suppressor genes, but most likely due to regulation of protein degradation through aggresome and controlling the Hsp90 chaperone activity [34].

HDAC6 is the only class II isoform that is able to deacetylate α -tubulin [35]. Furthermore, inhibition of HDAC6 results in acetylation of HSP90 and disruption of its chaperone activity. HDAC6 has a key role in degradation of misfolded proteins by using its ubiquitin-binding domain [36]. Additionally, HDAC6 is involved in tumorigenesis especially in Ras-induced transformation [37].

HDAC10 is the least characterized and the last isoform of class II that was discovered [38]. Even though it is in the same subclass as HDAC6 they are different in some aspects. For example, unlike HDAC6 that mostly resides in the cytoplasm and possesses two independent active sites, only one of the HDAC10 catalytic site is active and the other one is catalytically inactive. HDAC10 can be found both in cytoplasm and nucleus [38].

1.4.1.3. Class IV isoforms

The only isoform of class IV is HDAC11. HDAC11's structure is related to both class I and class II HDAC isoforms. It is mostly found in the nucleus and in tissues such as brain, heart, kidney, testis and skeletal muscle. HDAC 11 is a promising target for autoimmune diseases [39].

1.5. Histone Deacetylase inhibition

Since HDAC enzymes induce gene silencing and transcription factors repression, they are implicated in various diseases including cancer, malaria, and leishmanial [20]. Inhibition of HDAC activity can reverse epigenetic silencing associated with cancer. As a result, HDAC isoforms have become promising targets for drug discovery and development. HDACi induce cellular differentiation and migration, cell cycle arrest (mostly at the G₁/S checkpoint) and apoptosis [40], leading to growth arrest, DNA damage and tumor cell death. HDACi boost host immune response and decrease angiogenesis in tumor [41], [42].

1.6. Pharmacophoric model of HDACi

Despite all the structural differences among HDACi, they all follow a well-established pharmacophoric model (Figure 1.4). They all are comprised of three distinct groups, a variable surface recognition cap group that interacts at the protein surface, a linker group which travels through the tunnel of the active site, and a zinc binding group (ZBG) that chelates the zinc ion at the active site of the HDAC enzyme (Figure 1.5) [43].

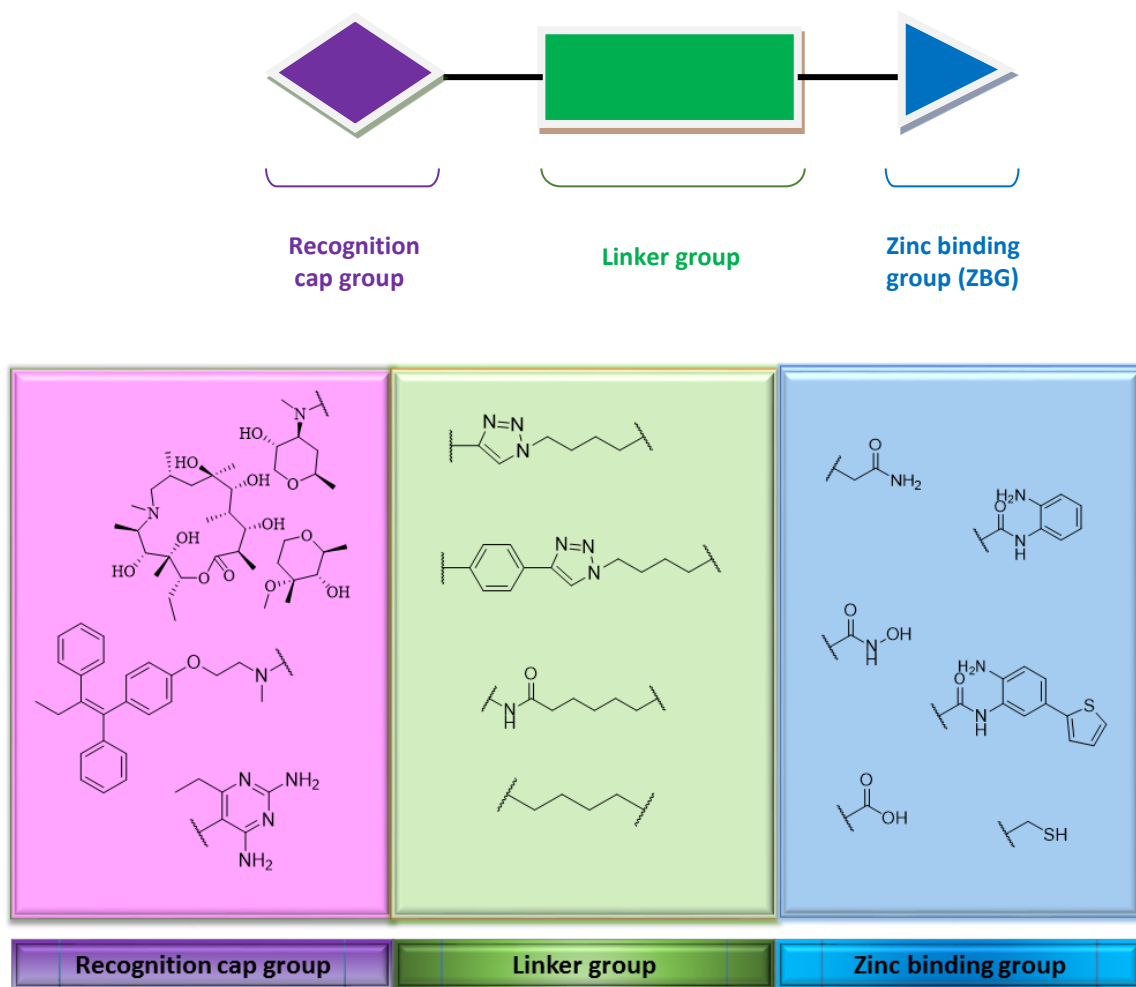


Figure 1.4. Pharmacophoric model of HDACi with selected examples of each group. All HDACi have surface recognition group that interacts with amino acid at the protein surface, a linker group that traverses the active site and a zinc binding group that chelates zinc atom in the active site pocket of the enzyme.

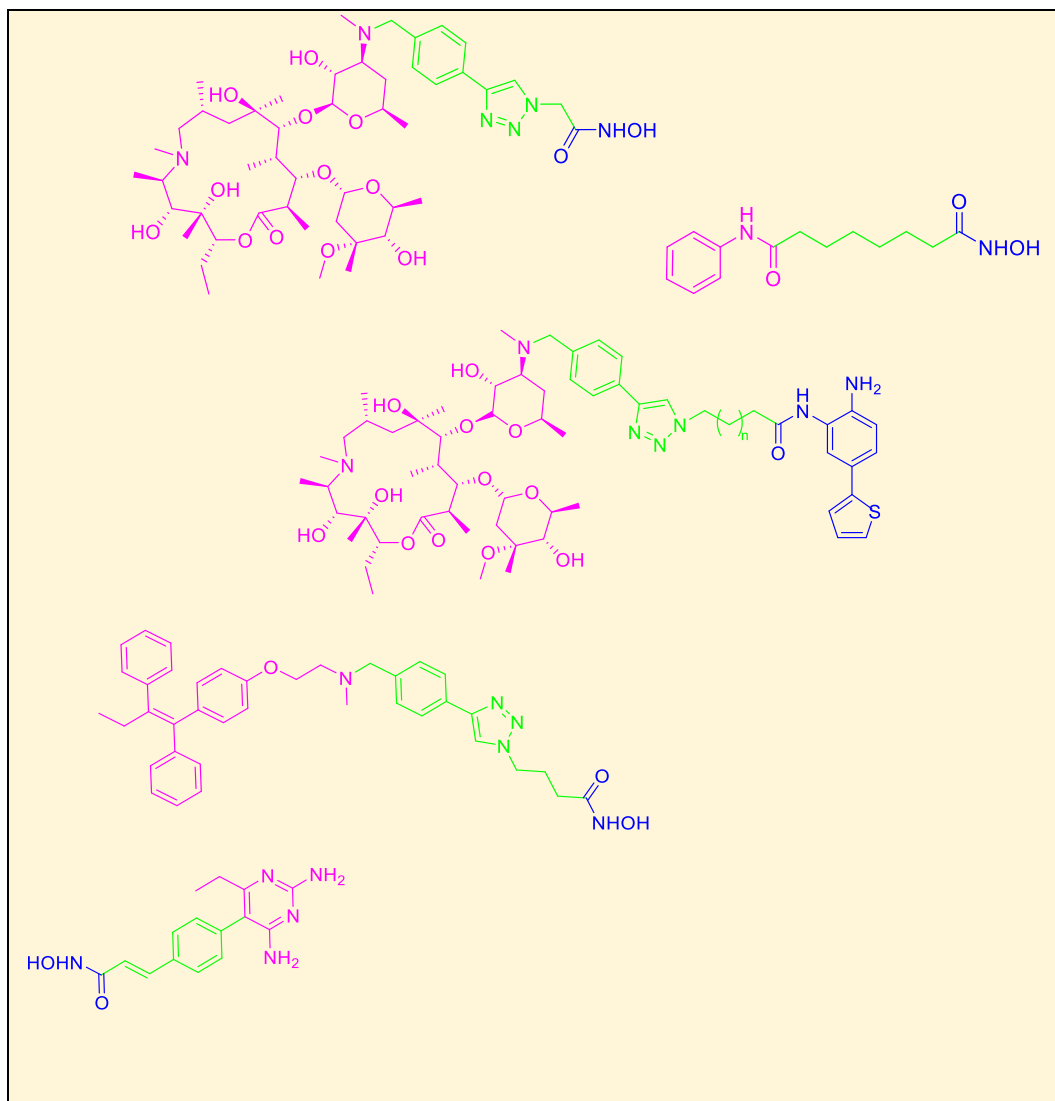


Figure 1.5. Selected examples of HDACi. Most HDACi follow a common three-motif pharmacophoric model comprising of recognition cap group, linker moiety and ZBG. (Note the color coding, purple indicates the cap recognition group, green shows the linker groups and blue indicates the ZBG).

1.6.1. Recognition cap group

The recognition cap group is generally a hydrophobic group that interacts with amino acids at the entrance of the active site and has an important role in inhibitory potency and isoform selectivity of HDACi [23].

Cyclic-peptide and depsipeptide recognition cap groups have been shown to impact class I isoform selectivity to HDACi. Their selectivity towards class I isoforms is due to their similarity to and/or imitation of the natural substrates of this class of HDAC proteins [44]. Natural products such as trapoxin A (TPX) (Figure 1.6), chlamydocin and Cyl-2 show great selectivity for class I isoforms. Romidepsin (depsipeptide, FK-228) is a FDA approved HDACi that shows a high selectivity for HDAC1 and HDAC2 compared to class II isoforms [45]. In addition to the similarities to the natural substrates, existence of two loops in class II isoforms prevents binding of bulky cap groups and makes it sterically unfavorable for cyclic peptides to bind and interact with the amino acids at the surface. The trends show that compounds with smaller cap groups have less isoform selectivity towards class I HDACs compared to the bulky ones. In fact using a bulky recognition cap group has turned into a strategy for developing class I isoform selective HDACi [23].

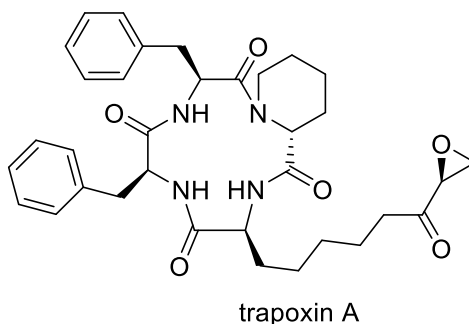


Figure 1.6. Chemical structure of trapoxin A, a naturally occurring selective class I isoform HDACi [46].

1.6.2. Linker group

The linker group traverses the tunnel leading to the active site and connects the surface recognition cap group to the zinc binding group. The linker domain typically consists of hydrophobic groups that interact with the lipophilic residues within the tunnel leading to the active site. The linker group can be a linear chain or a cyclic chain with

saturated or unsaturated bonds. Like two other compartment of the pharmacophoric model, this region can be modified to yield isoform selective HDACi as well. However, only a few class I selective HDACi have been reported up to date [23].

1.6.3. Zinc binding group

The ZBG, which chelates the Zn^{2+} ion in the active site pocket, is a major determinant of HDACi isoform selectivity and potency. However, the sequence similarity near the catalytic metal makes it very difficult to design and synthesize HDACi that are selective toward certain isoforms. Figure 1.7 illustrates zinc ion at the base of the catalytic pocket of HDAC 1, a class I isoform of HDAC enzymes.

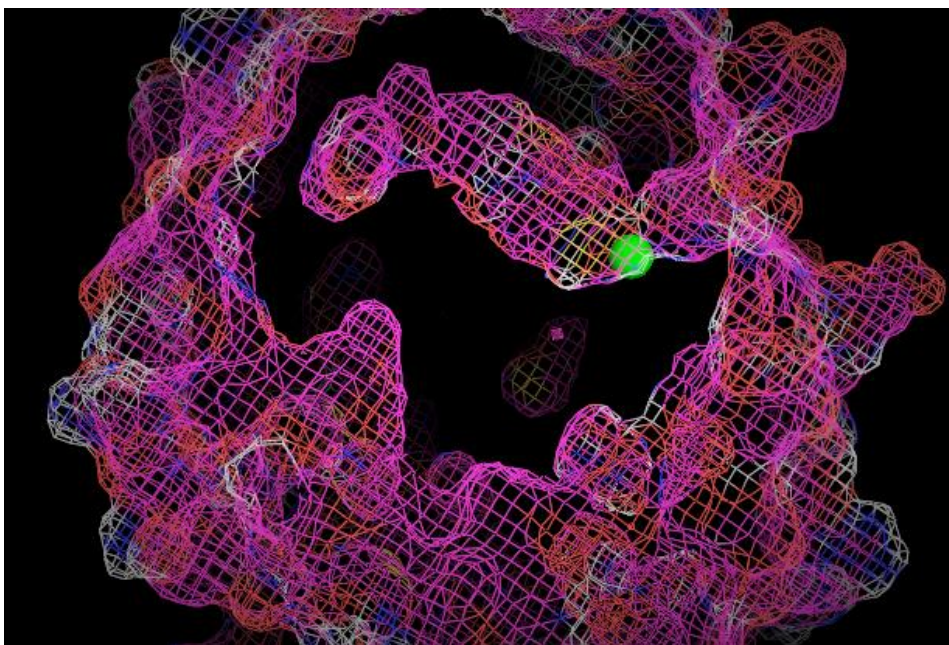


Figure 1.7. Zinc atom in the catalytic pocket of HDAC1, a class I HDAC isoform. Green sphere represents zinc atom.

The most common ZBG is hydroxamic acid. It owes its high potency to its strong bidentate chelation of zinc ion. The most well-known example of an HDACi with hydroxamic acid-based ZBG is suberoylanilide hydroxamic acid (SAHA) (also known as Vorinostat). The second common zinc binding group is alkyl thiol found in naturally

occurring depsipeptide prodrugs like largazole, FK228, or spiruchostatins. These prodrugs disulfide bridge is reduced to alkyl thiol ZBG upon their administration *in vivo*, resulting in isoform selective HDAC inhibition [45]. The third most common ZBG is the benzamide moiety which leads to class I isoform selectivity. Entinostat (MS-275) is a benzamide based HDACi which is currently in clinical trials for treating various types of cancers [22]. Additionally, there are other ZBGs that are not as common as the previously mentioned ones. These less common ZBGs include ketones, fluoroketones, carboxylic acids, carboxamide, thioamide, and epoxides (Table 1.2) [44].

Table 1.2. Selected examples of HDACi with various zinc binding groups [47].

Zinc binding group	Name	Isoform selectivity
Hydroxamic acid	Vorinostat (SAHA)	Pan inhibitor
	Belinostat (PXD101)	Pan inhibitor
	Panobinostat (LBH589)	Pan inhibitor
	Abexinostat (PCI 24781)	Pan inhibitor
	Pracinostat (SB939)	Pan inhibitor
	Givinostat (ITF2357)	Pan inhibitor
	Resminostat (4SC-201)	Pan inhibitor
Carboxamide	Azumamides	Class I

Table 1.2. Selected examples of HDACi with various zinc binding groups (continued).

Alkyl thiol	Romidepsin (FK228)	Class I
Benzamide	Entinostat (MS-275)	Class I
	Mocetinostat (MGCD0103)	Class I
Fatty acid	Valproic acid (VPA)	Class I
	Phenylbutyrate	Class I and II

1.6.3.1. Zinc dependent mechanism of lysine deacetylation

Finnin *et al.* [48] was the first to propose a mechanism for zinc dependent lysine deacetylation for HDLP which is almost similar for all zinc dependent HDAC enzymatic activity (Figure 1.8). In class I HDAC isoforms, the zinc ion in the active site is surrounded by two histidine-aspartic acid dyads (His131-Asp166 and His132-Asp173). Each histidine has a hydrogen bond with aspartic acid carboxylate oxygen, which is a characteristic of a charge-rely system found in the active site. The charge-rely system of His131-Asp166 is more buried in the active site than His132-Asp173. His131-Asp166 makes a hydrogen bond to the zinc bound water molecule. In class II isoforms in one of the dyads, one aspartic acid is replaced by asparagine, resulting in His-Asn pair. There is also a tyrosine residue (Tyr297) in class I HDAC isoforms that provides a proton. The tyrosine residue interacts with two aspartic acids (Asp258 and Asp168) as well as one

histidine (His170). In class II HDAC isoforms, the tyrosine residue is replaced with a histidine.

Lysine deacetylation starts with the zinc ion chelation of the water molecule as well as the carbonyl group of the acetyl lysine. The chelated water molecule is activated through H-bonding interaction with His131, resulting in nucleophilic attack of the carbonyl group of acetylated lysine. The resulting acyl anion is stabilized by the H-bonding with the hydroxyl group of Tyr297. The acyl anion then undergoes a rearrangement which results in formation of an acetate ion as well as a terminal ammonium on the terminal lysine residue of histone [49].

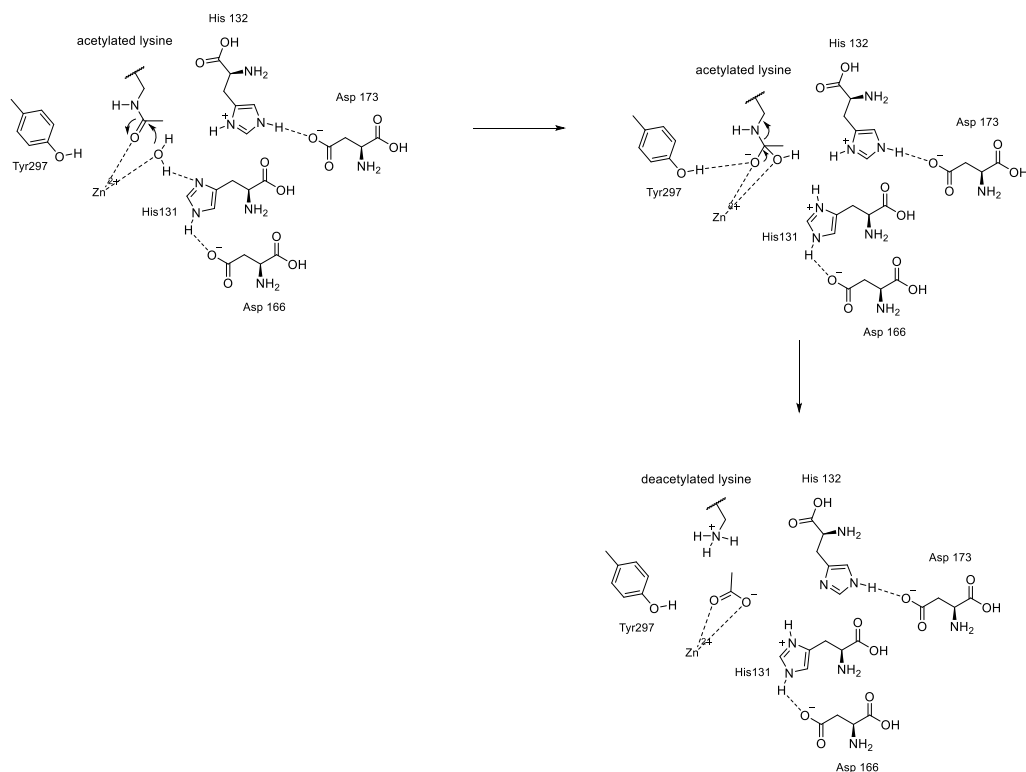


Figure 1.8. Proposed mechanism for lysine residue deacetylation by zinc-dependent HDAC enzymes [49]. Zinc atom chelates a water molecule and the carbonyl group of acetylated lysine ultimately leading to the hydrolysis of the acetyl group from the terminal lysine residues.

1.6.3.2. Hydroxamic acid derived HDACi

Hydroxamic acid based antiproliferative therapeutic agents were the first group of HDACi that were introduced. Hydroxamic acid-based HDACi are the broadest group of agents used in establishment of HDACi pharmacophoric model. Like all other classes of HDACi, this group is comprised of a bulky cap recognition group that interacts with the amino acids at the surface of the active site and a linker which helps position the hydroxamic acid ZBG for chelation to the zinc ion at the base of HDAC catalytic pocket and blocks the access of the substrate to the zinc atom [50]. The most well-known hydroxamic acid based HDACi is the FDA approved SAHA, which is pan inhibitor of HDAC isoforms [51].

Trichostatin A (TSA) (Figure 1.9), one of the first naturally occurring hydroxamic acid-based HDACi discovered, is isolated from *Streptomyces hygroscopicus* strain. TSA is known as an antifungal agent due to its ability to inhibit HDAC isoforms. TSA inhibits cell proliferation and induces growth arrest, differentiation, and apoptosis in various transformed cell lines. However its toxicity, relative instability, and lack of HDAC isoform selectivity led to the search for other substances. Many HDACi drug designs have been inspired by the structure of TSA [52].

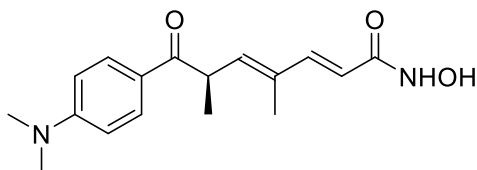


Figure 1.9. Chemical structure of trichostatin A (TSA), a naturally occurring non-selective HDACi. TSA was among the first naturally occurring HDACi to be described [44], [53].

1.6.3.3. Depsipeptide-derived HDACi

This class of HDACi has the most complex structure. They inhibit HDAC isoforms at nanomolar concentrations. They have also shown to be antiangiogenic by modulation of the expression of c-myc and regulatory genes [52]. Romidepsin (FK-228), a natural prodrug, is the most distinguished depsipeptide in this class. It is believed that its disulfide bond breaks and forms alkyl thiol once it is inside the cells. The 4-mercaptobut-1-enyl fits into the HDAC enzyme catalytic pocket and chelates the zinc atom at the base of the active site [45].

1.6.3.4. Benzamide-derived HDACi

This group of HDACi is less potent compared to their corresponding hydroxamic acid derivatives. However, several class I isoform-selective HDACi are derived from this group. Entinostat (MS-275) shows about 135 fold preference for HDAC1 and HDAC3 compared to HDAC6 and HDAC8 [54]. MS-275 is in clinical trials for treating patients with advanced and refractory solid tumors and lymphoma [55].

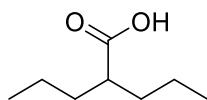
A crystallographic comparison between bacteria homologues of class I (HDLP) and class II (FB188HDAH) HDAC enzymes revealed the existence of a 14 Å hydrophobic internal cavity within the active site near the zinc ion. It is believed this internal cavity is an exit channel for releasing the acetate byproduct after deacetylation process [56]. The sequence difference in the internal cavity for HDLP and FB188HDAH can be used to design and synthesize isoform selective HDACi [57]. In fact, docking of MS-275 in the active site of an HDAC1 homology model revealed that more nonpolar substituents can be placed on the benzamide ring to favor the hydrophobic interactions with the lipophilic residues into the 14 Å internal cavity [58]. Furthermore, SAR study has shown the 2'-amino moiety of the benzanilide group is essential for HDAC inhibition [47]. The amino group is involved in zinc chelation in addition to interactions with histidines 140 and 141 through hydrogen binding [59].

1.6.3.5. Epoxide-derived HDACi

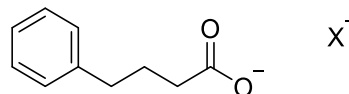
The HDAC inhibitory potency of epoxide-derived HDACi comes from their chelation of the active site zinc ion or an interaction with an amino acid within the active pocket. However, these compounds do not show much activity *in vivo* due to liability issues. Previously mentioned natural product, cyclic tetrapeptide trapoxin A is a member of this family [50].

1.6.3.6. Carboxylic acid (short fatty acid) HDACi

This group of HDACi has simple structures, and are less potent compared to the hydroxamic acid-derived HDACi. Two members of this group, valproic acid (VPA) and phenylbutyrate (Figure 1.10) are well-characterized and have already been approved for treating epilepsy. These two HDACi are in clinical trials for treating various types of cancer, including such as refractory solid tumors, lymphoma, prostate and breast cancers [60]. VPA promotes selective proteasomal degradation of HDAC2 [52] and shows growth suppression, proliferation inhibition and apoptosis induction [52]. VPA has been tested in many clinical trials both as a standalone and in combination therapies. It has been tested in a phase I study in patients with refractory solid or central nervous system tumors (CNS) [61]. VPA, in combination with 5-aza-2'-deoxycytidine (decitabine), was tested in patients with non-small cell lung cancer (NSCLC). Even though this combination therapy was found to be effective, it had to be terminated due to neurological toxicities at low doses [62].



Valproic acid



Phenylbutyrate

Figure 1.10. Chemical structures of valproic acid and phenylbutyrate, two well-established short fatty acid HDACi have been tested in clinical trials for treating various types of cancer [27].

1.7. FDA approved HDACi

In the last few years more than 490 clinical trials have been performed on a wide variety of HDACi [63], with phenylbutyrate being the first one enter clinical trials for treating various types of cancers such as prostate cancer, lymphoma and leukemia [64]. There are currently four FDA approved HDACi in the market. Vorinostat was the first to obtain FDA approval, followed by romidepsin and belinostat. Panobinostat is the latest HDACi which got approved in 2015 (Figure 1.11).

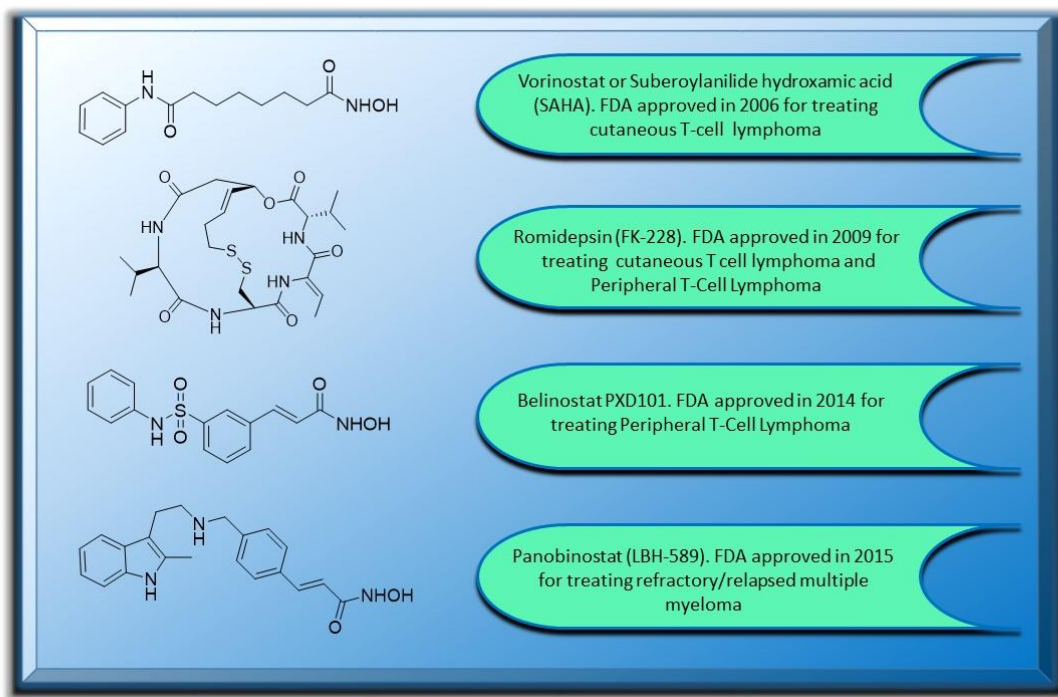


Figure 1.11. US FDA approved HDACi and their clinical indications [27].

1.7.1. Suberoylanilide hydroxamic acid (SAHA)

SAHA, also known as vorinostat, is the first HDACi in the clinic. It was approved by the US FDA in 2006 for treating relapsed and refractory cutaneous T-cell lymphoma (CTCL). Vorinostat is an orally active drug, manufactured by Merck & Co., Inc. [65]. Its approval was based on a phase II clinical trials in 74 patients with stage IB or higher CTCL, who already had two failed systematic therapies. This clinical trial only had 30% objective response rate [65], and nine patients had to stop taking the drug because of adverse side effects while eleven needed dose modification [66].

Vorinostat has been investigated in several clinical trials for treating solid tumors including relapsed and refractory breast and non-small cell lung cancers. Unfortunately vorinostat showed either a low or no activity in all of these trials [67]. Vorinostat is currently being studied in clinical trials in combination with other therapeutic agents [68]. For example, it is in phase I study in combination with bortezomib in patients with advanced, relapsed and refractory multiple myeloma [69], [70]. Additionally, vorinostat in combination with decitabine is in a phase I clinical trials for treatment of relapsed or newly diagnosed acute myelogenous leukemia or myelodysplastic syndrome [71]. Despite its potent HDAC inhibition vorinostat is a pan HDACi which suffers from toxic side effects possibly due to its lack of isoform selectivity [62].

1.7.2. Romidepsin (FK228)

Romidepsin (FK228) is the second HDACi and only depsipeptide that has so far obtained FDA approval. It was approved in 2009 for treating patients with cutaneous T-cell lymphoma as well as peripheral T-cell lymphoma (PTCL) who had received at least one failed systematic therapy. Romidepsin, is a potent, bicyclic class I isoform selective HDACi isolated from *chromobacterium violaceum*, a gram negative bacteria in a Japanese soil sample [72]. Romidepsin acts as a prodrug and its disulfide bond is reduced

by glutathione upon administration, leading to formation of a free thiol which is able to chelate and interact with the zinc ion in the HDAC enzyme pocket (Figure 1.12) [73].

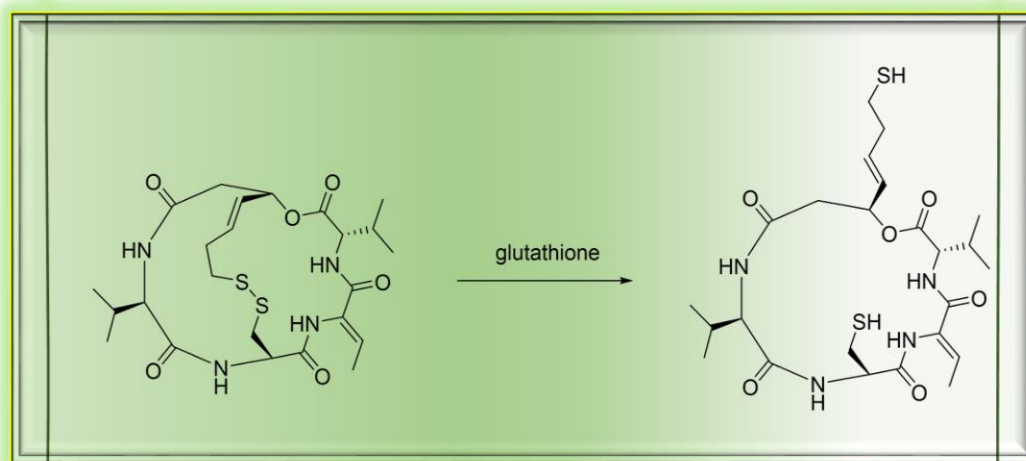


Figure 1.12. Reduction of romidepsin to its active form. Romidepsin is a prodrug, and its disulfide bond is reduced to alkyl thiol by glutathione *in vivo* [22].

1.7.3. Belinostat (PXD101)

Belinostat (PXD101) is a hydroxamic acid-based pan HDACi given FDA accelerated approval in 2014 for treating patients with relapsed or refractory peripheral T-cell lymphoma. Its approval was based on efficacy and safety data acquired from a single arm phase II trial. Belinostat has the trade name Beleodaq and it is manufactured by Spectrum Pharmaceuticals, Inc [65].

Belinostat inhibits tumor cell proliferation and like all other HDAC inhibitors, promotes expression of cycline dependent kinase inhibitor, p21, and apoptosis [74]. It inhibits growth of several human cell lines such as non-small cell lung, breast and prostate *in vitro*, and shows antitumor activity *in vivo* in human tumor xenografts [75]. Following the same trend for FDA approved HDACi, belinostat was tested in clinical trials for both solid and hematological cancers which resulted in no or poor activity. It is

suggested that HDACi lack of efficacy in treating solid tumors is due to their instability to reach the tumor site [27].

1.7.4. Panobinostat (LBH589)

Panobinostat (LBH589) is another potent hydroxamic acid-based pan HDACi. It is developed by Novartis with the trade name Farydak and can be administered both orally and intravenously. Panobinostat was granted FDA approval in 2015 based on progression free survival in pre-specified analysis of a phase III PANORAMA 1 trial [76]. Panobinostat is the first HDACi approved in US for treating patients with multiple myeloma who had received at least two prior treatments including the immunomodulatory agent, bortezomib. Panobinostat is undergoing more clinical trials as a combination therapy with other therapeutic agents in the relapsed, refractory and newly diagnosed patients with myeloma [77]. Currently, there is a regulatory submission for use of panobinostat in combination therapy for treating multiple myeloma in Europe and Japan [78].

1.8. Mechanism of HDACi-induced cell death

In general, HDACi induce tumor cell death through five mechanisms [26]. The first mechanism is through apoptosis which by itself has two aspects - extrinsic and intrinsic. Extrinsic or death receptor pathway occurs when a ligand like tumor necrosis factor-related apoptosis-induced ligand (TRAIL) binds to their death receptors and triggers activation of caspase-8 and recruitment of adaptor protein FADD. The promotion of TRAIL- induced apoptosis is due to blocking of the activity of HDAC1 and HDAC2 enzymes. The intrinsic or mitochondrial pathway is stress-stimulated, resulting in damage to the mitochondria membrane. This damage causes the release of proteins like cytochrome C and SMAC and eventually leads to apoptosis [79].

HDACi also trigger formation of reactive oxygen species (ROS) which has been suggested to induce cell death through intrinsic pathway [80].

Another mechanism of HDACi-induced tumor cell death involves angiogenesis inhibition. Angiogenesis is an essential process for tumor development and metastasis. HDACi have been shown to decrease the levels of pro-angiogenic factors including vascular endothelial growth factor (VEGF) and hypoxia-inducible factor 1 α (HIF1 α) [81].

The last putative mechanism of HDACi-induced tumor cell death is promotion of autophagy. Autophagy is a protein degradation system whose activation induces a necrotic-type cell death. However, autophagy acts as a double edge sword [82]. It can both mediate cell death, associated with HDACi antitumor activity improvement, or promotes tumor cell survival during nutrient or hypoxic stress which contributes to HDACi undesired side effects [83].

1.9. FDA approved HDACi in combination therapy

Despite the success of HDACi in treating hematological tumors such as CTCL, PTCL and multiple myeloma, they have been ineffective against solid tumors. It has been suggested that HDACi will be more effective if they are used in combination with other therapeutic agents. Specifically, HDACi are expected to reduce tumor cells threshold to undergo apoptosis induced by other agents, primarily due to their effect in lowering the levels of anti-apoptotic molecules such as XIAP, survivin and Bcl-2 and enhancing the levels pro-apoptotic molecules like bim, bid, and bmf [84], [85].

HDACi have been tested in combination therapy with direct activators of the apoptotic process, lexatumumab and mapatumumab, to improve their efficacy in treating cancer. Lexatumumab and mapatumumab are DR5 and DR4 agonist antibodies respectively that bind to death receptors on the surface of tumor cells to initiate extrinsic apoptosis [86]. In addition to inducing apoptosis, HDACi promote formation of the

death-inducing signaling complex (DISC) [87]. Combination of compounds that are agonists of death receptor with HDACi promotes both intrinsic and extrinsic apoptosis pathways. This strategy sensitizes TRAIL-resistance tumors to apoptosis [26]. HDACi also induce expression of p21 that leads to cell cycle arrest in G₁ phase [86]. Studies have shown that tumor cells are more sensitive to TRAIL-induced apoptosis when arrested in G₁ phase of cell cycle. Additionally p21-mediated induction by HDACi helps to inhibit Cdc2 activity which blocks the phosphorylation of survivin and promotes its degradation [86].

HDACi also have synergistic effects in combination with the proteasome inhibitor, bortezomib [26]. Both HDACi and bortezomib inhibit NF- κ B activity, a key factor for angiogenesis and tumor metastasis [89]. Furthermore, both agents induce ROS generation and endoplasmic reticular (ER) stress which enhances apoptosis [90]. Chloroquine and 3-methyladenine have been used in combinational therapy with HDACi to suppress their autophagy mediated cell survival effect and induce apoptosis [91].

1.10. HDACi in clinical trials

In addition to the four FDA approved HDACi, there are several more in various phases of clinical trials as a standalone or combination therapy for treating multiple cancer types (Figure 1.13).

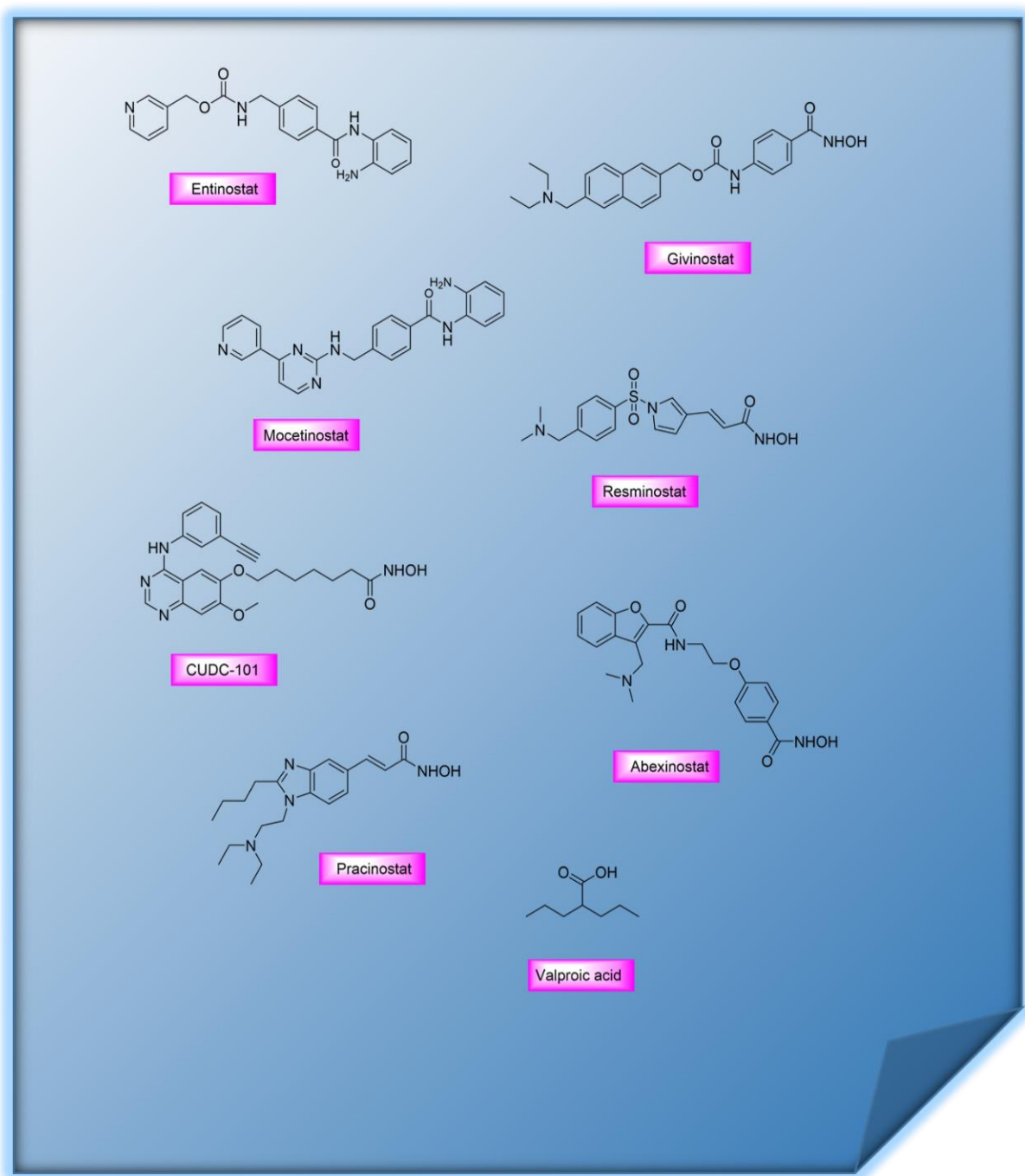


Figure 1.13. HDACi in clinical trials.

1.10.1. Abexinostat (PCI-24781)

Abexinostat is an orally available hydroxamic acid-based pan HDACi that has shown antitumor activity for a wide range of cancers. It has been in clinical trials as

monotherapy as well as combinational therapy. Abexinostat promotes apoptosis by cleaving caspase-3 and PARP. Its combination with the tyrosine kinase inhibitor, pazopanib was tested in phase I study in patients with metastatic solid tumor. The result from this study revealed a partial response and disease stabilization (clinical trial information NCT01543763). Currently, abexinostat is in combination therapy with cisplatin in phase I study in patients with advanced keratinizing nasopharyngeal carcinoma (NPC) (clinical trial information: ISRCTN96922360) [27].

1.10.2. Givinostat (ITF2357)

Givinostat is a hydroxamic acid-based pan HDACi with anti-inflammatory, anti-angiogenic, and antineoplastic activities. Givinostat has shown activity towards Hodgkin's lymphoma, multiple myeloma and chronic lymphocytic leukemia. It is currently undergoing a phase II clinical study for treatment of myeloproliferative neoplasms (MPN) [92].

1.10.3. Resminostat (4SC AG)

Resminostat is another hydroxamic acid-based pan HDACi has been tested in phase I study for treating advanced solid tumors [93]. It has also shown cell growth and apoptosis induction in multiple myeloma cell lines [94]. In a phase II study it was tested in relapsed and refractory Hodgkin lymphoma and showed promising results with a good safety profile [95]. Resminostat is in phase II clinical trial for treating liver cancer [96].

1.10.4. Pracinostat (SB939)

Pracinostat is a hydroxamic acid based-pan HDACi which is in phase II studies in patients with intermediate or high risk myelofibrosis (MF) [97] or advanced solid tumors [98]. Additionally, pracinostat is in a phase III study for acute myeloid leukemia treatment as well as a phase II study for treating myelodysplastic syndrome [96].

1.10.5. CUDC-101

CUDC-101 is a multi-target inhibitor of HDACs and epidermal growth factor (EGFR) and human epidermal growth factor receptor 2 (HER2). It shows anti-proliferative and pro-apoptotic activities *in vitro* and *in vivo* [99]. It has a hydroxamic acid moiety as its ZBG. Its dual inhibition activity makes it a potential therapeutic compound for treatment of drug-resistant tumors that cannot be treated with single target agents. CUDC is in clinical trials for treating advanced solid tumors [100].

1.10.6. Mocetinostat (MGCD0103)

Mocetinostat is a benzamide-based HDACi that is selective for class I isoforms. It showed anti-leukemia activity in a phase I trials in patients with leukemia or myelodysplastic syndromes (MDS) [101]. It shows synergetic growth arrest, cell death, and cell cycle arrest effects in treating pancreatic cancer when combined with tubastatin A (an HDAC 6 selective inhibitor) or MC1568 (a class IIa selective HDACi). Furthermore, it showed promising results in a phase II study for treating relapsed classical Hodgkin's lymphoma. However, the study had to be terminated due to four patients sudden death, which two of whom were probably treatment related deaths (clinical trial identifier: NCT00358982) [27], [102].

1.10.7. Entinostat (MS-275)

Entinostat is a benzamide derived class I selective HDACi which has been tested in many clinical trials for treating various types of cancer such as breast, colon, renal cell, non-small cell lung cancers, and lymphoblastic leukemia either as a monotherapy or combinational therapy [103]. Entinostat showed promising results when it was tested in a phase II clinical trial in combination with exemestane in patients with estrogen receptor positive advanced breast cancer [104]. Moreover, testing entinostat in patients with

refractory solid tumors and lymphomas resulted in disease stabilization and antitumor activities [105].

1.10.8. Valproic acid (VPA)

Valproic acid is a short fatty acid HDACi that has been in clinical trials as a standalone agent and in combination therapy. In a phase I study, treatment of patients with refractory solid or central nervous system tumors with VPA resulted in HDAC inhibition in half of the patients [61]. Combination of VPA and bevacizumab has been tested in patients with colorectal, prostate and gastroesophageal cancers [106].

1.11. HDACi deficiencies

Despite the HDACi encouraging results in treating CTCL, PTCL, and multiple myeloma, they suffer from various common side effects. The prevalent and predominant toxicities of HDACi are diarrhea, nausea, fatigue, vomiting, neutropenia, peripheral neuropathy [70], dehydration, and thrombocytopenia [107]. In addition to all these side effects, their lack of accumulation in solid tumors, as well as their cardiotoxicities has hampered their use [22].

1.11.1. Lack of accumulation in solid tumors

Up to date, none of the HDACi has shown benefits in treating solid tumors. HDACi have been tested extensively in various clinical trials to treat different solid tumors, such as breast, colorectal, prostate, head and neck, ovarian, and non-small cell lung cancers, but lack of potency and activation was observed when they were used as a single therapy. However their antitumor activity improved when they were used in combination with other therapeutic agents [108], [109].

1.11.2. Cardiotoxicity

HDACi are associated with serious cardiotoxicities, such as ST-segment depression, T-wave-fluttering and QT interval prolongation with the last one being the most severe and predominant one [22], [110]. QT prolongation is associated with torsades de pointes (TdP) which is a life threatening arrhythmia leading to syncope, ventricular and sudden cardiac death [111].

QT is considered prolonged when it is more than 430 msec for men and more than 450 msec for women. QT intervals can be influenced by ventricular conduction velocities as well as the velocity of repolarization. It is measured when the QRS complex starts and continues till T-wave ends. It demonstrates the time needed for ventricular depolarization. QT prolongation is mostly the result of factors that are able to prolong the action potential in most cases by delaying the repolarization phase 3, which can be caused either by blocking the ion channel cavity of hERG or triggering an abnormal trafficking that is essential for locating hERG subunit in the cell membrane [112].

Targeted therapeutic agents can affect cardiac and vascular function. Targeted anticancer drugs are usually associated with QT prolongation because of their influence on ventricular repolarization mostly through restricting the activating rectifier K^+ current (I_{kr}) carried by pore-forming α -subunit encoded by human ether-a-go-go-related gene potassium ion channels (hERG K^+) [113], [114]. It has been hypothesized that HDACi, anti-hER2, anti-VEGF, and tyrosine kinase inhibitors are associated with the risk of delayed ventricular repolarization and various life-threatening arrhythmias [115]. These drugs all block the potassium channel, resulting in increase in the repolarization time and hence QT interval prolongations [116]. The blockage of the hERG K^+ channel by various drugs is due to the interactions of lipophilic molecules with the hydrophobic aromatic residues in the channel's large inner cavity [111].

There are other suggested mechanisms for QT prolongation induced by targeted therapies in addition to blocking the hERG K^+ channel. The mechanism of QT prolongation in

some drugs lies in their ability to increase Na^+ current. For instance, alfuzosin, an α_1 -adrenergic receptor antagonist, which is designed to help men to urinate, increases QT prolongation by involving the Na^+ channel. In fact alfuzosin is one of the few examples of agents that cause cardiac repolarization through enhancing the sodium current [117].

Additionally, mutations or lack of proteins, such as Mink and Mink-related peptide 1 (MiRP1) that forms assemblies with hERG and are needed for its proper functioning *in vivo*, are associated with arrhythmia and changes in channel function thus leading to QT prolongation [118].

No major cardiotoxicity other than QT prolongation has been reported for vorinostat, belinostat and panobinostat; there was a report of death for romidepsin. Preclinical studies in dogs and rats have shown FK228 is able to induce myocardial inflammation and prolong QT intervals [119]. In a phase II study, a total of 15 patients with metastatic neuroendocrine tumors, received a 4-hour i.v. infusion of romidepsin at 14 mg/m^2 on days 1, 8, 15 every 28 days. This study had to be terminated because of a sudden death possibly related to ventricular arrhythmia, as well as a high number of cardiac side effects including 2 patients with asymptomatic grade 2 ventricular tachycardia (n=2), 3 patients with QT prolongation (n=3) [120]. Six patients out of the more than 500 patients who were treated with romidepsin died unexpectedly [119], [121].

Although observations from the use of HDACi in the clinic strongly suggest that they can induce cardiotoxicity, pre-existing cardiovascular diseases in cancer patients can contribute to cardiovascular adverse effects after treatments with anti-cancer agents. Sinus tachycardia, previous myocardial infection, atrial fibrillation as well as other cardiac abnormalities increases the chance of QT prolongation upon drug administration [122]. Furthermore, other factors such as obesity, gender, and age will elevate cardiotoxicity risk as well [123].

1.12. Mechanism of resistance to HDACi

Cancer cells have the ability to develop resistance to growth inhibitory and damaging factors. Tumorigenesis is a selection of malignant cells that are able to adjust to environmental constraints and be more independent from external proliferative and survival inhibitors. Factors including drug efflux, target overexpression and desensitization, epigenetic changes, anti-apoptotic and pro-survival mechanisms, and stress response mechanisms are involved in development of resistance to HDACi by the tumor cells [124]. However, in addition to the aforementioned factors, the tissue of origin, as well as genetic context are critical features in resistance development [124].

1.12.1. Efflux pump

Tumor overexpression of the ATP-binding cassette transporter family of efflux pumps is a hallmark of multidrug resistance. Various HDACi, including vorinostat, romidepsin and belinostat, have been tested in multidrug-resistant human cancer cell lines and only romidepsin has shown to be a substrate for a multidrug resistance associated protein [125].

1.12.2. Epigenetic changes

Inactivation and mutation of various isoforms of HDACs have been identified in different types of cancers. For instance, mutation in HDAC2 was observed in human colon and endometrial cancer cell lines with microsatellite instability [126]. Histone acetylation and DNA methylation activate or suppress gene transcription. However, DNA methylation is a predominant mechanism of tumor suppressor genes silencing, and has dominance over histone repressive markers in cancer cells [127]. Therefore, methylation of DNA impedes the ability of HDACi to restore expression of epigenetically silenced genes leading to resistance to HDACi. Studies have revealed that gene silencing induced

by DNA methylation cannot be overcome by the single action of HDACi and they need to be used with other hypomethylation-inducing agents [128].

1.12.3. Anti-apoptotic and pro-survival mechanisms

HDACi induced cell death is through apoptotic pathways involving mitochondria damage, cytochrome c release and production of reactive oxygen species. These cell-death mechanisms can be hindered by overexpression of anti-apoptotic proteins Bcl-2 and Bcl-X_L. It has been observed in various types of cancers that Bcl-2 was overexpressed while pro-apoptotic genes such as Bim and Bid were silenced. [129], [130]. It is suggested that changes in these proteins may be responsible for resistance to HDACi [126].

Additionally, the anti-apoptotic nuclear factor κ B (NF- κ B) is another mediator that may be involved in resistance to HDACi. In some cases inhibiting HDACs results in activation of NF- κ B via acetylation of the Rel/p65 subunit and stimulates expression of genes that interfere with triggered cell death [131]. In fact, it has been shown the activation of NF- κ B by some HDACi hinders apoptosis in non-small cell lung cancer [132] as well as leukemia [133].

The HDACi-mediated cyclin-dependent kinase inhibitor p21^(CIP1/WAF1) upregulation is involved in induction of cell cycle arrest, differentiation, and programmed cell death through p53-dependent and p53-independent pathway [134]. However, some studies have revealed that in U937 leukemia cell line, HDACi-mediated induction of p21^(CIP1/WAF1) protected cells from apoptosis [135].

1.12.4. Autophagy

Despite the role of autophagy in the death of some cancer cells, it has a protective role in some others which help them to adjust and manage the HDACi-induced cellular damage and apoptosis [136]. Combining HDACi with inhibitors of autophagy leads to

enhancement in efficacy of HDACi. For example, combination of chloroquine, an autophagy inhibitor, with vorinostat in treating imatinib-resistant chronic myeloid leukemia results in enhanced antineoplastic activity of vorinostat [91].

Based on the preceding discussion, several mechanisms of tumor resistance to HDACi have been described and many more are expected to be unraveled. Understanding these tumor resistance mechanisms is of great significance not only in design and development of new HDACi with higher potency and tumor selectivity but also in combinational therapy of the current HDACi with other therapeutic anticancer agents to develop optimum combination cocktails able to overcome the resistance pathways.

1.13. Improving HDACi efficacy in clinic

Despite HDACi potent antitumor activity, their use in clinic is hampered by their poor bioavailability, lack of accumulation in solid tumors, and off-target toxicities. In many cases they have to be used in combination with other anticancer drugs to compensate for their deficiencies [26], [27]. In the efforts to overcome HDACi deficiencies, developing non-viral and tumor selective delivery methods to enhance their concentration at the tumor site and diminish their off-target toxicities is of a great importance. Design and synthesis of isoform-selective HDACi, their localized administration or targeted delivery to the desired tissue and tumor site, as well as reducing their hERG binding affinity are strategies being pursued to improve their potency and activity and lower their adverse effects.

1.13.1. Localized administration

Localized administration is a target independent strategy for releasing the active ingredient near the area of the target site to avoid possible off-target toxicities. Local administration can be very beneficial in case of solid tumors which comprise about 85%

of human cancers [137]. It is used to overcome several drugs poor and variable oral bioavailability and adverse side effects. Additionally this strategy provides a sustainable and higher concentration of the drug in close proximity of target site [138].

In recent years, injection of therapeutic drugs as a means of localized administration has received much interest. In a study done by Eyupoglu, *et al.* intratumoral injection of HDACi MS-275 in rats to treat malignant gliomas showed enhanced level of acetylate H3 in brain tissue as well as low neurotoxicity, indicating MS-275 as a promising drug candidate for treating malignant gliomas [139].

Second strategy for localized administration is the topical application of the therapeutic agents. It has been shown that topically applying a drug which can easily and rapidly penetrate skin, enhances the pace of wound healing by accelerating the formation of granulation tissue even in severe tumor lesions [140]. HDACi are mainly used for treating CTCL. Despite their promising results for treating aforementioned cancer, they still suffer from cytotoxicity and lack of effectiveness when they are administered internally. This gets worse when it involves skin tumors, skin ulcer or repeated shedding of the skin. Indeed many CTCL patients die due to skin infections. To overcome the off-target toxicity of HDACi and to boost their potency and selectivity, some HDACi have been studied as viable candidates for topical therapy [141]. In a phase I study conducted by national Cancer Institute (NCI), a formulation of romidepsin was applied on the skin of patients with CTCL (clinical identifier number: NCT01445340). This study had to be terminated due to the side effects. Chung *et al.* also tested a topical formulation of two HDACi - PB (phenylbutyrate) and TSA - *in vivo* study to achieve increased level of local concentrations and avoid potential systematic adverse effects in treating rheumatoid arthritis. The topical formulations of these HDACi possessed high stability and high skin penetration ability with a low skin irritation and a long shelf-life. Additionally, a selective induction of cell cycle inhibitors in the synovium as well as pervasive suppression of TNF- α in affected tissues were observed once the prepared cream or ointment was

applied [142]. Another example of HDACi being investigated in phase I clinical trial as a topical therapy in treating CTCL is SHP-141, a HDACi derived from SAHA. In a study done by Kim.Y.H. *et al.* SHP-141 showed excellent tolerability and efficacy with no systematic HDACi related toxicity [143].

The last method for localized administration is utilizing surgically placed natural and synthetic biodegradable polymers, which can benefit from high drug concentration at the target site, longer drug exposure duration, and lower systematic toxicity [137].

1.13.2. Reduction of hERG binding

Cardiotoxicity of HDACi is one of the major and serious drawbacks that has hampered their use in clinics. As discussed earlier, the commonly accepted mechanism of cardiotoxicity of HDACi is their interactions with hERGK⁺ channel inner cavity residues which lead to blockage of human ether-a-go-go-related gene potassium ion channel. Understanding the link between HDACi cardiotoxicity and QT prolongation in relation to their hERG binding affinity is of great importance. This appreciation has been explored to design and synthesize novel potent HDACi that have lower affinity for hERG. Specifically, Novartis was able to design and synthesize non-cardiotoxic highly potent hydroxamic acid-based HDACi that show low or no hERG affinity [144].

1.13.3. Isoform-selective HDACi

Although, it is not completely clear if selective inhibition of one HDAC isoform yields less cardiotoxicity and more clinical benefit, it has nonetheless been hypothesized that the HDACi cytotoxicity and side effects are partially due to their lack of selectivity toward one HDAC isoform. It is believed HDAC5 and HDAC9 are modifiers of cardiac diseases phenotypes and their dysfunction results in susceptibility to cardiovascular diseases [145]. It has been shown that class I HDAC isoforms induce cardiomyocyte hypertrophy while class II HDAC enzymes suppress cardiomyocyte hypertrophy through

protein interactions in cardiomyocyte nucleus specifically with cardiomyocyte hypertrophy and not through their histone deacetylation mechanism [146]. Therefore inhibiting certain HDAC isoforms can have a great impact in diminishing some of HDACi-related cytotoxicity. Extensive efforts are currently on-going to design and synthesize isoform selective HDACi. In addition to class I selective, FDA approved romidepsin, there are several isoform selective HDACi in clinical or preclinical trials. Isoform selectivity can be achieved through utilizing certain groups as recognition cap group or ZBG [23].

1.13.3.1. Isoform selectivity through cap group modification

There has been substantial effort and research dedicated to modification of the cap group to achieve isoform selectivity. Surface recognition cap group interacts with the amino residues near the entrance of active site. The amino acid residues are specific to each HDAC enzyme class. Key examples of modification to the cap group which have resulted in isoform selective HDACi are the use of cyclic peptide which impacted class I isoform selectivity [21], and carboline in Tubastatin A which impacted exclusive HDAC6 selectivity [147].

1.13.3.2. Isoform-selectivity through ZBG modification

Although amino acids sequence similarity near the catalytic metal has made it problematic and challenging to design and develop isoform-selective HDACi, isoform selectivity has also been achieved through modification to HDACi ZBG. As a prime example, benzamide group is a ZBG that provides class I selectivity due to its interactions with the lipophilic residues in 14 Å° internal cavity. An example of benzamide based HDACi in clinical trial is MS-275 which is under investigation for treating NSCL, breast cancer, and advanced solid tumors, refractory solid tumors and lymphoma [27]. Epidaza (chidamide) is another benzamide-derived HDACi which was

recently approved by the Chinese regulatory authority to treat peripheral T cell lymphoma [148].

1.13.4. Targeted delivery

Targeted drug delivery is a promising strategy to improve anticancer agents' therapeutic window and their target to non-target ratio. Targeted delivery has several advantages including decreasing the drug off-target toxicity, increasing the drug concentration at the site of tumor and lowering the minimum effective dose of the drug which all lead to improvement in drug efficacy and potency [149].

Several approaches are plausible to achieve targeted delivery of HDACi to tumor site. Approaches mentioned below are the ones that are the focus of this thesis study. The first approach is to employ FDA approved drugs that are known to accumulate in certain tissues as the surface recognition group.

The second approach in targeted HDACis design is, equipping them with FDA approved targeting ligands such as anti-folate, anti-androgen, and anti-estrogen that have a preference for a certain receptor, which is overexpressed in particular cancers resulting in their selective accumulation in malignant cells [153], [154].

These targeting delivery strategies have the potential to result in selective delivery of HDACi to the site of tumor and lead to higher efficacy and therapeutic properties as well as and greater potency and lower off-target toxicity.

1.13.4.1. Tissue selective FDA approved drugs as the 'cap group'

One of the FDA approved class of drugs that selectively accumulate in lung tissue is macrolides [143]. Macrolides are a class of natural product with antibiotic and antifungal activity. They consist of a large macrocyclic lactone ring which is attached to deoxy sugars mostly cladinose and desosamine. Azithromycin is a macrolide which is approved for treating bacterial infection. It has been shown that azithromycin mostly

accumulates in lungs ¹, which is due to its high accumulation in macrophage cells [144]. Although macrophages are in almost all tissues, it has been proved that they mainly reside in lung and liver [145], which in return results in azithromycin high accumulation in these tissues. Different macrolides such as azithromycin, clarithromycin, or telithromycin can be modified through their sugar rings to serve as surface recognition cap group in HDACi pharmacophoric model. In fact in an *in vivo* study done by my labmate Dr. Will Guerrant (unpublished data), it was shown that macrolide based HDACi maintain their lung accumulation even after modification.

Herein, following our lab's previous work, I designed, developed and synthesized various classes of azithromycin conjugated HDACi with two different zinc binding groups for treating lung cancer (chapter 2 and chapter 3). Based on our unpublished data, these conjugated HDACi are anticipated to accumulate selectively in lung tissue by taking advantage of azithromycin selective accumulation in macrophage cells which predominantly reside in lung tissue [155], [156]. Chapter 2 is focused on azithromycin conjugated hydroxamic acid based HDACi, while chapter 3 is devoted to azithromycin conjugated N-(2-amino-5-(thiophen-2-yl)phenyl)acylamide derived HDACi, as isoform selective HDACi. These classes of HDACi exhibited nanomolar range HDAC inhibition potency toward all or selected zinc-dependent HDAC enzymes based on their zinc binding groups. Furthermore, evaluation of their antiproliferative activity against various transformed cell lines, showed a high nanomolar to low macromolar range cytotoxicity to cancer cells with less cytotoxicity against healthy cells compared to FDA approved HDACi SAHA. In fact, one of these azithromycin conjugated HDACi currently under investigation in animal models for further studies of its tumor regression ability.

1.13.4.2. Tumor receptor antagonist as the “cap group”

Estrogen receptor (ER) is overexpressed on tumor cells. Tamoxifen, an antagonist of estrogen receptor alpha (ER α), competes with estrogen for binding to ER α in ER α positive breast cancers. Conjugating tamoxifen as the cap group to HDACi, results in tissue selective accumulation of the target compounds due to tamoxifen high affinity for ER α . Additionally, it improves tamoxifen efficacy in ER α negative or tamoxifen resistant-developed tumors because of HDACi-mediated induction of ER expression.

It was previously shown in our lab that tamoxifen conjugated HDACi, have antiestrogen activity similar to tamoxifen with improved antiproliferative activity and nanomolar range HDAC inhibitory potency [157]. I synthesized various tamoxifen conjugated HDACis with different zinc binding groups and evaluated their antiproliferative activity as well as HDAC inhibitory potency. In addition to nanomolar range HDAC inhibitory activity, one class of these target compounds, tamoxifen conjugated hydroxamic acid HDACis, exhibited greater antiproliferative activity toward ER α positive breast cancer cells compared to tamoxifen, the most common and first line therapy for ER α positive breast cancer. Furthermore, many of these compounds were more selective toward ER α positive breast cancer cells relative to ER α negative breast cancer cells compared to tamoxifen that shows no selective antiproliferative activity between ER α positive and ER α negative breast cancer cells.

The promising results of HDAC inhibition potency and antiproliferative activity of these class of compounds encouraged us to continue our studies further and test these compounds in animal models. Tamoxifen conjugated hydroxamic acid HDACis are currently under *in vivo* study.

1.14. Thesis Overview

I have designed and synthesized various HDACi with different cap recognition group and ZBG that have the potential to selectively accumulate in the macrophage and

lung tissues as well as have HDAC isoform selectivity. Additionally, in some cases, such as tamoxifen conjugated HDACi, synthesizing a dual functioning compounds, improved the therapeutic efficacy of the HDACi through dual effects which resulted in more anti-cancer activity and potency.

In all cases, cytotoxicity of designed conjugated HDACi were enhanced against transformed cell lines, while their cytotoxicity to healthy cells were reduced.

Furthermore, in case of tamoxifen conjugated HDACi, in addition to an improved antiproliferative activity, I was able to achieve selectivity toward ER α positive breast cancer cells over ER α negative breast cancer cells, in comparison to tamoxifen which possesses the same antiproliferative activity toward ER α positive and ER α negative breast cancer cells.

1.15. References:

1. Siegel, R. L.; Miller, K. D.; Jemal, A. Cancer statistics, 2016. *CA: A cancer journal for clinicians* **2015**.
2. Harding, M. C.; Sloan, C. D.; Merrill, R. M.; Harding, T. M.; Thacker, B. J.; Thacker, E. L. Abstract MP67: Transition From Cardiovascular Disease to Cancer as the Leading Cause of Death in US States, 1999-2013. *Circulation* **2016**, 133, AMP67-AMP67.
3. <http://www.cancer.gov/about-cancer/what-is-cancer/statistics>)
4. McKinnell, R. G. *The biological basis of cancer*. Cambridge University Press: 1998.
5. Pérez-Herrero, E.; Fernández-Medarde, A. Advanced targeted therapies in cancer: Drug nanocarriers, the future of chemotherapy. *European Journal of Pharmaceutics and Biopharmaceutics* **2015**, 93, 52-79.
6. Hanahan, D.; Weinberg, R. A. Hallmarks of cancer: the next generation. *cell* **2011**, 144, 646-674.
7. <http://www.cancer.gov/about-cancer/what-is-cancer/statistics>
8. <http://www.cancer.org/cancer/cancerbasics/what-is-cancer>.

9. Papac, R. J. Origins of cancer therapy. *The Yale journal of biology and medicine* **2001**, 74, 391.
10. Chabner, B. A.; Roberts, T. G. Chemotherapy and the war on cancer. *Nature Reviews Cancer* **2005**, 5, 65-72.
11. Egger, G.; Liang, G.; Aparicio, A.; Jones, P. A. Epigenetics in human disease and prospects for epigenetic therapy. *Nature* **2004**, 429, 457-463.
12. Hansen, J. C.; Tse, C.; Wolffe, A. P. Structure and function of the core histone N-termini: more than meets the eye. *Biochemistry* **1998**, 37, 17637-17641.
13. Wolffe, A. P.; Guschin, D. Review: chromatin structural features and targets that regulate transcription. *Journal of structural biology* **2000**, 129, 102-122.
14. Luger, K.; Richmond, T. J. The histone tails of the nucleosome. *Current opinion in genetics & development* **1998**, 8, 140-146.
15. Marks, P. A.; Rifkind, R. A.; Richon, V. M.; Breslow, R.; Miller, T.; Kelly, W. K. Histone deacetylases and cancer: causes and therapies. *Nature Reviews Cancer* **2001**, 1, 194-202.
16. Zaidi, S.; Choi, M.; Wakimoto, H.; Ma, L.; Jiang, J.; Overton, J. D.; Romano-Adesman, A.; Bjornson, R. D.; Breitbart, R. E.; Brown, K. K. De novo mutations in histone-modifying genes in congenital heart disease. *Nature* **2013**, 498, 220-223.
17. Turner, B. Histone acetylation as an epigenetic determinant of long-term transcriptional competence. *Cellular and Molecular Life Sciences CMLS* **1998**, 54, 21-31.
18. Allfrey, V. G. In *Structural modifications of histones and their possible role in the regulation of ribonucleic acid synthesis*, Proceedings. Canadian Cancer Conference, 1965; 1965; pp 313-335.
19. Lee, D. Y.; Hayes, J. J.; Pruss, D.; Wolffe, A. P. A positive role for histone acetylation in transcription factor access to nucleosomal DNA. *Cell* **1993**, 72, 73-84.
20. Minucci, S.; Pelicci, P. G. Histone deacetylase inhibitors and the promise of epigenetic (and more) treatments for cancer. *Nature Reviews Cancer* **2006**, 6, 38-51.
21. Glozak, M.; Seto, E. Histone deacetylases and cancer. *Oncogene* **2007**, 26, 5420-5432.
22. Gryder, B. E.; Sodji, Q. H.; Oyelere, A. K. Targeted cancer therapy: giving histone deacetylase inhibitors all they need to succeed. *Future medicinal chemistry* **2012**, 4, 505-524.
23. Bieliauskas, A. V.; Pflum, M. K. H. Isoform-selective histone deacetylase inhibitors. *Chemical Society Reviews* **2008**, 37, 1402-1413.

24. Dokmanovic, M.; Clarke, C.; Marks, P. A. Histone deacetylase inhibitors: overview and perspectives. *Molecular cancer research* **2007**, 5, 981-989.
25. Lemoine, M.; Younes, A. Histone deacetylase inhibitors in the treatment of lymphoma. *Discovery medicine* **2010**, 10, 462-470.
26. Carew, J. S.; Giles, F. J.; Nawrocki, S. T. Histone deacetylase inhibitors: mechanisms of cell death and promise in combination cancer therapy. *Cancer letters* **2008**, 269, 7-17.
27. Mottamal, M.; Zheng, S.; Huang, T. L.; Wang, G. Histone deacetylase inhibitors in clinical studies as templates for new anticancer agents. *Molecules* **2015**, 20, 3898-3941.
28. Yang, X.-J.; Seto, E. The Rpd3/Hda1 family of lysine deacetylases: from bacteria and yeast to mice and men. *Nature reviews Molecular cell biology* **2008**, 9, 206-218.
29. Guenther, M. G.; Yu, J.; Kao, G. D.; Yen, T. J.; Lazar, M. A. Assembly of the SMRT-histone deacetylase 3 repression complex requires the TCP-1 ring complex. *Genes & development* **2002**, 16, 3130-3135.
30. Ayer, D. E. Histone deacetylases: transcriptional repression with SINers and NuRDs. *Trends in cell biology* **1999**, 9, 193-198.
31. Gregoret, I.; Lee, Y.-M.; Goodson, H. V. Molecular evolution of the histone deacetylase family: functional implications of phylogenetic analysis. *Journal of molecular biology* **2004**, 338, 17-31.
32. Watson, P. J.; Millard, C. J.; Riley, A. M.; Robertson, N. S.; Wright, L. C.; Godage, H. Y.; Cowley, S. M.; Jamieson, A. G.; Potter, B. V.; Schwabe, J. W. Insights into the activation mechanism of class I HDAC complexes by inositol phosphates. *Nature communications* **2016**, 7.
33. Fischle, W.; Dequiedt, F.; Hendzel, M. J.; Guenther, M. G.; Lazar, M. A.; Voelter, W.; Verdin, E. Enzymatic activity associated with class II HDACs is dependent on a multiprotein complex containing HDAC3 and SMRT/N-CoR. *Molecular cell* **2002**, 9, 45-57.
34. West, A. C.; Johnstone, R. W. New and emerging HDAC inhibitors for cancer treatment. *The Journal of clinical investigation* **2014**, 124, 30-39.
35. Hubbert, C.; Guardiola, A.; Shao, R.; Kawaguchi, Y.; Ito, A.; Nixon, A.; Yoshida, M.; Wang, X.-F.; Yao, T.-P. HDAC6 is a microtubule-associated deacetylase. *Nature* **2002**, 417, 455-458.
36. Kovacs, J. J.; Murphy, P. J.; Gaillard, S.; Zhao, X.; Wu, J.-T.; Nicchitta, C. V.; Yoshida, M.; Toft, D. O.; Pratt, W. B.; Yao, T.-P. HDAC6 regulates Hsp90 acetylation

and chaperone-dependent activation of glucocorticoid receptor. *Molecular cell* **2005**, 18, 601-607.

37. Kawaguchi, Y.; Kovacs, J. J.; McLaurin, A.; Vance, J. M.; Ito, A.; Yao, T.-P. The deacetylase HDAC6 regulates aggresome formation and cell viability in response to misfolded protein stress. *Cell* **2003**, 115, 727-738.

38. Kao, H.-Y.; Lee, C.-H.; Komarov, A.; Han, C. C.; Evans, R. M. Isolation and characterization of mammalian HDAC10, a novel histone deacetylase. *Journal of Biological Chemistry* **2002**, 277, 187-193.

39. Thaler, F.; Mercurio, C. Towards selective inhibition of histone deacetylase isoforms: what has been achieved, where we are and what will be next. *ChemMedChem* **2014**, 9, 523-536.

40. Marks, P. A.; Richon, V. M.; Rifkind, R. A. Histone deacetylase inhibitors: inducers of differentiation or apoptosis of transformed cells. *Journal of the National Cancer Institute* **2000**, 92, 1210-1216.

41. Zhang, L.; Han, Y.; Jiang, Q.; Wang, C.; Chen, X.; Li, X.; Xu, F.; Jiang, Y.; Wang, Q.; Xu, W. Trend of histone deacetylase inhibitors in cancer therapy: isoform selectivity or multitargeted strategy. *Medicinal research reviews* **2015**, 35, 63-84.

42. Gu, W.; Roeder, R. G. Activation of p53 sequence-specific DNA binding by acetylation of the p53 C-terminal domain. *Cell* **1997**, 90, 595-606.

43. Rodrigues, D. A.; Ferreira-Silva, G.; Ferreira, A. C.; Fernandes, R.; Kwee, J. K.; Sant'Anna, C. M. R.; Ionta, M.; Fraga, C. A. M. Design, Synthesis and Pharmacological Evaluation of Novel N-Acylhydrazones as Potent Histone Deacetylase 6/8 Dual Inhibitors. *Journal of medicinal chemistry* **2015**.

44. Furumai, R.; Komatsu, Y.; Nishino, N.; Khochbin, S.; Yoshida, M.; Horinouchi, S. Potent histone deacetylase inhibitors built from trichostatin A and cyclic tetrapeptide antibiotics including trapoxin. *Proceedings of the National Academy of Sciences* **2001**, 98, 87-92.

45. Furumai, R.; Matsuyama, A.; Kobashi, N.; Lee, K.-H.; Nishiyama, M.; Nakajima, H.; Tanaka, A.; Komatsu, Y.; Nishino, N.; Yoshida, M. FK228 (depsipeptide) as a natural prodrug that inhibits class I histone deacetylases. *Cancer research* **2002**, 62, 4916-4921.

46. Kijima, M.; Yoshida, M.; Sugita, K.; Horinouchi, S.; Beppu, T. Trapoxin, an antitumor cyclic tetrapeptide, is an irreversible inhibitor of mammalian histone deacetylase. *Journal of Biological Chemistry* **1993**, 268, 22429-22435.

47. Hrabeta, J.; Stiborova, M.; Adam, V.; Kizek, R.; Eckschlager, T. Histone deacetylase inhibitors in cancer therapy. A review. *Biomedical Papers* **2014**, 158, 161-169.

48. Finnin, M. S.; Donigian, J. R.; Cohen, A.; Richon, V. M.; Rifkind, R. A.; Marks, P. A.; Breslow, R.; Pavletich, N. P. Structures of a histone deacetylase homologue bound to the TSA and SAHA inhibitors. *Nature* **1999**, 401, 188-193.
49. Bertrand, P. Inside HDAC with HDAC inhibitors. *European journal of medicinal chemistry* **2010**, 45, 2095-2116.
50. Villar-Garea, A.; Esteller, M. Histone deacetylase inhibitors: understanding a new wave of anticancer agents. *International Journal of Cancer* **2004**, 112, 171-178.
51. Miller, T. A.; Witter, D. J.; Belvedere, S. Histone deacetylase inhibitors. *Journal of medicinal chemistry* **2003**, 46, 5097-5116.
52. Acharya, M. R.; Sparreboom, A.; Venitz, J.; Figg, W. D. Rational development of histone deacetylase inhibitors as anticancer agents: a review. *Molecular pharmacology* **2005**, 68, 917-932.
53. Kim, S. H.; Ahn, S.; Han, J.-W.; Lee, H.-W.; Lee, H. Y.; Lee, Y.-W.; Kim, M. R.; Kim, K. W.; Kim, W. B.; Hong, S. Apicidin is a histone deacetylase inhibitor with anti-invasive and anti-angiogenic potentials. *Biochemical and biophysical research communications* **2004**, 315, 964-970.
54. Beckers, T.; Burkhardt, C.; Wieland, H.; Gimmnich, P.; Ciossek, T.; Maier, T.; Sanders, K. Distinct pharmacological properties of second generation HDAC inhibitors with the benzamide or hydroxamate head group. *International journal of cancer* **2007**, 121, 1138-1148.
55. Ryan, Q. C.; Headlee, D.; Acharya, M.; Sparreboom, A.; Trepel, J. B.; Ye, J.; Figg, W. D.; Hwang, K.; Chung, E. J.; Murgo, A. Phase I and pharmacokinetic study of MS-275, a histone deacetylase inhibitor, in patients with advanced and refractory solid tumors or lymphoma. *Journal of Clinical Oncology* **2005**, 23, 3912-3922.
56. Wang, D.-F.; Wiest, O.; Helquist, P.; Lan-Hargest, H.-Y.; Wiech, N. L. On the function of the 14 Å long internal cavity of histone deacetylase-like protein: implications for the design of histone deacetylase inhibitors. *Journal of medicinal chemistry* **2004**, 47, 3409-3417.
57. Wang, D.-F.; Helquist, P.; Wiech, N. L.; Wiest, O. Toward selective histone deacetylase inhibitor design: homology modeling, docking studies, and molecular dynamics simulations of human class I histone deacetylases. *Journal of medicinal chemistry* **2005**, 48, 6936-6947.
58. Methot, J. L.; Chakravarty, P. K.; Chenard, M.; Close, J.; Cruz, J. C.; Dahlberg, W. K.; Fleming, J.; Hamblett, C. L.; Hamill, J. E.; Harrington, P. Exploration of the internal cavity of histone deacetylase (HDAC) with selective HDAC1/HDAC2 inhibitors (SHI-1: 2). *Bioorganic & medicinal chemistry letters* **2008**, 18, 973-978.

59. Moradei, O. M.; Mallais, T. C.; Frechette, S.; Paquin, I.; Tessier, P. E.; Leit, S. M.; Fournel, M.; Bonfils, C.; Trachy-Bourget, M.-C.; Liu, J. Novel aminophenyl benzamide-type histone deacetylase inhibitors with enhanced potency and selectivity. *Journal of medicinal chemistry* **2007**, 50, 5543-5546.
60. Gore, S. D.; Weng, L.-J.; Figg, W. D.; Zhai, S.; Donehower, R. C.; Dover, G.; Grever, M. R.; Griffin, C.; Grochow, L. B.; Hawkins, A. Impact of prolonged infusions of the putative differentiating agent sodium phenylbutyrate on myelodysplastic syndromes and acute myeloid leukemia. *Clinical Cancer Research* **2002**, 8, 963-970.
61. Su, J. M.; Li, X.-N.; Thompson, P.; Ou, C.-N.; Ingle, A. M.; Russell, H.; Lau, C. C.; Adamson, P. C.; Blaney, S. M. Phase 1 study of valproic acid in pediatric patients with refractory solid or CNS tumors: a children's oncology group report. *Clinical Cancer Research* **2011**, 17, 589-597.
62. Chu, B.; Karpenko, M.; Liu, Z.; Aimiwu, J.; Villalona-Calero, M.; Chan, K.; Grever, M.; Otterson, G. Phase I study of 5-aza-2'-deoxycytidine in combination with valproic acid in non-small-cell lung cancer. *Cancer chemotherapy and pharmacology* **2013**, 71, 115-121.
63. Rotili, D.; Simonetti, G.; Savarino, A.; Palamara, A. T.; Migliaccio, A. R.; Mai, A. Non-Cancer Uses of Histone Deacetylase Inhibitors: Effects on Infectious Diseases and β -Hemoglobinopathies+. *Current topics in medicinal chemistry* **2009**, 9, 272-291.
64. Gilbert, J.; Baker, S. D.; Bowling, M. K.; Grochow, L.; Figg, W. D.; Zabelina, Y.; Donehower, R. C.; Carducci, M. A. A phase I dose escalation and bioavailability study of oral sodium phenylbutyrate in patients with refractory solid tumor malignancies. *Clinical Cancer Research* **2001**, 7, 2292-2300.
65. Mann, B. S.; Johnson, J. R.; Cohen, M. H.; Justice, R.; Pazdur, R. FDA approval summary: vorinostat for treatment of advanced primary cutaneous T-cell lymphoma. *The oncologist* **2007**, 12, 1247-1252.
66. Rangwala, S.; Zhang, C.; Duvic, M. HDAC inhibitors for the treatment of cutaneous T-cell lymphomas. *Future medicinal chemistry* **2012**, 4, 471-486.
67. Kim, H.-J.; Bae, S.-C. Histone deacetylase inhibitors: molecular mechanisms of action and clinical trials as anti-cancer drugs. *Am J Transl Res* **2011**, 3, 166-179.
68. Duvic, M.; Dimopoulos, M. The safety profile of vorinostat (suberoylanilide hydroxamic acid) in hematologic malignancies: A review of clinical studies. *Cancer Treatment Reviews* **2016**, 43, 58-66.
69. Weber, D. M.; Graef, T.; Hussein, M.; Sobecks, R. M.; Schiller, G. J.; Lupinacci, L.; Hardwick, J. S.; Jagannath, S. Phase I trial of vorinostat combined with bortezomib for the treatment of relapsing and/or refractory multiple myeloma. *Clinical Lymphoma Myeloma and Leukemia* **2012**, 12, 319-324.

70. Badros, A.; Burger, A. M.; Philip, S.; Niesvizky, R.; Kolla, S. S.; Goloubeva, O.; Harris, C.; Zwiebel, J.; Wright, J. J.; Espinoza-Delgado, I. Phase I study of vorinostat in combination with bortezomib for relapsed and refractory multiple myeloma. *Clinical Cancer Research* **2009**, 15, 5250-5257.
71. Kirschbaum, M.; Gojo, I.; Goldberg, S. L.; Bredeson, C.; Kujawski, L. A.; Yang, A.; Marks, P.; Frankel, P.; Sun, X.; Tosolini, A. A phase 1 clinical trial of vorinostat in combination with decitabine in patients with acute myeloid leukaemia or myelodysplastic syndrome. *British journal of haematology* **2014**, 167, 185-193.
72. Coiffier, B.; Pro, B.; Prince, H. M.; Foss, F.; Sokol, L.; Greenwood, M.; Caballero, D.; Morschhauser, F.; Wilhelm, M.; Pinter-Brown, L. Romidepsin for the treatment of relapsed/refractory peripheral T-cell lymphoma: pivotal study update demonstrates durable responses. *J Hematol Oncol* **2014**, 7, 11.
73. VanderMolen, K. M.; McCulloch, W.; Pearce, C. J.; Oberlies, N. H. Romidepsin (Istodax, NSC 630176, FR901228, FK228, depsipeptide): a natural product recently approved for cutaneous T-cell lymphoma. *The Journal of antibiotics* **2011**, 64, 525-531.
74. Steele, N.; Plumb, J.; Vidal, L.; Tjørnelund, J.; Knoblauch, P.; Buhl-Jensen, P.; Molife, R.; Brown, R.; De Bono, J.; Evans, T. Pharmacokinetic and pharmacodynamic properties of an oral formulation of the histone deacetylase inhibitor Belinostat (PXD101). *Cancer chemotherapy and pharmacology* **2011**, 67, 1273-1279.
75. Plumb, J. A.; Finn, P. W.; Williams, R. J.; Bandara, M. J.; Romero, M. R.; Watkins, C. J.; La Thangue, N. B.; Brown, R. Pharmacodynamic response and inhibition of growth of human tumor xenografts by the novel histone deacetylase inhibitor PXD101. *Molecular cancer therapeutics* **2003**, 2, 721-728.
76. San Miguel, J. F.; Hungria, V.; Yoon, S.-S.; Beksac, M.; Dimopoulos, M. A.; Elghandour, A.; Jedrzejczak, W. W.; Guenther, A.; Na Nakorn, T.; Siritanaratkul, N. In *Panobinostat plus bortezomib and dexamethasone in patients with relapsed or relapsed and refractory multiple myeloma who received prior bortezomib and IMiDs: A predefined subgroup analysis of PANORAMA 1*, ASCO Annual Meeting Proceedings, 2015; 2015; p 8526.
77. Laubach, J. P.; Moreau, P.; San-Miguel, J. F.; Richardson, P. G. Panobinostat for the treatment of multiple myeloma. *Clinical Cancer Research* **2015**, 21, 4767-4773.
78. Garnock-Jones, K. P. Panobinostat: first global approval. *Drugs* **2015**, 75, 695-704.
79. Rosato, R. R.; Almenara, J. A.; Dai, Y.; Grant, S. Simultaneous activation of the intrinsic and extrinsic pathways by histone deacetylase (HDAC) inhibitors and tumor necrosis factor-related apoptosis-inducing ligand (TRAIL) synergistically induces mitochondrial damage and apoptosis in human leukemia cells. *Molecular Cancer Therapeutics* **2003**, 2, 1273-1284.

80. Sade, H.; Sarin, A. Reactive oxygen species regulate quiescent T-cell apoptosis via the BH3-only proapoptotic protein BIM. *Cell Death & Differentiation* **2004**, *11*, 416-423.
81. Deroanne, C. F.; Bonjean, K.; Servotte, S.; Devy, L.; Colige, A.; Clausse, N.; Blacher, S.; Verdin, E.; Foidart, J.-M.; Nusgens, B. V. Histone deacetylases inhibitors as anti-angiogenic agents altering vascular endothelial growth factor signaling. *Oncogene* **2002**, *21*, 427-436.
82. Carew, J. S.; Nawrocki, S. T.; Cleveland, J. L. Modulating autophagy for therapeutic benefit. *Autophagy* **2007**, *3*, 464-467.
83. Shao, Y.; Gao, Z.; Marks, P. A.; Jiang, X. Apoptotic and autophagic cell death induced by histone deacetylase inhibitors. *Proceedings of the National Academy of Sciences* **2004**, *101*, 18030-18035.
84. Zhang, X. D.; Gillespie, S. K.; Borrow, J. M.; Hersey, P. The histone deacetylase inhibitor suberic bishydroxamate regulates the expression of multiple apoptotic mediators and induces mitochondria-dependent apoptosis of melanoma cells. *Molecular cancer therapeutics* **2004**, *3*, 425-435.
85. Ruefli, A. A.; Ausserlechner, M. J.; Bernhard, D.; Sutton, V. R.; Tainton, K. M.; Kofler, R.; Smyth, M. J.; Johnstone, R. W. The histone deacetylase inhibitor and chemotherapeutic agent suberoylanilide hydroxamic acid (SAHA) induces a cell-death pathway characterized by cleavage of Bid and production of reactive oxygen species. *Proceedings of the National Academy of Sciences* **2001**, *98*, 10833-10838.
86. Nawrocki, S. T.; Carew, J. S.; Douglas, L.; Cleveland, J. L.; Humphreys, R.; Houghton, J. A. Histone deacetylase inhibitors enhance lexatumumab-induced apoptosis via a p21Cip1-dependent decrease in survivin levels. *Cancer research* **2007**, *67*, 6987-6994.
87. Inoue, S.; MacFarlane, M.; Harper, N.; Wheat, L.; Dyer, M.; Cohen, G. Histone deacetylase inhibitors potentiate TNF-related apoptosis-inducing ligand (TRAIL)-induced apoptosis in lymphoid malignancies. *Cell Death & Differentiation* **2004**, *11*, S193-S206.
88. Jin, Z.; Dicker, D. T.; El-Deiry, W. S. Enhanced sensitivity of G1 arrested human cancer cells suggests a novel therapeutic strategy using a combination of simvastatin and TRAIL. *Cell cycle* **2002**, *1*, 79-86.
89. Adachi, M.; Zhang, Y.; Zhao, X.; Minami, T.; Kawamura, R.; Hinoda, Y.; Imai, K. Synergistic effect of histone deacetylase inhibitors FK228 and m-carboxycinnamic acid bis-hydroxamide with proteasome inhibitors PSI and PS-341 against gastrointestinal adenocarcinoma cells. *Clinical cancer research* **2004**, *10*, 3853-3862.

90. Pei, X.-Y.; Dai, Y.; Grant, S. Synergistic induction of oxidative injury and apoptosis in human multiple myeloma cells by the proteasome inhibitor bortezomib and histone deacetylase inhibitors. *Clinical Cancer Research* **2004**, *10*, 3839-3852.
91. Carew, J. S.; Nawrocki, S. T.; Kahue, C. N.; Zhang, H.; Yang, C.; Chung, L.; Houghton, J. A.; Huang, P.; Giles, F. J.; Cleveland, J. L. Targeting autophagy augments the anticancer activity of the histone deacetylase inhibitor SAHA to overcome Bcr-Abl-mediated drug resistance. *Blood* **2007**, *110*, 313-322.
92. Rambaldi, A.; Dellacasa, C. M.; Finazzi, G.; Carobbio, A.; Ferrari, M. L.; Guglielmelli, P.; Gattoni, E.; Salmoiraghi, S.; Finazzi, M. C.; Di Tollo, S. A pilot study of the Histone-Deacetylase inhibitor Givinostat in patients with JAK2V617F positive chronic myeloproliferative neoplasms. *British journal of haematology* **2010**, *150*, 446-455.
93. Fouliard, S.; Robert, R.; Jacquet-Bescond, A.; du Rieu, Q. C.; Balasubramanian, S.; Loury, D.; Lorient, Y.; Hollebecque, A.; Kloos, I.; Soria, J.-C. Pharmacokinetic/pharmacodynamic modelling-based optimisation of administration schedule for the histone deacetylase inhibitor abexinostat (S78454/PCI-24781) in phase I. *European Journal of Cancer* **2013**, *49*, 2791-2797.
94. Mandl-Weber, S.; Meinel, F. G.; Jankowsky, R.; Oduncu, F.; Schmidmaier, R.; Baumann, P. The novel inhibitor of histone deacetylase resminostat (RAS2410) inhibits proliferation and induces apoptosis in multiple myeloma (MM) cells. *British journal of haematology* **2010**, *149*, 518-528.
95. Walewski, J.; Paszkiewicz-Kozik, E.; Borsaru, G.; Moicean, A.; Warszevska, A.; Strobel, K.; Biggi, A.; Hauns, B.; Mais, A.; Henning, S. W. In *Resminostat in relapsed or refractory Hodgkin lymphoma: initial results of the SAPHIRE phase II trial with a Novel Oral Histone Deacetylase (HDAC) Inhibitor*, Proceedings of the 52nd ASH Annual Meeting and Exposition, Orlando, FL, USA, 2010; 2010; pp 4-7.
96. Guha, M. HDAC inhibitors still need a home run, despite recent approval. *Nature Reviews Drug Discovery* **2015**, *14*, 225-226.
97. Quintás-Cardama, A.; Kantarjian, H.; Estrov, Z.; Borthakur, G.; Cortes, J.; Verstovsek, S. Therapy with the histone deacetylase inhibitor pracinostat for patients with myelofibrosis. *Leukemia research* **2012**, *36*, 1124-1127.
98. Razak, A.; Hotte, S.; Siu, L.; Chen, E.; Hirte, H.; Powers, J.; Walsh, W.; Stayner, L.; Laughlin, A.; Novotny-Diermayr, V. Phase I clinical, pharmacokinetic and pharmacodynamic study of SB939, an oral histone deacetylase (HDAC) inhibitor, in patients with advanced solid tumours. *British journal of cancer* **2011**, *104*, 756-762.
99. Lai, C.-J.; Bao, R.; Tao, X.; Wang, J.; Atoyan, R.; Qu, H.; Wang, D.-G.; Yin, L.; Samson, M.; Forrester, J. CUDC-101, a multitargeted inhibitor of histone deacetylase, epidermal growth factor receptor, and human epidermal growth factor receptor 2, exerts potent anticancer activity. *Cancer Research* **2010**, *70*, 3647-3656.

100. Shimizu, T.; LoRusso, P. M.; Papadopoulos, K. P.; Patnaik, A.; Beeram, M.; Smith, L. S.; Rasco, D. W.; Mays, T. A.; Chambers, G.; Ma, A. Phase I first-in-human study of CUDC-101, a multitargeted inhibitor of HDACs, EGFR, and HER2 in patients with advanced solid tumors. *Clinical Cancer Research* **2014**, 20, 5032-5040.
101. Garcia-Manero, G.; Assouline, S.; Cortes, J.; Estrov, Z.; Kantarjian, H.; Yang, H.; Newsome, W. M.; Miller, W. H.; Rousseau, C.; Kalita, A. Phase 1 study of the oral isotype specific histone deacetylase inhibitor MGCD0103 in leukemia. *Blood* **2008**, 112, 981-989.
102. Younes, A.; Oki, Y.; Bociek, R. G.; Kuruvilla, J.; Fanale, M.; Neelapu, S.; Copeland, A.; Buglio, D.; Galal, A.; Besterman, J. Mocetinostat for relapsed classical Hodgkin's lymphoma: an open-label, single-arm, phase 2 trial. *The lancet oncology* **2011**, 12, 1222-1228.
103. Pili, R.; Salumbides, B.; Zhao, M.; Altiok, S.; Qian, D.; Zwiebel, J.; Carducci, M.; Rudek, M. Phase I study of the histone deacetylase inhibitor entinostat in combination with 13-cis retinoic acid in patients with solid tumours. *British journal of cancer* **2012**, 106, 77-84.
104. Yardley, D. A.; Ismail-Khan, R. R.; Melichar, B.; Lichinitser, M.; Munster, P. N.; Klein, P. M.; Cruickshank, S.; Miller, K. D.; Lee, M. J.; Trepel, J. B. Randomized phase II, double-blind, placebo-controlled study of exemestane with or without entinostat in postmenopausal women with locally recurrent or metastatic estrogen receptor-positive breast cancer progressing on treatment with a nonsteroidal aromatase inhibitor. *Journal of Clinical Oncology* **2013**, 31, 2128-2135.
105. Gore, L.; Rothenberg, M. L.; O'Bryant, C. L.; Schultz, M. K.; Sandler, A. B.; Coffin, D.; McCoy, C.; Schott, A.; Scholz, C.; Eckhardt, S. G. A phase I and pharmacokinetic study of the oral histone deacetylase inhibitor, MS-275, in patients with refractory solid tumors and lymphomas. *Clinical Cancer Research* **2008**, 14, 4517-4525.
106. Wheler, J. J.; Janku, F.; Falchook, G. S.; Jackson, T. L.; Fu, S.; Naing, A.; Tsimberidou, A. M.; Moulder, S. L.; Hong, D. S.; Yang, H. Phase I study of anti-VEGF monoclonal antibody bevacizumab and histone deacetylase inhibitor valproic acid in patients with advanced cancers. *Cancer chemotherapy and pharmacology* **2014**, 73, 495-501.
107. Luu, T. H.; Morgan, R. J.; Leong, L.; Lim, D.; McNamara, M.; Portnow, J.; Frankel, P.; Smith, D. D.; Doroshow, J. H.; Gandara, D. R. A phase II trial of vorinostat (suberoylanilide hydroxamic acid) in metastatic breast cancer: a California Cancer Consortium study. *Clinical Cancer Research* **2008**, 14, 7138-7142.
108. Qiu, T.; Zhou, L.; Zhu, W.; Wang, T.; Wang, J.; Shu, Y.; Liu, P. Effects of treatment with histone deacetylase inhibitors in solid tumors: a review based on 30 clinical trials. *Future Oncology* **2013**, 9, 255-269.

109. Chun, P. Histone deacetylase inhibitors in hematological malignancies and solid tumors. *Archives of pharmacal research* **2015**, 38, 933-949.
110. Raedler, L. A. Farydak (Panobinostat): First HDAC Inhibitor Approved for the Treatment of Patients with Relapsed Multiple Myeloma.
111. Hoffmann, P.; Warner, B. Are hERG channel inhibition and QT interval prolongation all there is in drug-induced torsadogenesis? A review of emerging trends. *Journal of pharmacological and toxicological methods* **2006**, 53, 87-105.
112. Ponte, M. L.; Keller, G. A.; Girolamo, G. D. Mechanisms of drug induced QT interval prolongation. *Current drug safety* **2010**, 5, 44-53.
113. Bagnes, C.; Panchuk, P. N.; Recondo, G. Antineoplastic chemotherapy induced QTc prolongation. *Current drug safety* **2010**, 5, 93-96.
114. Hedhli, N.; S Russell, K. Cardiotoxicity of molecularly targeted agents. *Current cardiology reviews* **2011**, 7, 221-233.
115. Munster, P. N.; Rubin, E. H.; Van Belle, S.; Friedman, E.; Patterson, J. K.; Van Dyck, K.; Li, X.; Comisar, W.; Chodakewitz, J. A.; Wagner, J. A. A single suprathreshold dose of vorinostat does not prolong the QTc interval in patients with advanced cancer. *Clinical Cancer Research* **2009**, 15, 7077-7084.
116. Wolbrette, D. L. Drugs that cause torsades de pointes and increase the risk of sudden cardiac death. *Current cardiology reports* **2004**, 6, 379-384.
117. Lacerda, A. E.; Kuryshev, Y. A.; Chen, Y.; Renganathan, M.; Eng, H.; Danthi, S. J.; Kramer, J. W.; Yang, T.; Brown, A. M. Alfuzosin delays cardiac repolarization by a novel mechanism. *Journal of Pharmacology and Experimental Therapeutics* **2008**, 324, 427-433.
118. Abbott, G. W.; Sesti, F.; Splawski, I.; Buck, M. E.; Lehmann, M. H.; Timothy, K. W.; Keating, M. T.; Goldstein, S. A. MiRP1 forms I Kr potassium channels with HERG and is associated with cardiac arrhythmia. *Cell* **1999**, 97, 175-187.
119. Strevel, E. L.; Ing, D. J.; Siu, L. L. Molecularly targeted oncology therapeutics and prolongation of the QT interval. *Journal of Clinical Oncology* **2007**, 25, 3362-3371.
120. Shah, M. H.; Binkley, P.; Chan, K.; Xiao, J.; Arbogast, D.; Collamore, M.; Farra, Y.; Young, D.; Grever, M. Cardiotoxicity of histone deacetylase inhibitor depsipeptide in patients with metastatic neuroendocrine tumors. *Clinical Cancer Research* **2006**, 12, 3997-4003.
121. Bates, S. E.; Rosing, D. R.; Fojo, T.; Piekarz, R. L. Challenges of evaluating the cardiac effects of anticancer agents. *Clinical Cancer Research* **2006**, 12, 3871-3874.

122. Barbey, J. T.; Pezzullo, J. C.; Soignet, S. L. Effect of arsenic trioxide on QT interval in patients with advanced malignancies. *Journal of clinical oncology* **2003**, *21*, 3609-3615.
123. Wood, A. J.; Roden, D. M. Drug-induced prolongation of the QT interval. *New England Journal of Medicine* **2004**, *350*, 1013-1022.
124. Fantin, V. R.; Richon, V. M. Mechanisms of resistance to histone deacetylase inhibitors and their therapeutic implications. *Clinical cancer research* **2007**, *13*, 7237-7242.
125. Xiao, J. J.; Huang, Y.; Dai, Z.; Sadée, W.; Chen, J.; Liu, S.; Marcucci, G.; Byrd, J.; Covey, J. M.; Wright, J. Chemoresistance to depsipeptide FK228 [(E)-(1S, 4S, 10S, 21R)-7-[(Z)-ethylidene]-4, 21-diisopropyl-2-oxa-12, 13-dithia-5, 8, 20, 23-tetraazabicyclo [8, 7, 6]-tricos-16-ene-3, 6, 9, 22-pentanone] is mediated by reversible MDR1 induction in human cancer cell lines. *Journal of Pharmacology and Experimental Therapeutics* **2005**, *314*, 467-475.
126. Ropero, S.; Fraga, M. F.; Ballestar, E.; Hamelin, R.; Yamamoto, H.; Boix-Chornet, M.; Caballero, R.; Alaminos, M.; Setien, F.; Paz, M. F. A truncating mutation of HDAC2 in human cancers confers resistance to histone deacetylase inhibition. *Nature genetics* **2006**, *38*, 566-569.
127. Fahrner, J. A.; Eguchi, S.; Herman, J. G.; Baylin, S. B. Dependence of histone modifications and gene expression on DNA hypermethylation in cancer. *Cancer research* **2002**, *62*, 7213-7218.
128. Ou, J.-N.; Torrisani, J.; Unterberger, A.; Provençal, N.; Shikimi, K.; Karimi, M.; Ekström, T. J.; Szyf, M. Histone deacetylase inhibitor Trichostatin A induces global and gene-specific DNA demethylation in human cancer cell lines. *Biochemical pharmacology* **2007**, *73*, 1297-1307.
129. Maiso, P.; Carvajal-Vergara, X.; Ocio, E. M.; López-Pérez, R.; Mateo, G.; Gutiérrez, N.; Atadja, P.; Pandiella, A.; San Miguel, J. F. The histone deacetylase inhibitor LBH589 is a potent antimyeloma agent that overcomes drug resistance. *Cancer research* **2006**, *66*, 5781-5789.
130. Lindemann, R.; Newbold, A.; Whitecross, K.; Cluse, L.; Frew, A.; Ellis, L.; Williams, S.; Wiegmans, A.; Dear, A.; Scott, C. Analysis of the apoptotic and therapeutic activities of histone deacetylase inhibitors by using a mouse model of B cell lymphoma. *Proceedings of the National Academy of Sciences* **2007**, *104*, 8071-8076.
131. Mayo, M. W.; Denlinger, C. E.; Broad, R. M.; Yeung, F.; Reilly, E. T.; Shi, Y.; Jones, D. R. Ineffectiveness of histone deacetylase inhibitors to induce apoptosis involves the transcriptional activation of NF- κ B through the Akt pathway. *Journal of Biological Chemistry* **2003**, *278*, 18980-18989.

132. Rundall, B. K.; Denlinger, C. E.; Jones, D. R. Combined histone deacetylase and NF- κ B inhibition sensitizes non-small cell lung cancer to cell death. *Surgery* **2004**, 136, 416-425.
133. Dai, Y.; Rahmani, M.; Dent, P.; Grant, S. Blockade of histone deacetylase inhibitor-induced RelA/p65 acetylation and NF- κ B activation potentiates apoptosis in leukemia cells through a process mediated by oxidative damage, XIAP downregulation, and c-Jun N-terminal kinase 1 activation. *Molecular and cellular biology* **2005**, 25, 5429-5444.
134. Ju, R.; Muller, M. T. Histone deacetylase inhibitors activate p21WAF1 expression via ATM. *Cancer research* **2003**, 63, 2891-2897.
135. Vrana, J.; Decker, R.; Johnson, C.; Wang, Z.; Jarvis, W.; Richon, V.; Ehinger, M.; Fisher, P.; Grant, S. Induction of apoptosis in U937 human leukemia cells by suberoylanilide hydroxamic acid (SAHA) proceeds through pathways that are regulated by Bcl-2/Bcl-XL, c-Jun, and p21CIP1, but independent of p53. *Oncogene* **1999**, 18, 7016-7025.
136. Kondo, Y.; Kanzawa, T.; Sawaya, R.; Kondo, S. The role of autophagy in cancer development and response to therapy. *Nature Reviews Cancer* **2005**, 5, 726-734.
137. De Souza, R.; Zahedi, P.; Allen, C. J.; Piquette-Miller, M. Polymeric drug delivery systems for localized cancer chemotherapy. *Drug delivery* **2010**, 17, 365-375.
138. Larsen, S. W.; Østergaard, J.; Yaghmur, A.; Jensen, H.; Larsen, C. Use of in vitro release models in the design of sustained and localized drug delivery systems for subcutaneous and intra-articular administration. *Journal of Drug Delivery Science and Technology* **2013**, 23, 315-324.
139. Eyüpoglu, I. Y.; Hahnen, E.; Tränkle, C.; Savaskan, N. E.; Siebzehnriibl, F. A.; Buslei, R.; Lemke, D.; Wick, W.; Fahlbusch, R.; Blümcke, I. Experimental therapy of malignant gliomas using the inhibitor of histone deacetylase MS-275. *Molecular cancer therapeutics* **2006**, 5, 1248-1255.
140. Freeman, F.; Sheehan, P. Device for topical localized administration of zinc to tissue. In Google Patents: 2000.
141. Bates, S. E.; Fojo, A. T.; Piekarz, R. L.; Wright, J. J.; Grimes, G. J.; Schweikart, K. M. Topical Formulations of Histone Deacetylase Inhibitors and Methods Using the Same. In Google Patents: 2006.
142. Chung, Y.-L.; Lee, M.-Y.; Wang, A.-J.; Yao, L.-F. A therapeutic strategy uses histone deacetylase inhibitors to modulate the expression of genes involved in the pathogenesis of rheumatoid arthritis. *Molecular Therapy* **2003**, 8, 707-717.
143. Kim, Y. H.; Krathen, M.; Duvic, M.; Wong, H.; Porcu, P.; Tacastacas, J.; Korman, N. J.; Guitart, J.; Bradner, J. E.; Landau, S. B. In *A phase 1b study in cutaneous*

T-cell lymphoma (CTCL) with the novel topically applied skin-restricted histone deacetylase inhibitor (HDAC-i) SHP-141, 50th Annual Meeting of the American Society of Clinical Oncology, 2014; 2014.

144. Shultz, M. D.; Cao, X.; Chen, C. H.; Cho, Y. S.; Davis, N. R.; Eckman, J.; Fan, J.; Fekete, A.; Firestone, B.; Flynn, J. Optimization of the in vitro cardiac safety of hydroxamate-based histone deacetylase inhibitors. *Journal of medicinal chemistry* **2011**, 54, 4752-4772.

145. Backs, J.; Olson, E. N. Control of cardiac growth by histone acetylation/deacetylation. *Circulation research* **2006**, 98, 15-24.

146. Eom, G. H.; Kook, H. Role of histone deacetylase 2 and its posttranslational modifications in cardiac hypertrophy. *BMB reports* **2015**, 48, 131.

147. Butler, K. V.; Kalin, J.; Brochier, C.; Vistoli, G.; Langley, B.; Kozikowski, A. P. Rational design and simple chemistry yield a superior, neuroprotective HDAC6 inhibitor, tubastatin A. *Journal of the American Chemical Society* **2010**, 132, 10842-10846.

148. Ning, Z.-Q.; Li, Z.-B.; Newman, M. J.; Shan, S.; Wang, X.-H.; Pan, D.-S.; Zhang, J.; Dong, M.; Du, X.; Lu, X.-P. Chidamide (CS055/HBI-8000): a new histone deacetylase inhibitor of the benzamide class with antitumor activity and the ability to enhance immune cell-mediated tumor cell cytotoxicity. *Cancer chemotherapy and pharmacology* **2012**, 69, 901-909.

149. Sudimack, J.; Lee, R. J. Targeted drug delivery via the folate receptor. *Advanced drug delivery reviews* **2000**, 41, 147-162.

150. Mwakwari, S. C.; Patil, V.; Guerrant, W.; Oyelere, A. K. Macrocyclic histone deacetylase inhibitors. *Current topics in medicinal chemistry* **2010**, 10, 1423.

151. Dreaden, E. C.; Raji, I. O.; Austin, L. A.; Fathi, S.; Mwakwari, S. C.; Humphries, W. H.; Kang, B.; Oyelere, A. K.; El-Sayed, M. A. P-Glycoprotein-Dependent Trafficking of Nanoparticle-Drug Conjugates. *small* **2014**, 10, 1719-1723.

152. Laskin, D. L.; Weinberger, B.; Laskin, J. D. Functional heterogeneity in liver and lung macrophages. *Journal of leukocyte biology* **2001**, 70, 163-170.

153. Dreaden, E. C.; Mwakwari, S. C.; Sodji, Q. H.; Oyelere, A. K.; El-Sayed, M. A. Tamoxifen– poly (ethylene glycol)– thiol gold nanoparticle conjugates: enhanced potency and selective delivery for breast cancer treatment. *Bioconjugate chemistry* **2009**, 20, 2247-2253.

154. Dreaden, E. C.; Gryder, B. E.; Austin, L. A.; Tene Defo, B. A.; Hayden, S. C.; Pi, M.; Quarles, L. D.; Oyelere, A. K.; El-Sayed, M. A. Antiandrogen gold nanoparticles dual-target and overcome treatment resistance in hormone-insensitive prostate cancer cells. *Bioconjugate chemistry* **2012**, 23, 1507-1512.

155. Mwakwari, S. C.; Guarrant, W.; Patil, V.; Khan, S. I.; Tekwani, B. L.; Gurard-Levin, Z. A.; Mrksich, M.; Oyelere, A. K. Non-peptide macrocyclic histone deacetylase inhibitors derived from tricyclic ketolide skeleton. *Journal of medicinal chemistry* **2010**, 53, 6100-6111.
156. Oyelere, A. K.; Chen, P. C.; Guarrant, W.; Mwakwari, S. C.; Hood, R.; Zhang, Y.; Fan, Y. Non-peptide macrocyclic histone deacetylase inhibitors. *Journal of medicinal chemistry* **2008**, 52, 456-468.
157. Gryder, B. E.; Rood, M. K.; Johnson, K. A.; Patil, V.; Raftery, E. D.; Yao, L.-P. D.; Rice, M.; Azizi, B.; Doyle, D. F.; Oyelere, A. K. Histone deacetylase inhibitors equipped with estrogen receptor modulation activity. *Journal of medicinal chemistry* **2013**, 56, 5782-5796.

CHAPTER 2

STRUCTURE ACTIVITY RELATIONSHIP

OFAZITHROMYCIN DERIVED HISTONE DEACETYLASE

INHIBITORS WITH HYDROXAMIC ACID AS ZINC BINDING

GROUP

This work has been published in:

S. Tapadar, **S. Fathi**, I. Raji, W. Omesiete, J. Kornacki, S. Mwakwari, M. Miyata, K. Mitsutake, J. Li, M. Mrksich, M. Oyelerel. A structure–activity relationship of non-peptide macrocyclic histone deacetylase inhibitors and their anti-proliferative and anti-inflammatory activities. *Bioorganic & Medicinal Chemistry*, **2015**, 23 (24), 7543-7564.

2.1. Introduction

Histone acetyltransferase (HAT) together with histone deacetylase (HDAC) control the acetylation state of histone proteins as well as non-histone proteins including p53, HSP90 and ER α [1]. Inhibition of the enzymatic activity of HDACs has become a potentially viable therapeutic approach for treating many human diseases such as malaria, leishmanial infection, and cancer [2], therefore various small molecule histone deacetylase inhibitors (HDACi) have been designed and synthesized.

HDACi cause growth arrest, differentiation and apoptosis with a high potency both *in vitro* and *in vivo*. To date four HDACi have been approved by FDA for cutaneous/peripheral T-cell lymphoma and multiple myeloma, and there are many more in different stages of clinical trials for treating solid tumors as well as hematological malignancies [3]. The approved HDACi are suberoylanilide hydroxamic acid (SAHA) approved in 2006 for cutaneous T-cell lymphoma [4], romidepsin (FK228) approved in 2009 for cutaneous T-cell lymphoma and peripheral T-cell lymphoma [5], belinostat

(PXD101) approved in 2014 for peripheral T-cell lymphoma [6], and panobinostat (SB939) approved in 2015 for multiple myeloma [7]. Additionally, chidamide is a benzamide based HDACi which is only approved in China for refractory peripheral T-cell lymphoma. Chidamide is in phase I and phase II clinical trials for treating non-small cell lung cancer and breast cancer in the U.S., respectively [8], [9].

All HDACi follow a three-motif pharmacophoric model with a recognition cap group, linker group, and a zinc binding group (ZBG) (Figure 2.1) [10]. To date, several classes of small molecule HDACi have been designed and synthesized following this pharmacophoric model. Macrocyclic HDACi including cyclic tetrapeptides and depsipeptides possess the most complicated cap group that are able to maintain optimum interactions with the amino acid residues near the entrance of the HDAC enzyme active site. Despite the nanomolar range anticancer activity of this class of HDACi, their clinical development has been hampered by the drawbacks affiliated with peptide moieties and complex synthesis required to conduct structure activity relationship (SAR), [11]. To overcome these disadvantages, there has been an extensive research going on to replace the cap group with nonpeptide macrocyclic ones [12].

We have previously shown that macrocycles derived from 15-membered azalide ring azithromycin mimic the peptide backbone of macrocyclic HDACi [13]. Our design is based on the hypothesis that replacing the cyclic peptide moiety of a cyclic peptide HDACi with macrolide skeleton will lead to a new class of potent HDACi [14].

Azithromycin belongs to a class of glycosylated polyketide antibiotics called macrolides which comprise of a large macrocyclic lactone ring with two deoxy sugars, mostly cladinose and desosamine [15]. Macrolides have been in the market for treating respiratory tract infections for more than half a century now. They are endowed with additional non-antibiotic effects such as anti-inflammatory and immunomodulatory effects [16].

Moreover, we envisioned that equipping HDACi with macrolides, as the recognition cap group, will result in developing therapeutic agents with selective lung tissue accumulation property, due to macrolides accumulation in macrophage cells. Although macrophage cells reside in almost all tissues, they are highly concentrated in the liver (Kupffer cells), the lung (alveolar macrophages) and linings of splenic and lymph node medullary sinusoids to filter foreign materials [17], where they are responsible for nonspecific host defense as well as in specific immune responses in each tissue [18]. Macrophage cell accumulation in lungs consequently leads to macrolide selective accumulation in lung tissue. Therefore, conjugating azithromycin as the recognition cap group to HDACi could result in HDACi with selective tissue accumulation property [19], [20].

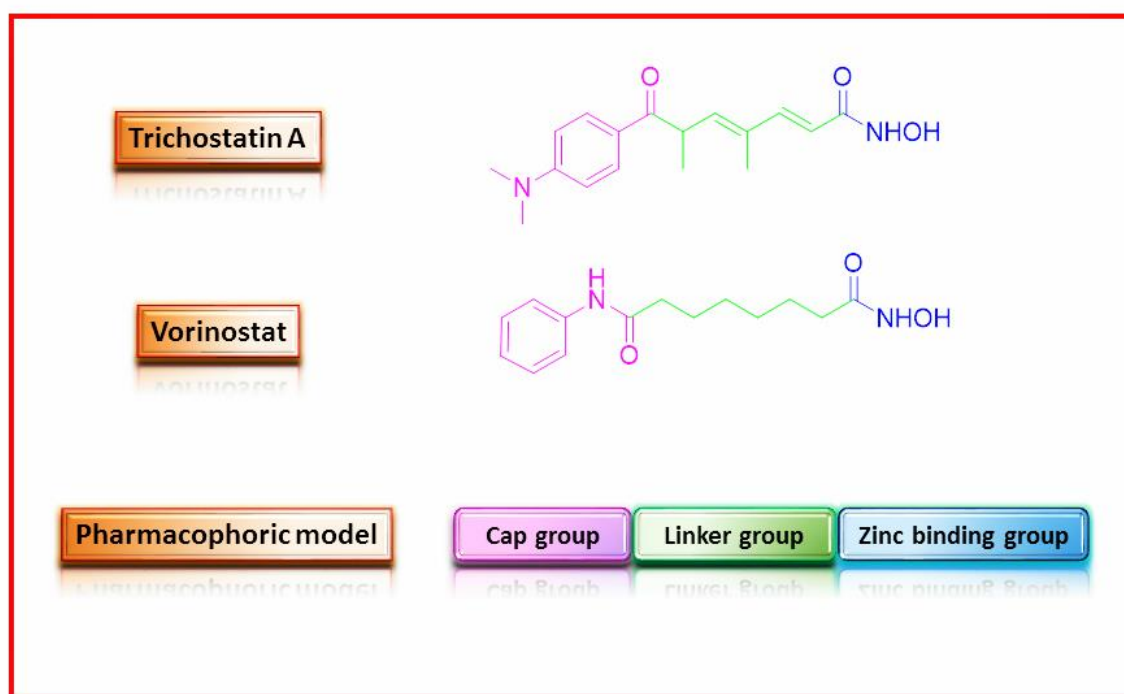


Figure 2.1. Naturally occurring HDACi trichostatin A and FDA approved HDACi SAHA. All following the three-motif pharmacophoric model of HDACi.

2.2. Azithromycin derived HDACi design

Following the three motif pharmacophoric model of HDACi, and inspired by previous study done in our lab [14], [25], I designed and disclosed three different classes of macrolide conjugated HDACi with different point of aryl-triazole moiety attachment, where azithromycin served as the recognition cap group and hydroxamic acid as the ZBG

To further define the depth of the structure activity relationship (SAR) of these azithromycin-derived HDACi, they were synthesized with various linker length (Figure 2.2). The influence of linker length on their HDAC inhibitory, anti-proliferative and anti-inflammatory activities was then investigated.

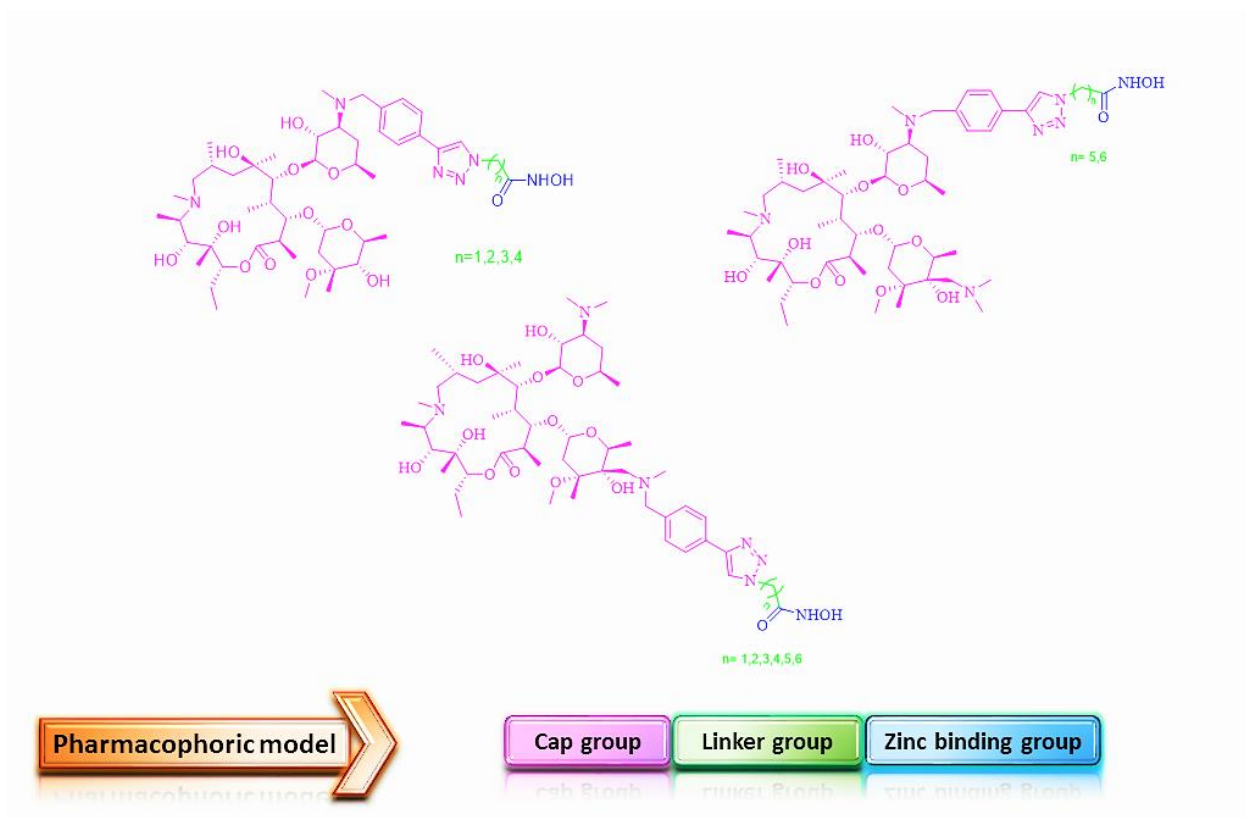
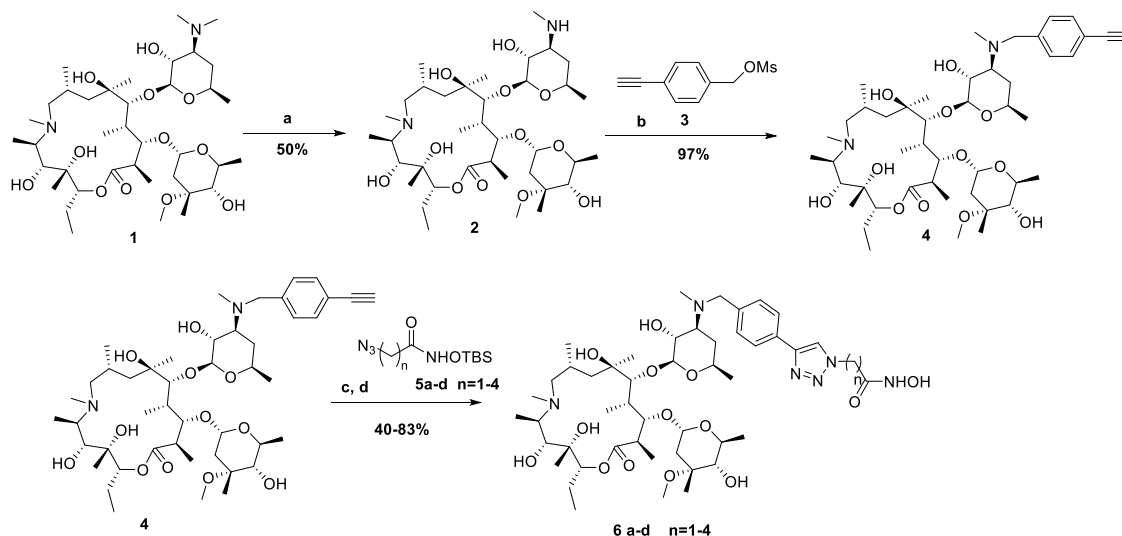


Figure 2.2. Structure activity relationship of azithromycin conjugated HDACis by modifying desosamine and cladinose sugar rings.

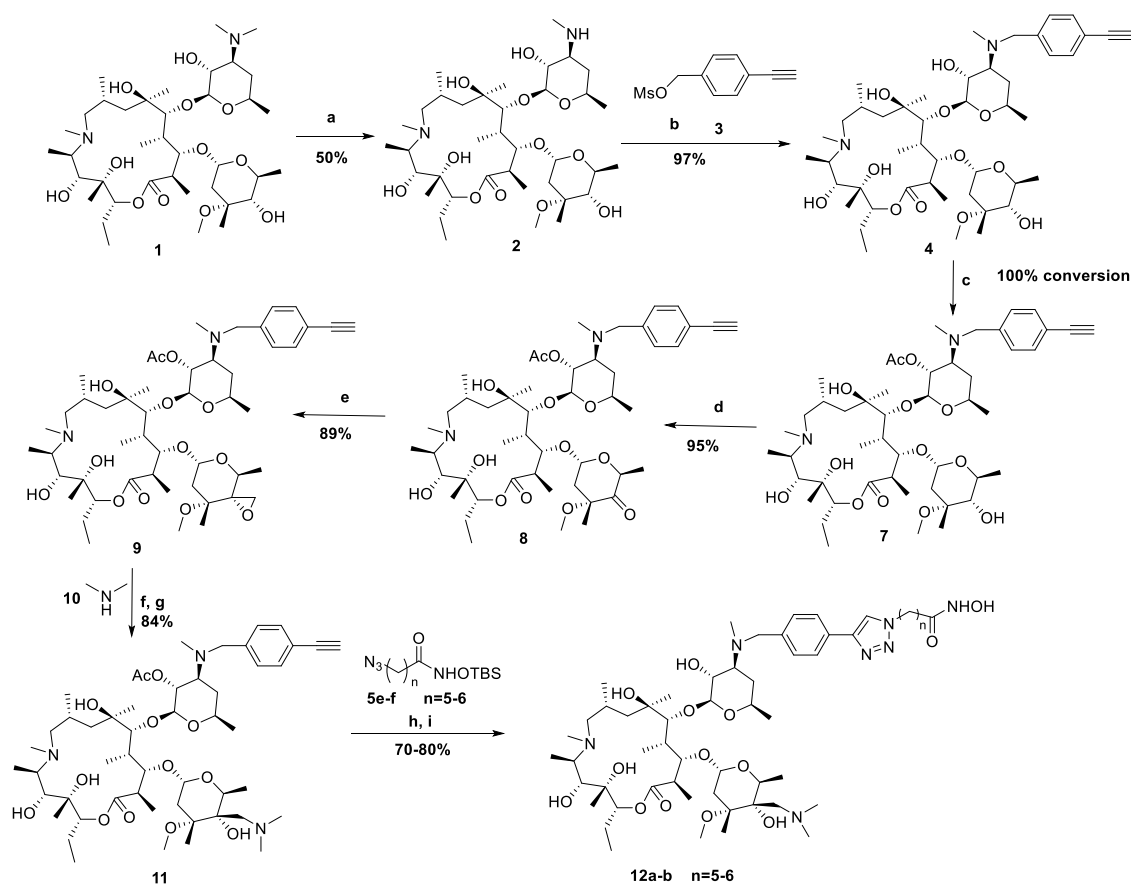
2.3. Chemistry and synthesis

To synthesize the first group of azithromycin derived HDACi, the ethynylbenzyl moiety was installed at desosamine sugar after removing one of the methyl groups and formation of the secondary amine **2** [21]. Subsequently, copper (I) catalyzed azide-alkyne-cycloaddition (AAC) reaction [22] between TBS-protected azidohydroxamates **5a-d** and compound **4**, followed by removal of TBS-group [23] afforded the final compounds **6a-d** (Scheme 2.1). Compounds **6e-f** ($n=5-6$) were previously synthesized by Dr. Subhasish Tapadar and are tested as controls.



Scheme 2.1. (a) I_2 , NaOAc, MeOH, 50 °C, 2 h, 50% (b) Hünig's base, DMSO, 85 °C, 3 h, 97%; (c) CuI (15 mol%), Hünig's base, THF-DMSO (1:1), 40 °C, 12 h; (d) CsF, MeOH, rt, 30 min (40-83%, c and d).

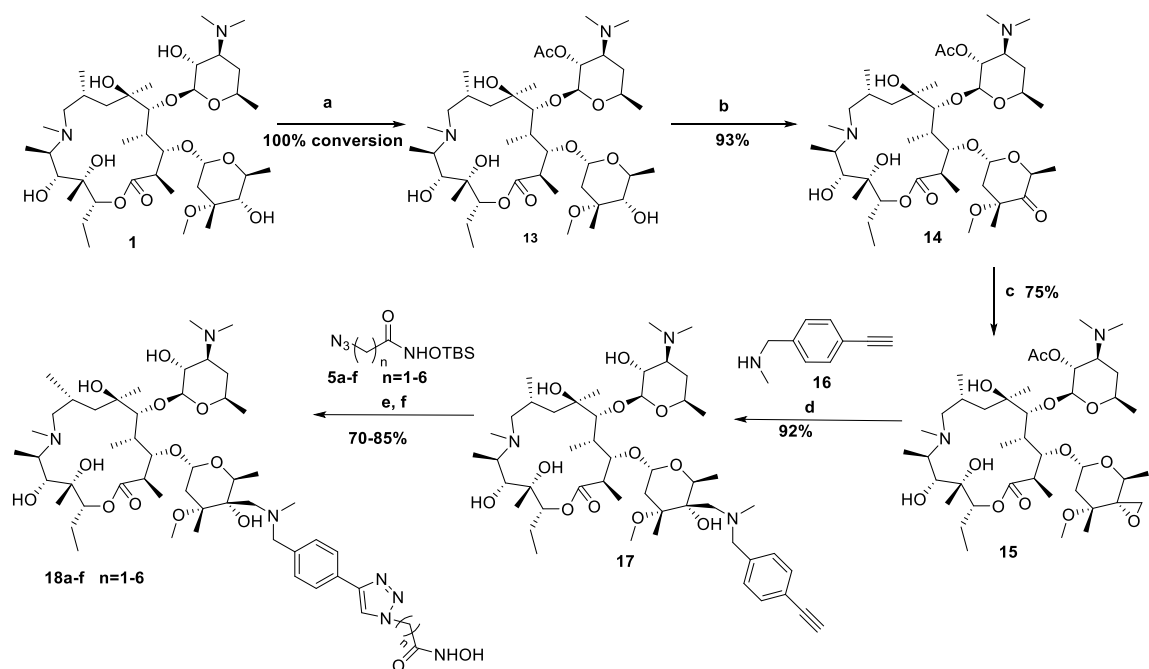
For the synthesis of the second group of azithromycin derived HDACi, a dimethyl amine group was installed at the C4'' position of cladinose sugar of **4**, a substitution that may influence the acid stability of the cladinose sugar glycosidic bond [24] (Scheme 2.2).



Scheme 2.2. (a) I_2 , NaOAc, MeOH, 50 °C, 2 h, 50% (b) Hünig's base, DMSO, 85 °C, 3 h, 97%; (c) acetic anhydride, CH_2Cl_2 , 40 °C, 48 h, 100% conversion; (d) NCS, DMS, TEA, CH_2Cl_2 , -15 °C, 6 h, 95%; (e) $(\text{CH}_3)_3\text{SO}^+\text{I}^-$, NaH, DMSO, THF, rt, 4 h, 89%; (f) KI, MeOH, 60 °C, 6 h; (g) MeOH, 90 °C, 3 days, (84%, f and g); (h) CuI (15 mol%), Hünig's base, THF, rt, 12 h; (i) CsF, MeOH, rt, 2 h (70-80%, h and i).

Finally, the third group of azithromycin derived HDACi was synthesized through the introduction of the ethynylbenzyl to cladinose sugar of azithromycin in four steps [21]. Acetic anhydride treatment of azithromycin **1** in dichloromethane selectively gave 2'-O-acetylazithromycin **13**. Corey-Kim oxidation on **13** followed by Corey-Chaykovsky epoxidation of intermediate 4''-oxo-2'-O-acetylazithromycin **14** yielded epoxy compounds **15**. Regioselective opening of epoxide ring of **15** with 4-ethynylbenzyl-*N*-

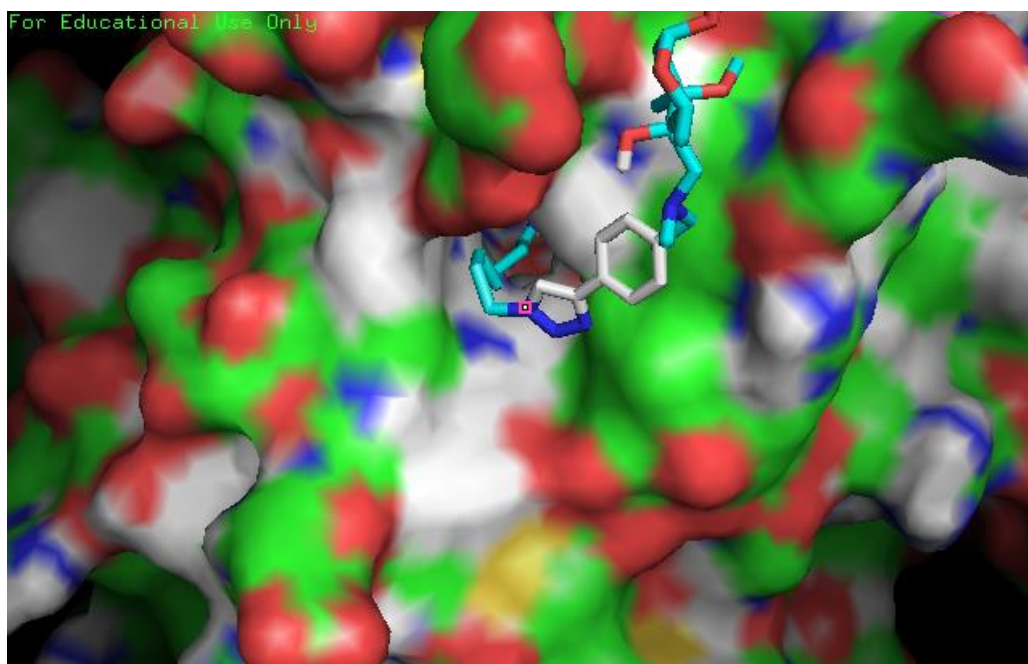
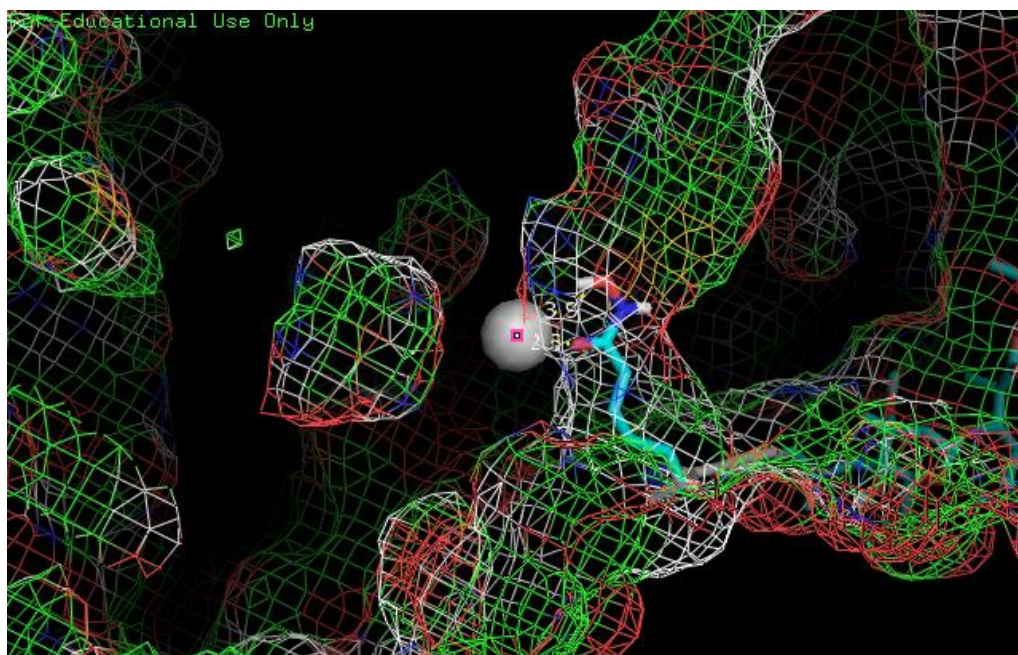
methyamine **16** in methanol, followed by a concomitant acetyl group deprotection, gave key intermediate **17**. Then it was subjected to AAC reaction with various TBS-protected azido hydroxamates **5a-f** followed by removal of TBS-group to give target molecules **18a-f** in moderate to good yields (Scheme 2. 3).



Scheme 2.3. (a) CH_2Cl_2 , Ac_2O , rt, 3 h, 100% conversion; (b) NCS, DMS, TEA, CH_2Cl_2 , -15°C , 4.5 h, 93%; (c) $(\text{CH}_3)_3\text{SO}^+\text{I}^-$, NaH, DMSO, THF, rt, 4 h, 75%; (d) KI, MeOH, 60°C , 6 h, 92%; (e) CuI (15 mol%), Hünig's base, THF, rt, 12 h; (f) CsF, MeOH, rt, 2 h, (70-85%, e and f) .

2.4. Docking study

Docking studies on different azithromycin conjugated HDACis were performed using AutoDock Vina. These compounds were docked against various isoforms of HDACs. Compounds with more than four methylene groups exhibited more potent HDAC inhibition potency which is in correlation with obtained HDAC inhibitory potency in table 2.1(Figure 2.3).



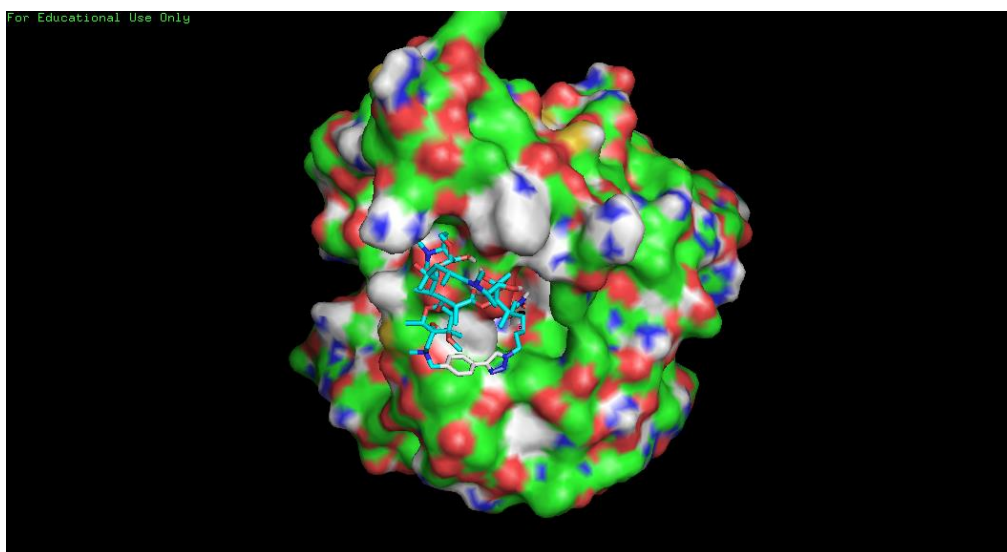
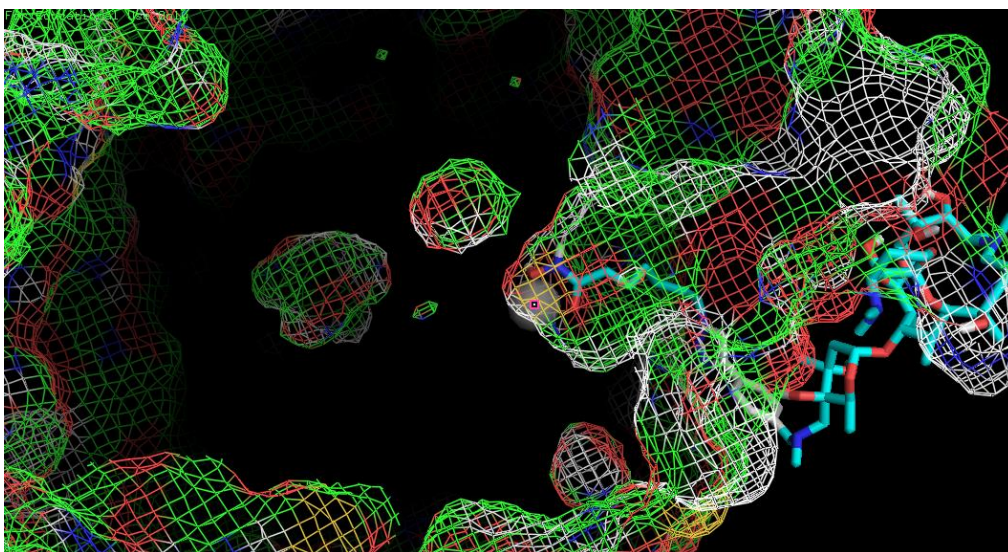


Figure 2.3. Docking studies of example cladinose modified azithromycin HDACi with six methylene linker group (18f) against HDAC1 and HDAC6. As illustrated, these compounds chelate zinc atom and show HDAC inhibition potency. The first two figures show zinc ion chelation in the active pocket of HDAC1 isoform. The grey spheres

illustrates the zinc atom. The last two figures show zinc ion chelation in the active site of HDAC6. The grey sphere represents zinc ion.

2.5. HDAC inhibitory activity

All the three groups of azithromycin derived HDACi and previously synthesized controls [14], [25] and compounds were tested against class I (HDAC1 and HDAC8) and class IIb (HDAC6) enzymes to evaluate their anti-HDAC activities. HDAC activity was determined using label-free mass spectrometry-based SAMDI assay [26]. As expected from previous observations, most of these new HDACis were less active against HDAC8 (Table 2.1).

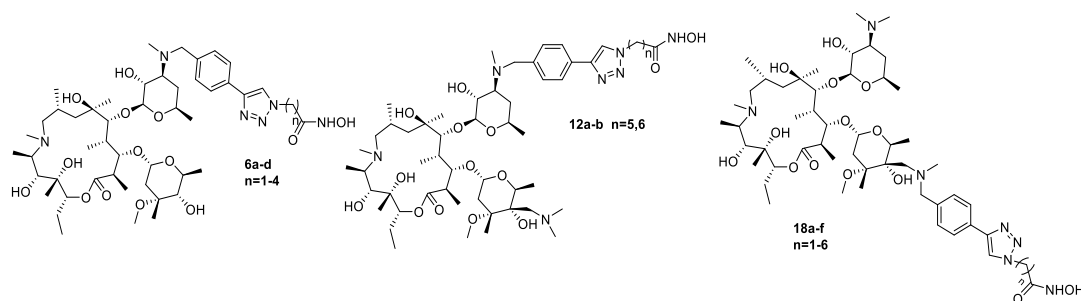


Table 2.1. HDAC 1, HDAC6, and HDAC8 inhibition activities of azithromycin derived hydroxamic acid compounds.

Compound	n	HDAC1 nM	HDAC6 nM	HDAC8 nM
6a	1	>10 μ M	5660 \pm 320	>10 μ M
6b	2	>10 μ M	2170 \pm 200	>10 μ M
6c	3	>10 μ M	106 \pm 13	>10 μ M
6d	4	1650 \pm 456	145 \pm 42	5380 \pm 650
6e	5	316 \pm 61	14.3 \pm 0.6	644 \pm 244
6f	6	68.6 \pm 3.3	7.29 \pm 0.56	314 \pm 90
18a	1	>10 μ M	>10 μ M	4510 \pm 660

Table 2.1. HDAC 1, HDAC6, and HDAC8 inhibition activities of azithromycin derived hydroxamic acid compounds (continued).

18b	2	>10 μ M	2030 \pm 300	2230 \pm 560
18c	3	>10 μ M	181 \pm 24	1180 \pm 210
18d	4	531 \pm 79	95.3 \pm 12.3	709 \pm 141
18e	5	203 \pm 35	31.9 \pm 1.2	786 \pm 176
18f	6	50.4 \pm 8.4	31.3 \pm 1.3	817 \pm 308
12a	5	160 \pm 66	14.7 \pm 1.8	1090 \pm 240
12b	6	79.5 \pm 54	18.9 \pm 3.4	749 \pm 98
SAHA	-	42	34	2800

(HDAC inhibition assay was performed by Dr. James Kornaki at Northwestern University)

Analysis of the HDAC1 and HDAC6 inhibitory effects of these macrolide derived HDACi revealed that their potency is largely dependent on the macrolide template as well as the length of the methylene spacer-group connecting the triazolyl group to the ZBG, hydroxamic acid. An increase in the length of the linker group (C1 to C6) led to an increase in HDAC1 and HDAC6 potencies. Introduction of the dimethylamino methyl group at cladinose sugar of azithromycin had moderate impact on HDAC inhibition (Table 1, compare **6e-f** and **12a-b**). Points of attachment of the aryl triazolyl hydroxamate group on the macrolide template also influenced HDAC inhibition potency. Attachment of the aryl-triazolyl cap group to cladinose sugar of azithromycin did not negatively impact HDAC1 inhibition while it only moderately attenuated HDAC6 inhibition potency (Table 1, compare **6e-f** and **18e-f**). Overall, the optimum HDAC1 and HDAC6 inhibition was obtained for the five and six methylene spacers. .

2.6. Anti-proliferative activity

To determine if the HDAC inhibitory activities of these macrolide derived HDACi translate to anti-proliferative activity, representative members from each class

were tested against three cell lines, two transformed cell lines, lung (A549) and breast (MCF-7) cancers as well as one normal cell line (VERO- monkey kidney epithelial cell). The selected compounds have diverse HDAC inhibitory activities ranging from weak to potent HDAC inhibition.

Compound **6c** is inactive against all transformed cell lines tested. The lack of cytotoxicity of **6c** may be due to its poor HDAC inhibition activity. The other two compounds tested – **12b** and **18f** have broad HDAC inhibition activity. Surprisingly however, only **12b** displayed the characteristic broad cytotoxicity activity of HDACi against all the cell lines investigated (Table 2.2). The reason for the lack of whole cell effect of **18f** is not apparent from this study. Relative to the previously synthesized **6f** and **12b** has slightly weaker anti-proliferative activity.

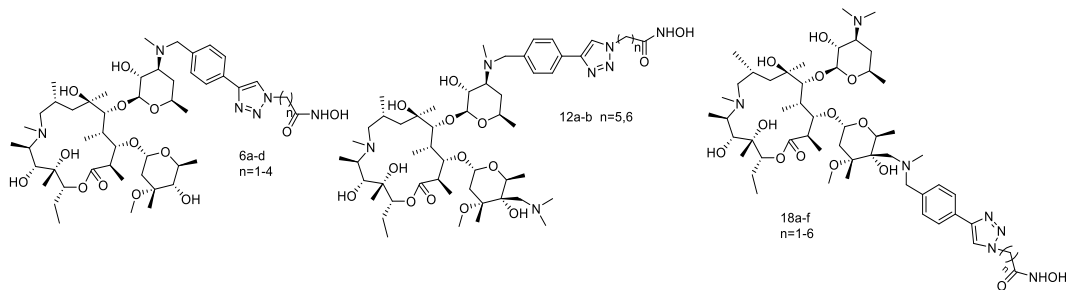


Table 2.2. Anti-proliferative activity of selected azithromycin conjugated HDACi (IC₅₀ values in μ M).

Compound	A549	MCF-7	Vero
6c	NI	NI	NT
6f	2.32 ± 0.53	4.08 ± 1.03	5.90 ± 0.18
18f	NI	NI	NT
12b	6.80 ± 0.50	5.92 ± 1.82	5.73 ± 0.49
SAHA	5.00 ± 0.24	3.27 ± 0.05	1.03 ± 0.09

Each value is obtained from a duplicate of three simultaneous experiments. NI=No inhibition, NT=not tested.

2.7. Anti-inflammatory activity

Cancer, especially lung cancer and many other lung diseases are associated with inflammation [27]. The transcriptional regulator nuclear factor- κ B (NF- κ B) is the main driver of inflammation [28], [28]. In 1863, Virchow discovered that cancer occurs at the site of chronic inflammation, and chronic inflammatory diseases are affiliated with higher risk of cancer [29]. It has been shown that HDACs play an important role in regulating inflammation [30], [31]. HDAC activity is essential for initiation of NF- κ B mediated transcription of inflammatory genes. HDACis such as SAHA [32], entinostat [33], and trichostatin A [34] diminish inflammation by inhibiting NF- κ B activation and signaling as well as promoting blockage of pro-inflammatory cytokine release [31].

To determine azithromycin conjugated HDACi anti-inflammatory activity, their effects on NF- κ B activity in BEAS-2B cell infected with nontypeable *Haemophilus influenza* (NTHi) was evaluated using NF- κ B luciferase assay [35]. *NTHi*, a Gram-negative bacterium, causes infection in the human respiratory tract [36]. This infection leads to activation of NF- κ B in human epithelial cell by translocating it from cytoplasm to nucleus and consequently up-regulating certain pro-inflammatory cytokines such as IL-1 β , IL-6, and TNF- α . For prescreening, these azithromycin derived HDACi were first treated with NTHi infected BEAS-2B cells at 1 μ M. It was observed that the compounds ability to inhibit NF- κ B had a direct correlation with their HDAC inhibitory potency. Analogs lacking or possessing weak anti-HDAC activities did not suppress NF- κ B activation while those with potent anti-HDAC activities suppressed NF- κ B activation to varying degrees with a close correlation with their HDAC inhibition potency.

Subsequently, selected compounds were screened to determine the IC₅₀ of their NF- κ B inhibitory activity. SAHA was used as the positive control. It was observed that these compounds suppressed the NTHi-induced NF- κ B activation with IC₅₀ ranging from low to high nanomolar (Table 2.3). Azithromycin did not show any effect in this assay as

its relative percentage luciferase activity was indistinguishable from no drug treatment in presence of NTHi (100%), which indicates that the anti-inflammatory activity of these compounds is derived from their HDAC inhibition activities.

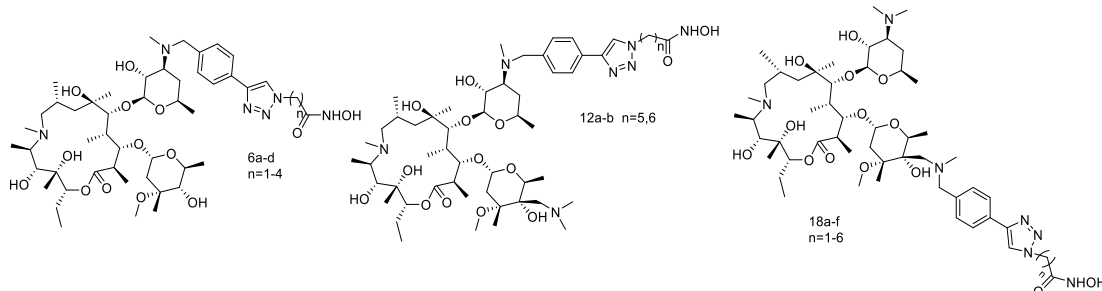


Table 2.3. Anti-inflammatory activity (NF- κ B inhibition) of selected HDACis

Compound	IC ₅₀ (nM)	*I _{max} %
6f	280	41.4
18e	368	46.1
12b	575	43.4
SAHA	88	37.4

*I_{max} (%) at 1 μ M. Anti-inflammatory activity was performed at Dr. Li lab at Georgia State University

2.8. Conclusion

Toward delineating the SAR of macrolide derived HDACi, I synthesized three new classes of hydroxamic acid-based HDACis derived from azithromycin. A subset of these compounds showed nanomolar range HDAC inhibitory activity. Compounds with more potent HDAC inhibition activity, exhibited low micromolar cytotoxicity against lung (A549) and breast (MCF-7) cancer cell lines. They were less cytotoxic against healthy cells (VERO) compared to the FDA approved HDACi SAHA that is more cytotoxic against healthy cells rather than transformed cells. Additionally, selected compounds exhibited anti-inflammatory activity in NTHi infected BSAS-2B cells.

2.9. Experimental

2.9.1. Materials and methods

Azithromycin was purchased from Greenfield chemical. 4-ethynylbenzyl alcohol was purchased from Sigma-Aldrich. All commercially available starting materials were used without purification. Reaction solvents were high performance liquid chromatography (HPLC) grade or American Chemical Society (ACS) grade and used without purification. Analtech silica gel plates (60 F₂₅₄) were used for analytical TLC, and Analtech preparative TLC plates (UV 254, 2000 µm) were used for purification. UV light and anisaldehyde/iodine stain were used to visualize the spots. 200-400 Mesh silica gel was used in column chromatography. Nuclear magnetic resonance (NMR) spectra were recorded on a Varian-Gemini 400 MHz or Bruker 500 MHz magnetic resonance spectrometer. ¹H NMR Spectra were recorded in parts per million (ppm) relative to the residual peaks of CHCl₃ (7.24 ppm) in CDCl₃ or CHD₂OD (4.78 ppm) in CD₃OD or DMSO-*d*₅ (2.49 ppm) in DMSO-*d*₆. ¹³C spectra were recorded relative to the central peak of the CDCl₃ triplet (77.0 ppm) or CD₃OD septet (49.3 ppm) or DMSO-*d*₆ septet (39.7 ppm) and were recorded with complete hetero-decoupling. Original 'fid' files were processed using MestReNova LITE (version 5.2.5-5780) program. High-resolution mass spectra were recorded at the Georgia Institute of Technology mass spectrometry facility in Atlanta.

2.9.2. Cell viability assay

All cell lines used in this study were maintained in Dulbecco's Modified Eagle Medium (DMEM) (Lonza, GA), supplemented with 10% fetal bovine serum (FBS) (Atlanta Biologicals, Atlanta, GA) and 1% *Penicillin-Streptomycin*. Cells were incubated in 96 well plates for 24 h prior to treatment and then treated with various drugs' concentration for 72 h. Drug anti-proliferative activity was measured using the MTS

assay (CellTiter 96 Aqueous One Solution and CellTiter 96 Non-Radioactive Cell Proliferation Assays, Promega, Madison, WI) as described by the manufacturer. All drugs solution were made in DMEM while DMSO concentration was maintained at 0.1%.

2.9.3. SAMDI assay (*In vitro* HDAC inhibition, performed by Dr. James Kornaki at Northwestern University)

HDAC1, HDAC6 were purchased from BPS Biosciences. To obtain IC₅₀ values, in 96-well microtiter plates (60 min, 37 °C), isoform- optimized substrates (50 µM) were incubated with enzyme (250nM) and inhibitor (at concentrations ranging from .1 nM to 1.0 mM) in HDAC buffer (25.0 mM Tris-HCl, pH 8.0, 140 mM NaCl, 3.0 mM KCl, 1.0 mM MgCl₂, and 0.1 mg/mL BSA). Solution-phase deacetylation reactions were quenched with trichostatin A (TSA) and transferred to SAMDI plates to immobilize the substrate components. SAMDI plates consist of an array of self-assembled monolayers (SAMs) presenting maleimide in standard 384-well format for high-throughput handling capability. Following immobilization, plates were washed to remove buffer constituents, enzyme, inhibitor, and any unbound substrate and analyzed by MALDI mass spectrometry using automated protocols. Deacetylation yields in each triplicate sample were obtained from the integrated peak intensities of the molecular ions for the substrate and the deacetylated product ion by taking the ratio of the former over the sum of both. Yields were plotted with respect to inhibitor concentration and fitted to obtain IC₅₀ values for each isoform–inhibitor pair.

Isoform-optimized substrates were prepared by traditional Fmoc solid-phase peptide synthesis (Anaspec) and purified by semi-preparative HPLC on a reverse-phase C18 column (Waters). The peptide GRK^{ac}FGC was used for HDAC1 and HDAC8 assays, whereas the peptide GRK^{ac}YGC was used for HDAC6 assays.

2.9.4. Anti-inflammatory assay (Performed at Dr. Li lab at Georgia State University)

Luciferase assay was used for measuring NF- κ B activity. BEAS-2B cells were transfected with NF- κ B luciferase reporter construct in pGL3 basic vector [35]. 24 hours after transfection, the cells were treated with drugs for 1 hour followed by stimulation with NTHi for 5 hours. Then cells were lysed with cell lysis buffer (250 mM Tris HCl (pH 7.5), 0.1% Triton-X, 1 mM DTT) and luciferase activity was measured by luciferase assay system (promega). Relative luciferase activity (RLA) was evaluated using the equation: $RLA = \text{luciferase unit of the cells treated with NTHi and drug} / \text{luciferase unit of the cells treated with mock}$. IC_{50} was determined by treating the cells with a serial dose of the drug followed by luciferase assay. % Inhibition was calculated using the equation: $\% \text{ inhibition} = RLA \text{ of the cells treated with indicated concentration of the drug} / RLA \text{ of the cells treated with mock}$.

2.9.5. Synthesis

Desmethylazithromycin **2**, 3'-N-(4-Ethynylbenzyl) azithromycin **4**, 4-ethynylbenzyl methanesulfonate **30**, and linker **5c** were synthesized as previously described in [14], [25].

2.9.5.1. 3'-Desmethylazithromycin (2)

To a 50 mL solution of azithromycin (20 g, 0.02 mmol) and sodium acetate (29 g, 0.21 mmol) in 80% aqueous methanol at 90°C. Iodine (7 g, 0.03 mmol) was added in three batches within 5 min. The mixture was maintained at pH 8-9 by addition of 1 M NaOH (once at 10 min of reaction time), and stirring continued for 3 h. The mixture was poured into cold water containing 5% sodium thiosulfate and extracted with CH_2Cl_2 (2×40 mL). The aqueous layer was basified with concentrated NH_4OH and extracted with

10% MeOH in CH₂Cl₂ (3×40 mL), and the organic layer was dried over Na₂SO₄. Solvent was evaporated off to give 17.7 g of compound **2** as an off-white solid (>90% purity, TLC, CH₂Cl₂/MeOH/NH₄OH 12:1:0.1). The crude **2** was used without further purification.

2.9.5.2. 4-Ethynylbenzyl methanesulfonate (**3**)

4-Ethynyl benzyl alcohol (1.20 g, 9.08 mmol) was dissolved in anhydrous DCM (15 mL) at rt. Triethyl amine (2.52 mL, 18.16 mmol) was added and reaction mixture stirred for 10 minutes. Then cooled to -15 °C and methane sulfonyl chloride (1.25 g, 13.62 mmol) was added. The reaction mixture stirred at -15 °C for 40 minutes. Then reaction mixture was quenched with NaHCO₃ followed by Brine (work up). The organic layer was separated and dried over Na₂SO₄. The crude product was purified by column chromatography (Silica gel, 2:3 Hex: DCM) to give the product (1.46 g, 88%) as a pale yellow solid.

2.9.5.3. (3'-N-(4-Ethynylbenzyl)) azithromycin (**4**)

Desmethyl azithromycin **2** (2.72 g, 3.70 mmol) was dissolved in anhydrous acetonitrile (20 mL), followed by addition of 4-Ethynylbenzyl methanesulfonate **3** (1.46 g, 6.94 mmol) and K₂CO₃ (3.58 g, 25.91 mmol). The reaction stirred at 80 °C for 3 h. Then it was washed with EtOAc (3×30 mL), NaHCO₃ and then brine solution and dried over Na₂SO₄ and concentrated *in vacuo*. The crude product was purified by column chromatography (Silica gel, 12:1:0.5 DCM: MeOH: NH₄OH) to give the product (3.03 g, 96%) as a white solid.

2.9.5.4. 4-Azido-N-((tert-butyldimethylsilyl)oxy)butanamide (**5c**)

2-Azidoacetic acid (540 mg, 5.34 mmol) was dissolved in anhydrous dichloromethane (20 mL). The solution was cooled to 0 °C and then TBTU (2.06 g, 6.41 mmol) was added and the solution was stirred for another 15 min at 0 °C. After that O-

(*tert*-butyldimethylsilyl) hydroxylamine (1.28 g, 6.95 mmol) dissolved in 5 mL of anhydrous dichloromethane containing Hünig's base (2 mL, 10.69 mmol) was added and the resulting reaction mixture was stirred at room temperature for 12 h. Reaction was quenched by adding water (5 mL) and the organic layer was separated. The aqueous layer was extracted twice with dichloromethane (10 mL) and the combined organic layer was washed with saturated aqueous NaHCO₃ solution (5 mL), water (10 mL), brine (10 mL), dried over anhydrous Na₂SO₄, filtered, and concentrated in *vacuo*. The crude was purified by column chromatography (Silica gel, 15% ethyl acetate in hexane) to afford the target compound **5c** (438 mg, 35%) as colorless oil ¹H NMR (CDCl₃, 400 MHz) δ (ppm) 7.79 (bs, 1H), 3.33 (t, *J* = 6.9 Hz, 2H), 2.17 (t, *J* = 6.9 Hz, 2H), 1.89 (q, *J* = 6.9 Hz and 4.3 Hz, 2H), 0.93 (s, 9H), 0.16 (s, 6H).

2.9.5.5. (Azithromycin-3'-(*N*-(4-triazolylbenzyl)))-*N*-hydroxyacetamide (**6a**)

(3'-*N*-(4-ethynylbenzyl))azithromycin **4** (0.10 g, 0.12 mmol) and 2-Azido-*N*-((*tert*-butyldimethyl silyl)oxy) ethanamide **5a** (0.05 g, 0.22 mmol) were dissolved in degassed anhydrous THF (5 mL). CuI (0.01 g, 0.06 mmol) and Hünig's base (0.04 mL, 0.24 mmol) were added to the reaction and the resulting reaction was stirred at room temperature for another 12h. Then, the reaction mixture was diluted with excess ethyl acetate (30 mL) and was transferred to a separatory funnel and then the ethyl acetate layer was washed with a solution (20 mL) of 4:1 mixture of saturated aqueous NH₄Cl solution /NH₄OH solution, water (10 mL), brine (10 mL), dried over anhydrous Na₂SO₄, filtered, and concentrated *in vacuo*. The crude was dissolved in 5 mL of anhydrous methanol and to that the solution caesium fluoride (0.03 g, 0.18 mmol) was added and the reaction was stirred at room temperature for 2 h. Afterward, water (10 mL) and ethyl acetate (30 mL) were added to the reaction and the organic layer was separated and then the organic layer was washed with brine (10 mL), dried over anhydrous Na₂SO₄, filtered and concentrated *in vacuo*. The crude was purified by preparative chromatography

(Silica gel, 5:1:1 EtOAc/MeOH/NH₄OH) to give the title compound **6a** as light yellow solid (0.045 g, 40% yield). ¹H NMR (400 MHz, CD₃OD) δ (ppm) 8.47 (d, J = 2.4 Hz, 1H), 7.96 (d, J = 7.0 Hz, 2H), 7.62 (d, J = 7.4 Hz, 2H), 5.13 (d, J = 4.6 Hz, 2H), 4.66 (d, J = 7.2 Hz, 1H), 4.31 – 4.20 (m, 2H), 4.15 (d, J = 12.9 Hz, 1H), 3.86 (d, J = 12.7 Hz, 2H), 3.76 – 3.70 (m, 2H), 3.52 (d, J = 6.9 Hz, 2H), 3.43 (dd, J = 3.2, 1.6 Hz, 3H), 3.29 (s, 3H), 3.20 – 3.12 (m, 2H), 3.07 (s, 1H), 3.01 – 2.97 (m, 1H), 2.88 (s, 3H), 2.55 (s, 3H), 2.30 (d, J = 14.2 Hz, 2H), 2.09 – 2.01 (m, 28H), 1.69 (dd, J = 15.2, 5.1 Hz, 2H), 1.56 (s, 3H), 1.44 (s, 3H), 1.32 (s, 3H), 1.17 (s, 3H), 1.03 (t, J = 7.4 Hz, 3H). ¹³C NMR (126 MHz, CD₃OD) δ (ppm) 180.7, 177.2, 149.5, 141.0, 140.9, 131.7, 127.5, 124.5, 104.7, 102.3, 97.6, 85.1, 80.1, 78.9, 76.8, 76.7, 76.2, 75.5, 73.2, 70.2, 70.1, 67.5, 66.8, 65.4, 59.3, 52.0, 51.0, 50.1, 49.3, 47.5, 44.1, 43.5, 38.4, 37.7, 36.7, 33.8, 32.7, 31.6, 29.1, 27.7, 24.5, 22.8, 19.8, 18.2, 16.5, 12.3, 10.6, 8.9. HMRS (ESI) $m+2/2z$ Calcd for C₄₈H₈₂N₆O₁₄ [M+2H⁺]: 483.2939, found for 483.2935.

2.9.5.6. Azithromycin-3'-(*N*-(4-triazolylbenzyl)))-*N*-hydroxypropanamide (**6b**)

Reaction of (3'-*N*-(4-ethynylbenzyl))azithromycin **4** (0.18 g, 0.22 mmol) and 3-Azido-*N*-((tert-butyldimethyl silyl)oxy) propanamide **5b** (0.08 g, 0.33 mmol) followed by TBS deprotection with caesium fluoride as described for the synthesis of **6a**, gave **6b** as light yellow solid (170 mg, 79%). ¹H NMR (400 MHz, CD₃OD) δ (ppm) 8.39 (s, 1H), 7.93 (d, J = 8.0 Hz, 2H), 7.61 (d, J = 8.3 Hz, 2H), 5.14 (d, J = 4.5 Hz, 1H), 4.88 (s, 3H), 4.67 (d, J = 7.3 Hz, 1H), 4.23 (d, 2H), 4.15 (d, J = 13.2 Hz, 1H), 3.86 (d, J = 13.3 Hz, 2H), 3.77 – 3.71 (m, 2H), 3.62 – 3.52 (m, 2H), 3.46 – 3.41 (m, 3H), 3.30 (s, 3H), 3.16 (d, J = 9.5 Hz, 2H), 2.91 (s, 3H), 2.55 (s, 3H), 2.32 (s, 1H), 2.15 – 2.01 (m, 24H), 1.70 (d, J = 10.6 Hz, 2H), 1.57 (s, 3H), 1.48 (d, J = 6.9 Hz, 2H), 1.43 (s, 3H), 1.38 – 1.33 (m, 2H), 1.29 (s, 3H), 1.20 (s, 3H), 1.16 (s, 3H), 1.03 (t, J = 7.4 Hz, 3H). ¹³C NMR (126 MHz, CD₃OD) δ (ppm) 178.3, 175.0, 147.1, 138.1, 129.6, 125.4, 102.5, 95.4, 83.0, 78.4, 77.8, 76.5, 73.9, 73.2, 72.3, 70.7, 70.0, 69.8, 65.4, 64.7, 60.8, 57.1, 55.4, 51.2, 48.2, 48.0, 47.9,

47.2, 46.1, 45.7, 45.3, 45.2, 41.9, 41.1, 36.1, 35.6, 31.7, 29.4, 29.1, 25.5, 22.7, 22.4, 20.6, 16.1, 13.2, 12.9, 10.1, 8.5, 6.9. HRMS (ESI) m/z Calcd. for $C_{49}H_{83}N_6O_{14}$ $[M+H]^+$: 979.5962, found for 979.5958.

2.9.5.7. Azithromycin-3'-(*N*-(4-triazolylbenzyl)))-*N*-hydroxybutanamide (**6c**)

Reaction of (3'-*N*-(4-ethynylbenzyl))azithromycin **4** (0.15 g, 0.17 mmol) and 4-Azido-*N*-((tert-butyldimethyl silyl)oxy) butanamide **5c** (0.08 g, 0.32 mmol) followed by TBS deprotection with caesium fluoride as described for the synthesis of **6a**, gave **6c** as light yellow solid (110 mg, 62%). 1H NMR (400 MHz, CD_3OD) δ (ppm) 8.21 (s, 1H), 7.66 (d, $J = 7.5$ Hz, 2H), 7.33 (d, $J = 6.2$ Hz, 2H), 4.35 (d, $J = 7.1$ Hz, 2H), 3.97 – 3.88 (m, 1H), 3.66 – 3.55 (m, 1H), 3.42 (s, 3H), 3.26 (d, $J = 10.4, 7.0$ Hz, 3H), 3.13 – 3.11 (m, 2H), 2.96 (s, 3H), 2.92 – 2.78 (m, 1H), 2.66 (dd, $J = 12.4, 7.4$ Hz, 3H), 2.59 (s, 3H), 2.29 (s, 3H), 2.18 (d, $J = 15.0$ Hz, 2H), 2.00 (dd, $J = 20.2, 12.5$ Hz, 2H), 1.81 (d, $J = 7.6$ Hz, 2H), 1.75 (s, 24H), 1.39 (dd, $J = 15.2, 9.7$ Hz, 2H), 1.26 (s, 3H), 1.16 (d, $J = 6.8$ Hz, 3H), 1.11 (d, $J = 3.8$ Hz, 3H), 1.06 – 1.00 (m, 1H), 0.96 (s, 3H), 0.88 (d, $J = 7.4$ Hz, 3H), 0.84 (d, $J = 6.8$ Hz, 3H), 0.71 (t, $J = 7.3$ Hz, 3H). ^{13}C NMR (126 MHz, CD_3OD) δ (ppm) 180.5, 177.2, 172.2, 149.5, 131.7, 131.6, 127.5, 123.1, 104.7, 97.6, 85.2, 80.6, 80.1, 78.8, 76.7, 76.1, 75.6, 75.1, 73.1, 70.1, 65.4, 59.4, 51.5, 50.8, 50.5, 50.2, 50.1, 49.5, 47.6, 44.1, 38.2, 37.7, 36.7, 32.8, 31.6, 31.5, 31.3, 31.2, 28.1, 27.8, 22.9, 22.9, 22.8, 22.4, 19.8, 18.2, 16.5, 12.3, 10.6, 9.0. HRMS (ESI) m/z Calcd for $C_{50}H_{85}N_6O_{14}$ $[M+H]^+$: 993.6118, found 993.6113

2.9.5.8. Azithromycin-3'-(*N*-(4-triazolylbenzyl)))-*N*-hydroxypentanamide (**6d**)

Reaction of (3'-*N*-(4-ethynylbenzyl))azithromycin **4** (0.14 g, 0.16 mmol) and 5-Azido-*N*-((tert-butyldimethyl silyl)oxy) pentanamide **5d** (0.07 g, 0.24 mmol) followed by TBS deprotection with caesium fluoride as described for the synthesis of **6a**, gave **6d** as light yellow solid (110 mg, 66%). 1H NMR (400 MHz, CD_3OD) δ (ppm) 8.28 (s, 1H),

7.73 (d, $J = 7.7$ Hz, 2H), 7.40 (d, $J = 7.9$ Hz, 2H), 4.47 (d, $J = 7.2$ Hz, 1H), 4.41 (s, 2H), 4.12 (d, $J = 17.0$ Hz, 2H), 3.80 (d, $J = 13.0$ Hz, 1H), 3.68 (s, 1H), 3.64 – 3.50 (m, 4H), 3.35 – 3.24 (m, 2H), 3.13 (s, 3H), 3.00 – 2.91 (m, 2H), 2.76 (dd, $J = 7.5, 4.4$ Hz, 2H), 2.65 (d, $J = 11.8$ Hz, 1H), 2.39 (s, 3H), 2.32 (d, $J = 15.0$ Hz, 2H), 2.24 (s, 3H), 2.15 – 2.09 (m, 3H), 1.98 – 1.86 (m, 22H), 1.31 (s, 3H), 1.23 (d, $J = 5.9$ Hz, 5H), 1.18 – 1.09 (m, 7H), 1.06 (s, 3H), 1.01 (d, $J = 7.5$ Hz, 4H), 0.91 (s, 2H), 0.84 (t, $J = 7.3$ Hz, 3H). ^{13}C NMR (126 MHz, CD_3OD) δ (ppm) 180.5, 177.2, 149.5, 141.7, 131.6, 131.4, 127.4, 122.9, 104.8, 97.3, 85.3, 80.5, 80.2, 78.9, 76.3, 76.2, 76.1, 75.1, 73.3, 70.0, 67.3, 65.3, 59.6, 51.8, 50.8, 50.3, 50.1, 50.0, 49.8, 49.5, 49.3, 47.5, 44.3, 43.9, 38.2, 37.6, 36.8, 32.8, 31.5, 28.5, 28.3, 24.4, 23.1, 22.9, 22.5, 19.8, 18.2, 16.5, 12.4, 10.7, 8.6. HRMS (ESI) m/z Calcd. for $\text{C}_{51}\text{H}_{87}\text{N}_6\text{O}_{14}$ [$\text{M}+\text{H}^+$]: 1007.6275, found 1007.6272.

2.9.5.9. ((3'-O-Acetyl)-4'-N-(4-ethynylbenzyl))azithromycin (7)

To the solution of (4'-ethynylbenzyl)azithromycin **4** (1.00 g, 1.18 mmol) in DCM (10 mL) was added acetic anhydride (0.13 mL, 1.41 mmol). Then the mixture was heated to 40 °C in a pressure tube and stirring continued for 48 h. The reaction mixture was cooled and diluted with DCM (100 mL) and washed with saturated NaHCO_3 (50 mL), water (50 mL), and brine (50 mL). The organic layer was dried over anhydrous Na_2SO_4 , filtered and concentrated *in vacuo*. The solid crude product **7** (1.1 g, 95%) was sufficiently pure to be used for the next reaction without any further purification. ^1H NMR (400 MHz, CDCl_3) δ (ppm) 7.38 (d, $J = 8.1$ Hz, 2H), 7.17 (d, $J = 8.1$ Hz, 2H), 5.06 – 5.00 (m, 1H), 4.94 (dd, $J = 10.6, 2.3$ Hz, 1H), 4.86 (dd, $J = 10.5, 7.6$ Hz, 1H), 4.79 (d, $J = 4.4$ Hz, 1H), 4.45 (d, $J = 7.6$ Hz, 1H), 4.13 (t, $J = 5.6$ Hz, 1H), 3.97 (dq, $J = 12.5, 6.2$ Hz, 1H), 3.64 (d, $J = 13.8$ Hz, 1H), 3.57 – 3.44 (m, 2H), 3.40 (d, $J = 4.3$ Hz, 1H), 3.29 (dd, $J = 12.3, 4.8$ Hz, 1H), 3.20 (s, 3H), 3.02 – 2.94 (m, 2H), 2.74 (td, $J = 12.2, 4.2$ Hz, 1H), 2.67 – 2.58 (m, 1H), 2.53 (q, $J = 7.2$ Hz, 2H), 2.28 (d, $J = 14.9$ Hz, 2H), 2.19 (s, 3H), 2.14 (d, $J = 6.8$ Hz, 3H), 2.10 (d, $J = 7.4$ Hz, 3H), 2.04 (d, $J = 5.4$ Hz, 3H), 1.99 –

1.89 (m, 1H), 1.82 – 1.70 (m, 3H), 1.68 – 1.34 (m, 3H), 1.28 – 1.17 (m, 13H), 1.13 (d, J = 7.1 Hz, 6H), 1.04 – 0.91 (m, 10H), 0.89 – 0.80 (m, 3H). ^{13}C NMR (101 MHz, CDCl_3) δ (ppm) 176.5, 175.5, 171.0, 170.0, 140.8, 132.0, 128.4, 128.1, 128.0, 120.7, 101.4, 96.5, 84.3, 83.7, 80.6, 79.8, 77.9, 76.4, 75.3, 74.1, 72.9, 71.2, 69.0, 65.6, 61.9, 61.1, 58.2, 49.4, 48.9, 45.5, 42.9, 41.4, 36.9, 35.1, 34.4, 31.0, 29.6, 27.1, 25.2, 23.6, 21.9, 21.6, 20.6, 17.9, 14.1, 11.7, 11.1, 8.3. HRMS (ESI) $m+2/2z$ Calcd. for $\text{C}_{48}\text{H}_{80}\text{N}_2\text{O}_{13}$ [$\text{M} + 2\text{H}^+$]: 446.2825, found 446.2810.

2.9.5.10. ((4''-Oxo)-3'-O-acetyl)-4'-N-(4-ethynylbenzyl)azithromycin (**8**)

A solution of *N*-chlorosucciniamide (0.46 g, 3.47 mmol) in DCM (5 mL) was stirred at -15 °C for 10 min. Then DMS (0.30 mL, 3.90 mmol) was added drop wise to form a white solution. After stirring for 20 min a DCM (5 mL) solution of compound **7** (1.93 g, 2.17 mmol) was added over 30 min and the resulting suspension was stirred at -15 °C for 30 min. Subsequently, TEA (0.5 mL, 3.47 mmol) was added and the reaction cleared up within a minute. Stirring continued at -10 °C for 2 h and the reaction was quenched with saturated aqueous NaHCO_3 solution (20 mL), extra DCM (20 mL) was added and the organic layer was separated. The aqueous layer was again extracted with DCM (2 x 10 mL) and the combined organic layer was dried over anhydrous Na_2SO_4 , filtered, and concentrated *in vacuo*. The crude was purified by column chromatography (Silica gel, 12:1:0.5 DCM: MeOH: NH_4OH) to give the title compound **8** (1.79 g, 93% yield) as white solid. ^1H NMR (400 MHz, CDCl_3) δ (ppm) 7.37 (d, J = 8.1 Hz, 2H), 7.17 (d, J = 7.3 Hz, 2H), 5.18 – 5.04 (m, 1H), 5.05 – 4.73 (m, 2H), 4.65 (d, J = 9.7 Hz, 1H), 4.48 – 4.34 (m, 1H), 4.20 (d, J = 4.3 Hz, 1H), 4.16 – 4.06 (m, 1H), 3.95 (dd, J = 15.2, 8.5 Hz, 1H), 3.72 – 3.57 (m, 2H), 3.56 – 3.37 (m, 3H), 3.31 (dd, J = 16.4, 9.8 Hz, 1H), 3.23 (t, J = 5.2 Hz, 1H), 3.19 (s, 1H), 3.07 (d, J = 6.2 Hz, 1H), 3.05 – 2.91 (m, 2H), 2.86 – 2.55 (m, 2H), 2.49 (d, J = 10.1 Hz, 1H), 2.27 (dd, J = 11.5, 6.2 Hz, 3H), 2.20 (d, J = 5.6 Hz, 3H), 2.17 – 2.13 (m, 2H), 2.11 (d, J = 5.3 Hz, 2H), 2.08 – 1.95 (m, 5H), 1.83 – 1.70

(m, 2H), 1.66 – 1.46 (m, 2H), 1.44 – 1.34 (m, 3H), 1.34 – 1.16 (m, 14H), 1.13 (dd, $J = 6.8, 4.2$ Hz, 4H), 1.10 – 1.01 (m, 4H), 1.00 – 0.91 (m, 3H), 0.90 – 0.73 (m, 3H). ^{13}C NMR (126 MHz, CDCl_3) δ (ppm) 211.6, 177.2, 176.5, 170.0, 169.7, 140.6, 132.0, 128.3, 120.6, 100.5, 94.6, 83.6, 75.8, 75.3, 74.3, 73.9, 73.0, 72.4, 72.2, 71.2, 69.8, 69.0, 68.0, 65.6, 63.1, 61.8, 58.3, 51.2, 49.5, 48.9, 45.1, 37.1, 36.9, 35.2, 34.4, 29.5, 23.0, 22.1, 21.5, 21.1, 20.6, 18.1, 15.5, 14.3, 12.3, 11.3, 9.0, 7.7. HRMS (ESI) m/z Calcd. for $\text{C}_{48}\text{H}_{77}\text{N}_2\text{O}_{13}$ $[\text{M}+\text{H}^+]$: 889.5420, found 889.5412.

2.9.5.11. ((4''-Epoxy)-3'-*O*-acetyl)-4'-*N*-(4-ethynylbenzyl))azithromycin (**9**)

NaH (0.2 g, 4.67 mmol, 60% w/w) was added to an oven dried three necked flask and was washed with petroleum ether ($\times 3$). The flask was immediately flushed with Ar and dry DMSO (6 mL) was introduced through a septum. The mixture was stirred at room temperature under Ar. Then trimethyloxosulfonium iodide (1.05 g, 4.67 mmol) was added over a period of 5 min. After hydrogen gas ceased to evolve, the resulting yellow clear solution was treated with a solution of compound **8** (1.88 g, 2.12 mmol) in anhydrous THF (5 mL) over 10 min and stirring continued for 2 h after which TLC (4:1:0.5 Hex, EtOAc: EtOH) showed a near quantitative conversion to a new product. THF was evaporated off, EtOAc (20 mL) was added to the remaining residue and the mixture was washed with water several times to remove DMSO. The organic layer was dried over Na_2SO_4 and concentrated to give light yellow solid product **9** (1.63 g, 85% yield). ^1H NMR (400 MHz, CDCl_3) δ (ppm) 7.37 (d, $J = 8.0$ Hz, 2H), 7.18 (d, $J = 6.7$ Hz, 2H), 5.26 (s, 1H), 5.06 (d, $J = 10.0$ Hz, 1H), 4.98 (d, $J = 8.5$ Hz, 1H), 4.95 – 4.76 (m, 2H), 4.72 (dd, $J = 12.6, 6.2$ Hz, 1H), 4.62 (t, $J = 7.4$ Hz, 1H), 4.50 (s, 1H), 4.44 (d, $J = 7.6$ Hz, 1H), 4.09 (t, $J = 7.3$ Hz, 1H), 4.03 (dd, $J = 12.6, 5.9$ Hz, 1H), 3.70 – 3.60 (m, 1H), 3.60 – 3.52 (m, 1H), 3.51 – 3.42 (m, 1H), 3.34 (d, $J = 19.2$ Hz, 1H), 3.28 – 3.14 (m, 2H), 3.09 (d, $J = 7.6$ Hz, 1H), 3.01 (d, $J = 4.1$ Hz, 1H), 2.91 (d, $J = 4.3$ Hz, 1H), 2.82 – 2.61 (m, 3H), 2.61 – 2.52 (m, 1H), 2.35 – 2.25 (m, 1H), 2.24 – 2.11 (m, 6H), 2.10 – 2.00

(m, 4H), 1.95 – 1.84 (m, 2H), 1.83 – 1.64 (m, 4H), 1.56 (ddd, $J = 20.9, 13.1, 6.4$ Hz, 2H), 1.49 – 1.32 (m, 3H), 1.30 – 1.14 (m, 10H), 1.12 (d, $J = 8.3$ Hz, 2H), 1.06 (s, 3H), 1.03 (d, $J = 4.9$ Hz, 3H), 1.03 – 0.97 (m, 4H), 0.94 (dd, $J = 15.2, 8.7$ Hz, 3H), 0.91 – 0.75 (m, 3H). ^{13}C NMR (126 MHz, CDCl_3) δ (ppm) 182.2, 175.8, 173.7, 169.7, 145.2, 142.9, 140.2, 132.2, 131.9, 128.6, 128.1, 120.9, 106.6, 105.0, 103.7, 97.4, 83.7, 78.3, 75.5, 74.3, 73.7, 72.5, 71.0, 70.6, 69.9, 69.3, 65.5, 65.3, 61.7, 60.9, 59.3, 49.9, 49.4, 42.7, 40.4, 39.7, 37.0, 31.9, 29.2, 22.9, 21.5, 19.3, 17.9, 15.2, 14.1, 11.7, 11.0, 10.3, 8.8. HRMS (ESI) m/z Calcd. for $\text{C}_{49}\text{H}_{79}\text{N}_2\text{O}_{13}$ [$\text{M}+\text{H}^+$]: 903.5577, found 903.5568.

2.9.5.12. ((4''-(*N,N*-Dimethylaminomethyl)-4'-*N*-(4-ethynylbenzyl))azithromycin (**11**))

Reaction of compound **9** (2.00 g, 2.2 mmol) and *N,N*-dimethylmethyl amine **10** (8.92 mL, 168.3, 2M in THF) mmol) in anhydrous methanol (20 mL). The solution was heated at 60 °C for 6 h. MeOH and residual methylamine was evaporated off to give light yellow solid which was again dissolved in MeOH (10 mL) and heated at 90 °C for three days after which TLC showed complete conversion. Excess MeOH was evaporated off to give compound give **11** as white solid (2.0 g, 90%) after purification by column chromatography (Silica gel, 20:1:0.1 DCM, MeOH, and NH_4OH). ^1H NMR (400 MHz, CDCl_3) δ (ppm) 7.38 (t, $J = 5.6$ Hz, 2H), 7.19 (d, $J = 8.0$ Hz, 2H), 4.98 (d, $J = 4.7$ Hz, 1H), 4.80 (dd, $J = 10.7, 7.5$ Hz, 1H), 4.61 (dd, $J = 16.8, 8.0$ Hz, 1H), 4.53 – 4.47 (m, 1H), 4.32 (dd, $J = 11.6, 6.2$ Hz, 1H), 4.08 (t, $J = 7.2$ Hz, 1H), 4.02 (q, $J = 6.4$ Hz, 1H), 3.70 (dt, $J = 9.6, 5.5$ Hz, 1H), 3.67 – 3.59 (m, 2H), 3.54 (d, $J = 6.2$ Hz, 1H), 3.49 (s, 1H), 3.41 (ddd, $J = 22.7, 11.0, 6.6$ Hz, 2H), 3.31 (d, $J = 7.3$ Hz, 1H), 3.20 – 3.12 (m, 1H), 3.11 – 2.98 (m, 3H), 2.92 (d, $J = 3.3$ Hz, 1H), 2.85 (d, $J = 2.4$ Hz, 1H), 2.78 (dd, $J = 17.2, 10.1$ Hz, 1H), 2.73 (s, 1H), 2.65 (dd, $J = 14.3, 7.6$ Hz, 2H), 2.57 (d, $J = 9.5$ Hz, 1H), 2.45 (dt, $J = 23.1, 10.2$ Hz, 1H), 2.31 (d, $J = 11.6$ Hz, 7H), 2.24 – 2.16 (m, 3H), 2.13 (dd, $J = 11.4, 4.5$ Hz, 1H), 2.10 – 2.01 (m, 4H), 2.00 – 1.78 (m, 6H), 1.68 (dd, $J = 23.3, 12.9$ Hz, 2H), 1.23 (qd, $J = 15.5, 7.1$ Hz, 17H), 1.13 (dd, $J = 9.7, 4.5$ Hz, 3H), 1.09 – 0.98 (m, 8H), 0.86

(ddd, $J = 11.8, 10.2, 6.2$ Hz, 3H). ^{13}C NMR (101 MHz, CDCl_3) δ (ppm) 178.0, 169.7, 140.7, 131.8, 128.3, 120.5, 100.4, 95.6, 84.2, 83.5, 78.8, 76.8, 76.0, 74.9, 74.2, 73.3, 71.4, 70.2, 70.1, 67.5, 67.4, 61.9, 61.3, 58.4, 57.9, 53.6, 49.0, 47.3, 47.2, 45.1, 44.7, 41.9, 41.4, 40.1, 36.8, 36.5, 31.5, 30.6, 30.0, 27.0, 26.5, 21.7, 21.3, 20.9, 18.5, 16.1, 15.7, 14.7, 11.1, 9.38, 7.5. ESI MS m/z Calcd. for $\text{C}_{51}\text{H}_{86}\text{N}_3\text{O}_{13}$ $[\text{M}+\text{H}^+]$: 948.61.

2.9.5.12. (Azithromycin-(4'-N-(4-benzyltriazolyl))-4''-(N,N-dimethylaminomethyl))-N-hydroxyhexanamide (12a)

Compound **11** (0.17 g, 0.18 mmol) and 6-Azido-N-((tert-butyldimethyl silyl)oxy) hexanamide **5e** (0.08 g, 0.30 mmol) were dissolved in anhydrous THF (5 mL) and stirred under Ar at room temperature. Copper (I) iodide (0.02 g, 0.09 mmol) and Hunig's base (0.07 mL, 0.37 mmol) were added to the mixture and stirring continued for 12 h. Caesium fluoride (0.04 g, 0.28 mmol) and MeOH (4 mL) were added to the mixture to remove TBS protecting group and stirring continued for an additional 2h. A solution of 4:1 saturated $\text{NH}_4\text{Cl}/\text{NH}_4\text{OH}$ (30 mL) was added to the reaction mixture and extracted with 20% MeOH/ CH_2Cl_2 (3×30 mL). The organic layer was dried over Na_2SO_4 and concentrated *in vacuo*. The crude product was purified by preparative chromatography (Silica gel, 5:1:1 EtOAc: MeOH: NH_4OH) to give the product (0.16 g, 80%) as light yellow solid. ^1H NMR (400 MHz, CD_3OD) δ (ppm) 7.74 (s, 1H), 7.20 (d, $J = 7.8$ Hz, 2H), 6.83 (d, $J = 7.9$ Hz, 2H), 3.83 (s, 2H), 3.74 (d, $J = 7.3$ Hz, 1H), 3.60 – 3.46 (m, 2H), 3.26 (d, $J = 13.0$ Hz, 1H), 2.99 – 2.89 (m, 3H), 2.78 (s, 1H), 2.75 – 2.67 (m, 3H), 2.37 (d, $J = 3.6$ Hz, 3H), 2.23 – 2.10 (m, 2H), 1.96 (t, $J = 14.2$ Hz, 3H), 1.80 – 1.64 (m, 11H), 1.60 – 1.45 (m, 3H), 1.43 – 1.30 (m, 11H), 1.28 (s, 1H), 1.22 (d, $J = 6.6$ Hz, 1H), 1.13 (dd, $J = 24.4, 9.4$ Hz, 3H), 1.02 (d, $J = 15.3$ Hz, 2H), 0.93 – 0.81 (m, 1H), 0.74 (dd, $J = 14.2, 7.2$ Hz, 3H), 0.68 (dd, $J = 10.0, 4.1$ Hz, 5H), 0.67 – 0.58 (m, 3H), 0.55 (d, $J = 6.7$ Hz, 6H), 0.48 (d, $J = 4.3$ Hz, 6H), 0.38 (d, $J = 7.5$ Hz, 3H), 0.33 – 0.21 (m, 10H). ^{13}C NMR (126 MHz, CD_3OD) δ (ppm) 180.5, 178.8, 177.3, 173.7, 172.8, 149.4, 141.7,

131.8, 127.5, 122.8, 105.1, 102.9, 97.3, 86.5, 80.7, 78.8, 77.9, 76.3, 75.9, 73.7, 72.8, 71.4, 70.0, 69.2, 64.7, 63.2, 61.6, 60.1, 55.7, 53.1, 52.1, 50.9, 48.5, 47.3, 44.5, 44.1, 43.9, 38.3, 37.6, 32.9, 32.4, 32.3, 32.2, 31.9, 31.7, 30.2, 28.4, 27.9, 23.1, 22.7, 19.7, 18.1, 16.4, 12.4, 10.7, 8.4. HRMS (ESI) $m+2/2z$ Calcd. for $C_{55}H_{97}N_7O_{14}$ [$M + 2H^+$]: 539.8541, found 539.8549.

2.9.5.13. (Azithromycin-(4'-N-(4-benzyltriazolyl))-4''-(N,N-dimethylaminomethyl))-N-hydroxyheptanamide (**12b**)

Reaction of compound **11** (0.08 g, 0.09 mmol) with 7-Azido-N-((*tert*-butyldimethylsilyl)oxy)heptanamide **5f** (0.04 g, 0.14 mmol) followed by TBS removal with caesium fluoride as described for the synthesis of compound **12a**, gave **12b** as light yellow solid (0.069 g, 70%). 1H NMR (400 MHz, CD_3OD) δ (ppm) 7.46 (s, 1H), 6.92 (d, $J = 8.0$ Hz, 2H), 6.56 (d, $J = 8.0$ Hz, 2H), 3.55 (d, $J = 6.2$ Hz, 2H), 3.47 (d, $J = 7.2$ Hz, 1H), 3.33 – 3.17 (m, 2H), 2.99 (d, $J = 12.9$ Hz, 1H), 2.76 (d, $J = 13.2$ Hz, 1H), 2.67 (dd, $J = 14.5, 9.8$ Hz, 3H), 2.51 (s, 1H), 2.43 (ddd, $J = 6.2, 4.9, 2.3$ Hz, 2H), 2.26 (t, $J = 15.8$ Hz, 1H), 2.09 (d, $J = 5.7$ Hz, 3H), 1.98 – 1.83 (m, 2H), 1.69 (dd, $J = 14.5, 9.6$ Hz, 2H), 1.55 – 1.37 (m, 13H), 1.35 – 1.23 (m, 2H), 1.22 (d, $J = 13.4$ Hz, 3H), 1.16 – 1.01 (m, 11H), 0.87 (t, $J = 11.8$ Hz, 3H), 0.75 (d, $J = 15.1$ Hz, 3H), 0.46 (d, $J = 19.0$ Hz, 6H), 0.44 – 0.40 (m, 3H), 0.35 (dt, $J = 15.7, 9.2$ Hz, 6H), 0.32 – 0.25 (m, 6H), 0.20 (t, $J = 5.5$ Hz, 6H), 0.11 (d, $J = 7.5$ Hz, 3H), 0.07 – 0.06 (m, 6H). ^{13}C NMR (126 MHz, CD_3OD) δ (ppm) 180.4, 180.1, 177.3, 173.5, 172.7, 149.5, 141.7, 141.2, 131.8, 131.4, 127.4, 122.8, 105.1, 102.8, 97.3, 86.1, 80.3, 78.9, 76.5, 75.7, 73.7, 72.8, 71.5, 70.1, 69.2, 64.6, 63.5, 61.7, 60.1, 55.7, 53.2, 52.1, 51.0, 48.5, 47.6, 47.4, 44.1, 43.8, 38.5, 38.0, 37.6, 32.1, 31.5, 29.0, 28.8, 27.7, 26.8, 23.1, 22.4, 20.0, 18.2, 16.4, 16.0, 12.6, 10.8, 8.5. HRMS (ESI) $m+2/2z$ Calcd. for $C_{56}H_{99}N_7O_{14}$ [$M + 2H^+$]: 546.8620, found 546.8611.

2.9.5.14. 3'-O-Acetylazithromycin (**13**)

Acetic anhydride (0.8 mL, 8.34 mmol) was added to a solution of azithromycin **1** (2.50 g, 3.34 mmol) in DCM (10 mL) at room temperature. The resulting solution was stirred under Ar for 3 h. The reaction was quenched by adding saturated NaHCO₃ and the organic layer was separated. The aqueous layer was extracted twice with DCM (20 mL) and the combined organic layer was washed with water, brine, dried over anhydrous Na₂SO₄, filtered and concentrated *in vacuo* to give the target compound as a white solid (2.50 g, 95%). ¹H NMR (400 MHz, CDCl₃) δ (ppm) 5.25 (dd, *J* = 1.6, 0.9 Hz, 1H), 4.93 (s, 3H), 4.74 – 4.67 (m, 2H), 4.59 (d, *J* = 10.2 Hz, 2H), 4.51 (d, *J* = 7.5 Hz, 2H), 4.18 – 4.13 (m, 2H), 4.01 – 3.93 (m, 2H), 3.59 (s, 2H), 3.54 (d, *J* = 6.3 Hz, 2H), 3.30 (s, 3H), 3.23 (s, 2H), 2.96 (d, *J* = 9.0 Hz, 2H), 2.79 – 2.71 (m, 2H), 2.68 – 2.52 (m, 4H), 2.40 (d, *J* = 11.8 Hz, 2H), 2.28 (d, *J* = 13.8 Hz, 4H), 2.04 – 2.01 (m, 1H), 1.98 (d, *J* = 2.3 Hz, 3H), 1.94 – 1.85 (m, 3H), 1.64 (d, *J* = 13.7 Hz, 3H), 1.53 (dd, *J* = 15.3, 4.9 Hz, 2H), 1.28 – 1.23 (m, 7H), 1.20 (d, *J* = 6.4 Hz, 3H), 1.16 (d, *J* = 6.0 Hz, 3H), 1.11 (d, *J* = 8.3 Hz, 3H), 1.09 (s, 3H), 1.03 (d, *J* = 6.7 Hz, 3H), 0.99 (s, 3H). ¹³C NMR (101 MHz, CDCl₃) δ (ppm) 178.2, 176.2, 169.8, 166.3, 100.6, 95.4, 83.8, 78.7, 78.1, 75.8, 74.9, 74.4, 73.5, 72.6, 71.8, 70.1, 68.2, 65.6, 63.7, 61.9, 49.3, 45.1, 42.0, 40.7, 36.5, 35.1, 30.4, 27.2, 26.3, 22.5, 22.0, 21.6, 21.2, 21.1, 18.5, 16.3, 15.4, 11.3, 9.2, 7.8. HRMS (ESI) *m*+2/2*z* Calcd. for C₄₀H₇₆N₂O₁₃ [M+2H⁺]/2: 396.2668, found 396.2656.

2.9.5.15. 4''-Oxo-3'-O-acetylazithromycin (**14**)

N-Iodosuccinimide (0.75 g, 5.61 mmol) was dissolved in anhydrous DCM (20 mL) and the solution was cooled to -15 °C. After 10 min, dimethyl sulfide (0.5 mL, 6.32 mmol) was added drop wise. The white suspension was stirred at -15 °C for 20 min, then a DCM solution (5 mL) of compound **13** (2.78 g, 3.51 mmol) was added over 30 min. The resulting suspension was stirred at -15 °C for 30 min, and triethylamine (0.8 mL, 5.6 mmol) was added. The solution became clear in a minute and stirring was continued at -

10 °C for 2 h. The reaction was quenched by adding saturated aqueous NaHCO₃ solution and the organic layer was separated. The aqueous layer was extracted twice with DCM (2x 50 mL). The combined organic layer was washed with water (50 mL), brine (50 mL), dried over anhydrous Na₂SO₄, filtered, and concentrated *in vacuo*. The crude was purified by column chromatography (Silica gel, 12:1:0.5 DCM: MeOH: NH₄OH) to yield the product (2.49 g 90%) as white solid. ¹H NMR (400 MHz, CDCl₃) δ ¹H NMR (400 MHz, CDCl₃), 6.21 (d, *J* = 41.6 Hz, 2H), 5.27 (t, *J* = 6.6 Hz, 1H), 5.19 (s, 1H), 5.05 (t, *J* = 7.0 Hz, 1H), 5.00 – 4.93 (m, 1H), 4.93 – 4.87 (m, 1H), 4.72 – 4.54 (m, 1H), 4.39 (q, *J* = 6.6 Hz, 1H), 4.36 – 4.27 (m, 1H), 4.11 – 4.06 (m, 1H), 4.05 – 3.99 (m, 5H), 3.50 – 3.41 (m, 1H), 3.36 (d, *J* = 6.1 Hz, 1H), 3.29 (s, 1H), 3.26 (s, 3H), 3.24 – 3.20 (m, 5H), 3.18 – 3.12 (m, 1H), 2.70 – 2.51 (m, 4H), 2.41 (d, *J* = 12.0 Hz, 1H), 2.20 (dt, *J* = 16.6, 9.6 Hz, 4H), 2.15 – 2.08 (m, 2H), 2.01 (d, *J* = 4.6 Hz, 1H), 1.97 (s, 3H), 1.93 (s, 1H), 1.86 (s, 3H), 1.72 – 1.65 (m, 1H), 1.65 – 1.57 (m, 1H), 1.53 (d, *J* = 14.9 Hz, 1H), 1.47 – 1.38 (m, 1H), 1.34 – 1.28 (m, 7H), 1.22 (t, *J* = 6.2 Hz, 1H), 1.18 (d, *J* = 7.3 Hz, 1H), 1.09 (ddd, *J* = 23.5, 15.0, 8.7 Hz, 3H), 0.97 (d, *J* = 8.6 Hz, 3H), 0.84 (dd, *J* = 6.6, 3.3 Hz, 3H), 0.82 – 0.72 (m, 3H). ¹³C NMR (101 MHz, CDCl₃) δ 211.4, 210.7, 177.7, 176.6, 173.3, 170.0, 169.9, 101.8, 100.4, 97.7, 95.4, 85.1, 82.8, 81.2, 73.8, 72.6, 70.7, 69.2, 68.4, 63.2, 62.3, 60.7, 50.9, 49.8, 45.4, 44.5, 41.4, 40.2, 36.2, 29.3, 26.9, 24.0, 22.6, 20.7, 16.2, 14.5, 11.6, 10.8, 8.5, 7.8. HRMS (ESI) *m/z* Calcd. for C₄₀H₇₃N₂O₁₃ [*M* + 2H⁺]/2: 395.2590, found 395.2587.

2.9.5.16. 4''-Epoxy-3'-*O*-acetylazithromycin (15)

NaH (0.3 g, 7.18 mmol, 60% w/w) was added to an oven dried three necked round bottom flask and was washed with petroleum ether (×3). The flask was immediately flushed with argon and dry DMSO (6 mL) was introduced through a septum. The mixture was stirred at room temperature under Ar. Over a period of 5 min, trimethyloxosulfonium iodide (1.58 g, 7.18 mmol) was added to the reaction mixture.

When hydrogen gas ceased to evolve, the resulting yellow clear solution was treated with a solution of oxidized azithromycin **14** (2.57 g, 3.26 mmol) in anhydrous THF (5 mL) over 10 min, and left to stir for 2 h. TLC (4:3:1:0.1 Hexane: EtOAc: MeOH: NH₄OH) after 2 h showed 100% conversion to the product. THF was removed under vacuum and EtOAc (50 mL) was added to the remaining solution. The solution was washed severely with water to remove DMSO. Organic layer was dried over Na₂SO₄ and concentrated to give the product (2.48 g, 95% yield) as white solid. ¹H NMR (400 MHz, CDCl₃) δ 5.04 (d, *J* = 17.3 Hz, 2H), 4.83 (s, 1H), 4.68 (d, *J* = 11.2 Hz, 2H), 4.06 (s, 1H), 3.68 (s, 2H), 3.63 – 3.52 (m, 2H), 3.29 (p, *J* = 16.5 Hz, 7H), 2.86 (s, 2H), 2.72 – 2.39 (m, 9H), 2.11 (dd, *J* = 21.0, 9.5 Hz, 4H), 1.98 (d, *J* = 14.8 Hz, 2H), 1.83 (s, 3H), 1.66 – 1.47 (m, 5H), 1.41 (s, 3H), 1.27 (dt, *J* = 58.5, 7.3 Hz, 14H), 1.06 – 0.98 (m, 9H), 0.96 (s, 3H), 0.90 – 0.73 (m, 3H). ¹³C NMR (101 MHz, CDCl₃) δ 180.6, 167.0, 158.0, 127.9, 121.1, 104.1, 102.5, 95.8, 92.1, 74.2, 73.6, 64.7, 63.5, 60.3, 56.2, 50.0, 49.6, 46.4, 45.4, 43.3, 42.3, 41.2, 40.4, 37.1, 36.7, 31.9, 29.8, 28.4, 26.9, 25.5, 23.6, 22.6, 20.9, 18.3, 16.8, 15.4, 14.1, 13.9, 11.4, 8.9, 7.9. HRMS (ESI) *m/z* Calcd. for C₄₁H₇₄N₂O₁₃ [*M* + H⁺]: 803.5264, found 803.5262.

2.9.5.17. 1-(4-Ethynylphenyl)-*N*-methylethylmethanamine (**16**)

Methylamine (9.32 mL, 18.63 mmol, 2M in THF) was added to a solution of 4-ethynylbenzyl methanesulfonate (**3**) (0.39 g, 1.86 mmol) in THF (20 mL) and left to stir at 50 °C for 12 h. Methylamine was evaporated off and the residue dissolved in 1M HCl. This was then extracted multiple times with DCM. The aqueous layer was basified with 1M NaOH and extracted with DCM. Organic layer was dried over anhydrous Na₂SO₄ and concentrated *in vacuo*. The residue obtained was purified by column chromatography to give compound **16** as a yellow liquid (0.15g, 55%). ¹H NMR (400 MHz, CDCl₃) δ (ppm) 7.41 – 7.36 (d, 2H), 7.20 (d, *J* = 8.4 Hz, 2H), 3.65 (d, *J* = 9.0 Hz, 2H), 3.03 (d, *J* = 3.2

Hz, 1H), 2.65 (s, 1H), 2.34 (s, 3H). ^{13}C NMR (101 MHz, CDCl_3) δ (ppm) 140.5, 132.1, 128.1, 120.6, 83.7, 55.3, 35.6.

2.9.5.18. (4''-(Methylamino)-N(methyl)(4-ethynylbenzyl))azithromycin (17)

Compound **35** (1.057 g, 7.3 mmol) was added to a solution of compound **34** (1.95 g, 2.4 mmol) in MeOH (10 mL). The mixture was stirred under argon at 60 °C for 6 h, after that the solution was cooled to room temperature and diluted with excess ethyl acetate (100 mL). The organic layer was washed with saturated aqueous NaHCO_3 solution (30 mL), water (20 mL), brine (20 mL), dried over anhydrous Na_2SO_4 , filtered and concentrated *in vacuo*. The crude was purified by column chromatography column (Silica gel, 4:3:2:0.1 Hexane: EtOAc: MeOH: NH_4OH) to give compound **37** as light yellow solid (2.0 g, 92% yield). ^1H NMR (400 MHz, CDCl_3) δ (ppm) 7.43 (d, J = 8.2 Hz, 2H), 7.21(d, 2H), 5.04 (d, J = 4.6 Hz, 1H), 4.62 (d, J = 8.6 Hz, 1H), 4.44 (d, J = 6.0 Hz, 1H), 4.24 – 4.15 (m, 3H), 3.67 (d, J = 6.4 Hz, 2H), 3.63 (s, 3H), 3.46 (s, 3H), 3.26 (d, J = 21.0 Hz, 6H), 3.05 (s, 1H), 2.95 (d, J = 14.7 Hz, 3H), 2.81 (d, J = 7.1 Hz, 3H), 2.66 (s, 3H), 2.44 (d, J = 10.1 Hz, 2H), 2.31 (d, J = 10.5 Hz, 9H), 2.18 (s, 3H), 2.15 (d, J = 0.5 Hz, 1H), 2.02 (t, J = 11.7 Hz, 3H), 1.92 (dd, J = 15.0, 5.0 Hz, 2H), 1.29 (s, 3H), 1.21 (t, J = 6.9 Hz, 10H), 1.14 (s, 3H), 1.12 – 1.02 (m, 10H), 0.88 (t, J = 7.6 Hz, 3H). ^{13}C NMR (126 MHz, CDCl_3) δ (ppm) 178.6, 139.4, 132.2, 128.8, 121.2, 102.8, 95.0, 94.8, 83.8, 83.3, 76.8, 74.2, 73.5, 70.9, 70.1, 68.1, 67.2, 67.2, 65.7, 63.2, 62.6, 62.5, 56.9, 49.6, 49.5, 45.4, 45.2, 43.2, 42.3, 42.2, 41.1, 40.9, 40.5, 40.4, 36.2, 31.3, 29.0, 27.5, 26.7, 22.7, 21.9, 21.3, 18.8, 16.2, 15.0, 14.6, 11.2, 9.2, 7.2. HRMS (ESI) $m+2/2z$ Calcd. for $\text{C}_{49}\text{H}_{85}\text{N}_3\text{O}_{12}$ [$\text{M} + 2\text{H}^+$]: 453.8061, found 453.8055.

2.9.5.19. (Azithromycin-4''-(methylamino)-N(methyl)(4-benzyltriazolyl))-N-hydroxyacetamide (18a)

(4''-(Methylamino)-*N*-(methyl)(4-ethynylbenzyl))azithromycin **17** (0.14 g, 0.16 mmol) and 2-Azido-*N*-((tert-butyldimethyl silyl)oxy) ethaneamide **5a** (0.06 g, 0.23 mmol) were dissolved in anhydrous THF (5 mL) and purged with Ar for 15 min. Copper (I) iodide (0.01 g, 0.08 mmol) and Hunig's base (0.06 mL, 0.31 mmol) were then added to the reaction mixture. The reaction mixture was purged with Ar for additional 15 min and stirring continued for 12 h. Caesium fluoride (0.04 g, 0.24 mmol) and MeOH (5 mL) were added to the mixture to remove TBS protecting group and the reaction continued for an additional 2 h. The reaction was quenched by adding a solution of 4:1 saturated NH₄Cl/NH₄OH (30 mL) and extracted with 20% MeOH/ CH₂Cl₂ (3×30 mL). The organic layer was dried over Na₂SO₄ and concentrated *in vacuo*. The crude product was purified by preparative TLC (Silica gel, 5:1:1 EtOAc: MeOH: NH₄OH) to give the product (0.131 g, 80% yield) as light yellow solid. ¹H NMR (400 MHz, CD₃OD) δ (ppm) 8.33 (s, 1H), 7.79 (d, *J* = 6.5 Hz, 2H), 7.37 (d, *J* = 7.1 Hz, 2H), 5.46 (s, 1H), 5.07 (d, *J* = 4.6 Hz, 3H), 4.44 (d, *J* = 6.9 Hz, 1H), 4.32 – 4.18 (m, 3H), 3.69 (s, 2H), 3.64 – 3.56 (m, 3H), 3.48 (d, *J* = 25.5 Hz, 2H), 3.34 (s, 3H), 3.32 – 3.21 (m, 3H), 3.09 – 2.93 (m, 3H), 2.85 – 2.64 (m, 3H), 2.41 (t, *J* = 20.9 Hz, 12H), 2.33 – 2.20 (m, 3H), 2.19 – 2.09 (m, 3H), 2.00 (dd, *J* = 25.3, 18.4 Hz, 3H), 1.95 – 1.83 (m, 3H), 1.82 – 1.70 (m, 3H), 1.52 – 1.39 (m, 3H), 1.32 (s, 3H), 1.24 (d, *J* = 6.3 Hz, 3H), 1.22 – 1.12 (m, 13H), 1.08 (s, 3H), 1.03 (d, *J* = 7.2 Hz, 3H), 0.96 – 0.82 (m, 3H). ¹³C NMR (126 MHz, CD₃OD) δ (ppm) 180.5, 177.3, 149.4, 140.9, 131.9, 131.6, 127.7, 124.6, 105.0, 102.0, 97.7, 85.6, 80.3, 78.9, 78.3, 76.3, 76.0, 73.6, 73.2, 73.0, 71.0, 69.8, 69.5, 67.0, 65.5, 65.0, 59.0, 51.0, 47.6, 45.0, 44.5, 44.1, 41.4, 37.7, 33.9, 33.2, 32.6, 31.6, 31.4, 28.6, 28.2, 24.6, 23.2, 23.0, 20.2, 18.2, 16.5, 15.3, 12.3, 10.7, 8.8. HRMS (ESI) *m*+2/*z* Calcd. for C₅₁H₈₉N₇O₁₄ [*M* + 2H⁺]: 511.8228, found 511.8230.

2.9.5.20. (Azithromycin-4''-(methylamino)-N(methyl)(4-benzyltriazolyl))-N-hydroxypropanamide (18b)

Reaction of (4''-(methylamino)-N(methyl)(4-ethynylbenzyl))azithromycin **17** (0.20 g, 0.218 mmol) and 3-azido-N-((*tert*-butyldimethylsilyl)oxy)propanamide **5b** (0.08 g, 0.32 mmol) followed by TBS deprotection with cesium fluoride as described for the synthesis of **18a**, gave **18b** as light yellow solid (0.178 g, 79%). ¹H NMR (500 MHz, CD₃OD) δ (ppm) 8.26 (d, J = 10.7 Hz, 1H), 7.78 (d, J = 7.6 Hz, 2H), 7.39 (d, J = 7.8 Hz, 2H), 5.48 (s, 1H), 5.13 – 5.07 (m, 2H), 4.74 (s, 3H), 4.46 (d, J = 7.2 Hz, 2H), 4.32 – 4.22 (m, 1H), 3.69 (d, J = 18.3 Hz, 3H), 3.67 – 3.57 (m, 1H), 3.57 – 3.48 (m, 2H), 3.38 (d, J = 13.2 Hz, 3H), 3.33 – 3.25 (m, 1H), 3.02 (dd, J = 23.0, 16.2 Hz, 3H), 2.86 – 2.75 (m, 3H), 2.74 – 2.65 (m, 3H), 2.44 (s, 3H), 2.31 – 2.19 (m, 3H), 2.19 – 2.10 (m, 2H), 2.09 – 1.97 (m, 3H), 1.94 – 1.87 (m, 9H), 1.87 – 1.82 (m, 2H), 1.81 – 1.72 (m, 3H), 1.53 – 1.40 (m, 3H), 1.35 (d, J = 11.2 Hz, 3H), 1.27 (t, J = 11.9 Hz, 13H), 1.24 – 1.19 (m, 3H), 1.16 (d, J = 6.7 Hz, 3H), 1.10 (s, 3H), 1.05 (d, J = 7.5 Hz, 3H), 0.96 – 0.86 (s, 3H). ¹³C NMR (126 MHz, CD₃OD) δ (ppm) 180.4, 177.1, 169.8, 149.2, 140.8, 131.8, 131.3, 127.5, 123.5, 104.8, 97.3, 85.4, 80.3, 78.9, 78.3, 76.2, 76.0, 74.5, 73.4, 72.9, 70.9, 69.9, 69.2, 66.8, 65.6, 65.0, 63.0, 58.8, 57.0, 55.8, 50.9, 48.1, 47.5, 44.8, 43.9, 41.3, 37.7, 33.9, 32.7, 31.6, 28.3, 24.5, 23.3, 22.8, 21.2, 20.1, 18.2, 16.8, 15.2, 12.3, 10.8, 8.8. HRMS (ESI) m/z Calcd. for C₅₂H₉₀N₇O₁₄ [M+H⁺]: 1036.6540, found 1036.6550.

2.9.5.21. (Azithromycin-4''-(methylamino)-N(methyl)(4-benzyltriazolyl))-N-hydroxybutanamide (18c)

Reaction of (4''-(methylamino)-N(methyl)(4-ethynylbenzyl))azithromycin **17** (0.20 g, 0.18 mmol) and 4-azido-N-((*tert*-butyldimethylsilyl)oxy) butanamide **5c** (0.08 g, 0.31 mmol) followed by TBS deprotection with caesium fluoride as described for the synthesis of **18a**, gave **18c** as light yellow solid (0.173 g, 80%). ¹H NMR (400 MHz,

CD₃OD) δ (ppm) 8.30 (s, 1H), 7.76 (d, J = 7.2 Hz, 2H), 7.34 (d, J = 7.7 Hz, 2H), 5.44 (s, 1H), 5.06 (d, J = 4.7 Hz, 1H), 4.51 – 4.35 (m, 3H), 4.30 – 4.19 (m, 2H), 3.60 (dd, J = 23.4, 16.5 Hz, 3H), 3.45 (d, J = 25.7 Hz, 1H), 3.32 (s, 3H), 3.27 – 3.16 (m, 3H), 2.99 (d, J = 14.7 Hz, 1H), 2.84 – 2.69 (m, 2H), 2.63 – 2.43 (m, 2H), 2.30 (d, J = 14.5 Hz, 10H), 2.24 – 2.04 (m, 15H), 1.95 (dd, J = 13.7, 6.5 Hz, 3H), 1.91 – 1.77 (m, 3H), 1.77 – 1.64 (m, 3H), 1.49 – 1.30 (m, 3H), 1.27 (s, 3H), 1.21 (d, J = 6.0 Hz, 6H), 1.16 (d, J = 6.1 Hz, 11H), 1.03 (dd, J = 19.7, 6.7 Hz, 7H), 0.85 (dd, J = 14.1, 7.0 Hz, 3H). ¹³C NMR (126 MHz, CD₃OD) δ (ppm) 180.7, 177.2, 149.4, 141.0, 131.9, 131.6, 127.7, 123.7, 104.9, 97.6, 85.5, 80.4, 78.8, 78.4, 76.4, 76.2, 74.5, 73.6, 73.1, 70.9, 69.9, 69.4, 66.9, 65.7, 64.9, 57.2, 55.6, 51.1, 48.2, 47.5, 44.9, 44.3, 43.9, 41.5, 37.7, 34.0, 33.6, 33.4, 32.8, 31.7, 31.4, 28.5, 28.2, 24.6, 23.2, 22.7, 20.3, 18.2, 16.7, 15.3, 12.5, 10.8, 8.7. HRMS (ESI) $m+2/2z$ Calcd. for C₅₃H₉₃N₇O₁₄ [M+2H⁺]: 525.8385, found 525.8385.

2.9.5.22. (Azithromycin-4''-(methylamino)-N(methyl)(4-benzyltriazolyl))-N-hydroxypentanamide (**18d**)

Reaction of (4''-(methylamino)-N(methyl)(4-ethynylbenzyl))azithromycin **17** (0.14 g, 0.15 mmol) and 5-azido-N-((*tert*-butyldimethylsilyl)oxy) pentanamide **5d** (0.06 g, 0.23 mmol) followed by TBS deprotection with caesium fluoride as described for the synthesis of **18a**, gave **18d** as light yellow solid (0.125 g, 75%). ¹H NMR (400 MHz, CD₃OD) δ (ppm) 7.72 (s, 1H), 7.19 (d, J = 7.9 Hz, 2H), 6.77 (d, J = 8.0 Hz, 2H), 4.47 (d, J = 5.0 Hz, 1H), 3.85 (d, J = 6.7 Hz, 3H), 3.63 (dd, J = 17.6, 4.5 Hz, 2H), 3.09 (s, 2H), 3.04 – 2.97 (m, 3H), 2.75 (s, 3H), 2.68 (dt, J = 3.3, 1.6 Hz, 2H), 2.43 (d, J = 14.3 Hz, 2H), 2.19 (dd, J = 7.4, 4.6 Hz, 2H), 2.12 (d, J = 11.6 Hz, 1H), 1.89 (d, J = 18.4 Hz, 15H), 1.64 (d, J = 7.1 Hz, 5H), 1.59 – 1.46 (m, 6H), 1.37 (dd, J = 16.4, 7.9 Hz, 7H), 1.15 (t, J = 7.3 Hz, 1H), 1.03 (s, 3H), 0.85 (td, J = 14.5, 7.5 Hz, 3H), 0.73 (s, 3H), 0.60 (ddd, J = 18.8, 13.2, 6.4 Hz, 15H), 0.49 (s, 3H), 0.43 (d, J = 7.3 Hz, 3H), 0.32 (d, J = 6.8 Hz, 3H), 0.27 (t, J = 7.4 Hz, 3H). ¹³C NMR (126 MHz, CD₃OD) δ (ppm) 180.2, 176.9, 172.9,

149.1, 140.6, 131.6, 127.3, 122.8, 104.7, 97.1, 85.3, 80.1, 78.6, 78.0, 76.1, 75.8, 74.3, 73.1, 71.1, 69.7, 66.6, 64.6, 64.5, 62.8, 58.7, 56.9, 55.5, 52.7, 51.6, 50.8, 47.3, 44.5, 44.1, 43.9, 41.4, 37.3, 33.6, 33.0, 32.7, 31.3, 30.0, 28.6, 26.7, 24.2, 23.1, 22.7, 20.0, 17.9, 16.4, 16.1, 15.0, 12.2, 10.6, 8.2. HRMS (ESI) m/z Calcd. for $C_{54}H_{94}N_7O_{14}$ $[M+H^+]$: 1064.6853, found 1064.6854.

2.9.5.23. (Azithromycin-4''-(methylamino)-*N*(methyl)(4-benzyltriazolyl))-*N*-hydroxyhexanamide (**18e**)

Reaction of (4''-(methylamino)-*N*(methyl)(4-ethynylbenzyl))azithromycin **17** (0.09 g, 0.10 mmol) and 6-azido-*N*-((*tert*-butyldimethylsilyl)oxy)hexanamide **5e** (0.04 g, 0.16 mmol) followed by TBS deprotection with caesium fluoride as described for the synthesis of **18a**, gave **18e** as light yellow solid (0.090 g, 80%). 1H NMR (400 MHz, CD_3OD) δ (ppm) 8.27 (s, 1H), 7.74 (d, $J = 8.1$ Hz, 2H), 7.32 (d, $J = 8.1$ Hz, 2H), 5.05 (d, $J = 5.0$ Hz, 1H), 4.78 (dd, $J = 10.0, 2.3$ Hz, 3H), 4.37 (dd, $J = 15.3, 7.2$ Hz, 3H), 4.23 (dd, $J = 12.4, 5.5$ Hz, 2H), 4.00 (dq, $J = 13.6, 6.9$ Hz, 1H), 3.66 (d, $J = 17.8$ Hz, 1H), 3.60 – 3.52 (m, 2H), 3.46 (dd, $J = 9.9, 5.4$ Hz, 1H), 3.29 (d, $J = 12.7$ Hz, 3H), 3.26 – 3.16 (m, 3H), 3.02 – 2.93 (m, 1H), 2.78 – 2.68 (m, 2H), 2.59 – 2.46 (m, 1H), 2.27 (d, $J = 16.0$ Hz, 3H), 2.22 – 2.15 (m, 3H), 2.10 (t, $J = 8.1$ Hz, 2H), 2.03 (d, $J = 16.0$ Hz, 3H), 1.97 – 1.91 (m, 5H), 1.91 – 1.86 (m, 3H), 1.83 (d, $J = 3.9$ Hz, 2H), 1.73 – 1.63 (m, 2H), 1.60 – 1.47 (m, 3H), 1.32 (dd, $J = 21.9, 6.6$ Hz, 6H), 1.26 (d, $J = 5.2$ Hz, 3H), 1.23 – 1.17 (m, 6H), 1.17 – 1.08 (m, 11H), 1.01 (dd, $J = 17.4, 6.0$ Hz, 11H), 0.89 – 0.79 (m, 3H). ^{13}C NMR (126 MHz, CD_3OD) δ (ppm) 180.2, 177.0, 173.3, 149.2, 140.7, 131.8, 131.3, 127.4, 122.9, 104.8, 97.2, 85.4, 80.1, 78.8, 78.3, 76.4, 75.9, 73.3, 73.2, 71.3, 69.9, 69.1, 66.6, 64.9, 58.7, 55.6, 53.0, 52.0, 50.9, 47.5, 44.7, 44.2, 43.9, 41.4, 37.4, 34.2, 33.7, 33.1, 32.6, 31.6, 30.3, 28.5, 28.2, 27.5, 26.6, 24.4, 22.9, 22.7, 20.0, 18.0, 16.4, 16.1, 12.4, 10.6, 8.4. HRMS (ESI) $m+2/2z$ Calcd. for $C_{55}H_{97}N_7O_{14}$ $[M+2H^+]$: 539.8541, found 539.8539.

2.9.5.24. (Azithromycin-4''-(methylamino)-*N*(methyl)(4-benzyltriazolyl))-*N*-hydroxyheptanamide (**18f**)

Reaction of (4''-(methylamino)-*N*(methyl)(4-ethynylbenzyl))azithromycin **17** (0.16 g, 0.18 mmol) and 7-azido-*N*-((*tert*-butyldimethylsilyl)oxy)heptanamide **5f** (0.08 g, 0.27 mmol) followed by TBS deprotection with caesium fluoride as described for the synthesis of **18a**, gave **18f** as light yellow solid (0.154 g, 80%). ¹H NMR (400 MHz, CD₃OD) δ (ppm) 7.71 (s, 1H), 7.18 (d, *J* = 8.1 Hz, 2H), 6.77 (d, *J* = 8.1 Hz, 2H), 4.49 (d, *J* = 5.0 Hz, 1H), 3.83 (dd, *J* = 10.2, 7.1 Hz, 3H), 3.72 – 3.63 (m, 2H), 3.50 – 3.40 (m, 1H), 3.11 (d, *J* = 16.2 Hz, 1H), 3.02 (d, *J* = 7.0 Hz, 1H), 2.99 – 2.95 (m, 1H), 2.90 (dd, *J* = 17.7, 14.2 Hz, 1H), 2.75 (s, 3H), 2.71 – 2.62 (m, 3H), 2.43 (d, *J* = 14.7 Hz, 1H), 2.24 (d, *J* = 7.0 Hz, 1H), 2.18 (dd, *J* = 7.5, 4.6 Hz, 1H), 2.00 (t, *J* = 14.8 Hz, 1H), 1.75 (d, *J* = 10.6 Hz, 9H), 1.70 – 1.58 (m, 6H), 1.55 – 1.44 (m, 3H), 1.44 – 1.34 (m, 3H), 1.33 – 1.30 (m, 3H), 1.31 – 1.25 (m, 3H), 1.19 – 1.10 (m, 2H), 1.04 (d, *J* = 7.4 Hz, 3H), 0.76 (dd, *J* = 20.3, 12.8 Hz, 3H), 0.70 (s, 3H), 0.68 – 0.61 (m, 6H), 0.60 (dt, *J* = 12.7, 4.4 Hz, 12H), 0.53 – 0.46 (m, 10H), 0.43 (d, *J* = 7.5 Hz, 5H), 0.34 – 0.24 (m, 3H). ¹³C NMR (126 MHz, CD₃OD) δ (ppm) 180.5, 177.4, 173.6, 149.4, 149.0, 140.7, 132.3, 131.9, 131.5, 127.6, 123.2, 122.9, 105.1, 97.3, 85.6, 80.2, 78.9, 78.2, 76.5, 75.8, 73.5, 71.6, 70.1, 69.3, 66.7, 65.1, 64.7, 58.7, 55.8, 53.3, 52.2, 50.9, 47.7, 44.9, 44.5, 44.3, 41.8, 37.7, 34.4, 33.4, 32.9, 32.0, 31.6, 30.7, 30.3, 28.9, 28.0, 27.4, 23.3, 20.2, 18.4, 16.7, 16.5, 12.6, 10.9, 8.6. HRMS (ESI) *m*+2/2 \bar{z} Calcd. for C₅₆H₉₉N₇O₁₄ [*M*+2H⁺]: 546.8620, found 546.8621.

2.10. References

1. Marks, P. Discovery and development of SAHA as an anticancer agent. *Oncogene* **2007**, 26, 1351-1356.
2. Patil, V.; Guerrant, W.; Chen, P. C.; Gryder, B.; Benicewicz, D. B.; Khan, S. I.; Tekwani, B. L.; Oyelere, A. K. Antimalarial and antileishmanial activities of histone

deacetylase inhibitors with triazole-linked cap group. *Bioorganic & medicinal chemistry* **2010**, 18, 415-425.

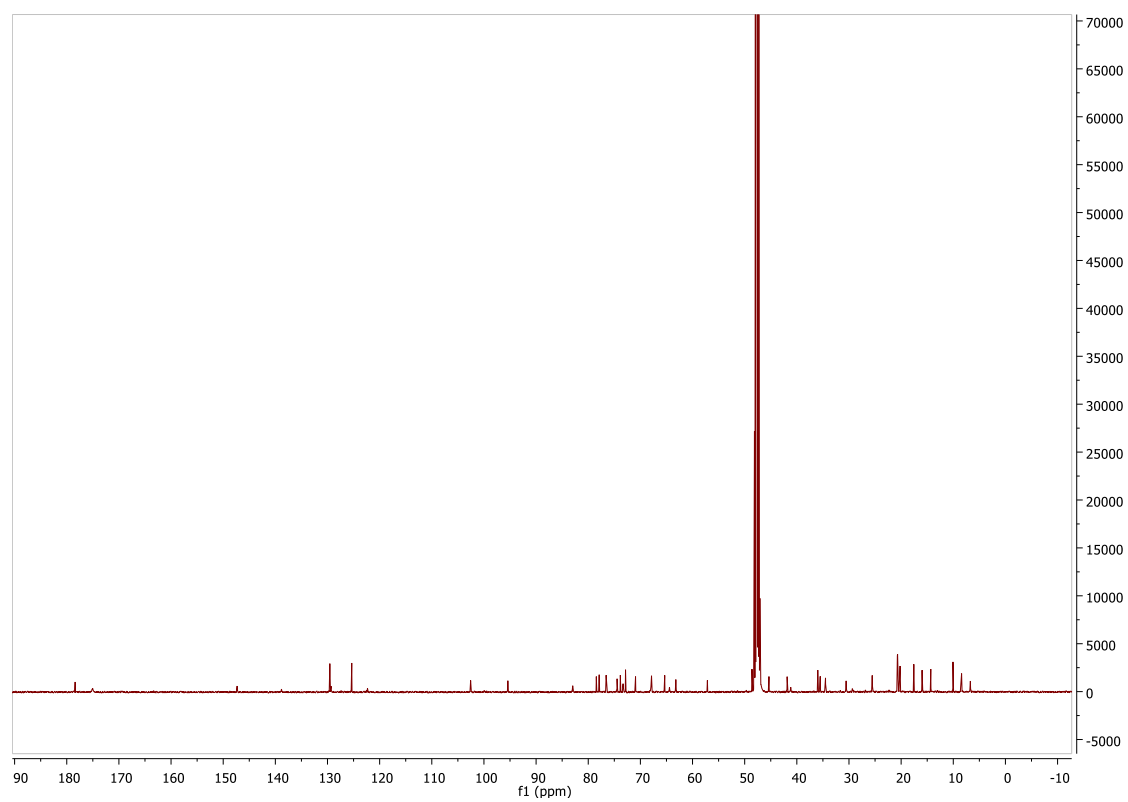
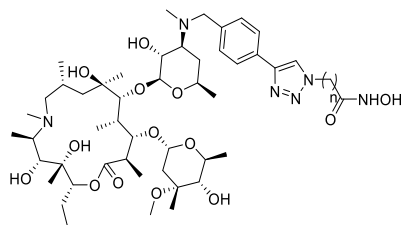
3. Mottamal, M.; Zheng, S.; Huang, T. L.; Wang, G. Histone deacetylase inhibitors in clinical studies as templates for new anticancer agents. *Molecules* **2015**, 20, 3898-3941.
4. Grant, S.; Easley, C.; Kirkpatrick, P. Vorinostat. *Nature reviews Drug discovery* **2007**, 6, 21-22.
5. Campas-Moya, C. Romidepsin for the treatment of cutaneous T-cell lymphoma. *Drugs of today (Barcelona, Spain: 1998)* **2009**, 45, 787-795.
6. Rashidi, A.; Cashen, A. F. Belinostat for the treatment of relapsed or refractory peripheral T-cell lymphoma. *Future Oncology* **2015**, 11, 1659-1664.
7. Neri, P.; Bahlis, N. J.; Lonial, S. Panobinostat for the treatment of multiple myeloma. *Expert opinion on investigational drugs* **2012**, 21, 733-747.
8. Gong, K.; Xie, J.; Yi, H.; Li, W. CS055 (Chidamide/HBI-8000), a novel histone deacetylase inhibitor, induces G1 arrest, ROS-dependent apoptosis and differentiation in human leukaemia cells. *Biochemical Journal* **2012**, 443, 735-746.
9. Flick, A. C.; Ding, H. X.; Leverett, C. A.; Kyne, R. E.; Liu, K. K.-C.; Fink, S. J.; O'Donnell, C. J. Synthetic approaches to the 2014 new drugs. *Bioorganic & medicinal chemistry* **2016**, 24, 1937-1980.
10. Miller, T. A.; Witter, D. J.; Belvedere, S. Histone deacetylase inhibitors. *Journal of medicinal chemistry* **2003**, 46, 5097-5116.
11. Yurek-George, A.; Cecil, A. R. L.; Mo, A. H. K.; Wen, S.; Rogers, H.; Habens, F.; Maeda, S.; Yoshida, M.; Packham, G.; Ganesan, A. The first biologically active synthetic analogues of FK228, the depsipeptide histone deacetylase inhibitor. *Journal of medicinal chemistry* **2007**, 50, 5720-5726.
12. Meutermans, W. D.; Bourne, G. T.; Golding, S. W.; Horton, D. A.; Campitelli, M. R.; Craik, D.; Scanlon, M.; Smythe, M. L. Difficult macrocyclizations: new strategies for synthesizing highly strained cyclic tetrapeptides. *Organic letters* **2003**, 5, 2711-2714.
13. Mwakwari, S. C.; Patil, V.; Guerrant, W.; Oyelere, A. K. Macrocyclic histone deacetylase inhibitors. *Current topics in medicinal chemistry* **2010**, 10, 1423.
14. Mwakwari, S. C.; Guerrant, W.; Patil, V.; Khan, S. I.; Tekwani, B. L.; Gurard-Levin, Z. A.; Mrksich, M.; Oyelere, A. K. Non-peptide macrocyclic histone deacetylase inhibitors derived from tricyclic ketolide skeleton. *Journal of medicinal chemistry* **2010**, 53, 6100-6111.

15. Alvarez-Elcoro, S.; Enzler, M. J. In *The macrolides: erythromycin, clarithromycin, and azithromycin*, Mayo Clinic Proceedings, 1999; Elsevier: 1999; pp 613-634.
16. Tsai, W. C.; Standiford, T. J. Immunomodulatory effects of macrolides in the lung: lessons from in-vitro and in-vivo models. *Current pharmaceutical design* **2004**, 10, 3081-3093.
17. Laskin, D. L.; Weinberger, B.; Laskin, J. D. Functional heterogeneity in liver and lung macrophages. *Journal of leukocyte biology* **2001**, 70, 163-170.
18. Nicod, L. Pulmonary defence mechanisms. *Respiration* **1999**, 66, 2-11.
19. Dreaden, E. C.; Mwakwari, S. C.; Austin, L. A.; Kieffer, M. J.; Oyelere, A. K.; El-Sayed, M. A. Small molecule–gold nanorod conjugates selectively target and induce macrophage cytotoxicity towards breast cancer cells. *Small* **2012**, 8, 2819-2822.
20. Dreaden, E. C.; Raji, I. O.; Austin, L. A.; Fathi, S.; Mwakwari, S. C.; Humphries, W. H.; Kang, B.; Oyelere, A. K.; El-Sayed, M. A. P-Glycoprotein-Dependent Trafficking of Nanoparticle-Drug Conjugates. *small* **2014**, 10, 1719-1723.
21. Mutak, S. Azalides from azithromycin to new azalide derivatives. *The Journal of antibiotics* **2007**, 60, 85-122.
22. Rostovtsev, V. V.; Green, L. G.; Fokin, V. V.; Sharpless, K. B. A stepwise Huisgen cycloaddition process: copper (I)-catalyzed regioselective “ligation” of azides and terminal alkynes. *Angewandte Chemie* **2002**, 114, 2708-2711.
23. Cosner, C. C.; Helquist, P. Concise, Convergent Syntheses of (±)-Trichostatin A Utilizing a Pd-Catalyzed Ketone Enolate α -Alkenylation Reaction. *Organic letters* **2011**, 13, 3564-3567.
24. Miljkovic, M. *Carbohydrates: synthesis, mechanisms, and stereoelectronic effects*. Springer Science & Business Media: 2009.
25. Oyelere, A. K.; Chen, P. C.; Guerrant, W.; Mwakwari, S. C.; Hood, R.; Zhang, Y.; Fan, Y. Non-peptide macrocyclic histone deacetylase inhibitors. *Journal of medicinal chemistry* **2008**, 52, 456-468.
26. Min, D.-H.; Yeo, W.-S.; Mrksich, M. A method for connecting solution-phase enzyme activity assays with immobilized format analysis by mass spectrometry. *Analytical chemistry* **2004**, 76, 3923-3929.
27. Vaguliene, N.; Zemaitis, M.; Lavinskiene, S.; Miliauskas, S.; Sakalauskas, R. Local and systemic neutrophilic inflammation in patients with lung cancer and chronic obstructive pulmonary disease. *BMC immunology* **2013**, 14, 36.

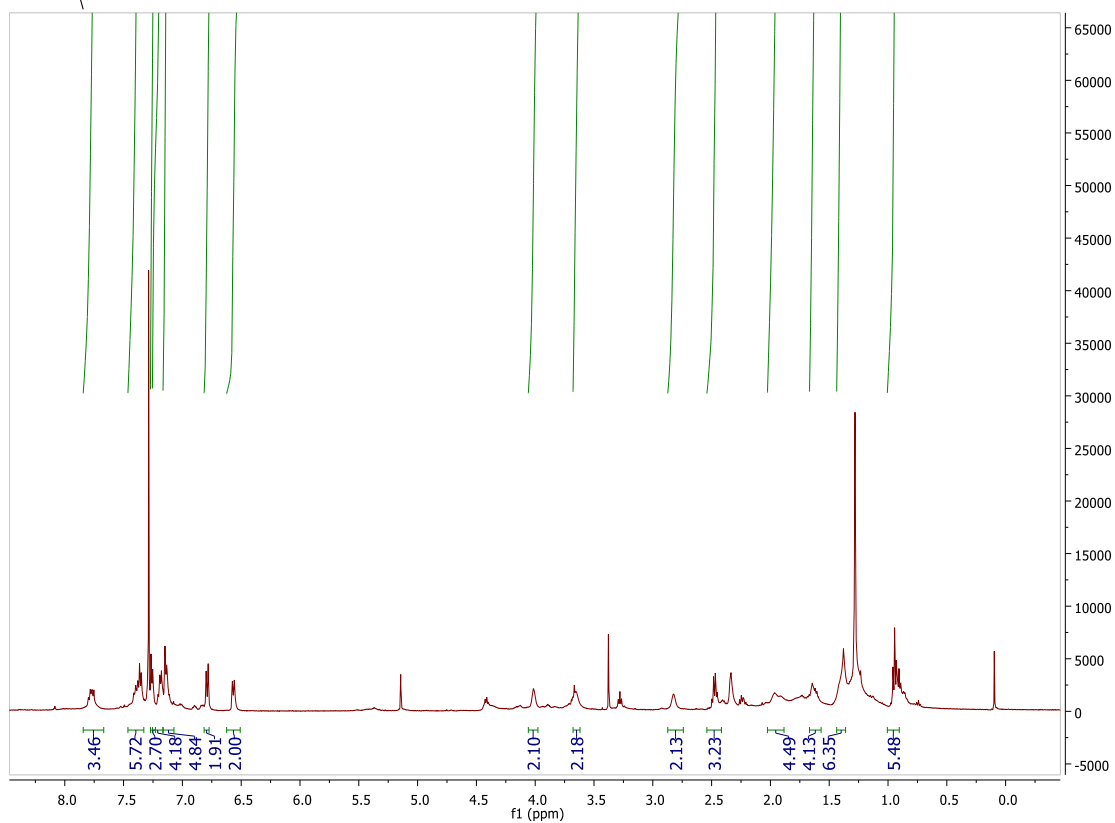
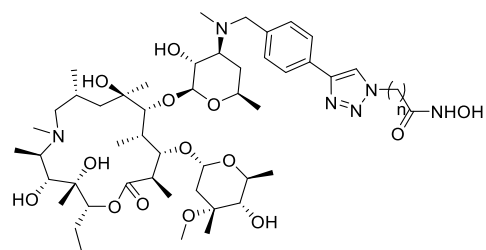
28. Azad, N.; Rojanasakul, Y.; Vallyathan, V. Inflammation and lung cancer: roles of reactive oxygen/nitrogen species. *Journal of Toxicology and Environmental Health, Part B* **2008**, 11, 1-15.
29. Balkwill, F.; Mantovani, A. Inflammation and cancer: back to Virchow? *The lancet* **2001**, 357, 539-545.
30. Johnstone, R. W. Histone-deacetylase inhibitors: novel drugs for the treatment of cancer. *Nature reviews Drug discovery* **2002**, 1, 287-299.
31. Tang, J.; Yan, H.; Zhuang, S. Histone deacetylases as targets for treatment of multiple diseases. *Clinical science* **2013**, 124, 651-662.
32. Shi, Z.-j.; Ouyang, D.-y.; Zhu, J.-s.; Xu, L.-h.; He, X.-h. Histone deacetylase inhibitor suberoylanilide hydroxamic acid exhibits anti-inflammatory activities through induction of mitochondrial damage and apoptosis in activated lymphocytes. *International immunopharmacology* **2012**, 12, 580-587.
33. Choo, Q.-Y.; Ho, P. C.; Tanaka, Y.; Lin, H.-S. The histone deacetylase inhibitors MS-275 and SAHA suppress the p38 mitogen-activated protein kinase signaling pathway and chemotaxis in rheumatoid arthritic synovial fibroblastic E11 cells. *Molecules* **2013**, 18, 14085-14095.
34. Furumai, R.; Ito, A.; Ogawa, K.; Maeda, S.; Saito, A.; Nishino, N.; Horinouchi, S.; Yoshida, M. Histone deacetylase inhibitors block nuclear factor- κ B-dependent transcription by interfering with RNA polymerase II recruitment. *Cancer science* **2011**, 102, 1081-1087.
35. Ishinaga, H.; Jono, H.; Lim, J. H.; Kweon, S. M.; Xu, H.; Ha, U. H.; Xu, H.; Koga, T.; Yan, C.; Feng, X. H. TGF- β induces p65 acetylation to enhance bacteria-induced NF- κ B activation. *The EMBO journal* **2007**, 26, 1150-1162.
36. Poolman, J. T.; Bakaletz, L.; Cripps, A.; Denoel, P. A.; Forsgren, A.; Kyd, J.; Lobet, Y. Developing a nontypeable *Haemophilus influenzae* (NTHi) vaccine. *Vaccine* **2000**, 19, S108-S115.

2.11. Supplementary data

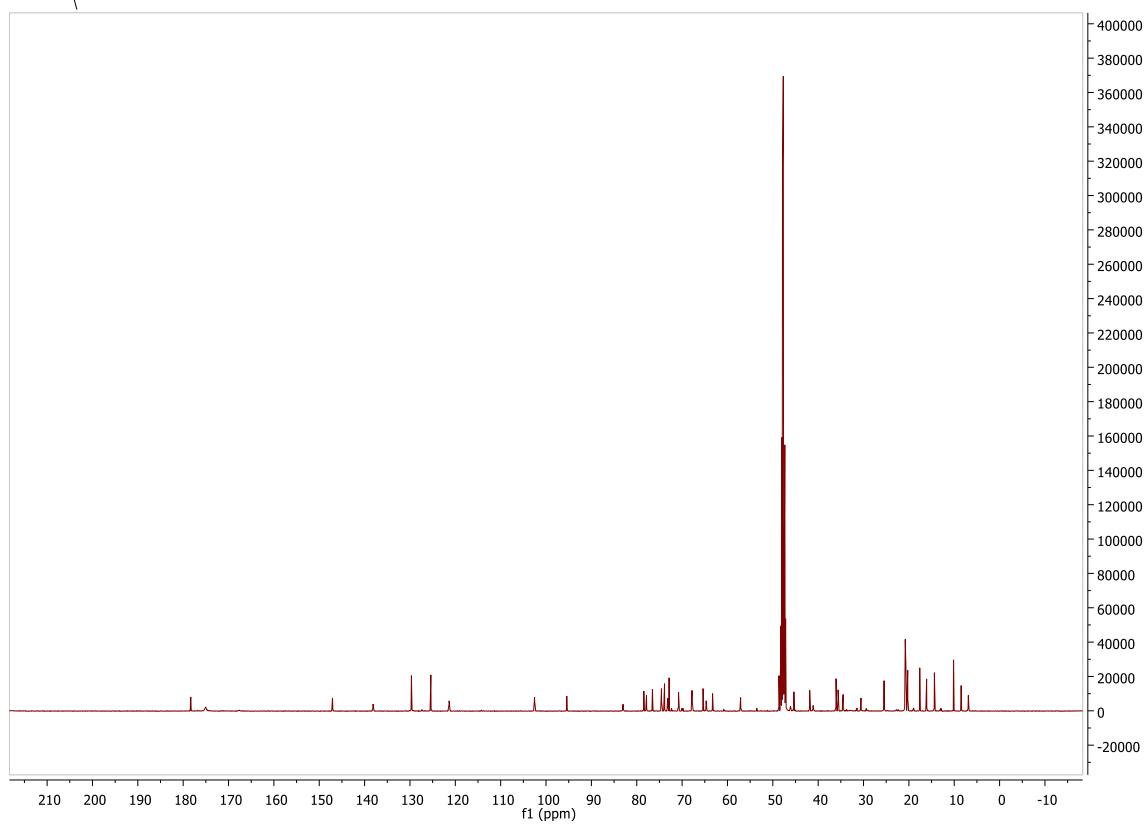
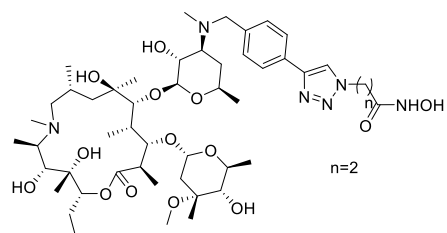
6a ^{13}C NMR



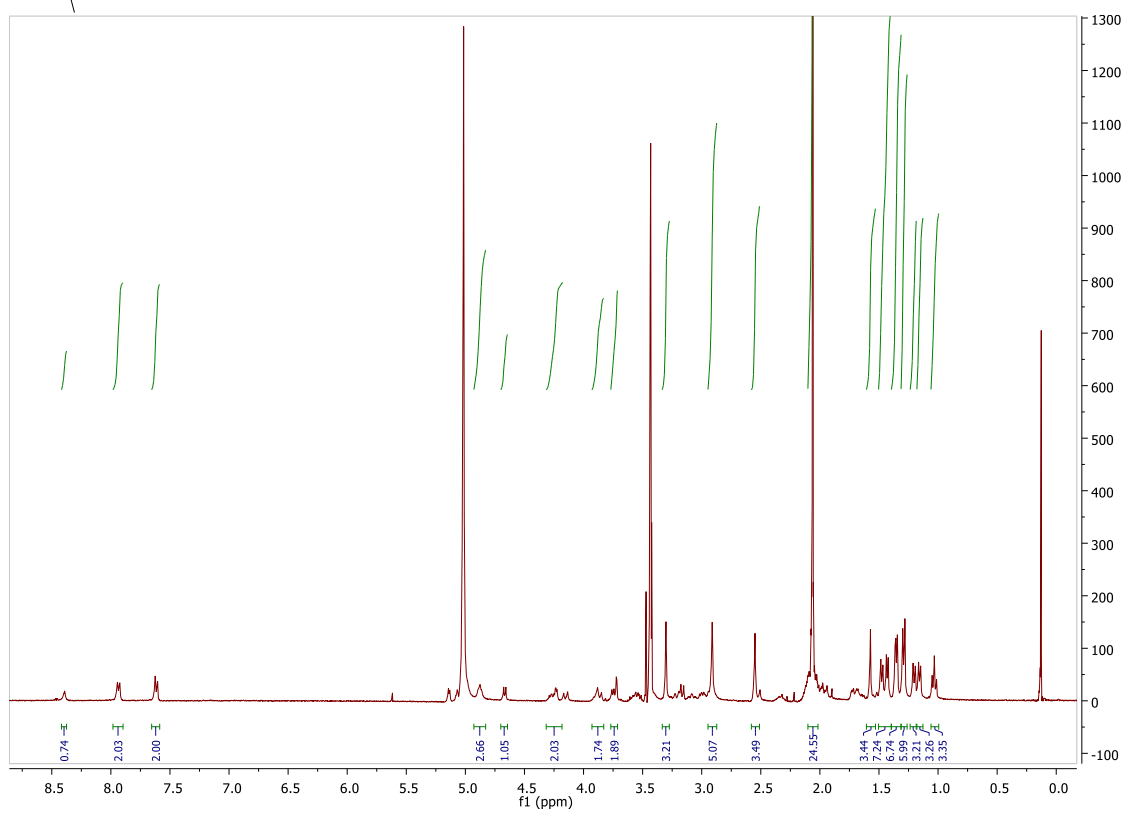
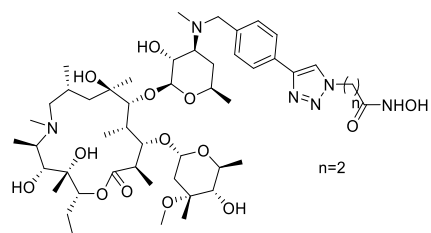
6a ^1H NMR



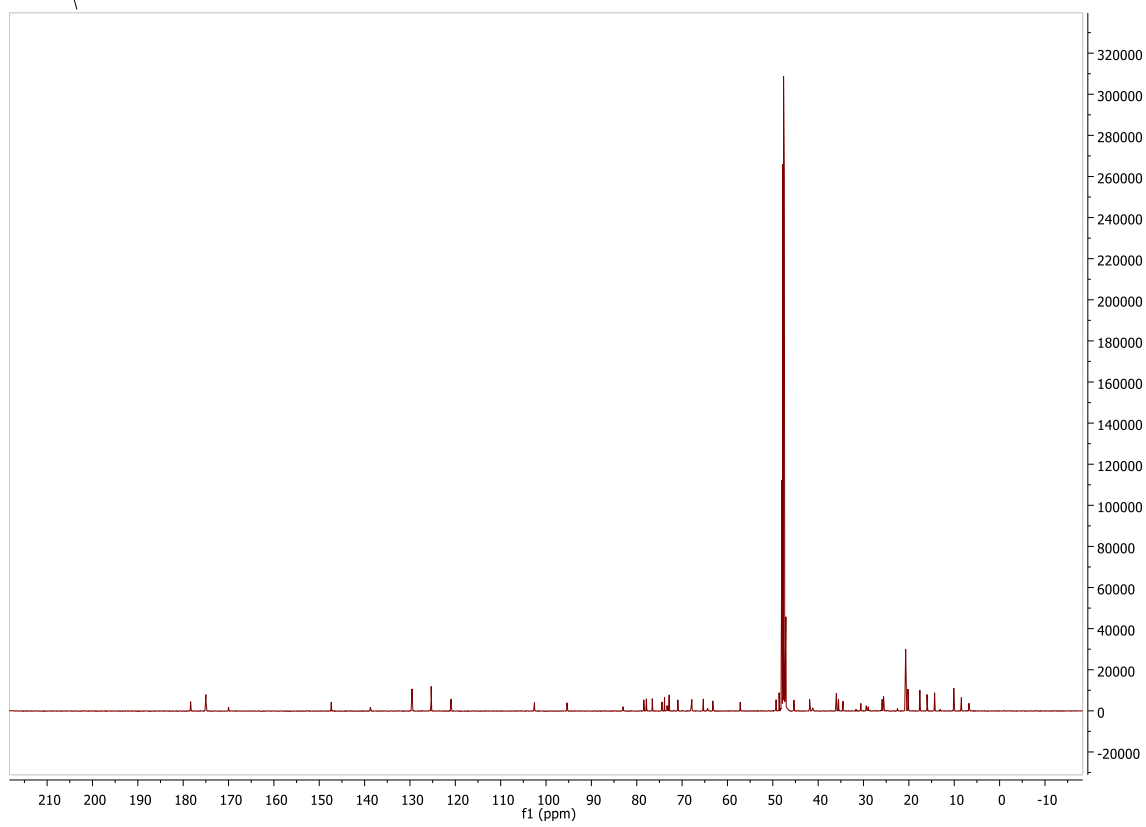
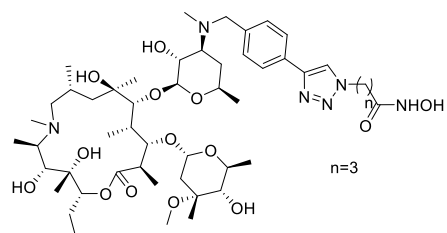
6b ^{13}C NMR



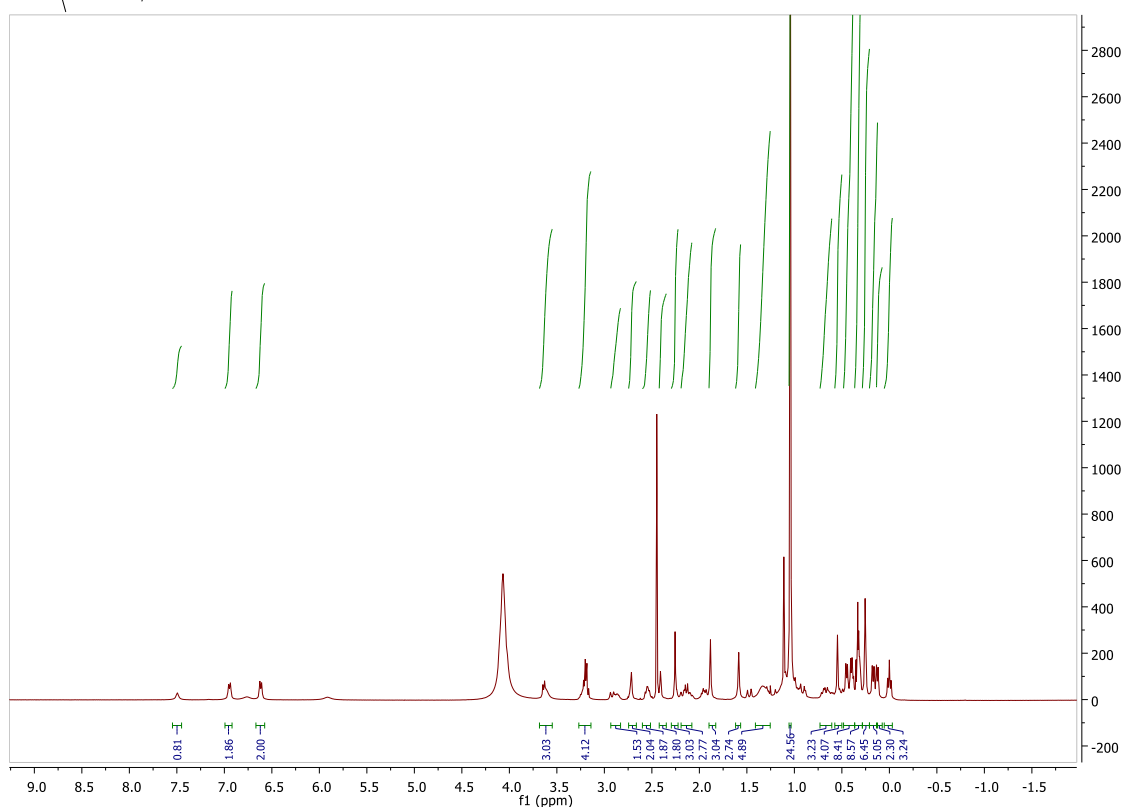
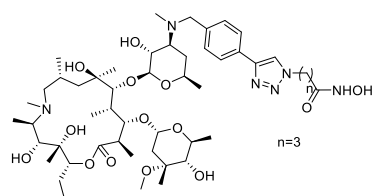
6b ^1H NMR



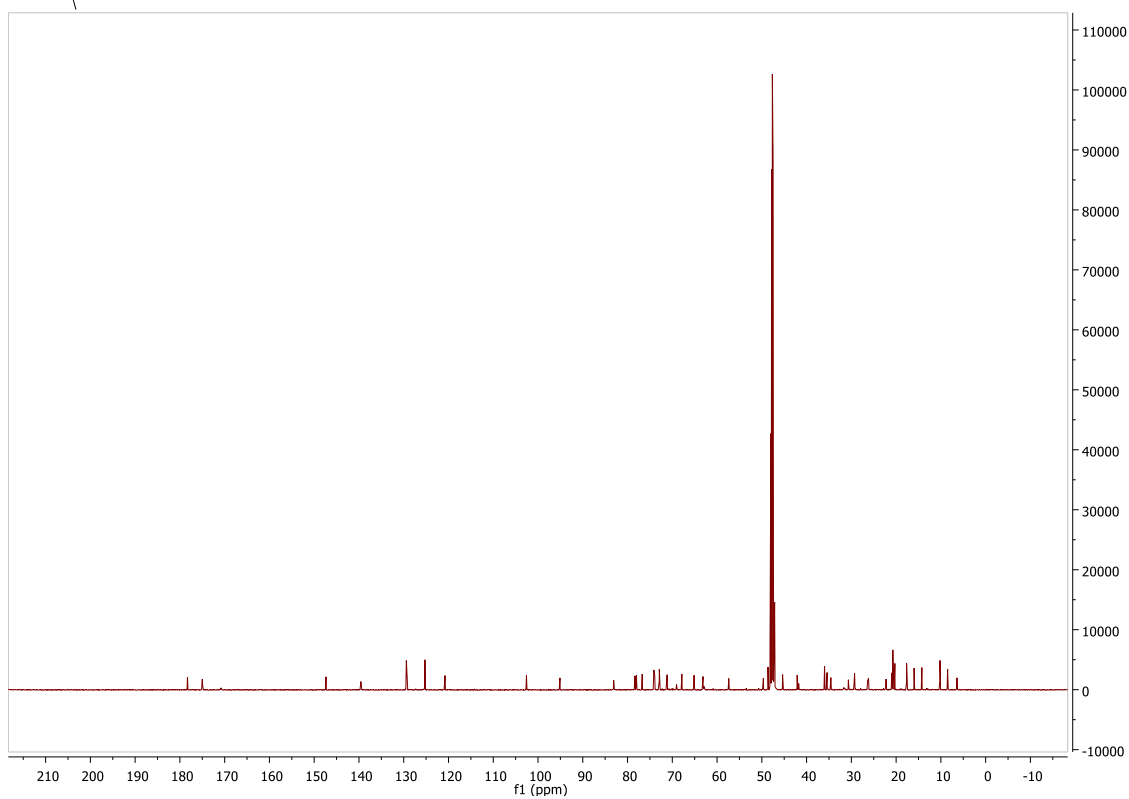
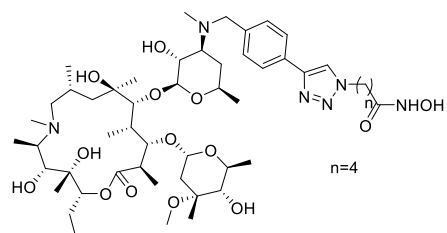
6c ^{13}C NMR



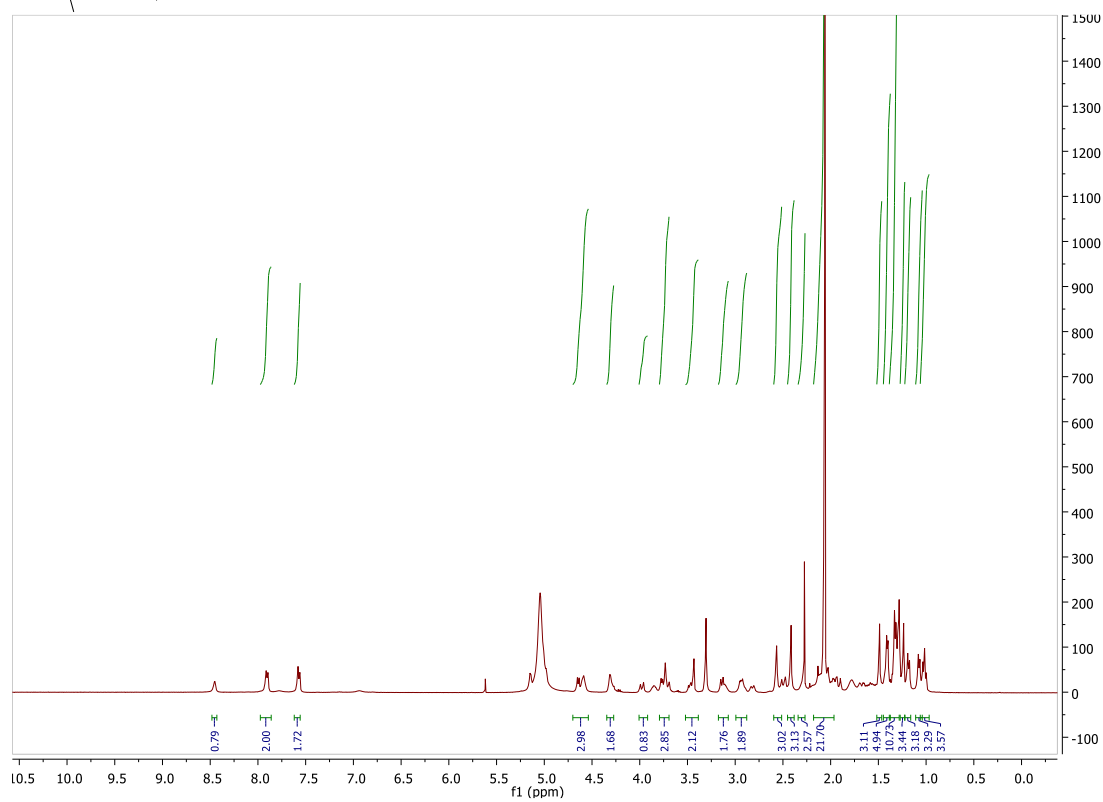
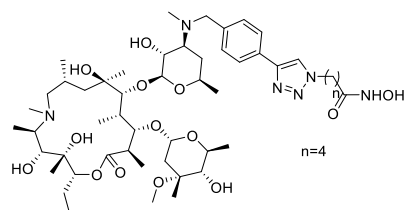
6c ^1H NMR



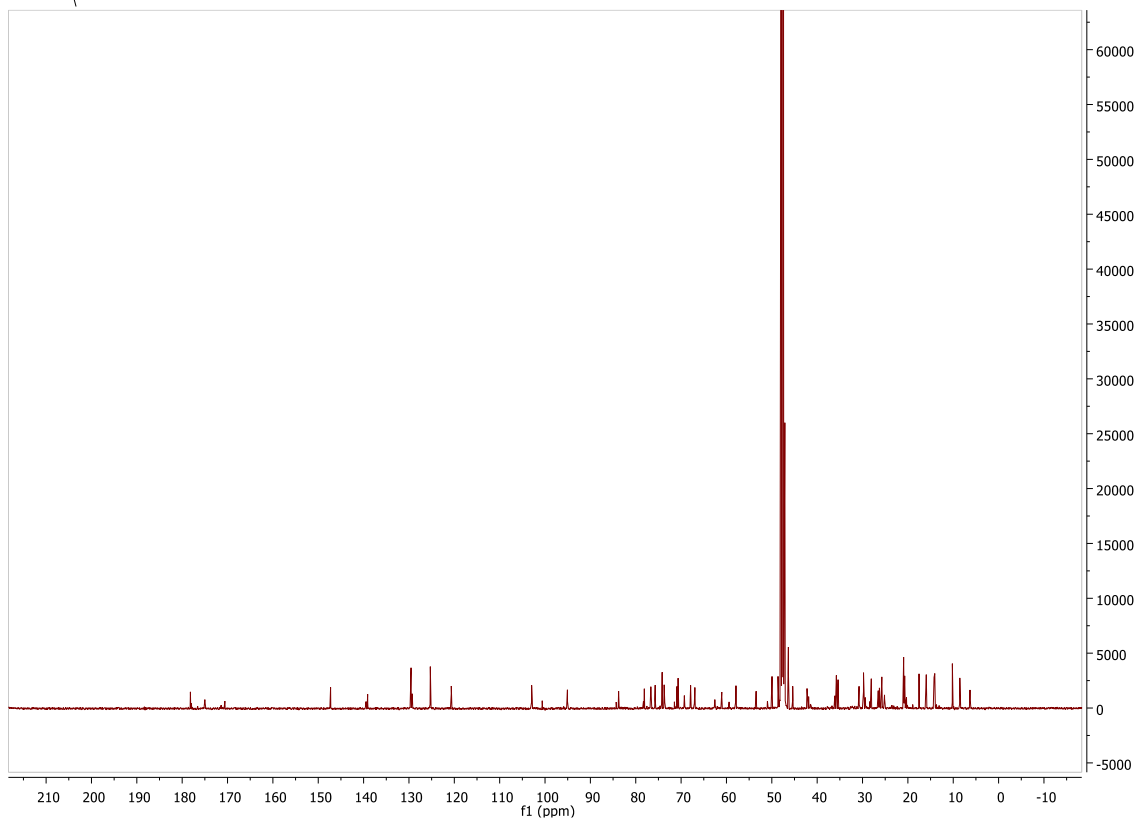
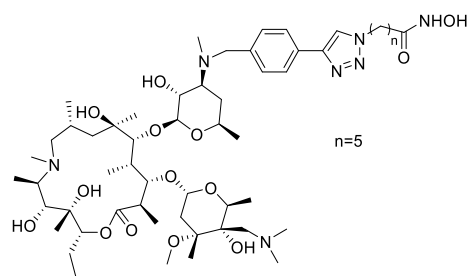
6d ^{13}C NMR



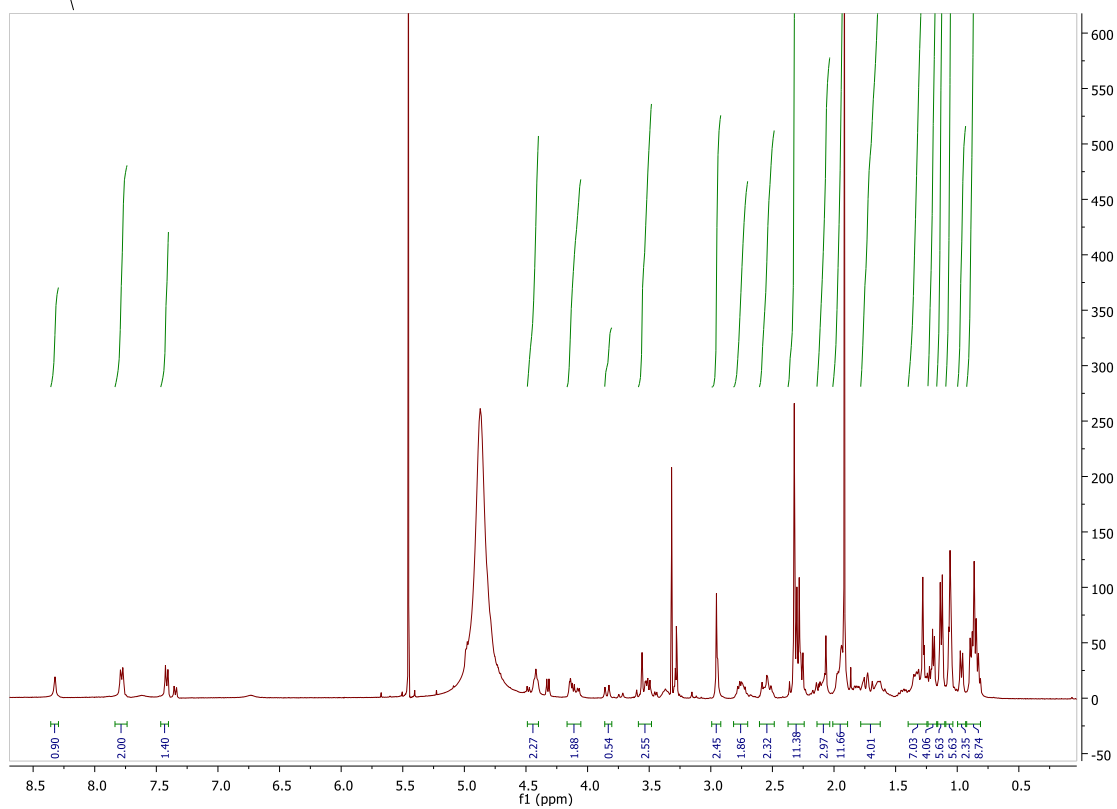
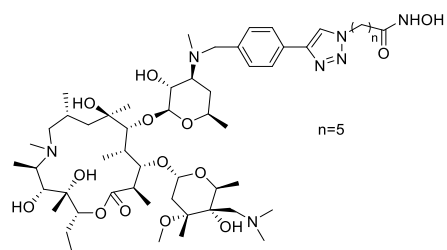
6d ^1H NMR



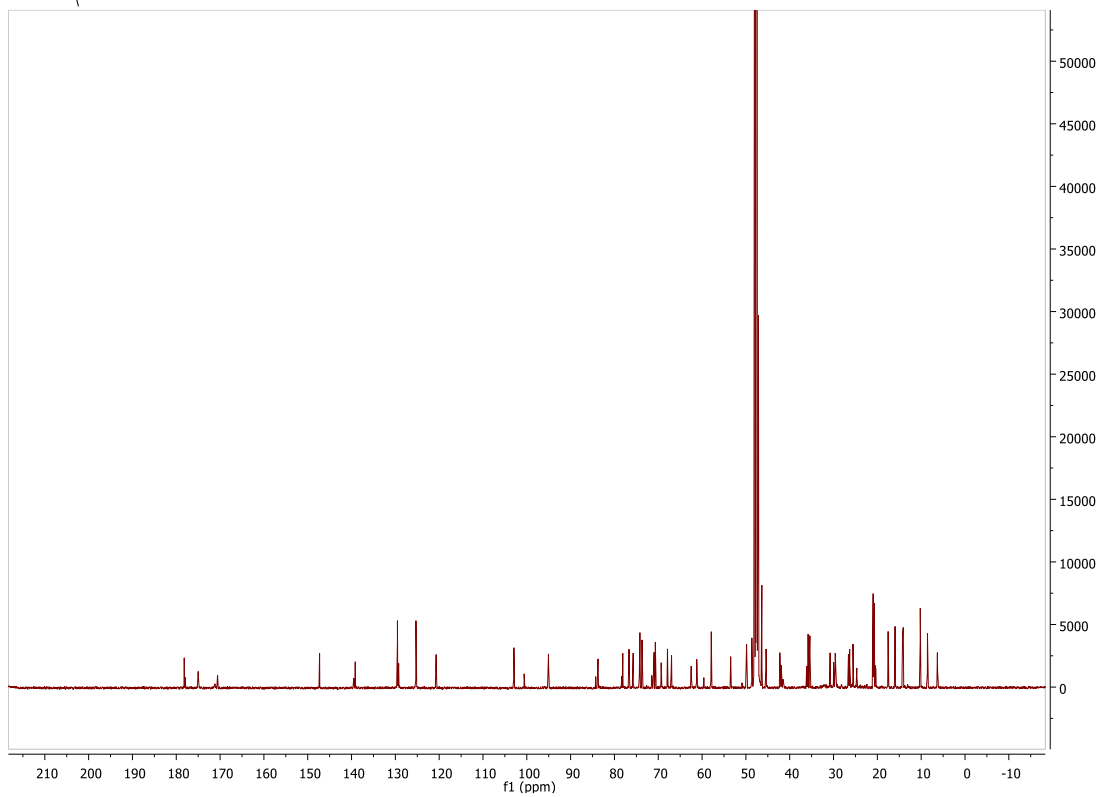
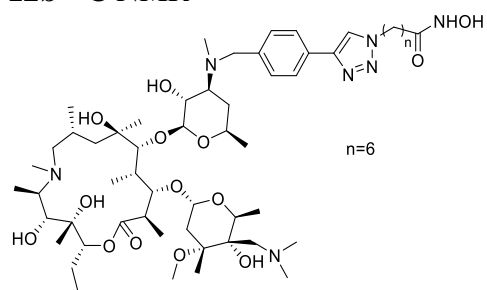
12a ^{13}C NMR



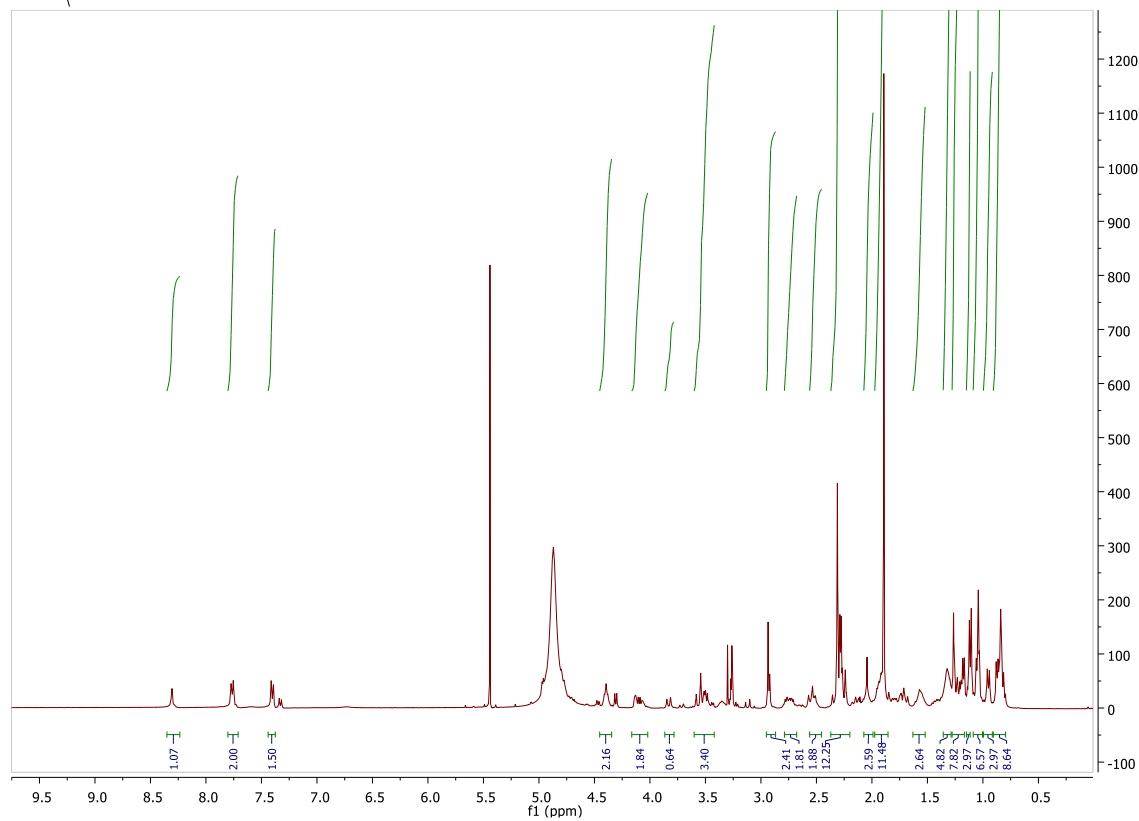
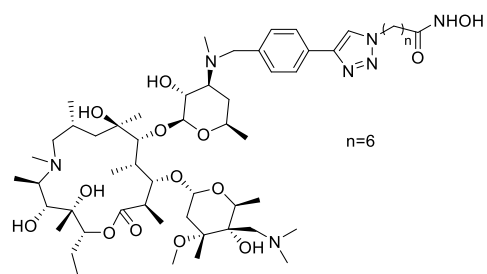
12a ^1H NMR



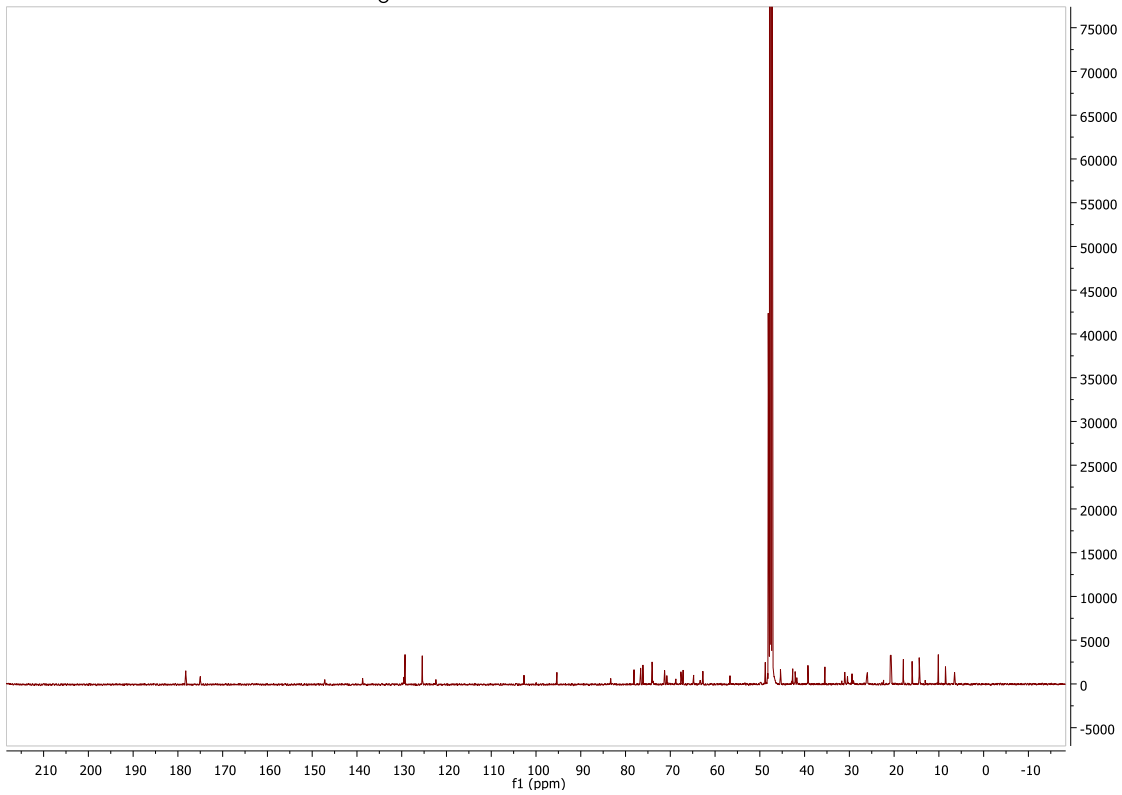
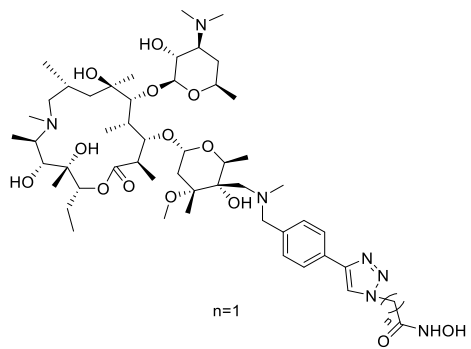
12b ^{13}C NMR



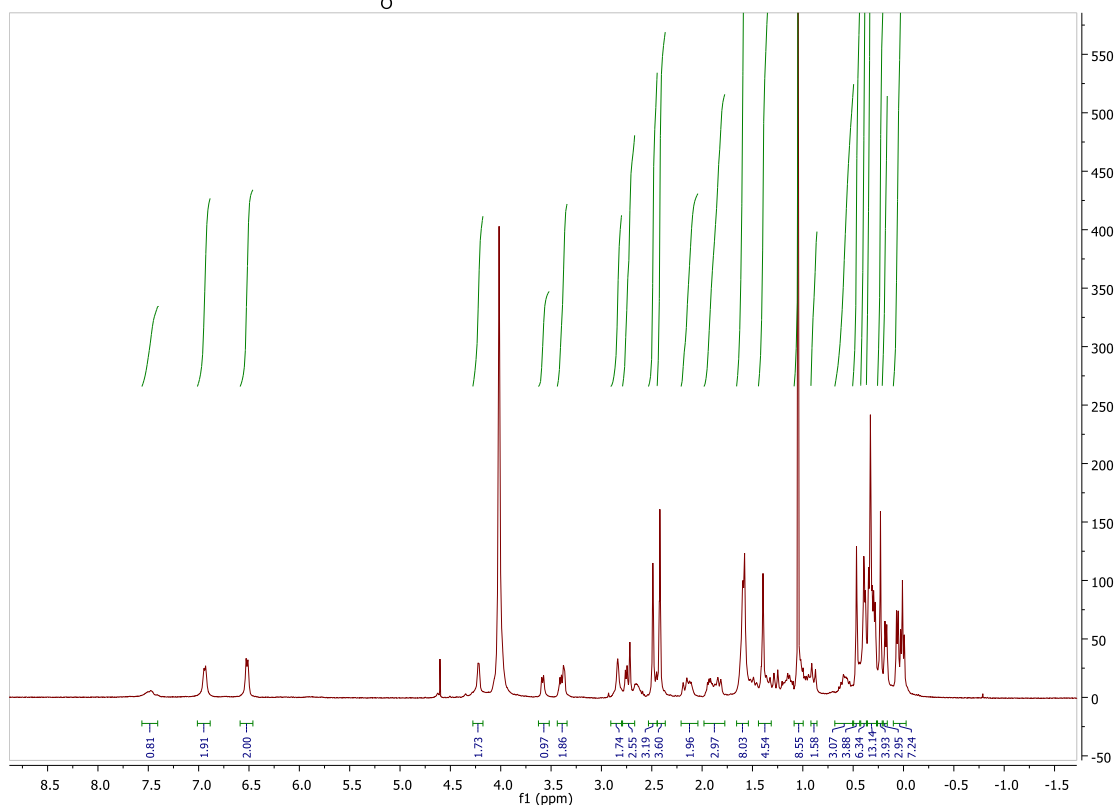
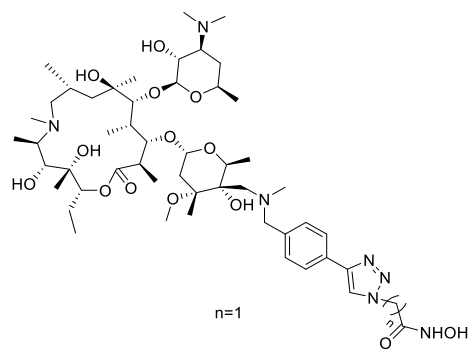
12b ^1H NMR



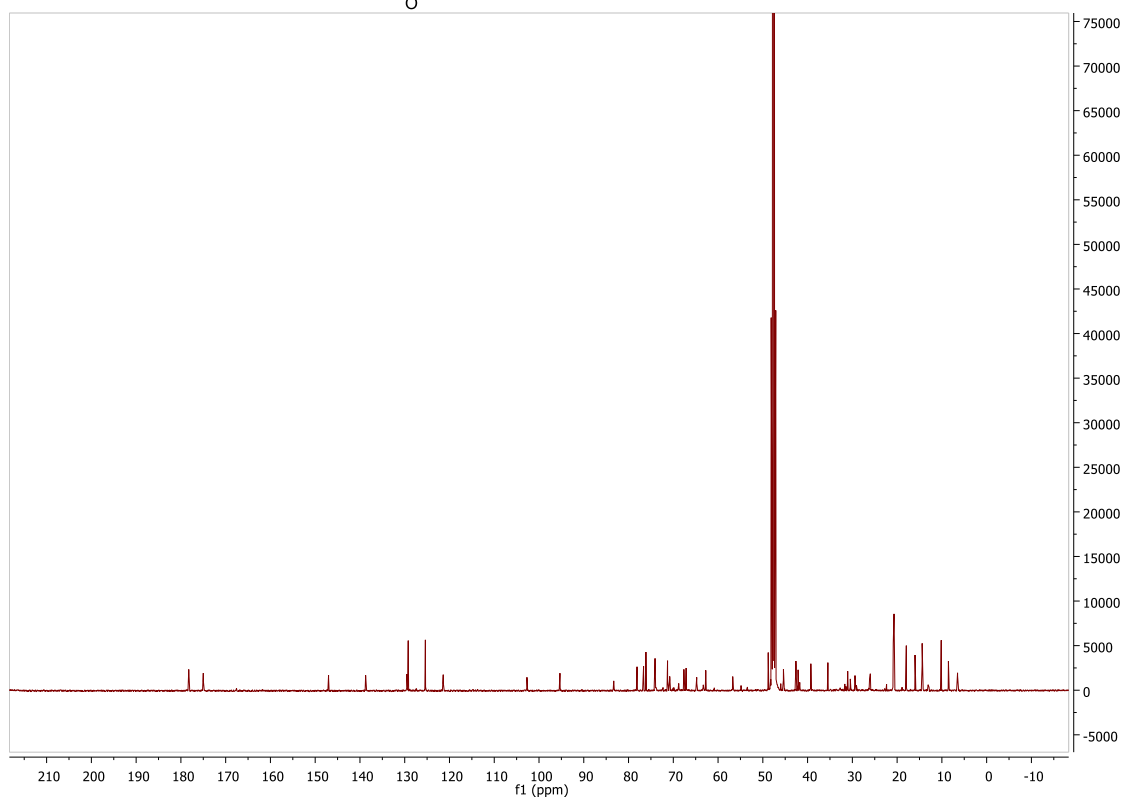
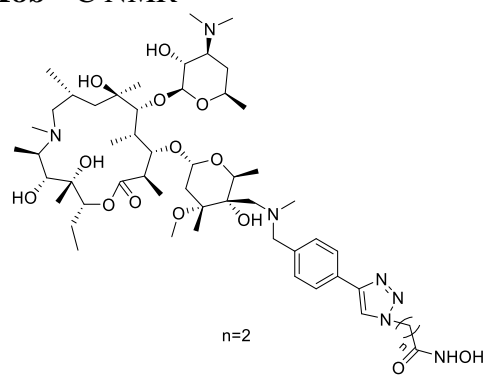
18a ^{13}C NMR



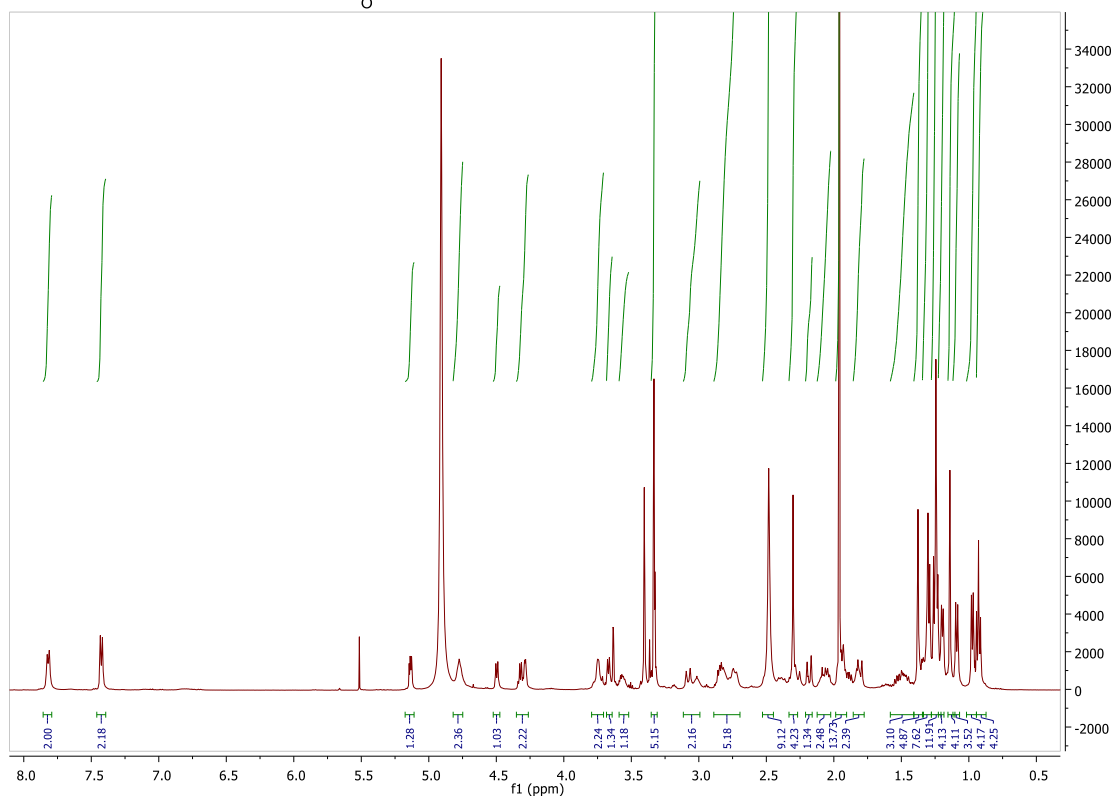
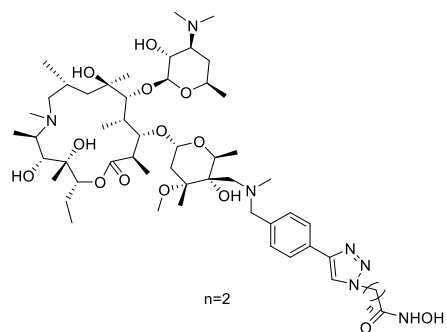
18a ^1H NMR



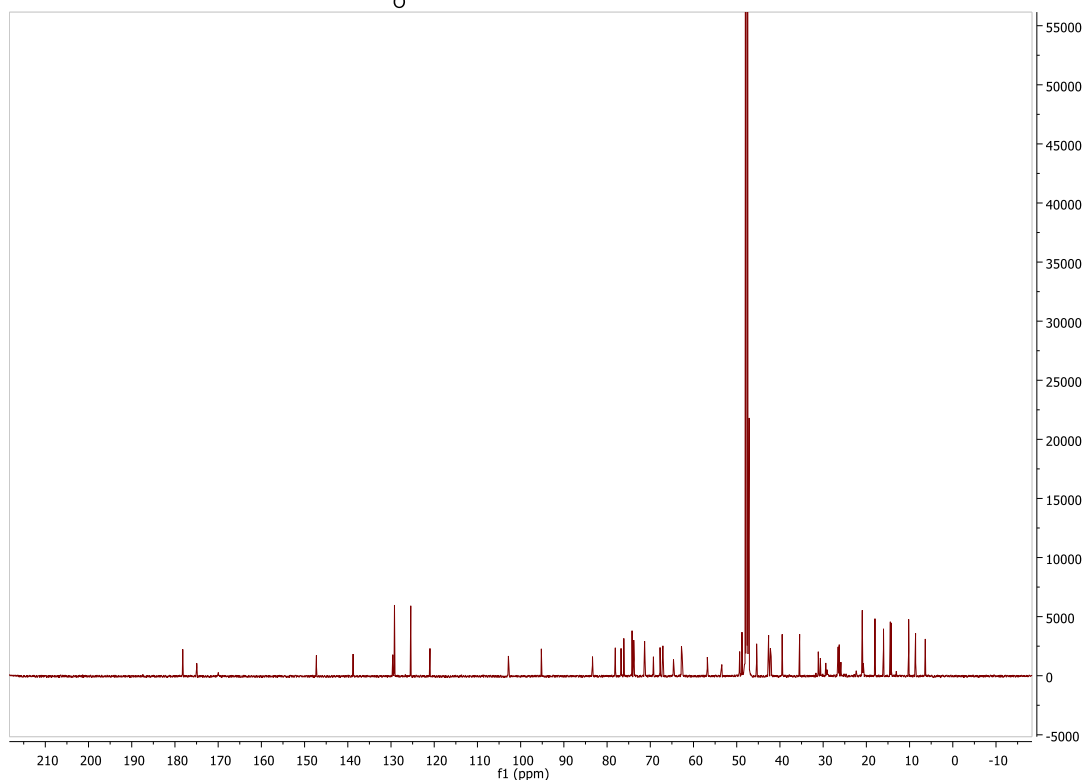
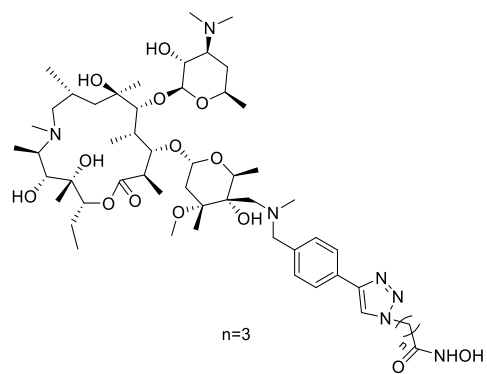
18b ^{13}C NMR



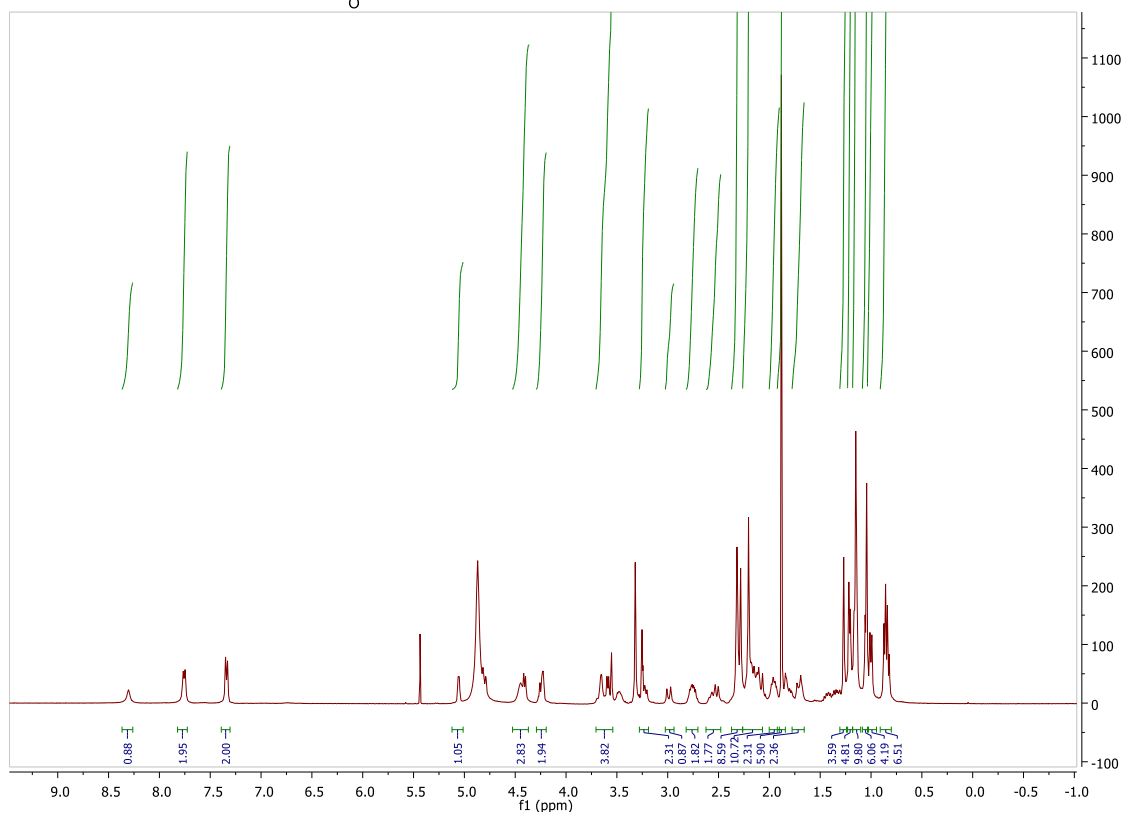
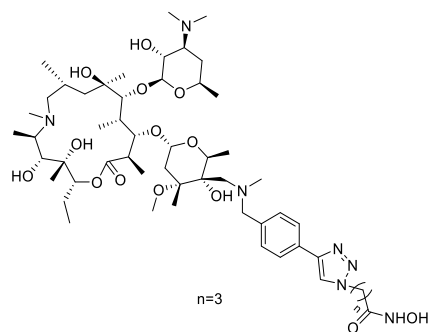
18b ^1H NMR



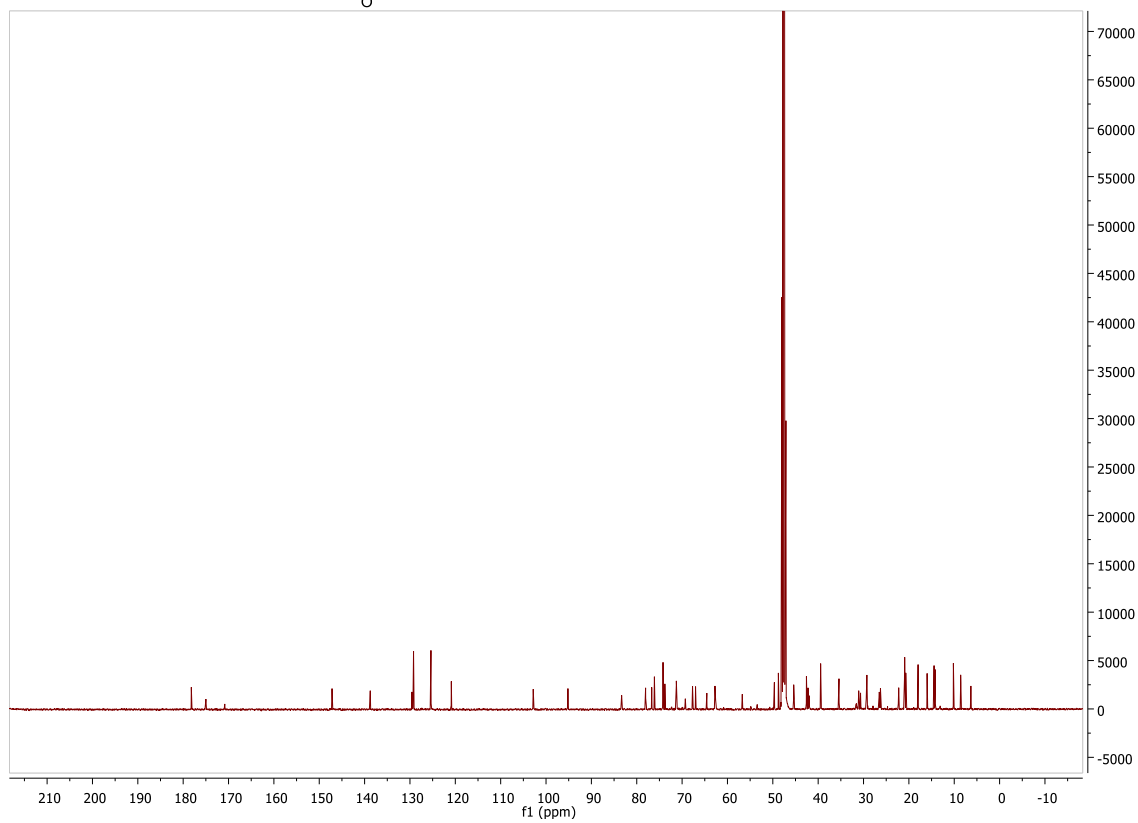
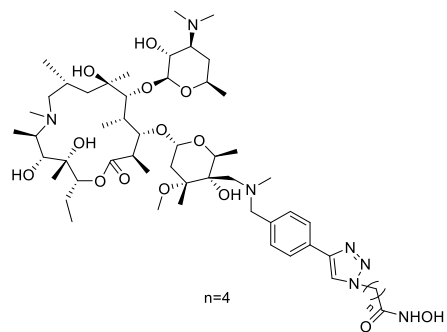
18c ^{13}C NMR



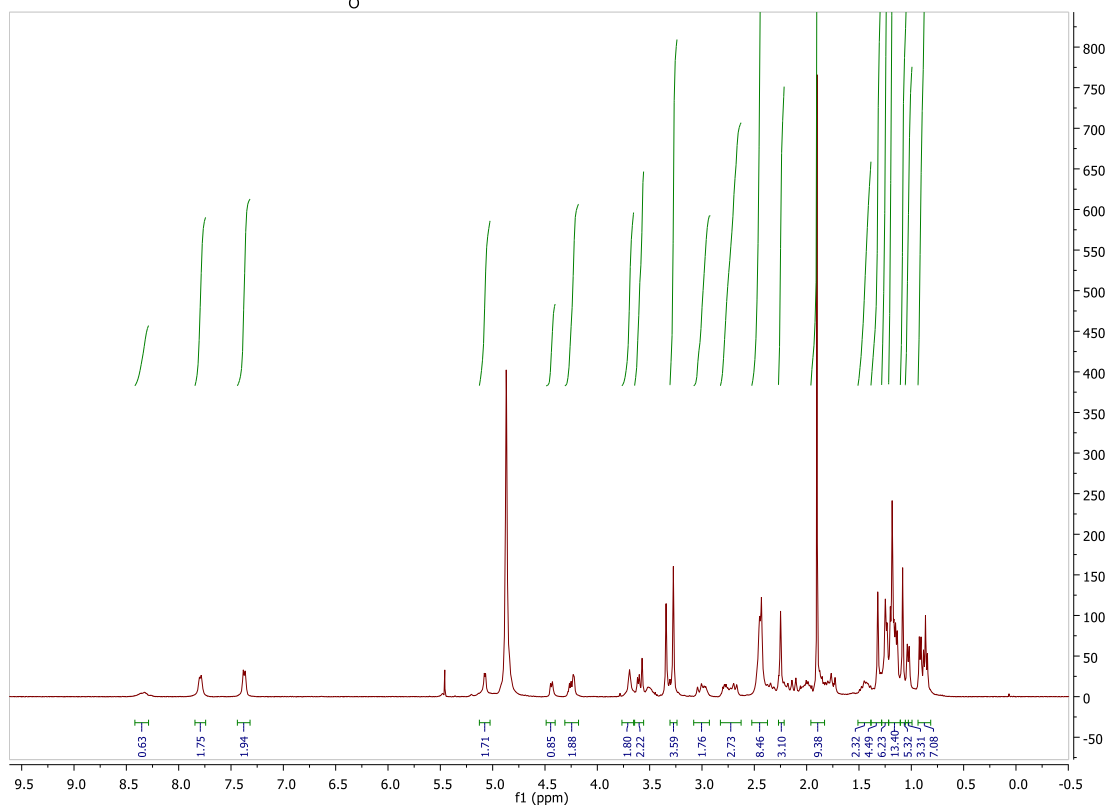
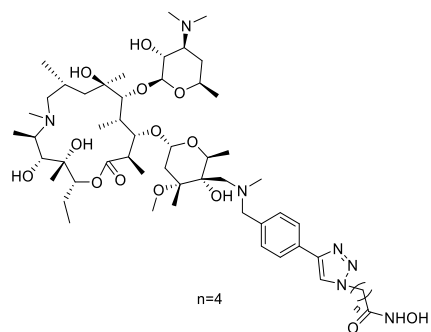
18c ^1H NMR



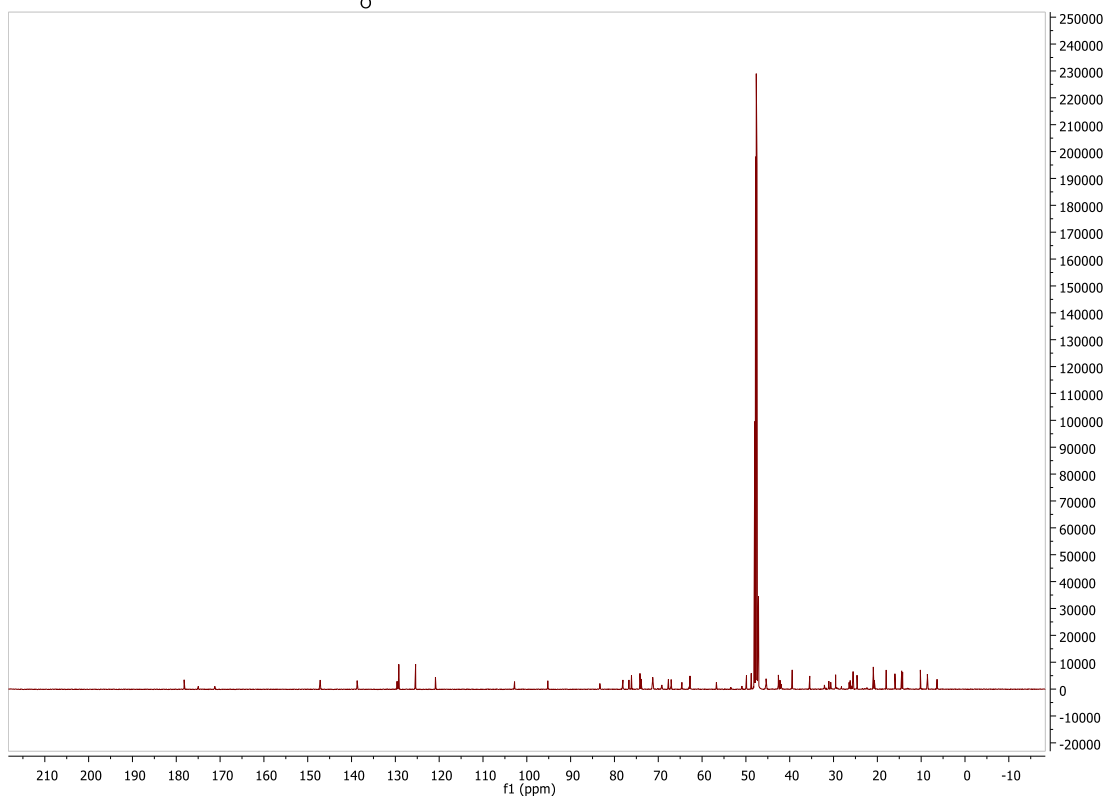
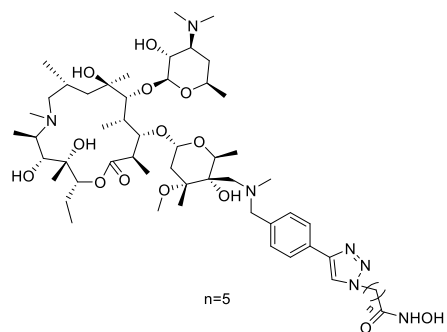
18d ^{13}C NMR



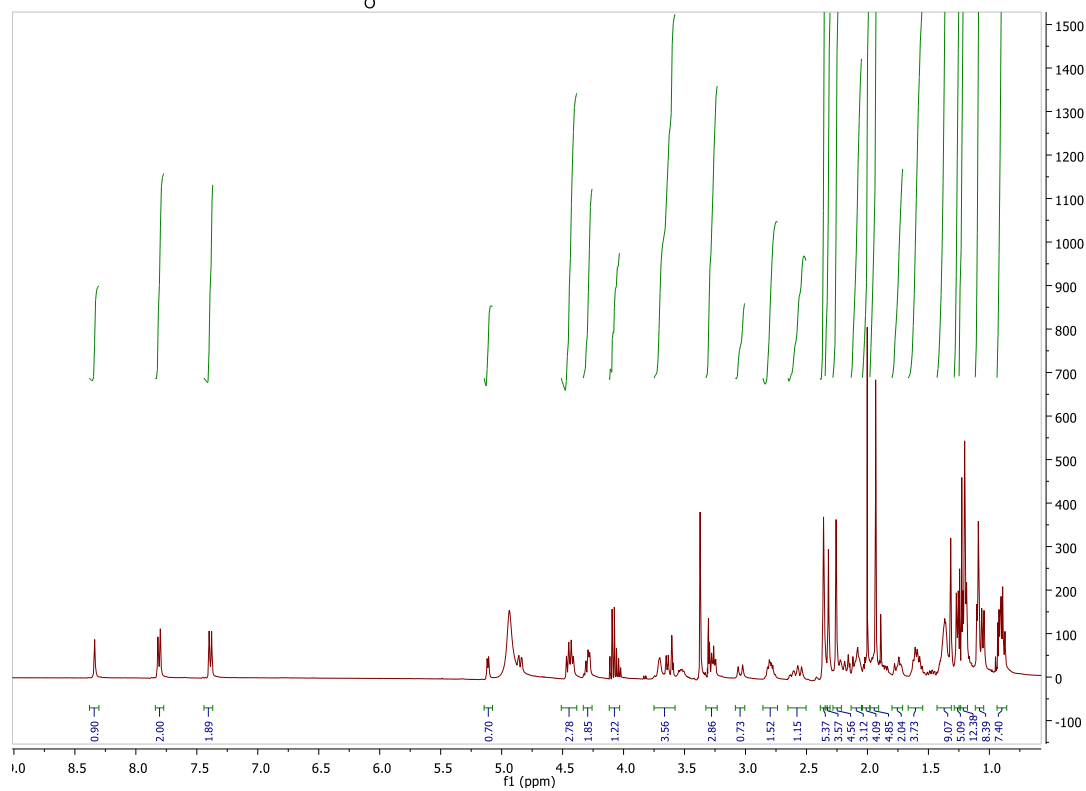
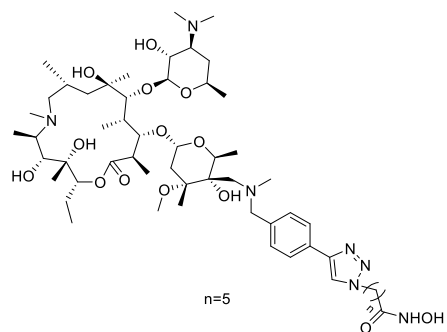
18d ^1H NMR



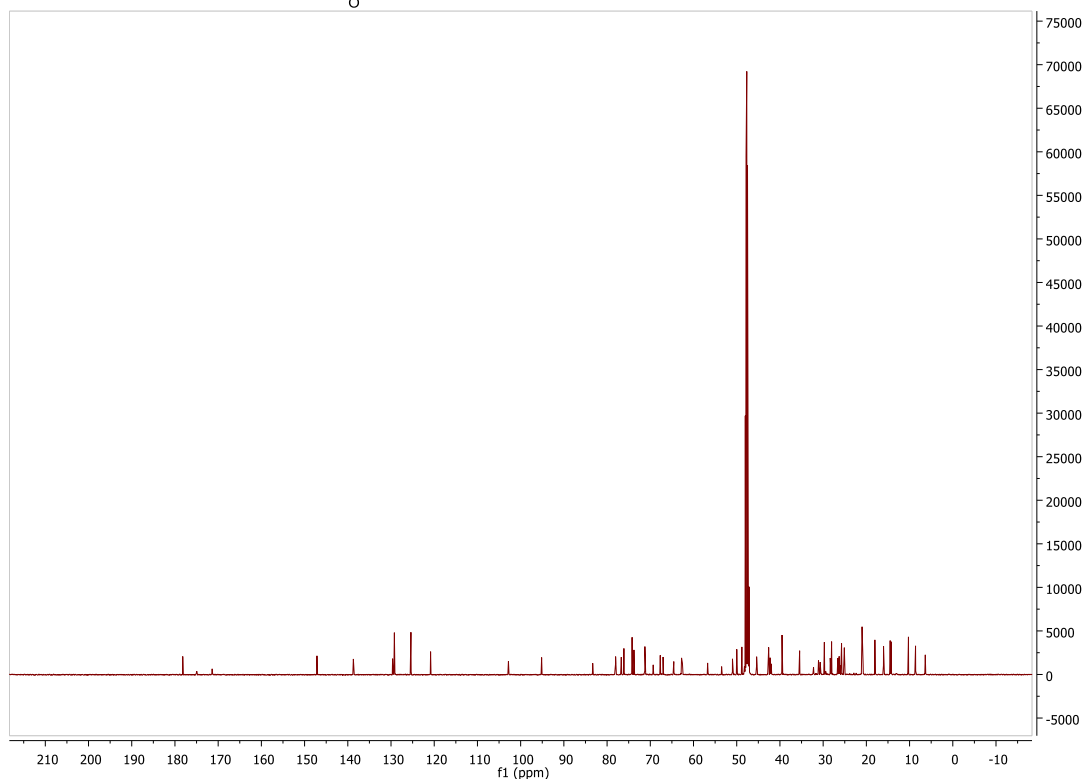
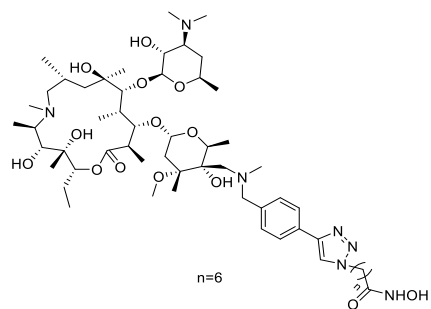
18e ^{13}C NMR



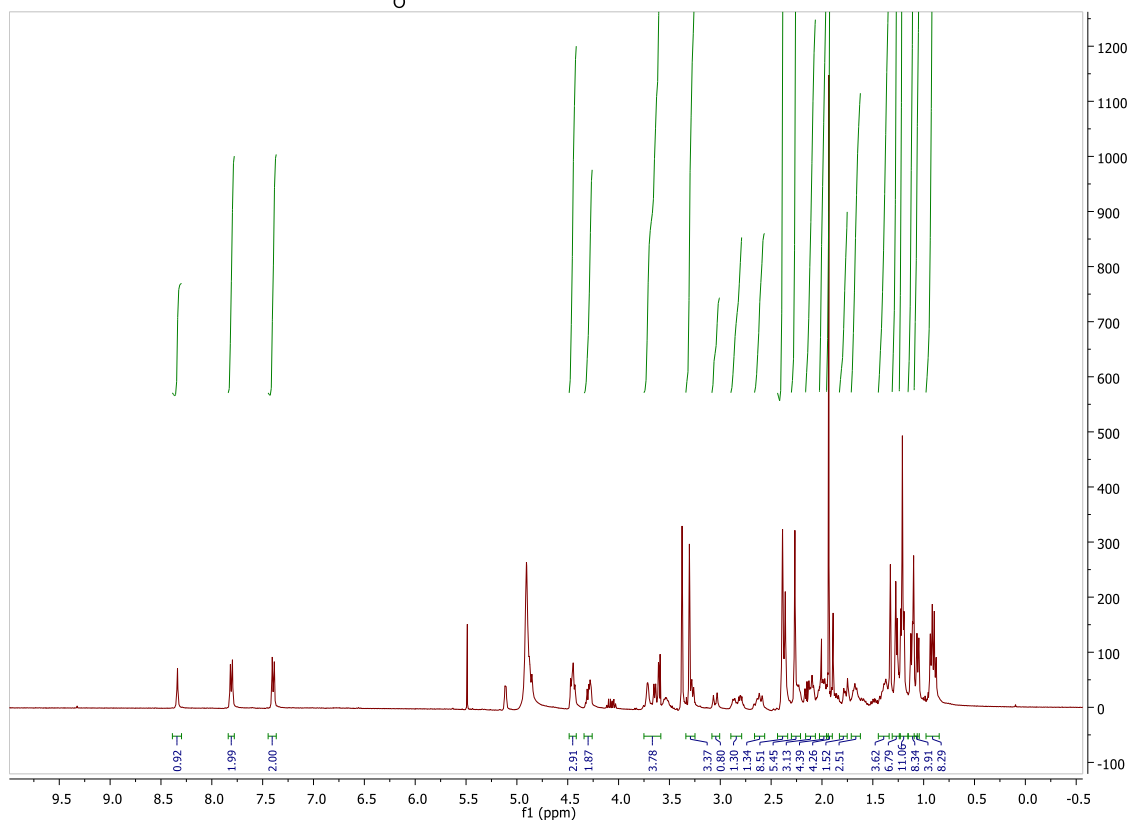
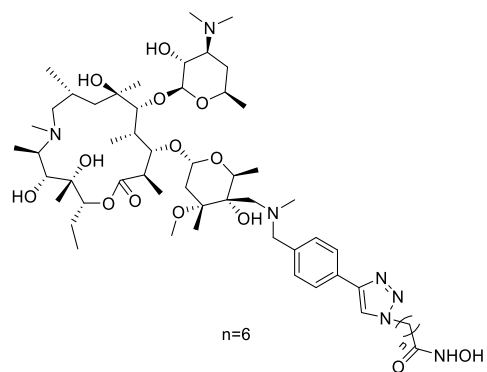
18e ^1H NMR



18f ^{13}C NMR



18f ^1H NMR



CHAPTER 3

ISOFORM SELECTIVE AZITHROMYCIN HDAC INHIBITOR CONJUGATES

3.1. Introduction

Epigenetic irregularities are key factors in many human diseases including cancer [1]. One class of epigenetic regulators is histone deacetylase (HDAC) that, together with histone acetyl transferase (HAT), regulate the chromatin structure by determining the histone acetylation state [2].

HDACs repress gene expression by removing the acetyl group from the terminal lysine of histone tail. There are 18 HDAC isoforms divided into two groups of zinc and NAD^+ dependent. Class I (HDAC1, 2, 3, 8), class IIa (HDAC4, 5, 7, 9), class IIb (HDAC6, 10), and class IV (HDAC11) are zinc dependent and have a zinc cation in their active site pockets [3] while class III (SIRT 1-7) is NAD^+ dependent. HDACs dysfunction including overexpression has been observed in many cancerous pathologies. Various HDAC isoforms are expressed in different tumor tissues, therefore, they have emerged as encouraging therapeutic targets over the past few decades [4].

It has been shown that small molecules can modulate HDAC enzymes biological activities [5]. There has been extensive research on the design and synthesis of HDAC inhibitors (HDACi) and this has so far led to FDA approval of suberoylanilide hydroxamic acid (SAHA) for cutaneous T-cell lymphoma [6], romidepsin (FK228) for cutaneous T-cell lymphoma and refractory peripheral T-cell lymphoma [7], belinostat (PXD101) for relapsed and refractory peripheral T-cell lymphoma [8], and recent accelerated approval of panobinostat (SB939) for multiple myeloma [9]. Chidamide (epidaza), is another HDACi that was developed and approved in China for relapsed and refractory peripheral T cell lymphoma [10]. Chidamide is currently in clinical trials in US [11].

However, despite the promising results of HDACi, they are associated with several side effects possibly due to the role of HDAC enzymes in regulation of various proteins involved in different normal biological processes [12]. Clinical studies revealed that non-selective inhibition of HDAC enzymes (Figure 3.1) lead to adverse effects including bone marrow depression, fatigue, diarrhea, weight lost, and cardiac toxicities and arrhythmias [13]. Thus, there is an unmet need to design and synthesize isoform-selective HDACis to impede only cancerous pathologies rather than affecting the normal cells in order to avoid side effects.

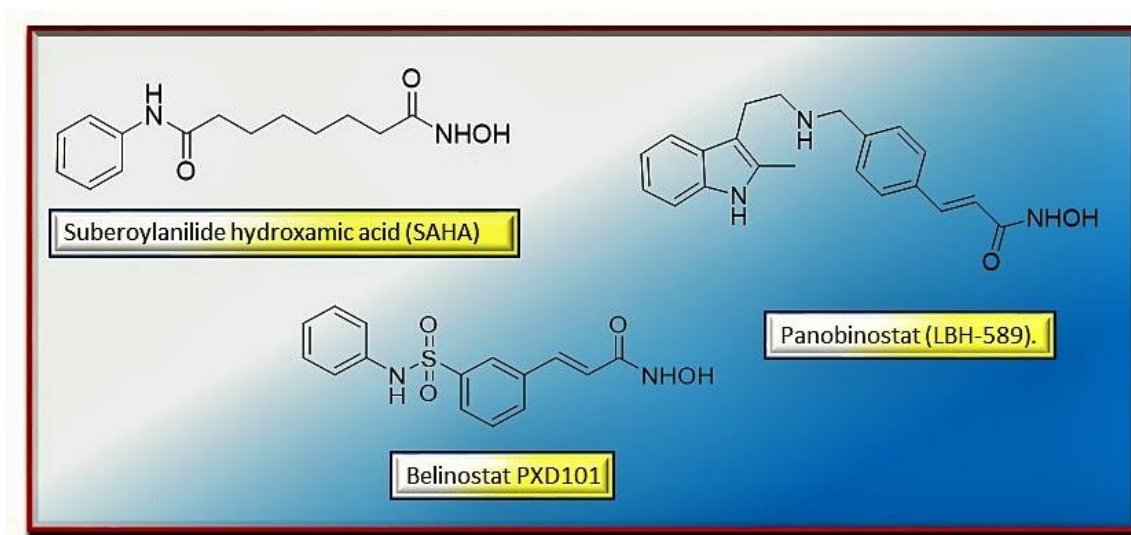


Figure 3.1. US FDA approved pan-HDACis. These HDACi are affiliated with numerous side effects mostly due to their non-selective HDAC inhibition.

3.2. Isoform selective HDACi

Hydroxamate zinc binding group (ZBG) is associated with poor bioavailability as well as short half-life due to its enzymatic hydrolysis [14]. FDA approved HDACi bearing hydroxamate moiety are pan-inhibitors and lack isoform selectivity. They show poor pharmacokinetics and rapid clearance as well as various off-target interactions including inhibition of the hERG cardiac channel leading to cardiotoxicity [15]. However, in contrast, there is a hope that more selective HDACi will have wider

therapeutic index [16], [17]. There has been extensive effort aimed at developing isoform selective HDACi. Much of these studies have focused on replacing the common HDACi hydroxamate ZBG with alternatives that, in addition to being more stable and have longer half-lives, possess isoform selective HDAC inhibitory activity.

Previous study has shown that substitution of hydroxamate with benzamide resulted in HDACi with class I isoform selectivity [18]. Crystallographic comparison of bacterial homologues of class I and class II revealed the existence of a 14 Å internal cavity within the HDAC active site near the catalytic metal cation (Figure 3.2) [19], [20], which is postulated to act as a channel for the release of the acetate byproduct after deacetylation of histone tail [21], [22]. The hydrophobic nature of the inner cavity suggested that hydrophobic substituents can be placed on the benzamide to enhance binding affinity to HDACs 1, 2 and 3[23].

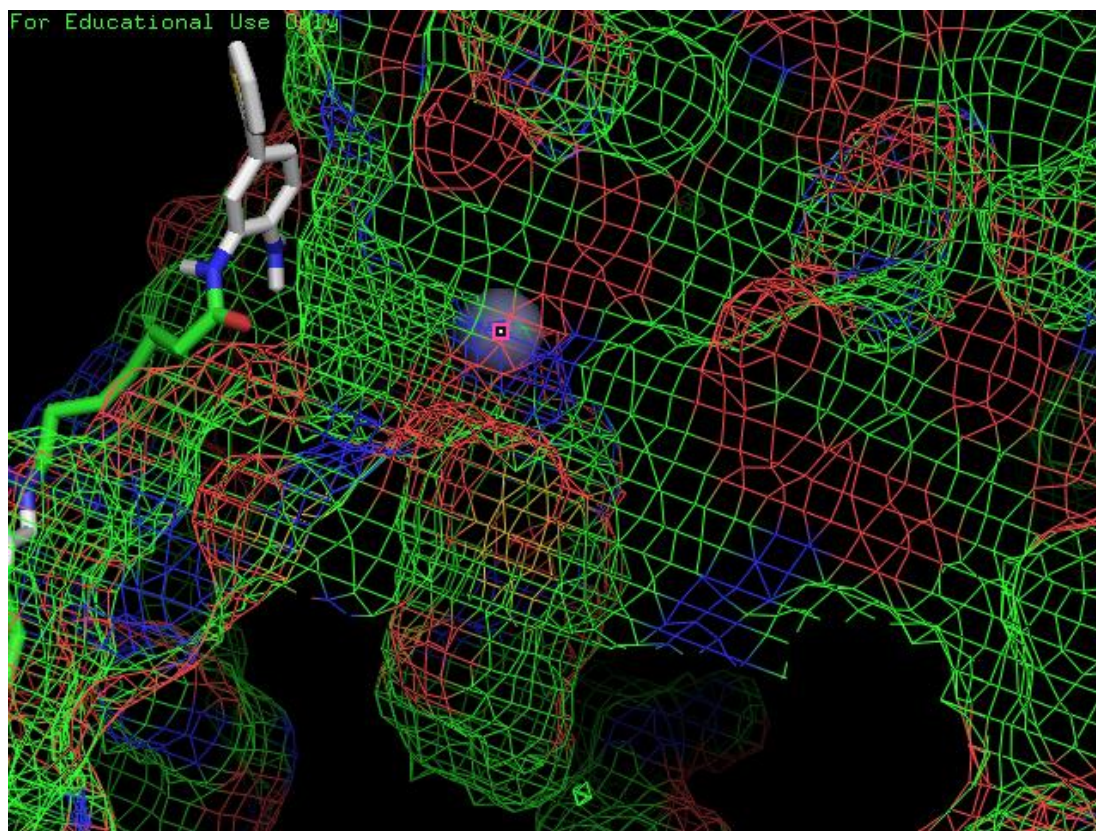


Figure 3.2. Docking study of our proposed design of N-(2-amino-5-(thiophen-2-yl)phenyl)acylamide derived azithromycin against HDAC2. The grey sphere represents zinc ion in the active pocket of HDAC2.

To date, several class I isoform selective HDACi containing benzamide ZBG have been synthesized. Chidamide (CS055), is a benzamide derived HDACi that has been used for relapsed and refractory peripheral T-cell lymphoma in China, and is in clinical trials in US [10]. Etenostat (MS-275) is a benzamide derived class I HDACi that is in clinical trials both as a monotherapy and in combination with other therapeutic agents for treating advanced and refractory solid tumors, non-small cell lung cancer (NSCLC) and breast cancer [24]. Mocetinostat (MGCD0103) is another HDACi with benzamide zinc binding group that is selective toward class I and class IV HDAC isoforms. Mocetinostat is in clinical trials as a standalone therapy for treating leukemia, myelodysplastic syndrome (MDS), chronic lymphocytic leukemia (CLL), advanced solid tumors, and relapsed Hodgkin's lymphoma (Figure 3.3) [25], [26].

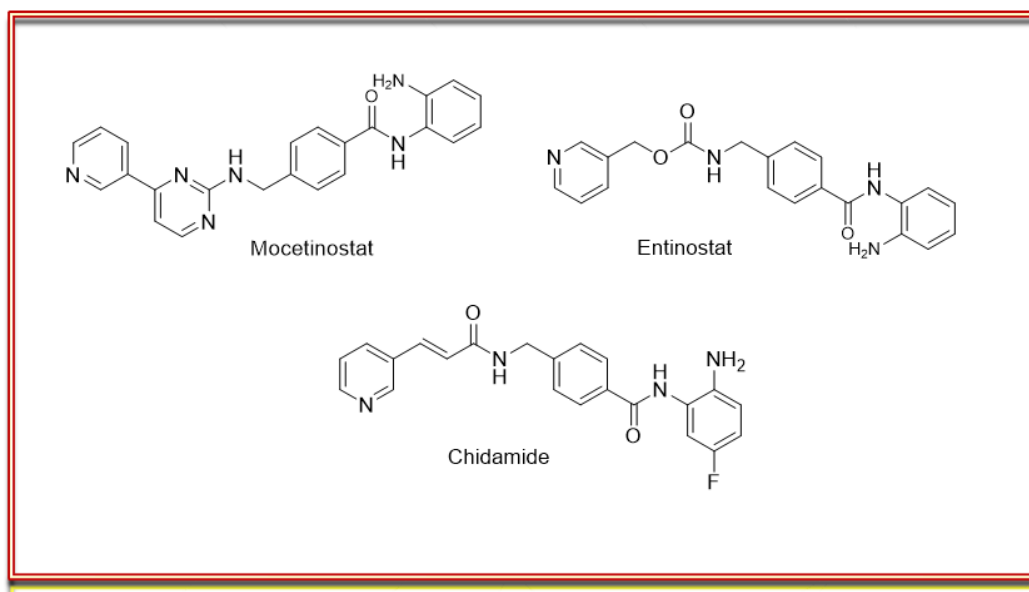


Figure 3.3. Mocetinostat, etenostat, and chidamide: three benzamide-derived HDACi in clinical trials for treating various types of cancers [11], [27].

3.3. Isoform selective HDACi design

To design and develop more selective HDACi, various benzamide-derived HDACi have been evaluated [23], [28]. MS-275 was the first reported benzamide derived HDACi with strong HDAC inhibitory potency, suggesting that the 2'-substituent of benzanilide has hydrogen bonding and electrostatic interactions with the enzyme amino acid residues [29], [30]. In 2007, Moradei O. M. *et al.* reported isoform selective benzamide derived HDACi with enhanced potency and selectivity bearing an aminophenyl group attached to the benzamide zinc bonding group. Their most potent synthesized HDACi with a thienyl substitution on the benzamide exhibited a nanomolar range HDAC inhibitory potency toward HDAC1 and HDAC2 as well as nanomolar range cytotoxicity toward HCT116, human colon cancer cell line [23].

In chapter 1, I had synthesized non-peptide macrocyclic pan HDACi with hydroxamic acid as the ZBG, derived from azithromycin that mimic the peptide backbone of macrocyclic HDACi [2], [31]. I hypothesized that replacement of the hydroxamic acid ZBG of azithromycin conjugated HDACi with benzamide ZBG will result in class I isoform selective HDACi [27]. Therefore, following the three motif pharmacophoric model of HDACi, I designed and synthesized a new class of azithromycin conjugated HDACi by changing the ZBG from hydroxamic acid to the thienyl benzamide in order to achieve isoform selective HDACi [23], [32]. Aryl triazole group was attached to the cap recognition group to enhance HDAC inhibition potency (Figure 3.4) [31], [33].

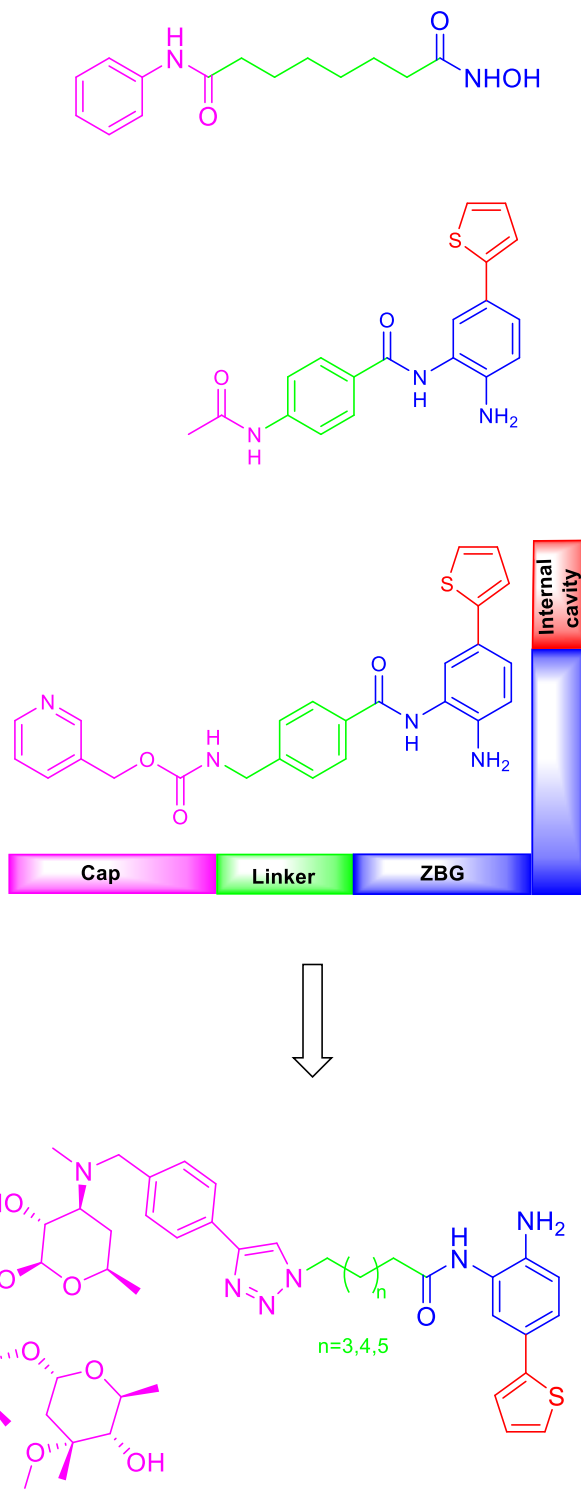


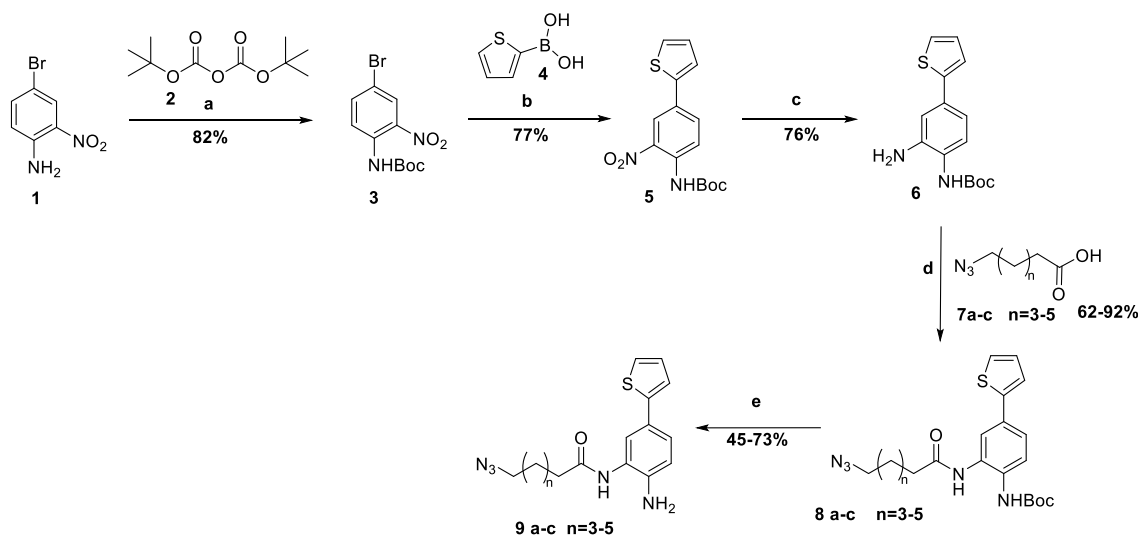
Figure 3.4. Three-motif pharmacophoric model of SAHA as well as selected examples of designed and published class I selective N-(2-amino-5-(thiophen-2-yl)phenyl)acylamide derived HDACi, which led to the design of azithromycin conjugated N-(2-amino-5-

(thiophen-2-yl)phenyl)acylamide derived HDACi. The thienyl group fits favorably in the 14 Å internal cavity of HDAC enzyme and improve the HDAC inhibitory potency through hydrophobic interactions with lipophilic amino acids residues of the cavity [22].

Additionally, a structure activity relationship (SAR) was performed on the linker length to attain the optimal length for maximum HDAC inhibitory potency. Our previous study in designing macrolide conjugated HDACi revealed that the methylene spacers of the linker moiety ranging from one to four methylene groups exhibits no or low HDAC inhibition potency. While five and six methylene spacers had the maximum HDAC inhibitory activity [2]. Thus, in this design the linker length is varied from five to seven methylene spacers.

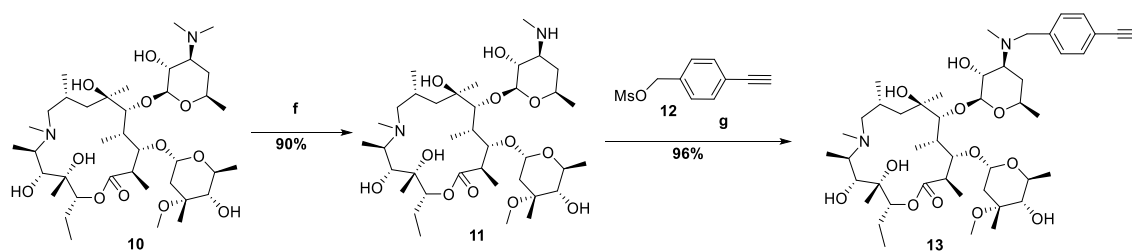
3.4. Chemistry

The azido N-(2-amino-5-(thiophen-2-yl)phenyl)acylamide intermediates **9a-c** were synthesized as described in the literature [32], [28]. Starting from 4-bromo-2-nitroaniline **1**. Boc protection of **1**, followed by Suzuki coupling [34], [35] with 2-thiophenyl boronic acid **4** and reduction of the nitro group to amine using zinc powder [36] gave the Boc protected 2-amino-4-(thiophen-2-yl)phenyl **6**. Coupling of compound **6** with the azido carboxylic acid derivatives **8a-c** [37], [38] followed by acid-promoted removal of the Boc protecting group yielded **9a-c** (Scheme 3.1).



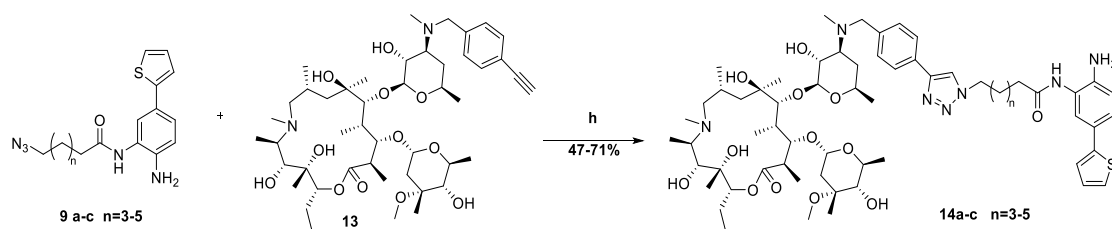
Scheme 3.1. (a) Et₃N, DCM, reflux, overnight, 82%; (b) Pd(PPh₃)₄, K₂CO₃, THF, 70 °C, 77%; (c) Zn, H₂O: Dioxane (1:4), 70 °C, 3 days, 76%; (d) EDCI, HOBT, DMF, 70 °C, 6 h, 62-92%; (e) TFA (1%), DCM, rt, 2h, 45-73%.

The surface recognition cap group, 3'-N-(4-ethynylbenzyl) azithromycin **13** was synthesized by removing the methyl group and formation of desmethyl azithromycin **11**, followed by introduction of ethynylbenzyl on the desosamine sugar ring (Scheme 3.2) [2], [31], [39].



Scheme 3.2. (f) I₂, NaOAc, MeOH, 50 °C, 2 h, 90%; (b) Hünig's base, DMSO, 85 °C, 3 h, 96%.

Azithromycin conjugated N-(2-amino-5-(thiophen-2-yl)phenyl)acylamide derived HDACi **14a-c** were synthesized through copper (I) catalyzed azide-alkyne-cycloaddition (AAC) reaction [40] of 2-thienyl benzamide zinc binding group **9a-c** with 3'-N-(4-ethynylbenzyl) azithromycin **13** (Scheme 3.3).



Scheme 3.3. (h) CuI, Hunig's base, THF, rt, overnight, 47-71%.

3.5. HDAC inhibitory activity (Performed by Dr. James Kornaki at Northwestern University and BPS BioScience)

To investigate the HDAC inhibition activities of azithromycin conjugated N-(2-amino-5-(thiophen-2-yl)phenyl)acylamide derived HDACi **14a-c**, they were tested against class I (HDAC1, 2, 3 and 8) and class IIb (HDAC6) enzymes. We used the previously synthesized hydroxamate derivative of azithromycin **15** (synthesized by Dr. Subhasish Tapadar) and SAHA as positive controls. HDAC inhibition activity was determined using the label-free mass spectrometry-based SAMDI assay. As expected azithromycin conjugated N-(2-amino-5-(thiophen-2-yl)phenyl)acylamide derived HDACi showed class I isoform selectivity with no HDAC inhibition activity against HDAC6, while azithromycin derived hydroxamate HDACi hit HDAC6 as well and exhibited no selectivity for HDAC isoforms (Table 3.1). We then screened lead **15** and compound **14b** against all Zn-dependent HDAC isoforms using the Fluor de Lys assay available through BPS Bioscience (San Diego, USA). Fluorescent intensity was measured at certain wavelengths. The IC₅₀ values were obtained employing fluorescent intensity in related equations to determine the concentration leading to half maximal percent activity (Table 3.2).

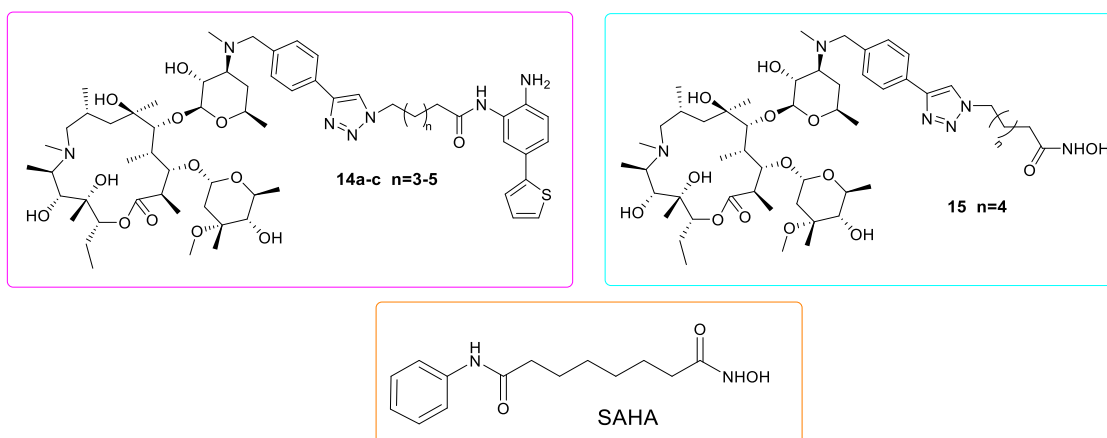


Table 3.1. HDAC 1, 2, 3, 6, and 8 inhibition activities of azithromycin conjugated N-(2-amino-5-(thiophen-2-yl)phenyl)acylamide derived HDACi compounds (IC₅₀ in nM) obtained using label-free mass spectrometry-based SAMDI assay, and their comparison with azithromycin derived hydroxamate and FDA approved pan- HDACi SAHA.

Compound	HDAC1	HDAC2	HDAC3	HDAC6	HDAC8
14a	125±28	NI	123	NI	NI
14b	232±28	159±17	NI	NI	NI
14c	217±23	65.1±23	29.4±7.8	NI	NI
15	50.4±8.4	NT	NT	31.3±1.3	817±308
SAHA	42	190	20	34	2800

NI= No Inhibition. NT= Not Tested

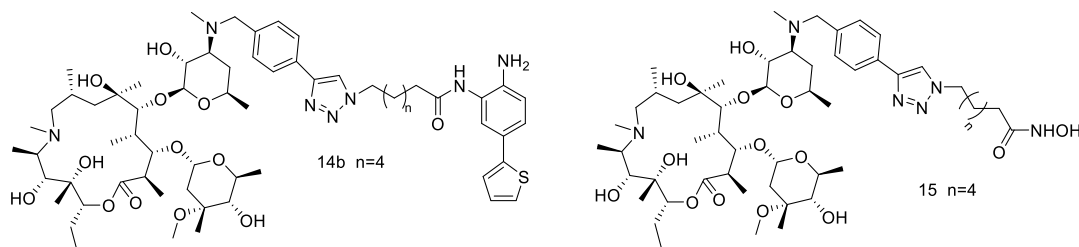


Table 3.2. HDAC inhibition potency against all Zn-dependent HDAC isoforms using the Fluor de Lys assay available through BPS Bioscience.

HDAC inhibition	15	14b
HDAC1	2.7	509
HDAC2	8.1	3454
HDAC3/NCOR2	1.7	NI
HDAC4	1904	NI
HDAC5	1773	NI
HDAC6	1.7	NI
HDAC7	2621	NI
HDAC8	839	NI
HDAC9	6910	NI
HDAC10	4.5	2285
HDAC11	7361	NI

SAMDI assay was analyzed by SAMDI-MS and compounds were characterized by their m/z shifts after their acetyl loss. Fluor de Lys assay was analyzed by measuring the fluorescent signal generated after adding the developer to the substrate combination, by fluorescent plate scanner. The fluorescent signal was compared to positive and negative controls.

3.6. Docking study

Docking studies on azithromycin conjugated HDACi against HDAC isoforms were performed using AutoDock Vina. This study revealed a strong chelation of the zinc

ion at the bottom of the active pocket of class I isoforms to the benzamide ZBG (Figure 3.5). This docking study confirmed the observed class I HDAC selectivity.

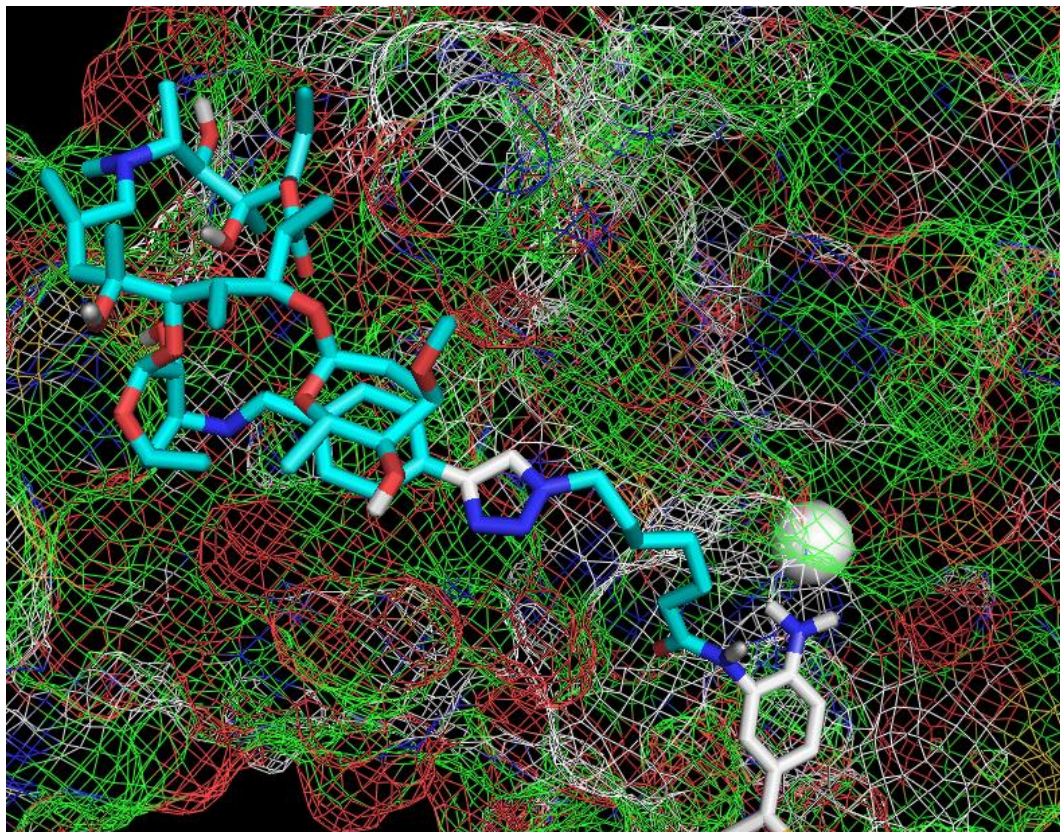


Figure 3.5. Docked structure of azithromycin-HDACi conjugate with six methylene linker group (14b) against HDAC2.

3.7. Anti-proliferative activity

The azithromycin conjugated N-(2-amino-5-(thiophen-2-yl)phenyl)acylamide derived HDACi **14a-c** were tested against three transformed cell lines, lung (A549), Estrogen receptor (ER) positive (MCF-7) and ER negative (MDA-MB231) breast cancers as well as one normal cell line (VERO) monkey kidney epithelial cell. We used hydroxamate derivative of azithromycin **15** and SAHA as positive controls. Despite their considerably weaker HDAC inhibition activities, compounds **14a-c** possessed potent anti-

proliferative activities against the tested tumor cell lines with **14b** inherently more cytotoxic and tumor cell selective relative to **15** and SAHA (Table 3.2).

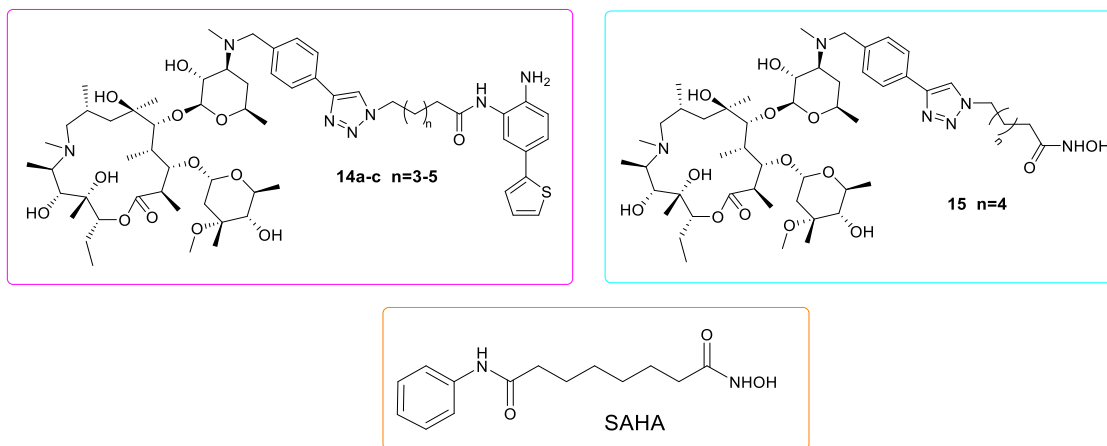


Table 3.3. Anti-proliferative activity of azithromycin conjugated HDACi (IC₅₀ values in μ M).

Compound	A549	MCF-7	MDA-MB231	VERO
14a	2.24 \pm 0.35	0.85 \pm 0.19	2.10 \pm 0.67	2.54 \pm 0.27
14b	1.72 \pm 0.09	0.83 \pm 0.07	1.20 \pm 0.058	6.46 \pm 1.15
14c	1.70 \pm 0.25	1.50 \pm 0.53	0.84 \pm 0.48	3.48 \pm 0.60
15	2.32 \pm 0.53	4.08 \pm 0.30	NT	5.90 \pm 0.18
SAHA	5.00 \pm 0.24	3.27 \pm 0.05	3.40 \pm 0.20	1.03 \pm 0.97

Each value is obtained from a duplicate of three simultaneous experiments. NT=not tested

Compound **14b** was synthesized in a larger scale (1.5 g) sent to Augusta University (Professor Muthusamy Thangaraju's Lab) for animal study.

3.8. *In vivo* study (Performed by Professor Muthusamy Thangaraju's Lab at Augusta University)

For *in vivo* studies, MMTV-PyMT-Tg mice were chosen since their mammary tumors mimic formation and progression of human breast cancer and they eventually metastasize to lung tissues. At the beginning tumors possess ER expression but ultimately they turn into ER negative breast tumors [41]. Mice with metastatic breast cancer were treated with 40 mg/kg body of compounds **14b** (azithromycin conjugated N-(2-amino-5-(thiophen-2-yl)phenyl)acylamide derived HDACi) and **15** (azithromycin conjugated hydroxamic acid derived HDACi) 3 times a week. After 6 weeks mice were sacrificed and the tumor volume in each case was measured (Figure 3.6).

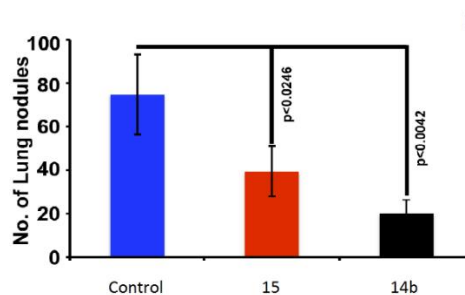
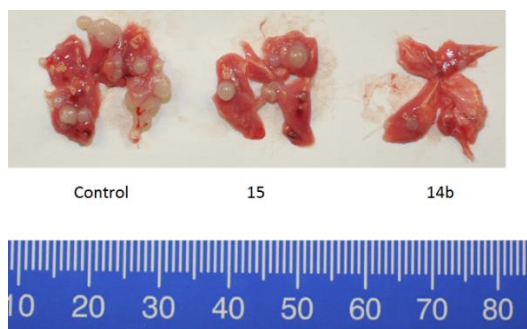
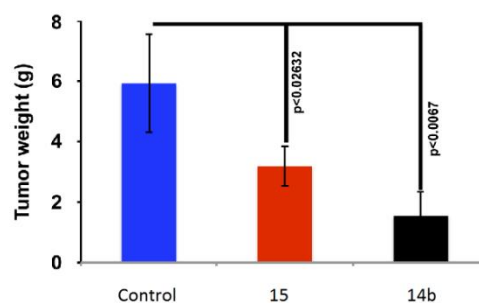
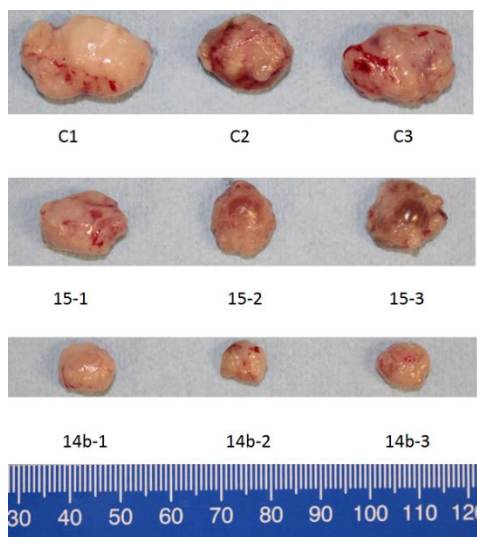


Figure 3.6. (A) Tumor regression and (B) number of nodules in MMTV-PyMT-Tg mice with metastatic lung cancer that were treated with compounds 14b and 15. Compound 14b an isoform selective HDACi resulted in a better tumor regression compared to compound 15 a pan HDACi (**Performed by Professor Muthusamy Thangaraju's Lab at Augusta University**).

Compound **14b**, a class I isoform selective HDACi, resulted in a greater tumor size regression compared to compound **15** a pan HDACi (Figure 3.7). HDAC1 strongly influences breast cancer progression. It promotes tumorigenesis and colony formation by suppressing the induction of ER α expression and its transcription activity [42]. ER α plays an important role in modulating tumor growth in breast cancer and loss of its expression and activity results in significant increase in tumor cell proliferation [43], [44], [45]. Therefore, selective inhibition of HDAC1 leads to a better breast cancer progression repression through re-expression of ER α -mRNA and its proteins [43].

3.9. Conclusion

I synthesized a new class of non-peptide macrocyclic N-(2-amino-5-(thiophen-2-yl)phenyl)acylamide derived HDACi that exhibited isoform selectivity toward class I HDAC isoforms, unlike their hydroxamate analogue and FDA approved pan-HDACin SAHA which show no selectivity for any classes of HDAC isoform. These azithromycin conjugated HDACi had a better therapeutic window and showed a low macromolar, and in some cases, high nanomolar cytotoxicity against transformed cell lines, lung (A549), ER positive (MCF-7) and ER negative (MDA-MB231) breast cancer, and less cytotoxicity toward healthy cell line (VERO) compared to SAHA.

3.10. Experimental

3.10.1. Materials and methods

Azithromycin was purchased from Greenfield chemical. 4-ethynylbenzyl alcohol, thiophen-2-ylboronic acid, and 4-bromo-2-nitroaniline were purchased from Sigma-Aldrich. All commercially available starting materials were used without purification. Reaction solvents were high performance liquid chromatography (HPLC) grade or American Chemical Society (ACS) grade and used without purification. Analtech silica gel plates (60 F₂₅₄) were used for analytical TLC, and Analtech preparative TLC plates (UV 254, 2000 μ m) were used for purification. UV light and anisaldehyde/iodine stain were used to visualize the spots. 200-400 Mesh silica gel was used in column chromatography. Nuclear magnetic resonance (NMR) spectra were recorded on a Varian-Gemini 400 MHz or Bruker 500 MHz magnetic resonance spectrometer. ¹H NMR Spectra were recorded in parts per million (ppm) relative to the residual peaks of CHCl₃ (7.24 ppm) in CDCl₃ or CHD₂OD (4.78 ppm) in CD₃OD or DMSO-*d*₅ (2.49 ppm) in DMSO-*d*₆. ¹³C spectra were recorded relative to the central peak of the CDCl₃ triplet (77.0 ppm) or CD₃OD septet (49.3 ppm) or DMSO-*d*₆ septet (39.7 ppm) and were recorded with complete hetero-decoupling. Original 'fid' files were processed using MestReNova LITE (version 5.2.5-5780) program. High-resolution mass spectra were recorded at the Georgia Institute of Technology mass spectrometry facility in Atlanta. Compounds **3**, **5**, **6**, **8a-c**, **9a-c**, **11** and **13** were synthesized as described before [2], [32].

3.10.1.1. *tert*-butyl (4-bromo-2-nitrophenyl) carbamate (**3**)

4-Bromo-2-nitroaniline **1** (10 g, 0.046 mol) was dissolved in anhydrous dichloromethane (15 mL). Boc anhydride **2** (22.12 g, 0.1 mol) followed by triethyl amine (14 mL, 0.1 mol) were added to the reaction mixture. Reaction stirred at reflux overnight. Reaction mixture was washed with NaHCO₃ (10 mL) and brine solution (10 mL) and

dried over Na₂SO₄ and concentrated *in vacuo*. The crude product was purified by column chromatography (Silica gel, 10:1 Hex: EtOAc) to give the product (12.02 g, 82%) as a pale yellow solid. ¹H NMR (400 MHz, CDCl₃) δ 8.51 (d, *J* = 9.2 Hz, 1H), 8.33 (dd, *J* = 2.4, 0.8 Hz, 1H), 7.69 (dd, *J* = 9.2, 2.4 Hz, 1H), 1.60 – 1.47 (m, 9H).

3.10.1.2. *tert*-butyl (2-nitro-4-(thiophen-2-yl)phenyl)carbamate (5)

Compound **3** (12.02 g, .038 mol) was dissolved in anhydrous THF (30 mL) followed by K₂CO₃ (15.71 g, 0.11 mol). After purging with argon for 20 minutes, thiophen-2-ylboronic acid **4** (6.30 g, 0.05 mol) was added followed by Pd(PPh₃)₄ (4.38 g, 0.003 mol). The reaction mixture stirred at reflux overnight. Then it was washed with NaHCO₃ (15 mL) and brine solution (20 mL) and dried over Na₂SO₄ and concentrated *in vacuo*. The crude product was purified by column chromatography (Silica gel, 10:1 Hex: EtOAc) to give the product (9.25 g, 77%) as a pale yellow solid. ¹H NMR (400 MHz, CDCl₃) δ 9.66 (s, 1H), 8.57 (dd, *J* = 13.2, 8.7 Hz, 1H), 8.40 (d, *J* = 2.3 Hz, 1H), 7.82 (dd, *J* = 8.9, 2.3 Hz, 1H), 7.38 – 7.27 (m, 1H), 7.10 (ddd, *J* = 13.6, 6.8, 4.9 Hz, 1H), 1.63 – 1.47 (m, 9H).

3.10.1.3. *tert*-butyl (2-amino-4-(thiophen-2-yl)phenyl)carbamate (6)

Compound **5** (8.86 g, 0.027 mmol) was dissolved in 1,4-dioxane and water (20 mL, 4:1). The mixture stirred at room temperature till all the starting material dissolved completely. Then zinc powder was added and the mixture stirred for three days at 70 °C. The reaction mixture stirred at reflux overnight. Then it was washed with NaHCO₃ (15 mL) and brine solution (15 mL) and dried over Na₂SO₄ and concentrated *in vacuo*. The crude product was purified by column chromatography (Silica gel, 3:1 Hex: EtOAc) to give the product (6.1 g, 76%) a brown solid. ¹H NMR (400 MHz, CDCl₃) δ 7.36 – 7.16 (m, 3H), 7.08 – 6.91 (m, 3H), 1.64 – 1.42 (m, 9H).

3.10.1.4. *tert*-butyl (2-(4-azidohexanamido)-4-(thiophen-2-yl)phenyl)carbamate (**8a**)

4-Azidohexanoic acid **7a** (60 mg, 0.38 mmol) was dissolved in anhydrous DMF (5 mL) followed by adding EDCI (73 mg, 0.38 mmol) and HOBT (52 mg, 0.38 mmol). After 30 minutes of stirring at room temperature, compound **6** (80 mg, 0.27 mmol) was added and then the reaction mixture was heated to 70 °C for 6 h. The reaction mixture stirred at reflux overnight. Then it was washed with water (3×5 mL) NaHCO₃ (5 mL) and brine solution (5 mL) and dried over Na₂SO₄ and concentrated *in vacuo*. The crude product was purified by preparative TLC (Silica gel, 30:1 DCM: Acetone) to give the product (109 mg, 92%) as a pale yellow solid. ¹H NMR (400 MHz, CDCl₃) δ 8.12 (s, 1H), 7.73 (s, 1H), 7.38 (p, *J* = 8.5 Hz, 2H), 7.11 – 6.95 (m, 1H), 6.85 (s, 1H), 3.25 (dt, *J* = 14.6, 6.6 Hz, 2H), 2.39 (t, *J* = 7.4 Hz, 2H), 1.82 – 1.68 (m, 2H), 1.63 (dd, *J* = 14.8, 7.3 Hz, 2H), 1.56 – 1.47 (m, 9H), 1.50 – 1.34 (m, 2H).

3.10.1.5. *tert*-butyl (2-(4-azidoheptanamido)-4-(thiophen-2-yl)phenyl)carbamate (**8b**)

4-Azidoheptanoic acid **7b** (687 mg, 4.01 mmol) was dissolved in anhydrous DMF (10 mL) followed by adding EDCI (767 mg, 4.01 mmol) and HOBT (542 mg, 4.01 mmol). After 30 minutes of stirring at room temperature, compound **6** (832 mg, 2.87 mmol) was added and then the reaction mixture was heated to 70 °C for 6 h. The reaction mixture stirred at reflux overnight. Then it was washed with water (3×10 mL), NaHCO₃ (5 mL) and brine solution (5 mL) and dried over Na₂SO₄ and concentrated *in vacuo*. The crude product was purified by column chromatography (Silica gel, 40:1 DCM: Acetone) to give the product (953 mg, 75%) as a pale yellow solid. ¹H NMR (400 MHz, CDCl₃) δ 8.02 (s, 1H), 7.75 (s, 1H), 7.48 – 7.28 (m, 2H), 7.05 (dd, *J* = 5.0, 3.7 Hz, 1H), 6.83 (s, 1H), 3.26 (dd, *J* = 16.5, 9.5 Hz, 2H), 2.40 (t, *J* = 7.4 Hz, 2H), 1.72 (d, *J* = 31.7 Hz, 2H), 1.66 – 1.58 (m, 2H), 1.54 (d, *J* = 15.0 Hz, 9H), 1.39 (d, *J* = 25.7 Hz, 2H).

3.10.1.6. *tert*-butyl (2-(4-azidooctanamido)-4-(thiophen-2-yl)phenyl)carbamate (**8c**)

4-Azidooctanoic acid **7c** (808 mg, 4.36 mmol) was dissolved in anhydrous DMF (10 mL) followed by adding EDCI (833 mg, 4.36 mmol) and HOBT (589 mg, 4.36 mmol). After 30 minutes of stirring at room temperature, compound **6** (908 mg, 3.11 mmol) was added and then the reaction mixture was heated to 70 °C for 6 h. The reaction mixture stirred at reflux overnight. Then it was washed with water (3×10 mL), NaHCO₃ (10 mL) and brine solution (10 mL) and dried over Na₂SO₄ and concentrated *in vacuo*. The crude product was purified by column chromatography (Silica gel, 40:1 DCM: Acetone) to give the product (882 mg, 62%) as a pale yellow solid. ¹H NMR (400 MHz, CDCl₃) δ 7.98 (s, 1H), 7.75 (s, 1H), 7.40 (s, 2H), 7.13 – 6.95 (m, 1H), 6.83 (s, 1H), 3.25 (dd, *J* = 14.3, 7.5 Hz, 2H), 2.40 (t, *J* = 7.4 Hz, 2H), 1.70 (d, *J* = 44.0 Hz, 2H), 1.61 – 1.55 (m, 2H), 1.60 – 1.42 (m, 9H), 1.39 (s, 2H).

3.10.1.7. N-(2-amino-5-(thiophen-2-yl)phenyl)-4-azidohexanamide (**9a**)

Compound **8a** (224 mg, 0.52 mmol) was dissolved in 1% TFA (1 mL) in DCM (5 mL). The reaction mixture stirred for 1h at rt. The reaction mixture was quenched with NaHCO₃ (5 mL) and then brine solution (5 mL) and dried over Na₂SO₄ and concentrated *in vacuo*. The crude product was purified by column chromatography (Silica gel, 40:1 DCM: Acetone) to give the product (180 mg, 73%) a pale yellow solid. ¹H NMR (400 MHz, CDCl₃) δ 7.42 (d, *J* = 2.0 Hz, 1H), 7.31 (dt, *J* = 10.1, 5.1 Hz, 1H), 7.15 (dd, *J* = 3.6, 1.2 Hz, 1H), 7.02 (dd, *J* = 5.0, 3.6 Hz, 1H), 6.79 (d, *J* = 8.3 Hz, 1H), 3.35 – 3.21 (m, 2H), 2.42 (t, *J* = 7.5 Hz, 2H), 1.78 (dt, *J* = 15.1, 7.4 Hz, 2H), 1.64 (dd, *J* = 14.6, 7.1 Hz, 2H), 1.53 – 1.41 (m, 2H). ¹³C NMR (126 MHz, CDCl₃) δ 171.6, 144.1, 140.5, 127.7, 126.8, 126.4, 125.0, 124.4, 123.5, 123.0, 121.8, 118.6, 51.1, 36.5, 28.5, 26.6, 25.2. HRMS (ESI) *m/z* Calcd. for C₁₆H₂₀N₅S [M+H⁺]: 330.1383, found for 330.1382.

3.10.1.8. N-(2-amino-5-(thiophen-2-yl)phenyl)-4-azidoheptanamide (9b)

Compound **8b** (953 mg, 2.15 mmol) was dissolved in 1% TFA (1 mL) in DCM (5 mL). The reaction mixture stirred for 1 h at rt. The reaction mixture was quenched with NaHCO₃ (5 mL) and then brine solution (5 mL) and dried over Na₂SO₄ and concentrated *in vacuo*. The crude product was purified by column chromatography (Silica gel, 7:1 DCM: Acetone) to give the product (496 mg, 67%) a pale yellow solid. ¹H NMR (400 MHz, CDCl₃) δ 7.39 (t, *J* = 16.6 Hz, 1H), 7.31 (dt, *J* = 10.0, 5.0 Hz, 1H), 7.21 – 7.13 (m, 2H), 7.02 (dd, *J* = 5.0, 3.6 Hz, 1H), 6.79 (d, *J* = 8.2 Hz, 1H), 3.93 (s, 2H), 3.37 – 3.19 (m, 2H), 2.54 – 2.23 (m, 2H), 1.77 (d, *J* = 6.9 Hz, 2H), 1.63 – 1.55 (m, 2H), 1.41 (dd, *J* = 10.2, 6.3 Hz, 2H). ¹³C NMR (126 MHz, CDCl₃) δ 171.6, 144.1, 140.5, 128.0, 126.1, 125.2, 124.5, 123.5, 122.8, 121.8, 118.6, 51.4, 36.8, 29.0, 28.7, 26.4, 25.4. HRMS (ESI) *m/z* Calcd. for C₁₇H₂₂ON₅S [M+H⁺]: 344.1540, found for 344.1537.

3.10.1.9. N-(2-amino-5-(thiophen-2-yl)phenyl)-4-azido-octanamide (9c)

Compound **8c** (882 mg, 1.93 mmol) was dissolved in 1% TFA (1 mL) in DCM (5 mL). The reaction mixture stirred for 1 h at rt. The reaction mixture was quenched with NaHCO₃ (5 mL) and then brine solution (5 mL) and dried over Na₂SO₄ and concentrated *in vacuo*. The crude product was purified by column chromatography (Silica gel, 70:1 DCM: Acetone) to give the product (163 mg, 45%) a pale yellow solid. ¹H NMR (400 MHz, CDCl₃) δ 10.62 (s, 1H), 7.79 (d, *J* = 1.4 Hz, 1H), 7.53 (dt, *J* = 8.4, 5.0 Hz, 2H), 7.25 – 7.16 (m, 1H), 7.05 (dd, *J* = 5.1, 3.6 Hz, 1H), 3.09 (dt, *J* = 14.7, 7.1 Hz, 2H), 2.97 (t, *J* = 7.7 Hz, 2H), 1.95 – 1.75 (m, 2H), 1.42 (ddd, *J* = 17.0, 12.1, 11.1 Hz, 2H), 1.31 – 1.07 (m, 4H).

3.10.1.10. 3'-Desmethylazithromycin (**11**)

To a solution of azithromycin **10** (20 g, 0.02 mmol) and sodium acetate (29 g, 0.21 mmol) in 80% aqueous methanol (50 mL) at 90 °C. Iodine (7 g, 0.03 mmol) was added in three batches within 5 min. The mixture was maintained at pH 8-9 by addition of 1 M NaOH (once at 10 min of reaction time), and stirring continued for 3 h. The mixture was poured into cold water containing 5% sodium thiosulfate and extracted with CH₂Cl₂ (2×40 mL). The aqueous layer was basified with concentrated NH₄OH and extracted with 10% MeOH in CH₂Cl₂ (3×40 mL), and the organic layer was dried over Na₂SO₄. Solvent was evaporated off to give 17.7 g of compound **13** as an off-white solid (>90% purity, TLC, CH₂Cl₂/MeOH/NH₄OH 12:1:0.1). The crude **13** was used without further purification.

3.10.1.11. (3'-N-(4-ethynylbenzyl)) azithromycin (**13**)

Desmethyl azithromycin **11** (2.72 g, 3.70 mmol) was dissolved in anhydrous acetonitrile (15 mL), followed by addition of 4-ethynylbenzyl methanesulfonate **12** (1.46 g, 6.94 mmol) and K₂CO₃ (3.58 g, 25.91 mmol). The reaction stirred at 80 °C for 3 h. Then it was washed with EtOAc (3×30 mL), NaHCO₃ (10 mL) and brine solution (10 mL) and dried over Na₂SO₄ and concentrated *in vacuo*. The crude product was purified by column chromatography (Silica gel, 12:1:0.5 DCM: MeOH: NH₄OH) to give the product (3.03 g, 96%) as a white solid.

3.10.1.12. Azithromycin-3'-(N-(4-triazolylbenzyl))- N-(2-amino-5-(thiophen-2-yl)phenyl) hexanamide (**14a**)

(3'-N-(4-Ethynylbenzyl))azithromycin **13** (127 mg, 0.15 mmol) and N-(2-amino-5-(thiophen-2-yl)phenyl)-4-azidohexanamide **9a** (49 mg, 0.15 mmol) were dissolved in degassed anhydrous THF (5 mL). CuI (8 mg, 0.075 mmol) and Hünig's base (0.05 mL, 0.30 mmol) were added to the reaction and the resulting reaction was stirred at room

temperature overnight. Then, the reaction mixture was diluted with excess ethyl acetate (30 mL) and was transferred to a separatory funnel and then the ethyl acetate layer was washed with a solution (20 mL) of 4:1 mixture of saturated aqueous NH_4Cl solution / NH_4OH solution, water (10 mL), brine (10 mL), dried over anhydrous Na_2SO_4 , filtered, and concentrated *in vacuo*. The crude was purified by preparative chromatography (Silica gel, 30:1:0.5 EtOAc/MeOH/ NH_4OH) to give the title compound **14a** (111 mg, 63%) as a light yellow solid. ^1H NMR (400 MHz, CD_3OD) δ 8.33 (s, 1H), 7.76 (d, J = 8.3 Hz, 2H), 7.43 (d, J = 8.1 Hz, 2H), 7.30 (dd, J = 8.3, 2.1 Hz, 1H), 7.22 (d, J = 5.1 Hz, 1H), 7.20 – 7.13 (m, 1H), 7.00 (dd, J = 5.1, 3.6 Hz, 1H), 6.84 (d, J = 8.3 Hz, 1H), 4.98 (d, J = 18.1 Hz, 2H), 4.48 (dd, J = 17.6, 7.1 Hz, 2H), 4.25 – 3.98 (m, 3H), 3.61 (d, J = 16.0 Hz, 3H), 3.16 (s, 2H), 2.99 (d, J = 9.4 Hz, 1H), 2.79 (s, 2H), 2.42 (dd, J = 19.9, 12.7 Hz, 3H), 2.31 (d, J = 21.5 Hz, 4H), 2.06 – 1.93 (m, 6H), 1.95 – 1.84 (m, 14H), 1.76 (d, J = 8.7 Hz, 3H), 1.39 (dd, J = 57.2, 29.4 Hz, 10H), 1.32 – 1.18 (m, 8H), 1.19 (dd, J = 16.9, 11.3 Hz, 8H), 1.13 (d, J = 14.6 Hz, 3H), 1.08 (d, J = 17.2 Hz, 4H), 1.08 – 0.98 (m, 3H), 0.98 – 0.85 (m, 6H). ^{13}C NMR (126 MHz, CD_3OD) δ 178.4, 175.1, 173.7, 155.3, 147.3, 144.2, 141.7, 129.4, 127.5, 125.6, 125.0, 124.4, 123.8, 122.8, 122.3, 121.1, 120.7, 117.1, 102.5, 83.2, 77.7, 76.3, 74.0, 72.6, 71.2, 67.9, 65.0, 63.9, 62.7, 60.3, 60.1, 57.0, 56.0, 55.8, 49.9, 45.2, 42.0, 35.3, 34.6, 30.4, 29.2, 28.0, 25.6, 24.9, 21.1, 20.6, 20.2, 20.0, 19.5, 18.8, 17.6, 16.2, 15.8, 13.8, 13.2, 12.6, 12.2, 10.3, 8.4. HRMS (ESI) m/z Calcd. for $\text{C}_{62}\text{H}_{97}\text{O}_{13}\text{N}_7\text{S}$ [$\text{M}+2\text{H}^+/2$]: 589.8424, found for 589.8421.

3.10.1.13. Azithromycin-3'-(N-(4-triazolylbenzyl)))- N-(2-amino-5-(thiophen-2-yl)phenyl) heptanamide (**14b**)

(3'-N-(4-Ethynylbenzyl))azithromycin **13** (257 mg, 0.30 mmol) and N-(2-amino-5-(thiophen-2-yl)phenyl)-4-azidoheptanamide **9b** (104 mg, 0.30 mmol) were dissolved in degassed anhydrous THF (5 mL). CuI (29 mg, 0.15 mmol) and Hünig's base (0.10 mL, 0.60 mmol) were added to the reaction and the resulting reaction was stirred at room

temperature overnight. Then, the reaction mixture was diluted with excess ethyl acetate (30 mL) and was transferred to a separatory funnel and then the ethyl acetate layer was washed with a solution (20 mL) of 4:1 mixture of saturated aqueous NH_4Cl solution / NH_4OH solution, water (10 mL), brine (10 mL), dried over anhydrous Na_2SO_4 , filtered, and concentrated *in vacuo*. The crude was purified by preparative chromatography (Silica gel, 30:1:0.5 EtOAc/MeOH/ NH_4OH) to give the title compound **14b** (256 mg, 71%) as a light yellow solid. ^1H NMR (400 MHz, CD_3OD) δ 8.16 (s, 1H), 7.61 (d, J = 8.2 Hz, 2H), 7.27 (dd, J = 9.4, 5.1 Hz, 3H), 7.16 (dd, J = 8.3, 2.2 Hz, 1H), 7.10 – 7.03 (m, 2H), 7.03 (dd, J = 3.6, 1.0 Hz, 1H), 6.86 (dd, J = 5.1, 3.6 Hz, 1H), 6.71 (d, J = 8.3 Hz, 1H), 4.85 (t, J = 12.7 Hz, 1H), 4.71 (dd, J = 10.1, 2.5 Hz, 2H), 4.34 (dd, J = 22.9, 7.1 Hz, 2H), 4.31 (t, J = 6.9 Hz, 2H), 4.12 – 3.95 (m, 2H), 3.68 (d, J = 13.1 Hz, 1H), 3.50 (ddd, J = 45.5, 18.6, 8.4 Hz, 4H), 3.21 – 3.11 (m, 4H), 3.03 (s, 3H), 2.85 (d, J = 9.5 Hz, 1H), 2.64 (dt, J = 18.8, 9.2 Hz, 3H), 2.29 (t, J = 7.4 Hz, 2H), 2.21 (d, J = 15.5 Hz, 4H), 2.13 (s, 4H), 1.85 (dd, J = 14.2, 7.0 Hz, 4H), 1.76 – 1.54 (m, 5H), 1.44 – 1.21 (m, 8H), 1.17 (d, J = 24.4 Hz, 6H), 1.12 (t, J = 7.9 Hz, 4H), 1.09 – 0.98 (m, 7H), 0.96 (dd, J = 20.5, 14.4 Hz, 8H), 0.91 (d, J = 7.5 Hz, 4H), 0.76 (dd, J = 15.3, 7.6 Hz, 6H). ^{13}C NMR (101 MHz, CD_3OD) δ 209.7, 178.1, 173.6, 163.1, 157.6, 148.5, 145.8, 144.2, 129.3, 128.6, 127.4, 126.0, 125.2, 124.5, 123.1, 122.6, 121.1, 120.5, 117.4, 115.9, 114.7, 114.0, 105.9, 102.5, 94.9, 82.9, 78.1, 77.6, 76.7, 74.3, 72.9, 71.2, 67.8, 65.9, 65.2, 62.8, 57.3, 52.3, 49.9, 38.9, 35.8, 35.3, 35.0, 34.6, 30.7, 29.5, 28.1, 26.4, 26.0, 25.2, 21.2, 20.7, 20.2, 17.8, 15.9, 14.2, 10.4, 8.5, 5.4, 5.1, 1.3. HRMS (ESI) m/z Calcd. for $\text{C}_{63}\text{H}_{99}\text{O}_{13}\text{N}_7\text{S}$ [$\text{M}+2\text{H}^+/2$]: 596.8505, found for 598.8502.

3.10.1.14. Azithromycin-3'-(*N*-(4-triazolylbenzyl)))- *N*-(2-amino-5-(thiophen-2-yl)phenyl) octanamide (**14c**)

(3'-*N*-(4-Ethynylbenzyl))azithromycin **13** (118 mg, 0.14 mmol) and *N*-(2-amino-5-(thiophen-2-yl)phenyl)-4-azidooctanamide **9c** (50 mg, 0.14 mmol) were dissolved in

degassed anhydrous THF (5 mL). CuI (13 mg, 0.07 mmol) and Hünig's base (0.05 mL, 0.27 mmol) were added to the reaction and the resulting reaction was stirred at room temperature overnight. Then, the reaction mixture was diluted with excess ethyl acetate (30 mL) and was transferred to a separatory funnel and then the ethyl acetate layer was washed with a solution (20 mL) of 4:1 mixture of saturated aqueous NH_4Cl solution / NH_4OH solution, water (10 mL), brine (10 mL), dried over anhydrous Na_2SO_4 , filtered, and concentrated *in vacuo*. The crude was purified by preparative chromatography (Silica gel, 30:1:0.5 EtOAc/MeOH/ NH_4OH) to give the title compound **14c** (78 mg, 47%) as a light yellow solid. ^1H NMR (400 MHz, CDCl_3) δ 7.74 (dd, J = 15.3, 12.0 Hz, 3H), 7.50 (t, J = 5.8 Hz, 1H), 7.40 – 7.29 (m, 3H), 7.15 (dd, J = 8.0, 4.3 Hz, 2H), 7.01 (dd, J = 5.0, 3.7 Hz, 1H), 6.78 (d, J = 8.4 Hz, 1H), 5.05 (d, J = 4.4 Hz, 1H), 4.70 (s, 1H), 4.39 (dt, J = 16.8, 8.5 Hz, 3H), 4.23 (d, J = 2.8 Hz, 1H), 4.07 – 3.90 (m, 2H), 3.83 – 3.71 (m, 1H), 3.66 (d, J = 22.0 Hz, 1H), 3.60 (d, J = 7.2 Hz, 1H), 3.53 – 3.38 (m, 3H), 3.36 (d, J = 10.6 Hz, 1H), 2.98 (t, J = 9.8 Hz, 1H), 2.87 (s, 1H), 2.75 (s, 2H), 2.54 (s, 2H), 2.40 (dd, J = 18.5, 10.7 Hz, 5H), 2.26 (d, J = 19.7 Hz, 5H), 2.17 (s, 1H), 2.12 – 2.01 (m, 2H), 2.02 – 1.81 (m, 5H), 1.82 – 1.65 (m, 4H), 1.57 – 1.45 (m, 2H), 1.45 – 1.28 (m, 13H), 1.24 (dt, J = 20.9, 9.4 Hz, 11H), 1.19 – 1.13 (m, 4H), 1.07 (t, J = 12.9 Hz, 8H), 1.03 (d, J = 7.5 Hz, 3H), 0.99 – 0.79 (m, 6H). ^{13}C NMR (126 MHz, CDCl_3) δ 178.9, 172.2, 147.5, 144.4, 140.5, 129.8, 129.5, 128.0, 127.4, 126.1, 125.9, 124.8, 123.6, 123.0, 121.8, 119.6, 118.4, 102.9, 94.6, 83.5, 74.2, 73.8, 73.3, 72.8, 70.6, 69.9, 68.7, 65.5, 64.2, 61.7, 57.7, 56.0, 50.3, 49.3, 45.4, 42.6, 42.1, 36.9, 36.6, 36.3, 34.6, 32.0, 30.1, 29.6, 29.3, 28.8, 28.3, 27.5, 26.8, 26.0, 25.4, 22.7, 22.1, 21.5, 21.3, 18.0, 16.4, 14.6, 14.2, 11.3, 8.9, 7.5. HRMS (ESI) m/z Calcd. for $\text{C}_{63}\text{H}_{101}\text{O}_{13}\text{N}_7\text{S}$ [$\text{M}+2\text{H}^+/2$]: 603.8584, found for 603.8591.

3.10.2. Cell viability assay

All cell lines used in this study were maintained in phenol red free Dulbecco's Modified Eagle Medium (DMEM) (Corning, VA), supplemented with 10% fetal bovine serum (FBS) (Atlanta Biologicals, Atlanta, GA) and 1% *Penicillin-Streptomycin*. Cells were incubated in 96 well plate for 24 h prior to treatment and then treated with various drugs' concentration for 72 h. Their anti-proliferative activity was measured using the MTS assay (CellTiter 96 Aqueous One Solution and CellTiter 96 Non-Radioactive Cell Proliferation Assays, Promega, Madison, WI) as described by the manufacturer. All drugs solution were made in DMEM while DMSO concentration was maintained at 0.1%.

3.10.3. SAMDI assay (*In vitro* HDAC inhibition, performed by Dr. James Kornaki at Northwestern University)

HDAC1, 2, 3, and 6 were purchased from BPS Biosciences. To obtain IC₅₀ values, in a 96-well microtiter plates (60 min, 37 °C), isoform- optimized substrates (50 µM) were incubated with enzyme (250nM) and inhibitor (at concentrations ranging from 0.1 nM to 1.0 mM) in HDAC buffer (25.0 mM Tris-HCl, pH 8.0, 140 mM NaCl, 3.0 mM KCl, 1.0 mM MgCl₂, and 0.1 mg/mL BSA). Solution-phase deacetylation reactions were quenched with trichostatin A (TSA) and transferred to SAMDI plates to immobilize the substrate components. SAMDI plates were consist of an array of self-assembled monolayers (SAMs) presenting maleimide in standard 384-well format for high-throughput handling capability. Following immobilization, plates were washed to remove buffer constituents, enzyme, inhibitor, and any unbound substrate and analyzed by MALDI mass spectrometry using automated protocols. Deacetylation yields in each triplicate sample were obtained from the integrated peak intensities of the molecular ions

for the substrate and the deacetylated product ion by taking the ratio of the former over the sum of both. Yields were plotted with respect to inhibitor concentration and fitted to obtain IC₅₀ values for each isoform–inhibitor pair.

Isoform-optimized substrates were prepared by traditional Fmoc solid-phase peptide synthesis (Anaspec) and purified by semi-preparative HPLC on a reverse-phase C18 column (Waters). The peptide GRK^{ac}FGC was prepared for HDAC1 and HDAC8 experiments, whereas the peptide GRK^{ac}YGC was prepared for HDAC6 experiments.

3.10.4. *In vitro* HDAC inhibition (Performed through contractual agreement with BPS Bioscience)

HDAC inhibition was performed via Fluor de Lys assay. This assay is based on Fluorimetric Histone deAcetylaseLysyl substrate and developer combination. First the substrate with the acetylated lysine chain is incubated with HDAC enzymes. Then the developer is added which results in generating a fluorophore.

To perform the *in vitro* HDAC inhibition assay, different concentration of HDACi with 10% DMSO in HDAC assay buffer were prepared and added to the enzymatic reaction containing HDAC assay buffer, BSA, substrate and enzyme (all the HDAC isoforms) in 96 well plate. Developer was then added to each well and the plate was incubated at room temperature for 15 minutes. Fluorescent intensity at the certain wavelengths was measured using Biotek Synergy microplate reader. Fluorescent intensities were measured in the absence and presence of the compounds as well as in the absence of HDAC, and the data was analyzed using Graphpad Prism. IC₅₀ value for each compound was determined by the concentration leading to a half-maximal percent inhibition.

3.11. References

1. Falkenberg, K. J.; Johnstone, R. W. Histone deacetylases and their inhibitors in cancer, neurological diseases and immune disorders. *Nature reviews Drug discovery* **2014**, 13, 673-691.
2. Tapadar, S.; Fathi, S.; Raji, I.; Omesiete, W.; Kornacki, J. R.; Mwakwari, S. C.; Miyata, M.; Mitsutake, K.; Li, J.-D.; Mrksich, M. A structure–activity relationship of non-peptide macrocyclic histone deacetylase inhibitors and their anti-proliferative and anti-inflammatory activities. *Bioorganic & Medicinal Chemistry* **2015**, 23, 7543-7564.
3. Lee, Y.-H.; Seo, D.; Choi, K.-J.; Andersen, J. B.; Won, M.-A.; Kitade, M.; Gómez-Quiroz, L. E.; Judge, A. D.; Marquardt, J. U.; Raggi, C. Antitumor effects in hepatocarcinoma of isoform-selective inhibition of HDAC2. *Cancer research* **2014**, 74, 4752-4761.
4. Gryder, B. E.; Sodji, Q. H.; Oyelere, A. K. Targeted cancer therapy: giving histone deacetylase inhibitors all they need to succeed. *Future medicinal chemistry* **2012**, 4, 505-524.
5. Di Micco, S.; Chini, M. G.; Terracciano, S.; Bruno, I.; Riccio, R.; Bifulco, G. Structural basis for the design and synthesis of selective HDAC inhibitors. *Bioorganic & medicinal chemistry* **2013**, 21, 3795-3807.
6. Marks, P. A.; Breslow, R. Dimethyl sulfoxide to vorinostat: development of this histone deacetylase inhibitor as an anticancer drug. *Nature biotechnology* **2007**, 25, 84-90.
7. Furumai, R.; Matsuyama, A.; Kobashi, N.; Lee, K.-H.; Nishiyama, M.; Nakajima, H.; Tanaka, A.; Komatsu, Y.; Nishino, N.; Yoshida, M. FK228 (depsipeptide) as a natural prodrug that inhibits class I histone deacetylases. *Cancer research* **2002**, 62, 4916-4921.
8. Campbell, P.; Thomas, C. M. Belinostat for the treatment of relapsed or refractory peripheral T-cell lymphoma. *Journal of Oncology Pharmacy Practice* **2016**, 1078155216634178.
9. Kjær, A. S. H. K.; Brinkmann, C. R.; Dinarello, C. A.; Olesen, R.; Østergaard, L.; Søgaaard, O. S.; Tolstrup, M.; Rasmussen, T. A. The histone deacetylase inhibitor panobinostat lowers biomarkers of cardiovascular risk and inflammation in HIV patients. *Aids* **2015**, 29, 1195-1200.
10. Pan, D.-S.; Yang, Q.-J.; Fu, X.; Shan, S.; Zhu, J.-Z.; Zhang, K.; Li, Z.-B.; Ning, Z.-Q.; Lu, X.-P. Discovery of an orally active subtype-selective HDAC inhibitor, chidamide, as an epigenetic modulator for cancer treatment. *MedChemComm* **2014**, 5, 1789-1796.

11. Chang, C.; Zhao, S.; Guo, J.; Zhao, Y.; Fei, C.; Gu, S.; Li, X. Chidamide, a Novel Histone Deacetylase Inhibitor, Displays Potent Antitumor Activity Against MDS Cells Mainly through JAK2/STAT3 Signaling Inhibition. *Blood* **2015**, 126, 5233-5233.
12. Bruserud, O.; Stapnes, C.; Ersvaer, E.; Gjertsen, B.; Rynningen, A. Histone deacetylase inhibitors in cancer treatment: a review of the clinical toxicity and the modulation of gene expression in cancer cells. *Current pharmaceutical biotechnology* **2007**, 8, 388-400.
13. Witt, O.; Deubzer, H. E.; Milde, T.; Oehme, I. HDAC family: What are the cancer relevant targets? *Cancer letters* **2009**, 277, 8-21.
14. Frey, R. R.; Wada, C. K.; Garland, R. B.; Curtin, M. L.; Michaelides, M. R.; Li, J.; Pease, L. J.; Glaser, K. B.; Marcotte, P. A.; Bouska, J. J. Trifluoromethyl ketones as inhibitors of histone deacetylase. *Bioorganic & medicinal chemistry letters* **2002**, 12, 3443-3447.
15. Shen, S.; Kozikowski, A. P. Why Hydroxamates May Not Be the Best Histone Deacetylase Inhibitors—What Some May Have Forgotten or Would Rather Forget? *ChemMedChem* **2015**.
16. Balasubramanian, S.; Verner, E.; Buggy, J. J. Isoform-specific histone deacetylase inhibitors: the next step? *Cancer letters* **2009**, 280, 211-221.
17. Guha, M. HDAC inhibitors still need a home run, despite recent approval. *Nature Reviews Drug Discovery* **2015**, 14, 225-226.
18. Wong, J. C.; Hong, R.; Schreiber, S. L. Structural biasing elements for in-cell histone deacetylase paralog selectivity. *Journal of the American Chemical Society* **2003**, 125, 5586-5587.
19. Bressi, J. C.; Jennings, A. J.; Skene, R.; Wu, Y.; Melkus, R.; De Jong, R.; O'Connell, S.; Grimshaw, C. E.; Navre, M.; Gangloff, A. R. Exploration of the HDAC2 foot pocket: Synthesis and SAR of substituted N-(2-aminophenyl) benzamides. *Bioorganic & medicinal chemistry letters* **2010**, 20, 3142-3145.
20. Finnin, M. S.; Donigian, J. R.; Cohen, A.; Richon, V. M.; Rifkind, R. A.; Marks, P. A.; Breslow, R.; Pavletich, N. P. Structures of a histone deacetylase homologue bound to the TSA and SAHA inhibitors. *Nature* **1999**, 401, 188-193.
21. Wang, D.-F.; Wiest, O.; Helquist, P.; Lan-Hargest, H.-Y.; Wiech, N. L. On the function of the 14 Å long internal cavity of histone deacetylase-like protein: implications for the design of histone deacetylase inhibitors. *Journal of medicinal chemistry* **2004**, 47, 3409-3417.
22. Wang, D.-F.; Helquist, P.; Wiech, N. L.; Wiest, O. Toward selective histone deacetylase inhibitor design: homology modeling, docking studies, and molecular

dynamics simulations of human class I histone deacetylases. *Journal of medicinal chemistry* **2005**, 48, 6936-6947.

23. Moradei, O. M.; Mallais, T. C.; Frechette, S.; Paquin, I.; Tessier, P. E.; Leit, S. M.; Fournel, M.; Bonfils, C.; Trachy-Bourget, M.-C.; Liu, J. Novel aminophenyl benzamide-type histone deacetylase inhibitors with enhanced potency and selectivity. *Journal of medicinal chemistry* **2007**, 50, 5543-5546.

24. Mottamal, M.; Zheng, S.; Huang, T. L.; Wang, G. Histone deacetylase inhibitors in clinical studies as templates for new anticancer agents. *Molecules* **2015**, 20, 3898-3941.

25. Garcia-Manero, G.; Assouline, S.; Cortes, J.; Estrov, Z.; Kantarjian, H.; Yang, H.; Newsome, W. M.; Miller, W. H.; Rousseau, C.; Kalita, A. Phase 1 study of the oral isotype specific histone deacetylase inhibitor MGCD0103 in leukemia. *Blood* **2008**, 112, 981-989.

26. Blum, K. A.; Advani, A.; Fernandez, L.; Van Der Jagt, R.; Brandwein, J.; Kambhampati, S.; Kassis, J.; Davis, M.; Bonfils, C.; Dubay, M. Phase II study of the histone deacetylase inhibitor MGCD0103 in patients with previously treated chronic lymphocytic leukaemia. *British journal of haematology* **2009**, 147, 507-514.

27. Bieliauskas, A. V.; Pflum, M. K. H. Isoform-selective histone deacetylase inhibitors. *Chemical Society Reviews* **2008**, 37, 1402-1413.

28. Methot, J. L.; Chakravarty, P. K.; Chenard, M.; Close, J.; Cruz, J. C.; Dahlberg, W. K.; Fleming, J.; Hamblett, C. L.; Hamill, J. E.; Harrington, P. Exploration of the internal cavity of histone deacetylase (HDAC) with selective HDAC1/HDAC2 inhibitors (SHI-1: 2). *Bioorganic & medicinal chemistry letters* **2008**, 18, 973-978.

29. Saito, A.; Yamashita, T.; Mariko, Y.; Nosaka, Y.; Tsuchiya, K.; Ando, T.; Suzuki, T.; Tsuruo, T.; Nakanishi, O. A synthetic inhibitor of histone deacetylase, MS-27-275, with marked in vivo antitumor activity against human tumors. *Proceedings of the National Academy of Sciences* **1999**, 96, 4592-4597.

30. Suzuki, T.; Ando, T.; Tsuchiya, K.; Fukazawa, N.; Saito, A.; Mariko, Y.; Yamashita, T.; Nakanishi, O. Synthesis and histone deacetylase inhibitory activity of new benzamide derivatives. *Journal of medicinal chemistry* **1999**, 42, 3001-3003.

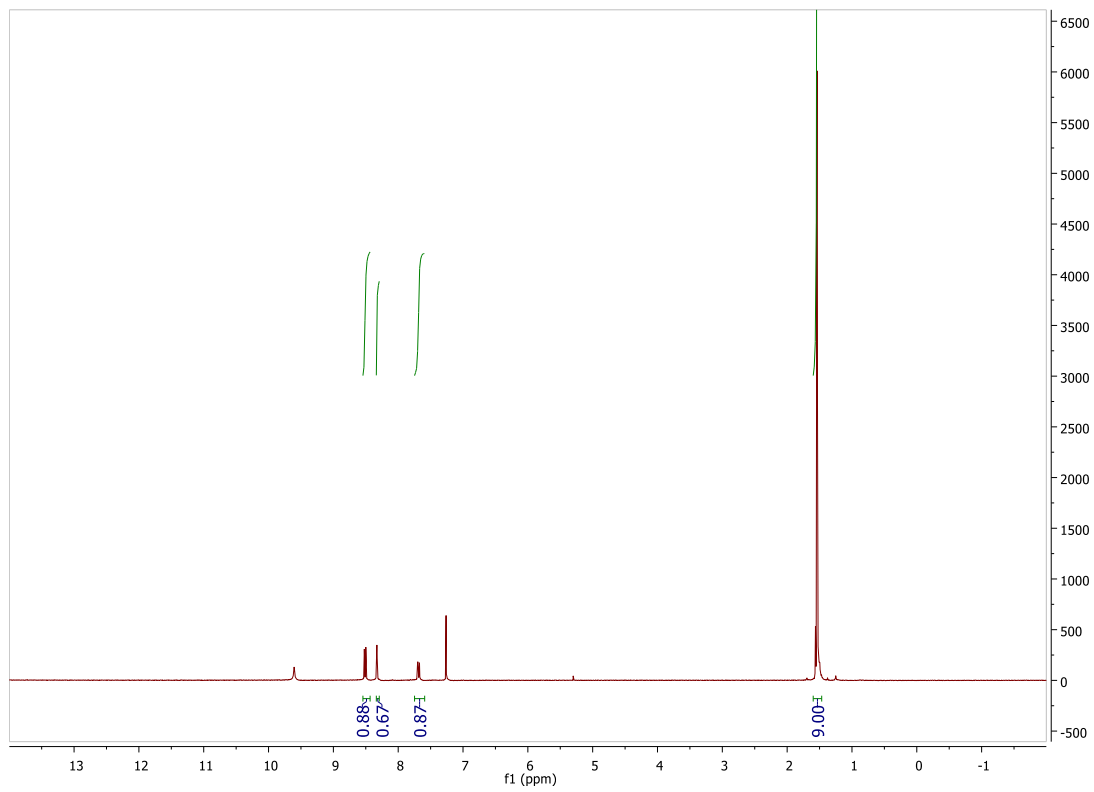
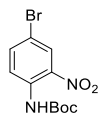
31. Mwakwari, S. C.; Guerrant, W.; Patil, V.; Khan, S. I.; Tekwani, B. L.; Gurard-Levin, Z. A.; Mrksich, M.; Oyelere, A. K. Non-peptide macrocyclic histone deacetylase inhibitors derived from tricyclic ketolide skeleton. *Journal of medicinal chemistry* **2010**, 53, 6100-6111.

32. Sodji, Q. H.; Kornacki, J. R.; McDonald, J. F.; Mrksich, M.; Oyelere, A. K. Design and structure activity relationship of tumor-homing histone deacetylase inhibitors conjugated to folic and pteric acids. *European journal of medicinal chemistry* **2015**, 96, 340-359.

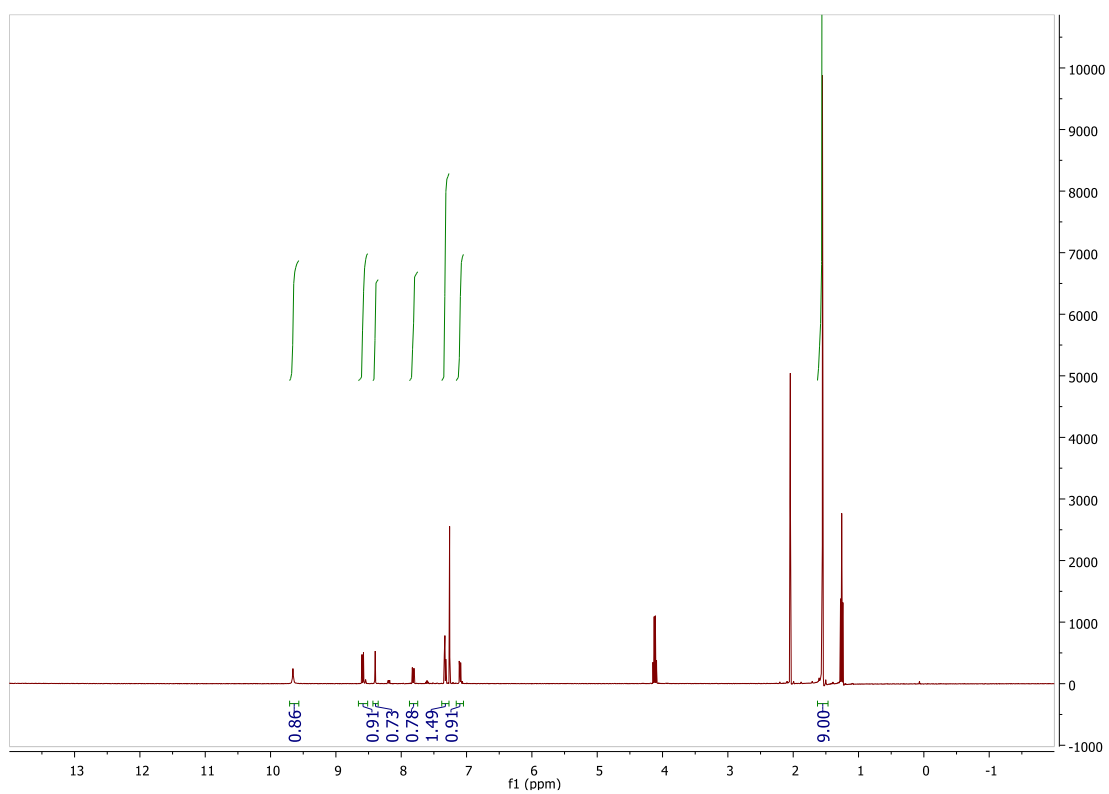
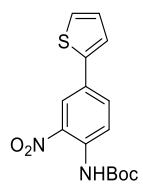
33. Mwakwari, S. C.; Patil, V.; Guerrant, W.; Oyelere, A. K. Macrocyclic histone deacetylase inhibitors. *Current topics in medicinal chemistry* **2010**, 10, 1423.
34. Miyaura, N.; Yanagi, T.; Suzuki, A. The palladium-catalyzed cross-coupling reaction of phenylboronic acid with haloarenes in the presence of bases. *Synthetic Communications* **1981**, 11, 513-519.
35. Miyaura, N.; Suzuki, A. Palladium-catalyzed cross-coupling reactions of organoboron compounds. *Chemical reviews* **1995**, 95, 2457-2483.
36. Boix, C.; Poliakoff, M. Selective reductions of nitroarenes to anilines using metallic zinc in near-critical water. *J. Chem. Soc., Perkin Trans. I* **1999**, 1487-1490.
37. Gryder, B. E.; Akbashev, M. J.; Rood, M. K.; Raftery, E. D.; Meyers, W. M.; Dillard, P.; Khan, S.; Oyelere, A. K. Selectively targeting prostate cancer with antiandrogen equipped histone deacetylase inhibitors. *ACS chemical biology* **2013**, 8, 2550-2560.
38. Han, S.-Y.; Kim, Y.-A. Recent development of peptide coupling reagents in organic synthesis. *Tetrahedron* **2004**, 60, 2447-2467.
39. Oyelere, A. K.; Chen, P. C.; Guerrant, W.; Mwakwari, S. C.; Hood, R.; Zhang, Y.; Fan, Y. Non-peptide macrocyclic histone deacetylase inhibitors. *Journal of medicinal chemistry* **2008**, 52, 456-468.
40. Rostovtsev, V. V.; Green, L. G.; Fokin, V. V.; Sharpless, K. B. A stepwise Huisgen cycloaddition process: copper (I)-catalyzed regioselective "ligation" of azides and terminal alkynes. *Angewandte Chemie* **2002**, 114, 2708-2711.
41. Fantozzi, A.; Christofori, G. Mouse models of breast cancer metastasis. *Breast Cancer Research* **2006**, 8, 1.
42. Senese, S.; Zaragoza, K.; Minardi, S.; Muradore, I.; Ronzoni, S.; Passafaro, A.; Bernard, L.; Draetta, G. F.; Alcalay, M.; Seiser, C. Role for histone deacetylase 1 in human tumor cell proliferation. *Molecular and cellular biology* **2007**, 27, 4784-4795.
43. Kawai, H.; Li, H.; Avraham, S.; Jiang, S.; Avraham, H. K. Overexpression of histone deacetylase HDAC1 modulates breast cancer progression by negative regulation of estrogen receptor α . *International journal of cancer* **2003**, 107, 353-358.
44. Zhang, Z.; Yamashita, H.; Toyama, T.; Sugiura, H.; Omoto, Y.; Ando, Y.; Mita, K.; Hamaguchi, M.; Hayashi, S.-i.; Iwase, H. HDAC6 expression is correlated with better survival in breast cancer. *Clinical Cancer Research* **2004**, 10, 6962-6968.
45. Saji, S.; Kawakami, M.; Hayashi, S.-i.; Yoshida, N.; Hirose, M.; Horiguchi, S.-i.; Itoh, A.; Funata, N.; Schreiber, S. L.; Yoshida, M. Significance of HDAC6 regulation via estrogen signaling for cell motility and prognosis in estrogen receptor-positive breast cancer. *Oncogene* **2005**, 24, 4531-4539.

3.12. Supplementary data

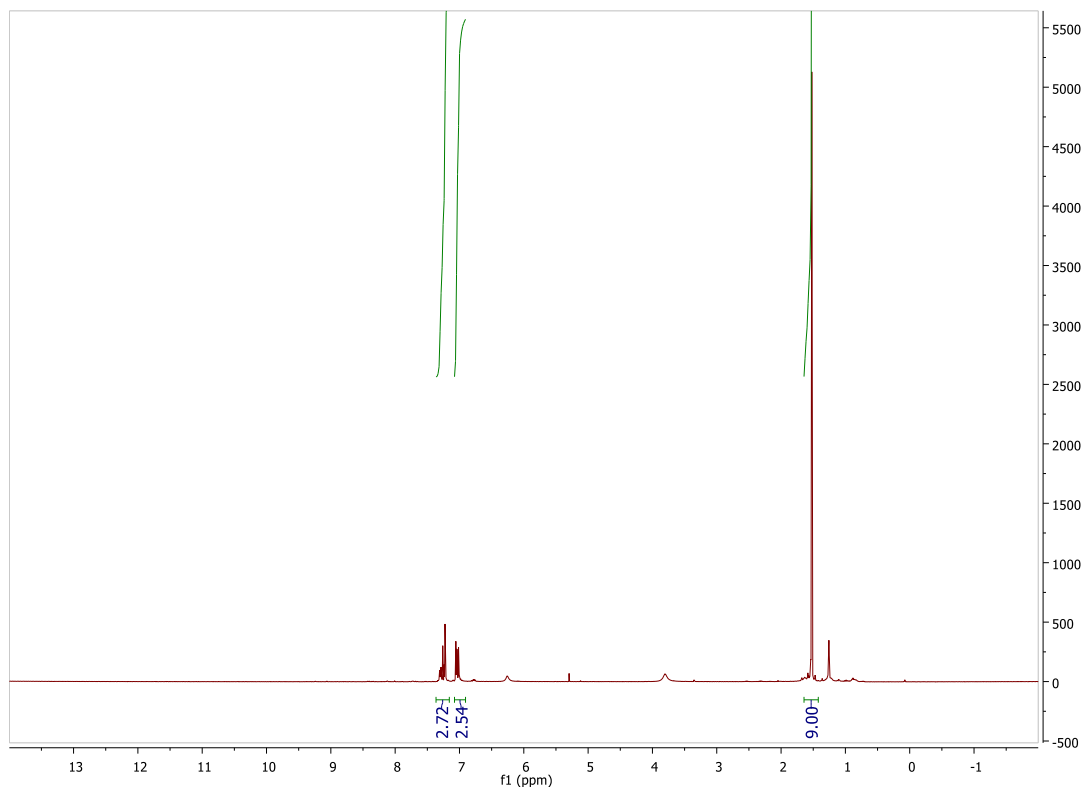
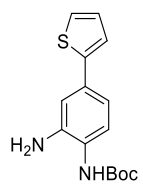
3 ¹HNMR



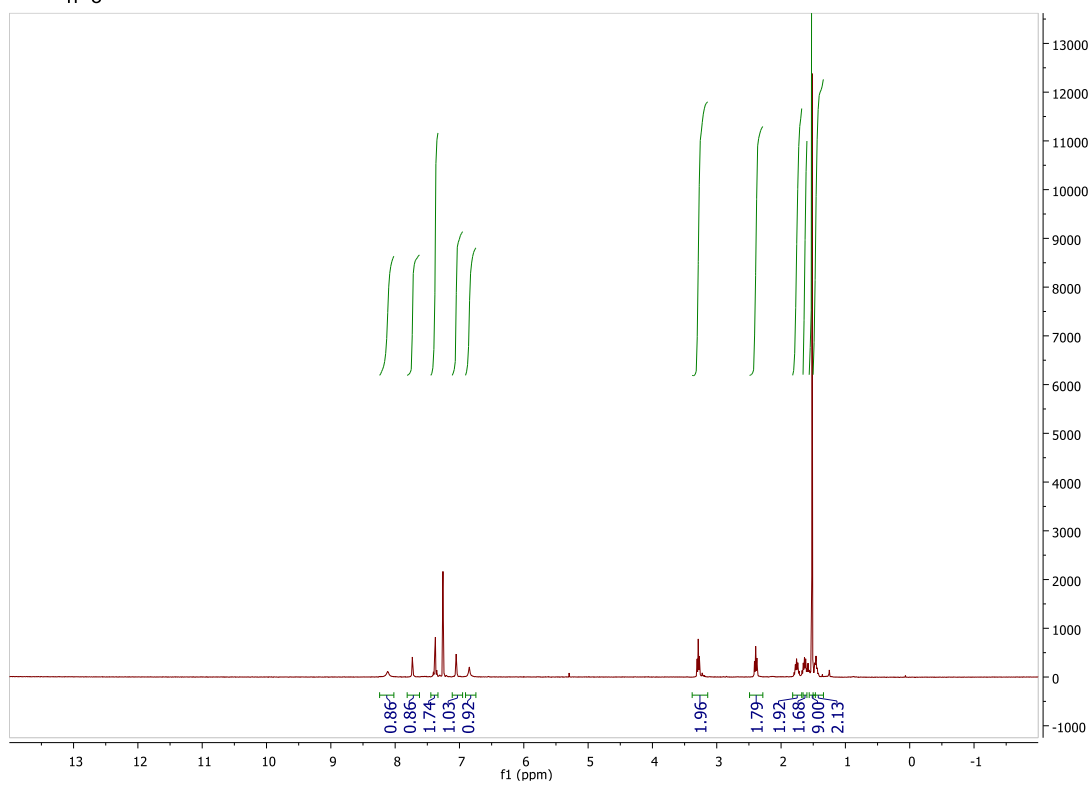
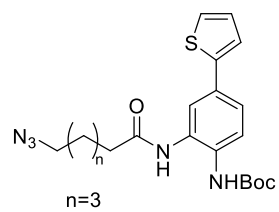
5 ¹H NMR



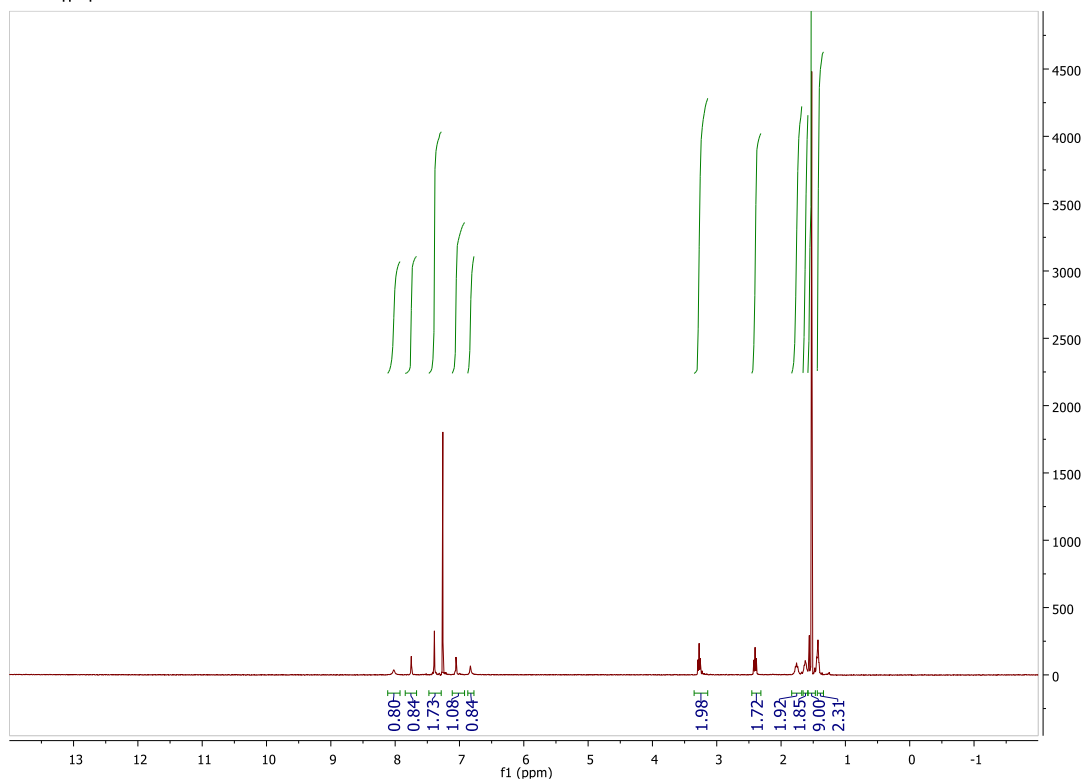
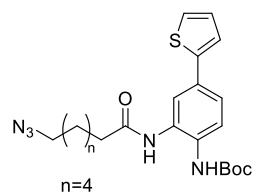
6 ^1H NMR

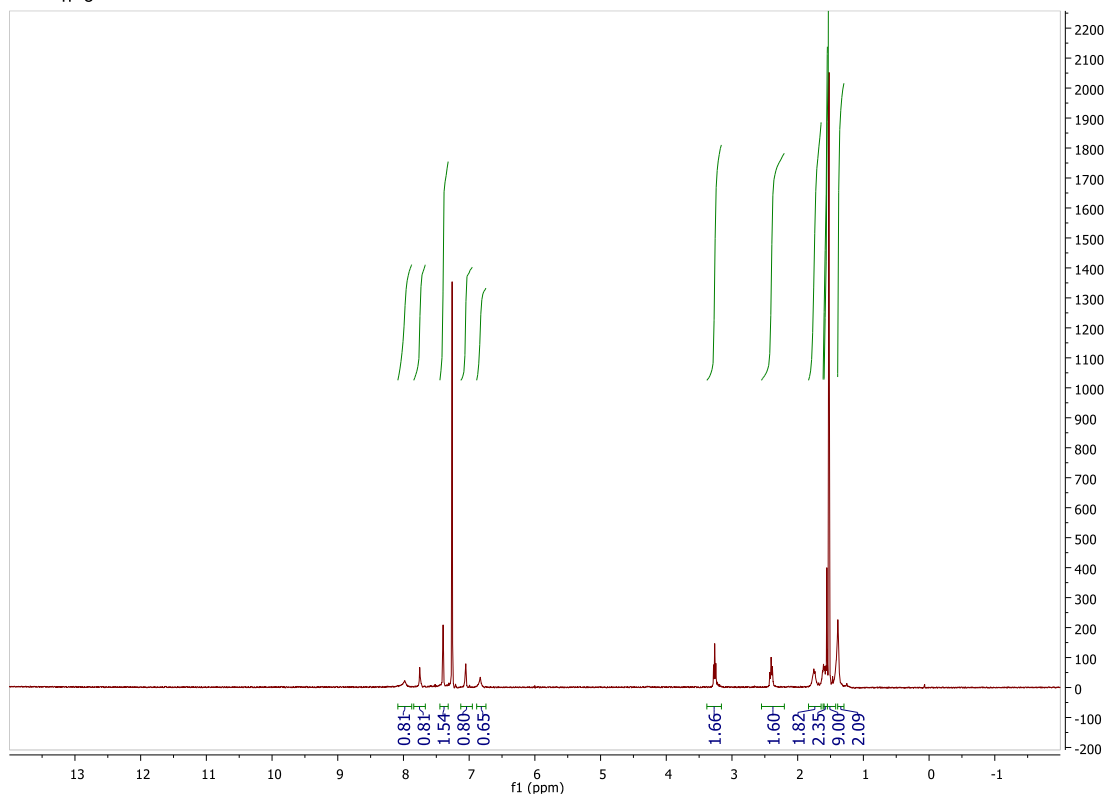


8a ^1H NMR

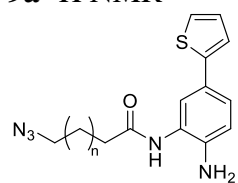


8b ^1H NMR

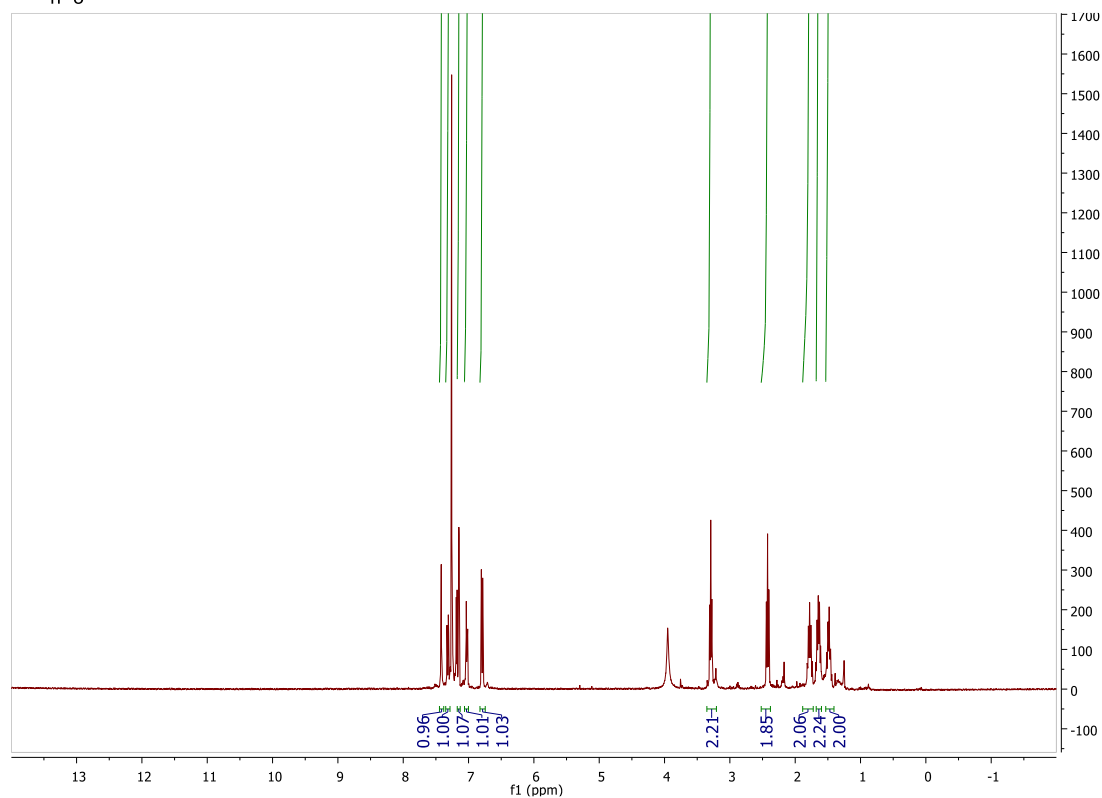


CN(C(=O)CNC1=CC=C(C=C1)SC2=CC=CC=C2S3CCCCC3)c4ccccc4
n=5

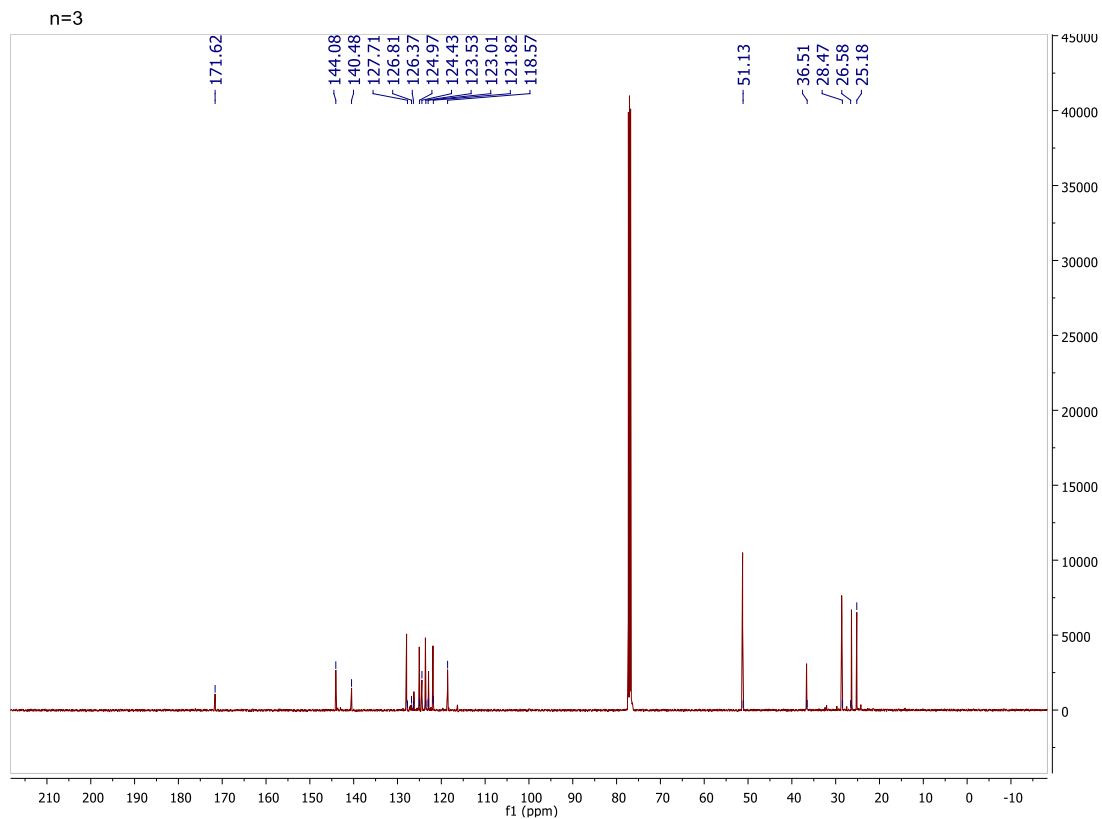
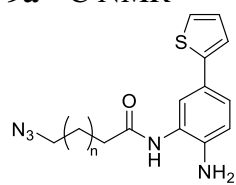
9a ^1H NMR



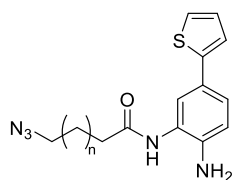
n=3



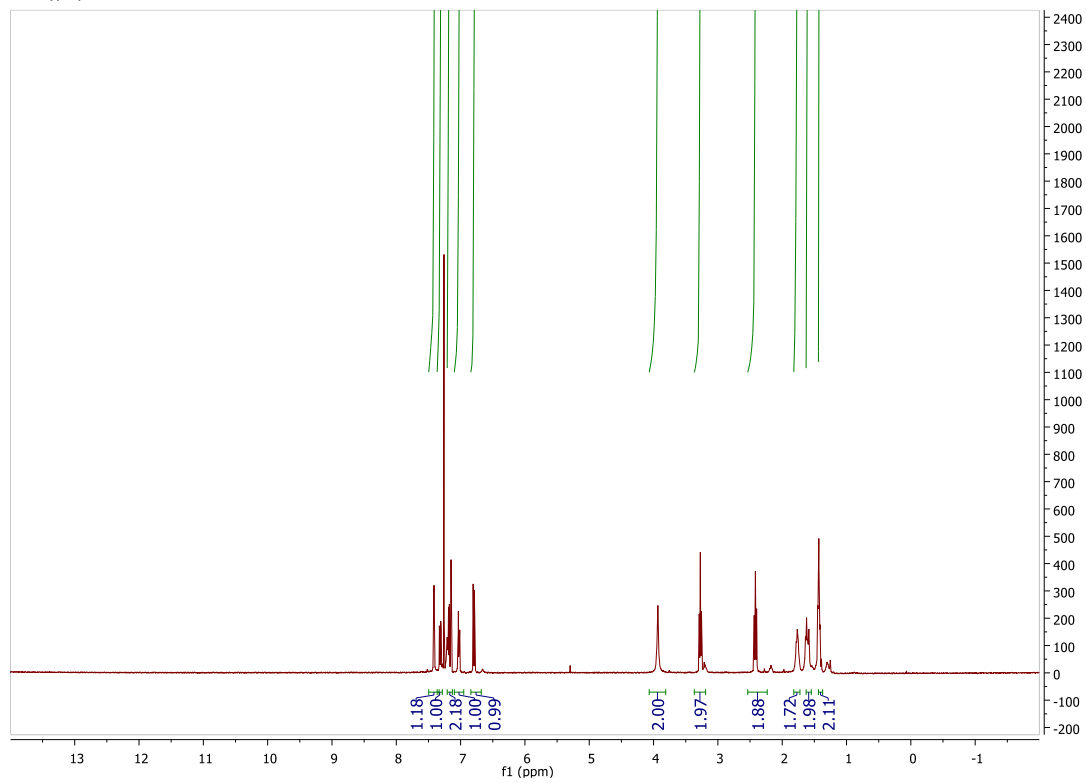
9a ^{13}C NMR



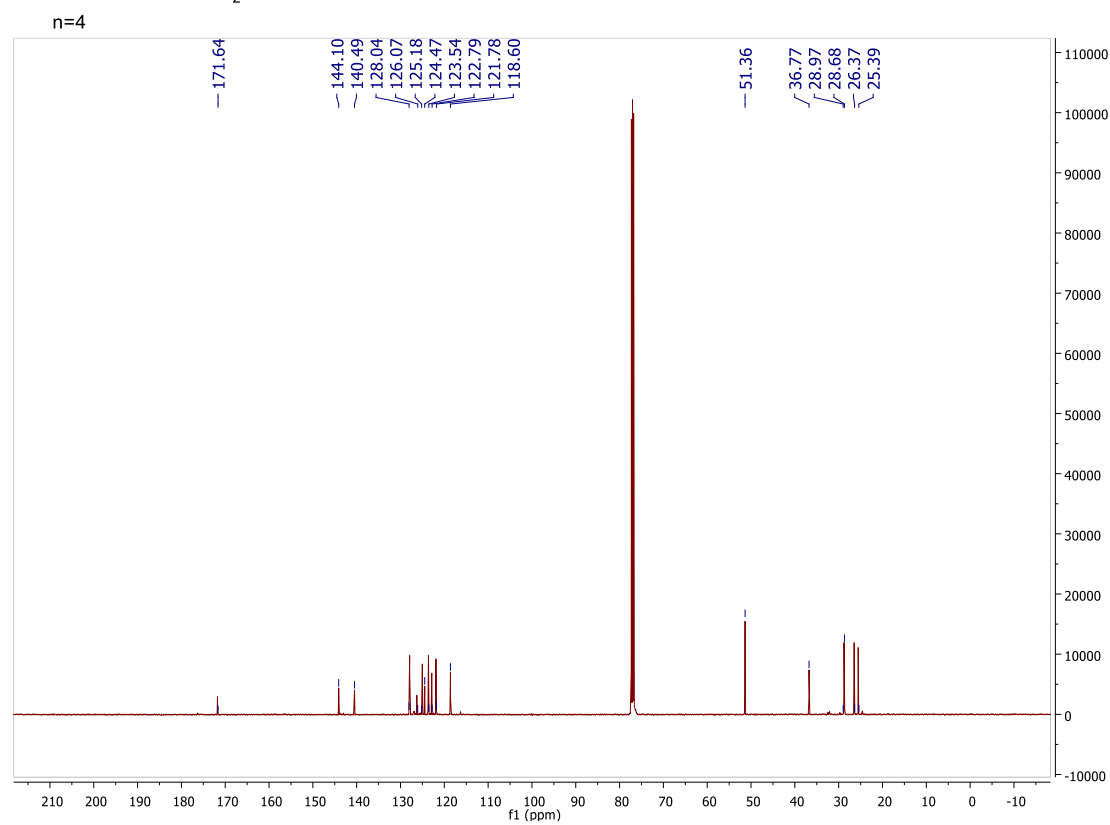
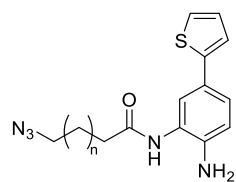
9b ^1H NMR



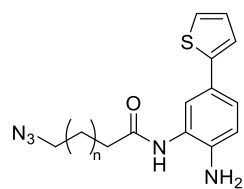
n=4



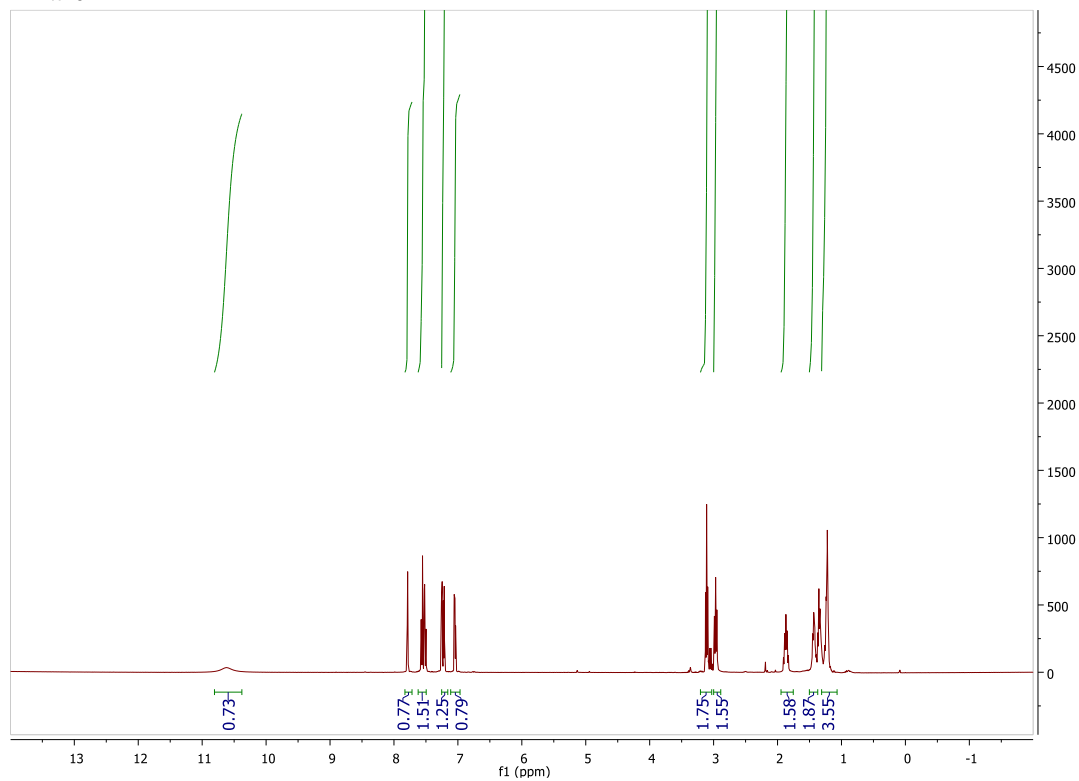
9b ^{13}C NMR



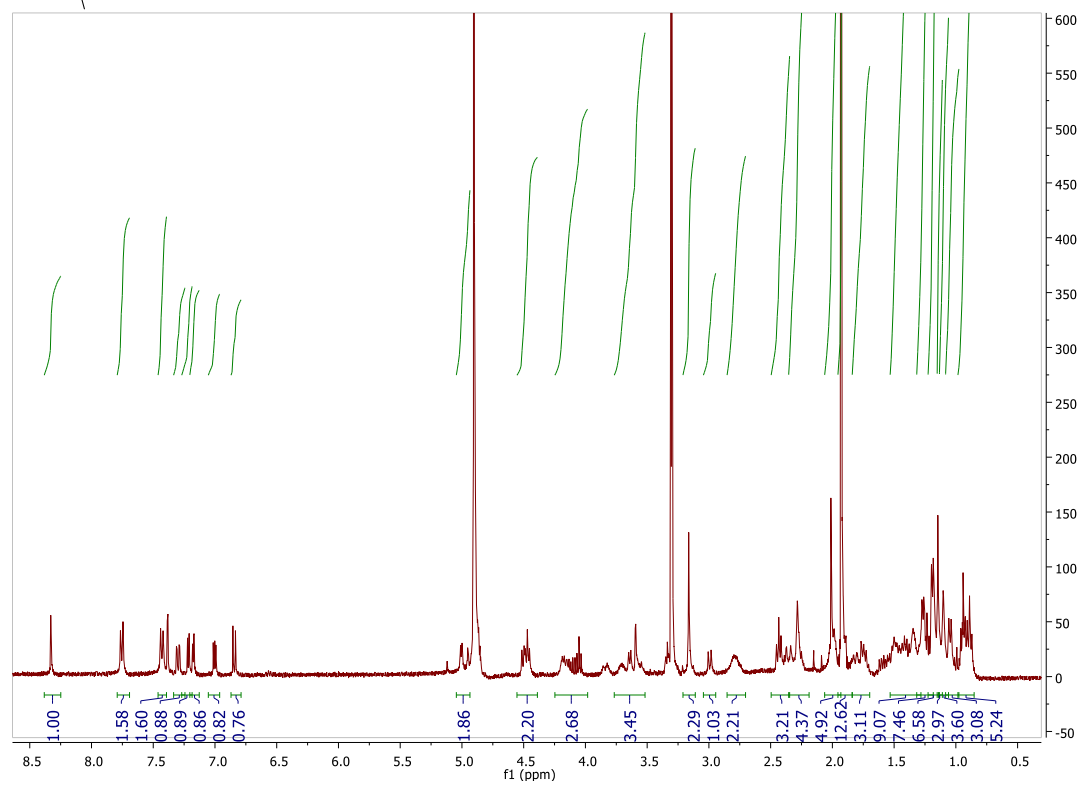
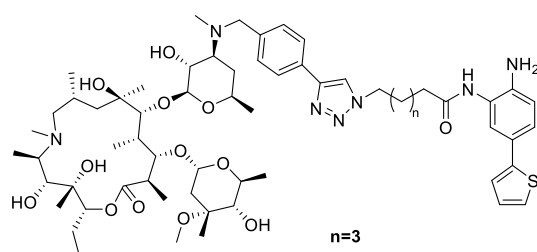
9c ^1H NMR



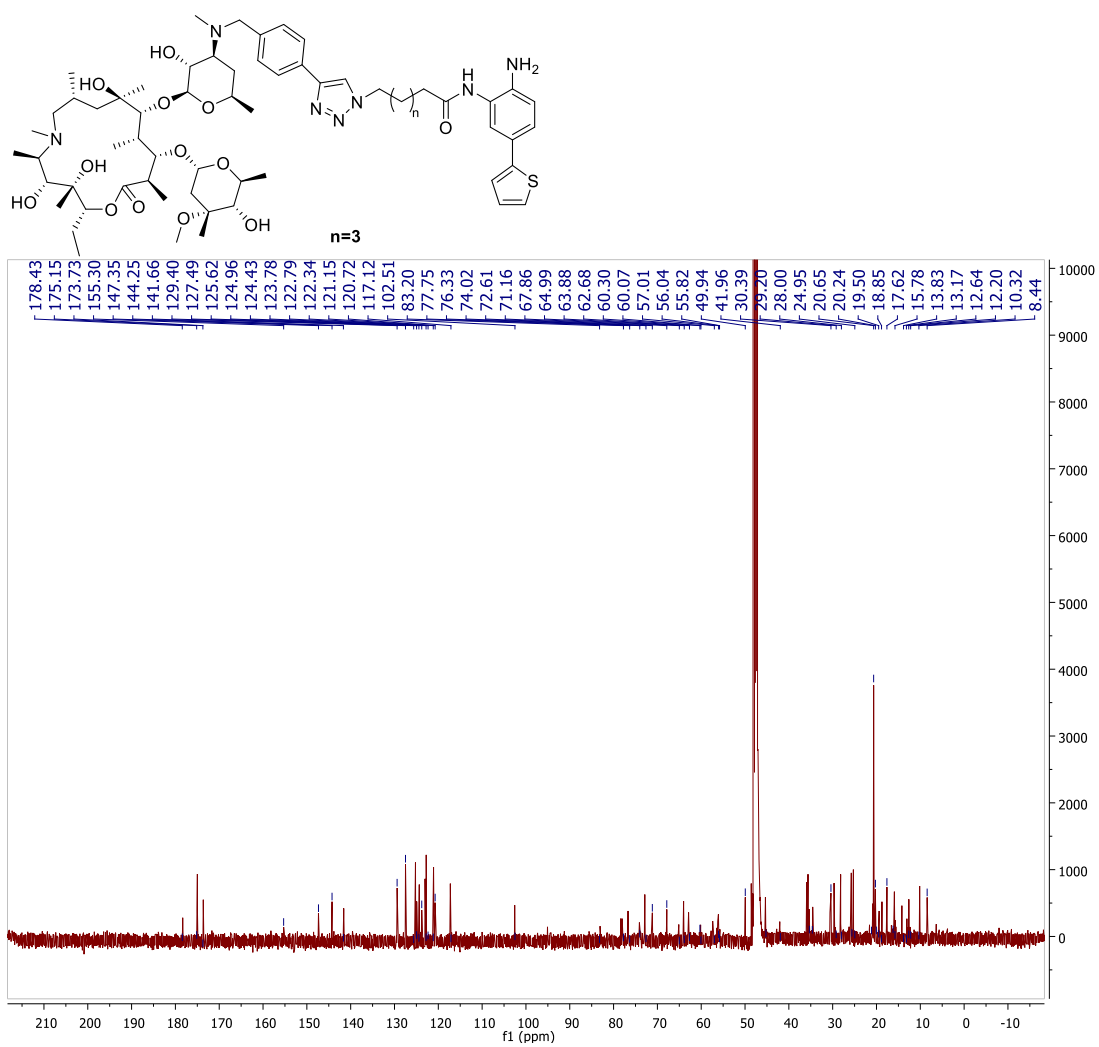
n=5



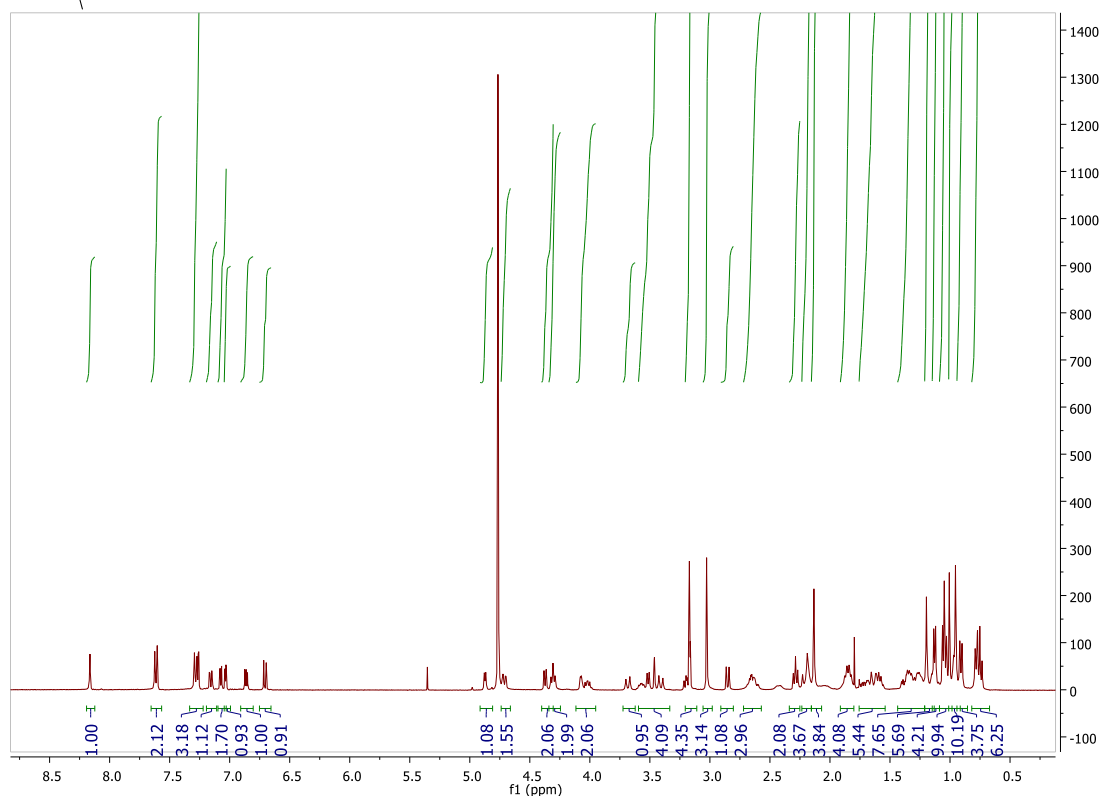
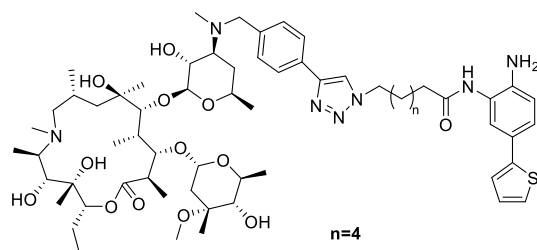
14a ^1H NMR



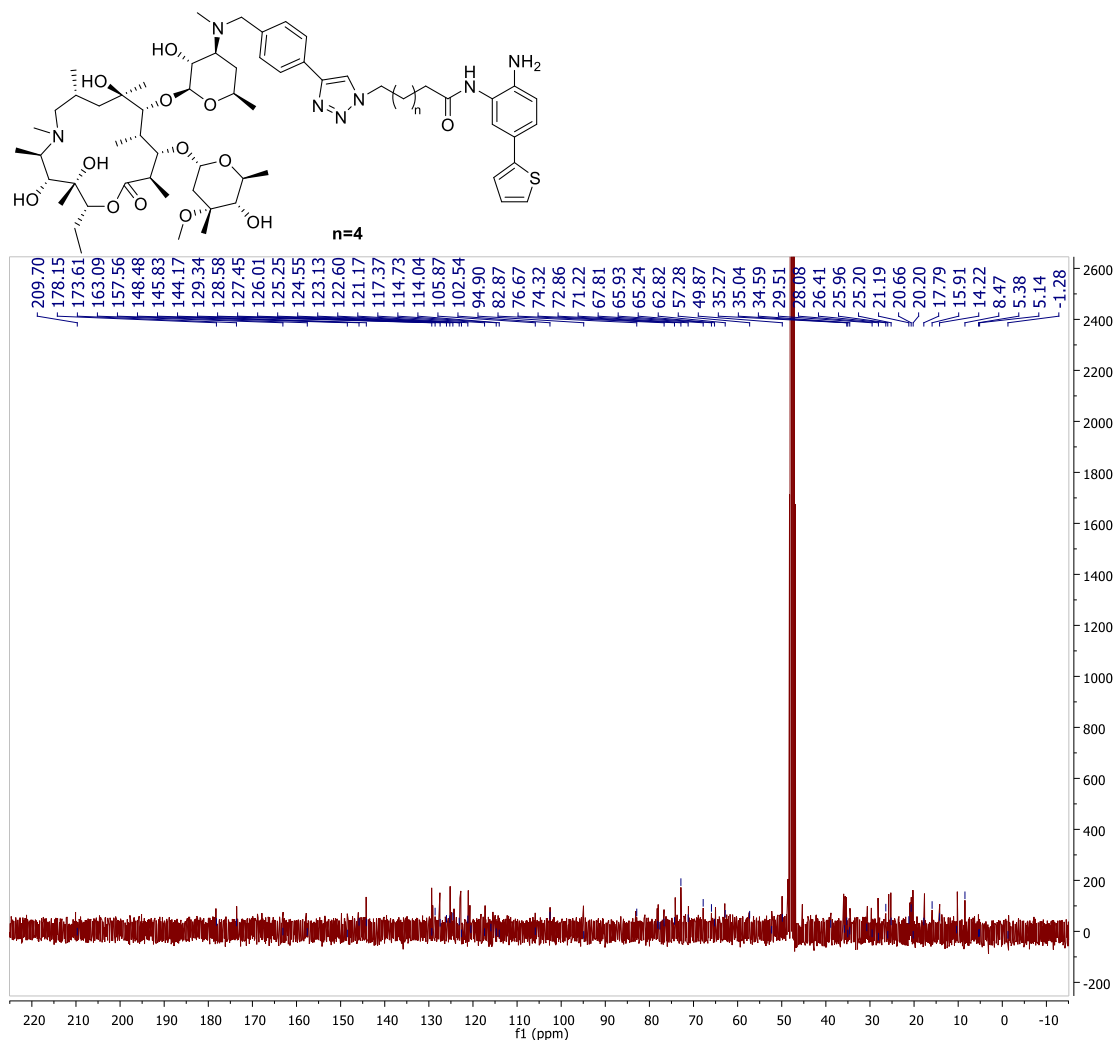
14a ^{13}C NMR



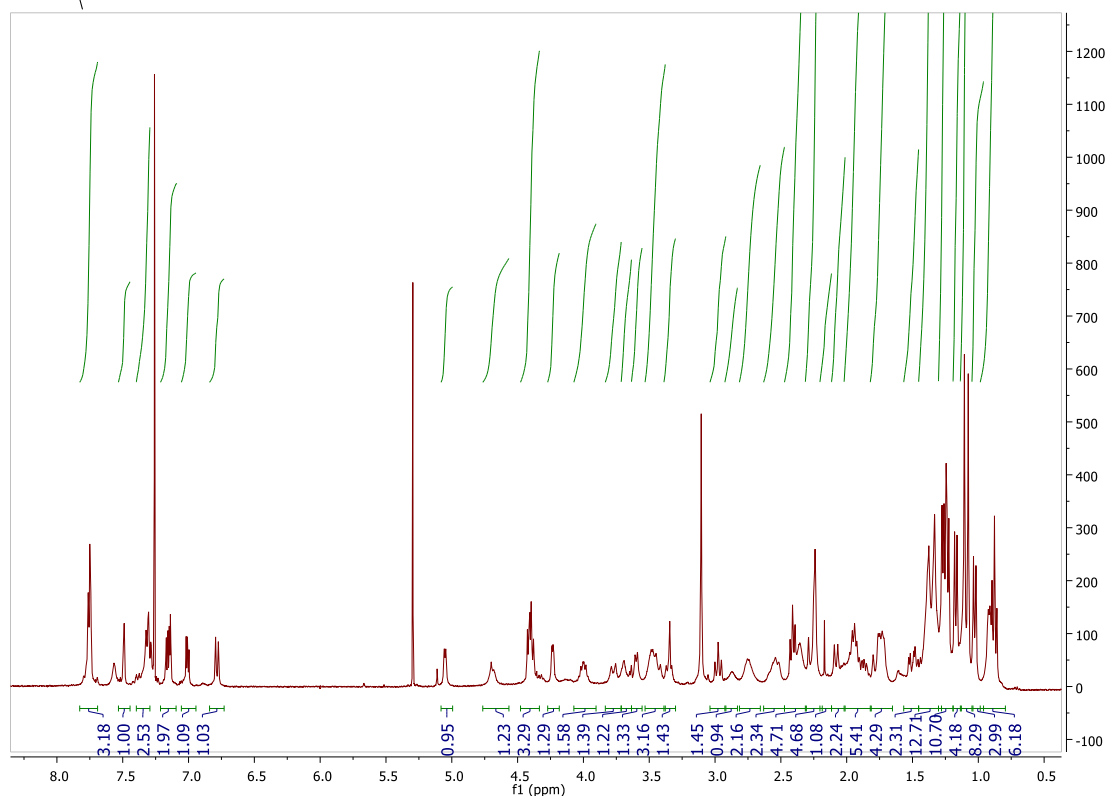
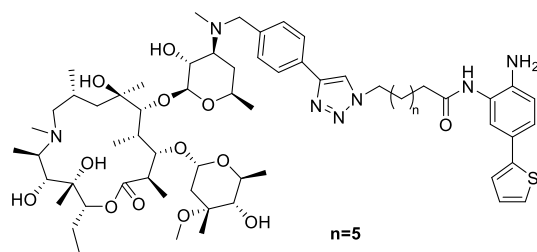
14b ^1H NMR



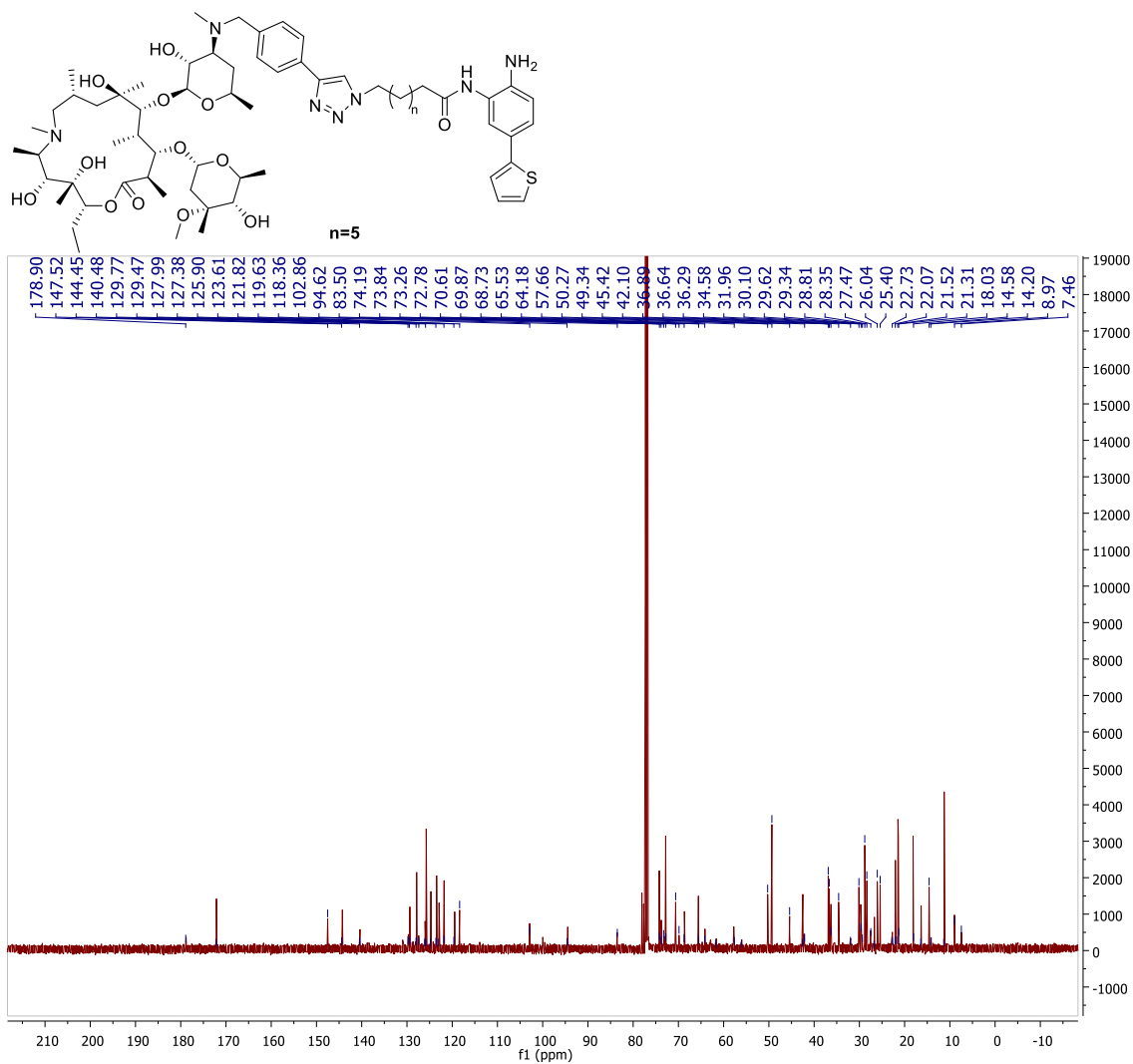
14b ^{13}C NMR



14c ^1H NMR



14c ^{13}C NMR



CHAPTER 4

HISTONE DEACETYLASE INHIBITORS EQUIPPED WITH ESTROGEN RECEPTOR MODULATORS FOR SELECTIVELY TARGETING BREAST CANCER

4.1. Introduction

Histone deacetylase enzymes (HDAC) are among the most promising targets in cancer therapy due to their critical role in chromatin remodeling and gene expression regulation. Through their deacetylase activities, HDACs are not only involved in regulating DNA-histone interaction, they regulate non-histone protein functions as well [1]. Removal of the acetyl group by HDAC enzymes from lysine residue of the histone proteins leads to a condensed chromatin and transcriptional repression [2], while addition of the acetyl group by HAT results in an open and accessible chromatin and favors the expression of tumor suppresser genes [3].

Epigenetic changes leading to gene expression modulations are responsible for cancer progression, therefore, inhibiting HDACs activity has emerged as a potential strategy to invert changes that are affiliated with cancer, and an ongoing research has been dedicated to develop potent and selective HDACi. Currently, there are four US FDA approved HDACi, with many others in various stages of clinical trials [4]. SAHA was the first FDA approved HDACi in the clinic. SAHA obtained approval in 2006 for treating cutaneous T-cell lymphoma [5], followed by approval of FK228 in 2009 for cutaneous T-cell lymphoma and peripheral T-cell lymphoma [6], and belinostat in 2014 for peripheral T-cell lymphoma [7]. Panobinostat is the last HDACi that received accelerated FDA approval in 2015 for treating multiple myeloma [8]. Chidamide (CS055) is a HDACi only approved in China for treating relapsed/refractory peripheral T-cell lymphoma. Chidamide is currently being investigated in phase II clinical trials in US [9]. Despite

promising results in treating certain types of cancer, HDACi share common drawbacks including lack of isoform selectivity and poor solid tumor accumulation as well as poor bioavailability and cardiotoxicity [10].

Studies have shown HDACi are more potent and have a greater efficiency when they are used in combination with other therapeutic agents [11], [12]. One promising example of HDACi combinational therapy is their use in hormone resistant breast cancer together with selective estrogen receptor modulators (SERM) such as tamoxifen (Tam). Tamoxifen is a potent estrogen receptor (ER) antagonist [13]. It is considered one of the essential drugs by world health organization (WHO) and is a first line therapy and the most commonly used treatment for endocrine dependent breast cancer. However its use is limited since almost all patients with metastatic breast cancer, 40% of whom received tamoxifen as an adjuvant therapy, relapse and acquire resistance to it and eventually die [14], [15]. Although the mechanism of tamoxifen resistance development is not fully defined to date, it is however clear that tamoxifen resistant tumors still exhibit ER expression 70% of the time in form of ER α or upregulation of ER β expression, a closely related ER α isoform [16]. In some cases, however, tumors are ER negative due to epigenetic silencing of ER α subtypes [17]. Tamoxifen sensitivity in ER negative breast cancers can be restored by inducing ER α expression, using DNA demethylating agents such as [5-aza-2'-deoxycytidine (5-aza-dC)] and HDACi like SAHA or trichostatin A [17], [18], [19].

One potential strategy to extend the therapeutic utility of antiestrogens to ER expressing, antiestrogen resistant breast tumors is to use design-multiple ligand approach [20] wherein a prototypical antiestrogen such as tamoxifen is covalently linked to a moiety having independent anticancer activity [21], [22] Recent studies have shown that covalent linkage of ER antagonist ligands to HDACi resulted in bifunctional agents with improved *in vitro* therapeutic indices and anti-proliferative activity [23], [24].

In our effort to achieve more potent HDACi with targeted delivery to the site of tumor we designed three classes of SERM-HDACi. We hypothesized that dual-acting SERM-HDACi not only could result in targeted delivery of compounds to the breast tissue due to tamoxifen affinity for ER but also could explore cell ER expression status to achieve higher concentrations in ER antagonist resistant, ER expressing breast tumors and subsequent HDAC inhibition by the HDACi moiety of these agents will result in selective tumor growth inhibition.

ERs reside in cytoplasm while they are bound to heat shock proteins. Upon binding to estrogen they get activated and are translocated to nucleus. However, small populations of ERs that are involved in modulating cell survival and proliferation exist on the plasma membrane [25] of target tumor cells. These ERs can facilitate tumor selective uptake of SERM conjugated HDACi [26].

A previous study by Gryder *et al* revealed that incorporation of tamoxifen into HDACi surface recognition group furnished dual-acting SERM-HDACi with antagonist activity similar to tamoxifen and exhibiting nanomolar range HDAC6 inhibition activity. These dual-acting SERM-HDACi also demonstrated more potent anti-proliferative activity against MCF-7 (ER α positive breast cancer cell line) compared to tamoxifen.

In order to complete the SAR from the previous project, I synthesized various tamoxifen conjugated HDACi having different zinc binding groups and compared activities for compounds with various linker lengths to determine the optimal length.

4.2. Synthesis of Tamoxifen-derived Dual-acting SERM-HDACi

Following the previously disclosed dual-acting SERM-HDACi template [24], [27], I designed three classes of tamoxifen conjugated HDACi having different zinc binding groups and methylene linker lengths to evaluate the impact of these modification on HDAC inhibitory potency.

Based on our previous work, the optimal linkers were predicted to be five or six methylene groups [28]. Therefore, I limited my SAR study on the linkers having between five and eight methylene groups. Additionally, Gryder *et al* [24] disclosed that having the triazolyl moiety attached to benzyl-tamoxifen moiety results in a better HDAC inhibitory potency and anti-proliferative activity.

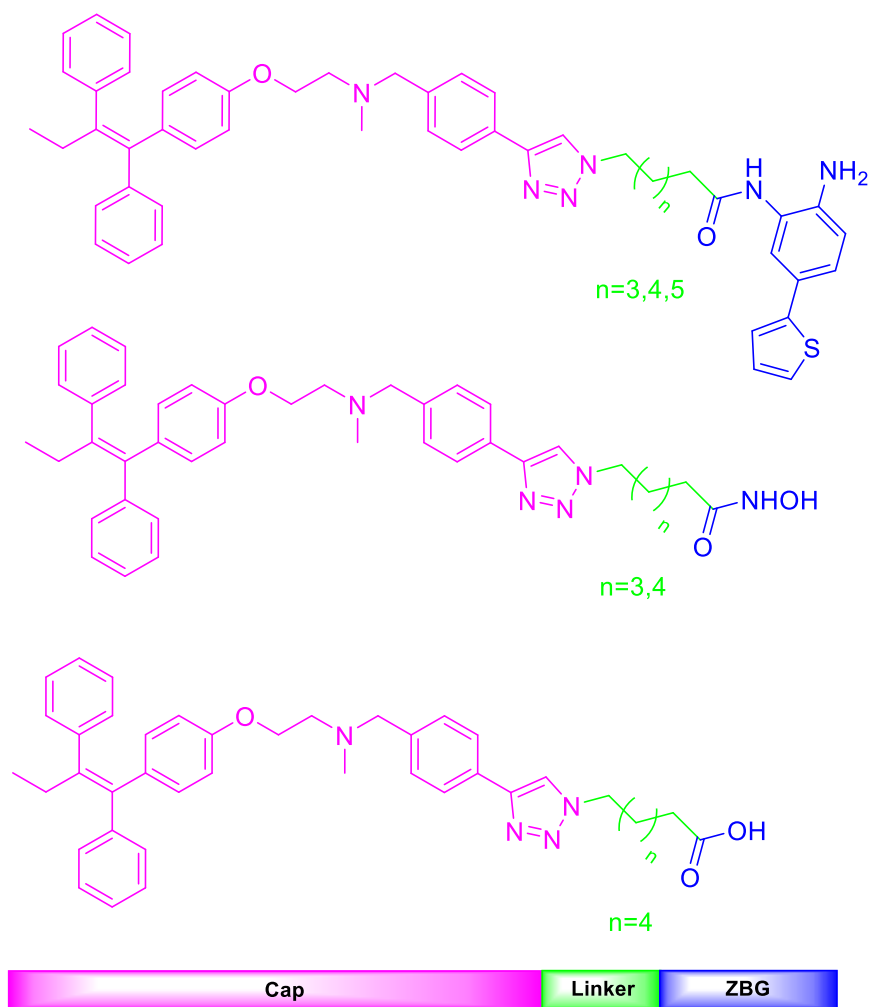
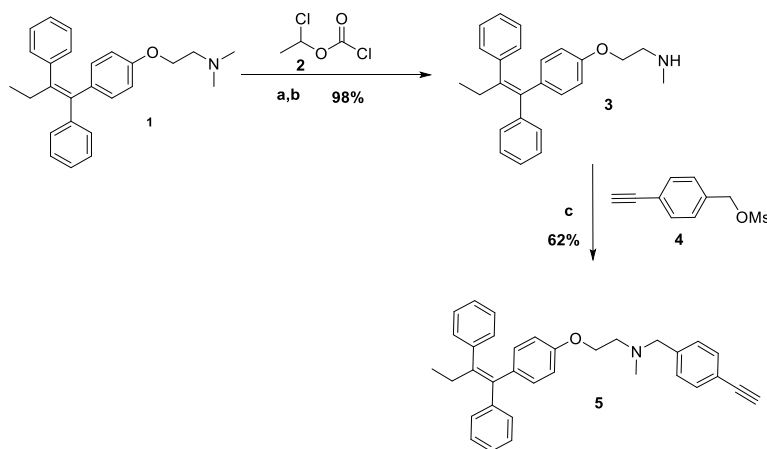


Figure 4.1. Three classes of tamoxifen conjugated HDACi with different ZBG and linker length.

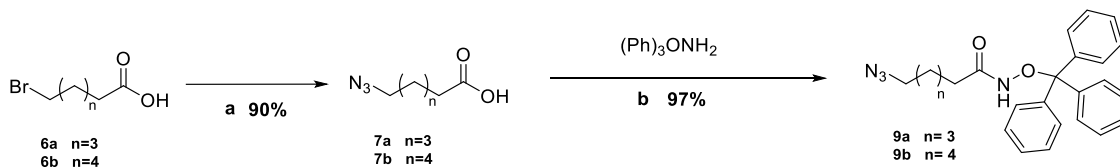
4.3. Chemistry and synthesis

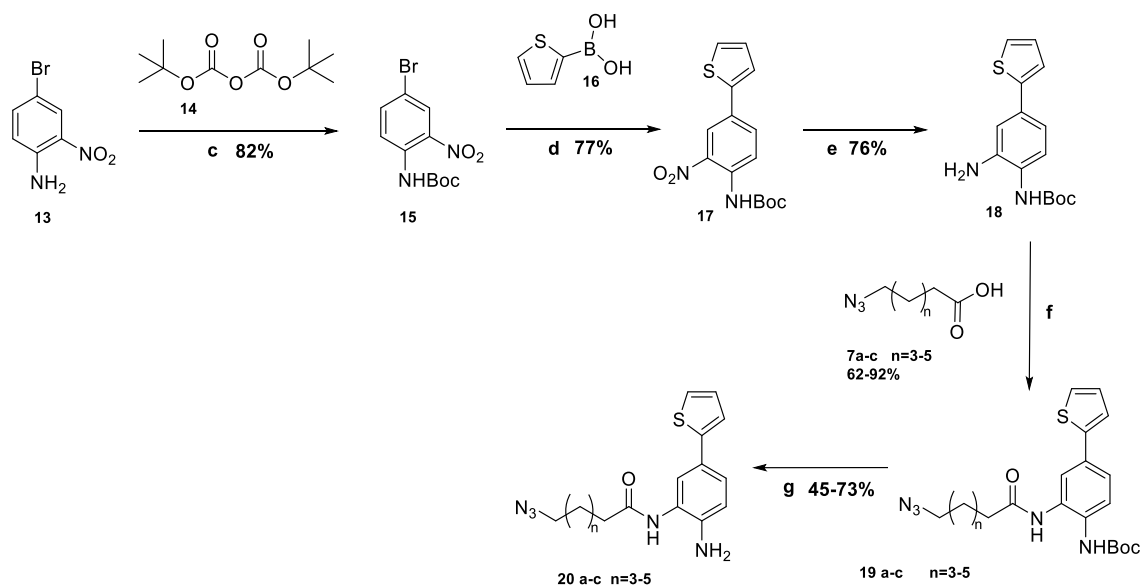
N-Desmethyl tamoxifen **3** was obtained through demethylation of tamoxifen **1** by reacting it with 1-chloroethyl chloroformate **2** [29]. Compound **3** was then reacted with 4-ethynylbenzyl methanesulfonate **4** to yield *N*-alkynated tamoxifen **5** (Scheme 4.1) [30].



Scheme 4.1. (a) DCM, 30 min; (b) MeOH, reflux, overnight 98% (a and b); (c) Hunig's base, DMSO, 85 °C, 4 h, 62%.

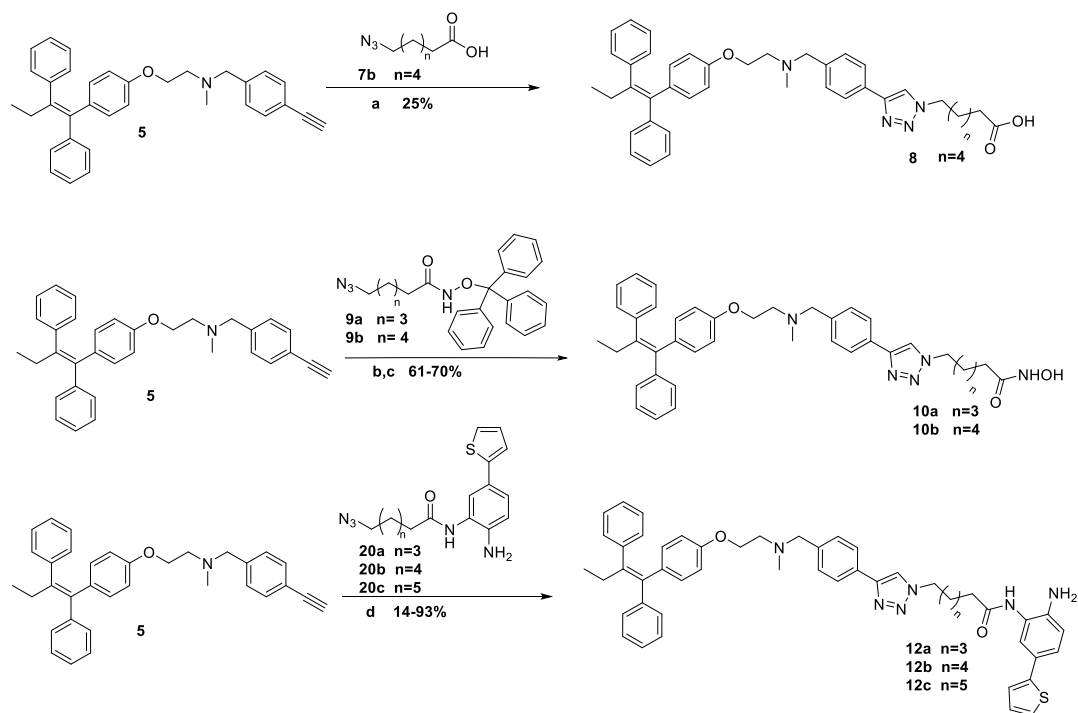
The reaction of bromo alkanolic acids **6a-b** with sodium azide resulted in azide alkanolic acids **7a-b** which was then coupled with *O*-trityl hydroxylamine [31] to yield **9a-b**. Additionally, the azido thiophene-benzamide **20a-c** were synthesized as described in literature and chapter 3 (Scheme 4.2) [32].





Scheme 4.2. (a) NaN_3 , DMF, 80 °C, overnight, 90%; (b) *N*-Methyl morpholine, *O*-tritylhydroxyl amine, isobutyl chloroformate, THF, 3h, 97%; (c) Et_3N , DCM, reflux, overnight, 82%; (d) $\text{Pd}(\text{PPh}_3)_4$, K_2CO_3 , THF, 70 °C, 77%; (e) Zn, H_2O : Dioxane (1:4), 70 °C, 3 days, 76%; (f) EDCI, HOBT, DMF, 70 °C, 6 h, 62-92%; (g) TFA (1%), DCM, rt, 2h, 45-73%.

All the three classes of tamoxifen conjugated HDACi were synthesized through Cu (I) catalyzed azide-alkyne cycloaddition reaction between benzyl-alkynyl tamoxifen **5** and azides **9a-b** and **20a-c** to furnish the requisite compounds **10a-b** and **12a-c** [24], [33], [34]. Control carboxylic compound **8** was similarly synthesized from **5** and azido acid **7b** (Scheme 4.3) [35].



Scheme 4.3. (a) THF, CuI, Hunig's base, rt, overnight, 25%; (b) THF, CuI, Hunig's base, rt, overnight; (c) TFA, TIPS, DCM, rt, 1 h, 61-70% (b and c); (d) THF, CuI, Hunig's base, rt, overnight, 14-93%.

4.4. HDAC inhibitory potency (Performed by Lindsey Szymczak at Northwestern University)

All three classes of synthesized tamoxifen conjugated HDACi were tested against class I HDAC isoforms and HDAC6 to evaluate their HDAC inhibitory potency as it has been established that these HDAC isoforms are involved in breast cancer [36], [37]. HDAC activity was determined by the label-free mass spectrometry-based SAMDI assay [38].

As expected, the thiophene-benzamide-based compounds **12a-c** were selective toward HDAC1 and HDAC2 and did not inhibit other HDAC isoforms [39], while the hydroxamate-based compounds **10a-b** showed low to mid nanomolar range HDAC inhibitory potency toward all tested isoforms. Compound **8** did not exhibit any HDAC

inhibitory potency. Based on this finding, the tamoxifen-derived hydroxamic acid compounds **10a-b** were the most potent HDACi among these three groups (Table 4.1).

Table 4.1. HDAC 1, 2, 3, 6, and HDAC8 inhibition activities of three different classes of tamoxifen conjugated HDACi (IC₅₀ in nM).

Compound	n	HDAC1	HDAC2	HDAC3	HDAC6	HDAC8
8	4	NI	NI	NI	1880±540	NI
10a*	3	524	ND	ND	567	ND
10b	4	317±29	785±66	96±12	33±7.6	3050±250
12a	3	635±110	281±25	NI	NI	NI
12b	4	543±82	281±39	NI	NI	NI
12c	5	NI	1130±120	NI	NI	NI
SAHA	-	42	190	20	34	2800

ND: Not determind, NI: No inhibition. * HDAC inhibitory potency of compound 10a was previously reported by Gryder *et al* and performed by BPS BioScience [24].

4.5. Anti-proliferative activity and therapeutic index

After obtaining the HDAC inhibitory activity of tamoxifen conjugated HDACi, they were tested against three cell lines, two transformed cell lines, ER positive (MCF-7) and ER negative (MDA-MB231) breast cancers as well as one non-cancerous mamalian cell line (VERO- monkey kidney epithelial cell). These compounds were compared to tamoxifen, the first line therapy for treating ER positive breast cancer, and SAHA, an FDA approved HDACi. As anticipated, the control carboxylic acid compound **8** was inactive against all tested cell lines. Surprisingly, the benzamide compounds **12a-c** did not show cytotoxicity against these cancer cell lines despite their class I HDAC selectivity. The reason for the lack of antiproliferative activity of compounds **12a-c** is not apparent from this study. Gratifyingly, we observed that the hydroxamic acid compounds

10a-b displayed ER dependent antiproliferative activity. Relative to tamoxifen, **10a-b** were about 8 fold more potent toward ER positive breast cancer cells and about 2 fold more potent toward ER negative breast cancer cells (Table 4.2).

Furthermore, compounds **10a-b** displayed tumor-selective cytotoxicity with *in vitro* therapeutic index (IVTI) of 4.3 and 1.4 while tamoxifen and SAHA showed no tumor-selective cytotoxicity (Table 4.2).

Table 4.2. Anti-proliferative activity of selected azithromycin conjugated HDACi (IC₅₀ values in μ M).

Compound	n	MCF-7	MDA-MB231	VERO	<i>In vitro</i> therapeutic index $\frac{\text{IC}_{50} \text{ in VERO}}{\text{IC}_{50} \text{ in MCF-7}}$
8	4	NI	NI	NI	-
10a	3	2.1 \pm 0.1	10 \pm 0.5*	9.1 \pm 2.8	4.3
10b	4	2.4 \pm 0.4	6.4 \pm 0.5	3.4 \pm 0.1	1.4
12a	3	NI	NI	NI	-
12b	4	NI	NI	NI	-
12c	5	NI	NI	NI	-
Tamoxifen	-	15.6 \pm 1.3	17 \pm 1.2	16 \pm 0.1	1.1
SAHA	-	3.3 \pm 0.1	3.4 \pm 0.2	1 \pm 0.1	0.2

Each value is obtained from a duplicate of three simultaneous experiments. NI=No inhibition. * Value reported previously by

Gryder, *et al* [24].

IVTI is safety window for comparing the therapeutic efficacy of drug candidates [40]. It is a comparison between drug cytotoxicity to transformed cells and healthy cells. The higher the therapeutic index, the safer the drug is expected to be.

Overall, these tamoxifen-derived dual-acting SERM-HDACi are more selective toward breast cancer cells compared to SAHA. The promising anti-proliferative activity and HDAC inhibitory potency results of compounds **10a** and **10b** encouraged us to synthesize these two compounds in a larger scale to study their activity in animal models. Compounds **10a** and **10b** are currently under *in vivo* investigation.

4.6. Conclusion

Tamoxifen is the most common therapy for treating ER positive breast cancer [41], however, many patients relapse and acquire resistance during the course of treatment. A high percentage of the tamoxifen resistant tumors still express ER, either in form of ER α or ER β . Additionally, in tumors that are ER negative, ER expression can be stimulated by using HDACi as an adjuvant therapy [42].

I have identified tamoxifen-derived dual-acting SERM-HDACi that displayed enhanced potency and improved IVTI. Unlike tamoxifen that exhibits no selectivity for ER positive and ER negative breast cancer cells, these compounds are more potent and cytotoxic toward ER positive breast cancer cells (MCF-7). Furthermore, compared to the FDA approved HDACi SAHA which is significantly toxic to VERO cells, these SERM-HDACi are less cytotoxic toward healthy cells. The improvement in potency and IVTI could potentially be due cell to ER expression status dependent cell uptake and/or intracellular retention of these SERM-HDACi.

4.7. Experimental

4.7.1. Materials and methods

Tamoxifen was purchased from Cayman chemical company. 4-ethynylbenzyl alcohol and 1-chloroethyl chloroformate were purchased from Sigma-Aldrich. All commercially available starting materials were used without purification. Reaction solvents were high performance liquid chromatography (HPLC) grade or American

Chemical Society (ACS) grade and used without purification. Analtech silica gel plates (60 F₂₅₄) were used for analytical TLC, and Analtech preparative TLC plates (UV 254, 2000 μ m) were used for purification. UV light and anisaldehyde/iodine stain were used to visualize the spots. 200-400 Mesh silica gel was used in column chromatography. Nuclear magnetic resonance (NMR) spectra were recorded on a Varian-Gemini 400 MHz or Bruker 500 MHz magnetic resonance spectrometer. ¹H NMR Spectra were recorded in parts per million (ppm) relative to the residual peaks of CHCl₃ (7.24 ppm) in CDCl₃ or CHD₂OD (4.78 ppm) in CD₃OD or DMSO-*d*₅ (2.49 ppm) in DMSO-*d*₆. ¹³C spectra were recorded relative to the central peak of the CDCl₃ triplet (77.0 ppm) or CD₃OD septet (49.3 ppm) or DMSO-*d*₆ septet (39.7 ppm) and were recorded with complete hetero-decoupling. Original 'fid' files were processed using MestReNova LITE (version 5.2.5-5780) program. High-resolution mass spectra were recorded at the Georgia Institute of Technology mass spectrometry facility in Atlanta. Compounds **3**, **5**, **7a-b**, **9a-b**, and **10a** were synthesized as it was discussed before [24], [28], [30], [31], [43]. Compounds **4**, **20a-c** were synthesized as described in chapter 2 and 3.

4.7.1.1. *N*-Desmethyltamoxifen (**3**)

Tamoxifen **1** (2.3 g, 6.2 mmol) was dissolved in DCM (10 mL). The reaction mixture was purged for 15 minutes, then cooled to 0 °C, and then 1-chloroethyl chloroformate **2** (2.7 mL, 24.8 mmol) was added dropwise and stirred for another 15 minutes. Then it was refluxed overnight. Solvent was evaporated. Then reaction mixture was quenched with NaHCO₃ (10 mL) and brine (10 mL). The organic layer was separated and dried over Na₂SO₄. The crude product was purified by column chromatography (Silica gel, 3:2:0.1 EtOAc: Hex: NEt₃) to give the product (2.1 g, 98%) as a white solid. ¹H NMR (400 MHz, CDCl₃) δ 7.41 – 7.32 (m, 2H), 7.32 – 7.24 (m, 3H), 7.23 – 7.19 (m, 1H), 7.17 – 7.08 (m, 3H), 7.04 – 6.96 (m, 1H), 6.95 – 6.90 (m, 1H), 6.86 – 6.79 (m, 2H),

6.62 – 6.54 (m, 2H), 3.94 (t, $J = 5.1$ Hz, 2H), 2.90 (dd, $J = 6.8, 3.1$ Hz, 2H), 2.51 (dd, $J = 12.3, 4.8$ Hz, 2H), 2.47 (d, $J = 8.2$ Hz, 3H), 0.98 (dd, $J = 11.8, 4.4$ Hz, 3H).

4.7.1.2. 4-(4-Ethynylbenzyl)-Tamoxifen (**5**)

To a stirring solution of desmethyl tamoxifen **3** (572.2 mg, 1.28 mmol) in DMSO (5 mL), compound **4** (350 mg, 1.7 mmol) and Hunig's base (0.7 mL, 4.1 mmol) were added. The reaction mixture was heated for 4 h at 85 °C. Then reaction mixture was washed with water (3×10 mL) EtOAc (5 mL) and quenched with NaHCO₃ (5 mL) and brine (5 mL). The organic layer was separated and dried over Na₂SO₄. The crude product was purified by column chromatography (Silica gel, 1:3:0.1 EtOAc: Hex: NEt₃) to give the product (373 mg, 62%) as a pale yellow solid. ¹H NMR (400 MHz, CD₃OD) δ 7.36 (dt, $J = 7.3, 3.7$ Hz, 2H), 7.32 – 7.29 (m, 2H), 7.27 – 7.14 (m, 5H), 7.15 – 7.01 (m, 5H), 6.73 (dt, $J = 4.9, 2.2$ Hz, 2H), 6.56 – 6.46 (m, 2H), 4.91 (t, $J = 1.1$ Hz, 1H), 3.90 (dd, $J = 7.2, 3.9$ Hz, 2H), 3.50 (d, $J = 17.8$ Hz, 2H), 2.67 (t, $J = 5.5$ Hz, 2H), 2.42 (q, $J = 7.4$ Hz, 2H), 2.21 (d, $J = 1.8$ Hz, 3H), 0.95 – 0.82 (m, 3H).

4.7.1.3. 7-Azido heptanoic acid (**7b**)

Sodium azide (1.95 g, 30 mmol) was added to a stirring solution of 7-bromo heptanoic acid **6b** (3.1 g, 15 mmol) in DMF (10 mL). Reaction stirred overnight. After TLC indicated the complete consumption of the starting material, DMF was evaporated off, and then reaction mixture was dissolved in EtOAc (10 mL) and acidify to pH=3. Then it was washed with brine (5 mL) and organic layer was separated and dried over Na₂SO₄. It yielded product (2.5 g, 97%) as a light brown oil. ¹H NMR (400 MHz, CDCl₃) δ 11.86 (s, 1H), 3.26 – 3.10 (m, 2H), 2.27 (t, $J = 7.0$ Hz, 2H), 1.61 – 1.42 (m, 4H), 1.32 (d, $J = 2.5$ Hz, 4H).

4.7.1.4. 4-Azido-N-(trityloxy)heptanamide (**9b**)

7-Azido heptanoic acid **7b** (2.5 g, 14.5 mmol) was dissolved in anhydrous THF (15 mL). *N*-methyl morpholine (1.6 mL, 14.5 mmol) was added to the solution. The reaction mixture was then cooled to -15 °C and stirred for 5 min. Isobutyl chloroformate (1.9 mL, 14.5 mmol) was added and the mixture stirred for another 10 min at -15°C. *O*-Tritylhydroxyl amine (4.0 g, 14.5 mmol) was added followed by additional 2 eq of *N*-methyl morpholine (3.2 mL, 29 mmol). Stirring continued for another 15 min at -15°C and 2 h at room temperature. Reaction mixture was acidified with 1N HCl to pH=3 to neutralize excess amine, followed by work up. The organic layer was separated and dried over Na₂SO₄. The crude product was purified by column chromatography (Silica gel, 1:2 EtOAc: Hex) to give the product (3.3 mg, 53%) as a white solid. ¹H NMR (400 MHz, CDCl₃) δ 7.46 (d, *J* = 26.8 Hz, 3H), 7.29 (dd, *J* = 38.2, 18.5 Hz, 13H), 3.17 (s, 2H), 1.57 (d, *J* = 27.1 Hz, 1H), 1.54 – 1.33 (m, 3H), 1.22 (tt, *J* = 35.4, 17.9 Hz, 4H), 1.07 (s, 2H).

4.7.1.5. Tamoxifen-*N*-(4-triazolylbenzyl)-*N*-heptanoic Acid (**8**)

4-(4-Ethynylbenzyl)-Tamoxifen **5** (92.5 mg, 0.2 mmol) and 7-azido heptanoic acid **7b** (36.9 mg, 0.2 mmol) were dissolved in degassed anhydrous THF (5 mL). CuI (18.6 mg, 0.1 mmol) and Hünig's base (0.07 mL, 0.4 mmol) were added to the reaction and the resulting reaction was stirred at room temperature overnight. Then, the reaction mixture was diluted with excess ethyl acetate (30 mL) and was transferred to a separatory funnel and then the ethyl acetate layer was washed with a solution (20 mL) of 4:1 mixture of saturated aqueous NH₄Cl solution /NH₄OH solution, water (10 mL), brine (10 mL), dried over anhydrous Na₂SO₄, filtered, and concentrated *in vacuo*. The crude was purified by preparative chromatography (Silica gel, 10:2:0.5 EtOAc/Hex/NEt₃) to give the title compound **8** (31.8 mg, 25%) as a light yellow solid. ¹H NMR (400 MHz, CDCl₃) δ 7.88 – 7.70 (m, 3H), 7.47 – 7.36 (m, 2H), 7.33 (t, *J* = 7.2 Hz, 2H), 7.24 (dt, *J* = 8.0, 6.0 Hz, 3H), 7.13 (dq, *J* = 14.7, 7.4 Hz, 5H), 6.77 (d, *J* = 8.7 Hz, 2H), 6.53 (d, *J* = 8.6 Hz, 2H), 4.37 (t,

$J = 7.1$ Hz, 2H), 4.06 (s, 2H), 3.80 (s, 2H), 3.01 (d, $J = 37.8$ Hz, 2H), 2.47 (dd, $J = 15.8$, 8.7 Hz, 2H), 2.41 (d, $J = 6.5$ Hz, 3H), 2.25 (d, $J = 22.6$ Hz, 2H), 1.93 (s, 2H), 1.37 (s, 3H), 1.25 (s, 3H), 0.90 (dd, $J = 14.5$, 7.1 Hz, 3H). ^{13}C NMR (126 MHz, CDCl_3) δ 177.8, 156.3, 147.3, 143.8, 143.2, 142.4, 141.5, 138.2, 136.0, 132.0, 130.8, 130.6, 130.4, 129.7, 129.5, 128.1, 127.9, 127.8, 127.3, 126.5, 126.1, 125.8, 119.7, 114.1, 113.4, 64.8, 61.4, 56.0, 54.9, 50.4, 41.6, 31.9, 30.2, 29.7, 29.0, 28.5, 26.3, 24.8, 22.7, 14.2, 13.6. HRMS (ESI) m/z Calcd. for $\text{C}_{41}\text{H}_{47}\text{O}_3\text{N}_4$ $[\text{M}+\text{H}^+]$: 643.3643, found for 643.3637.

4.7.1.6. Tamoxifen-*N*-(4-triazolylbenzyl)-*N*-hydroxyhexanamide (**10a**)

4-(4-Ethynylbenzyl)-tamoxifen **5** (264.5 mg, 0.5 mmol) and 6-azido-*N*-(trityloxy)hexanamide **9a** (279.0 mg, 0.7 mmol) were dissolved in degassed anhydrous THF (5 mL). CuI (53.3 mg, 0.3 mmol) and Hünig's base (0.2 mL, 1.1 mmol) were added to the reaction and the resulting reaction was stirred at room temperature overnight. Then, the reaction mixture was diluted with excess ethyl acetate (30 mL) and was transferred to a separatory funnel and then the ethyl acetate layer was washed with a solution (20 mL) of 4:1 mixture of saturated aqueous NH_4Cl solution / NH_4OH solution, water (10 mL), brine (10 mL), dried over anhydrous Na_2SO_4 , filtered, and concentrated *in vacuo*. The crude was then dissolved in DCM: TFA (1: 0.2 mL) solution. Triisopropyl silane was added dropwise until the color transformed from dark yellow to pale yellow. TLC indicated the complete consumption of the starting material after 1 h. Solvent and TFA were evaporated off, then reaction mixture was quenched with NaHCO_3 followed by work up and dried over anhydrous Na_2SO_4 , filtered, and concentrated *in vacuo*. The crude was purified by preparative chromatography (Silica gel, 12:1:0.1 DCM/MeOH/ NH_4OH) to give the title compound **10a** (196.0 mg, 61%) as a white solid. ^1H NMR (400 MHz, CD_3OD) δ 8.22 (s, 1H), 7.77 (d, $J = 7.3$ Hz, 2H), 7.39 – 7.28 (m, 2H), 7.30 – 7.21 (m, 2H), 7.17 (t, $J = 7.3$ Hz, 3H), 7.03 (dt, $J = 14.1$, 6.3 Hz, 5H), 6.72 (d, $J = 8.5$ Hz, 2H), 6.49 (d, $J = 8.4$ Hz, 2H), 4.32 (s, 2H), 3.88 (s, 2H), 3.58 (s, 2H), 2.72 (s, 2H), 2.44 – 2.31

(m, 2H), 2.24 (s, 3H), 2.06 (s, 2H), 1.87 (s, 2H), 1.61 (s, 2H), 1.26 (d, $J = 21.4$ Hz, 2H), 0.84 (t, $J = 7.4$ Hz, 3H). ^{13}C NMR (101 MHz, CD_3OD) δ 156.6, 147.1, 143.6, 142.2, 141.2, 138.3, 137.1, 135.5, 131.7, 129.9, 129.1, 128.0, 127.6, 126.7, 126.0, 125.5, 120.9, 113.1, 64.9, 61.6, 55.2, 49.9, 41.5, 29.5, 28.6, 25.5, 24.7, 12.8. HRMS (ESI) m/z Calcd. for $\text{C}_{40}\text{H}_{44}\text{O}_3\text{N}_5$ $[\text{M}+\text{H}^+]$: 642.3439, found for 642.3451.

4.7.1.7. Tamoxifen-*N*-(4-triazolylbenzyl)-*N*-hydroxyheptanamide (**10b**)

4-(4-Ethynylbenzyl)-Tamoxifen **5** (617.3 mg, 1.3 mmol) and 7-azido-*N*-(trityloxy)hexanamide **9b** (673.1 mg, 1.6 mmol) were dissolved in degassed anhydrous THF (5 mL). CuI (123.8 mg, 0.6 mmol) and Hünig's base (0.5 mL, 2.6 mmol) were added to the reaction and the resulting reaction was stirred at room temperature overnight. Then, the reaction mixture was diluted with excess ethyl acetate (30 mL) and was transferred to a separatory funnel and then the ethyl acetate layer was washed with a solution (20 mL) of 4:1 mixture of saturated aqueous NH_4Cl solution / NH_4OH solution, water (10 mL), brine (10 mL), dried over anhydrous Na_2SO_4 , filtered, and concentrated *in vacuo*. The crude was then dissolved in DCM: TFA (1: 0.2 mL) solution. Triisopropyl silane was added dropwise until the color transformed from dark yellow to pale yellow. TLC indicated the complete consumption of the starting material after 1 h. Solvent and TFA were evaporated off, then reaction mixture was quenched with NaHCO_3 followed by work up and dried over anhydrous Na_2SO_4 , filtered, and concentrated *in vacuo*. The crude was purified by column chromatography (Silica gel, 12:1:0.1 DCM/MeOH/ NH_4OH) to give the title compound **10b** (60.0 mg, 70%) as a white solid. ^1H NMR (400 MHz, CD_3OD) δ 8.19 (s, 1H), 7.76 (s, 2H), 7.40 – 7.18 (m, 4H), 7.12 (d, $J = 28.3$ Hz, 3H), 7.04 (s, 5H), 6.71 (d, $J = 7.4$ Hz, 2H), 6.47 (d, $J = 6.6$ Hz, 2H), 4.29 (s, 2H), 3.83 (s, 2H), 3.49 (s, 2H), 2.64 (s, 2H), 2.37 (d, $J = 5.8$ Hz, 2H), 2.17 (s, 3H), 2.07 (d, $J = 14.9$ Hz, 2H), 1.82 (s, 2H), 1.54 (s, 2H), 1.26 (s, 4H), 0.83 (s, 3H). ^{13}C NMR (101 MHz, CD_3OD) δ 171.4, 156.7, 147.1, 143.6, 142.3, 141.1, 138.4, 137.8, 135.5, 131.7,

129.9, 129.5, 129.1, 128.0, 127.7, 126.4, 125.8, 125.3, 120.9, 113.3, 104.9, 65.2, 61.6, 55.4, 49.9, 41.8, 32.4, 29.8, 28.6, 27.8, 25.7, 25.0, 12.8. HRMS (ESI) m/z Calcd. for $C_{41}H_{48}O_3N_5$ $[M+H]^+$: 658.3752, found for 658.3746.

4.7.1.8. Tamoxifen-*N*-(4-triazolylbenzyl)-*N*-(2-amino-5-(thiophen-2-yl)phenyl)hexanamide (**12a**)

4-(4-Ethynylbenzyl)-tamoxifen **5** (50 mg, 0.1 mmol) and *N*-(2-amino-5-(thiophen-2-yl)phenyl)-4-azidohexanamide **9a** (38.4 mg, 0.1 mmol) were dissolved in degassed anhydrous THF (5 mL). CuI (10 mg, 0.05 mmol) and Hünig's base (0.04 mL, 0.2 mmol) were added to the reaction and the resulting reaction was stirred at room temperature overnight. Then, the reaction mixture was diluted with excess ethyl acetate (30 mL) and was transferred to a separatory funnel and then the ethyl acetate layer was washed with a solution (20 mL) of 4:1 mixture of saturated aqueous NH_4Cl solution/ NH_4OH solution, water (10 mL), brine (10 mL), dried over anhydrous Na_2SO_4 , filtered, and concentrated *in vacuo*. The crude was purified by preparative TLC (Silica gel, 12:1:0.1 DCM/MeOH/ NH_4OH) to give the title compound **12a** (72.0 mg, 85%) as a yellow oil. 1H NMR (400 MHz, $CDCl_3$) δ 7.95 (s, 1H), 7.77 – 7.66 (m, 3H), 7.40 (dd, J = 14.9, 4.1 Hz, 1H), 7.39 – 7.28 (m, 5H), 7.29 – 7.27 (m, 1H), 7.25 – 7.22 (m, 2H), 7.18 – 7.08 (m, 7H), 7.02 – 6.93 (m, 1H), 6.80 – 6.72 (m, 2H), 6.59 – 6.51 (m, 2H), 4.33 (dd, J = 19.0, 12.1 Hz, 2H), 4.01 – 3.87 (m, 2H), 2.76 (t, J = 5.9 Hz, 2H), 2.51 – 2.39 (m, 2H), 2.34 (dd, J = 9.3, 5.1 Hz, 2H), 2.26 (d, J = 10.5 Hz, 3H), 1.90 (td, J = 14.3, 7.0 Hz, 2H), 1.77 – 1.62 (m, 2H), 1.30 (dt, J = 16.6, 5.0 Hz, 4H), 0.92 (t, J = 7.4 Hz, 3H). ^{13}C NMR (101 MHz, $CDCl_3$) δ 171.9, 156.7, 147.6, 144.3, 143.8, 142.4, 141.4, 140.6, 138.3, 135.6, 131.9, 129.7, 129.6, 129.4, 128.1, 127.9, 127.7, 127.3, 126.5, 126.0, 125.8, 125.6, 124.8, 124.6, 123.5, 123.0, 121.6, 119.8, 118.3, 113.2, 66.0, 62.2, 55.7, 50.0, 42.7, 36.2, 29.9, 29.6, 29.1, 26.1, 25.0, 13.7. HRMS (ESI) m/z Calcd. for $C_{50}H_{53}O_2N_6S$ $[M+H]^+$: 801.3952, found for 801.3941.

4.7.1.9. Tamoxifen-*N*-(4-triazolylbenzyl)-*N*-(2-amino-5-(thiophen-2-yl)phenyl)heptanamide (**12b**)

4-(4-Ethynylbenzyl)-tamoxifen **5** (50 mg, 0.1 mmol) and *N*-(2-amino-5-(thiophen-2-yl)phenyl)-4-azidoheptanamide **9b** (36.4 mg, 0.1 mmol) were dissolved in degassed anhydrous THF (5 mL). CuI (10 mg, 0.05 mmol) and Hünig's base (0.04 mL, 0.2 mmol) were added to the reaction and the resulting reaction was stirred at room temperature overnight. Then, the reaction mixture was diluted with excess ethyl acetate (30 mL) and was transferred to a separatory funnel and then the ethyl acetate layer was washed with a solution (20 mL) of 4:1 mixture of saturated aqueous NH₄Cl solution /NH₄OH solution, water (10 mL), brine (10 mL), dried over anhydrous Na₂SO₄, filtered, and concentrated *in vacuo*. The crude was purified by preparative TLC (Silica gel, 12:1:0.1 DCM/MeOH/NH₄OH) to give the title compound **12b** (80.0 mg, 93%) as a yellow oil. ¹H NMR (400 MHz, CDCl₃) δ 7.81 – 7.67 (m, 3H), 7.47 – 7.39 (m, 1H), 7.39 – 7.29 (m, 4H), 7.29 – 7.19 (m, 4H), 7.20 – 7.04 (m, 8H), 7.03 – 6.92 (m, 1H), 6.81 – 6.74 (m, 2H), 6.55 (d, *J* = 8.8 Hz, 2H), 4.32 (dd, *J* = 8.8, 5.0 Hz, 2H), 3.96 (t, *J* = 5.8 Hz, 2H), 2.76 (t, *J* = 5.8 Hz, 2H), 2.48 (dq, *J* = 14.8, 7.4 Hz, 2H), 2.40 – 2.30 (m, 2H), 2.27 (d, *J* = 10.1 Hz, 3H), 1.87 (d, *J* = 7.0 Hz, 2H), 1.70 (t, *J* = 18.5 Hz, 2H), 1.30 (ddd, *J* = 31.5, 16.0, 7.3 Hz, 6H), 0.99 – 0.87 (m, 3H). ¹³C NMR (101 MHz, MeOD) δ 174.9, 158.0, 148.6, 145.5, 145.0, 143.7, 142.6, 139.7, 138.8, 137.0, 133.0, 131.2, 130.9, 130.4, 129.2, 129.0, 128.9, 128.3, 127.7, 127.1, 126.7, 126.4, 125.8, 125.2, 124.3, 124.1, 122.7, 122.5, 122.2, 118.7, 114.3, 66.5, 63.0, 56.6, 51.2, 43.3, 37.0, 31.3, 30.1, 29.4, 27.2, 26.7, 14.3. HRMS (ESI) *m/z* Calcd. for C₅₁ H₅₅ O₂ N₆ S [M+H⁺]: 815.4102, found for 815.4084.

4.7.1.10. Tamoxifen-*N*-(4-triazolylbenzyl)-*N*-(2-amino-5-(thiophen-2-yl)phenyl)octanamide (**12c**)

4-(4-Ethynylbenzyl)-tamoxifen **5** (60 mg, 0.1 mmol) and *N*-(2-amino-5-(thiophen-2-yl)phenyl)-4-azidooctanamide **9c** (50 mg, 0.1 mmol) were dissolved in degassed anhydrous THF (5 mL). CuI (12 mg, 0.06 mmol) and Hünig's base (0.04 mL, 0.2 mmol) were added to the reaction and the resulting reaction was stirred at room temperature overnight. Then, the reaction mixture was diluted with excess ethyl acetate (30 mL) and was transferred to a separatory funnel and then the ethyl acetate layer was washed with a solution (20 mL) of 4:1 mixture of saturated aqueous NH₄Cl solution /NH₄OH solution, water (10 mL), brine (10 mL), dried over anhydrous Na₂SO₄, filtered, and concentrated *in vacuo*. The crude was purified by preparative TLC (Silica gel, 12:1:0.1 DCM/MeOH/NH₄OH) to give the title compound **12a** (13.0 mg, 14%) as a yellow oil. ¹H NMR (500 MHz, CDCl₃) δ 7.84 – 7.67 (m, 3H), 7.46 – 7.33 (m, 6H), 7.26 (d, *J* = 7.0 Hz, 3H), 7.21 (dd, *J* = 22.4, 14.8 Hz, 4H), 7.16 – 7.07 (m, 5H), 6.79 (d, *J* = 8.6 Hz, 2H), 6.57 (d, *J* = 8.3 Hz, 2H), 4.02 (s, 2H), 3.66 (d, *J* = 5.8 Hz, 2H), 2.83 (s, 2H), 2.46 (dt, *J* = 25.8, 13.0 Hz, 3H), 1.96 (s, 4H), 1.67 – 1.57 (m, 4H), 1.38 (s, 6H), 1.01 – 0.90 (m, 5H). ¹³C NMR (126 MHz, CDCl₃) δ 168.1, 143.8, 142.4, 138.2, 136.5, 131.9, 131.8, 129.7, 129.5, 128.1, 127.9, 127.8, 126.5, 126.2, 126.0, 125.9, 125.6, 124.7, 119.4, 115.7, 114.1, 113.9, 113.4, 100.0, 56.1, 51.5, 42.6, 32.0, 31.1, 31.0, 30.1, 29.7, 29.7, 29.4, 29.0, 28.9, 28.8, 28.8, 26.6, 26.2, 25.3, 25.1, 22.6, 17.0, 16.8, 14.1, 13.6. HRMS (ESI) *m/z* Calcd. for C₅₂ H₅₅ O₂ N₆ S [M+H⁺]: 827.4102, found for 827.4100.

4.7.2. Cell viability assay

All cell lines used in this study were maintained in phenol red free Dulbecco's Modified Eagle Medium (DMEM) and Eagles's Minimum Essential Medium (EMEM) (Corning, VA), supplemented with 10% fetal bovine serum (FBS) (Atlanta Biologicals, Atlanta, GA) and 1% *Penicillin-Streptomycin*. Cells were incubated in 96 well plate 24 h prior to treatment and then treated with various drugs' concentration for 72 h. Their anti-proliferative activity was measured using the MTS assay (CellTiter 96 Aqueous One

Solution and CellTiter 96 Non-Radioactive Cell Proliferation Assays, Promega, Madison, WI) as described by the manufacturer. All drugs solution were made in DMEM and EMEM while DMSO concentration was maintained at 0.1%.

4.7.3. SAMDI assay (*In vitro* HDAC inhibition, performed by Lindsey Szymczak at Northwestern University)

HDAC1, 2, 3, 8 and 6 were purchased from BPS Biosciences. To obtain IC₅₀ values, in a 96-well microtiter plates (60 min, 37 °C), isoform- optimized substrates (50 µM) were incubated with enzyme (250nM) and inhibitor (at concentrations ranging from .1 nM to 1.0 mM) in HDAC buffer (25.0 mM Tris-HCl, pH 8.0, 140 mM NaCl, 3.0 mM KCl, 1.0 mM MgCl₂, and 0.1 mg/mL BSA). Solution-phase deacetylation reactions were quenched with trichostatin A (TSA) and transferred to SAMDI plates to immobilize the substrate components. SAMDI plates were consist of an array of self-assembled monolayers (SAMs) presenting maleimide in standard 384-well format for high-throughput handling capability. Following immobilization, plates were washed to remove buffer constituents, enzyme, inhibitor, and any unbound substrate and analyzed by MALDI mass spectrometry using automated protocols. Deacetylation yields in each triplicate sample were obtained from the integrated peak intensities of the molecular ions for the substrate and the deacetylated product ion by taking the ratio of the former over the sum of both. Yields were plotted with respect to inhibitor concentration and fitted to obtain IC₅₀ values for each isoform–inhibitor pair.

Isoform-optimized substrates were prepared by traditional Fmoc solid-phase peptide synthesis (Anaspec) and purified by semi-preparative HPLC on a reverse-phase C18 column (Waters). The peptide GRK^{ac}FGC was prepared for HDAC1 and HDAC8 experiments, whereas the peptide GRK^{ac}YGC was prepared for HDAC6 experiments.

4.8. References

1. Bolden, J. E.; Peart, M. J.; Johnstone, R. W. Anticancer activities of histone deacetylase inhibitors. *Nature reviews Drug discovery* **2006**, 5, 769-784.
2. Thiagalingam, S.; CHENG, K. H.; Lee, H. J.; Mineva, N.; Thiagalingam, A.; Ponte, J. F. Histone deacetylases: unique players in shaping the epigenetic histone code. *Annals of the New York Academy of Sciences* **2003**, 983, 84-100.
3. Roth, S. Y.; Denu, J. M.; Allis, C. D. Histone acetyltransferases. *Annual review of biochemistry* **2001**, 70, 81-120.
4. Afifi, S.; Michael, A.; Azimi, M.; Rodriguez, M.; Lendvai, N.; Landgren, O. Role of Histone Deacetylase Inhibitors in Relapsed Refractory Multiple Myeloma: A Focus on Vorinostat and Panobinostat. *Pharmacotherapy: The Journal of Human Pharmacology and Drug Therapy* **2015**, 35, 1173-1188.
5. Hegde, M.; Mantelingu, K.; Pandey, M.; Pavankumar, C. S.; Rangappa, K. S.; Raghavan, S. C. Combinatorial Study of a Novel Poly (ADP-ribose) Polymerase Inhibitor and an HDAC Inhibitor, SAHA, in Leukemic Cell Lines. *Targeted oncology* **2016**, 1-11.
6. Calderwood, C.; Jones, M.; Hoile, L.; Thatcher, T.; Sime, P.; Maher, T.; O'Reilly, K.; Davies, D.; Davies, E. The Depsipeptide Hdac Inhibitor Fk228 Has Potent Anti-Fibrotic Properties In IpF Fibroblasts And Decreases The Expression Of Lysyl Oxidase A Potential IpF Biomarker. *Am J Respir Crit Care Med* **2013**, 187, A3993.
7. Johnston, P. B.; Cashen, A. F.; Nikolinakos, P. G.; Beaven, A. W.; Barta, S. K.; Bhat, G.; Song, T.; Choi, M. R.; Allen, L. F.; de Vos, S. Safe and effective treatment of patients with peripheral T-cell lymphoma (PTCL) with the novel HDAC inhibitor, Belinostat, in combination with CHOP: results of the Bel-CHOP phase 1 trial. *Blood* **2015**, 126, 253-253.
8. Wahaib, K.; Beggs, A. E.; Campbell, H.; Kodali, L.; Ford, P. D. Panobinostat: A histone deacetylase inhibitor for the treatment of relapsed or refractory multiple myeloma. *American Journal of Health-System Pharmacy* **2016**, 73.
9. Shi, Y.-K.; Dong, M.; Hong, X.-N.; Zhang, W.-J.; Feng, J.-F.; Zhu, J.; Yu, L.; Ke, X.-Y.; Huang, H.-Q.; Shen, Z.-X. In *Phase II study of chidamide (CS055), a new subtype-selective oral histone deacetylase inhibitor, in patients with relapsed or refractory peripheral T-cell lymphoma*, ASCO Annual Meeting Proceedings, 2013; 2013; p 8525.
10. Gryder, B. E.; Sodji, Q. H.; Oyelere, A. K. Targeted cancer therapy: giving histone deacetylase inhibitors all they need to succeed. *Future medicinal chemistry* **2012**, 4, 505-524.

11. Mottamal, M.; Zheng, S.; Huang, T. L.; Wang, G. Histone deacetylase inhibitors in clinical studies as templates for new anticancer agents. *Molecules* **2015**, *20*, 3898-3941.
12. Carew, J. S.; Giles, F. J.; Nawrocki, S. T. Histone deacetylase inhibitors: mechanisms of cell death and promise in combination cancer therapy. *Cancer letters* **2008**, *269*, 7-17.
13. Mandlekar, S.; Yu, R.; Tan, T.-H.; Kong, A.-N. T. Activation of caspase-3 and c-Jun NH2-terminal kinase-1 signaling pathways in tamoxifen-induced apoptosis of human breast cancer cells. *Cancer Research* **2000**, *60*, 5995-6000.
14. Ring, A.; Dowsett, M. Mechanisms of tamoxifen resistance. *Endocrine-related cancer* **2004**, *11*, 643-658.
15. Lv, W.; Liu, J.; Skaar, T. C.; Flockhart, D. A.; Cushman, M. Design and synthesis of norendoxifen analogues with dual aromatase inhibitory and estrogen receptor modulatory activities. *Journal of medicinal chemistry* **2015**, *58*, 2623-2648.
16. Speirs, V.; Malone, C.; Walton, D. S.; Kerin, M. J.; Atkin, S. L. Increased expression of estrogen receptor β mRNA in tamoxifen-resistant breast cancer patients. *Cancer Research* **1999**, *59*, 5421-5424.
17. Sharma, D.; Saxena, N. K.; Davidson, N. E.; Vertino, P. M. Restoration of tamoxifen sensitivity in estrogen receptor-negative breast cancer cells: tamoxifen-bound reactivated ER recruits distinctive corepressor complexes. *Cancer research* **2006**, *66*, 6370-6378.
18. Schneider, B. J.; Kalemkerian, G. P.; Bradley, D.; Smith, D. C.; Egorin, M. J.; Daignault, S.; Dunn, R.; Hussain, M. Phase I study of vorinostat (suberoylanilide hydroxamic acid, NSC 701852) in combination with docetaxel in patients with advanced and relapsed solid malignancies. *Investigational new drugs* **2012**, *30*, 249-257.
19. Webb, P.; Nguyen, P.; Kushner, P. J. Differential SERM effects on corepressor binding dictate ER α activity in vivo. *Journal of Biological Chemistry* **2003**, *278*, 6912-6920.
20. Morphy, R.; Rankovic, Z. Designed multiple ligands. An emerging drug discovery paradigm. *Journal of medicinal chemistry* **2005**, *48*, 6523-6543.
21. Dao, K.-L.; Sawant, R. R.; Hendricks, J. A.; Ronga, V.; Torchilin, V. P.; Hanson, R. N. Design, Synthesis, and Initial Biological Evaluation of a Steroidal Anti-Estrogen-Doxorubicin Bioconjugate for Targeting Estrogen Receptor-Positive Breast Cancer Cells. *Bioconjugate chemistry* **2012**, *23*, 785-795.
22. Peng, K.-w.; Wang, H.; Qin, Z.; Wijewickrama, G. T.; Lu, M.; Wang, Z.; Bolton, J. L.; Thatcher, G. R. Selective estrogen receptor modulator delivery of quinone

warheads to DNA triggering apoptosis in breast cancer cells. *ACS chemical biology* **2009**, 4, 1039-1049.

23. Li, C.; Tang, C.; Hu, Z.; Zhao, C.; Li, C.; Zhang, S.; Dong, C.; Zhou, H.-B.; Huang, J. Synthesis and structure–activity relationships of novel hybrid ferrocenyl compounds based on a bicyclic core skeleton for breast cancer therapy. *Bioorganic & medicinal chemistry* **2016**, 24, 3062-3074.

24. Gryder, B. E.; Rood, M. K.; Johnson, K. A.; Patil, V.; Raftery, E. D.; Yao, L.-P. D.; Rice, M.; Azizi, B.; Doyle, D. F.; Oyelere, A. K. Histone deacetylase inhibitors equipped with estrogen receptor modulation activity. *Journal of medicinal chemistry* **2013**, 56, 5782-5796.

25. Levin, E. R. Plasma membrane estrogen receptors. *Trends in Endocrinology & Metabolism* **2009**, 20, 477-482.

26. Cheng, S.-B.; Graeber, C. T.; Quinn, J. A.; Filardo, E. J. Retrograde transport of the transmembrane estrogen receptor, G-protein-coupled-receptor-30 (GPR30/GPER) from the plasma membrane towards the nucleus. *Steroids* **2011**, 76, 892-896.

27. Bertrand, P. Inside HDAC with HDAC inhibitors. *European journal of medicinal chemistry* **2010**, 45, 2095-2116.

28. Tapadar, S.; Fathi, S.; Raji, I.; Omesiete, W.; Kornacki, J. R.; Mwakwari, S. C.; Miyata, M.; Mitsutake, K.; Li, J.-D.; Mrksich, M. A structure–activity relationship of non-peptide macrocyclic histone deacetylase inhibitors and their anti-proliferative and anti-inflammatory activities. *Bioorganic & Medicinal Chemistry* **2015**, 23, 7543-7564.

29. Olofson, R.; Martz, J. T.; Senet, J. P.; Piteau, M.; Malfroot, T. A new reagent for the selective, high-yield N-dealkylation of tertiary amines: improved syntheses of naltrexone and nalbuphine. *The Journal of Organic Chemistry* **1984**, 49, 2081-2082.

30. Oyelere, A. K.; Chen, P. C.; Guerrant, W.; Mwakwari, S. C.; Hood, R.; Zhang, Y.; Fan, Y. Non-peptide macrocyclic histone deacetylase inhibitors. *Journal of medicinal chemistry* **2008**, 52, 456-468.

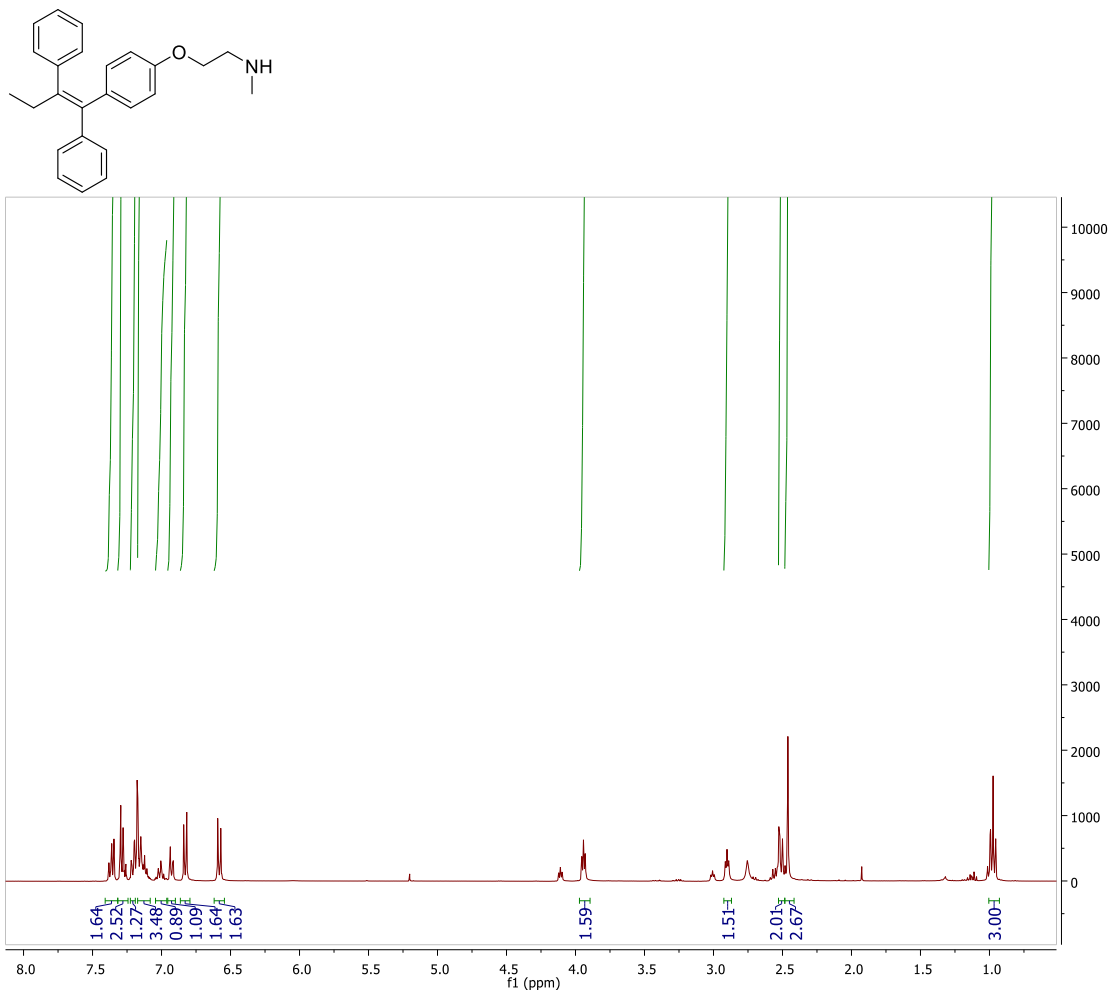
31. Gryder, B. E.; Akbashev, M. J.; Rood, M. K.; Raftery, E. D.; Meyers, W. M.; Dillard, P.; Khan, S.; Oyelere, A. K. Selectively targeting prostate cancer with antiandrogen equipped histone deacetylase inhibitors. *ACS chemical biology* **2013**, 8, 2550-2560.

32. Sodji, Q. H.; Kornacki, J. R.; McDonald, J. F.; Mrksich, M.; Oyelere, A. K. Design and structure activity relationship of tumor-homing histone deacetylase inhibitors conjugated to folic and pteric acids. *European journal of medicinal chemistry* **2015**, 96, 340-359.

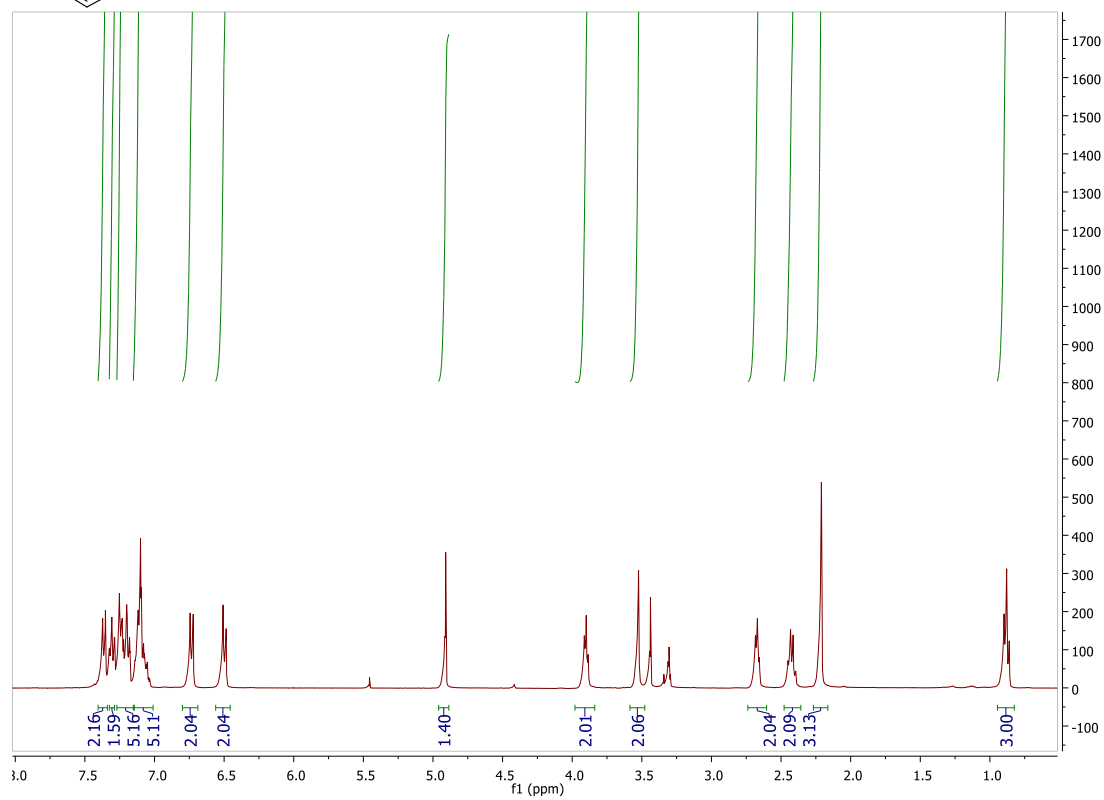
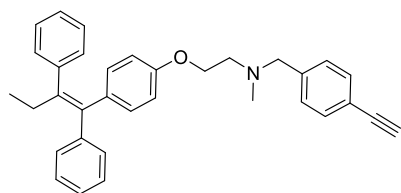
33. Bock, V. D.; Hiemstra, H.; Van Maarseveen, J. H. CuI-Catalyzed Alkyne–Azide “Click” Cycloadditions from a Mechanistic and Synthetic Perspective. *European Journal of Organic Chemistry* **2006**, 2006, 51-68.
34. Díaz, D. D.; Punna, S.; Holzer, P.; McPherson, A. K.; Sharpless, K. B.; Fokin, V. V.; Finn, M. Click chemistry in materials synthesis. 1. Adhesive polymers from copper-catalyzed azide-alkyne cycloaddition. *Journal of Polymer Science Part A: Polymer Chemistry* **2004**, 42, 4392-4403.
35. Rostovtsev, V. V.; Green, L. G.; Fokin, V. V.; Sharpless, K. B. A stepwise huisgen cycloaddition process: copper (I)-catalyzed regioselective “ligation” of azides and terminal alkynes. *Angewandte Chemie* **2002**, 114, 2708-2711.
36. Park, S. Y.; Jun, J.; Jeong, K. J.; Heo, H. J.; Sohn, J. S.; Lee, H. Y.; Park, C. G.; Kang, J. Histone deacetylases 1, 6 and 8 are critical for invasion in breast cancer. *Oncology reports* **2011**, 25, 1677-1681.
37. Witt, O.; Deubzer, H. E.; Milde, T.; Oehme, I. HDAC family: What are the cancer relevant targets? *Cancer letters* **2009**, 277, 8-21.
38. Min, D.-H.; Yeo, W.-S.; Mrksich, M. A method for connecting solution-phase enzyme activity assays with immobilized format analysis by mass spectrometry. *Analytical chemistry* **2004**, 76, 3923-3929.
39. Moradei, O. M.; Mallais, T. C.; Frechette, S.; Paquin, I.; Tessier, P. E.; Leit, S. M.; Fournel, M.; Bonfils, C.; Trachy-Bourget, M.-C.; Liu, J. Novel aminophenyl benzamide-type histone deacetylase inhibitors with enhanced potency and selectivity. *Journal of medicinal chemistry* **2007**, 50, 5543-5546.
40. Muller, P. Y.; Milton, M. N. The determination and interpretation of the therapeutic index in drug development. *Nature reviews Drug discovery* **2012**, 11, 751-761.
41. Group, E. B. C. T. C. Tamoxifen for early breast cancer: an overview of the randomised trials. *The Lancet* **1998**, 351, 1451-1467.
42. Yang, X.; Phillips, D. L.; Ferguson, A. T.; Nelson, W. G.; Herman, J. G.; Davidson, N. E. Synergistic activation of functional estrogen receptor (ER)- α by DNA methyltransferase and histone deacetylase inhibition in human ER- α -negative breast cancer cells. *Cancer research* **2001**, 61, 7025-7029.
43. Mwakwari, S. C.; Guerrant, W.; Patil, V.; Khan, S. I.; Tekwani, B. L.; Gurard-Levin, Z. A.; Mrksich, M.; Oyelere, A. K. Non-peptide macrocyclic histone deacetylase inhibitors derived from tricyclic ketolide skeleton. *Journal of medicinal chemistry* **2010**, 53, 6100-6111.

4.9. Supplementary data

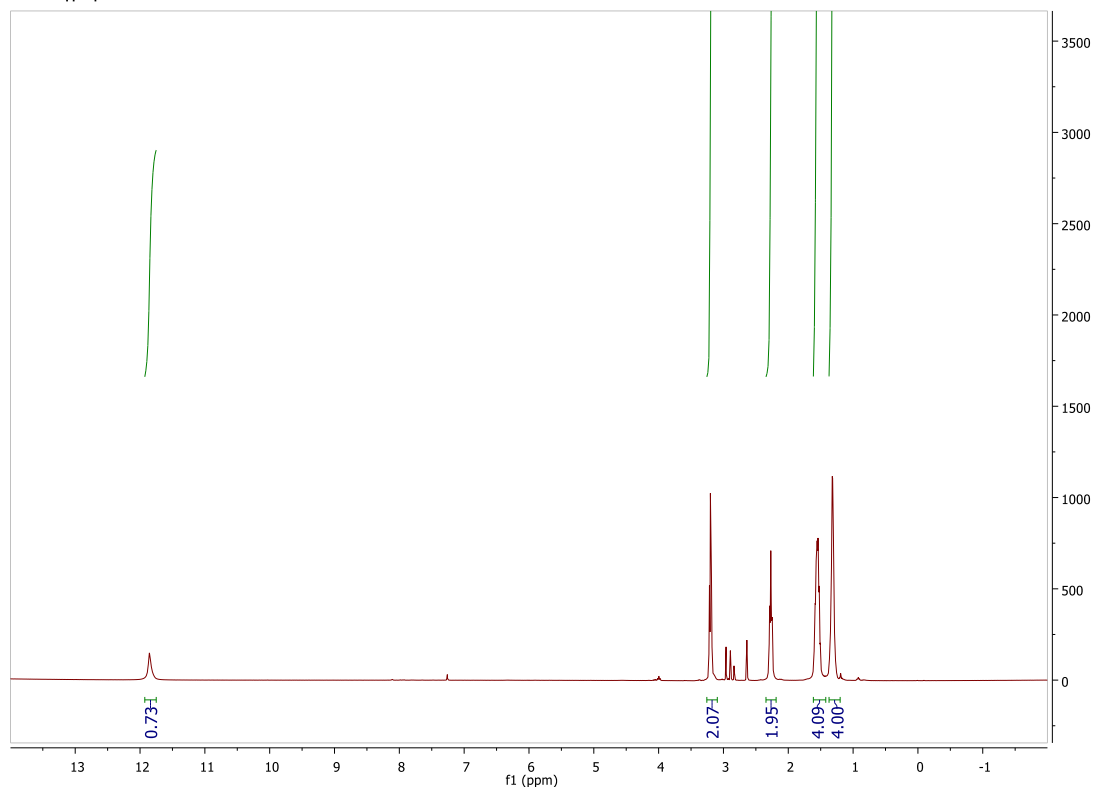
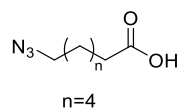
3 ^1H NMR



5 ^1H NMR

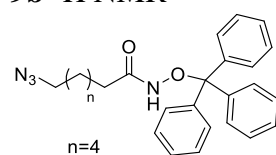


7b ¹H NMR

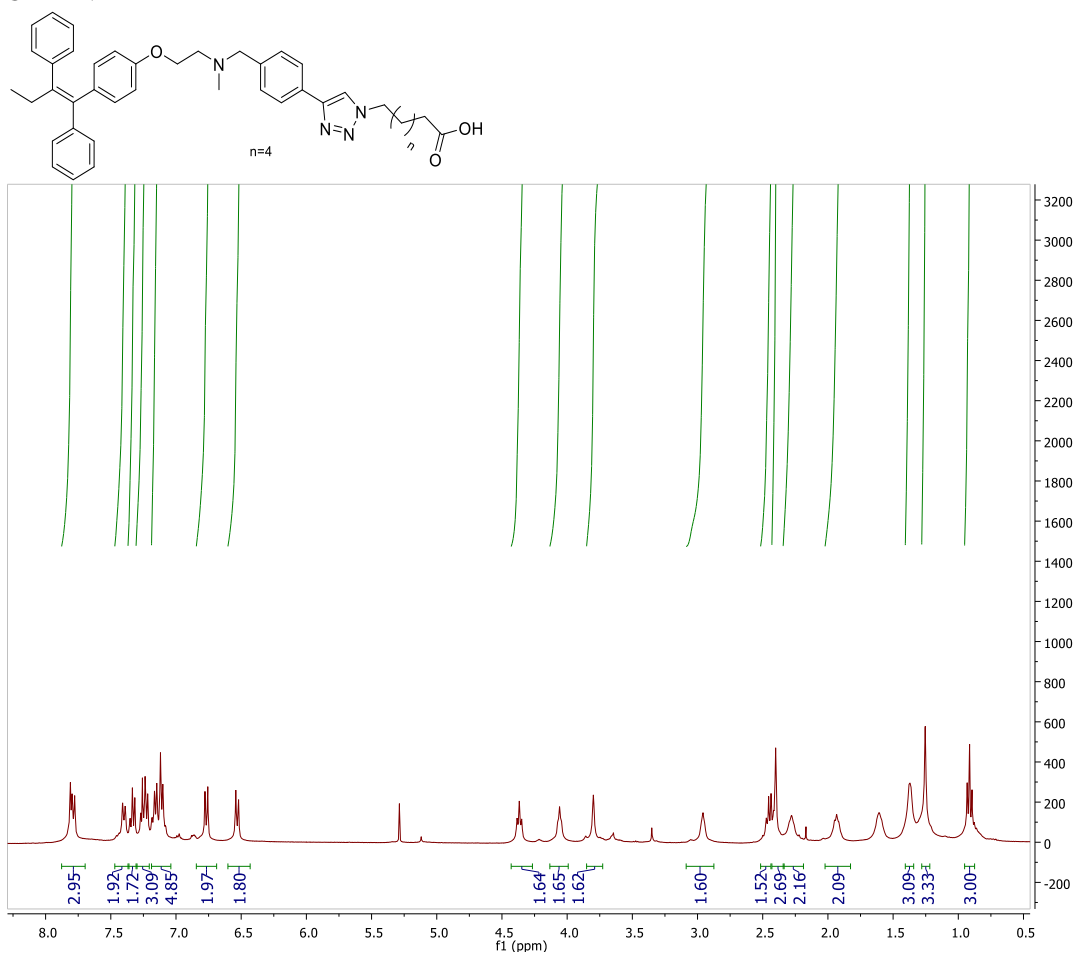


N=[N+]#NCCCC(=O)Nc1ccccc1C2(c3ccccc3)c4ccccc24

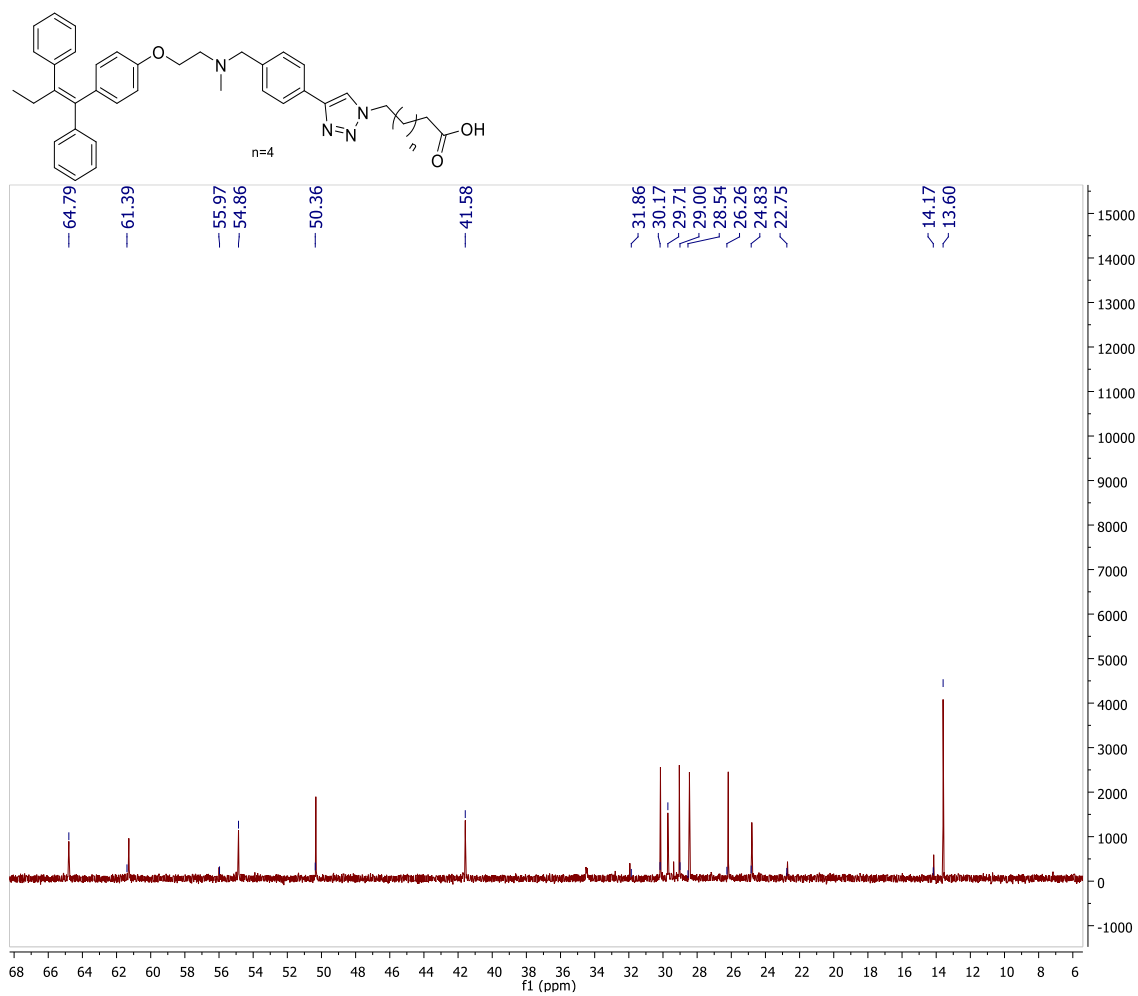
$n=4$



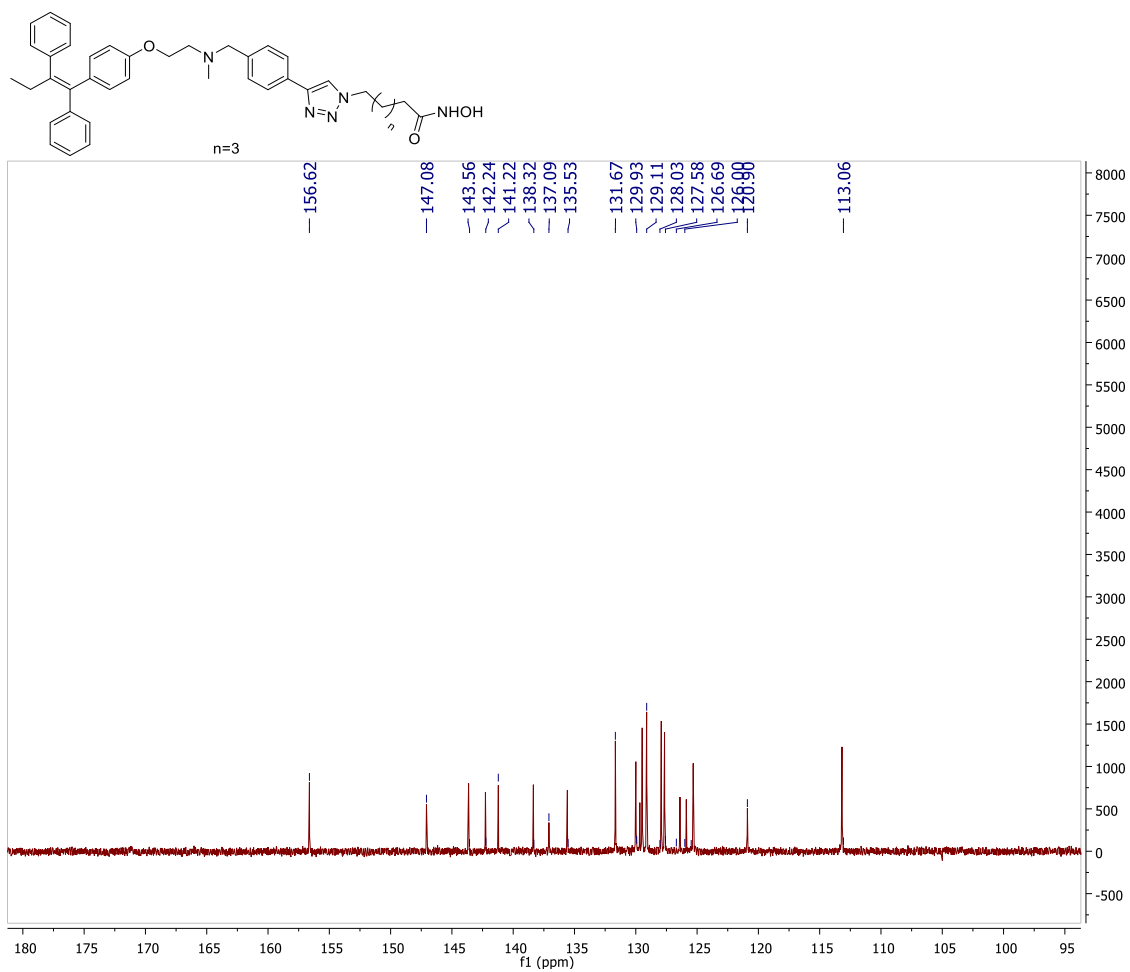
8 ¹H NMR



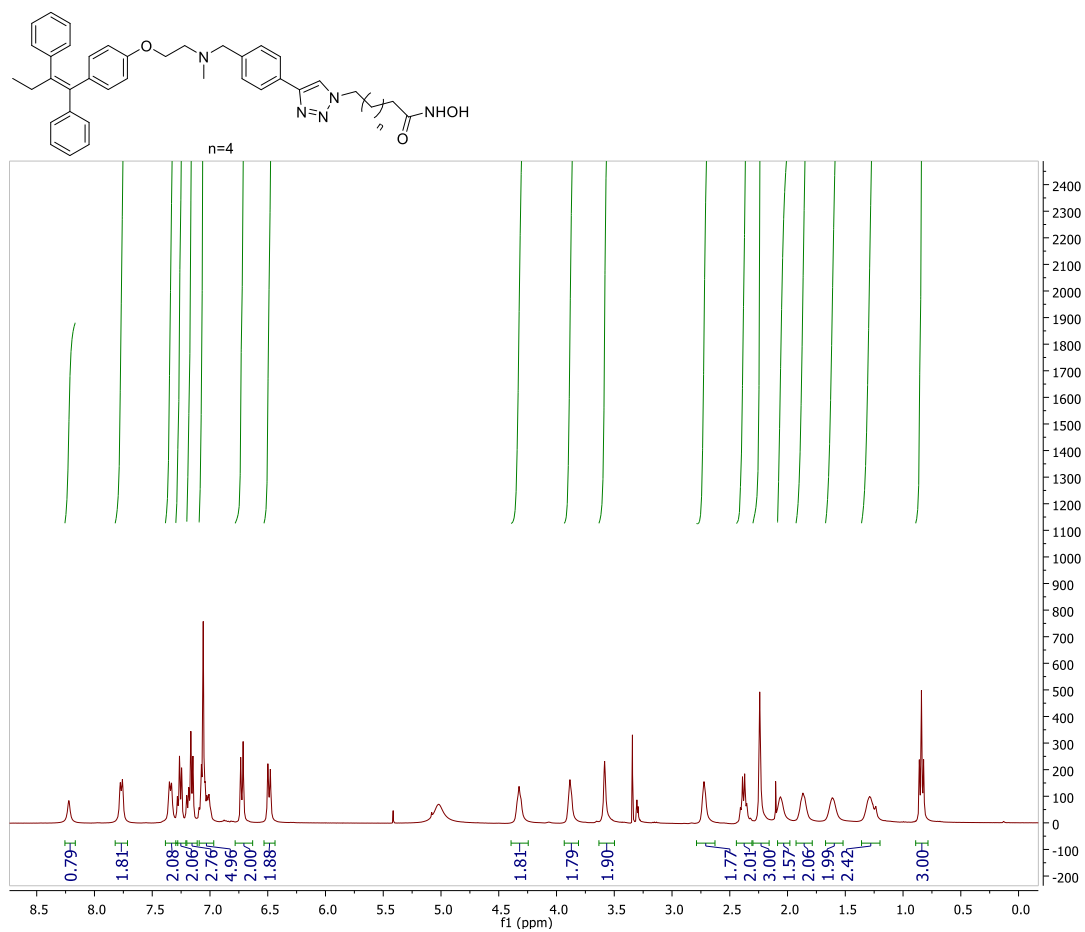
8 ^{13}C NMR



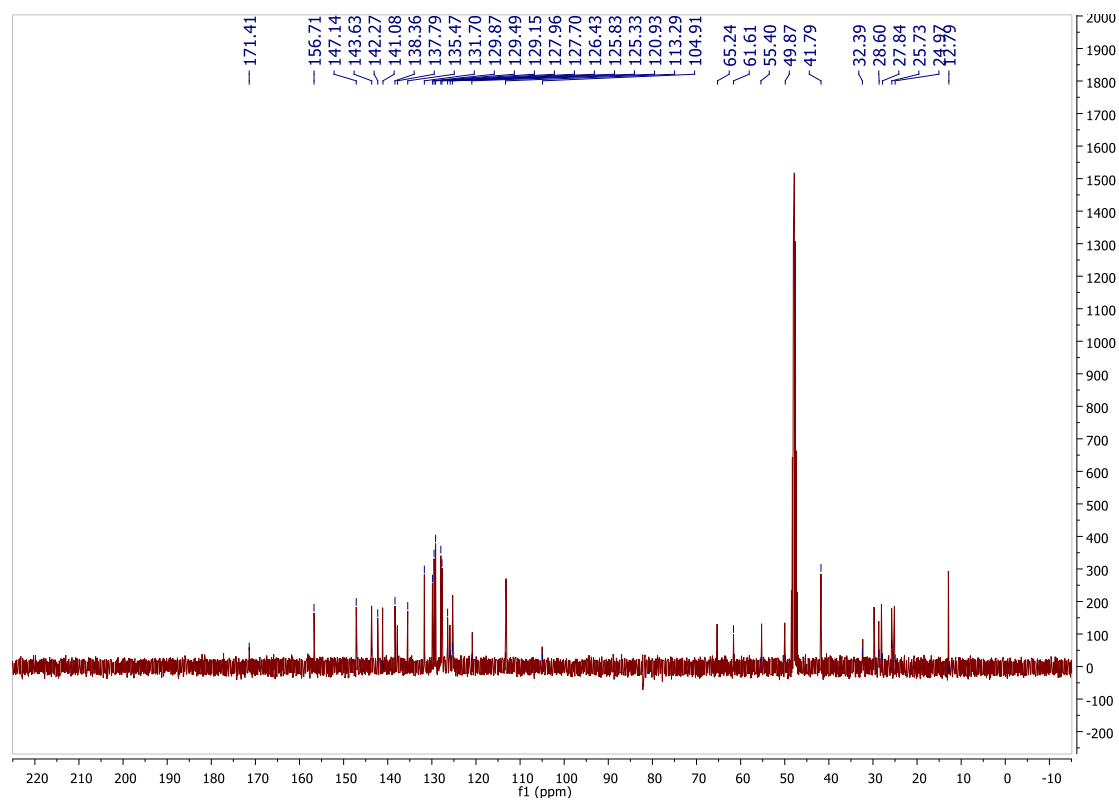
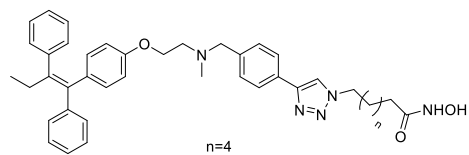
10a ^{13}C NMR



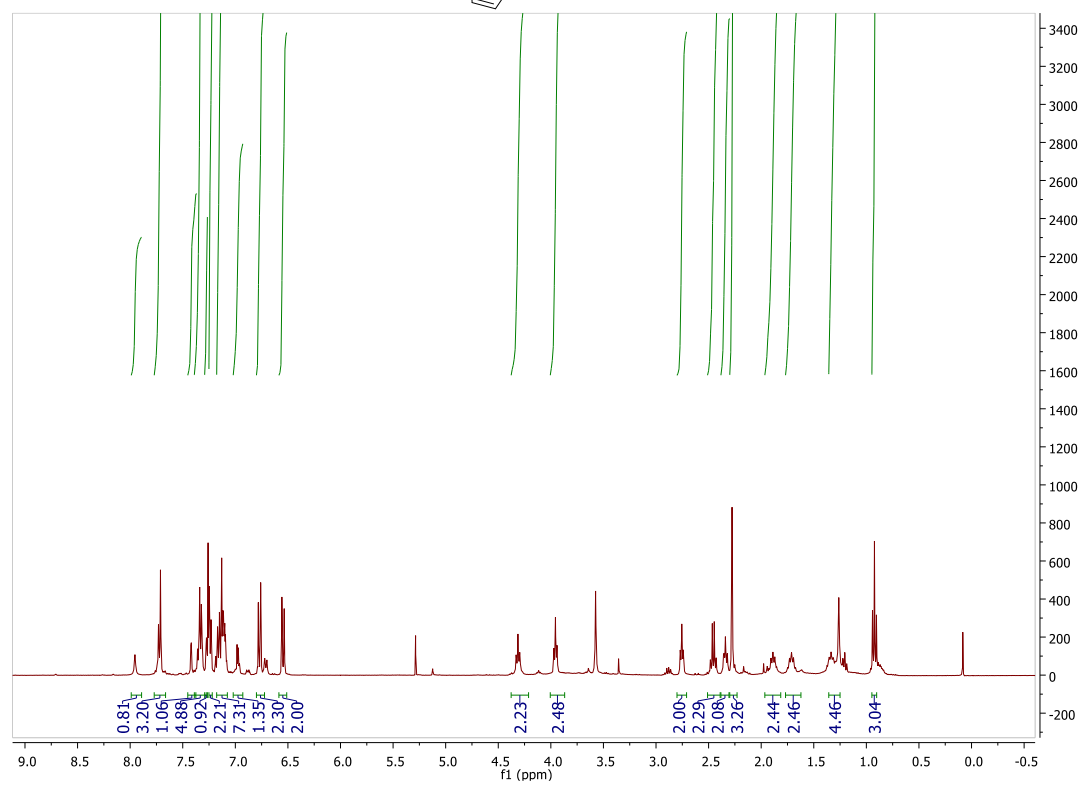
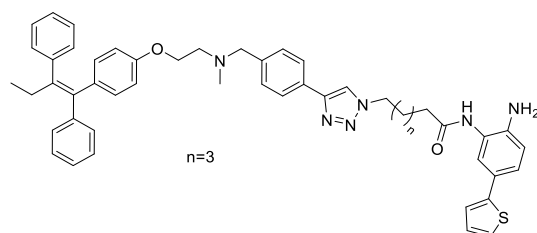
10b ^1H NMR



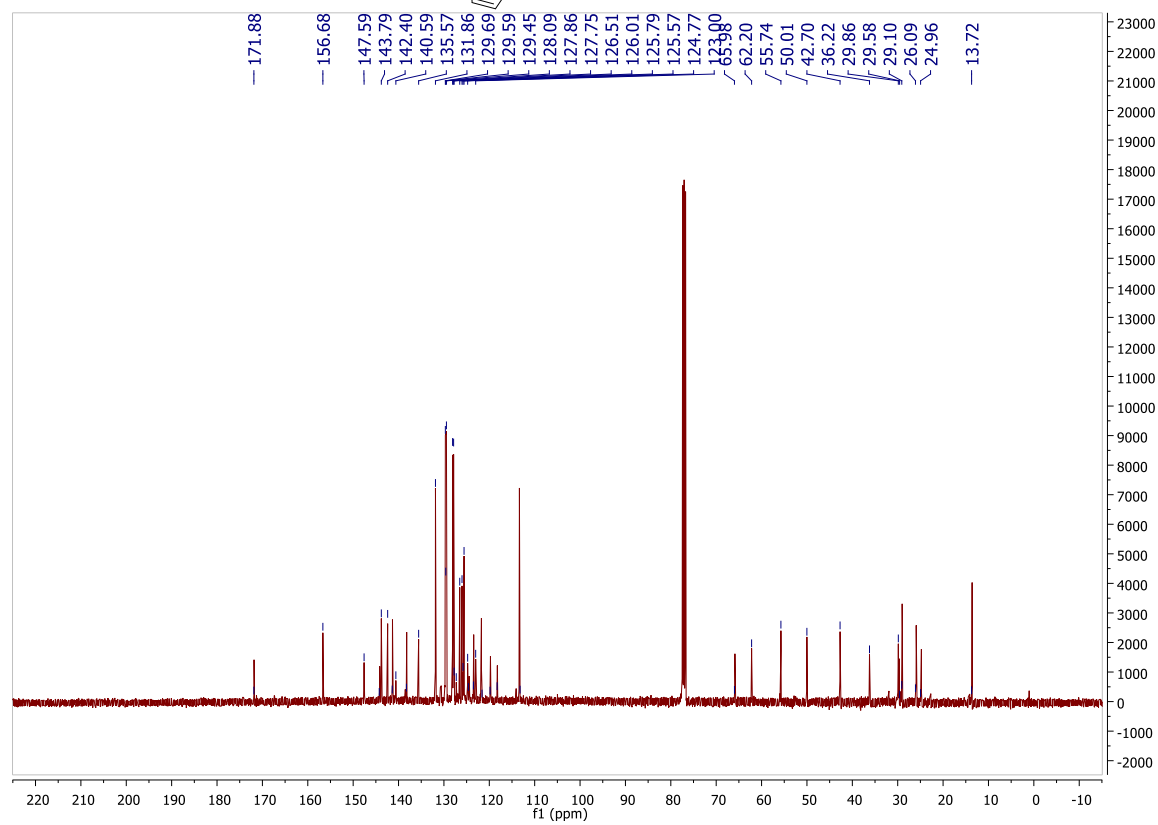
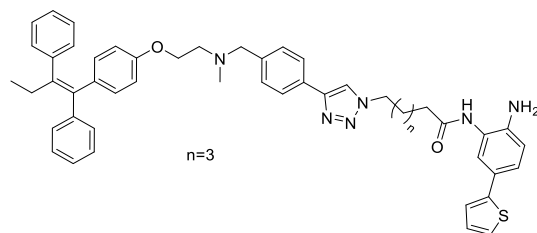
10b ^{13}C NMR



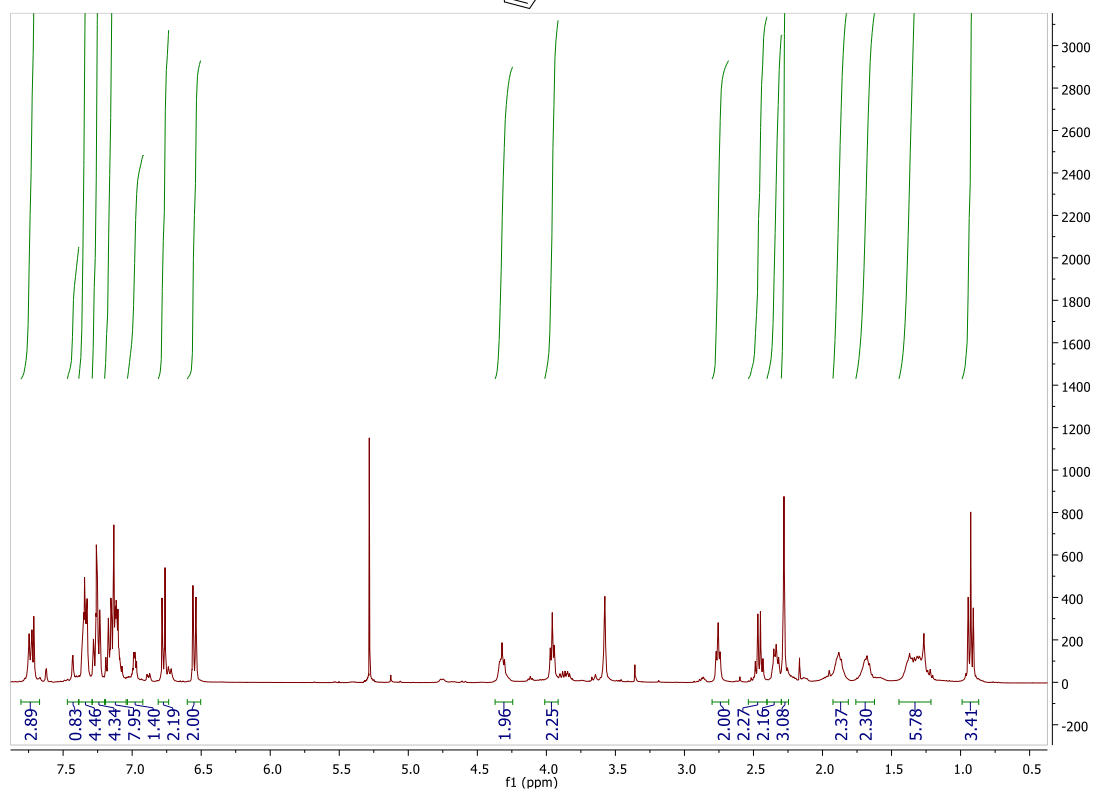
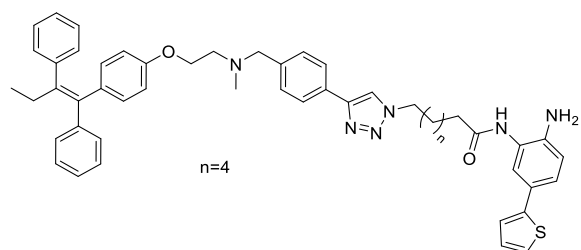
12a ^1H NMR



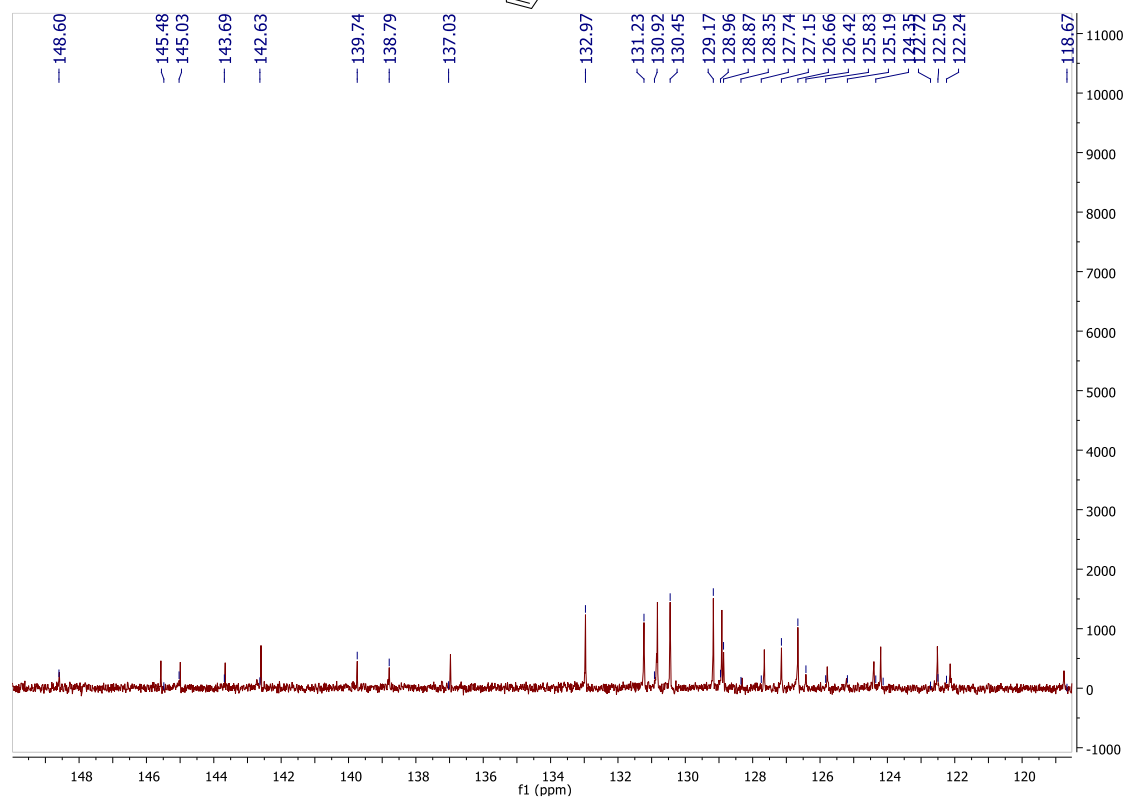
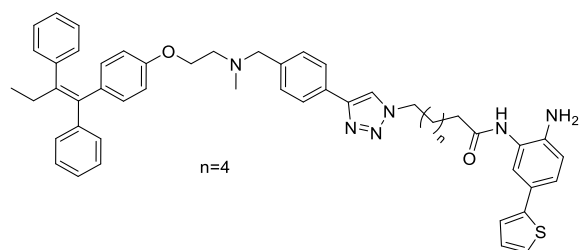
12a ^{13}C NMR



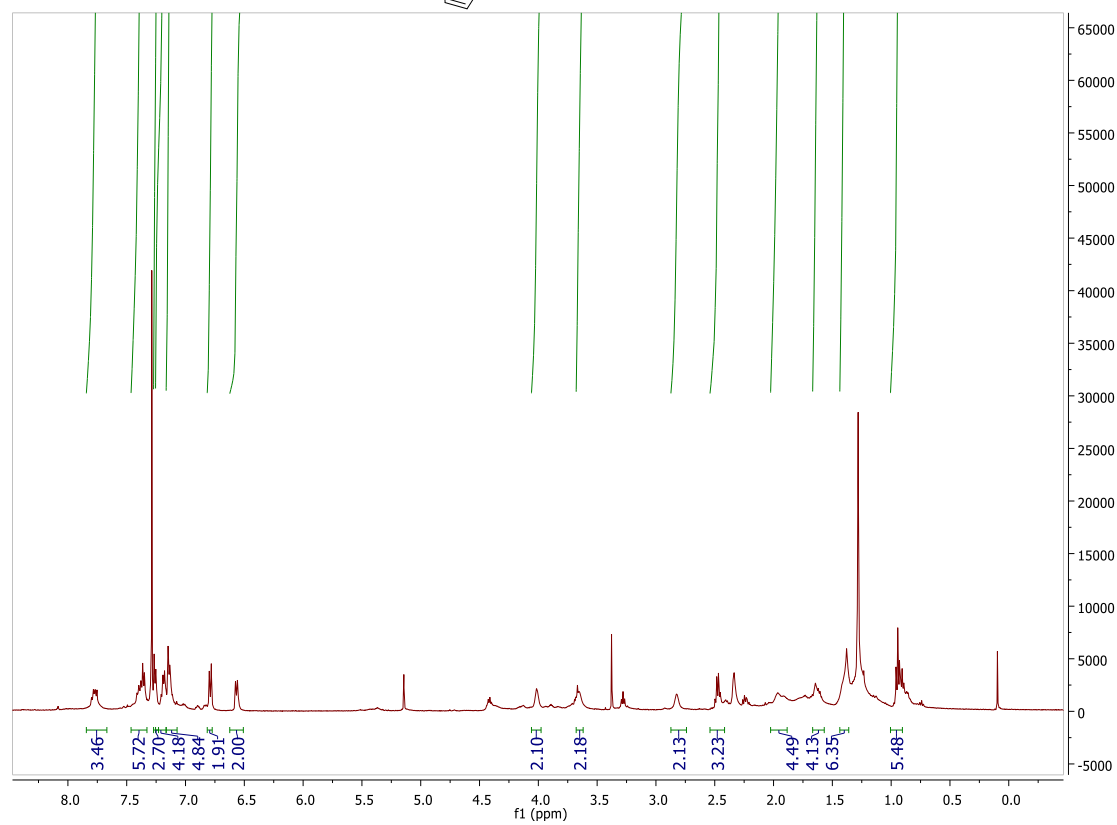
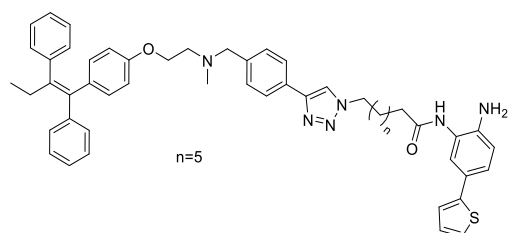
12b ^1H NMR



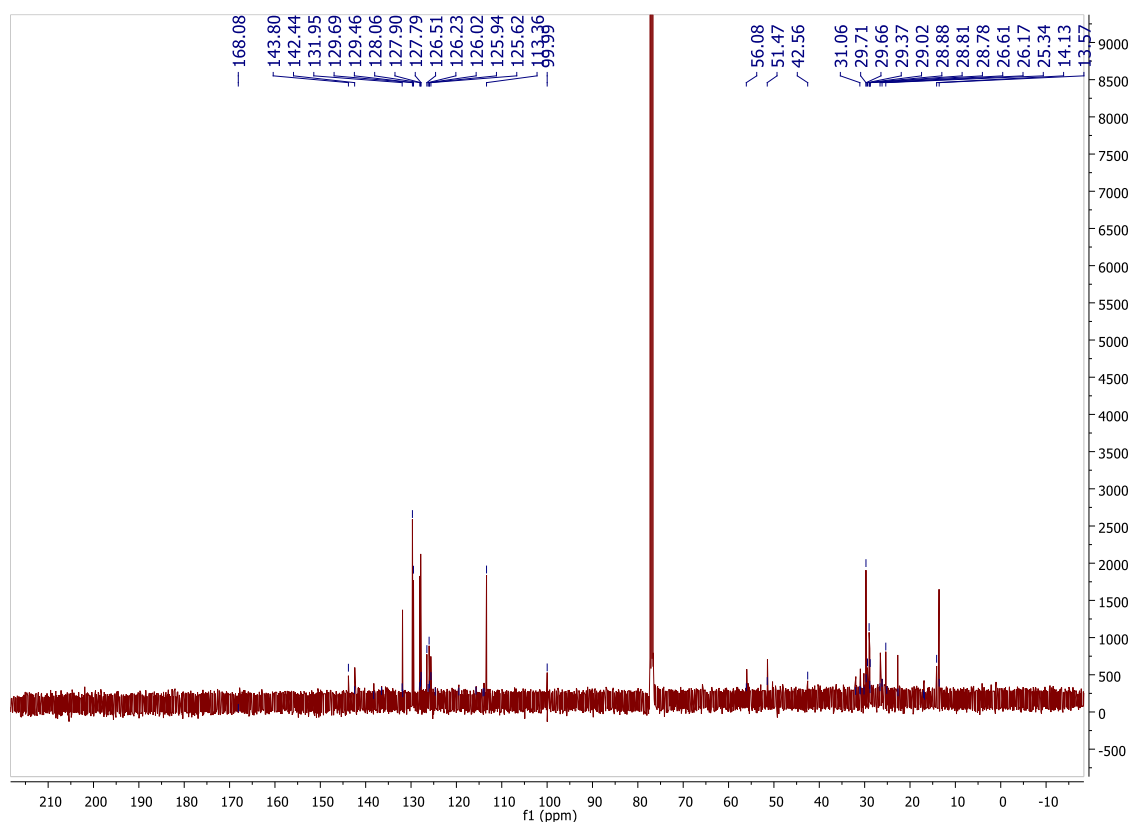
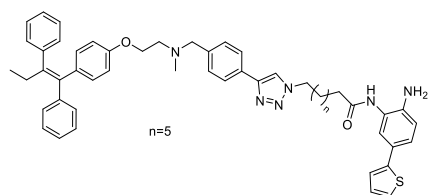
12b ^{13}C NMR



12c ^1H NMR



12c ^{13}C NMR



CHAPTER 5

BIFUNCTIONAL STAT3/HISTONE DEACETYLASE

INHIBITORS FOR TREATING STAT3 DEPENDENT TUMORS

5.1. Introduction

Pyrimethamine is an antifolate drug used as an antimalarial agent (Figure 5.1) [1] and has also been used in chemotherapy along with other drugs such as proguanil for few decades [2]. Its antimalarial activity originates from its ability to specifically bind and inhibit dihydrofolate reductase (DHFR, 5,6,7,8-tetrahydrofolate: NADP⁺ oxidoreductase, EC 1.5.1.3) in *Plasmodium falciparum* and some other protozoa [3], [4]. DHFR is critical for folate metabolism and has been a drug target for fungal, protozoal and bacterial infections and cancer. It facilitates an NADPH-dependent reduction of dihydrofolate to tetrahydrofolate, a cofactor necessary for the biosynthesis of thymidylate, purine nucleotides, and many other essential amino acids required for protein, RNA and DNA synthesis [5]. DHFR inhibition by antifolate compounds interferes with these pathways, resulting in cell cycle arrest and cell death [6].

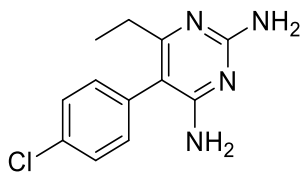


Figure 5.1. Structure of pyrimethamine, an antifolate drug with antimalarial activity. Pyrimethamine is a STAT3 inhibitor and is currently in clinical trial for treating relapsed chronic lymphocytic leukemia (CLL) and small lymphocytic lymphoma (SLL).

Unfortunately, pyrimethamine's use as a standalone antimalarial agent has been hampered by naturally occurrence of drug resistance in the parasite [1]. Mutations in the gene encoding dihydrofolate reductase-thymidylate synthesis are responsible for the

developed drug resistance [7], [8]. To overcome the developed resistance obstacle, pyrimethamine has been used in combination therapy with other drugs such as sulfadoxine to treat malaria. However, parasite mutations in DHFR conferred sulfadoxine- pyrimethamine- resistant as well [9].

However, despite the pyrimethamine failure in treating malaria recent years, studies have shown it inhibits proliferation of acute myeloid leukemia (AML) by targeting a protein in tumor cells called STAT3 (Signal transducer and activator of transcription 3) [10], [11], [12]. In fact, pyrimethamine is currently in phase I/II clinical trials for the treatment of relapsed chronic lymphocytic leukemia (CLL) and small lymphocytic lymphoma (SLL) (ClinicalTrials.gov Identifier: NCT01066663).

STAT proteins, a family of seven members (STAT1, 2, 3, 4, 5a, 5b, 6), were discovered in 1993 by Shuai *et al* [13]. STAT3, an oncogenic transcription factor with critical role in the signaling of a number of cytokines and growth factors, confers resistance to apoptosis in various cell types [14] and is activated in many cancers [15], [11]. STAT3 activation through its tyrosine phosphorylation by JAK (Janus kinase) or IL-6 signaling cascade [16] enhances its dimerization and translocation from cytoplasm to nucleus where it can bind to certain DNA sequences and regulates genes expression involved in various cellular processes. Tyrosine phosphorylation is not the only way to activate STAT3. It can be activated through other processes such as serine phosphorylation, acetylation, methylation and glutathionylation [17], [18], [19]. Once STAT3 is activated it enhances various cell processes such as cell proliferation, differentiation, survival and angiogenesis that contribute to malignant transformation and progression in many cancers such as breast, ovary, and prostate [20]. Although STAT3 has non-transcriptional responsibilities, such as regulation of mitochondrial function, most of its oncogenic activities is related to its gene regulation in nucleus [12].

Activation of STAT3 is tightly regulated in normal conditions, however in cancer, it is highly activated and leads to malignant cancer cells phenotype [21]. Therefore,

inhibiting STAT3 can be a promising strategy for cancer therapy as a wide variety of cancers depend on STAT3 for their survival. Additionally, there is less chance for developing resistance due to convergence of many cellular pathways on STAT3. STAT3 inhibitors exhibit synergetic effect with other therapeutic agents in inhibiting tumor stem cells, leading to improved therapeutic indices for these agents.

Histone deacetylase (HDAC) enzymes are a class of proteins that play an important role in regulating STAT3 activation [22]. HDACs along with histone acetyl transferase (HAT) control gene expression, chromatin condensation and play an essential role in transcriptional activation by regulating acetylation state of histone proteins [23]. In addition to histone proteins, several non-histone proteins, including transcription factors (E2F, STAT3, P53, NF- κ B), estrogen receptor (ER α), androgen receptor (AR), α -tubulin, and chaperons (HSP90) are regulated by HDAC and HAT activity [24]. Due to critical role of HDACs in regulating a wide range of cellular pathways such as cell survival, differentiation, cell cycle progression, angiogenesis and immunity, HDACs are considered as promising targets, and their inhibition has emerged as a potential strategy in treating various diseases like malaria, leishmania, and most importantly cancer [25], [26]. To date, there are four US FDA approved HDACis, namely, SAHA (suberoylanilide hydroxamic acid, vorinostat) approved in 2006 for relapsed and refractory cutaneous T-cell lymphoma (CTCL) [27], romidepsin (FK228) approved in 2009 for relapsed/refractory peripheral T-cell lymphoma [28], belinostat (PXD101) approved in 2014 for relapsed/refractory peripheral T-cell lymphoma [29], and lastly panobinostat (LBH589) in 2015 for treating acute myeloma (Figure 5.2) [30]. Chidamide (CS055) is another HDACi which is only approved in China for treating relapsed/ refractory peripheral T-cell lymphoma. Chidamide is in phase II clinical trials in US [31].

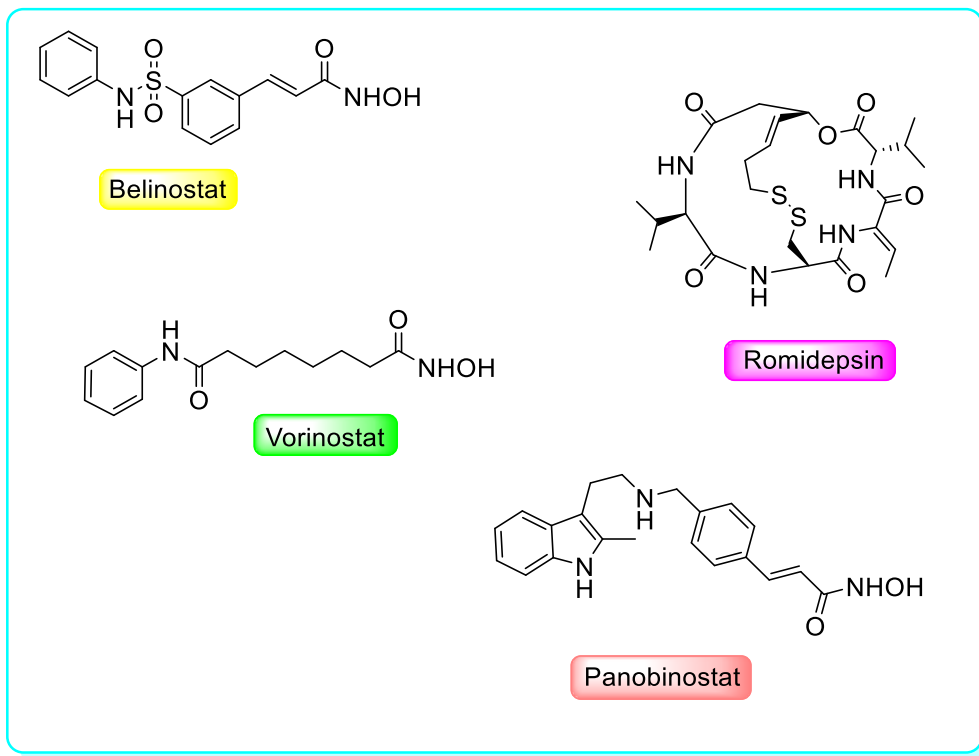


Figure 5.2. US FDA approved HDACi.

Inhibition and knockdown of class I HDAC, specifically HDAC3, has been shown to result in upregulated STAT3Lys685 acetylation, attenuated STAT3Tyr705 phosphorylation and inhibition of survival of pSTAT3-positive diffuse large B-cell lymphoma (DLBCL) cells. The DLBCL cytotoxicity is linked to downregulation of the direct STAT3 target myeloid leukemia cell differentiation protein (Mcl-1), a pro-cell survival protein encoded by *MCL1* gene [32]. Therefore, targeting STAT3-positive DLBCL cells with HDACi is another potentially viable therapeutic option for managing CLL and DLBCL tumors. We hypothesized that designed multiple ligands comprising pyrimethamine and HDAC inhibition chemotype will integrate direct stat3- and HDAC-inhibition, and downregulation of Mcl-1 within a single molecular template. These pyrimethamine-HDACi conjugates are anticipated to be more efficient inhibitors of

proliferation of CLL, DLBCL and possibly other tumors which are exquisitely dependent on STAT3 signaling pathway.

5.2. Design of Pyrimethamine-HDACi Conjugates

The three-motif HDACi pharmacophoric model consists of a recognition cap group, linker group, and zinc binding group (ZBG) (Figure 5.3) [33]. Pyrimethamine structure closely resembles HDACi aryl-derived cap group. Moreover, substitution of the pyrimithamine halogen group with alkyl, aryl and ring systems have been shown to be compatible with DHFR inhibition. Based on these observations, I designed two classes of pyrimethamine-HDACi conjugates using pyrimethamine as a surrogate for HDACi cap group.

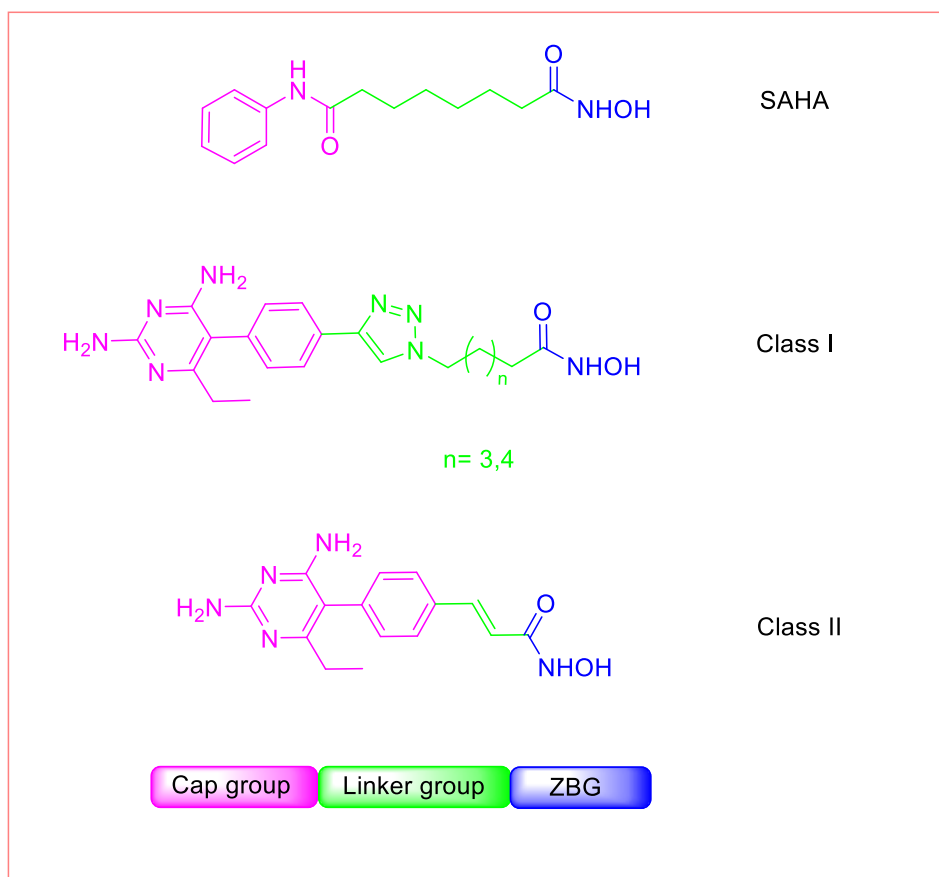
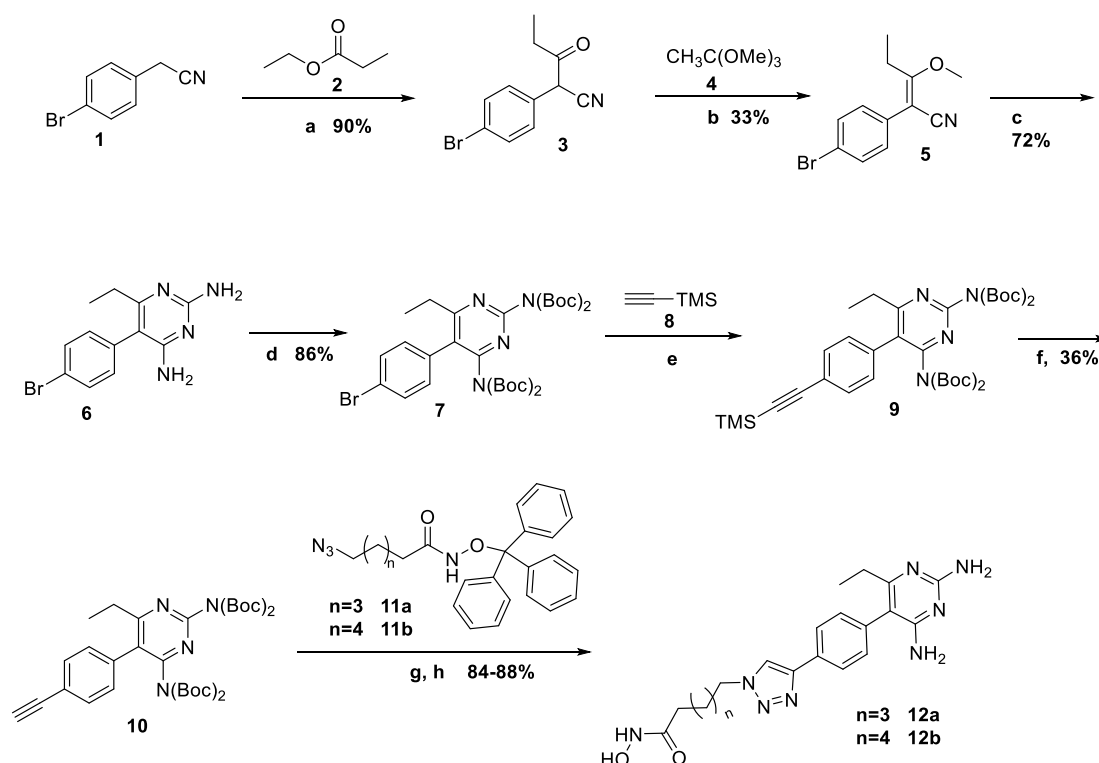


Figure 5.3. Pharmacophoric model of HDACi, and the two classes of pyrimethamine HDACi-conjugates.

For aryl triazolyl HDACi, we had previously shown that five and six methylenes are ideal length of for linker group to ensure optimal zinc chelation [25]. Therefore, I limited the linker length to five and six methylene groups in my design.

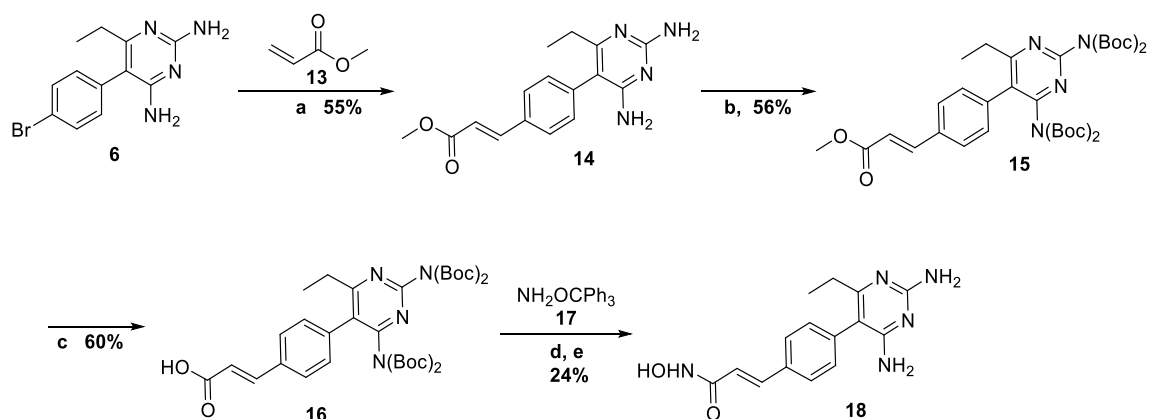
5.3. Chemistry and synthesis

To synthesizethe the class I pyrimethamine-HDACi conjugates, 4-bromophenyl acetonitrile **1** was reacted with ethyl propanoate **2** under basic condition to yield β -ketonitrile **3** [34] the keto group of which was then converted to methoxy **5** using trimethyl orthoformate **4** [35]. Pyrimidine ring was formed through cyclization reaction with guanidine hydrochloride [36]. Boc protection of amine groups [37], [38] followed by sonogashira reaction with trimethylsilylacetylene **8** resulted in compound **9** [39]. Trimethylsilyl group was removed using potasium carbonate to afford alkyne **10**. Subsequently, copper (I) catalyzed azide-alkyne-cycloaddition (AAC) reaction [40] between alkyne **10** and compounds **11a-b**, followed by removal of trityl- protecting group resulted the final product **12a-b**. Compounds **11a-b** were synthesized as described in chapter 4 [41] (Scheme 5.1).



Scheme 5.1. (a) KOtBu Amyl 25% toluene, THF, rt, 20 min, 90%; (b) 6 h, 107 °C, 33%; (c) Guanidine hydrochloride, NaHCO₃, DMSO, 100 °C, 6 h, 72%; (d) Boc₂O, THF, DMAP, 45 °C, THF, 86%; (e) Hunig's base, Pd(PPh₃)₄, acetonitrile, CuI, 75 °C, overnight; (f) K₂CO₃, MeOH, 0 °C, 2 h, 36% (e and f); (g) CuI, Hunig's base, rt, overnight; (h) TFA, DCM, rt, 2 h, 84-88% (g and h).

To synthesize the class II pyrimethamine-HDACi conjugates, a Heck reaction was performed on intermediate **6** with methyl acrylate **13** [42]. After the Boc protection, the ester group was converted to carboxylic acid **16** using sodium hydroxide [43]. The final hydroxamic acid derivative **18** was synthesized through coupling of carboxylic acid **16** and *O*-trityl hydroxylamine **17** followed by trityl deprotection (Scheme 5.2) [41].



Scheme 5.2 . (a) Tri-*O*-tolyl phosphine, Pd(OAc)₂, TEA, DMF, 120 °C, overnight, 55%; (b) Boc₂O, THF, DMAP, 45 °C, THF, 56%; (c) NaOH, H₂O, Dioxane, 20 °C, 12 h, 60%; (d) EDCI, HOBT, DCM, rt, 6 h; (e) TFA, DCM, rt, 2 h, 24% (d and e).

5.4. HDAC inhibitory potency (Performed by BPS Bioscience)

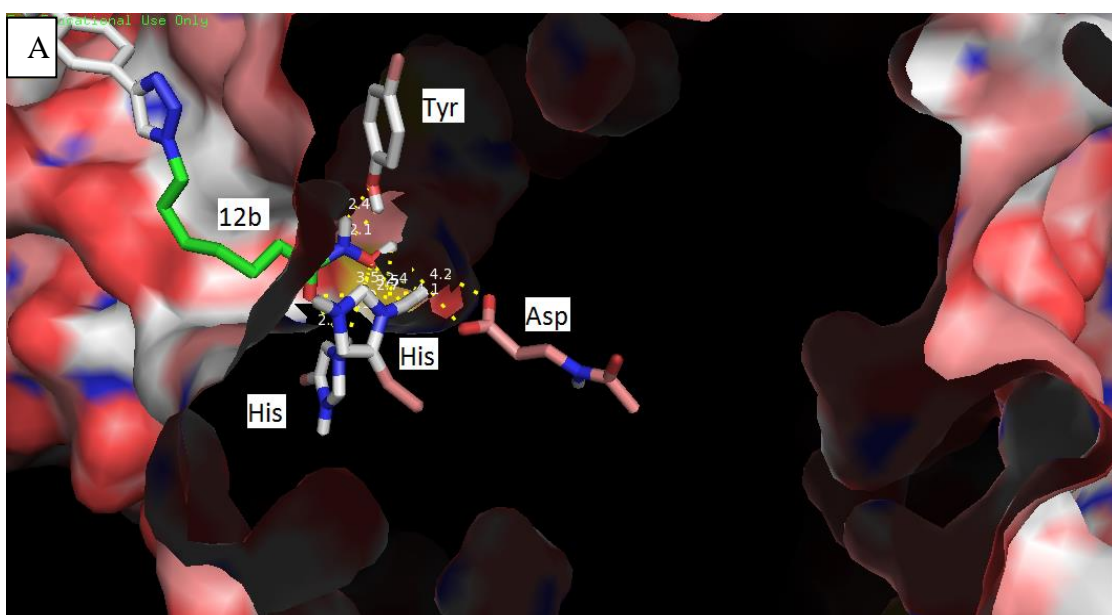
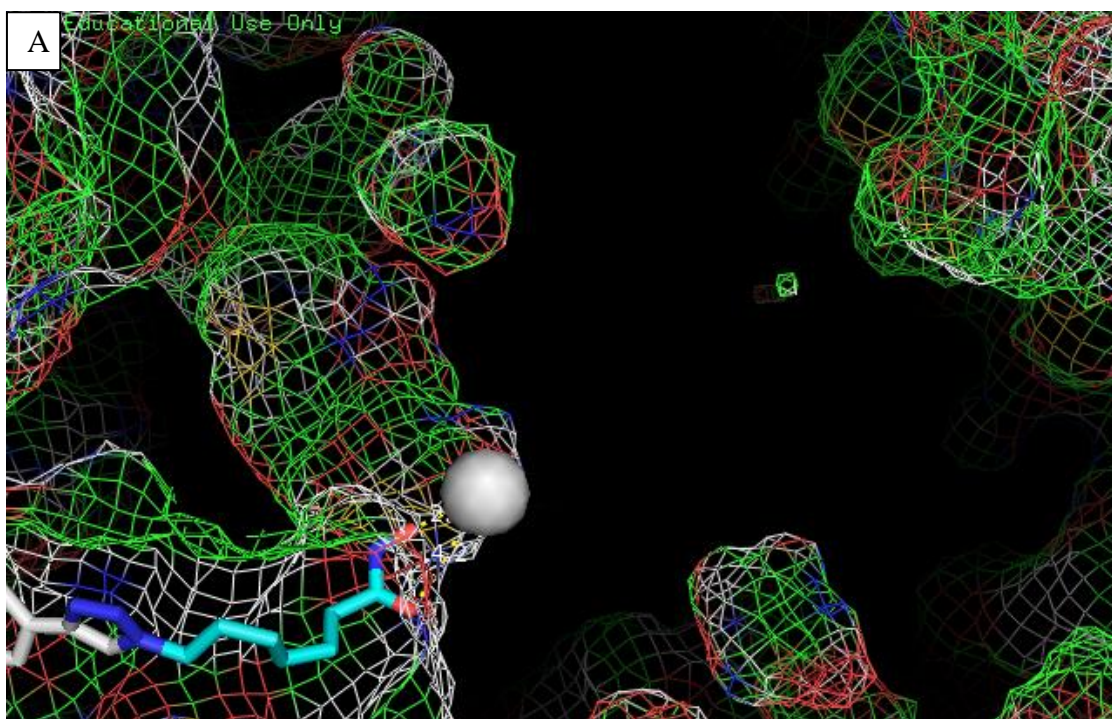
All three pyrimethamine conjugated HDACi were tested against HDAC isoforms 1, 6 and 8. Compounds **12a** and **12b** showed both HDAC1 and HDAC6 inhibition activity while compound **18** exhibited HDAC inhibition potency more selectively toward HDAC6.

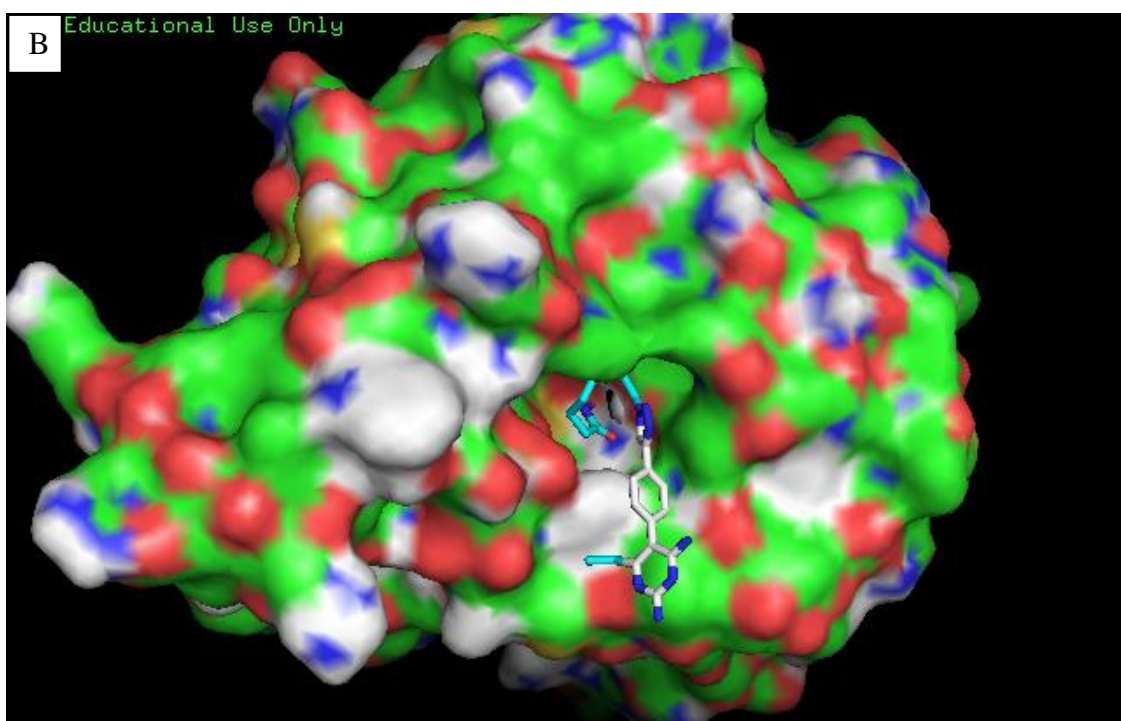
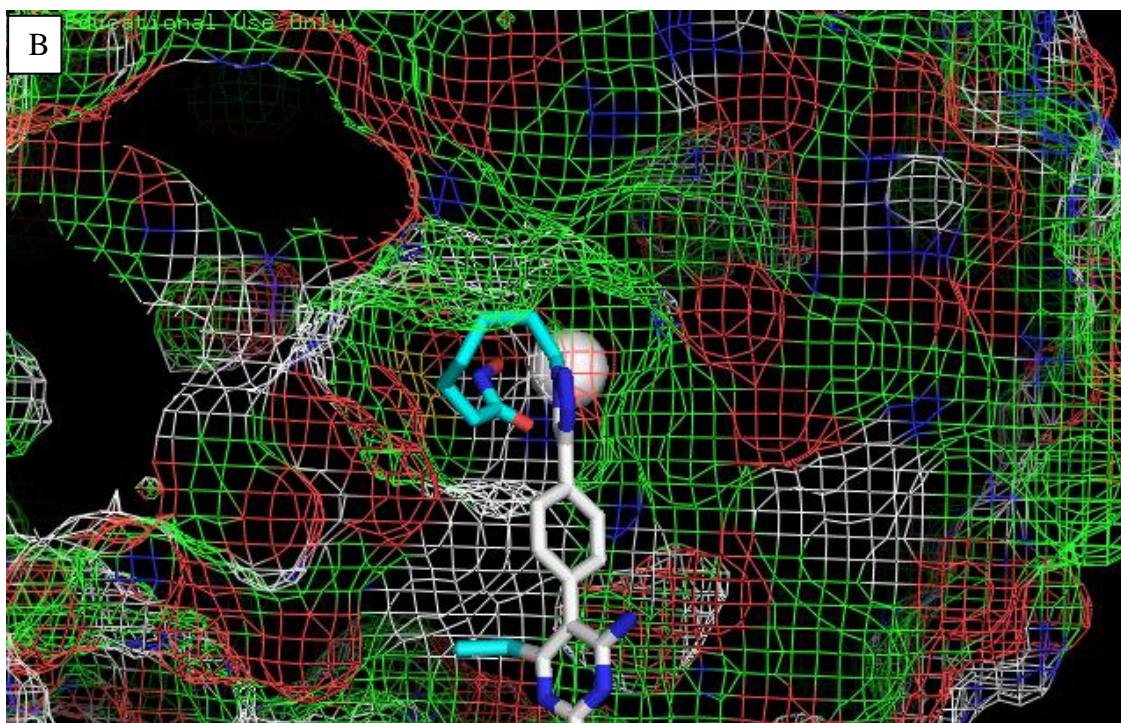
Table 5.1. HDAC inhibition activities of pyrimethamine-HDACi conjugates (IC₅₀ in μM).

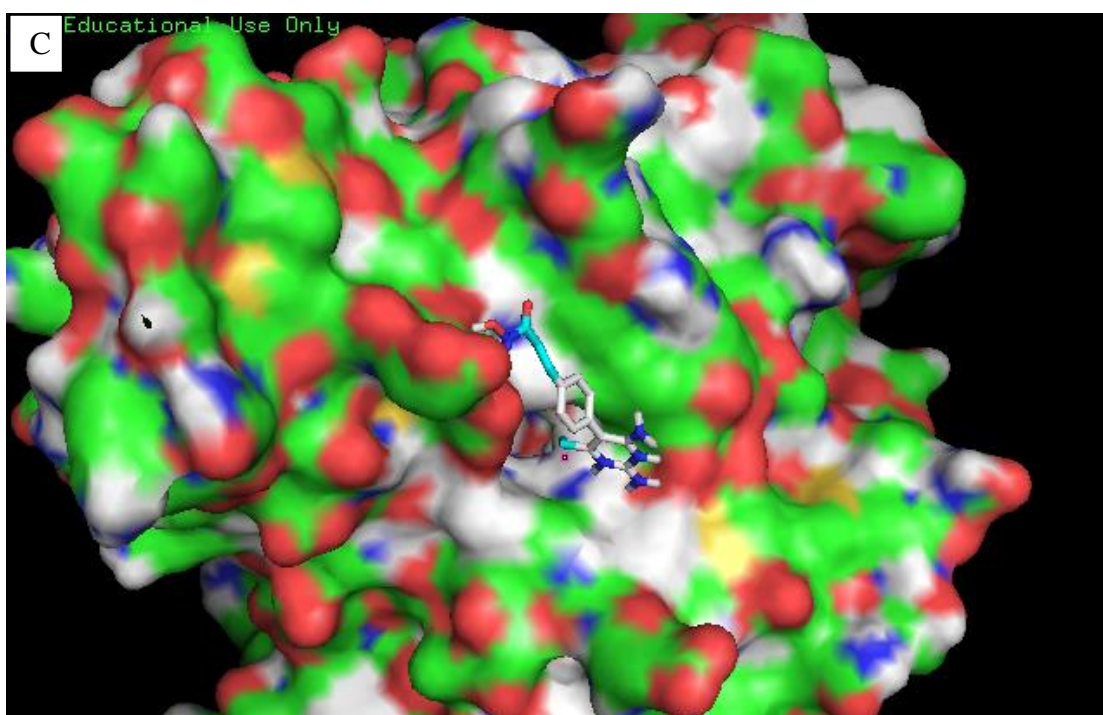
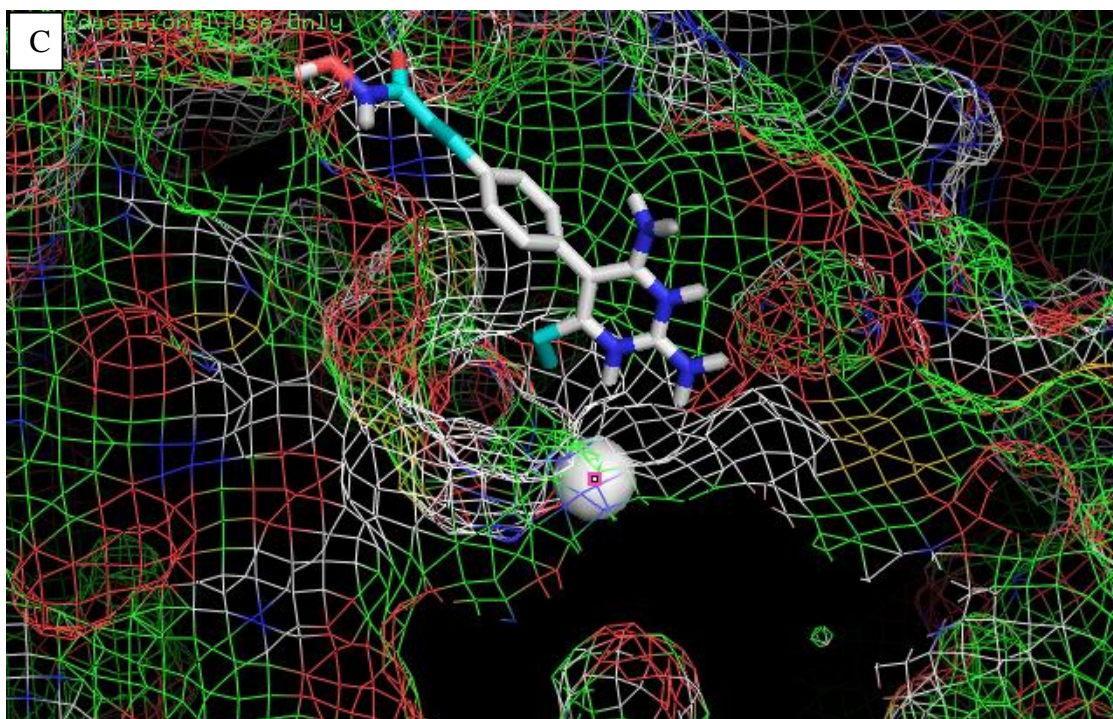
Compound	HDAC1	HDAC6	HDAC8
12a	0.26	0.046	2.8
12b	0.045	0.017	0.78
18	2.2	0.40	1.8
SAHA	0.042	0.034	2.8

5.5. Docking study

Molecular docking analyses using AutoDock Vina confirmed that compounds **12a** and **12b** chelates the zinc ion in the active site of both HDAC1 and HDAC6 while compound **18** only chelates the zinc ion in the pocket of HDAC6 and does not exhibit HDAC1 inhibition potency (Figure 5.4).







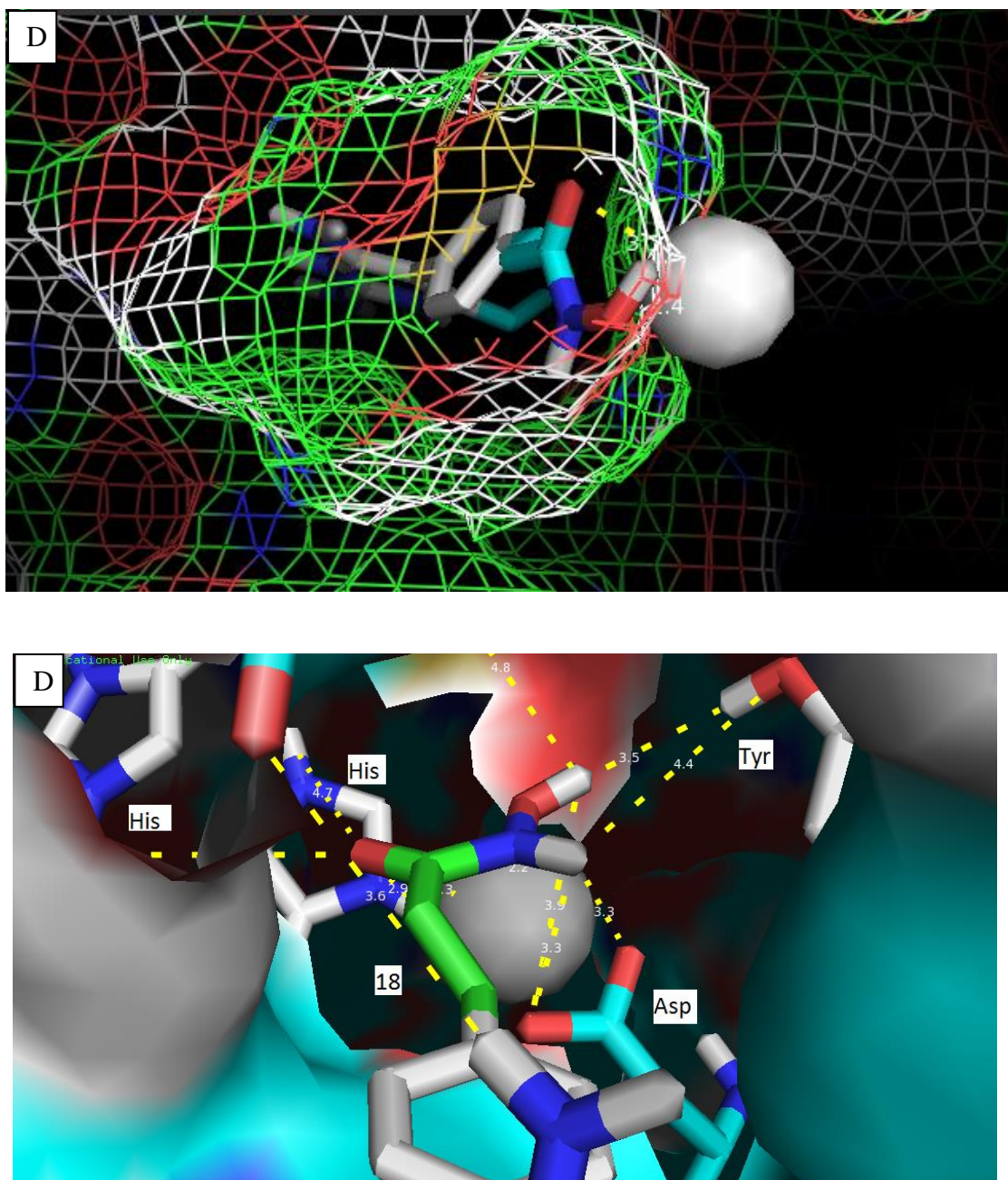


Figure 5.4. Docking structures of various pyrimethamin conjugated HDACi. Grey sphere represents zinc ion in the active site of HDAC isoform. (A) **12b** against HDAC1 (B) **12b** against HDAC6 (C) **18** against HDAC1 (D) **18** against HDAC6.

5.6. Antiproliferative activity

The pyrimethamine-HDACi conjugates were tested against four cell lines. Three transformed cell lines, lung (A549), ER positive (MCF-7), ER negative (MDA-MB231) cancer cell lines, and one healthy cell line (VERO- monkey kidney epithelial cell). SAHA, the FDA approved HDACi, was used as the control.

As expected compound **18** did not show anti-proliferative activity towards transformed cell lines, since it did not exhibit HDAC inhibitory activity. Additionally, compound **12b** was a more potent HDAC inhibitor compared to **12a**, therefore it was more cytotoxic towards transformed cell lines than **12a**.

Furthermore, The data showed that pyrimethamine conjugated HDACi **12a** and **12b** were most cytotoxic toward MDA-MB231 with STAT3 activity. STAT3 is not activated in other cell lines, therefore the pyrimethamine conjugated HDACi did not show parent anti-proliferative activity towards them.

Table 5.2. Anti-proliferative activity of pyrimethamine-HDACi conjugates (IC₅₀ values in μ M).

Compound	A549	MCF-7	MDA-MB231	VERO	Hs.505 T
12a	NI	NI	38.38 \pm 1.0	ND	ND
12b	26.27 \pm 3.0	52.6 \pm 6.2	1.11 \pm 0.2	11.5 \pm 2.7	ND
18	NI	NI	NI	ND	ND
SAHA	5.00 \pm 0.24	3.27 \pm 0.05	3.40 \pm 0.20	1.03 \pm 0.97	52 \pm 2.2

Each value is obtained from a duplicate of three simultaneous experiments. NI: No Inhibition. ND: Not Determined at maximum concentration of 50 μ M.

5.7. Conclusion

I designed and synthesized two classes of pyrimethamine conjugated HDACi. Compounds **12a** and **12b** inhibited both HDAC1 and HDAC6 activity while compound **18** was a very weak HDAC inhibitor. Additionally, it was 5 fold more selective toward HDAC6 compared to HDAC1. Compound **18** did not show HDAC anti-proliferative activity due to lack of HDAC inhibition potency.

These pyrimethamine HDACi conjugates were most cytotoxic toward STAT3 activated transformed cell line such as MDA-MB231.

5.8. Experimental

5.8.1. Materials and methods

4-Bromophenyl acetonitrile, ethyl propionate, *O*-tritylhydroxylamine, methyl acrylate, were purchased from Sigma-Aldrich. Trimethylsilylacetylene was purchased from Alfa Aesar. All commercially available starting materials were used without purification. Reaction solvents were high performance liquid chromatography (HPLC) grade or American Chemical Society (ACS) grade and used without purification. Analtech silica gel plates (60 F₂₅₄) were used for analytical TLC, and Analtech preparative TLC plates (UV 254, 2000 μ m) were used for purification. UV light and anisaldehyde/iodine stain were used to visualize the spots. 200-400 Mesh silica gel was used in column chromatography. Nuclear magnetic resonance (NMR) spectra were recorded on a Varian-Gemini 400 MHz or Bruker 500 MHz magnetic resonance spectrometer. ¹H NMR Spectra were recorded in parts per million (ppm) relative to the residual peaks of CHCl₃ (7.24 ppm) in CDCl₃ or CHD₂OD (4.78 ppm) in CD₃OD or DMSO-*d*₅ (2.49 ppm) in DMSO-*d*₆. ¹³C spectra were recorded relative to the central peak

of the CDCl₃ triplet (77.0 ppm) or CD₃OD septet (49.3 ppm) or DMSO-*d*₆ septet (39.7 ppm) and were recorded with complete hetero-decoupling. Original 'fid' files were processed using MestReNova LITE (version 5.2.5-5780) program. High-resolution mass spectra were recorded at the Georgia Institute of Technology mass spectrometry facility in Atlanta.

5.8.1.1. 2-(4-Bromophenyl)-3-oxopentanenitrile (**3**)

To a solution of 4-bromophenyl acetonitrile (1.4 g, 7 mmol) in THF (10 mL), potassium tert-pentylate (25% in toluene) (12.2 mL, 21 mmol) was added dropwise, followed by addition of ethyl propanoate. The reaction mixture stirred for 20 minutes, and then diluted with 1N HCl solution to pH=7, and water (5 mL) and EtOAc (10 mL). The organic layer was then washed with water (10 mL) and brine (10 mL) and dried over Na₂SO₄. Crude product was purified by column chromatography using (Silica gel, 4:1, Hex: EtOAc) and yielded the product (1.6 g, 90%) as yellow oil. ¹H NMR (400 MHz, CD₃OD) δ 7.62 – 7.53 (m, 2H), 7.49 – 7.41 (m, 2H), 2.71 – 2.55 (m, 2H), 1.31 – 1.23 (m, 3H). ¹³C NMR (101 MHz, CD₃OD) δ 173.5, 132.1, 131.9, 130.9, 130.0, 128.9, 120.0, 119.4, 85.6, 28.8, 11.2. HRMS (ESI) *m/z* Calcd. for C₁₁ H₁₀ N O Br [M+H⁺]: 250.9946, found for 250.9946.

5.8.1.2. 2-(4-Bromophenyl)-3-methoxypent-2-enenitrile (**5**)

Compound **3** (3.1 mg, 12.5 mmol) and trimethyl orthoacetate **4** (12.3 ml, 96.5 mmol) were heated at 107 °C for 6 h. The reaction mixture was washed with water (15 ml), NaHCO₃ (15 ml), and brine (15 ml). The organic layer was dried over Na₂SO₄. Crude product was purified by column chromatography using (Silica gel, 3:1, Hex: EtOAc) and yielded the product (1.1 g, 33%) as yellow oil. ¹H NMR (400 MHz, CDCl₃) δ 7.57 – 7.35 (m, 4H), 2.77 (q, *J* = 7.6 Hz, 2H), 1.32 – 1.26 (m, 3H). ¹³C NMR (101

MHz, CDCl₃) δ 173.1, 131.4, 130.8, 129.8, 120.7, 119.7, 91.5, 56.4, 24.1, 12.8. HRMS (ESI) m/z Calcd. for C₁₂ H₁₂ N O Br [M+H⁺]: 265.0102, found for 265.0103.

5.8.1.3. 5-(4-Bromophenyl)-6-ethylpyrimidine-2,4-diamine (6)

A mixture of compound 5 (846 mg, 3.2 mmol), sodium hydrogen carbonate (588 mg, 7mmol) and guanidine hydrochloride (668 mg, 7 mmol) in dry DMSO (10 mL) was heated at 100 °C for 5 h. The reaction mixture was washed with water (15×3 mL) and 10% MeOH: DCM (15 mL). Organic layer was separated and washed with brine (10 mL), and dried over Na₂SO₄. Crude product was purified by precipitation with EtOAc and yielded the product (670 mg, 72%) as a white powder. ¹H NMR (400 MHz, CD₃OD) δ 7.62 (d, J = 8.5 Hz, 2H), 7.16 (d, J = 8.5 Hz, 2H), 2.22 (q, J = 7.6 Hz, 2H), 1.03 (t, J = 7.6 Hz, 3H). ¹³C NMR (126 MHz, DMSO) δ 166.8, 162.6, 162.4, 135.9, 133.4, 132.3, 121.0, 105.9, 49.1, 27.9, 13.7. HRMS (ESI) m/z Calcd. for C₁₂ H₁₄ N₄ Br [M+H⁺]: 293.0396, found for 293.0399.

5.8.1.4. Di-tert-butyl (5-(4-bromophenyl)-6-ethylpyrimidine-2,4-diyl)bis((tert-butoxycarbonyl)carbamate) (7)

Compound 6 (104.4 mg, 0.3 mmol) and DMAP (4.3 mg, 0.03 mmol) were dissolved in THF (5 mL) and flushed with argon. Boc₂O (622.7 mg, 2.8 mmol) was added to the solution. Reaction went overnight at 40 °C. The reaction mixture was washed with water (5 mL) and DCM (5 mL) and the organic layer was separated and washed with brine (5 mL), and dried over Na₂SO₄. The crude product was purified on preparative TLC using 4:1 (Hex: EtOAc) to yield the product (204 mg, 86% conversion) as a yellow oil. ¹H NMR (400 MHz, CDCl₃) δ 7.56 – 7.48 (m, 2H), 7.14 – 7.03 (m, 2H), 2.59 (q, J = 7.5 Hz, 2H), 1.42 (s, 18H), 1.31 (s, 18H), 1.13 (t, J = 7.5 Hz, 3H). ¹³C NMR (101 MHz, CDCl₃) δ 173.9, 158.6, 157.4, 150.3, 149.8, 132.0, 131.7, 130.8, 128.3, 122.6,

83.5, 83.1, 28.4, 27.9, 13.0. HRMS (ESI) m/z Calcd. for $C_{32}H_{46}O_8N_4Br$ $[M+H]^+$: 693.2494, found for 693.2493.

5.8.1.5. *Di-tert-butyl (6-ethyl-5-(4-((trimethylsilyl)ethynyl)phenyl)pyrimidine-2,4-diyl)bis((tert-butoxycarbonyl)carbamate) (9).*

Compound **7** (315 mg, 0.4 mmol), $Pd(PPh_3)_4$ (26 mg, 0.02 mmol), and CuI (8.6 mg, 0.04 mmol) were dissolved in acetonitrile (5 mL) under argon. Trimethylsilylacetylene (0.1 mL, 0.9 mmol) was added, followed by Hunig's base (0.2 mL, 0.9 mmol). The reaction mixture was heated to 75 °C overnight. The reaction mixture was washed with water (3 mL) and DCM (5 mL). The organic layer was separated and washed with brine (5 mL), and dried over Na_2SO_4 . Crude product was used in the next step without purification.

5.8.1.6. *Di-tert-butyl (6-ethyl-5-(4-ethynylphenyl)pyrimidine-2,4-diyl)bis((tert-butoxycarbonyl)carbamate) (10)*

Potassium carbonate (74 mg, 0.5 mmol) was added to a solution of crude compound **9** (190 mg) in methanol (3 mL). The reaction mixture stirred for 2 h at rt. The reaction mixture was washed with water (1 mL) and DCM (3 mL). The organic layer was separated and washed with brine (3 mL), and dried over Na_2SO_4 . The crude product was purified on preparative TLC using 8:1:1 (Hex: EtOAc: Ether) and yielded the product (93 mg, 36% overall yield of **9** and **10**) as a white powder. 1H NMR (400 MHz, $CDCl_3$) δ 7.57 – 7.49 (m, 2H), 7.25 – 7.18 (m, 2H), 3.14 (s, 1H), 2.61 (dt, $J = 7.5, 6.0$ Hz, 2H), 1.45 (s, 18H), 1.34 (s, 18H), 1.17 (q, $J = 7.6$ Hz, 3H). ^{13}C NMR (101 MHz, $CDCl_3$) δ 173.8, 158.7, 157.1, 150.9, 150.0, 134.0, 132.3, 129.5, 128.8, 122.4, 83.8, 83.5, 83.1, 78.4, 28.5, 27.7, 13.0. HRMS (ESI) m/z Calcd. for $C_{34}H_{47}O_8N_4$ $[M+H]^+$: 639.3388, found for 639.3382.

5.8.1.7. 4-(4-(4-(2,4-Diamino-6-ethylpyrimidin-5-yl)phenyl)-1H-1,2,3-triazol-1-yl)-N-hydroxyhexanamide (**12a**)

Compound **10** (41 mg, 0.06 mmol) and 4-azido-N-(trityloxy)hexanamide **11a** (32 mg, 0.08 mmol) were dissolved in anhydrous THF (5 mL) and purged with argon for 15 min. Copper (I) iodide (6 mg, 0.03 mmol) and Hunig's base (0.02 mL, 0.1 mmol) were then added to the reaction mixture. The reaction mixture was purged with argon for additional 15 min and stirring continued for overnight 12 h. The crude was then dissolved in DCM: TFA (1: 0.2 mL) solution. Triisopropyl silane was added dropwise until the color transformed from dark yellow to pale yellow. TLC indicated the complete consumption of the starting material after 1 h. Solvent and TFA were evaporated off. The crude product was purified by precipitation in EtOAc to give the title compound (23 mg, 88%) as a pale yellow solid. ¹H NMR (500 MHz, MeOD) δ 8.46 (s, 1H), 8.02 (d, *J* = 7.7 Hz, 2H), 7.40 (dd, *J* = 15.1, 8.0 Hz, 2H), 4.50 (d, *J* = 6.2 Hz, 2H), 2.42 (q, *J* = 7.2 Hz, 2H), 2.21 – 2.04 (m, 2H), 2.02 (s, 2H), 1.71 (s, 2H), 1.41 (s, 2H), 1.21 – 1.12 (m, 3H). ¹³C NMR (126 MHz, MeOD) δ 165.2, 155.5, 154.6, 146.9, 131.6, 130.9, 126.7, 121.4, 108.8, 71.2, 50.1, 29.8, 29.2, 25.6, 24.6, 23.9, 17.3, 11.8. HRMS (ESI) *m/z* Calcd. for C₂₀H₂₇O₂N₈ [M+H⁺]: 411.2251, found for 411.2246.

5.8.1.8. 4-(4-(4-(2,4-Diamino-6-ethylpyrimidin-5-yl)phenyl)-1H-1,2,3-triazol-1-yl)-N-hydroxyheptanamide (**12b**)

Compound **10** (40 mg, 0.06 mmol) and 4-azido-N-(trityloxy)heptanamide **11b** (32 mg, 0.08 mmol) were dissolved in anhydrous THF (5 mL) and purged with argon for 15 min. Copper (I) iodide (6 mg, 0.03 mmol) and Hunig's base (0.02 mL, 0.1 mmol) were then added to the reaction mixture. The reaction mixture was purged with argon for additional 15 min and stirring continued for overnight 12 h. The crude was then dissolved in DCM: TFA (1: 0.2 mL) solution. Triisopropyl silane was added dropwise until the color transformed from dark yellow to pale yellow. TLC indicated the complete

consumption of the starting material after 1 h. Solvent and TFA were evaporated off. The crude product was purified by precipitation in EtOAc to give the title compound (22 mg, 84%) as a pale yellow solid. ^1H NMR (400 MHz, CD_3OD) δ 8.43 (s, 1H), 7.99 (d, J = 6.4 Hz, 2H), 7.37 (s, 2H), 4.47 (s, 2H), 2.39 (s, 2H), 2.19 (d, J = 31.3 Hz, 2H), 1.99 (d, J = 11.8 Hz, 2H), 1.60 (s, 2H), 1.38 (s, 4H), 1.14 (d, J = 6.1 Hz, 3H). ^{13}C NMR (126 MHz, MeOD) δ 164.9, 155.4, 154.8, 146.7, 131.4, 130.9, 130.6, 126.5, 121.4, 108.8, 50.1, 29.8, 29.4, 28.1, 26.1, 25.0, 23.7, 23.0, 11.8. HRMS (ESI) m/z Calcd. for $\text{C}_{21}\text{H}_{29}\text{O}_2\text{N}_8$ $[\text{M}+\text{H}^+]$: 425.2408, found for 425.2402.

5.8.1.9. Methyl-3-(4-(2,4-diamino-6-ethylpyrimidin-5-yl)phenyl)acrylate (**14**)

Compound **6** (90 mg, 0.3 mmol), methyl acrylate **13** (0.09 mL, 0.9 mmol), TEA (0.1 mL, 0.8 mmol), and tri-*O*-tolylphosphine (28 mg, 0.09 mmol) were dissolved in DMF (3 mL). The reaction mixture was purged with argon for 15 min, then $\text{Pd}(\text{OAc})_2$ (10.3 mg, 0.05 mmol) was added, and then was heated at 120 °C overnight. The reaction mixture was washed with water (10 mL) and DCM (10 mL). The organic layer was separated and washed with brine (5 mL), and dried over Na_2SO_4 . Crude product was purified on preparative TLC using 10:1:0.5 (EtOAc: Hex: NEt_3) and yielded the product (50 mg, 55%) as a pale yellow powder. ^1H NMR (400 MHz, CD_3OD) δ 7.74 (d, J = 8.2 Hz, 3H), 7.32 (d, J = 7.7 Hz, 2H), 6.60 (d, J = 16.2 Hz, 1H), 2.38 – 2.21 (m, 2H), 1.10 (t, J = 7.4 Hz, 3H). ^{13}C NMR (126 MHz, MeOD) δ 167.4, 164.1, 157.7, 144.1, 134.6, 134.2, 130.9, 128.7, 118.6, 107.9, 70.3, 51.1, 31.8, 29.2, 25.4, 12.0. HRMS (ESI) m/z Calcd. $\text{C}_{16}\text{H}_{19}\text{O}_2\text{N}_4$ $[\text{M}+\text{H}^+]$: 299.1503, found for 299.1503.

5.8.1.10. Methyl-3-(4-(2,4-bis(bis(tert-butoxycarbonyl)amino)-6-ethylpyrimidin-5-yl)phenyl)acrylate (**15**)

Compound **14** (27 mg, 0.09 mmol) and DMAP (1.1 mg, 0.009 mmol) were dissolved in THF (3 mL) and flushed with argon. Boc_2O was added to the solution.

Reaction went overnight at 40 °C. The reaction mixture was washed with water (1 mL) and DCM (3 mL) and the organic layer was separated and washed with brine (3 mL), and dried over Na₂SO₄. The crude product was purified on preparative TLC using 3:1 (Hex: EtOAc) to yield the product (35 mg, 56%) as a white solid. ¹H NMR (400 MHz, CD₃OD) δ 7.77 (s, 1H), 7.74 (d, *J* = 7.0 Hz, 2H), 7.34 (dd, *J* = 17.5, 8.2 Hz, 2H), 6.63 (dd, *J* = 16.1, 10.6 Hz, 1H), 3.80 (s, 3H), 2.80 – 2.57 (m, 2H), 1.48 (s, 18H), 1.35 (d, *J* = 4.3 Hz, 18H), 1.19 (t, *J* = 7.5 Hz, 3H). ¹³C NMR (101 MHz, CDCl₃) δ 173.8, 167.3, 158.6, 157.4, 150.9, 149.8, 143.8, 135.3, 134.5, 129.8, 128.0, 118.7, 82.2, 81.3, 70.4, 51.9, 51.8, 29.7, 29.0, 28.6, 28.2, 28.0, 27.9, 27.8, 27.7, 13.2, 12.9. HRMS (ESI) *m/z* Calcd. C₃₆ H₅₁ O₁₀ N₄ [M+H⁺]: 699.3600, found for 699.3595.

5.8.1.11. 3-(4-(2,4-Bis(bis(tert-butoxycarbonyl)amino)-6-ethylpyrimidin-5-yl)phenyl)acrylic acid (**16**)

Compound **15** (60 mg, 0.08 mmol) was dissolved in 1,4-dioxane (3 mL) and added dropwise to an aqueous solution (3 mL) containing hydroxylamine (6 mg, 0.2 mmol) and sodium hydroxide (10.2 mg, 0.2 mmol) at rt, and stirred for 12 h and concentrated under vacume to remove organic solvent. The aqueous solution was adjusted to pH=1 with 1N HCl. The resulting precipitate was collected by filtration and dried to give the product (35 mg, 60%) as a pale yellow solid. ¹H NMR (400 MHz, CDCl₃) δ 7.70 (s, 1H), 7.60 – 7.52 (m, 2H), 7.27 (d, *J* = 5.2 Hz, 1H), 7.22 (d, *J* = 8.1 Hz, 1H), 6.54 (s, 1H), 2.62 (dq, *J* = 15.2, 7.5 Hz, 2H), 1.51 (d, *J* = 15.4 Hz, 6H), 1.50 – 1.44 (m, 12H), 1.32 (s, 18H), 1.24 (d, *J* = 3.9 Hz, 3H). ¹³C NMR (101 MHz, CDCl₃) δ 174.3, 158.9, 158.2, 157.6, 156.7, 150.7, 150.5, 150.0, 130.0, 129.5, 128.8, 128.1, 125.5, 81.5, 29.7, 29.0, 28.6, 28.3, 28.0, 27.8, 27.7, 13.1, 12.9. HRMS (ESI) *m/z* Calcd. C₃₅ H₄₉ O₁₀ N₄ [M+H⁺]: 685.3443, found for 685.3434.

5.8.1.12. 3-(4-(2,4-Diamino-6-ethylpyrimidin-5-yl)phenyl)-N-hydroxyacrylamide (**18**)

Compound **16** (35 mg, 0.05 mmol), EDCI (9.5 mg, 0.05 mmol) and HOBT (6.9 mg, 0.05 mmol) were dissolved in DCM (3 mL) at 0 °C. After stirring at 0 °C for 15 min, amine (20.6 mg, 0.07 mmol) and Hunig's base (0.03 mL, 0.15 mmol) were added. And the reaction mixture stirred for 12 h at rt. The reaction mixture was washed with water (1 mL) and DCM (3 mL) and the organic layer was separated and washed with brine, and dried over Na₂SO₄. The crude was then dissolved in DCM: TFA (1: 0.2 mL) solution. Triisopropyl silane was added dropwise until the color transformed from dark yellow to pale yellow. TLC indicated the complete consumption of the starting material after 1 h. Solvent and TFA were evaporated off. The crude product was purified by precipitation in EtOAc to give the title compound (3.6 mg, 24%) as a pale yellow solid. ¹H NMR (500 MHz, MeOD) δ 7.75 (d, *J* = 7.4 Hz, 2H), 7.66 (d, *J* = 15.6 Hz, 1H), 7.37 (d, *J* = 6.9 Hz, 2H), 6.59 (d, *J* = 15.3 Hz, 1H), 2.38 (d, *J* = 7.4 Hz, 2H), 1.15 (t, *J* = 7.3 Hz, 3H). ¹³C NMR (126 MHz, MeOD) δ 171.8, 165.2, 158.0, 155.3, 144.8, 135.7, 130.7, 128.7, 120.4, 29.6, 27.2, 23.9, 12.0. HRMS (ESI) *m/z* Calcd. C₁₅ H₁₈ O₂ N₅ [M+H⁺]: 300.1455, found for 300.1451.

5.8.2. Cell viability assay

All cell lines used in this study were maintained in phenol red free Dulbecco's Modified Eagle Medium (DMEM) (Corning, VA), supplemented with 10% fetal bovine serum (FBS) (Atlanta Biologicals, Atlanta, GA) and 1% *Penicillin-Streptomycin*. Cells were incubated in 96 well plate for 24 h prior to treatment and then treated with various drugs' concentration for 72 h. Their anti-proliferative activity was measured using the MTS assay (CellTiter 96 Aqueous One Solution and CellTiter 96 Non-Radioactive Cell Proliferation Assays, Promega, Madison, WI) as described by the manufacturer. All

drugs solution were made in DMEM while DMSO concentration was maintained at 0.1%.

5.8.3. *In vitro* HDAC inhibition (Performed through contractual agreement with BPS Bioscience)

HDAC inhibition was performed via Fluor de Lys assay. This assay is based on Fluorimetric Histone deAcetylaseLysyl substrate and developer combination. First the substrate with the acetylated lysine chain is incubated with HDAC enzymes. Then the developer is added which results in generating a fluorophore.

To perform the *in vitro* HDAC inhibition assay, different concentration of HDACi with 10% DMSO in HDAC assay buffer were prepared and added to the enzymatic reaction containing HDAC assay buffer, BSA, substrate and enzyme (HDAC1, HDAC6 and HDAC8) in 96 well plate. Developer was then added to each well and the plate was incubated at room temperature for 15 minutes. Fluorescent intensity at the certain wavelengths was measured using Biotek Synergy microplate reader. Fluorescent intensities were measured in the absence and presence of the compounds as well as in the absence of HDAC, and the data was analyzed using Graphpad Prism. IC₅₀ value for each compound was determined by the concentration leading to a half-maximal percent inhibition.

5.9. References

1. Cowman, A. F.; Morry, M. J.; Biggs, B. A.; Cross, G.; Foote, S. J. Amino acid changes linked to pyrimethamine resistance in the dihydrofolate reductase-thymidylate synthase gene of *Plasmodium falciparum*. *Proceedings of the National Academy of Sciences* **1988**, 85, 9109-9113.
2. Curd, F.; Davey, D.; Rose, F. Studies on Synthetic Antimalarial Drugs: X.—Some Biguanide Derivatives as New Types of Antimalarial Substances with Both Therapeutic and Causal Prophylactic Activity. *Annals of Tropical Medicine & Parasitology* **1945**, 39, 208-216.

3. Peterson, D. S.; Walliker, D.; Wellems, T. E. Evidence that a point mutation in dihydrofolate reductase-thymidylate synthase confers resistance to pyrimethamine in *falciparum* malaria. *Proceedings of the National Academy of Sciences* **1988**, 85, 9114-9118.
4. Ferone, R.; Roland, S. Dihydrofolate reductase: thymidylate synthase, a bifunctional polypeptide from *Crithidia fasciculata*. *Proceedings of the National Academy of Sciences* **1980**, 77, 5802-5806.
5. Kompis, I. M.; Islam, K.; Then, R. L. DNA and RNA synthesis: antifolates. *Chemical reviews* **2005**, 105, 593-620.
6. Li, R.; Sirawaraporn, R.; Chitnumsub, P.; Sirawaraporn, W.; Wooden, J.; Athappilly, F.; Turley, S.; Hol, W. G. Three-dimensional structure of *M. tuberculosis* dihydrofolate reductase reveals opportunities for the design of novel tuberculosis drugs. *Journal of molecular biology* **2000**, 295, 307-323.
7. Peterson, D. S.; Milhous, W. K.; Wellems, T. E. Molecular basis of differential resistance to cycloguanil and pyrimethamine in *Plasmodium falciparum* malaria. *Proceedings of the National Academy of Sciences* **1990**, 87, 3018-3022.
8. Foote, S. J.; Galatis, D.; Cowman, A. F. Amino acids in the dihydrofolate reductase-thymidylate synthase gene of *Plasmodium falciparum* involved in cycloguanil resistance differ from those involved in pyrimethamine resistance. *Proceedings of the National Academy of Sciences* **1990**, 87, 3014-3017.
9. Kublin, J. G.; Dzinjalama, F. K.; Kamwendo, D. D.; Malkin, E. M.; Cortese, J. F.; Martino, L. M.; Mukadam, R. A.; Rogerson, S. J.; Lescano, A. G.; Molyneux, M. E. Molecular markers for failure of sulfadoxine-pyrimethamine and chlorproguanil-dapsone treatment of *Plasmodium falciparum* malaria. *Journal of infectious diseases* **2002**, 185, 380-388.
10. Murphy, C.; Blanchard, J.; Ganser, A.; Brown, E.; Hassell, J.; Humphries, R.; Morgan, M.; Heuser, M. High-throughput drug screening identifies pyrimethamine as a potent and selective inhibitor of acute myeloid leukemia. *Current cancer drug targets* **2016**.
11. Chaudhari, S.; Desai, J. S.; Adam, A.; Mishra, P. Jak/stat as a novel target for treatment of leukemia. *Int J Pharm Pharm Sci* **2014**, 6, 1-7.
12. Yeh, J. E.; Frank, D. A. STAT3-Interacting Proteins as Modulators of Transcription Factor Function: Implications to Targeted Cancer Therapy. *ChemMedChem* **2015**.
13. Shuai, K.; Ziemiecki, A.; Wilks, A. F.; Harpur, A. G.; Sadowski, H. B.; Gilman, M. Z.; Darnell, J. E. Polypeptide signalling to the nucleus through tyrosine phosphorylation of Jak and Stat proteins. **1993**.

14. Weimbs, T.; Talbot, J. J. STAT3 signaling in polycystic kidney disease. *Drug Discovery Today: Disease Mechanisms* **2013**, 10, e113-e118.
15. Miklossy, G.; Hilliard, T. S.; Turkson, J. Therapeutic modulators of STAT signalling for human diseases. *Nature reviews Drug discovery* **2013**, 12, 611-629.
16. Spitzner, M.; Ebner, R.; Wolff, H. A.; Ghadimi, B. M.; Wienands, J.; Grade, M. STAT3: a novel molecular mediator of resistance to chemoradiotherapy. *Cancers* **2014**, 6, 1986-2011.
17. Kim, E.; Kim, M.; Woo, D.-H.; Shin, Y.; Shin, J.; Chang, N.; Oh, Y. T.; Kim, H.; Rhee, J.; Nakano, I. Phosphorylation of EZH2 activates STAT3 signaling via STAT3 methylation and promotes tumorigenicity of glioblastoma stem-like cells. *Cancer cell* **2013**, 23, 839-852.
18. Butturini, E.; de Prati, A. C.; Chiavegato, G.; Rigo, A.; Cavalieri, E.; Darra, E.; Mariotto, S. Mild oxidative stress induces S-glutathionylation of STAT3 and enhances chemosensitivity of tumoural cells to chemotherapeutic drugs. *Free Radical Biology and Medicine* **2013**, 65, 1322-1330.
19. Lee, H.; Zhang, P.; Herrmann, A.; Yang, C.; Xin, H.; Wang, Z.; Hoon, D. S.; Forman, S. J.; Jove, R.; Riggs, A. D. Acetylated STAT3 is crucial for methylation of tumor-suppressor gene promoters and inhibition by resveratrol results in demethylation. *Proceedings of the National Academy of Sciences* **2012**, 109, 7765-7769.
20. Alvarez, J. V.; Febbo, P. G.; Ramaswamy, S.; Loda, M.; Richardson, A.; Frank, D. A. Identification of a genetic signature of activated signal transducer and activator of transcription 3 in human tumors. *Cancer research* **2005**, 65, 5054-5062.
21. Nelson, E. A.; Sharma, S. V.; Settleman, J.; Frank, D. A. A chemical biology approach to developing STAT inhibitors: molecular strategies for accelerating clinical translation. *Oncotarget* **2011**, 2, 518-524.
22. Kabra, D. G.; Pfuhmann, K.; García-Cáceres, C.; Schriever, S. C.; García, V. C.; Kebede, A. F.; Fuente-Martin, E.; Trivedi, C.; Heppner, K.; Uhlénhaut, N. H. Hypothalamic leptin action is mediated by histone deacetylase 5. *Nature communications* **2016**, 7.
23. Gryder, B. E.; Sodji, Q. H.; Oyelere, A. K. Targeted cancer therapy: giving histone deacetylase inhibitors all they need to succeed. *Future medicinal chemistry* **2012**, 4, 505-524.
24. Mottamal, M.; Zheng, S.; Huang, T. L.; Wang, G. Histone deacetylase inhibitors in clinical studies as templates for new anticancer agents. *Molecules* **2015**, 20, 3898-3941.
25. Tapadar, S.; Fathi, S.; Raji, I.; Omesiete, W.; Kornacki, J. R.; Mwakwari, S. C.; Miyata, M.; Mitsutake, K.; Li, J.-D.; Mrksich, M. A structure–activity relationship of

non-peptide macrocyclic histone deacetylase inhibitors and their anti-proliferative and anti-inflammatory activities. *Bioorganic & Medicinal Chemistry* **2015**, 23, 7543-7564.

26. Lemoine, M.; Younes, A. Histone deacetylase inhibitors in the treatment of lymphoma. *Discovery medicine* **2010**, 10, 462-470.

27. Mann, B. S.; Johnson, J. R.; Cohen, M. H.; Justice, R.; Pazdur, R. FDA approval summary: vorinostat for treatment of advanced primary cutaneous T-cell lymphoma. *The oncologist* **2007**, 12, 1247-1252.

28. Coiffier, B.; Pro, B.; Prince, H. M.; Foss, F.; Sokol, L.; Greenwood, M.; Caballero, D.; Morschhauser, F.; Wilhelm, M.; Pinter-Brown, L. Romidepsin for the treatment of relapsed/refractory peripheral T-cell lymphoma: pivotal study update demonstrates durable responses. *Journal of hematology & oncology* **2014**, 7, 1.

29. Plumb, J. A.; Finn, P. W.; Williams, R. J.; Bandara, M. J.; Romero, M. R.; Watkins, C. J.; La Thangue, N. B.; Brown, R. Pharmacodynamic response and inhibition of growth of human tumor xenografts by the novel histone deacetylase inhibitor PXD101. *Molecular cancer therapeutics* **2003**, 2, 721-728.

30. Surati, M.; Valla, K.; Shah, K. S.; Panjic, E. H.; Lonial, S. Panobinostat for the treatment of multiple myeloma. *Expert Opinion on Orphan Drugs* **2015**, 3, 229-238.

31. Ning, Z.-Q.; Li, Z.-B.; Newman, M. J.; Shan, S.; Wang, X.-H.; Pan, D.-S.; Zhang, J.; Dong, M.; Du, X.; Lu, X.-P. Chidamide (CS055/HBI-8000): a new histone deacetylase inhibitor of the benzamide class with antitumor activity and the ability to enhance immune cell-mediated tumor cell cytotoxicity. *Cancer chemotherapy and pharmacology* **2012**, 69, 901-909.

32. Gupta, K.; Gulen, F.; Sun, L.; Aguilera, R.; Chakrabarti, A.; Kiselar, J.; Agarwal, M.; Wald, D. N. GSK3 is a regulator of RAR-mediated differentiation. *Leukemia* **2012**, 26, 1277-1285.

33. Mwakwari, S. C.; Guerrant, W.; Patil, V.; Khan, S. I.; Tekwani, B. L.; Gurard-Levin, Z. A.; Mrksich, M.; Oyelere, A. K. Non-peptide macrocyclic histone deacetylase inhibitors derived from tricyclic ketolide skeleton. *Journal of medicinal chemistry* **2010**, 53, 6100-6111.

34. Ji, Y.; Trenkle, W. C.; Vowles, J. V. A high-yielding preparation of β -ketonitriles. *Organic letters* **2006**, 8, 1161-1163.

35. Kuroyanagi, J.-i.; Kanai, K.; Sugimoto, Y.; Fujisawa, T.; Morita, C.; Suzuki, T.; Kawakami, K.; Takemura, M. Novel antifungal agents: Triazolopyridines as inhibitors of β -1, 6-glucan synthesis. *Bioorganic & medicinal chemistry* **2010**, 18, 5845-5854.

36. Tropak, M. B.; Zhang, J.; Yonekawa, S.; Rigat, B. A.; Aulakh, V. S.; Smith, M. R.; Hwang, H.-J.; Ciufolini, M. A.; Mahuran, D. J. Pyrimethamine Derivatives: Insight

into Binding Mechanism and Improved Enhancement of Mutant β -N-acetylhexosaminidase Activity. *Journal of medicinal chemistry* **2015**, 58, 4483-4493.

37. Chan, D. C.; Fu, H.; Forsch, R. A.; Queener, S. F.; Rosowsky, A. Design, synthesis, and antifolate activity of new analogues of piritrexim and other diaminopyrimidine dihydrofolate reductase inhibitors with ω -carboxyalkoxy or ω -carboxy-1-alkynyl substitution in the side chain. *Journal of medicinal chemistry* **2005**, 48, 4420-4431.

38. Porcheddu, A.; Giacomelli, G.; Piredda, I.; Carta, M.; Nieddu, G. A Practical and Efficient Approach to PNA Monomers Compatible with Fmoc-Mediated Solid-Phase Synthesis Protocols. *European Journal of Organic Chemistry* **2008**, 2008, 5786-5797.

39. Dhokale, B.; Jadhav, T.; Mobin, S. M.; Misra, R. Meso alkynylated tetraphenylethylene (TPE) and 2, 3, 3-triphenylacrylonitrile (TPAN) substituted BODIPYs. *The Journal of organic chemistry* **2015**, 80, 8018-8025.

40. Rostovtsev, V. V.; Green, L. G.; Fokin, V. V.; Sharpless, K. B. A stepwise Huisgen cycloaddition process: copper (I)-catalyzed regioselective "ligation" of azides and terminal alkynes. *Angewandte Chemie* **2002**, 114, 2708-2711.

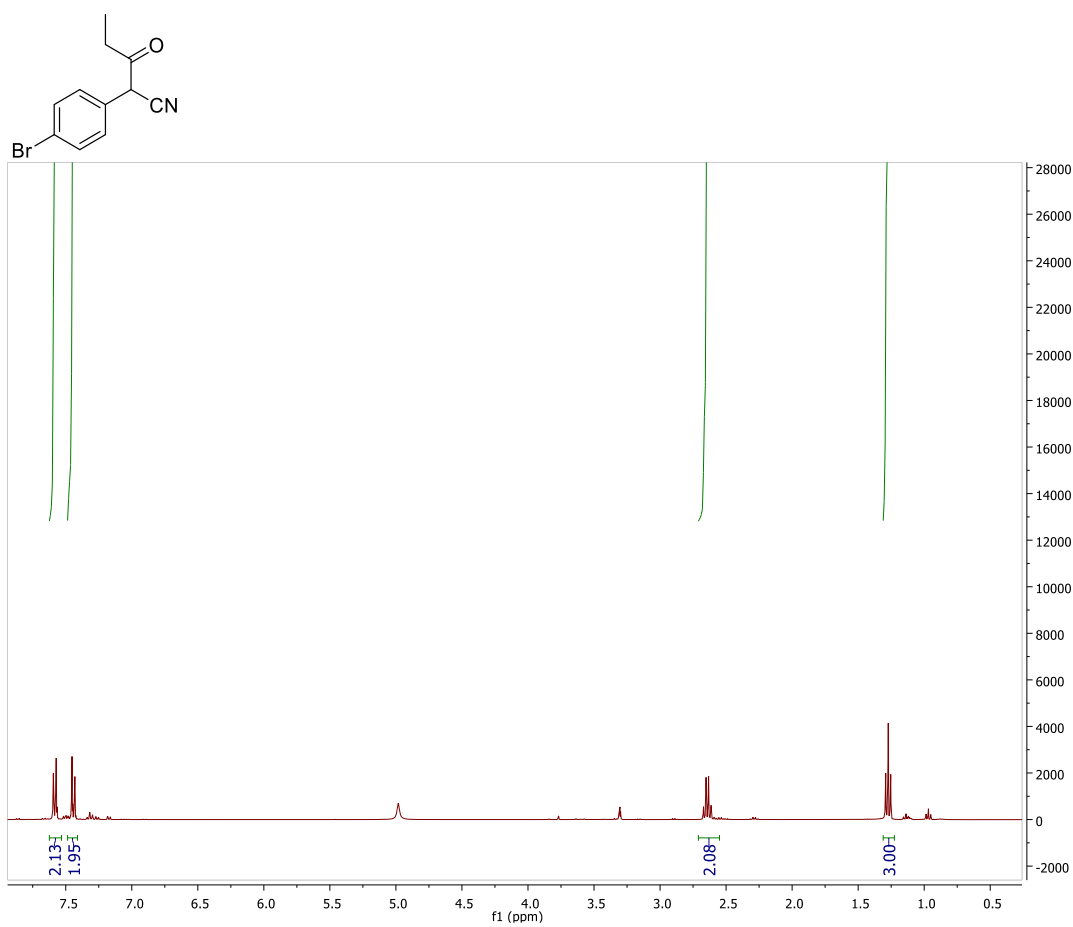
41. Gryder, B. E.; Akbashev, M. J.; Rood, M. K.; Raftery, E. D.; Meyers, W. M.; Dillard, P.; Khan, S.; Oyeler, A. K. Selectively targeting prostate cancer with antiandrogen equipped histone deacetylase inhibitors. *ACS chemical biology* **2013**, 8, 2550-2560.

42. De Savi, C.; Bradbury, R. H.; Rabow, A. A.; Norman, R. A.; de Almeida, C.; Andrews, D. M.; Ballard, P.; Buttar, D.; Callis, R. J.; Currie, G. S. Optimization of a Novel Binding Motif to (E)-3-(3, 5-Difluoro-4-((1 R, 3 R)-2-(2-fluoro-2-methylpropyl)-3-methyl-2, 3, 4, 9-tetrahydro-1 H-pyrido [3, 4-b] indol-1-yl) phenyl) acrylic Acid (AZD9496), a Potent and Orally Bioavailable Selective Estrogen Receptor Downregulator and Antagonist. *Journal of Medicinal Chemistry* **2015**, 58, 8128-8140.

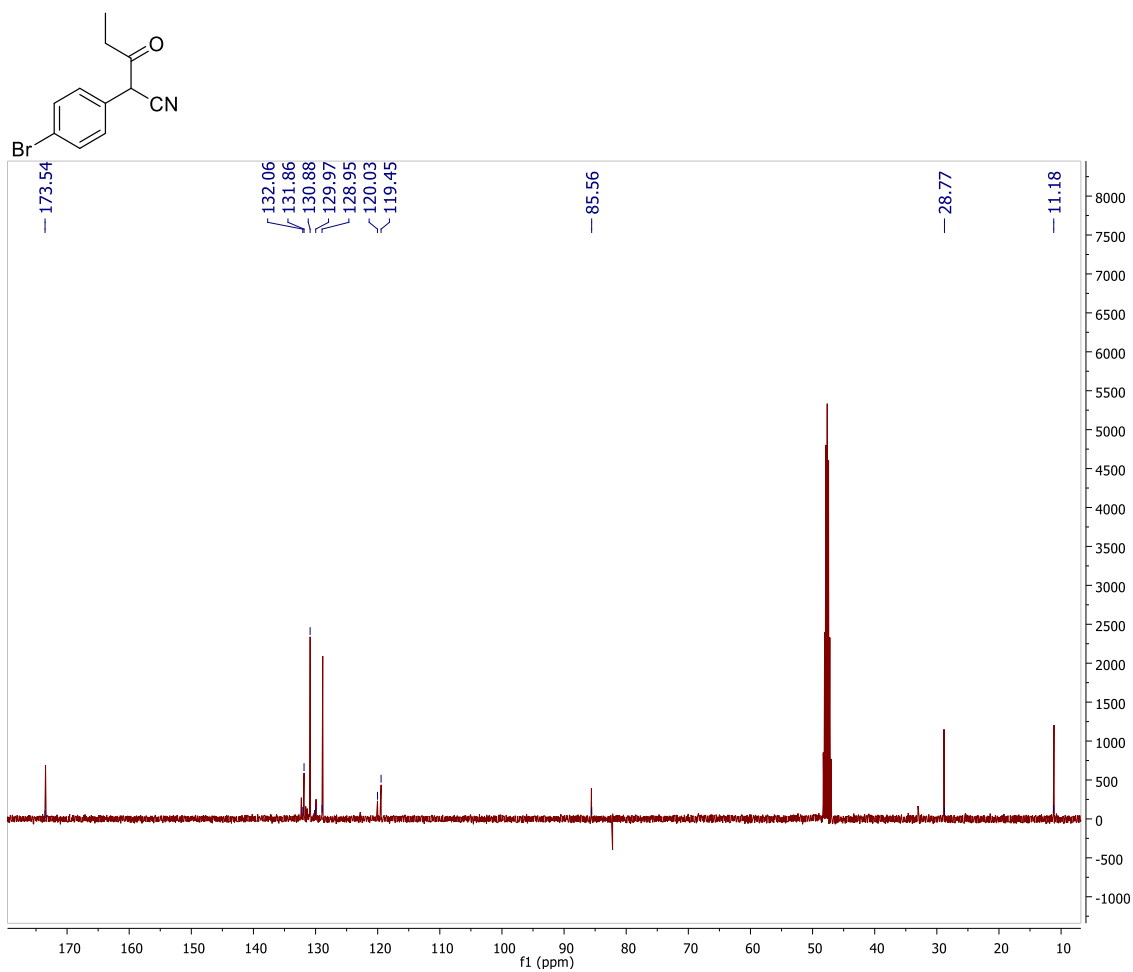
43. Liu, W.; Lau, F.; Liu, K.; Wood, H. B.; Zhou, G.; Chen, Y.; Li, Y.; Akiyama, T. E.; Castriota, G.; Einstein, M. Benzimidazolones: A new class of selective peroxisome proliferator-activated receptor γ (PPAR γ) modulators. *Journal of medicinal chemistry* **2011**, 54, 8541-8554.

5.9. Supplementary data

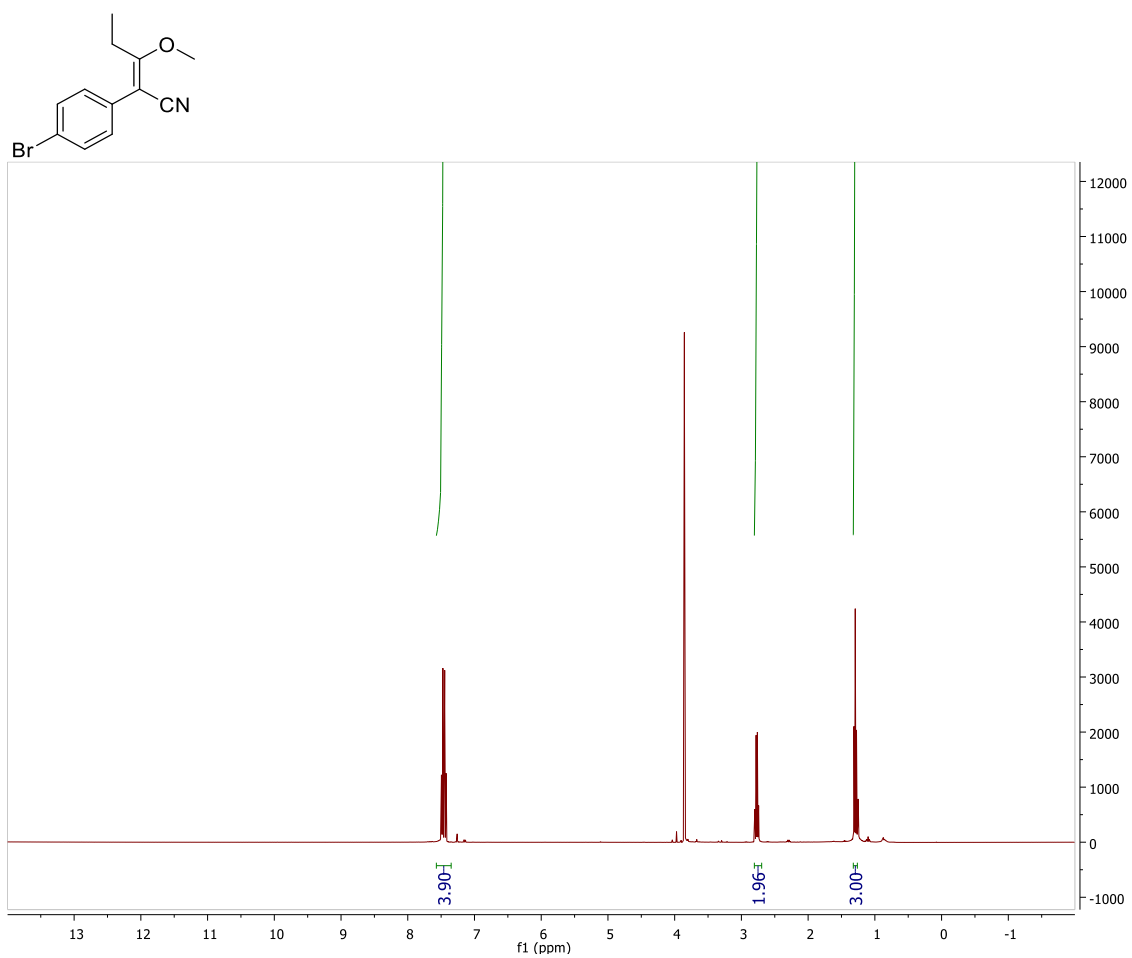
3 ^1H NMR



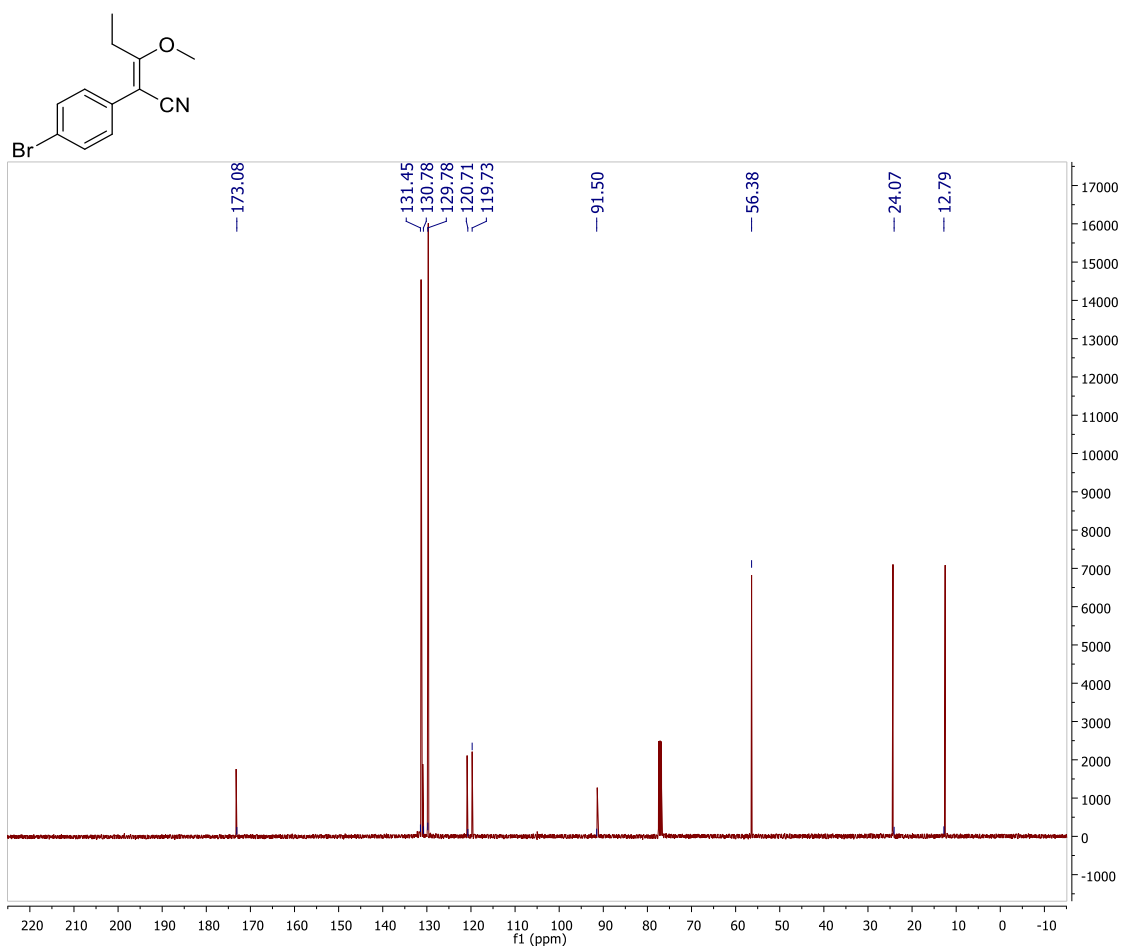
3 ^{13}C NMR



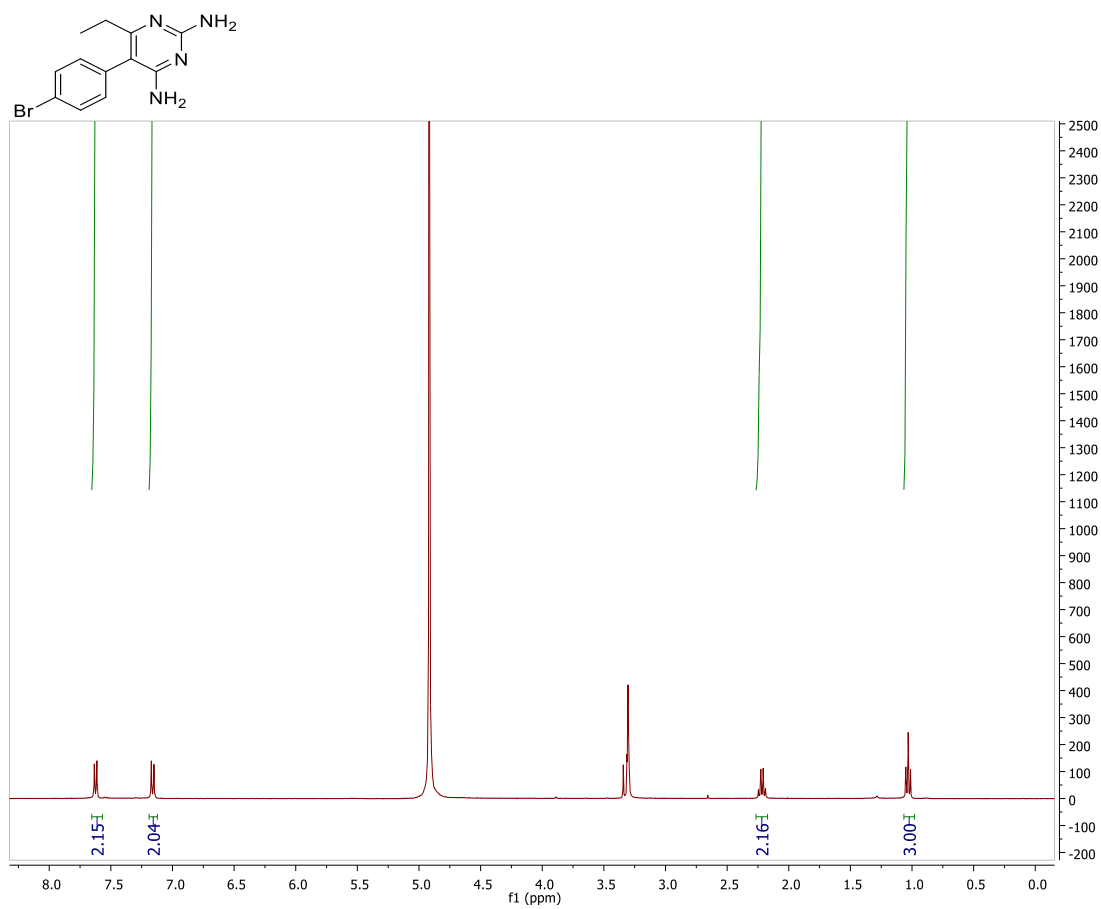
5 ^1H NMR



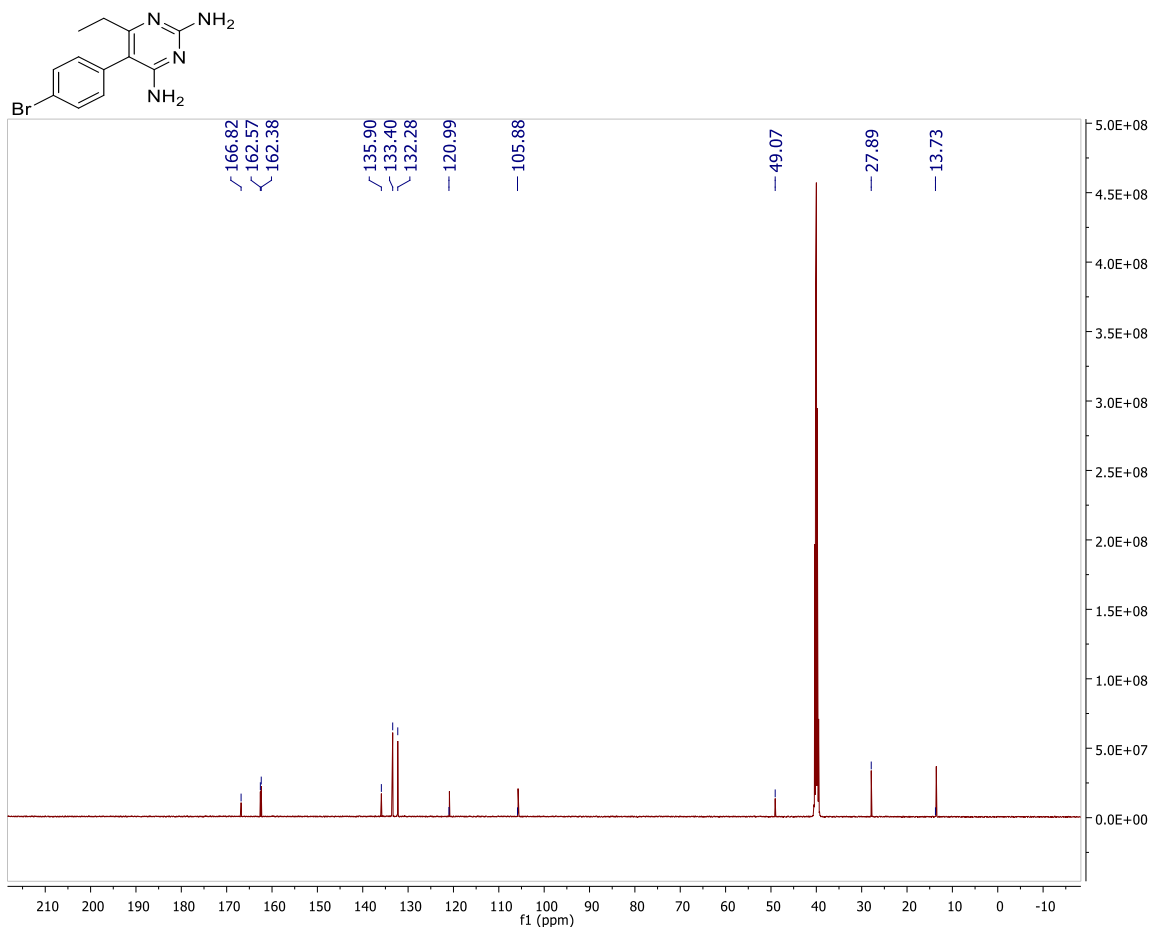
5 ^{13}C NMR



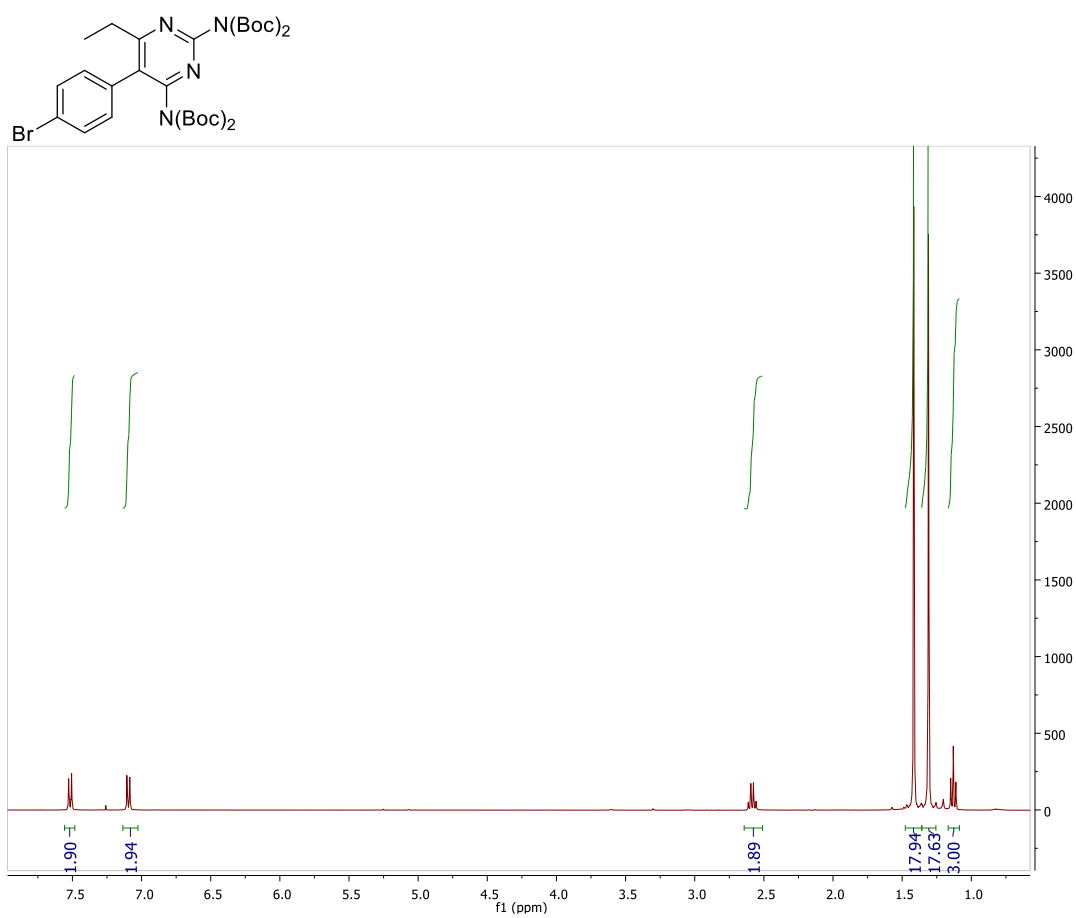
6 ^1H NMR



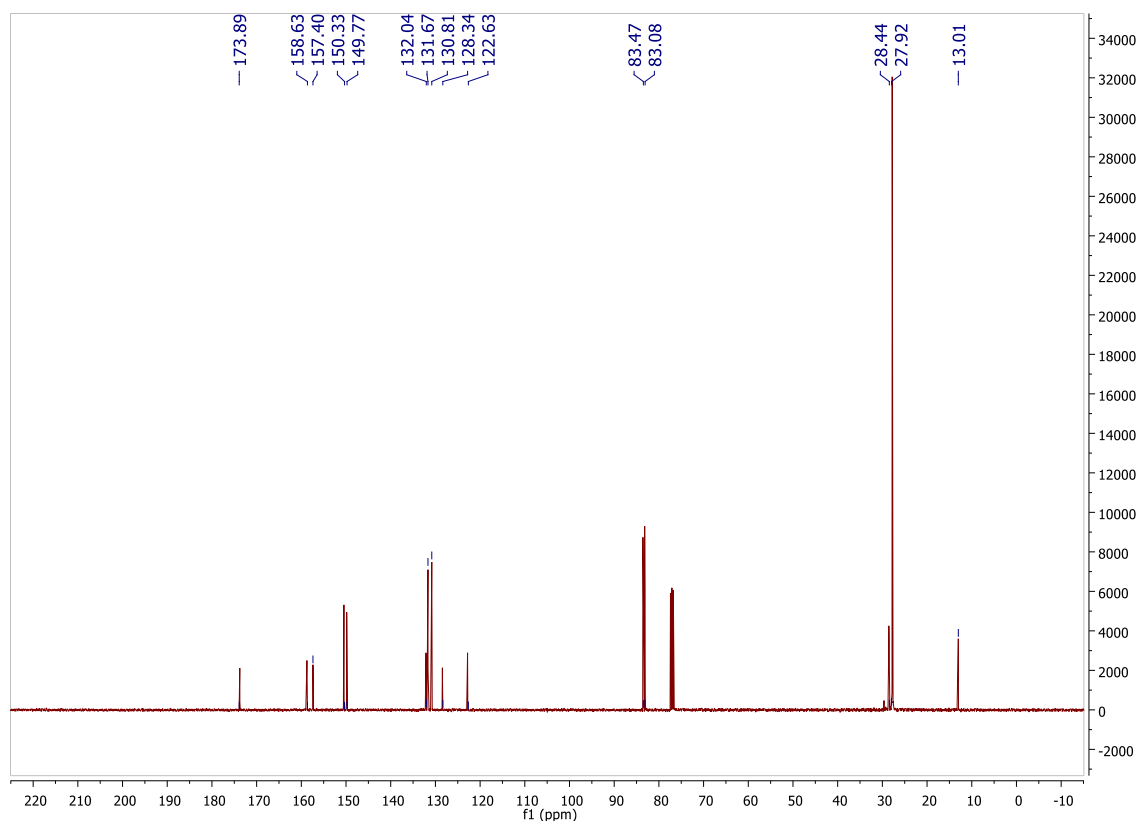
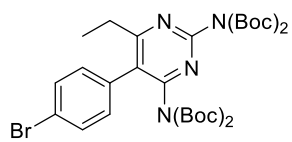
6 ^{13}C NMR



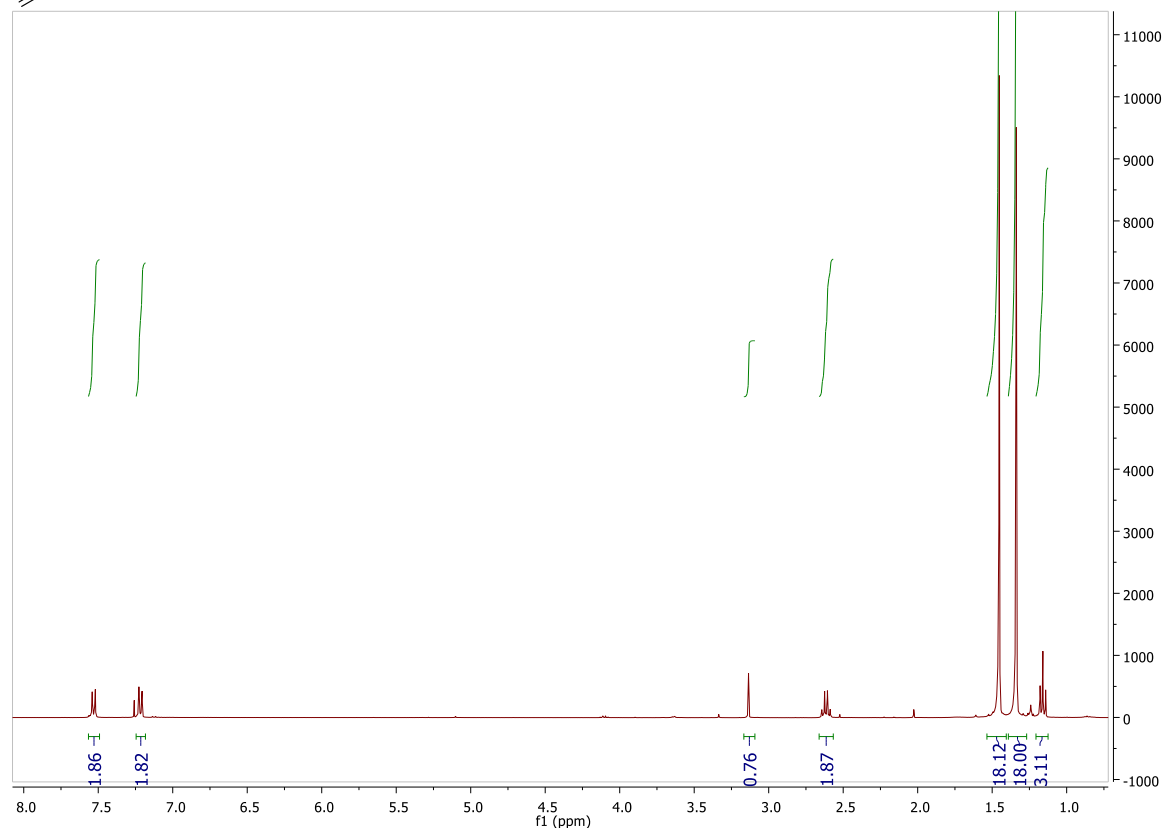
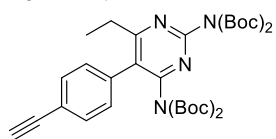
7 ^1H NMR



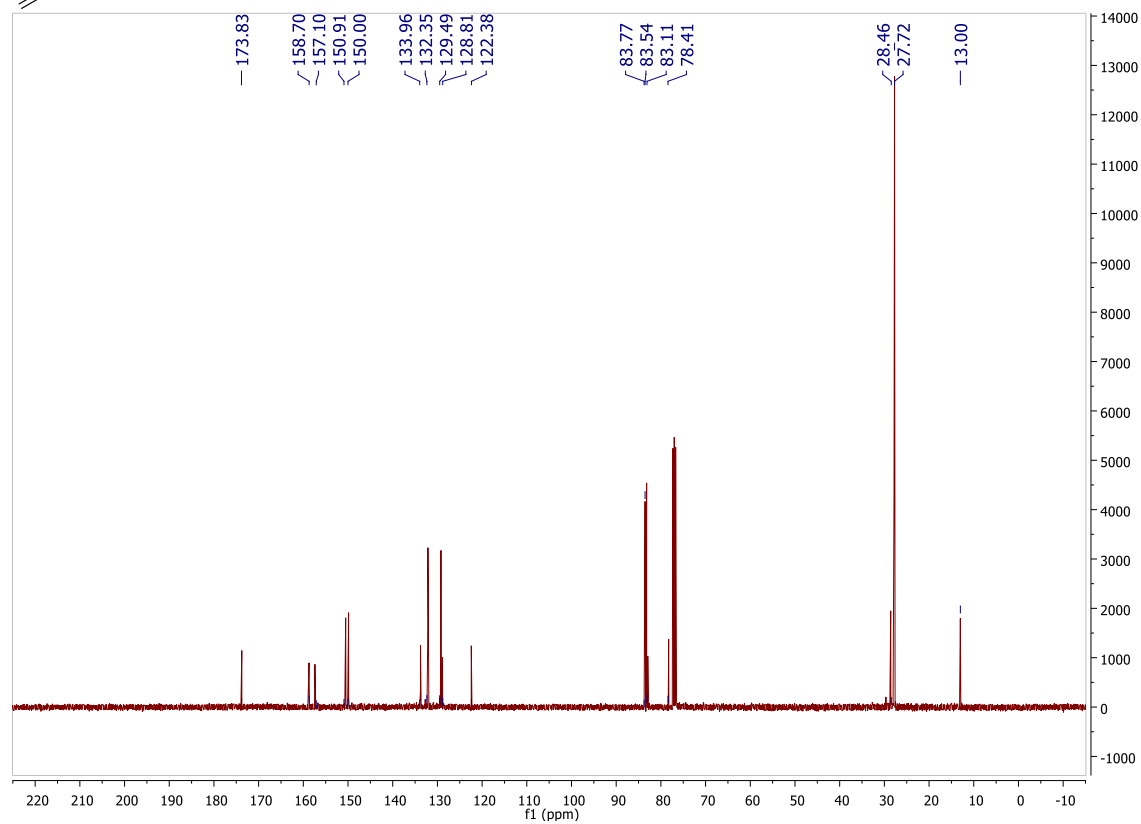
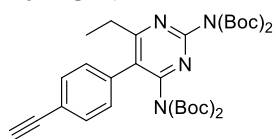
7 ¹³C NMR



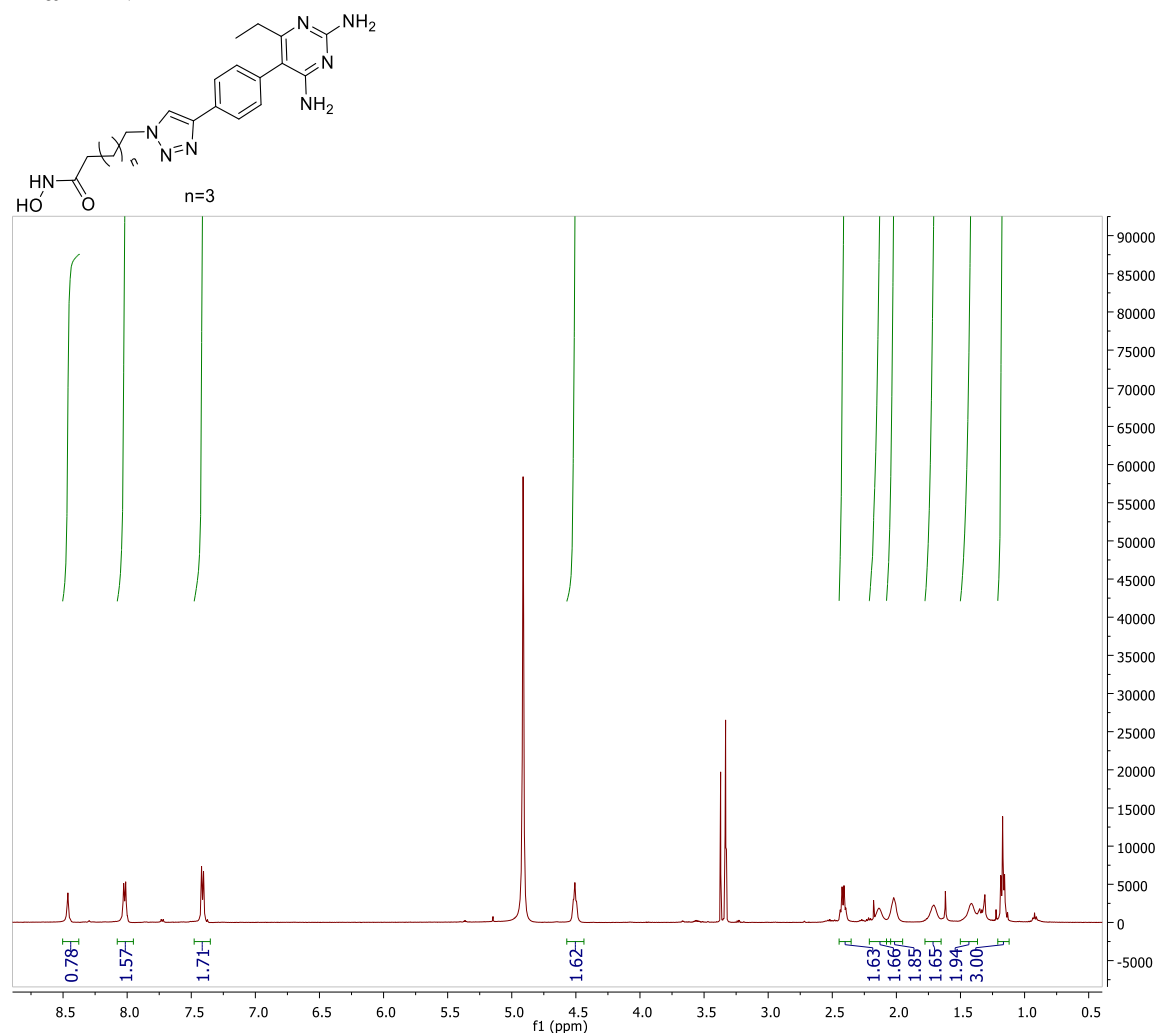
10 ^1H NMR



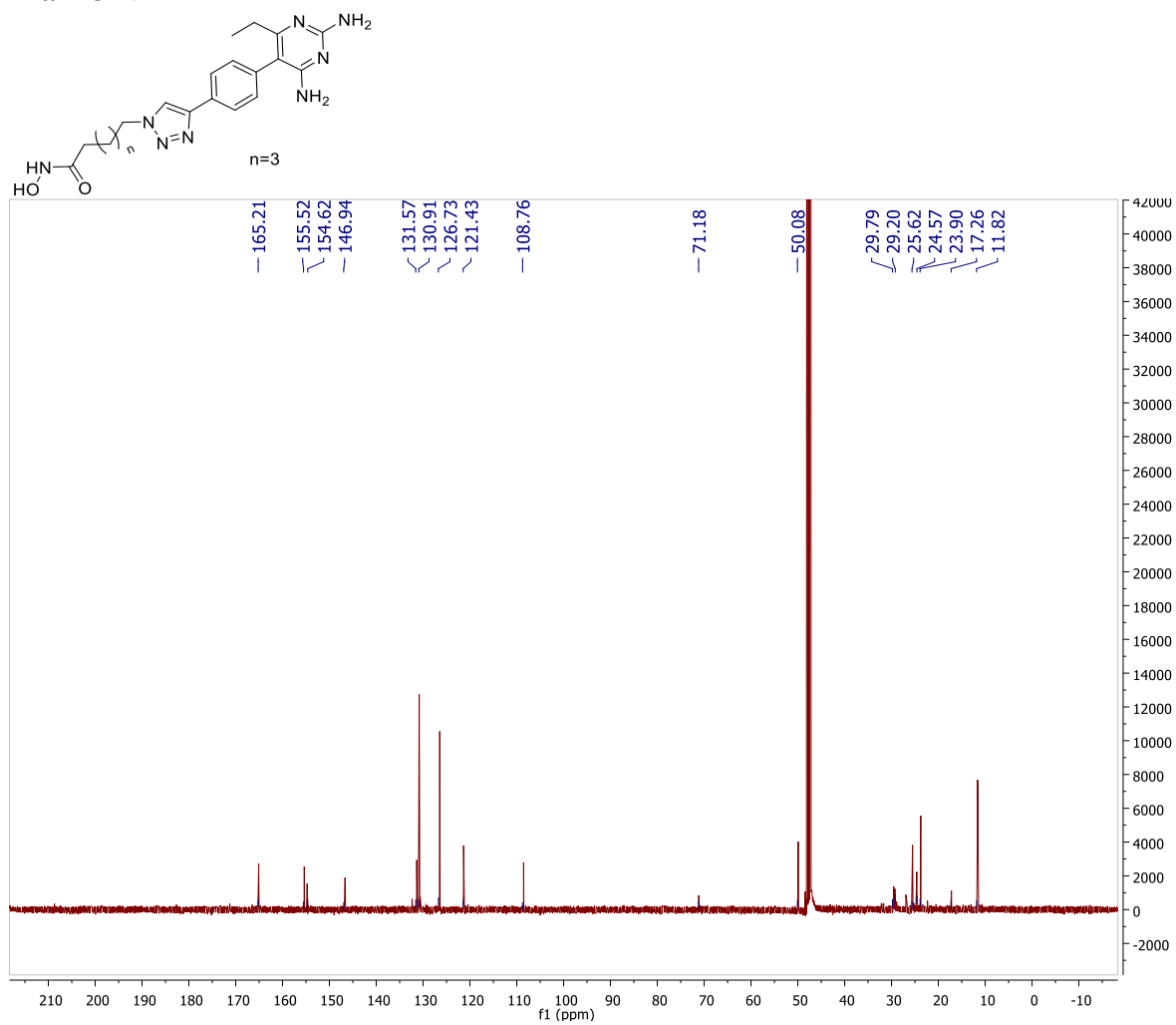
10 ^{13}C NMR



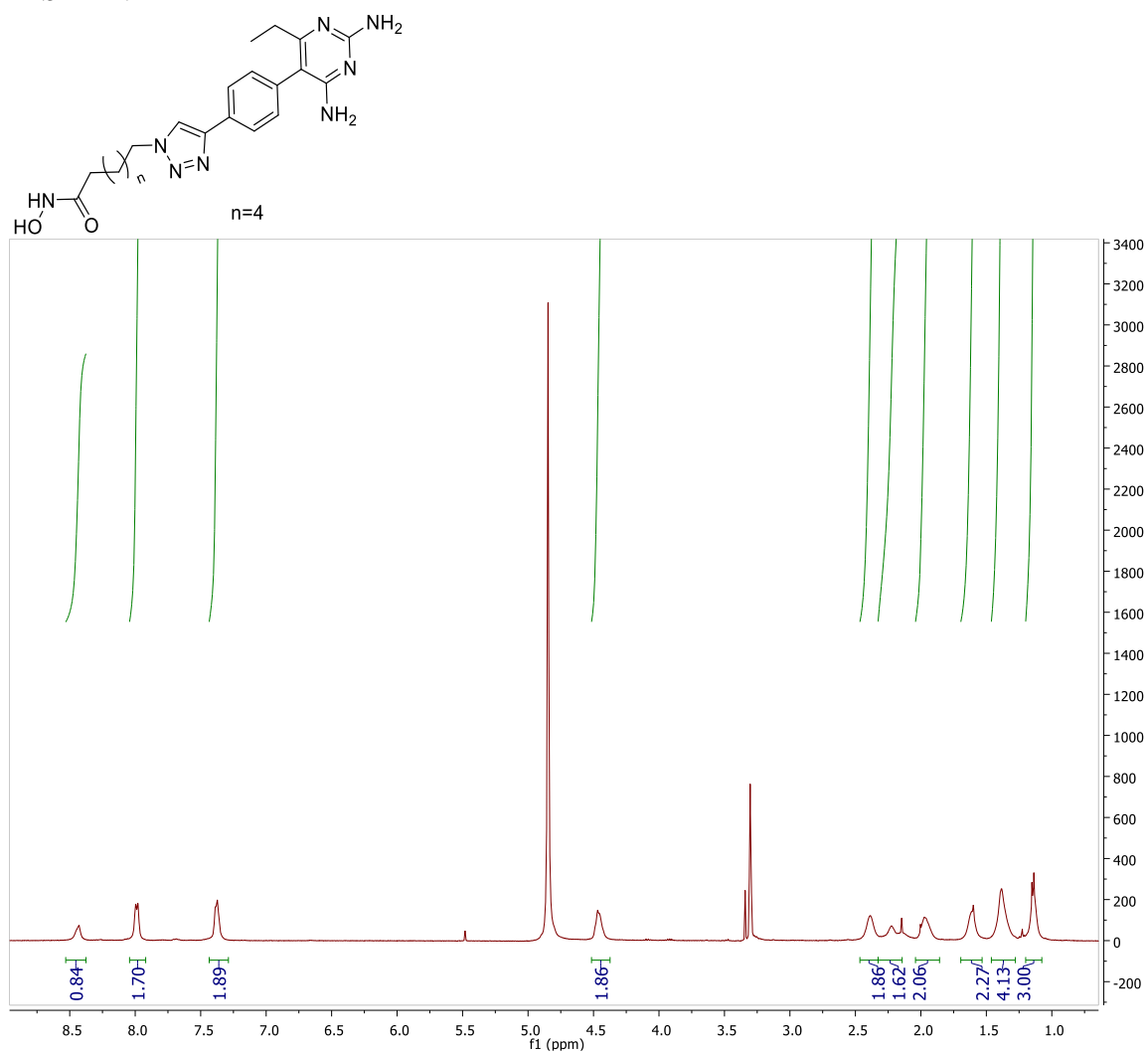
12a ^1H NMR



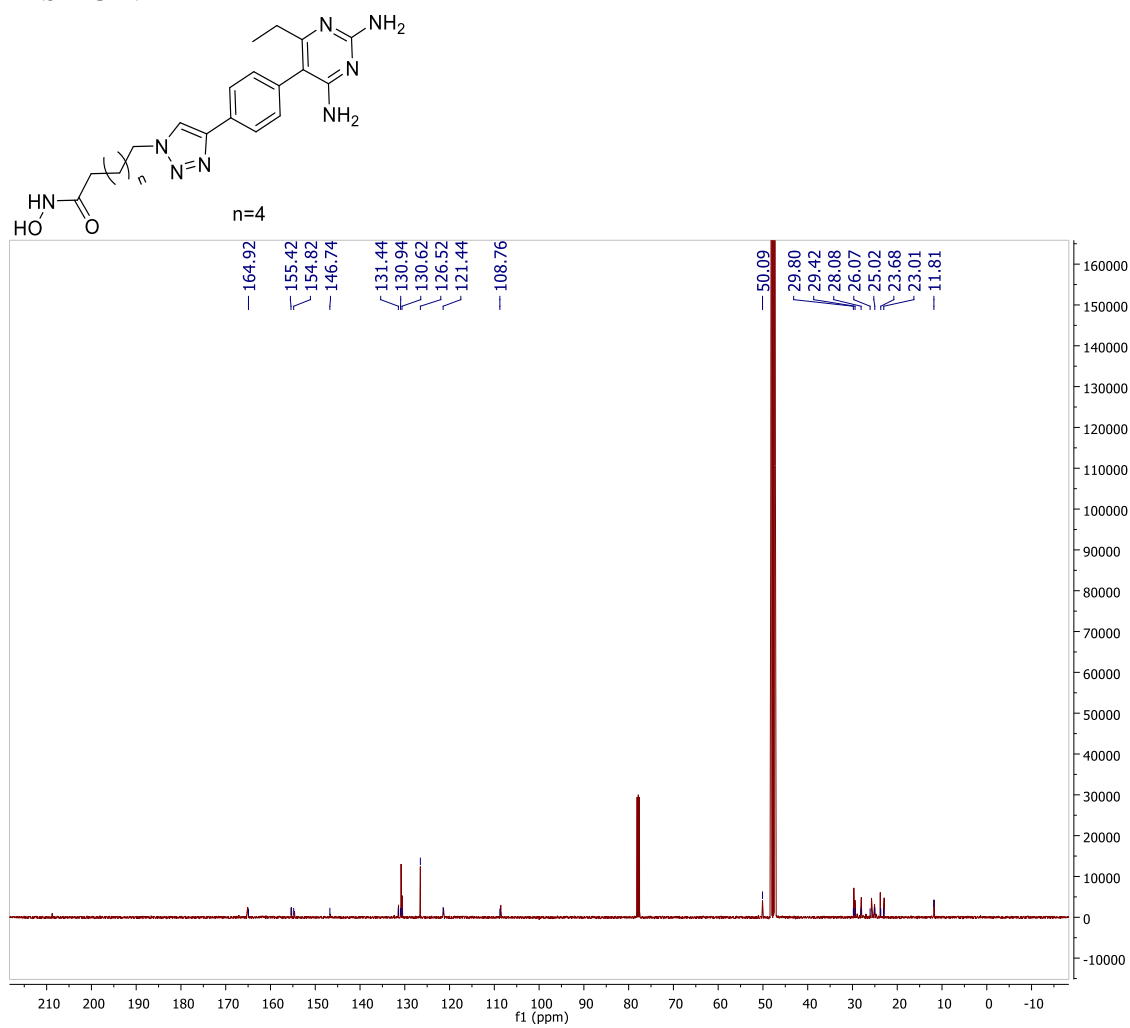
12a ^{13}C NMR



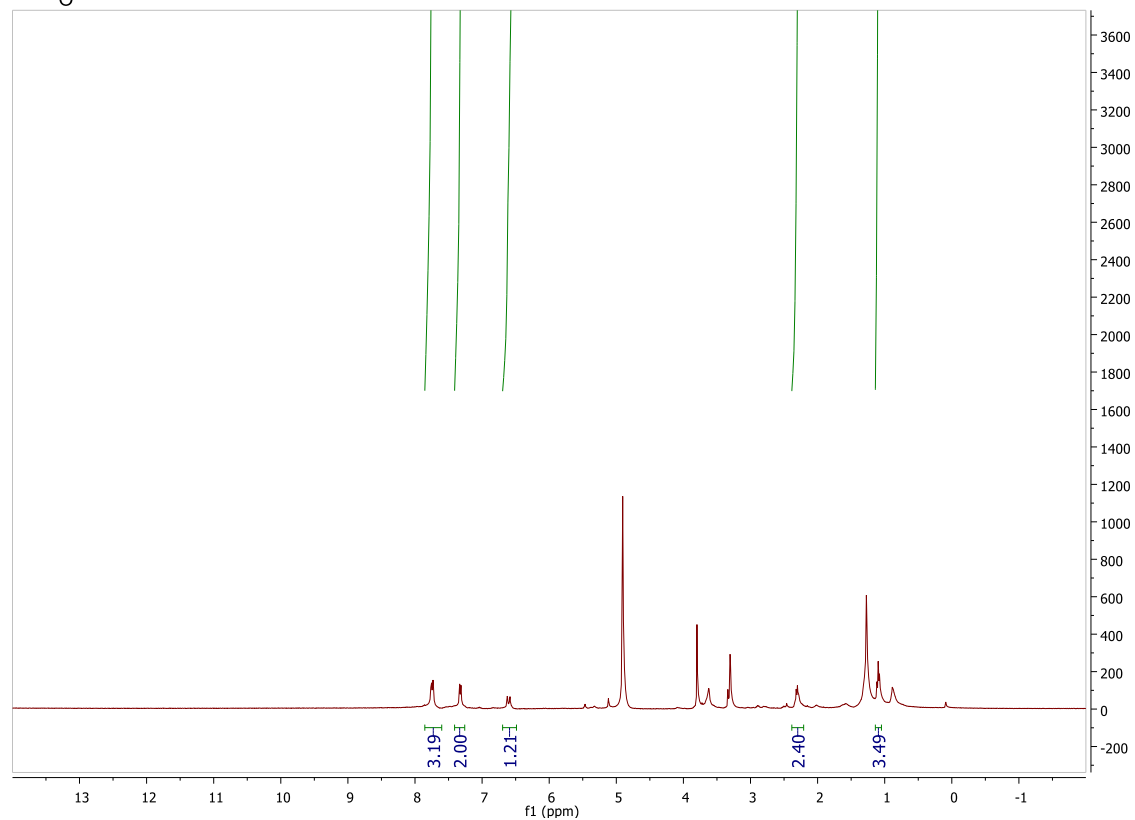
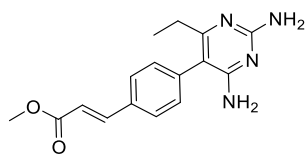
12b ^1H NMR



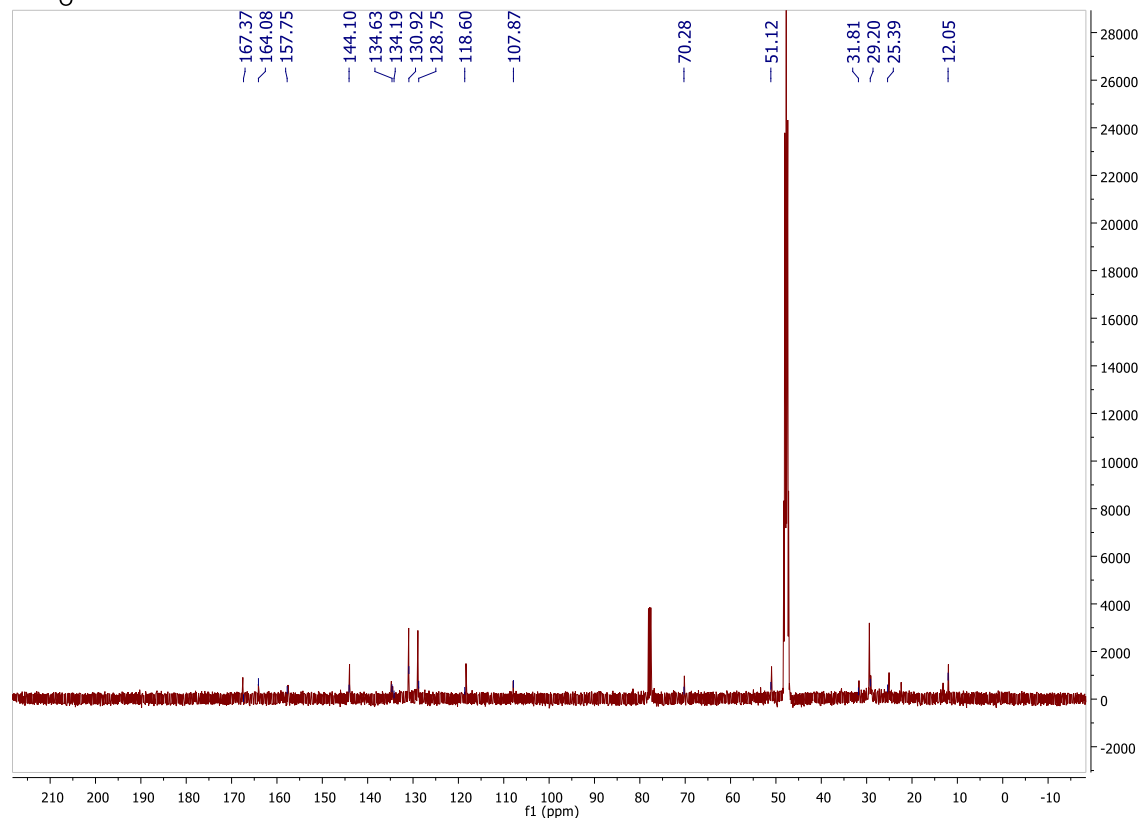
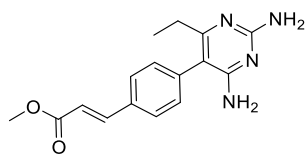
12b ^{13}C NMR



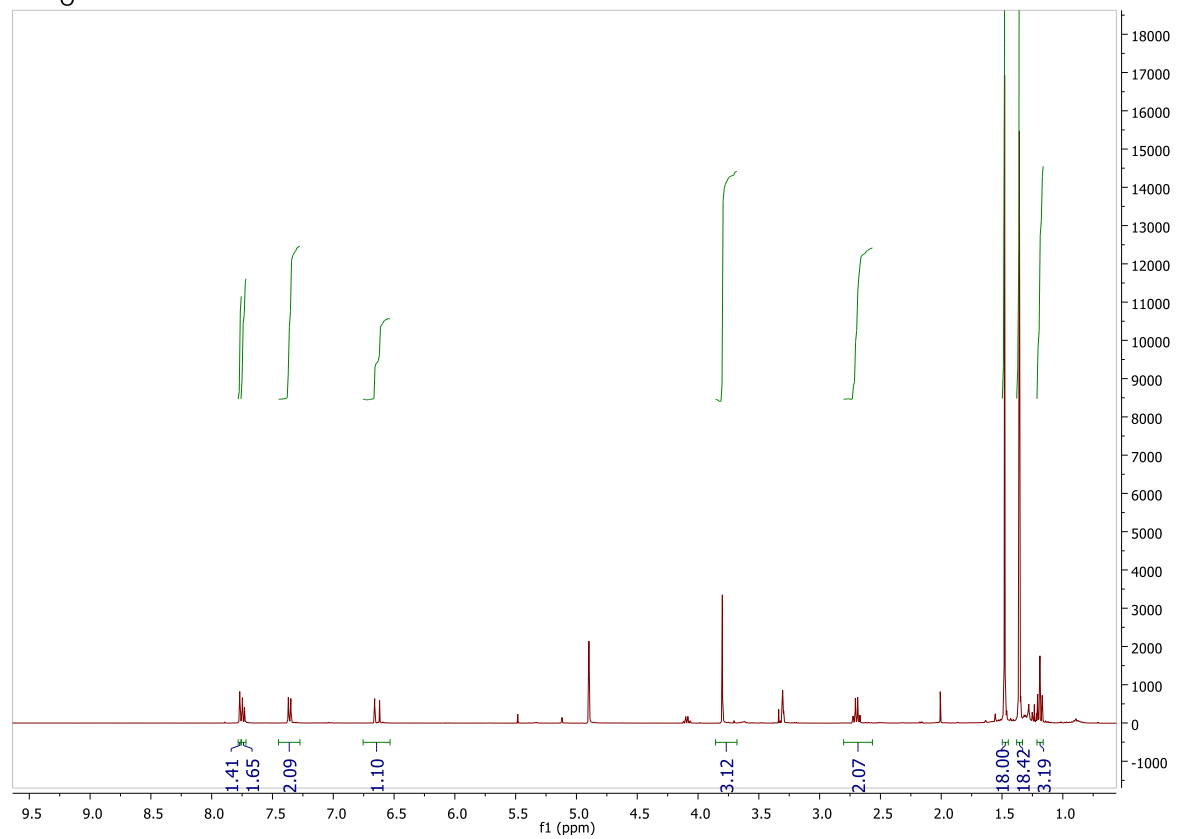
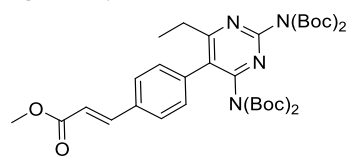
14 ^1H NMR



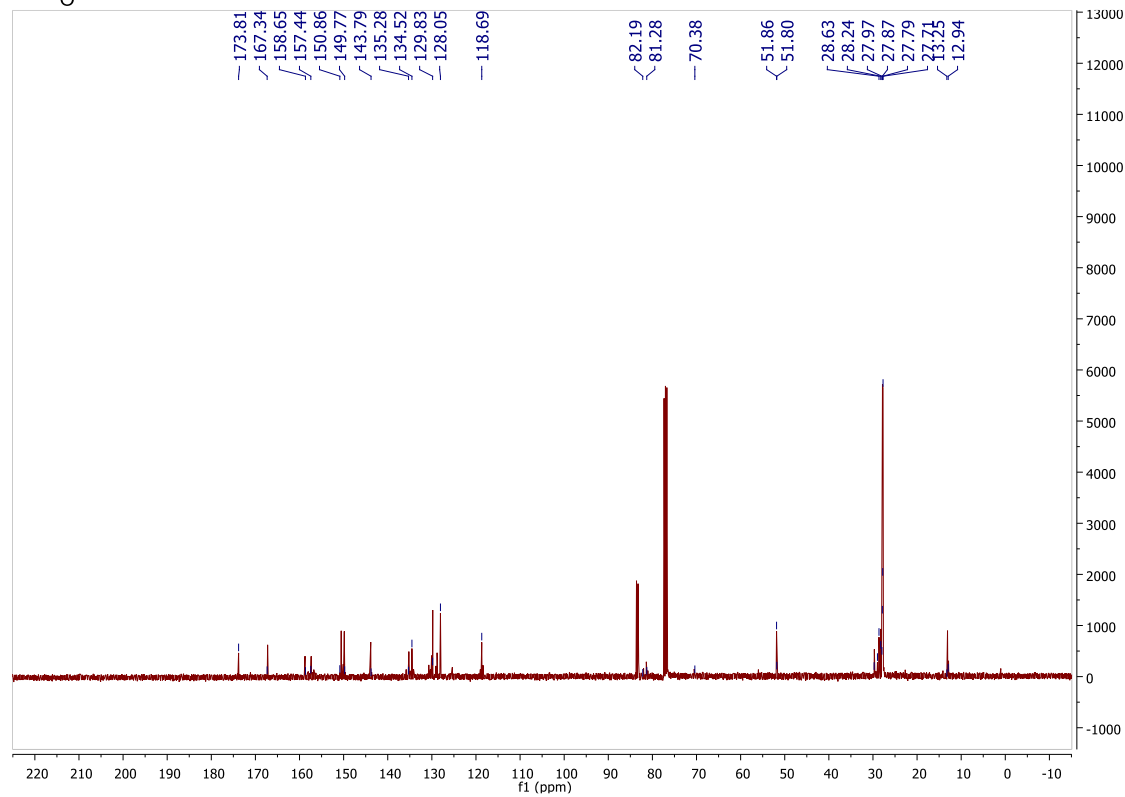
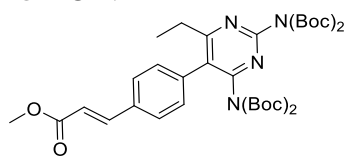
14 ^{13}C NMR



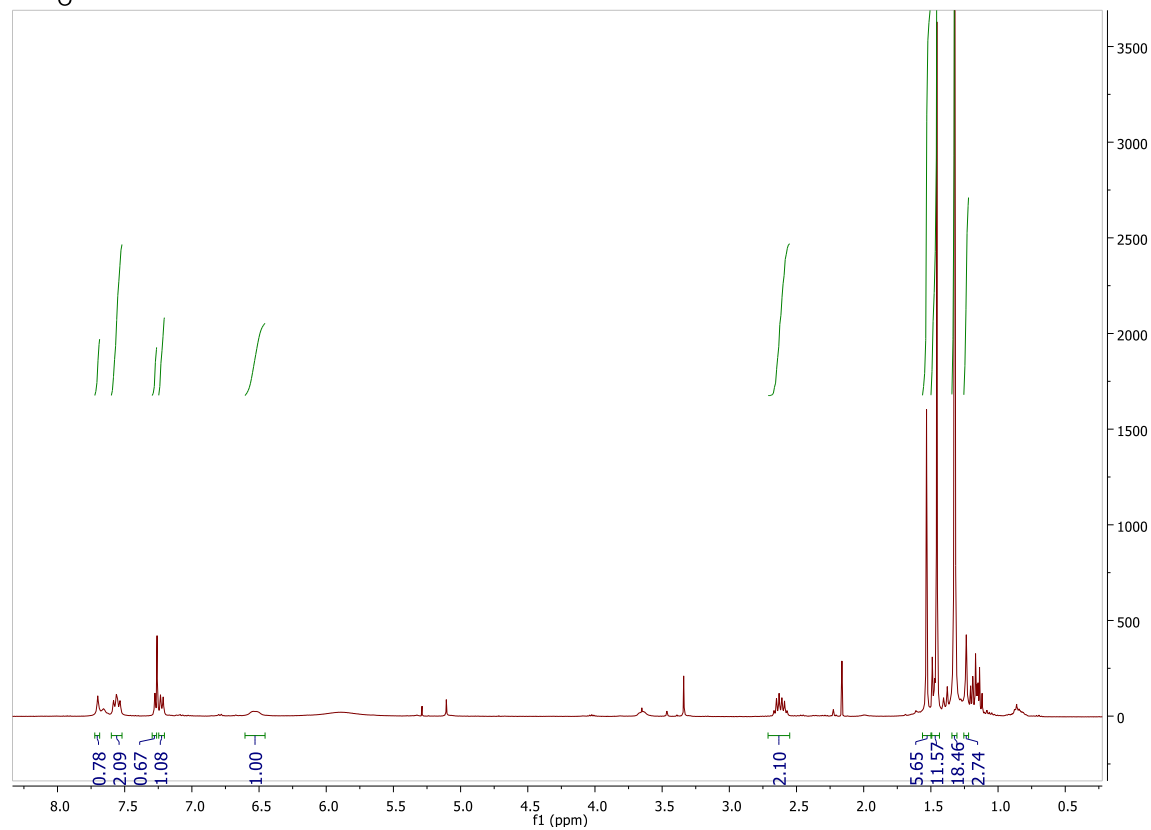
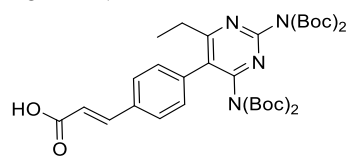
15 ¹H NMR

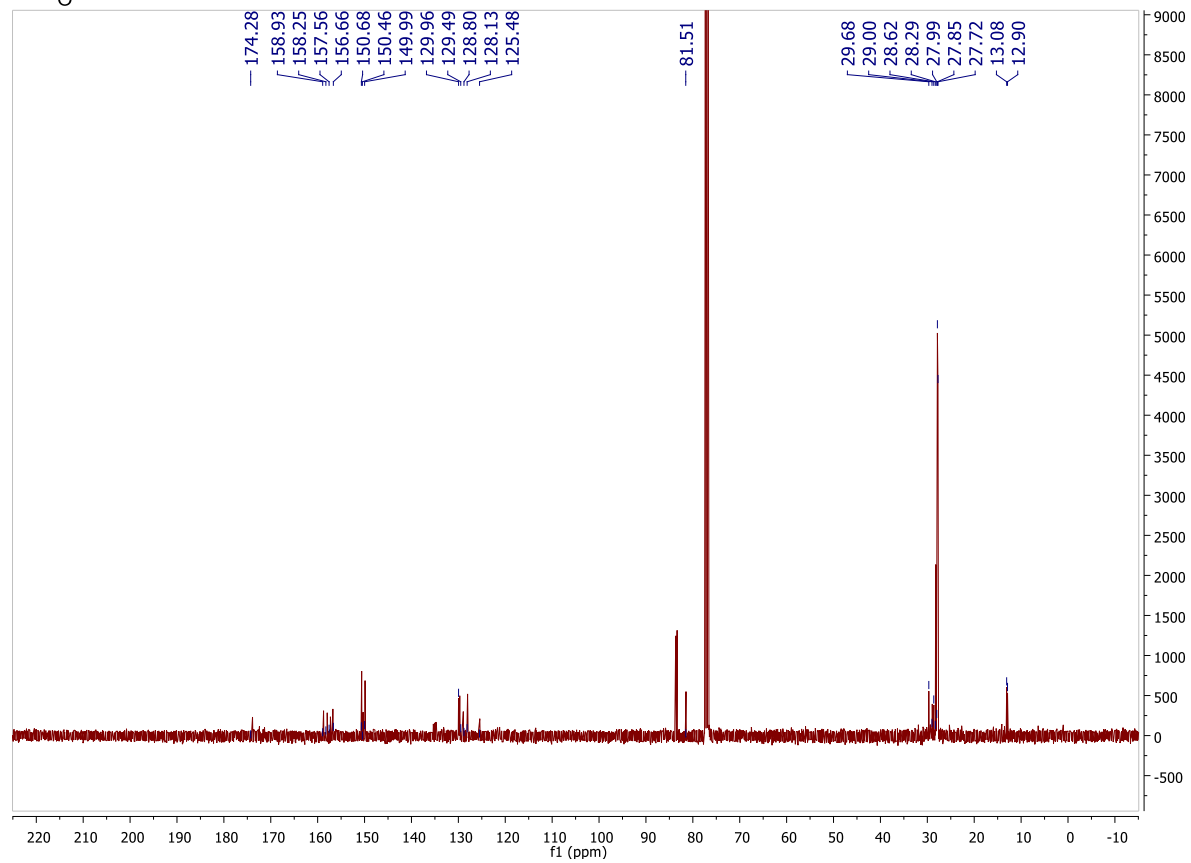


15 ¹³C NMR

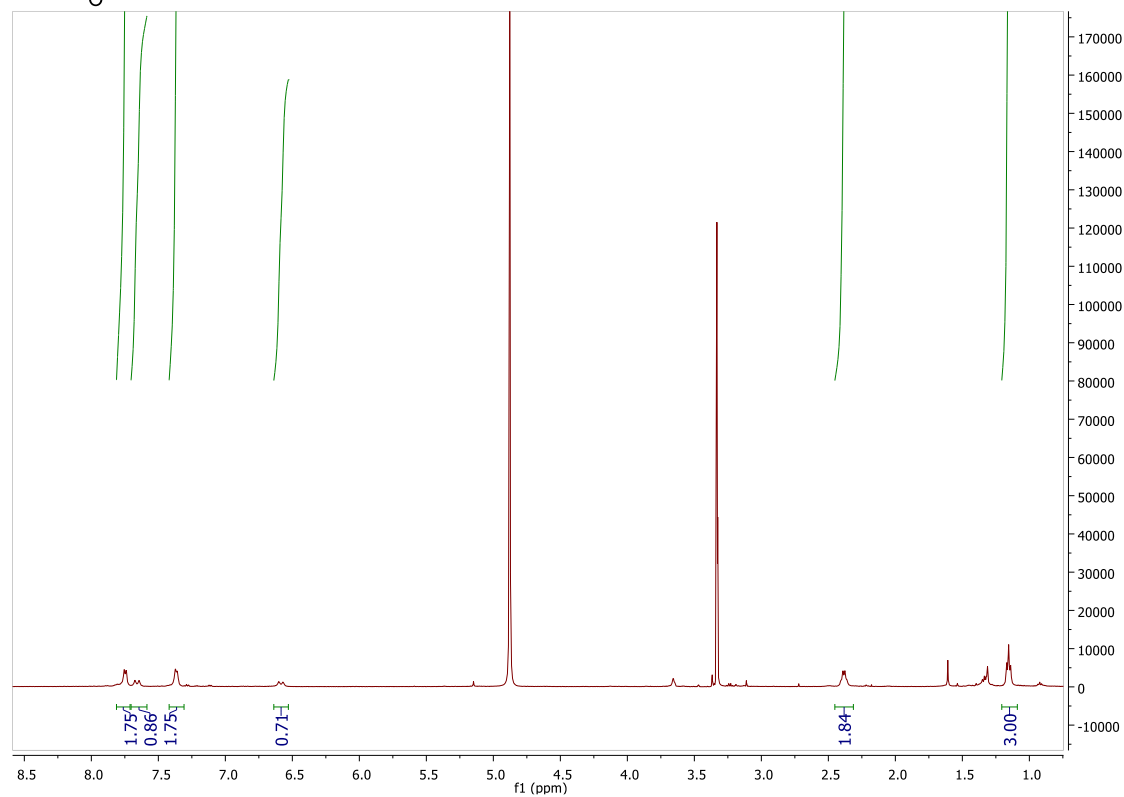
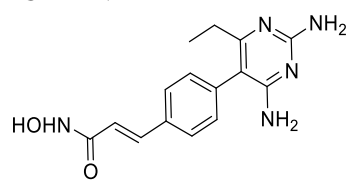


16 ^1H NMR

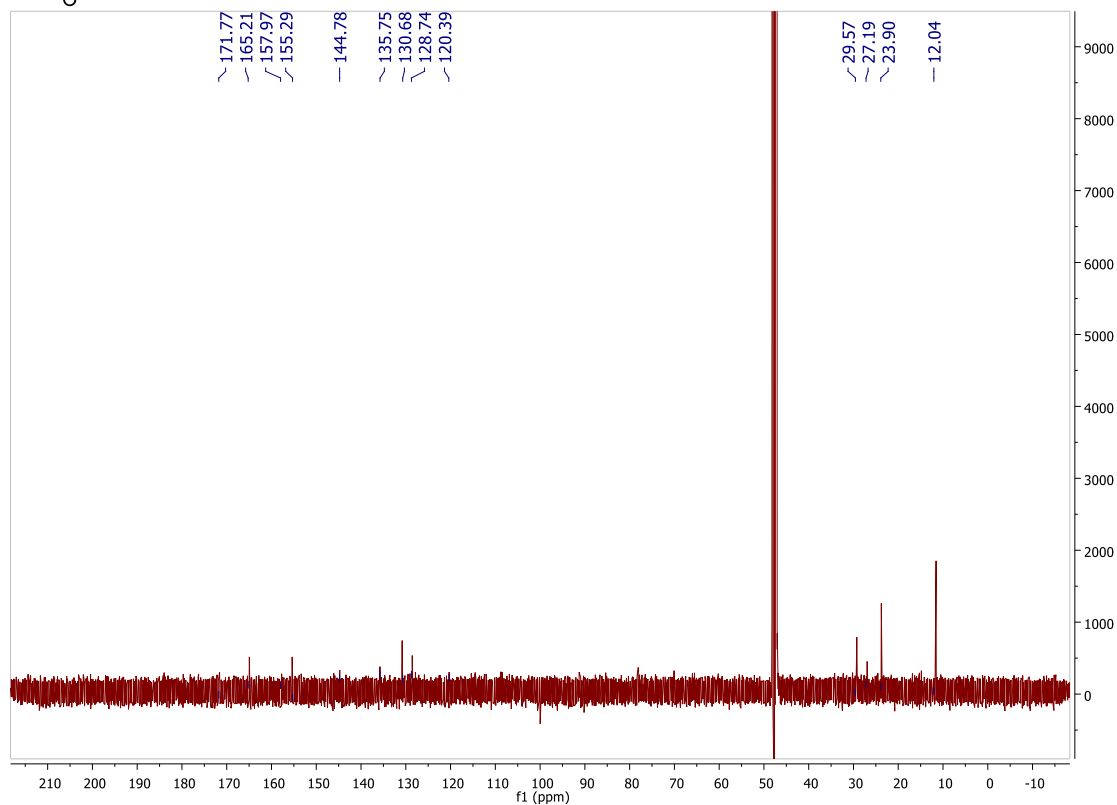
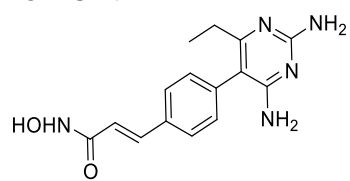


CC1=C(C(=N1)N(C(=O)OC(C)(C)C)C(=O)OC(C)(C)C)C2=CC=CC=C2/C=C/C(=O)O

18 ^1H NMR



18 ¹³C NMR



Chapter 6

CONCLUSION AND FUTURE STUDIES

6.1. Conclusion

Cancer is one of the leading causes of death worldwide [1]. Genetic and epigenetic alterations are involved in tumorigenesis, therefore, epigenetic regulations have become a new promising therapeutic strategy over the past few decades. Epigenetic regulation has various ways to modify DNA and histone state through processes such as DNA methylation, histone modification and remodeling via histone acetylation and deacetylation. Histone acetyl transferase (HAT) and histone deacetylase (HDAC) are able to add or remove acetyl group, respectively, from histone core tail, leading to an open or restricted chromatin. Histone modification impacts DNA access to transcription factors and, consequently, gene expressions [2].

Development of HDAC inhibitors (HDACi) that impede HDAC enzyme function and result in expression of tumor suppressor proteins such as p53 has emerged as an encouraging anticancer therapeutic approach [3]. To date, there are four US FDA approved HDACi for treating CTCL, PTCL and myeloma with many others being investigated in different phases of clinical trials [4]. Chidamide is another HDACi that is approved only in china for treating relapsed and refractory peripheral T-cell lymphoma and currently in phase II clinical trials in US [5]. Despite the promising results of these HDACi, they mostly suffer from poor bioavailability, lack of accumulation in solid tumors and side effects including severe cardiotoxicity [6]. Thus, there is an unmet medical need to develop a new class of HDACi that are more potent towards solid tumors and less cytotoxic to healthy cells.

This thesis focused on two approaches to overcome the common limitations of HDACi: 1) Design and development of isoform-selective HDACi. 2) Targeted delivery of HDACi to the site of tumor through their conjugation to FDA approved drugs that are

known to accumulate in certain tissues or target certain receptors overexpressed on tumor cells.

In chapter 2 and 3, I showed that HDACi that are conjugated to azithromycin, an FDA approved antibiotic, has the potential to target lung tissues, possibly due to azithromycin accumulation in macrophage cells [7], [8]. I described the designed and synthesis of pan HDACi and isoform selective HDACi conjugated to azithromycin for delivery to lung tissues, and evaluated their HDAC inhibitory potency and anti-proliferative activity. Interestingly, despite the lower HDAC potency of isoform selective HDACi they exhibited more potent anti-proliferative activity towards transformed cell lines. Additionally, data from *in vivo* efficacy study on a lead pan HDACi and isoform selective HDACi in mouse model strongly suggest that these azithromycin conjugated HDACi have the potential to accumulate in lung tissue and protect it from metastasis. Furthermore, the *in vivo* study also confirmed the general hypothesis that isoform selective HDACi have better efficacy and therapeutic outcome compared to pan HDACi. Animal model showed greater tumor regression as well as less number of lung nodules in the mice that were treated with the isoform selective HDACi compared to the ones that were treated with pan HDACi.

In chapter 4, a series of dual functioning compounds with both selective estrogen receptor modulator (SERM) and HDAC inhibition activities having various zinc binding groups was synthesized and tested against both ER α positive (MCF-7) and ER α negative (MDA-MB231) cell lines. In this project, tamoxifen, a SERM that is the most common and the first line therapy in treating ER α positive breast cancer [9], was used as the HDACi cap group. Conjugating tamoxifen to the HDACi resulted in their better uptake by ER α positive breast cancer cell line compared to ER α negative breast cancer cell line possibly due to tamoxifen's binding to ER α [10], [11]. The lead tamoxifen conjugated HDACi exhibited more selectivity and cytotoxicity toward ER α positive (MCF-7) rather

than ER α negative (MDA-MB231) compared to tamoxifen itself [12]. Leads compounds are currently being investigated in animal models.

The last chapter focused on design and synthesis of bifunctional STA3/ HDAC inhibitors, where pyrimethamine, a known STAT3 selective inhibitor [13] was used as the cap group. We hypothesized that multiple ligand compounds comprising of pyrimethamine and HDAC inhibitors will result in both STAT3 and HDAC inhibition. The anti-proliferative activity of these compounds were evaluated against three transformed cell lines, lung (A549), ER α positive (MCF-7), ER α negative (MDA-MB231) with activated STAT3 and one normal cell line (VERO). These compounds anti-proliferative activity was in correlation with their HDAC1 inhibition potency. The lead compound with the nanomolar range HDAC1 and HDAC6 inhibitory potency had the most potent anti-proliferative activity whereas the one with low HDAC inhibition potency (macromolar range) was not cytotoxic against cancer cells. Additionally, the lead compound exhibited the most cytotoxicity toward ER α negative (MDA-MB231) where STAT3 is activated. This data shows that pyrimethamine HDACi conjugates have the potential to inhibit proliferation of other tumors which are dependent on STAT3 signaling pathway including myeloma cell lines, INA6, and U266, and prostate cancer cell line DU145.

Pyrimethamine is currently in clinical trials for treating relapsed chronic lymphocytic leukemia and small lymphocytic lymphoma due to STAT3 activation in these cancers [14].

Furthermore, pyrimethamine is an FDA approved anti-folate and anti-malarial drug. However, its use as an anti-malarial therapeutic agent is hampered due to naturally developed resistance in the parasite [15], [16]. It has been shown that HDACi are associated with anti-parasitic activity, therefore, pyrimethamine conjugated HDACi have the potential to overcome the developed resistance to pyrimethamine in treating malarial.

Hence, these compounds anti-malarial activity is another important factor that needs to be evaluated.

Finally, to complete this project and SAR study, more pyrimethamine conjugated HDACi with different zinc binding groups need to be synthesized.

6.2. References

1. Siegel, R. L.; Miller, K. D.; Jemal, A. Cancer statistics, 2016. *CA: a cancer journal for clinicians* **2016**, 66, 7-30.
2. Egger, G.; Liang, G.; Aparicio, A.; Jones, P. A. Epigenetics in human disease and prospects for epigenetic therapy. *Nature* **2004**, 429, 457-463.
3. Marks, P. A.; Rifkind, R. A.; Richon, V. M.; Breslow, R.; Miller, T.; Kelly, W. K. Histone deacetylases and cancer: causes and therapies. *Nature Reviews Cancer* **2001**, 1, 194-202.
4. Mottamal, M.; Zheng, S.; Huang, T. L.; Wang, G. Histone deacetylase inhibitors in clinical studies as templates for new anticancer agents. *Molecules* **2015**, 20, 3898-3941.
5. Ning, Z.-Q.; Li, Z.-B.; Newman, M. J.; Shan, S.; Wang, X.-H.; Pan, D.-S.; Zhang, J.; Dong, M.; Du, X.; Lu, X.-P. Chidamide (CS055/HBI-8000): a new histone deacetylase inhibitor of the benzamide class with antitumor activity and the ability to enhance immune cell-mediated tumor cell cytotoxicity. *Cancer chemotherapy and pharmacology* **2012**, 69, 901-909.
6. Gryder, B. E.; Sodji, Q. H.; Oyelere, A. K. Targeted cancer therapy: giving histone deacetylase inhibitors all they need to succeed. *Future medicinal chemistry* **2012**, 4, 505-524.
7. Laskin, D. L.; Weinberger, B.; Laskin, J. D. Functional heterogeneity in liver and lung macrophages. *Journal of leukocyte biology* **2001**, 70, 163-170.

8. Dreaden, E. C.; Raji, I. O.; Austin, L. A.; Fathi, S.; Mwakwari, S. C.; Humphries, W. H.; Kang, B.; Oyelere, A. K.; El-Sayed, M. A. P-Glycoprotein-Dependent Trafficking of Nanoparticle-Drug Conjugates. *small* **2014**, 10, 1719-1723.
9. Mandlekar, S.; Yu, R.; Tan, T.-H.; Kong, A.-N. T. Activation of caspase-3 and c-Jun NH2-terminal kinase-1 signaling pathways in tamoxifen-induced apoptosis of human breast cancer cells. *Cancer Research* **2000**, 60, 5995-6000.
10. Gryder, B. E.; Rood, M. K.; Johnson, K. A.; Patil, V.; Raftery, E. D.; Yao, L.-P. D.; Rice, M.; Azizi, B.; Doyle, D. F.; Oyelere, A. K. Histone deacetylase inhibitors equipped with estrogen receptor modulation activity. *Journal of medicinal chemistry* **2013**, 56, 5782-5796
11. Peng, K.-w.; Wang, H.; Qin, Z.; Wijewickrama, G. T.; Lu, M.; Wang, Z.; Bolton, J. L.; Thatcher, G. R. Selective estrogen receptor modulator delivery of quinone warheads to DNA triggering apoptosis in breast cancer cells. *ACS chemical biology* **2009**, 4, 1039-1049.
12. Webb, P.; Nguyen, P.; Kushner, P. J. Differential SERM effects on corepressor binding dictate ER α activity in vivo. *Journal of Biological Chemistry* **2003**, 278, 6912-6920.
13. Murphy, C.; Blanchard, J.; Ganser, A.; Brown, E.; Hassell, J.; Humphries, R.; Morgan, M.; Heuser, M. High-throughput drug screening identifies pyrimethamine as a potent and selective inhibitor of acute myeloid leukemia. *Current cancer drug targets* **2016**.
14. Chaudhari, S.; Desai, J. S.; Adam, A.; Mishra, P. Jak/stat as a novel target for treatment of leukemia. *Int J Pharm Pharm Sci* **2014**, 6, 1-7.
15. Peterson, D. S.; Milhous, W. K.; Wellems, T. E. Molecular basis of differential resistance to cycloguanil and pyrimethamine in *Plasmodium falciparum* malaria. *Proceedings of the National Academy of Sciences* **1990**, 87, 3018-3022.

16. Foote, S. J.; Galatis, D.; Cowman, A. F. Amino acids in the dihydrofolate reductase-thymidylate synthase gene of *Plasmodium falciparum* involved in cycloguanil resistance differ from those involved in pyrimethamine resistance. *Proceedings of the National Academy of Sciences* **1990**, 87, 3014-3017.

APPENDIX A

LIPOSOMAL DRUG DELIVERY SYSTEMS FOR TARGETED CANCER THERAPY

This work was published Future Medicinal Chemistry.

S. Fathi, A. Oyelere, Future Med. Chem, (2016) 8(17), 2091–2112.

A.1. Introduction

Cancer is one of the leading causes of death worldwide. According to American Cancer Society, cancer is the second deadliest disease, after cardiovascular diseases [1], [2]. Mutations or damages to the genes, which occur due to genetic disposition or environmental factors, are the main cause of cancer. Cancer cells are prone to rapid division, metastasis and are resistant to cell death [3]. Available treatments - like surgery, chemotherapy, hormone therapy, or radiotherapy - have terrible side effects. Most chemotherapeutic agents are hampered by narrow therapeutic indices, poor pharmacokinetics and non-selective distribution in the body, leading to off-target toxicity. To date, one of the main obstacles in cancer treatment has been selective delivery of drugs to tumor site, a feat which holds great promise at enhancing drug therapeutic efficacy and lowering off-target toxicities [4]. Nanoparticles (NP) have emerged as a promising therapeutic agents in recent years as they facilitate increased uptake and accumulation of drugs at the tumor sites [5]. Among all classes of nanoparticles, liposomal drug delivery system has received the most attention over the past few decades [6].

The idea of a liposome as a delivery vehicle goes back to 1965. It was first introduced by Alec Bangham and colleagues [7]. Liposomes are self-assembled small and spherical vesicles consisting of an aqueous core which is surrounded by one or more

phospholipid bilayers. Because of their amphiphilic nature, liposomes are able to carry both hydrophobic and hydrophilic compounds [8] (Figure 1.A). Various types of small molecules including antifungal and anticancer drugs as well as macromolecules such as hormones, enzymes and different varieties of peptides have been incorporated into liposomes [9]. Liposomes' biocompatibility, bioavailability and site specific drug delivery properties have stimulated intense interest in them as unique drug carrier systems for delivery and release of therapeutic drugs at the site of a tumor to potentially enhance drug potency efficacy and minimize side effects [10]. Liposomes' pharmacokinetic properties depend greatly on size, surface charge, number of bilayers and fluidity [11]. They can be classified in multiple categories such as: conventional (first generation of liposomes), stealth (PEG grafted liposomes), long release, triggered release or ligand targeted [8], [12]. In some liposome conjugates, a drug molecule is linked to the carrier through covalent bonds that are usually acid cleavable or redox sensitive [13]. In other liposome systems, the therapeutic drug is encapsulated by the carrier, without a need for a covalent bond. These designs allow liposomes to carry multiple drugs simultaneously [14].

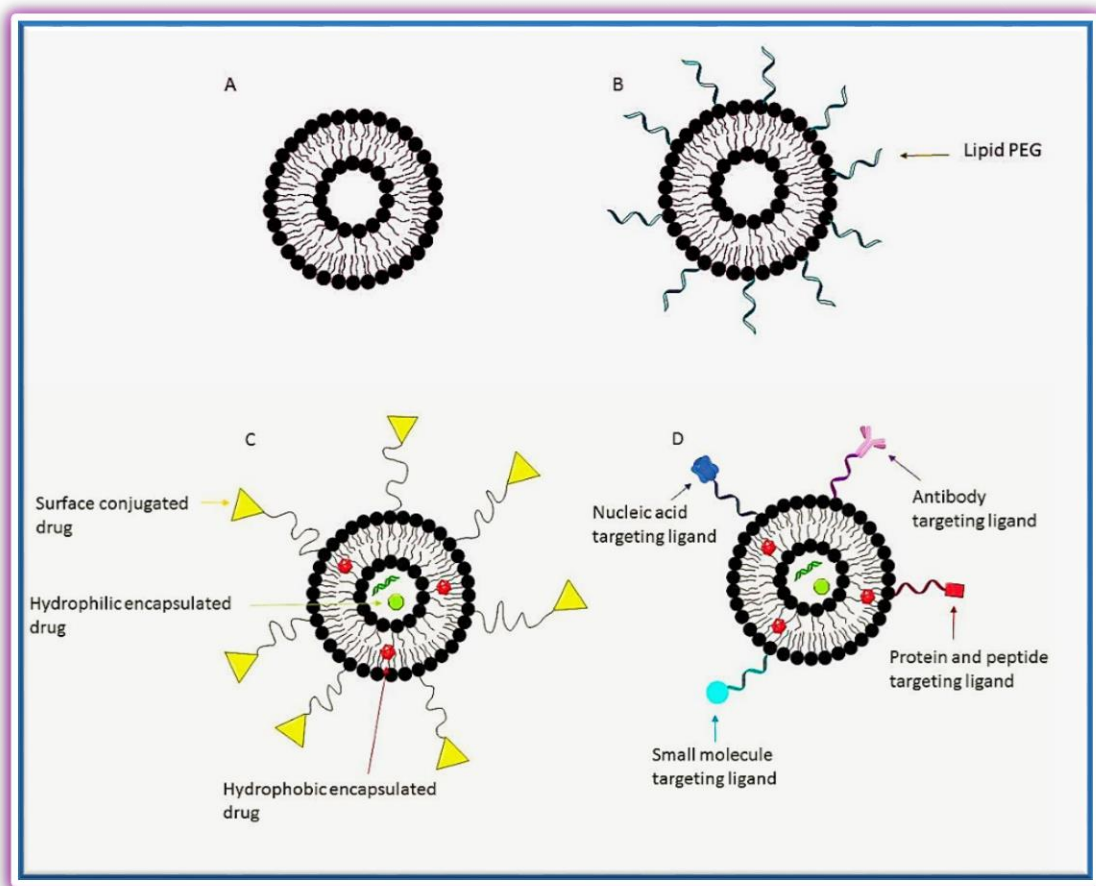


Figure A.1. Liposomes as carriers in drug delivery systems. They can be used to encapsulate one or several hydrophobic and hydrophilic therapeutic agents [15]. A) Conventional liposomes (The first generation of liposomes). B) Stealth liposomes (PEG grafted liposomes) - PEG conjugated lipids impede the liposome clearance by RES and enhance circulation time in bloodstream, increasing concentration at the tumor site. (C) Some drugs can be conjugated directly to the surface of the liposome. (D) Targeted liposomes - a ligand (proteins, antibodies, small molecule, etc.) is coupled to the surface of the liposome to increase selectivity toward tumors and reduces its off-target toxicity.

In 1986 Matsumura and Maeda suggested that the liposome facilitated tumor drug delivery is largely mediated through the enhanced permeability and retention (EPR) effect [16], [17] as solid tumors are made of vascular fenestrate that helps liposomes to

penetrate through tumor tissue [18]. It is becoming clear that the tumor vascular endothelial linings are usually more permeable than the vascular endothelial linings in healthy tissues. EPR relies on the permeability of tumor vasculature to sequester nanoparticles and therapeutic agents within its interstitial space. EPR also depends on tumor cell deficient lymphatic drainage to allow drugs to remain in the interstitial fluid compartment after being released from their carrier [19]. EPR is not effective for metastatic tumors or the ones with larger size. *In vivo* studies have revealed that these type of tumors suffer from low accumulation of pharmaceutical macromolecules, due to being hypovascular in the central area and consequently having less vascular leakage which results in a poor EPR effect and low drug accumulation within tumor tissue [17], [20], [21].

Tumor properties are not the only factors that determine EPR effect success. Liposome and pharmaceutical agent features are determining factors as well. Only liposomes with sizes as large as 200nm can penetrate tumor endothelia and are commonly used as drug delivery vehicles. These liposomes are being excluded from healthy tissues since they are limited to species smaller than 2nm [22]. Furthermore, circulation time of these liposomes needs to be long enough for the liposome to reach an effective concentration within the tumor interstitial space, and then accumulate in tumor tissue through EPR effect [23]. Therefore, optimization of tumor targeting and clearance mechanism is considered the next pressing step toward improved NP-based drug delivery systems [24]. In addition, pharmaceutical agent size influences EPR effect as very low molecular weight drugs diffuse back into blood stream and do not retain in the tumor interstitial fluid [19], [23].

Doxil[®], the first US Food and Drug Administration (FDA) approved liposome, encapsulates Doxorubicin. It received FDA approval in 1995 for treating refractory ovarian cancer and Kaposi sarcoma in AIDS. Since Doxil[®] approval, the scope of research into liposome facilitated drug delivery has widened. To date, twelve FDA

approved liposomes are available on the market (Table 1) and many more are in different phases of clinical trials.

Table A.1. FDA approved liposomal and lipid based formulations [7], [10], [12], [25], [26].

Platform	Drug	Indication	Marketed by	Year approved
Doxil	Doxorubicin	Refractory ovarian cancer and Kaposi sarcoma in AIDS	Alza Corporation	1995
DaunoXome	Daunorubicin	Kaposi sarcoma in AIDS	Gilead Sciences	1996
Marqibo	Vincristine	Acute lymphoblastic leukemia	Talen	2012
Ambisome	Amphotericin B	Serious fungal infections	Gilead Sciences	1990 (Europe), 1997 (USA), 2000
Myocet	Doxorubicin	Metastatic breast cancer	Elan Corporation	2000

Table A.1. FDA approved liposomal and lipid based formulations (continued)

Lipo-dox	Doxorubicin	Kaposi's sarcoma, ovarian and breast cancer	Taiwan- Liposome	2001 (Taiwan)
Estrasorb	Estrogen	Menopausal therapy	King	2003
Visudyne	Verteporfin	Age-related molecular degeneration	QLT	2000 (USA), 2003 (Japan)
Depocyt	Cytarabine	Neoplastic meningitis and lymphomatous meningitis	Pacira	1999
DepoDur	Morphine sulfate	Pain	Pacira	2004
Abelect	Amphotericin B	Serious fungal infections	Elan Corporation	1995
Amphotec	Amphotericin B	Serious fungal infections	Alza Corporation	1996

A.2. Liposome properties

Liposomes are made from cholesterol and non-toxic phospholipids. Their properties greatly depend on their size, surface charge, surface hydration and their lipid bilayer. Liposomes size ranges from 30 nm to several micrometers and this size variation influences circulation times and RES uptake rates. Liposomes of well-defined size are prepared by extrusion of lipids through filters containing pores having the desired size. However, liposomes that are made this way are about 20-50 % larger than the pore size [27]. Medium size liposomes ($150\text{nm} < d < 200\text{nm}$) have the highest circulation time. Liposomes with size greater than 300nm or smaller than 70nm commonly accumulate in liver and spleen [28] and cleared out from the blood circulation. Liposomes may compose of one (uni-lamellar) or multiple (multi-lamellar) lipid bilayers surrounding an aqueous layer. Polar and hydrophilic head groups are oriented towards the aqueous phase while the hydrophobic nonpolar tail groups are oriented away from water [29].

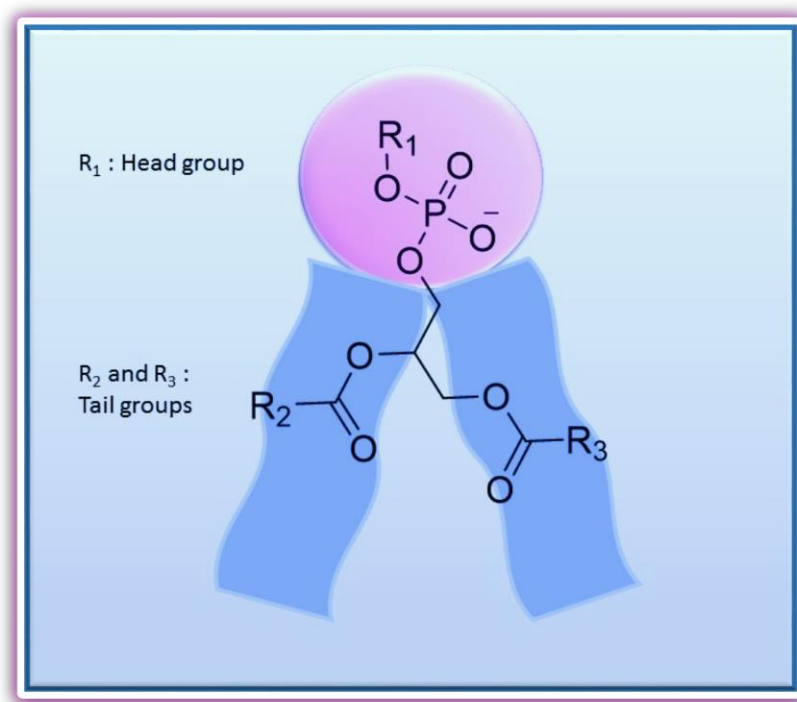


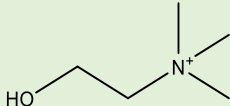
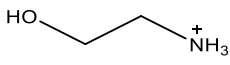
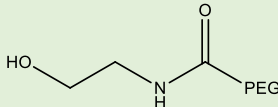
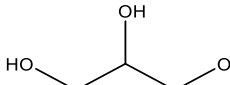
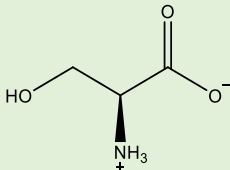
Figure A.2. General structure of phospholipid constituent of liposomes with the head and fatty acid tail groups [12].

Tail group (R_2 , R_3) of liposome (Figure A.2) is a fatty acid chain with a carbon length between C14 and C18. When R_2 and R_3 are saturated chains, rigidity is higher and fluidity is lower. When the fatty acid chain is unsaturated the bilayer is less stable and more permeable. Furthermore, longer chains lead to a thicker bilayer. The saturation status and length of fatty acid chains affect the degree of liposome membrane leakiness and the lipid phase transition temperature.

(R_1) represents the head group. The identity of the head group has a direct impact on surface hydration. Some head groups like Choline and ethanolamine are positively charged and make the overall charge of liposome neutral, while others such as serine, PEG amide of ethanolamine, and glycerol are neutral and thus result in a negatively charged liposome (Table A.2). A charge free liposome with ethanolamine as its head

group has a minimal degree of surface hydration whereas a negatively charged liposome with PEG (ethanolamine) as the head group has an enhanced surface hydration [12].

Table A.2. Different head groups and their effect on the liposome overall charge.

Compound	Structure	Liposome charge overall
Choline		Neutral
Ethanolamine		Neutral
PEG amide of ethanolamine		Negative
Glycerol		Negative
Serine		Negative

A.2.1. Liposome surface charge and hydration

Liposomes' lipid head groups and surface charge have a significant influence on liposome cell binding and endocytosis. Head group charge determines in large part liposome stability and bio-distribution. Due to the negative charge of DNA backbone, cationic or neutral liposomes are used for intracellular DNA delivery, while anionic liposomes are used for transporting other macromolecules to other targets [30]. Liposome surface charge is one of the most important factors which dictate how liposome will interact with cells and how fast it will be cleared by macrophages or cells of the reticuloendothelial system (RES). Neutral liposomes have a high tendency to aggregate and the least tendency to be cleared out by RES. In negatively charged liposomes, aggregation is reduced and they are more stable in suspensions. However, the negative charge can be recognized by receptors on the surface of many cells including macrophages [31], resulting in faster endocytosis and up take by RES and MPS [12]. The rapid clearance of negative liposomes limits their use compared to neutral liposomes. Positively charged liposomes are up taken faster than negatively charged or neutral liposomes. Their interaction with serum proteins increases endocytotic uptake and clearance by the lung, liver and spleen. The positively charged liposomes faster clearance results in a low *in vivo* transfection efficiency [12]. In general, the interaction of specific opsonizing proteins with phospholipid head groups is a major factor in liposome clearance. Both positively and negatively charged phospholipid head groups enhance opsonization. One common solution to preventing opsonization, consequently reducing liposome clearance rate, is to use poly ethylene glycol (PEG). The flexible polymeric chains of PEG form a shield that can mask the liposome's surface charge. An aqueous layer forms around the surface of liposome once PEG is installed onto its surface. Formation of this aqueous layer prevents liposome recognition by opsonins, resulting in longer circulation time and evading rapid uptake by RES [32]. PEG grafted liposomes are called "stealth" liposomes [23].

Additionally, in order to reduce aggregation and cellular uptake of liposomes by macrophages, the surface of the liposomes can be modified using hydrophilic polymers such as PEG to increase liposome thermodynamic stability. PEG addition to the surface of liposome prevents its recognition by macrophages and extends its blood circulation time [33]. This process is called surface hydration or steric modification [12], [34].

A.2.2. Fluidity of lipid bilayer

The fluidity of liposome membrane plays an important role in liposome mobility and morphology [35]. A liposome membrane can exist in both fluid and gel phases, which vary below and above T_c , the lipid phase transition temperature, where a liposome has maximum leakiness and both phases exist. Below T_c liposome is in gel phase and above T_c , it is in fluid phase. The lower membrane fluidity corresponds to a highly ordered structure [12]. The composition, length of phospholipid and the amount of cholesterol used in liposome formation has a direct impact on T_c and consequently liposome penetration [36]. Cholesterol content is a very vital factor in effectively delivering therapeutic agents to the site of a tumor [37]. Higher cholesterol content in the liposome formulation results in a lower drug encapsulation efficacy due to its possible effect on disruption of membrane linear structure [38].

A.2.3. Liposome bio-distribution in vivo

Liposome bio-distribution *in vivo* highly depends on lipid bilayer size, composition, charge, surface hydration and degree of saturation. For instance, liposomes with saturated fatty acyl chains have an improved bio-distribution compared to ones that contain unsaturated chains. The phase transition state of phospholipids is also another important factor. Liposomes with phospholipids of different transition phase such as PG and DSPC are retained less in the body and eliminated faster due to leakage and phase separation [39]. Additionally, PEG coated liposomes gain a longer circulation time and improved bio-distribution by introducing steric hindrance to the phagocyte system [40].

Liposomes can be injected via three routes: subcutaneous (sc), intravenous (iv) or intraperitoneal (ip). Each route results in a different bio-distribution pattern [37], thereby having a great influence on the delivery of an encapsulated drug to the site of a tumor. Liposome injection via a subcutaneous route results in a higher level of drug in the bloodstream. In such injections, smaller liposomes have the highest concentration and remain in the body 12 to 24 hours post injection, whereas larger liposomes do not circulate well and remain at the site of injection [41]. Intravenous and intraperitoneal injections of liposomes result in a lower half-life compared to subcutaneous injections [42].

Liposome's surface hydration and charge as well as size have direct impacts on bio-distribution, pathway and rate of cellular uptake [43] by affecting liposome's interaction with cells and thus its penetration through tumor tissue [44], [45]. For Liposome to maintain long circulation time in the body its size has to fit within a certain range. Liposomes smaller or larger than this size range are removed rapidly from blood stream. Positively and negatively charged liposomes are recognized and uptaken by RES faster compared to the charge free liposomes. Installing PEG on the surface of liposome prevents opsonization and liposome uptake by macrophages. To obtain a liposome that is optimal for drug delivery these factors have to be considered and be optimum. A neutral stealth liposome with a size range of 70-150 nm is one of the ideal candidates for drug delivery system.

A.3. Liposomes enhance delivery via triggered release

In spite of their versatility as drug delivery vehicles, liposomes suffer from key limitations. In particular, the rate of drug release once the liposomes are internalized in the tumor endosomal compartment can be slow. Also, liposomes internalized by tumor cells through endocytosis are eventually transferred to the lysosome, where the encapsulated drugs may be degraded if they are unable to escape the harsh lysosomal

environment. [46]. Various triggers mechanisms, which facilitate drug release, have been incorporated into liposome design. Therefore, applicable strategies should be developed to release the drug at the site of a tumor prior to degradation. The commonly used triggers for liposome cargo release rely on pH [47], [48], [49], light [50], [51], heat or temperature difference [52], [53], [54], specific enzymes, ultrasound, or magnetic field [55]. These triggers induce changes in the carrier assembly which leads to destabilization and release of the encapsulated drug. The logic behind the triggered release is not only to control the place and time the drug is released but also to decrease the injected dose and minimize side effects.

A.3.1. Acid triggered release

Acid triggered release was first suggested by Yatvin *et al.* in 1980 [48]. Since then extensive studies have been done on pH-sensitive liposomes [56], [57]. They are designed to introduce macromolecules or hydrophilic molecules to the cytoplasm of tumor cells and are generally made from phosphatidylethanolamine (PE) or its derivatives and a compound with an acidic group such as a carboxylic acid moiety which plays a stabilizing role at neutral pH [58]. Several acid sensitive liposomes contain dioleoylphosphatidylethanolamine (DOPE) in combination with Cholesteryl hemisuccinate (CHEMS) because of the fusogenic potential of these lipids, making them stable at physiological pH [59], [60], [61]. DOPE by itself does not form a liposome, but it can be stabilized and used to make liposomes by mixing with other PEG-coated lipids [46]. CHEMS gets protonated under acidic conditions and it loses its ability to stabilize the charged bilayer. The ensuing electrostatic repulsion causes liposome destabilization [62]. DOPE and CHEMS or a combination in the formulation of pH-sensitive liposomes have been used for encapsulating several anticancer and antibacterial agents such as doxorubicin, staurosporin, methotrexate, and gentamicin [60]. Acid triggered release liposomes are also grafted with a low molar ratio PEG to extend circulation time as

discussed earlier. Liposomes shielded with PEG-lipids have reduced sensitivity to acidic conditions and slower cargo release compared to conventional liposomes. Acid sensitive liposomes are stable at physiological pH (pH= 7.4), but undergo quick destabilization and degradation upon entering the acidic condition in the late endosomal environment ($5 < \text{pH} < 6.3$) [61], [63]. Once liposome is endocytosed by tumor cells, upon exposure to an acidic environment and cleavage of PEG lipids, it fuses the endosome membrane and releases the drug into the cytoplasm of the tumor cells [61]. It must be noted that the encapsulated drug has to be released from its carrier once it is in the late endosomal environment, and before liposome entrance to the harsh acidic environment of lysosome which degrades both carrier and cargo [64].

A.3.2. Light triggered release

Light activation is another approach for triggering the release of liposome cargoes that has been extensively studied. Light-dependent techniques that have been used to elicit cargo include photoisomerization, photocrosslinking, photosensitization-induced oxidation, surface plasmon absorption, and photothermal effects [65]. In photoisomerization, the part of the lipid components used to make the liposome has a double bond which changes configuration from trans to cis upon exposure to light [66]. Azobenzenes, moieties with a nitrogen-nitrogen double bond to which benzene rings are attached on each side, are the most commonly used compounds for photoisomerization. Once the compound is exposed to light, it changes its configuration from planar trans isomer to the less hydrophobic cis isomer which is less favorable for forming micelles [67]. Consequently, light radiation results in destabilization of the assembly and triggers release of the liposome encapsulated drug(s).

Photocrosslinking-mediated liposome cargo release was first introduced by Regen *et al.* [68]. Liposomes designed for photocrosslinking are made by doping the lipids with photocrosslinkable lipids such as 1, 2 bis-(tricoso-10, 12-dinoyl)-sn-glycero-3-

phosphocholine) (DC_{8,9}PC) or gelatin methacryloyl (GelMA) which have polymerizable triple and double bonds respectively [69], [70]. Photo irradiation of liposomes containing these polymerizable bonds results in polymers which disrupt the uniformity of the bilayer, creates pores, release the liposome encased drug(s).

Photosensitization-induced oxidation, which was first introduced by Anderson *et al.* in 1992 [71], utilizes lipids which are prone to photo-oxidation [72]. Photosensitization-induced oxidation occurs when oxidizing agents such as singlet oxygen are formed upon light exposure. These oxidizing agents cause damage to the liposome bio-membrane by oxidizing the plasmogenic lipids and inducing a transition from laminar to hexagonal phase which results in the leakage of cargo from the carrier [73]. Tissue is irradiated when the liposome is uptaken by tumor cells and has entered the endosome. Once the tissue is irradiated, the photosensitizer reagent contained in the liposome acts on the endosomal membrane, resulting in releasing the drug into the tumor cytosol.

Near infrared radiation (NIR) is the ideal light- triggered release mechanism since it can penetrate through blood and tissues up to 10 cm [74]. Upon irradiation with NIR light, liposomes convert the absorbed light into a thermal energy which increases the regional energy and temperature and leads to the cargo release [75]. However this method suffers from a lack of organic compounds which are capable of converting NIR light (700- 950nm) energy to a chemical response to trigger drug release. Gold nanoparticles are among the few agents that can absorb NIR light well, making them useful in photo-thermal therapy [76]. The first gold nanoparticle was introduced by Radt *et al.* [65] and since then extensive studies have been done on utilizing gold nanoparticles in surface plasmon absorption triggered release [75]. Wu *et al.* [77] showed that irradiating gold nanoshells can lead to almost complete release of an encapsulated drug.

A.3.3. Heat triggered release

Thermosensitive liposomes (TSL) respond to heat stimulus, such as IR lasers or microwave, to release the encapsulated drug. Most thermosensitive liposomes release their encapsulated drug at about 35-45 °C in a span of 30 minutes [78]. When TSLs are exposed to heat stimulation, their phase status changes from gel to liquid, making their bilayers become more permeable and releasing an encapsulated drug [79]. As mentioned earlier, melting temperature (T_m) depends on the character of the phospholipid used in forming the liposome [80]. However, for PEG grafted liposomes, the concentration of lipid-PEG applied on the liposome surface (in most cases 1, 2-distearoyl-sn-glycero-3-phosphoethanolamine-N-PEG2000 “DSPE2000”) matters as well since PEG can influence the permeability of the liposome bilayer [81]. Also, heat triggered release depends on tumor microvasculature features. Exposure to heat can influence tumor vessel leakiness and enhances tumor perfusion [82], leading to higher accumulation and concentration of liposome in the tumor endosome [83]. Cisplatin, doxorubicin, and methotrexate are some examples of anticancer drugs that have been encapsulated in heat sensitive liposomes [84], [85]. This method is generally combined with chemotherapy or radiation therapy to improve the treatment outcome. Improved survival rate has been noted in cohort of patients who undergo combination of chemotherapy and hyperthermia compared to the patients who receive only chemotherapy [86].

A.4. In-vivo liposomal drug delivery

Liposome mediated drug delivery *in vivo* occurs through two different targeting modes - passive and active targeting. Active targeting delivery development of liposomes is hindered by many barriers (discussed below) and hence is less advanced compared to passive targeting delivery [87]. In passive targeting, the liposome complex diffuses into leaky microvasculature such as tumors or inflamed tissues and shows selectivity toward any tissues with permeable endothelium cells. In active targeting, the liposome complex

incorporates a ligand that is specific for the epitope of a certain tissue or a distinct receptor that is overexpressed by cancer cells. Active targeting of liposomes has the potential to result in the delivery of elevated levels of drugs at disease sites with concomitant increase in drug efficacy [88].

A.4.1. Passive Targeting

Passive targeting of liposome is a means of delivery and transportation of the encapsulated drug into tumor cells through convection or passive diffusion. Convection is the movement of molecules within the fluid whereas diffusion is the transport of molecules across the membrane based on their concentration gradient (Figure A.3). Small molecules with low molecular weights mainly rely on diffusion for tissue distribution, while convection occurs when a large molecule is being transported through the large pores. [89]. However, since convection through the tumor interstitium is deficient, due to interstitial hypertension of tumors, diffusion is the main means for drug delivery in passive targeting. Following injection, liposome enters the tumor cytoplasm through the EPR effect. Maximum EPR effect is reached when a liposome has a longer circulation time in the body and it is not up-taken by RES organs quickly. To provide liposomes with longer blood circulation, they are often grafted with PEG to diminish their rapid clearance rate by RES.

Passive targeting relies on liposome size and tumor vasculature, and varies for different types of tumors based on their extravasation, angiogenesis, and vascularization. In solid tumors, passive targeting is not very efficient because of the interstitial fluid pressure. Tumor interstitial fluid pressure has a nonlinear correlation to its lymphatic drainage [90]. As the interstitial fluid pressure for a tumor gets higher, its lymphatic drainage decreases [91]. Tumor interstitial fluid pressure is a barrier in cancer therapy that results in inefficient therapeutic agents uptake [92].

Liposome size plays an important role in extraversion into tumor cells. As the liposome size gets larger, its clearance by RES or phagocyte systems (MPS) becomes more rapid. Liposomes of size below 400nm have enough circulation time in the bloodstream to extravasate into tumors, however, extraversion is more effective if liposomes have diameters lower than 200nm [23].

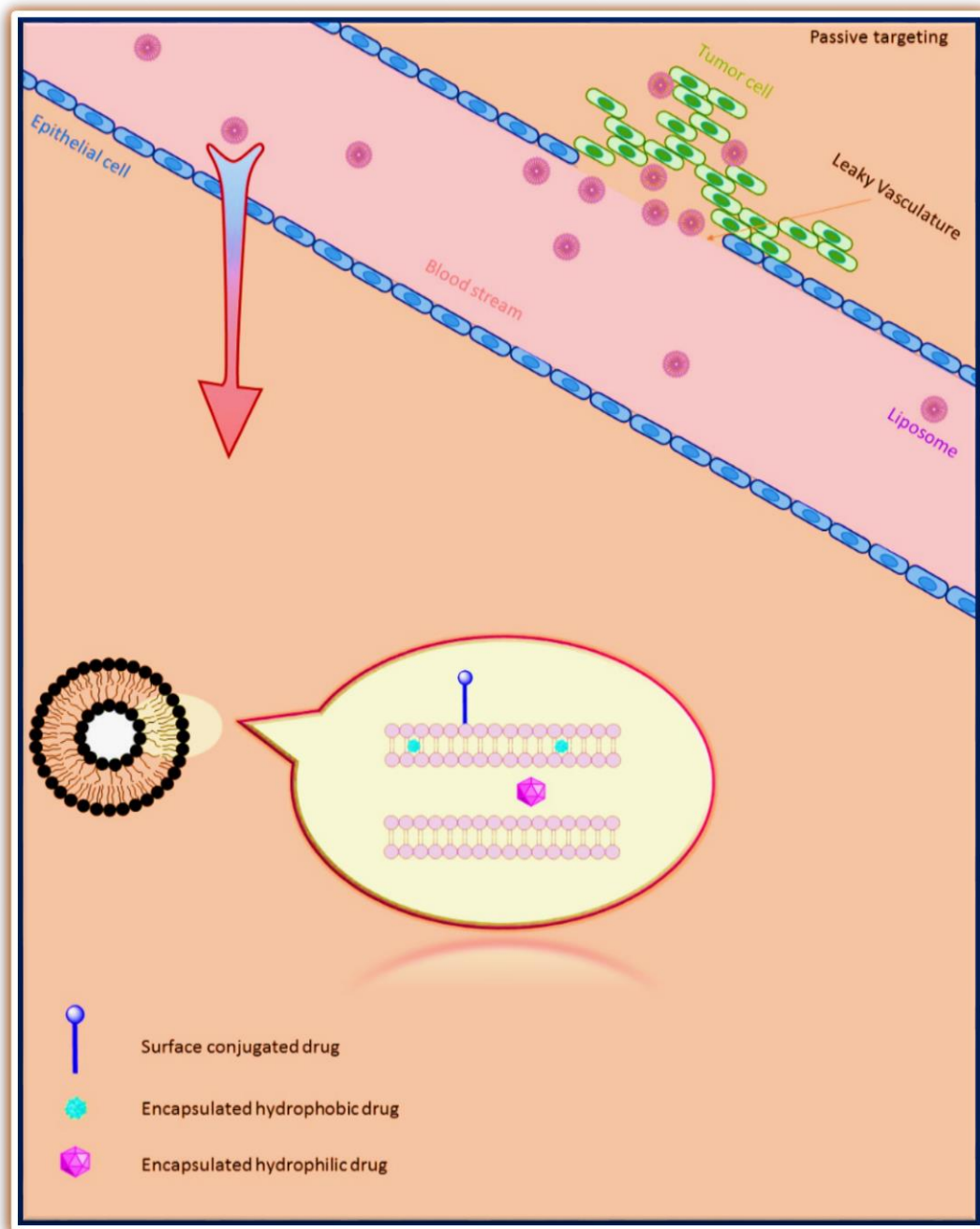


Figure A.3. Passive liposomal delivery. Liposomes reach the tumor site through diffusion and accumulate in tumor tissue via EPR effect.

Passive targeting through the EPR effect is applicable for targeting all tumor cells except prostate and pancreatic cancer cells [93], [94]. To date, there are many passive targeting liposomes that are FDA approved and there are many more currently in clinical trials. Liposomal encapsulated Doxorubicin, Vincristine, and cisplatin are examples of liposome formulated drugs in the market that function through passive targeting. The first two are conventional liposomes whereas the latter is categorized as a PEG grafted one. While conventional liposomes are uptaken rapidly by RES or macrophages in liver and spleen, PEGylated liposomes have longer half lives in the body, which in some cases can reach a couple of days [23].

A.4.2. Active Targeting/ Ligand Targeting Liposomes (LTL)

New strategies that may improve the tumor selective delivery of liposome encapsulated drugs are currently under active investigation. So far, ligand- targeting liposomes (LTL) have emerged as the most promising drug delivery tools [95], [96], [97]. In ligand targeting liposomes (LTLs) (Figure A.4), a ligand that selectively targets a specific receptor is coupled to the surface of the liposome. After EPR effect mediated selective accumulation within tumor interstitium, the attached ligand promotes tumor cell uptake of the [98]. Active targeting has been noted to enhance liposome delivery to diseased organs, tissues, or subcellular domains [99] and elevate therapeutic efficacy [100]. The ideal ligand is that for a receptor that is overexpressed by tumor cells relative to normal cells (Figure A.5) [101], [102]. The interaction between the ligand on liposome surface and the receptor overexpressed on cancer cells must be sufficiently strong and capable of receptor mediated endocytosis to enable efficient delivery of liposomes to the

site of a tumor and within the tumor cells. [103]. Receptors overexpressed on the tumor surface are more accessible, and therefore are better targets, compared to receptors overexpressed within the cancer cell nucleus or cytoplasm. For LTLs to reach the intracellular receptors, they have to be able to penetrate tumor cell membranes [104]. These non-selective targeted liposomes may enter the cytoplasm of healthy cells leading to unwanted side effects caused by damage to healthy cells along with cancer cells [105].

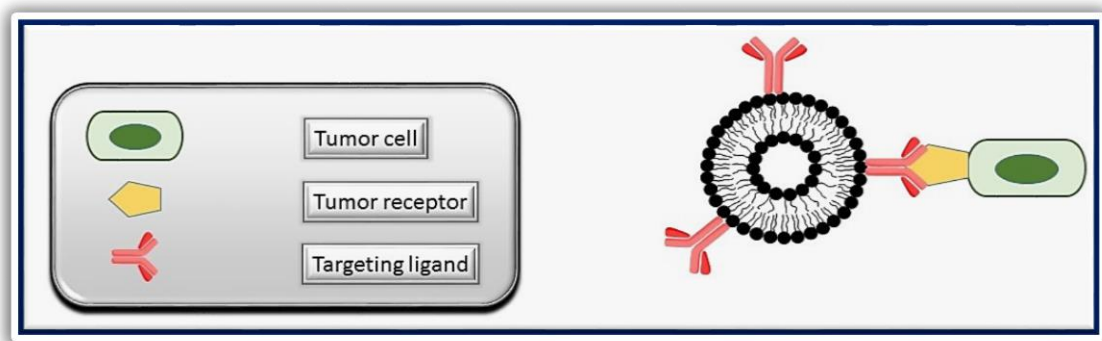


Figure A.4. Ligand targeted liposome. Liposome is conjugated to a targeting ligand that specifically interacts with a certain receptor which is overexpressed only by tumor cells.

Active targeting highly depends on the physicochemical properties of the ligand such as size, charge, orientation, and physical adsorption [106], [107]. The type of ligand, as well as its conjugation chemistry to the nanoparticle surface, has a great impact on the liposome's overall targeting efficacy. Nonspecific binding of the ligand to other proteins in the bloodstream is another important factor that should be taken into consideration [108], [109]. By far, covalent attachment is the most preferred approach for conjugating ligands on to the surface of liposomes.

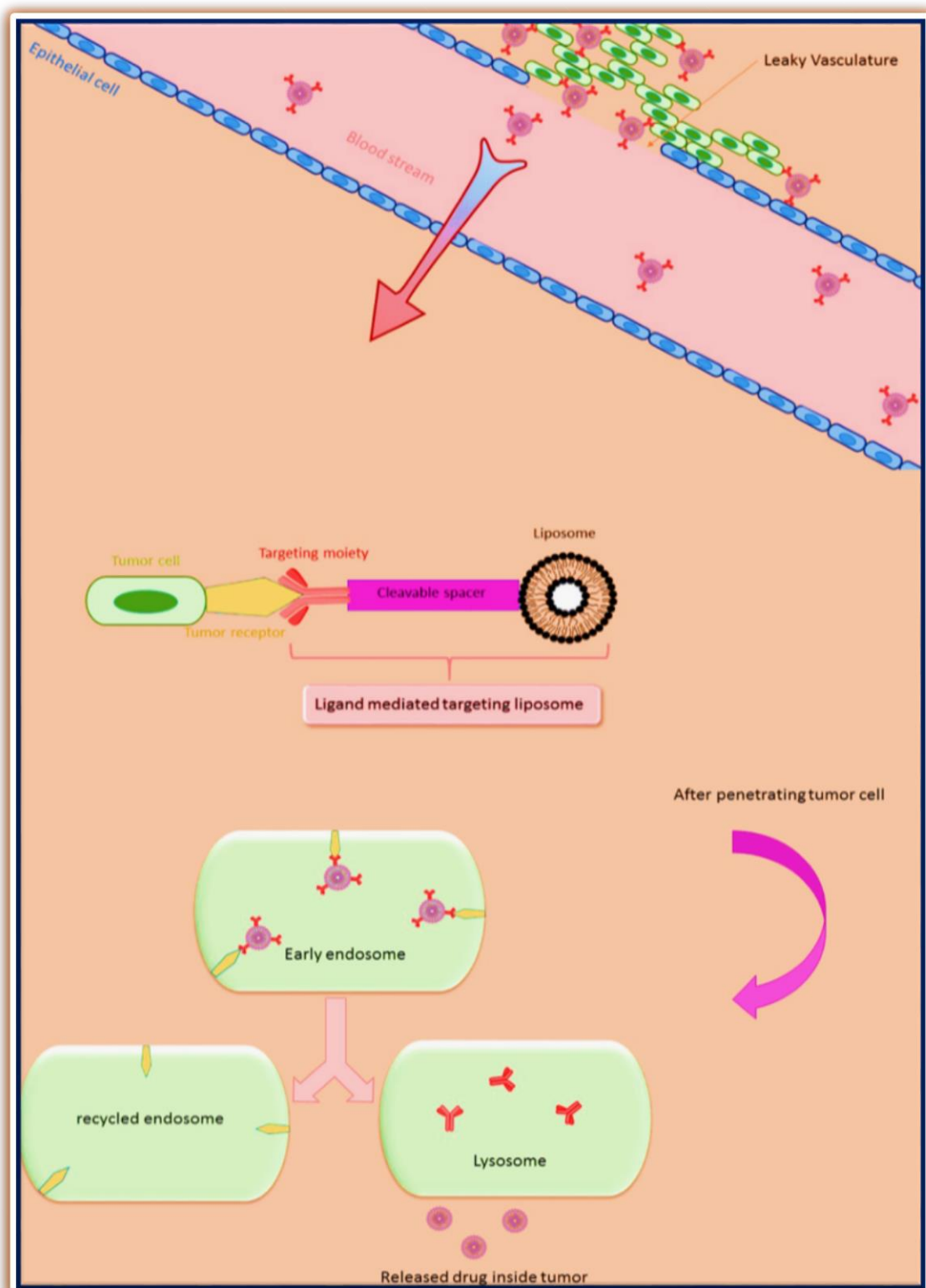


Figure A.5. Liposomal active targeting. A variety of targeting moieties can be coupled on the surface of liposome to enhance selective delivery to the site of tumor [110]. Ligand conjugated liposomes interact with the receptors overexpressed on the surface of tumor cells. In addition to increasing drug concentration at tumor site, this phenomena also decreases drug toxicity to healthy cells [111].

The targeting ligand can vary from proteins to a nucleic acids, peptides, small molecules, sugars or antibodies in order to target a sugar, protein, or nucleic acid existing in diseased tissues and organs [112], [113]. Using antibodies or antibody fragments as a targeting moiety is one of the more promising approaches to active targeting due to their high affinity and selectivity for target receptors. However, some studies revealed that using antibodies does not help tumor localization but instead helps with internalization in tumor tissue in animal models [103]. Peptides are another encouraging targeting ligand that are easy to prepare at low cost and can be modified to minimize potential enzyme degradation [22].

There are a few criteria that need to be considered in choosing the targeting ligand. Key among these criteria is target specificity. It is beneficial if the targeting ligand can recognize a receptor which is specific to tumor cells, to avoid targeting healthy cells that are expressing another isoform of targeted receptor [114]. The binding affinity between the targeting ligand and the tumor receptor is of importance as well. There is an inverse correlation between binding affinity and the concentration of liposome needed to reach tumor receptor binding saturation. When the targeting ligand has a high affinity to bind to the tumor receptor, a lower concentration of the liposome is needed [115]. Using ligands with a strong affinity for the tumor receptor reduces the liposome interaction with healthy cells and thus diminish its off-target toxicity. However, if a ligand with low affinity can be at higher concentration or a combination of various ligands can be used to compensate for not having a ligand with a strong affinity for tumor receptor [111], [116].

The size of the targeting ligand affects the overall size of liposome and hence influences the drug delivery via different mechanisms. When a liposome gets bigger it is cleared faster from the bloodstream by RES or MPS while smaller liposomes have a greater retention time. Additionally, smaller liposomes can extravasate better into the tumor interstitium. The ideal liposome size for tumor uptake is less than 200nm [117].

The point of ligand attachment impacts liposome drug delivery as well [107]. It is better to use functional groups such as amine, carboxylic acid, *etc.* that can be coupled to the liposome directly or indirect through as spacer group. However, it is possible that attaching the ligand to the liposome through these functional groups may compromise ligand's ability to interact with the tumor expressed receptor [111]. To forestall an attenuation of ligand-receptor interaction, regions of the ligand that will not hinder its affinity for tumor receptor should be identified prior to considering liposome conjugation.

Although active targeting is more efficient than free drug release in the blood circulation or even passive targeting, only a small fraction of the drug is uptaken by tumor cells. In active targeting, two factors are competing against each other: liposome clearance by RES and binding to the target site. One of the challenges in ligand-mediated liposomes is that for it to be recognized by the target tissue or cell, the liposome has to be in the locality of the target site [118]. To overcome this problem, the bloodstream circulation time must be extended [119]. As mentioned earlier, liposome uptake by RES can be avoided or delayed by using PEG grafted liposomes, elevating the drug concentration at the tumor site and consequently enhancing target binding of the liposome [120]. Presence of free PEG does not generally interfere with the liposome target binding.

Thus far, no targeted liposome has received FDA approval and there are few in clinical trials. Several reasons are responsible for this clinical failure. First, when liposomes are introduced in bloodstream they experience a rapid formation of a protein corona around them which hampers surface functionality. Protein corona was first

described by Dawson et.al in 2007 as involving an adsorption layer or atmosphere formed around nanoparticles by the proteins that are interacting with nanoparticles [121, 122]. Secondly, tumors grow quickly around endothelial barriers. When liposomes with targeting moieties get to the tumor site, they bind to the first receptor they see and may not even penetrate into the rest of tumor to bind other receptors [123]. Additionally, once inside tumor vasculature, there may be other barriers the liposomes have to cross. Finally, the existence of targeting moieties on the surface of the liposome can influence their uptake by RES, lowering circulation time in bloodstream. These drawbacks make targeted liposomal delivery essentially equal in efficiency to non-targeted delivery *in vivo* studies [124]. Despite their shortcomings, several clinical trials on targeted liposomes are currently underway. Doxorubicin and oxaliplatin liposomal formulations are examples of targeted liposomal delivery in clinical trials under the names MM302 (I) and MBP-426 (I), respectively. The former targets HER2 using an anti-ErbB2-scFv formulation for treating breast cancer [125] while the latter targets transferrin to treat gastroesophageal and esophageal adenocarcinoma [126].

Ligands for targeted liposomal drug delivery applications are divided into two groups of small molecule and macromolecule targeting ligands. Each group itself is further divided into subgroups. Small molecule targeting moieties are ligands with low molecular weight and smaller size. One example of small molecule targeting ligands is folic acid which shows affinity for folate receptor overexpressed on tumor cells. Unlike small molecule ligands, macromolecule targeting ligands such as proteins, antibodies and their fragments have larger size and higher molecular weight. In general, macromolecule targeting ligands have lower tumor cell permeability and are of limited applications compared to smaller sized ligands.

A.4.2.1. Small molecules as targeting ligands

Many anticancer drugs are known to be toxic toward healthy cells by restricting proliferation or inducing apoptosis. To minimize anticancer agent toxicities to healthy cells, several strategies have been developed to selectively target cancer cells through conjugation of anticancer agents to ligands selective for receptors overexpressed in tumors. The type of tumor targeting ligand has a significant impact on the efficiency of LTLs. Therefore, ligand selection should be done very carefully. Among natural and synthetic ligands, folic acid, ACUPA (*S,S*-2-[3-[5-amino-1-carboxypentyl]-ureido]-pentanedioic acid), and TPP (triphenylphosphonium) are common examples of small molecule ligands that have shown promise in liposomal active targeting [107]. Carbohydrates like mannose, glucose, and galactose and their derivatives are other small molecule targeting ligands that have been widely used [116].

A.4.2.1.1. Folic acid-drug conjugates

Folic acid (folate) (Figure A.6) has been widely used as a small molecule ligand to selectively target folic receptors (FR) [127]. FR are membrane proteins with molecular weight of 38-40 kDa, with two distinct isoforms (α and β) in humans [128], [129]. Isoform β has been found on CD34+ cells [130] and does not show affinity for folic acid or any folate derivatives. On the other hand, Isoform α is frequently overexpressed on the surface of broad range of human tumor cells, such as brain, ovarian, breast, and lung cancer.

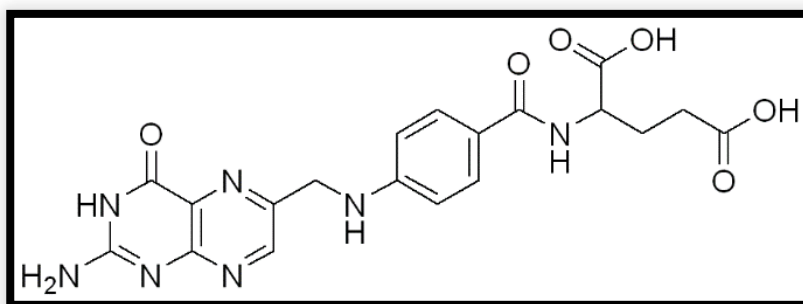


Figure A.6. Folic acid structure. High affinity for folate receptor is generally retained when folic acid is conjugated to folate receptor by the γ carboxylic acid [128].

Folic acid has several advantages that make it a better targeting moiety compared to many other targeting ligands. First, folic acid displays a high affinity ($K_D = \sim 10^{-9}$ M) and selectivity for tumor surface expressed FR. Second, folate is very stable and does not succumb to denaturation. Third, folate is readily available and its conjugation chemistry to the surface of liposome has been worked out. Furthermore, FR overexpression in some cancer cells exceeds 10^6 per cell. However, folate affinity can be compromised after conjugation to a drug molecule. The solution to this obstacle is to load more drug per folate carrier in order to compensate for its low affinity, or to replace the payload with much more potent drugs. Although conjugating more concentration of the same drug molecule to the targeting ligand seems appealing, it is simpler and more convenient to have one warhead that has a greater potency compared to installing many of the low potency drug on the same carrier. Additionally, in order for folate to be effective as a liposome tumor targeting ligand, it is coupled to the liposome surface via a PEG linker to overcome the steric hindrance at the interface of contact between the cell and the liposomes. Folate-conjugated liposomes designed in this way have shown a high affinity for tumors overexpressing FR [131].

Folate-conjugated liposome drug release after endocytosis and drug delivery capacity depends on environmental pH. Studies have shown folates are internalized into tumors with a low pH endosomal environment. Therefore, utilizing pH sensitive lipids in making the liposomes enhances folate conjugated liposome efficiency. One example of folate-targeted pH-sensitive liposomes is folate-LPDII, which is synthesized by mixing dioleoylphosphatidylethanolamine (DOPE)/cholesteryl hemisuccinate (CHEMS)/folate-PEG-DOPE (60:40:0.1, m/m) and the cationic DNA/polylysine (1:0.75, w/w) complexes. The first folate mediated targeted drugs that entered clinic, EC17, was designed to elevate

the immunogenicity of FR positive tumors (Figure A.6) [132]. And the first folate conjugated drug to be tested on humans was ^{111}In -DTPA-folate, a chelator of ^{111}In . ^{111}In -DTPA-folate binds to FR with 1 nM affinity [133] and mostly targets cancer cells but it is also found in kidney tissue [134]. Paclitaxel-liposome is another example of folate conjugated liposomes. Paclitaxel is an anticancer drug mainly used for treatment of breast and ovarian cancers. Paclitaxel and yttrium-90 conjugation with folic acid in liposomal active targeting has been shown to improve survival in a mouse xenograft model of ovarian cancer [135]. Additionally, recent studies have shown folic acid can be used to deliver imaging and therapeutic agents in both xenograft models as well as human cancer cells [136].

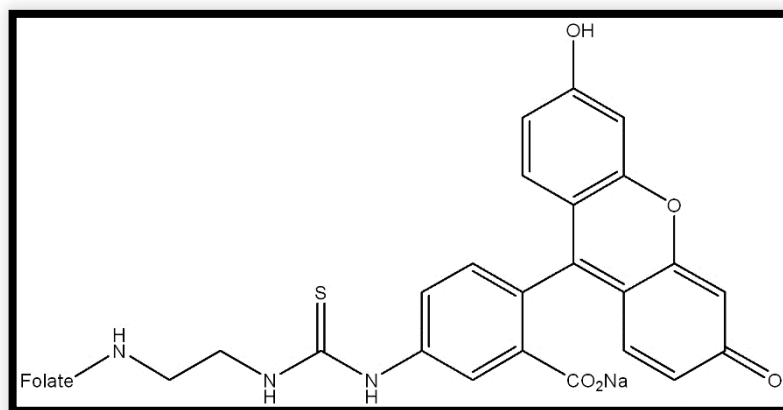


Figure A.7. Structure of EC17, the first folate ligand mediated targeting liposome in clinical trial.

Folate mediated cancer targeting does have its share of limitations. In addition to tumor cells, many healthy cells in different organs express FR on their surface. FR expression in normal cells mostly occurs in activated macrophages or monocytes, and tubules of the kidneys, lung, and thyroid [137], [138], [139]. This reduces folate

conjugated liposome selectivity toward cancer cells as well as increasing the chance of off-target toxicity. Activated macrophages often accumulate at the site of inflammation and have been most observed in inflammatory diseases such as, rheumatoid arthritis, osteoarthritis, and Crohn's disease or organ transplantation and infection [140]. Furthermore, FR overexpression varies for different patients and depends on the type of cancer. Although FR is overexpressed in about 40% of cancer patients, this overexpression varies widely from as low as 17% in case of testicular cancer to as high as 90% for breast, ovarian and uterus cancers [136].

A.4.2.1.2. TPP- drug conjugates

Many disorders in humans such as cancer, neurodegenerative diseases, Alzheimer disease, diabetes, or aging are characterized by mitochondria dysfunctions [141]. Some of the features associated with mitochondria diseases could be respiratory (respiratory failure, apnea), cardiac (heart failure), neurological or endocrinal [142]. The mitochondrion is an organelle located in the cytosol which functions to maintain energy producing oxidative metabolism as well as cellular mortality management. Unfortunately, there are currently no available treatments for mitochondrial related diseases other than treating symptoms. In recent years, targeting mitochondria has emerged as a promising approach to control many types of mitochondria related diseases. One of the obstacles in treating mitochondrial related diseases is to find a way to get the therapeutic drug inside the mitochondria of cells with a reasonable bio-distribution. This is hard to accomplish due to the controlled impermeability of the mitochondrial inner membrane. Clinical trials on several mitochondria-acting drugs failed due to the lack of an effective drug delivery approach to the mitochondria [143]. Many drugs will eventually reach mitochondrial vicinity through interaction with subcellular compartments but the main challenge to enter mitochondria still remains. Triphenylphosphonium (TPP) and its derivatives (Figure A.7) are examples of small molecule targeting ligand that are being used in liposomal

delivery for targeting mitochondria [144]. TPP is a hydrophobic molecule that can easily penetrate the cell membrane and accumulate inside cells. Studies have shown that the positive charge on TPP is responsible for its high accumulation within mitochondria, an attribute that is vital to its *in vitro* performance. However, TPP positive charge adversely affects *in vivo* blood exposure [144], [145]. One of the mitochondria targeting liposomes conjugated to TPP is stearyl TPP (STPP) bromide (Figure A.8). It is synthesized by ultrasonication after film rehydration [146]. STPP targeting liposomes have been widely used to deliver various therapeutic agents inside mitochondria. Recently, DOX and PTX were loaded inside STPP-derived targeting liposomes for delivery inside mitochondria [146]. Loading DOX inside a STPP-derived liposome enhanced its targeted delivery to the site of tumor. Additionally the liposome was further modified by adding folic acid on the surface, to increase its efficiency and potency by transforming it to a dual targeting motif. Similarly, utilizing ligand targeted liposome to deliver PTX to tumor tissue resulted in PTX greater bio-distribution and thus lower IC₅₀. To date, only a few liposomes are known to deliver mitochondrial-acting therapeutics, however none of them have been approved by FDA due to limited bioavailability and biocompatibility.

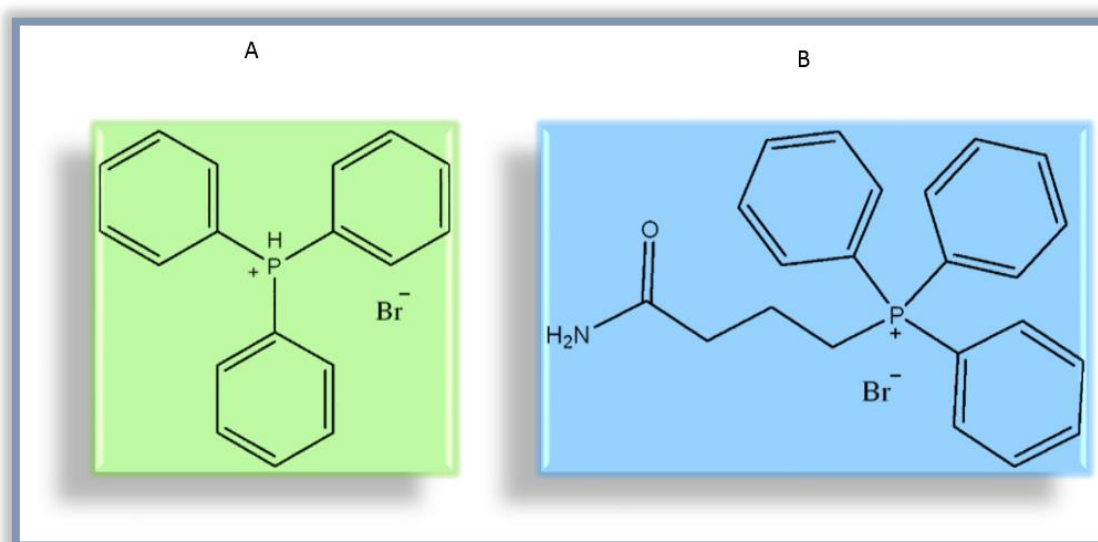


Figure A.8. A. Triphenylphosphonium (TPP) structure. Different groups can be added to the phosphonium ion to synthesize more potent targeting groups that have a higher affinity for entering mitochondria. B. Structure of stearyl TPP (STPP) bromide. STPP has been used widely as a small molecule targeting group in ligand-mediated liposomal delivery.

A.4.2.1.3. ACUPA- drug conjugates

Another very promising small molecule targeting ligands is S,S-2-[3-[5-amino-1-carboxypentyl]-ureido]-pentanedioic acid (ACUPA). ACUPA mediates molecular interaction between prostate specific membrane antigen (PSMA) and liposomes [6]. PSMA is overexpressed in prostate cancer cells as well as in non-prostate solid tumor neovasculature [147] and was first used as prostate cancer imaging agent [148]. One of the ACUPA mediated liposomes that has entered phase II clinical trial is ACUPA docetaxel-loaded PEG-PLGA, a pH sensitive liposome that effectively delivers the payload drug to the site of tumor [149]. Mice xerograph studies revealed that it enhances tumor accumulation and promotes prolonged growth suppression *in vivo* [6].

Furthermore, clinical studies in patients with advance solid tumor showed a lower dose tumor shrinkage compared to free docetaxel [150].

A.4.2.2. Macromolecules as targeting ligands

Utilizing macromolecule-derived targeting ligands, such as nucleic acid, peptides, proteins, and antibodies, in liposomal drug delivery has shown promising results in cancer therapy due largely to ligand related enhancements in efficacy, prolonged circulation time and targeted delivery to tumor sites. However, unlike small molecule ligand mediated targeting liposomes, macromolecule ligand use is limited by lower permeability through tumor vasculature due to the larger size [151]. Antibodies were the first macromolecule to be used as a targeting ligand and since then more macromolecules have been introduced [152]. This section focuses on a variety of macromolecules as targeting ligands and their properties such as size or molecular weight as well as their benefits and limitations in liposomal delivery systems.

A.4.2.2.1. Nucleic acid based- drug conjugates:

Nucleic acid aptamers are composed of oligonucleotides which fold by intramolecular interaction and form distinct three-dimensional conformations [153]. Nucleic acid aptamers have strong affinity and specificity for their substrate due to a distinctive structure that originated from Watson-Crick and non-Watson-Crick interactions. Because of their small size, ease of isolation and favorable immunogenicity profile, aptamer conjugated liposomes have emerged as promising drug delivery vehicles in targeted cancer therapy [154]. They are also being used in imaging and cell sorting applications. In addition to their strong affinity for cognate receptors, aptamers also benefit from ease and replicability of synthesis or chemical derivation. Additionally, aptamer conjugated liposomes have conformational flexibility and nuclease stability. Aptamer binding affinity depends on secondary and tertiary structures, which in turn

relies on target environment conditions such as pH and temperature. This can affect and reduce liposomal therapy efficiency *in vivo* experiments.

Nucleic acid aptamers are usually 75-100 nucleotides. This length provides an opportunity for vast variation in sequence, resulting in different conformations and different binding affinity. However, the negative charge associated with the phosphodiester backbone aptamers contributes to increase in liposome clearance rate by the spleen and kidney, thereby reducing circulation time in blood stream. The negative charge on liposomes also elevates non-specific interactions as well, leading to a reduction in substrate affinity. Additionally, long aptamers generate steric hindrance which leads to a barrier in conjugation to the liposome surface [155]. To overcome this obstacle, positively charged PEG linkers can be used to conjugate the aptamers to the liposome surface, this approach neutralizes both the liposome negative charge as well as decreases steric hindrance.

The first *in vitro* aptamer conjugated nanoparticle to target PSMA was reported in 2004. Following that research was conducted *in vivo*, which showed a reduction in tumor growth in comparison to non-targeted nanoparticles [154]. Despite the promising results of aptamer conjugated liposomes *in vitro*, they show limitations *in vivo*. Nucleic acids are easily degraded, which makes them unstable in biological environment. To overcome this problem and avoid ligand degradation on the surface of liposome, nucleic acids can be modified with fluoro, amine, or methoxy groups. Besides *in vivo* limitations, the high manufacturing cost of aptamers is one of the major reasons hampering their development.

A.4.2.2.2. Peptide- drug conjugates

Peptides, composed of up to 50 amino acids, have simpler three dimensional structures relative to proteins. Therefore, their conjugation to liposomal surfaces is easier. To increase drug efficacy by enhancing cellular uptake and maintaining liposomes within tumor tissue, many cell penetrating peptides have been designed and synthesized [100].

RGD (arginine–glycine–aspartic acid), which targets $\alpha\text{v}\beta 3$ integrin with a strong affinity, is the most commonly used peptide [156]. RGD with various linkers facilitating liposomal conjugation are commercially available. RGDs can be in both linear and cyclic forms, and studies have shown that cyclic RGD is more potent [157]. However, the use of RGD as a targeting ligand is being hampered by the fact that $\alpha\text{v}\beta 3$ integrin expression can be found on healthy cells in addition to tumor cells.

Another peptide targeting ligand that has been widely used for delivering anticancer drugs to the tumor site is NGR (asparagine-glycine-arginine). Like RGD, NGR has linear and cyclic forms, with the cyclic structure being more potent. NGR specifically binds to CD13/aminopeptidase N, which is overexpressed in tumor vasculature [158].

A.4.2.2.3. Protein- drug conjugates

Proteins have been widely used as targeting ligands due to their strong substrate binding and well defined three dimensional structures. Transferrin (Tf), a glycoprotein which binds to the transferrin receptor (Tf-R) with a high affinity and triggers endocytosis by taking advantage of clathrin-dependent pathway, is a commonly used targeting ligand. After internalization, Tf and TfR are recycled to the cellular surface through recycling pathway. Transferrin function is transportation and regulation of intracellular iron concentration. The transferrin receptor has been extensively used for drug targeting to tumors. Tf-R is overexpressed on cancer cells because of the need of iron for energy production, cell proliferation and heme synthesis [159]. Luckily, transferrin does not induce any immune response in patients [160], therefore using liposomes that are conjugated with Tf can be beneficial to deliver encapsulated drugs to the tumor site. Research has shown that transferrin can affect the efficacy of the encapsulated drug at cellular levels in addition to affecting targeting ability. In some studies, there was an increase in gene transfection and tumor size shrinkage [161]. MBP-

426 is a Tf conjugated liposome in clinical trials that encapsulates oxaliplatin. It is currently under investigation in phase II clinical trial for treating colorectal cancer.

In addition to naturally occurring proteins, there are variety of synthetic proteins such as affibodies and *ankyrin repeat proteins* which are being investigated for targeted delivery of anticancer therapeutic agents. Affibodies are polypeptide ligands of approximately 15kDa that are used for tissue-specific targeting and controlled release of encapsulated drugs in ligand conjugated nanoparticles. Their small size provides a high ratio of binding site to ligand size, which improves endocytosis by tumor cells. For instance, some affibodies selectively bind to extracellular domain of the human epidermal growth factor receptor 2 (HER-2) in tumors that overexpress HER-2 antigen [162], [163]. In addition to affibodies' selective targeting ability, their high stability in both *in vitro* and *in vivo* studies have made them a promising targeting ligand of choice in liposomal drug delivery [162].

Designed ankyrin repeat proteins (DARPin) are non-immunoglobulins binding proteins. The Ankyrin motif is composed of 33 amino acids which form a secondary structure consisting of 1 β turn and two antiparallel α -helices. Their small size, high stability, and high affinity against soluble or membrane bound antigens have made them excellent binders for tumor targeting. Winkler *et al* [164] designed DARPins that are specific for epithelial cell adhesion molecules (EpCAM) as a drug delivery vehicle for small interfering RNA (siRNA) complementary to the *bcl-2* mRNA. DARPin dimers were utilized as fusionproteins to deliver siRNA into cells. EpCAM is transmembrane glycoprotein responsible for cell proliferation, differentiation and signaling [165]. EpCAM is overexpressed in solid tumors, with a low expression in normal cells. Its overexpression is more common in breast, prostate, colon, and pancreas carcinomas. EpCAM is easily internalized by tumor cells and is suitable for the delivery of anticancer agents to tumor tissue [164].

Unfortunately, proteins suffer from several limitations. In some cases their size affects the efficiency of their installation on liposomal surfaces. The complexity of their amino acid residues makes conjugation chemistry difficult. Moreover, the chemistry used for protein conjugation to liposomal surfaces can significantly influence their secondary/tertiary structures which may affect antigen affinity.

A.4.2.2.4. Antibody- drug conjugates

Antibodies or immunoglobulin (Ig) are Y-shaped glycoproteins that [152] bind and interact with antigens through the binding site which is located at the tip of the antibody. The binding site, which is also called “hypervariable region (HVR)” or “F(ab')₂ fragment”, can have various structures in order to interact with different antigens. The antibody protein recognition part “Fc fragment” is located at the bottom of Y-shaped antibody (Figure A.9). It helps mononuclear phagocyte system and immune system to recognize proteins. [107]. The first evidence for their specific binding to tumor cells antigen was seen in 1975 [166].

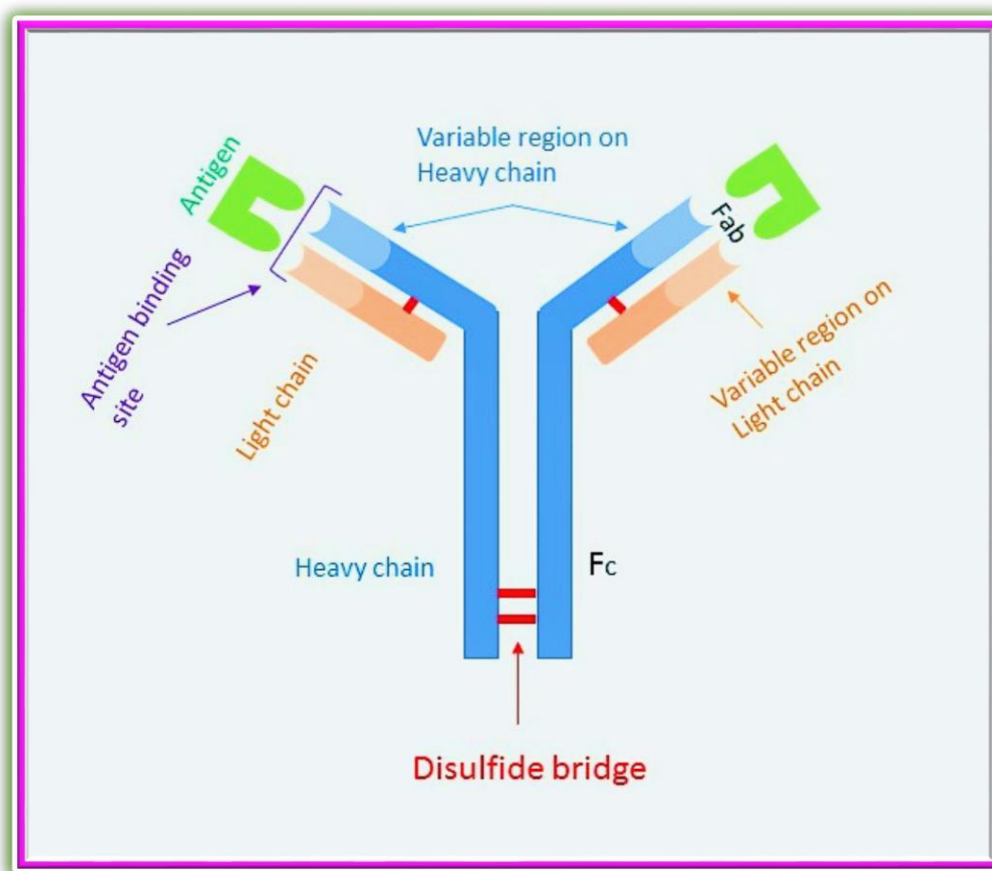


Figure A.9. Antibody Y-shaped structure. Protein recognition part (Fc) is located at the base, while antigen binding site (Fab) is positioned at the tip of antibody structure.

To date, several antibody targeted cancer treatment modalities have been approved by the US FDA [167]. Retoximab (Rituxan®) is anti-CD20 antibody being used for treating CD-20 positive B-cell non-Hodgkin's lymphoma. It was approved in 1997 and manufactured by IDEC pharmaceuticals. Ibritumomab tiuxetan (Zevalin®) is another anti-CD20 antibody manufactured by IDEC pharmaceuticals. It obtained FDA approval in 2002 and since then has been used for Rituximab-failed non-Hodgkins lymphoma [168]. Gemtuzumabozogamicin (Mylotarg®) is an anti-CD33 antibody manufactured by Wyeth Pharmaceuticals. It has been in the market since FDA approval

in 2000, for treating relapsed and refractory acute myelogenous leukemia [169]. These are only a few examples of antibody use for targeted cancer treatments. Studies have shown that using antibodies as targeting ligands is beneficial in delivery systems such as liposomes due to high affinity and selectivity for the target. Antibody conjugated liposomes can enhance the selective toxicity of therapeutic agents to cancer cells [170].

Unfortunately, even though antibody conjugated liposomes showed favorable results *in vitro*, their use in *in vivo* studies have been hampered by several limiting factors. Antibodies are very sensitive to environmental changes such as temperature, enzyme or salt concentration changes and are not stable in the presence of organic solvents. These factors, along with large size (150 kDa), make conjugation of antibodies to liposome surfaces complex. Furthermore, antibodies' large size increases the overall liposome size after conjugation and resulting antibody-conjugated liposomes have enhanced clearance rates by RES or MPS leading to low blood circulation time [171]. The main function of antibodies is to recognize antigens and induce clearance by MPS and the immune system. Decorating liposomes with antibodies inadvertently leads to faster clearance from the bloodstream, although, removal of Fc fragment slightly improves circulation time [172]. Newer coupling methods, where an antibody or its fragment is attached to the terminal end of a PEG linker and engrafted to the liposome surface, have been developed to minimize blood clearance [7], [131].

Despite all these limitations, several antibody conjugated liposomes have made their way to pre-clinical or clinical trials. For example, SGT-53 is a wildtype p53 sequence encapsulating cationic liposome with anti-transferrin receptor antibody. It is under investigation in phase II clinical trials for treating glioblastoma, solid tumors and pancreatic cancer. SGT-94 is another anti-transferrin receptor antibody liposome incorporating RB94 plasmid DNA. It is in phase I clinical trials for treating solid tumors [173]. MM-302 is an anti-Her-2 antibody conjugated liposome that encapsulates doxorubicin. It is in clinical trials for the treatment HER-2 positive breast cancer. Upon

administration, MM-302 binds to HER-2 overexpressing tumor cells and doxorubicin gets released upon endocytosis of the conjugated liposome into the tumor cell. The released doxorubicin then impedes topoisomerase II activity, inhibition of RNA synthesis and DNA replication; leading to retardation of tumor growth [174]. MCC-465 is another example of antibody conjugated liposome that encapsulates doxorubicin. It is in clinical trials for treating gastric cancer. It is conjugated to F(ab')₂ fragment of human monoclonal antibody GAH, which targets more than 90% of cancerous stomach tissue [175].

A.5. Future perspective and conclusion

With the FDA approval and success of several liposomes in recent years, liposomal drug delivery has become a promising targeted delivery system for cancer therapy. Liposomal drug delivery occurs through passive and active targeting. Active targeting can revolutionize cancer therapy and increase patient's life quality and survival by delivering anticancer drugs specifically to tumor sites, consequently diminishing cytotoxicity and minimizing side effects. However, despite all the research and efforts dedicated in active targeting liposomes studies, progress in the clinic has been so slow. Although active targeting liposomes enhance drug efficiency and efficacy by improving delivery to the target site as well as increasing tissue distribution and cellular uptake by tumor cells, their use in *in vivo* studies has been hampered by low penetration through tumor tissues and their quick recognition by the immune and reticuloendothelial systems due to formation of protein corona around liposome surface.

Additionally, some of the targeting ligands are not stable and soluble in organic solvents, a situation which makes their scale up synthesis very difficult.

Therefore, there is an unmet need to improve the design and stability of active targeting liposomes as therapeutic delivery systems. Factors such as liposome size, charge, PEG coating, and ligand size, charge, length and density cause formation and composition of

protein corona [176]. These factors should be optimized to obtain ligand targeted liposomes with higher potency and efficacy for cancer therapy.

A.6. References

1. Siegel, R. L.; Miller, K. D.; Jemal, A. Cancer statistics, 2016. *CA: a cancer journal for clinicians* **2016**, 66, 7-30.
2. Harding, M. C.; Sloan, C. D.; Merrill, R. M.; Harding, T. M.; Thacker, B. J.; Thacker, E. L. Abstract MP67: Transition From Cardiovascular Disease to Cancer as the Leading Cause of Death in US States, 1999-2013. *Circulation* **2016**, 133, AMP67-AMP67.
3. Pérez-Herrero, E.; Fernández-Medarde, A. Advanced targeted therapies in cancer: Drug nanocarriers, the future of chemotherapy. *European Journal of Pharmaceutics and Biopharmaceutics* **2015**, 93, 52-79.
4. Bertrand, N.; Leroux, J.-C. The journey of a drug-carrier in the body: an anatomo-physiological perspective. *Journal of Controlled Release* **2012**, 161, 152-163.
5. Jain, R. K.; Stylianopoulos, T. Delivering nanomedicine to solid tumors. *Nature reviews Clinical oncology* **2010**, 7, 653-664.
6. Hrkach, J.; Von Hoff, D.; Ali, M. M.; Andrianova, E.; Auer, J.; Campbell, T.; De Witt, D.; Figa, M.; Figueiredo, M.; Horhota, A. Preclinical development and clinical translation of a PSMA-targeted docetaxel nanoparticle with a differentiated pharmacological profile. *Science translational medicine* **2012**, 4, 128ra39-128ra39.
7. Allen, T. M.; Cullis, P. R. Liposomal drug delivery systems: from concept to clinical applications. *Advanced drug delivery reviews* **2013**, 65, 36-48.
8. Patil, Y. P.; Jadhav, S. Novel methods for liposome preparation. *Chemistry and physics of lipids* **2014**, 177, 8-18.
9. Chang, H.-I.; Yeh, M.-K. Clinical development of liposome-based drugs: formulation, characterization, and therapeutic efficacy. *International journal of nanomedicine* **2012**, 7, 49.
10. Pattni, B. S.; Chupin, V. V.; Torchilin, V. P. New Developments in Liposomal Drug Delivery. *Chemical reviews* **2015**.
11. Alexis, F.; Pridgen, E.; Molnar, L. K.; Farokhzad, O. C. Factors affecting the clearance and biodistribution of polymeric nanoparticles. *Molecular pharmaceutics* **2008**, 5, 505-515.

12. Lian, T.; Ho, R. J. Trends and developments in liposome drug delivery systems. *Journal of pharmaceutical sciences* **2001**, 90, 667-680.
13. Hamann, P. R.; Hinman, L. M.; Hollander, I.; Beyer, C. F.; Lindh, D.; Holcomb, R.; Hallett, W.; Tsou, H.-R.; Upeslakis, J.; Shochat, D. Gemtuzumab ozogamicin, a potent and selective anti-CD33 antibody-calicheamicin conjugate for treatment of acute myeloid leukemia. *Bioconjugate chemistry* **2002**, 13, 47-58.
14. Marcucci, F.; Lefoulon, F. Active targeting with particulate drug carriers in tumor therapy: fundamentals and recent progress. *Drug discovery today* **2004**, 9, 219-228.
15. Çağdaş, M.; Sezer, A. D.; Bucak, S. Liposomes as Potential Drug Carrier Systems for Drug Delivery. In INTECH: 2014.
16. Matsumura, Y.; Maeda, H. A new concept for macromolecular therapeutics in cancer chemotherapy: mechanism of tumoritropic accumulation of proteins and the antitumor agent smancs. *Cancer research* **1986**, 46, 6387-6392.
17. Fang, J.; Nakamura, H.; Maeda, H. The EPR effect: unique features of tumor blood vessels for drug delivery, factors involved, and limitations and augmentation of the effect. *Advanced drug delivery reviews* **2011**, 63, 136-151.
18. Gabizon, A.; Goren, D.; Horowitz, A. T.; Tzemach, D.; Lossos, A.; Siegal, T. Long-circulating liposomes for drug delivery in cancer therapy: a review of biodistribution studies in tumor-bearing animals. *Advanced Drug Delivery Reviews* **1997**, 24, 337-344.
19. Torchilin, V. Tumor delivery of macromolecular drugs based on the EPR effect. *Advanced drug delivery reviews* **2011**, 63, 131-135.
20. Nagamitsu, A.; Greish, K.; Maeda, H. Elevating blood pressure as a strategy to increase tumor-targeted delivery of macromolecular drug SMANCS: cases of advanced solid tumors. *Japanese journal of clinical oncology* **2009**, 39, 756-766.
21. Chattopadhyay, N.; Fonge, H.; Cai, Z.; Scollard, D.; Lechtman, E.; Done, S. J.; Pignol, J.-P.; Reilly, R. M. Role of antibody-mediated tumor targeting and route of administration in nanoparticle tumor accumulation in vivo. *Molecular pharmaceutics* **2012**, 9, 2168-2179.
22. Noble, G. T.; Stefanick, J. F.; Ashley, J. D.; Kiziltepe, T.; Bilgicer, B. Ligand-targeted liposome design: challenges and fundamental considerations. *Trends in biotechnology* **2014**, 32, 32-45.
23. Maruyama, K. Intracellular targeting delivery of liposomal drugs to solid tumors based on EPR effects. *Advanced drug delivery reviews* **2011**, 63, 161-169.

24. Owens, D. E.; Peppas, N. A. Opsonization, biodistribution, and pharmacokinetics of polymeric nanoparticles. *International journal of pharmaceutics* **2006**, 307, 93-102.
25. Fan, Y.; Zhang, Q. Development of liposomal formulations: from concept to clinical investigations. *Asian Journal of Pharmaceutical Sciences* **2013**, 8, 81-87.
26. Dawidczyk, C. M.; Kim, C.; Park, J. H.; Russell, L. M.; Lee, K. H.; Pomper, M. G.; Searson, P. C. State-of-the-art in design rules for drug delivery platforms: lessons learned from FDA-approved nanomedicines. *Journal of Controlled Release* **2014**, 187, 133-144.
27. Drummond, D. C.; Meyer, O.; Hong, K.; Kirpotin, D. B.; Papahadjopoulos, D. Optimizing liposomes for delivery of chemotherapeutic agents to solid tumors. *Pharmacological reviews* **1999**, 51, 691-744.
28. Litzinger, D. C.; Buiting, A. M.; van Rooijen, N.; Huang, L. Effect of liposome size on the circulation time and intraorgan distribution of amphipathic poly (ethylene glycol)-containing liposomes. *Biochimica et Biophysica Acta (BBA)-Biomembranes* **1994**, 1190, 99-107.
29. Akbarzadeh, A.; Rezaei-Sadabady, R.; Davaran, S.; Joo, S. W.; Zarghami, N.; Hanifehpour, Y.; Samiei, M.; Kouhi, M.; Nejati-Koshki, K. Liposome: classification, preparation, and applications. *Nanoscale Res Lett* **2013**, 8, 102.
30. Cuomo, F.; Mosca, M.; Murgia, S.; Ceglie, A.; Lopez, F. Oligonucleotides and polynucleotides condensation onto liposome surface: effects of the base and of the nucleotide length. *Colloids and Surfaces B: Biointerfaces* **2013**, 104, 239-244.
31. Miller, C. R.; Bondurant, B.; McLean, S. D.; McGovern, K. A.; O'Brien, D. F. Liposome-cell interactions in vitro: effect of liposome surface charge on the binding and endocytosis of conventional and sterically stabilized liposomes. *Biochemistry* **1998**, 37, 12875-12883.
32. Levchenko, T. S.; Rammohan, R.; Lukyanov, A. N.; Whiteman, K. R.; Torchilin, V. P. Liposome clearance in mice: the effect of a separate and combined presence of surface charge and polymer coating. *International journal of pharmaceutics* **2002**, 240, 95-102.
33. Lasic, D.; Martin, F.; Gabizon, A.; Huang, S.; Papahadjopoulos, D. Sterically stabilized liposomes: a hypothesis on the molecular origin of the extended circulation times. *Biochimica et Biophysica Acta (BBA)-Biomembranes* **1991**, 1070, 187-192.
34. Tirosh, O.; Barenholz, Y.; Katzhendler, J.; Priev, A. Hydration of polyethylene glycol-grafted liposomes. *Biophysical journal* **1998**, 74, 1371-1379.

35. Tan, C.; Zhang, Y.; Abbas, S.; Feng, B.; Zhang, X.; Xia, W.; Xia, S. Biopolymer–Lipid Bilayer Interaction Modulates the Physical Properties of Liposomes: Mechanism and Structure. *Journal of agricultural and food chemistry* **2015**, 63, 7277-7285.
36. Sinico, C.; Manconi, M.; Peppi, M.; Lai, F.; Valenti, D.; Fadda, A. M. Liposomes as carriers for dermal delivery of tretinoin: in vitro evaluation of drug permeation and vesicle–skin interaction. *Journal of Controlled Release* **2005**, 103, 123-136.
37. Coderch, L.; Fonollosa, J.; De Pera, M.; Estelrich, J.; De La Maza, A.; Parra, J. Influence of cholesterol on liposome fluidity by EPR: relationship with percutaneous absorption. *Journal of Controlled Release* **2000**, 68, 85-95.
38. Alam, M. I.; Paget, T.; Elkordy, A. A. Formulation and advantages of furazolidone in liposomal drug delivery systems. *European Journal of Pharmaceutical Sciences* **2016**.
39. Gabizon, A.; Price, D. C.; Huberty, J.; Bresalier, R. S.; Papahadjopoulos, D. Effect of liposome composition and other factors on the targeting of liposomes to experimental tumors: biodistribution and imaging studies. *Cancer research* **1990**, 50, 6371-6378.
40. Lee, C.-M.; Choi, Y.; Huh, E. J.; Lee, K. Y.; Song, H.-C.; Sun, M. J.; Jeong, H.-J.; Cho, C.-S.; Bom, H.-S. Polyethylene glycol (PEG) modified 99mTc-HMPAoliposome for improving blood circulation and biodistribution: the effect of the extent of PEGylation. *Cancer biotherapy & radiopharmaceuticals* **2005**, 20, 620-628.
41. Oussoren, C.; Zuidema, J.; Crommelin, D.; Storm, G. Lymphatic uptake and biodistribution of liposomes after subcutaneous injection.: II. Influence of liposomal size, lipid composition and lipid dose. *Biochimica et Biophysica Acta (BBA)-Biomembranes* **1997**, 1328, 261-272.
42. Allen, T.; Hansen, C.; Guo, L. Subcutaneous administration of liposomes: a comparison with the intravenous and intraperitoneal routes of injection. *Biochimica et Biophysica Acta (BBA)-Biomembranes* **1993**, 1150, 9-16.
43. Lu, F.; Wu, S. H.; Hung, Y.; Mou, C. Y. Size effect on cell uptake in well-suspended, uniform mesoporous silica nanoparticles. *Small* **2009**, 5, 1408-1413.
44. Lee, K. D.; Nir, S.; Papahadjopoulos, D. Quantitative analysis of liposome-cell interactions in vitro: rate constants of binding and endocytosis with suspension and adherent J774 cells and human monocytes. *Biochemistry* **1993**, 32, 889-899.
45. He, C.; Hu, Y.; Yin, L.; Tang, C.; Yin, C. Effects of particle size and surface charge on cellular uptake and biodistribution of polymeric nanoparticles. *Biomaterials* **2010**, 31, 3657-3666.

46. Andresen, T. L.; Jensen, S. S.; Jørgensen, K. Advanced strategies in liposomal cancer therapy: problems and prospects of active and tumor specific drug release. *Progress in lipid research* **2005**, 44, 68-97.
47. Ishida, T.; Kirchmeier, M.; Moase, E.; Zalipsky, S.; Allen, T. Targeted delivery and triggered release of liposomal doxorubicin enhances cytotoxicity against human B lymphoma cells. *Biochimica et Biophysica Acta (BBA)-Biomembranes* **2001**, 1515, 144-158.
48. Connor, J.; Yatvin, M. B.; Huang, L. pH-sensitive liposomes: acid-induced liposome fusion. *Proceedings of the National Academy of Sciences* **1984**, 81, 1715-1718.
49. Drummond, D. C.; Zignani, M.; Leroux, J.-C. Current status of pH-sensitive liposomes in drug delivery. *Progress in Lipid Research* **2000**, 39, 409-460.
50. Luo, D., et al., Doxorubicin encapsulated in stealth liposomes conferred with light-triggered drug release. *Biomaterials* **2016**, 75, 193-202.
51. Morgan, C.; Yianni, Y.; Sandhu, S.; Mitchell, A. Liposome fusion and lipid exchange on ultraviolet irradiation of liposomes containing a photochromic phospholipid. *Photochemistry and photobiology* **1995**, 62, 24-29.
52. Yatvin, M. B.; Weinstein, J. N.; Dennis, W. H.; Blumenthal, R. Design of liposomes for enhanced local release of drugs by hyperthermia. *Science* **1978**, 202, 1290-1293.
53. Needham, D.; Dewhirst, M. W. The development and testing of a new temperature-sensitive drug delivery system for the treatment of solid tumors. *Advanced drug delivery reviews* **2001**, 53, 285-305.
54. Gaber, M. H.; Hong, K.; Huang, S. K.; Papahadjopoulos, D. Thermosensitive sterically stabilized liposomes: formulation and in vitro studies on mechanism of doxorubicin release by bovine serum and human plasma. *Pharmaceutical research* **1995**, 12, 1407-1416.
55. Lamparski, H.; Liman, U.; Barry, J. A.; Frankel, D. A.; Ramaswami, V.; Brown, M. F.; O'Brien, D. F. Photoinduced destabilization of liposomes. *Biochemistry* **1992**, 31, 685-694.
56. Kirpotin, D.; Hong, K.; Mullah, N.; Papahadjopoulos, D.; Zalipsky, S. Liposomes with detachable polymer coating: destabilization and fusion of dioleoylphosphatidylethanolamine vesicles triggered by cleavage of surface-grafted poly (ethylene glycol). *Febs Letters* **1996**, 388, 115-118.
57. Saito, G.; Swanson, J. A.; Lee, K.-D. Drug delivery strategy utilizing conjugation via reversible disulfide linkages: role and site of cellular reducing activities. *Advanced drug delivery reviews* **2003**, 55, 199-215.

58. Duzgunes, N.; Straubinger, R.; Baldwin, P.; Papahadjopoulos, D.; Wilschut, J.; Hoekstra, D. pH-sensitive liposomes: introduction of foreign substances into cells. *Marcel Dekker, New York* **1991**, 713-730.
59. Cullis, P. t.; Kruijff, B. d. Lipid polymorphism and the functional roles of lipids in biological membranes. *Biochimica et Biophysica Acta (BBA)-Reviews on Biomembranes* **1979**, 559, 399-420.
60. Simões, S.; Moreira, J. N.; Fonseca, C.; Düzgüneş, N.; de Lima, M. C. P. On the formulation of pH-sensitive liposomes with long circulation times. *Advanced drug delivery reviews* **2004**, 56, 947-965.
61. Sudimack, J. J.; Guo, W.; Tjarks, W.; Lee, R. J. A novel pH-sensitive liposome formulation containing oleyl alcohol. *Biochimica et Biophysica Acta (BBA)-Biomembranes* **2002**, 1564, 31-37.
62. Subbarao, N. K.; Parente, R. A.; Szoka Jr, F. C.; Nadasdi, L.; Pongracz, K. The pH-dependent bilayer destabilization by an amphipathic peptide. *Biochemistry* **1987**, 26, 2964-2972.
63. Legendre, J.-Y.; Szoka Jr, F. C. Delivery of plasmid DNA into mammalian cell lines using pH-sensitive liposomes: comparison with cationic liposomes. *Pharmaceutical research* **1992**, 9, 1235-1242.
64. Ohkuma, S.; Poole, B. Fluorescence probe measurement of the intralysosomal pH in living cells and the perturbation of pH by various agents. *Proceedings of the National Academy of Sciences* **1978**, 75, 3327-3331.
65. Fomina, N.; Sankaranarayanan, J.; Almutairi, A. Photochemical mechanisms of light-triggered release from nanocarriers. *Advanced drug delivery reviews* **2012**, 64, 1005-1020.
66. Bisby, R. H.; Mead, C.; Morgan, C. G. Active uptake of drugs into photosensitive liposomes and rapid release on UV photolysis. *Photochemistry and photobiology* **2000**, 72, 57-61.
67. Kano, K.; Tanaka, Y.; Ogawa, T.; Shimomura, M.; Okahata, Y.; Kunitake, T. Photoresponsive membranes. Regulation of membrane properties by photoreversible cis-trans isomerization of azobenzenes. *Chemistry Letters* **1980**, 421-424.
68. Regen, S. L.; Singh, A.; Oehme, G.; Singh, M. Polymerized phosphatidyl choline vesicles. Stabilized and controllable time-release carriers. *Biochemical and biophysical research communications* **1981**, 101, 131-136.
69. Yavlovich, A.; Singh, A.; Blumenthal, R.; Puri, A. A novel class of photo-triggerable liposomes containing DPPC: DC 8, 9 PC as vehicles for delivery of doxorubicin to cells. *Biochimica et Biophysica Acta (BBA)-Biomembranes* **2011**, 1808, 117-126.

70. Kadri, R.; Messaoud, G. B.; Tamayol, A.; Aliakbarian, B.; Zhang, H.; Hasan, M.; Sánchez-González, L.; Arab-Tehrany, E. Preparation and characterization of nanofunctionalized alginate/methacrylated gelatin hybrid hydrogels. *RSC Advances* **2016**, 6, 27879-27884.
71. Anderson, V. C.; Thompson, D. H. Triggered release of hydrophilic agents from plasmalogen liposomes using visible light or acid. *Biochimica et Biophysica Acta (BBA)-Biomembranes* **1992**, 1109, 33-42.
72. Thompson, D. H.; Gerasimov, O. V.; Wheeler, J. J.; Rui, Y.; Anderson, V. C. Triggerable plasmalogen liposomes: improvement of system efficiency. *Biochimica et Biophysica Acta (BBA)-Biomembranes* **1996**, 1279, 25-34.
73. Girotti, A. W. Photodynamic lipid peroxidation in biological systems. *Photochemistry and Photobiology* **1990**, 51, 497-509.
74. Weissleder, R. A clearer vision for in vivo imaging. *Nature biotechnology* **2001**, 19, 316-317.
75. Prevo, B. G.; Esakoff, S. A.; Mikhailovsky, A.; Zasadzinski, J. A. Scalable Routes to Gold Nanoshells with Tunable Sizes and Response to Near-Infrared Pulsed-Laser Irradiation. *Small* **2008**, 4, 1183-1195.
76. Pashkovskaya, A.; Kotova, E.; Zorlu, Y.; Dumoulin, F.; Ahsen, V.; Agapov, I.; Antonenko, Y. Light-triggered liposomal release: membrane permeabilization by photodynamic action. *Langmuir* **2009**, 26, 5726-5733.
77. Wu, G.; Mikhailovsky, A.; Khant, H. A.; Fu, C.; Chiu, W.; Zasadzinski, J. A. Remotely triggered liposome release by near-infrared light absorption via hollow gold nanoshells. *Journal of the American Chemical Society* **2008**, 130, 8175-8177.
78. Dromi, S.; Frenkel, V.; Luk, A.; Traugher, B.; Angstadt, M.; Bur, M.; Poff, J.; Xie, J.; Libutti, S. K.; Li, K. C. Pulsed-high intensity focused ultrasound and low temperature-sensitive liposomes for enhanced targeted drug delivery and antitumor effect. *Clinical Cancer Research* **2007**, 13, 2722-2727.
79. Anyarambhatla, G. R.; Needham, D. Enhancement of the phase transition permeability of DPPC liposomes by incorporation of MPPC: a new temperature-sensitive liposome for use with mild hyperthermia. *Journal of Liposome Research* **1999**, 9, 491-506.
80. Li, L.; ten Hagen, T. L.; Schipper, D.; Wijnberg, T. M.; van Rhooen, G. C.; Eggermont, A. M.; Lindner, L. H.; Koning, G. A. Triggered content release from optimized stealth thermosensitive liposomes using mild hyperthermia. *Journal of Controlled Release* **2010**, 143, 274-279.

81. Nicholas, A. R.; Scott, M. J.; Kennedy, N. I.; Jones, M. N. Effect of grafted polyethylene glycol (PEG) on the size, encapsulation efficiency and permeability of vesicles. *Biochimica et Biophysica Acta (BBA)-Biomembranes* **2000**, 1463, 167-178.
82. Koning, G. A.; Eggermont, A. M.; Lindner, L. H.; ten Hagen, T. L. Hyperthermia and thermosensitive liposomes for improved delivery of chemotherapeutic drugs to solid tumors. *Pharmaceutical research* **2010**, 27, 1750-1754.
83. Gaber, M. H.; Wu, N. Z.; Hong, K.; Huang, S. K.; Dewhirst, M. W.; Papahadjopoulos, D. Thermosensitive liposomes: extravasation and release of contents in tumor microvascular networks. *International Journal of Radiation Oncology* Biology* Physics* **1996**, 36, 1177-1187.
84. Kong, G.; Anyarambhatla, G.; Petros, W. P.; Braun, R. D.; Colvin, O. M.; Needham, D.; Dewhirst, M. W. Efficacy of liposomes and hyperthermia in a human tumor xenograft model: importance of triggered drug release. *Cancer research* **2000**, 60, 6950-6957.
85. Weinstein, J. N.; Magin, R. L.; Cysyk, R. L.; Zaharko, D. S. Treatment of solid L1210 murine tumors with local hyperthermia and temperature-sensitive liposomes containing methotrexate. *Cancer research* **1980**, 40, 1388-1395.
86. Issels, R.; Lindner, L.; Wendtner, C.; Hohenberger, P.; Reichardt, P.; Daugaard, S.; Mansmann, U.; Hiddemann, W.; Blay, J.; Verweij, J. ILBA Impact of regional hyperthermia (RHT) on response to neo-adjuvant chemotherapy and survival of patients with high-risk soft-tissue sarcoma (HR-STS): Results of the randomized EORTC-ESHO intergroup trial (NCI-00003052). *European Journal of Cancer Supplements* **2009**, 7, 2.
87. Barenholz, Y. Liposome application: problems and prospects. *Current opinion in colloid & interface science* **2001**, 6, 66-77.
88. Malam, Y.; Loizidou, M.; Seifalian, A. M. Liposomes and nanoparticles: nanosized vehicles for drug delivery in cancer. *Trends in pharmacological sciences* **2009**, 30, 592-599.
89. Danhier, F.; Feron, O.; Préat, V. To exploit the tumor microenvironment: passive and active tumor targeting of nanocarriers for anti-cancer drug delivery. *Journal of Controlled Release* **2010**, 148, 135-146.
90. Rofstad, E. K.; Galappathi, K.; Mathiesen, B. S. Tumor interstitial fluid pressure—a link between tumor hypoxia, microvascular density, and lymph node metastasis. *Neoplasia* **2014**, 16, 586-594.
91. Lammers, T.; Hennink, W.; Storm, G. Tumour-targeted nanomedicines: principles and practice. *British journal of cancer* **2008**, 99, 392-397.

92. Heldin, C.-H.; Rubin, K.; Pietras, K.; Östman, A. High interstitial fluid pressure—an obstacle in cancer therapy. *Nature Reviews Cancer* **2004**, 4, 806-813.
93. Maeda, H.; Sawa, T.; Konno, T. Mechanism of tumor-targeted delivery of macromolecular drugs, including the EPR effect in solid tumor and clinical overview of the prototype polymeric drug SMANCS. *Journal of controlled release* **2001**, 74, 47-61.
94. Jain, R. K. Transport of molecules in the tumor interstitium: a review. *Cancer research* **1987**, 47, 3039-3051.
95. Béduneau, A.; Saulnier, P.; Benoit, J.-P. Active targeting of brain tumors using nanocarriers. *Biomaterials* **2007**, 28, 4947-4967.
96. Weinstein, J. N.; Blumenthal, R.; Sharrow, S. O.; Henkart, P. A. Antibody-mediated targeting of liposomes. Binding to lymphocytes does not ensure incorporation of vesicle contents into the cells. *Biochimica et Biophysica Acta (BBA)-Biomembranes* **1978**, 509, 272-288.
97. Chauhan, V. P.; Stylianopoulos, T.; Boucher, Y.; Jain, R. K. Delivery of molecular and nanoscale medicine to tumors: transport barriers and strategies. *Annual review of chemical and biomolecular engineering* **2011**, 2, 281-298.
98. Byrne, J. D.; Betancourt, T.; Brannon-Peppas, L. Active targeting schemes for nanoparticle systems in cancer therapeutics. *Advanced drug delivery reviews* **2008**, 60, 1615-1626.
99. Cheng, Z.; Al Zaki, A.; Hui, J. Z.; Muzykantov, V. R.; Tsourkas, A. Multifunctional nanoparticles: cost versus benefit of adding targeting and imaging capabilities. *Science* **2012**, 338, 903-910.
100. Kamaly, N.; Xiao, Z.; Valencia, P. M.; Radovic-Moreno, A. F.; Farokhzad, O. C. Targeted polymeric therapeutic nanoparticles: design, development and clinical translation. *Chemical Society Reviews* **2012**, 41, 2971-3010.
101. Peer, D.; Karp, J. M.; Hong, S.; Farokhzad, O. C.; Margalit, R.; Langer, R. Nanocarriers as an emerging platform for cancer therapy. *Nature nanotechnology* **2007**, 2, 751-760.
102. Shi, J.; Xiao, Z.; Kamaly, N.; Farokhzad, O. C. Self-assembled targeted nanoparticles: evolution of technologies and bench to bedside translation. *Accounts of chemical research* **2011**, 44, 1123-1134.
103. Kirpotin, D. B.; Drummond, D. C.; Shao, Y.; Shalaby, M. R.; Hong, K.; Nielsen, U. B.; Marks, J. D.; Benz, C. C.; Park, J. W. Antibody targeting of long-circulating lipidic nanoparticles does not increase tumor localization but does increase internalization in animal models. *Cancer research* **2006**, 66, 6732-6740.

104. Jeong, Y.; Xie, Y.; Xiao, G.; Behrens, C.; Girard, L.; Wistuba, I. I.; Minna, J. D.; Mangelsdorf, D. J. Nuclear receptor expression defines a set of prognostic biomarkers for lung cancer. *PLoS Med* **2010**, 7, e1000378.
105. Holbeck, S.; Chang, J.; Best, A. M.; Bookout, A. L.; Mangelsdorf, D. J.; Martinez, E. D. Expression profiling of nuclear receptors in the NCI60 cancer cell panel reveals receptor-drug and receptor-gene interactions. *Molecular endocrinology* **2010**, 24, 1287-1296.
106. Duncan, R.; Vicent, M.; Greco, F.; Nicholson, R. Polymer–drug conjugates: towards a novel approach for the treatment of endocrine-related cancer. *Endocrine-related cancer* **2005**, 12, S189-S199.
107. Bertrand, N.; Wu, J.; Xu, X.; Kamaly, N.; Farokhzad, O. C. Cancer nanotechnology: the impact of passive and active targeting in the era of modern cancer biology. *Advanced drug delivery reviews* **2014**, 66, 2-25.
108. Monopoli, M. P.; Åberg, C.; Salvati, A.; Dawson, K. A. Biomolecular coronas provide the biological identity of nanosized materials. *Nature nanotechnology* **2012**, 7, 779-786.
109. Jiang, W.; Kim, B. Y.; Rutka, J. T.; Chan, W. C. Nanoparticle-mediated cellular response is size-dependent. *Nature nanotechnology* **2008**, 3, 145-150.
110. Koshkaryev, A.; Sawant, R.; Deshpande, M.; Torchilin, V. Immunoconjugates and long circulating systems: origins, current state of the art and future directions. *Advanced drug delivery reviews* **2013**, 65, 24-35.
111. Srinivasarao, M.; Galliford, C. V.; Low, P. S. Principles in the design of ligand-targeted cancer therapeutics and imaging agents. *Nature Reviews Drug Discovery* **2015**, 14, 203-219.
112. Yu, B.; Tai, H. C.; Xue, W.; Lee, L. J.; Lee, R. J. Receptor-targeted nanocarriers for therapeutic delivery to cancer. *Molecular membrane biology* **2010**, 27, 286-298.
113. Saha, R. N.; Vasanthakumar, S.; Bende, G.; Snehathatha, M. Nanoparticulate drug delivery systems for cancer chemotherapy. *Molecular Membrane Biology* **2010**, 27, 215-231.
114. Reubi, J. C.; Schonbrunn, A. Illuminating somatostatin analog action at neuroendocrine tumor receptors. *Trends in pharmacological sciences* **2013**, 34, 676-688.
115. Kularatne, S. A.; Wang, K.; Santhapuram, H.-K. R.; Low, P. S. Prostate-specific membrane antigen targeted imaging and therapy of prostate cancer using a PSMA inhibitor as a homing ligand. *Molecular pharmaceutics* **2009**, 6, 780-789.

116. Lepenies, B.; Lee, J.; Sonkaria, S. Targeting C-type lectin receptors with multivalent carbohydrate ligands. *Advanced drug delivery reviews* **2013**, 65, 1271-1281.
117. Yuan, F.; Dellian, M.; Fukumura, D.; Leunig, M.; Berk, D. A.; Torchilin, V. P.; Jain, R. K. Vascular permeability in a human tumor xenograft: molecular size dependence and cutoff size. *Cancer research* **1995**, 55, 3752-3756.
118. Florence, A. T. "Targeting" nanoparticles: the constraints of physical laws and physical barriers. *Journal of controlled release* **2012**, 164, 115-124.
119. Pirollo, K. F.; Chang, E. H. Does a targeting ligand influence nanoparticle tumor localization or uptake? *Trends in biotechnology* **2008**, 26, 552-558.
120. Maruyama, K.; Ishida, O.; Takizawa, T.; Moribe, K. Possibility of active targeting to tumor tissues with liposomes. *Advanced drug delivery reviews* **1999**, 40, 89-102.
121. Tenzer, S.; Docter, D.; Kuharev, J.; Musyanovych, A.; Fetz, V.; Hecht, R.; Schlenk, F.; Fischer, D.; Kiouptsi, K.; Reinhardt, C. Rapid formation of plasma protein corona critically affects nanoparticle pathophysiology. *Nature nanotechnology* **2013**, 8, 772-781.
122. Caracciolo, G. Liposome–protein corona in a physiological environment: Challenges and opportunities for targeted delivery of nanomedicines. *Nanomedicine: Nanotechnology, Biology and Medicine* **2015**, 11, 543-557.
123. Lammers, T.; Kiessling, F.; Hennink, W. E.; Storm, G. Drug targeting to tumors: principles, pitfalls and (pre-) clinical progress. *Journal of controlled release* **2012**, 161, 175-187.
124. Choi, C. H. J.; Alabi, C. A.; Webster, P.; Davis, M. E. Mechanism of active targeting in solid tumors with transferrin-containing gold nanoparticles. *Proceedings of the National Academy of Sciences* **2010**, 107, 1235-1240.
125. Nellis, D. F.; Giardina, S. L.; Janini, G. M.; Shenoy, S. R.; Marks, J. D.; Tsai, R.; Drummond, D. C.; Hong, K.; Park, J. W.; Ouellette, T. F. Preclinical manufacture of anti-HER2 liposome-inserting, scFv-PEG-lipid conjugate. 2. Conjugate micelle identity, purity, stability, and potency analysis. *Biotechnology progress* **2005**, 21, 221-232.
126. Suzuki, R.; Takizawa, T.; Kuwata, Y.; Mutoh, M.; Ishiguro, N.; Utoguchi, N.; Shinohara, A.; Eriguchi, M.; Yanagie, H.; Maruyama, K. Effective anti-tumor activity of oxaliplatin encapsulated in transferrin–PEG-liposome. *International journal of pharmaceutics* **2008**, 346, 143-150.
127. Lu, Y.; Low, P. S. Folate-mediated delivery of macromolecular anticancer therapeutic agents. *Advanced drug delivery reviews* **2012**, 64, 342-352.

128. Sudimack, J.; Lee, R. J. Targeted drug delivery via the folate receptor. *Advanced drug delivery reviews* **2000**, 41, 147-162.
129. Antony, A. C. Folate receptors. *Annual review of nutrition* **1996**, 16, 501-521.
130. Reddy, J. A.; Haneline, L. S.; Srour, E. F.; Antony, A. C.; Clapp, D. W.; Low, P. S. Expression and functional characterization of the β -isoform of the folate receptor on CD34+ cells. *Blood* **1999**, 93, 3940-3948.
131. Lee, R. J.; Low, P. S. Delivery of liposomes into cultured KB cells via folate receptor-mediated endocytosis. *Journal of Biological Chemistry* **1994**, 269, 3198-3204.
132. Lu, Y.; Low, P. S. Folate targeting of haptens to cancer cell surfaces mediates immunotherapy of syngeneic murine tumors. *Cancer Immunology, Immunotherapy* **2002**, 51, 153-162.
133. Siegel, B. A.; Dehdashti, F.; Mutch, D. G.; Podoloff, D. A.; Wendt, R.; Sutton, G. P.; Burt, R. W.; Ellis, P. R.; Mathias, C. J.; Green, M. A. Evaluation of ¹¹¹In-DTPA-folate as a receptor-targeted diagnostic agent for ovarian cancer: initial clinical results. *Journal of Nuclear Medicine* **2003**, 44, 700-707.
134. Wang, S.; Luo, J.; Lantrip, D. A.; Waters, D. J.; Mathias, C. J.; Green, M. A.; Fuchs, P. L.; Low, P. S. Design and synthesis of [¹¹¹In] DTPA-folate for use as a tumor-targeted radiopharmaceutical. *Bioconjugate chemistry* **1997**, 8, 673-679.
135. Werner, M. E.; Karve, S.; Sukumar, R.; Cummings, N. D.; Copp, J. A.; Chen, R. C.; Zhang, T.; Wang, A. Z. Folate-targeted nanoparticle delivery of chemo- and radiotherapeutics for the treatment of ovarian cancer peritoneal metastasis. *Biomaterials* **2011**, 32, 8548-8554.
136. Low, P. S.; Kularatne, S. A. Folate-targeted therapeutic and imaging agents for cancer. *Current opinion in chemical biology* **2009**, 13, 256-262.
137. Zhao, X.; Li, H.; Lee, R. J. Targeted drug delivery via folate receptors. *Expert opinion on drug delivery* **2008**, 5, 309-319.
138. Salazar, M. D. A.; Ratnam, M. The folate receptor: what does it promise in tissue-targeted therapeutics? *Cancer and Metastasis Reviews* **2007**, 26, 141-152.
139. Weitman, S. D.; Lark, R. H.; Coney, L. R.; Fort, D. W.; Frasca, V.; Zurawski, V. R.; Kamen, B. A. Distribution of the folate receptor GP38 in normal and malignant cell lines and tissues. *Cancer research* **1992**, 52, 3396-3401.
140. Nakashima-Matsushita, N.; Homma, T.; Yu, S.; Matsuda, T.; Sunahara, N.; Nakamura, T.; Tsukano, M.; Ratnam, M.; Matsuyama, T. Selective Expression of Folate Receptor and its Possible Role in Methotrexate Transport in Synovial

Macrophages from Patients with Rheumatoid Arthritis. *ARTHRITIS AND RHEUMATISM-ATLANTA* **1999**, 42, 1609-1616.

141. Galluzzi, L.; Morselli, E.; Kepp, O.; Vitale, I.; Rigoni, A.; Vacchelli, E.; Michaud, M.; Zischka, H.; Castedo, M.; Kroemer, G. Mitochondrial gateways to cancer. *Molecular aspects of medicine* **2010**, 31, 1-20.

142. Guzman-Villanueva, D.; Mendiola, M. R.; Nguyen, H. X.; Weissig, V. Influence of Triphenylphosphonium (TPP) Cation Hydrophobization with Phospholipids on Cellular Toxicity and Mitochondrial Selectivity. **2015**.

143. Fulda, S.; Galluzzi, L.; Kroemer, G. Targeting mitochondria for cancer therapy. *Nature reviews Drug discovery* **2010**, 9, 447-464.

144. Smith, R. A.; Porteous, C. M.; Gane, A. M.; Murphy, M. P. Delivery of bioactive molecules to mitochondria in vivo. *Proceedings of the National Academy of Sciences* **2003**, 100, 5407-5412.

145. Marrache, S.; Dhar, S. Engineering of blended nanoparticle platform for delivery of mitochondria-acting therapeutics. *Proceedings of the National Academy of Sciences* **2012**, 109, 16288-16293.

146. Pathak, R. K.; Kolishetti, N.; Dhar, S. Targeted nanoparticles in mitochondrial medicine. *Wiley Interdisciplinary Reviews: Nanomedicine and Nanobiotechnology* **2015**, 7, 315-329.

147. Stylianopoulos, T.; Jain, R. K. Design considerations for nanotherapeutics in oncology. *Nanomedicine: Nanotechnology, Biology and Medicine* **2015**, 11, 1893-1907.

148. Hillier, S. M.; Maresca, K. P.; Femia, F. J.; Marquis, J. C.; Foss, C. A.; Nguyen, N.; Zimmerman, C. N.; Barrett, J. A.; Eckelman, W. C.; Pomper, M. G. Preclinical evaluation of novel glutamate-urea-lysine analogues that target prostate-specific membrane antigen as molecular imaging pharmaceuticals for prostate cancer. *Cancer research* **2009**, 69, 6932-6940.

149. Li, X.; Yang, W.; Zou, Y.; Meng, F.; Deng, C.; Zhong, Z. Efficacious delivery of protein drugs to prostate cancer cells by PSMA-targeted pH-responsive chimaeric polymersomes. *Journal of Controlled Release* **2015**, 220, 704-714.

150. Deng, C.; Jiang, Y.; Cheng, R.; Meng, F.; Zhong, Z. Biodegradable polymeric micelles for targeted and controlled anticancer drug delivery: promises, progress and prospects. *Nano Today* **2012**, 7, 467-480.

151. Maeda, H. The enhanced permeability and retention (EPR) effect in tumor vasculature: the key role of tumor-selective macromolecular drug targeting. *Advances in enzyme regulation* **2001**, 41, 189-207.

152. Allen, T. M. Ligand-targeted therapeutics in anticancer therapy. *Nature Reviews Cancer* **2002**, 2, 750-763.
153. Pinheiro, V. B.; Taylor, A. I.; Cozens, C.; Abramov, M.; Renders, M.; Zhang, S.; Chaput, J. C.; Wengel, J.; Peak-Chew, S.-Y.; McLaughlin, S. H. Synthetic genetic polymers capable of heredity and evolution. *Science* **2012**, 336, 341-344.
154. Farokhzad, O. C.; Jon, S.; Khademhosseini, A.; Tran, T.-N. T.; LaVan, D. A.; Langer, R. Nanoparticle-aptamer bioconjugates a new approach for targeting prostate cancer cells. *Cancer research* **2004**, 64, 7668-7672.
155. Xiao, Z.; Farokhzad, O. C. Aptamer-functionalized nanoparticles for medical applications: challenges and opportunities. *ACS nano* **2012**, 6, 3670-3676.
156. Dubey, P. K.; Mishra, V.; Jain, S.; Mahor, S.; Vyas, S. Liposomes modified with cyclic RGD peptide for tumor targeting. *Journal of drug targeting* **2004**, 12, 257-264.
157. Colombo, G.; Curnis, F.; De Mori, G. M.; Gasparri, A.; Longoni, C.; Sacchi, A.; Longhi, R.; Corti, A. Structure-activity relationships of linear and cyclic peptides containing the NGR tumor-homing motif. *Journal of Biological Chemistry* **2002**, 277, 47891-47897.
158. Negussie, A. H.; Miller, J. L.; Reddy, G.; Drake, S. K.; Wood, B. J.; Dreher, M. R. Synthesis and in vitro evaluation of cyclic NGR peptide targeted thermally sensitive liposome. *Journal of Controlled Release* **2010**, 143, 265-273.
159. Sakaguchi, N.; Kojima, C.; Harada, A.; Koiwai, K.; Emi, N.; Kono, K. Effect of Transferrin As a Ligand of pH-Sensitive Fusogenic Liposome– Lipoplex Hybrid Complexes. *Bioconjugate chemistry* **2008**, 19, 1588-1595.
160. Szwed, M.; Matusiak, A.; Laroche-Clary, A.; Robert, J.; Marszalek, I.; Jozwiak, Z. Transferrin as a drug carrier: cytotoxicity, cellular uptake and transport kinetics of doxorubicin transferrin conjugate in the human leukemia cells. *Toxicology in Vitro* **2014**, 28, 187-197.
161. Joshee, N.; Bastola, D. R.; Cheng, P.-W. Transferrin-facilitated lipofection gene delivery strategy: characterization of the transfection complexes and intracellular trafficking. *Human gene therapy* **2002**, 13, 1991-2004.
162. Alexis, F.; Basto, P.; Levy-Nissenbaum, E.; Radovic-Moreno, A. F.; Zhang, L.; Pridgen, E.; Wang, A. Z.; Marein, S. L.; Westerhof, K.; Molnar, L. K. HER-2-Targeted Nanoparticle–Affibody Bioconjugates for Cancer Therapy. *ChemMedChem* **2008**, 3, 1839-1843.
163. Sandström, M.; Lindskog, K.; Velikyan, I.; Wennborg, A.; Feldwisch, J.; Sandberg, D.; Tolmachev, V.; Orlova, A.; Sörensen, J.; Carlsson, J. Biodistribution and

radiation dosimetry of the anti-HER2 Affibody molecule ⁶⁸Ga-ABY-025 in breast cancer patients. *Journal of Nuclear Medicine* **2016**, jnumed. 115.169342.

164. Winkler, J.; Martin-Killias, P.; Plückthun, A.; Zangemeister-Wittke, U. EpCAM-targeted delivery of nanocomplexed siRNA to tumor cells with designed ankyrin repeat proteins. *Molecular cancer therapeutics* **2009**, 8, 2674-2683.

165. Trzpis, M.; McLaughlin, P. M.; de Leij, L. M.; Harmsen, M. C. Epithelial cell adhesion molecule: more than a carcinoma marker and adhesion molecule. *The American journal of pathology* **2007**, 171, 386-395.

166. Chari, R. V. Targeted delivery of chemotherapeutics: tumor-activated prodrug therapy. *Advanced drug delivery reviews* **1998**, 31, 89-104.

167. Glennie, M. J.; van de Winkel, J. G. Renaissance of cancer therapeutic antibodies. *Drug discovery today* **2003**, 8, 503-510.

168. Abou-Jawde, R.; Choueiri, T.; Alemany, C.; Mekhail, T. An overview of targeted treatments in cancer. *Clinical therapeutics* **2003**, 25, 2121-2137.

169. Brannon-Peppas, L.; Blanchette, J. O. Nanoparticle and targeted systems for cancer therapy. *Advanced drug delivery reviews* **2012**, 64, 206-212.

170. Leserman, L. D.; Barbet, J.; Kourilsky, F.; Weinstein, J. N. Targeting to cells of fluorescent liposomes covalently coupled with monoclonal antibody or protein A. **1980**.

171. Bartlett, D. W.; Su, H.; Hildebrandt, I. J.; Weber, W. A.; Davis, M. E. Impact of tumor-specific targeting on the biodistribution and efficacy of siRNA nanoparticles measured by multimodality in vivo imaging. *Proceedings of the National Academy of Sciences* **2007**, 104, 15549-15554.

172. Simard, P.; Leroux, J.-C. In vivo evaluation of pH-sensitive polymer-based immunoliposomes targeting the CD33 antigen. *Molecular pharmaceutics* **2010**, 7, 1098-1107.

173. Anselmo, A. C.; Mitragotri, S. Nanoparticles in the Clinic. *Bioengineering & Translational Medicine* **2016**.

174. Munster, P. N.; Miller, K.; Krop, I. E.; Dhindsa, N.; Niyikiza, C.; Nielsen, U.; Oduyungbo, A.; Rajarethinam, A.; Campbell, K.; Geretti, E. In *A Phase I study of MM-302, a HER2-targeted liposomal doxorubicin, in patients with advanced, HER2-positive (HER2+) breast cancer*, ASCO Annual Meeting. Chicago, IL, USA, 2012; 2012; pp 1-5.

175. Matsumura, Y.; Gotoh, M.; Muro, K.; Yamada, Y.; Shirao, K.; Shimada, Y.; Okuwa, M.; Matsumoto, S.; Miyata, Y.; Ohkura, H. Phase I and pharmacokinetic

study of MCC-465, a doxorubicin (DXR) encapsulated in PEG immunoliposome, in patients with metastatic stomach cancer. *Annals of Oncology* **2004**, 15, 517-525.

176. Albanese, A.; Tang, P. S.; Chan, W. C. The effect of nanoparticle size, shape, and surface chemistry on biological systems. *Annual review of biomedical engineering* **2012**, 14, 1-16.

177. Nie, S. Understanding and overcoming major barriers in cancer nanomedicine. *Nanomedicine* **2010**, 5, 523-528.

APPENDIX B

AZITHROMYCIN FUNCTIONALIZED LIPOSOMES

B.1. Introduction

Despite intensive research towards development of new therapies for treating cancer, it is still among the leading causes of death worldwide [1], [2]. Every year over 10 million people are diagnosed with cancer which results in thousands of death [3]. Cancer cells originate from normal healthy cells and because of their similarity to normal cell, it has proven very difficult to selectively target them [4]. The utility of most of the current cancer therapeutic agents is hampered by dose-limiting side effects and off-target toxicities [3]. One approach to solve this problem is the use of carriers, such as liposomes, to deliver anticancer drugs selectively to target tissues. Liposomal drug delivery method facilitates selective targeting of the cancerous tissues while reducing the off-target toxicities and increasing the drug's blood circulation time. Additionally, liposomal drug delivery formulation could be used to deliver multiple drugs, which target pathways, to various cancer types [5], [6].

Liposomes are lipid bilayers vesicles, designed to enhance the drug bioavailability and accumulation at the target site [7]. In some cases in order to increase the liposome blood circulation, they are coated with Poly Ethylene Glycol (PEG). These are called “stealth” liposomes and prevents liposome’s rapid uptake by immune system [3], [7]. Once the liposome is made and decorated with PEG and other ligands the anticancer drug can be inserted inside or it can be attached outside to the lipid bilayer based on the drug lipophilicity (Figure B.1). If the anticancer drug is hydrophilic it will be encapsulated into the liposome, since the interior part is surrounded by hydrophilic head groups. On the other hand, if it is hydrophobic it will be inserted in or attached to hydrophobic bilayer. There are more than ten FDA approved liposomal drug formulations [3].

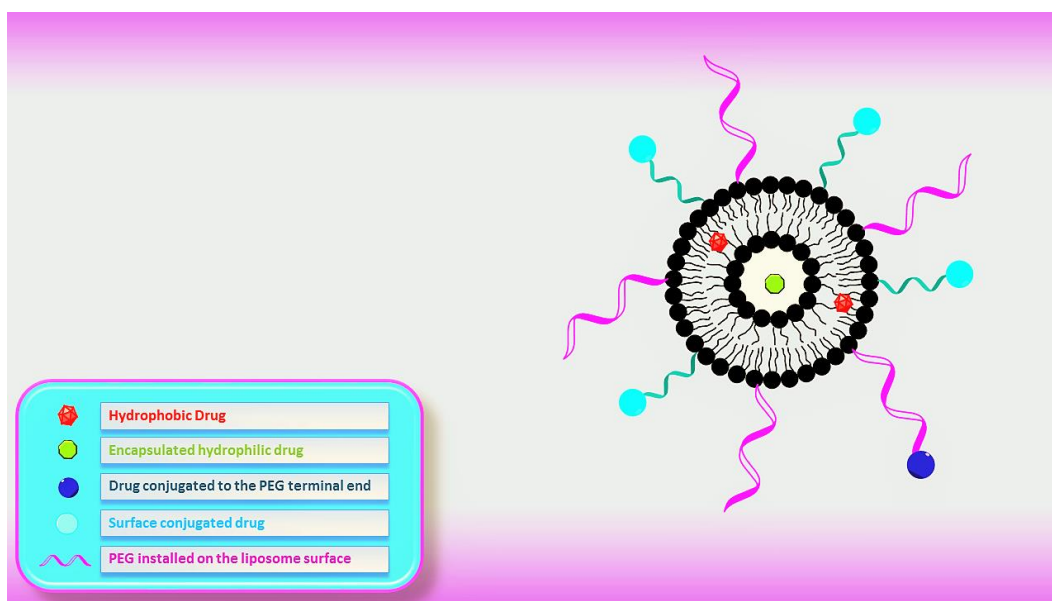


Figure B.1. Liposomal drug delivery system. Various therapeutic drugs can be encapsulated inside the liposome, within its bilayers or conjugated to its surface depending on their hydrophobicity. Installing PEG on the surface of liposome delays its recognition by reticulum endothelial system (RES) and macrophages.

B.2. Ligand functionalized liposome design

Liposomes function as drug delivery vehicles by encapsulating the therapeutic drug in the interior, within their bilayers or attaching it on the bilayer membrane [8], [9], [10]. Liposomes can be made based on three models. In the first model the ligand is directly attached to phospholipid head group. But the problem with this model is the liposome will be uptaken by immune system easily and rapidly. Hence, the circulation time of such liposome is short [11]. The second model is similar to the first one except that PEGylated phospholipids are incorporated into the liposome to increase the liposome blood circulation time. However, steric occlusion could prevent the accessibility of the targeting ligand by the receptors expressed in the target tissue. In the third model, the ligand is attached to the distal end of PEG coating. This model is called “post insertion” model and it usually facilitates long blood circulation time and high selectivity (Figure B.2) [12].

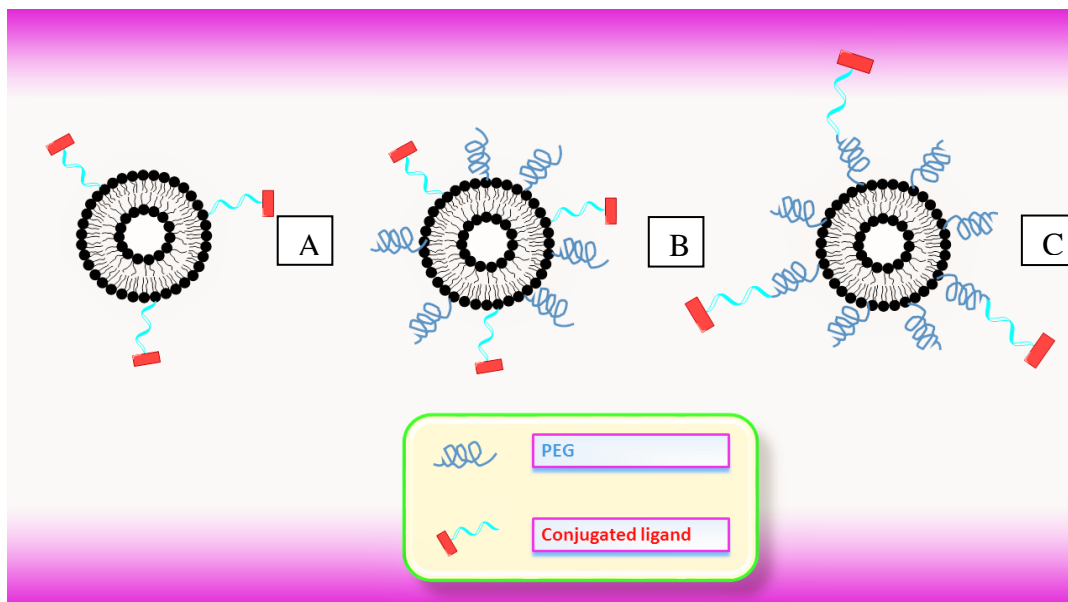


Figure B.2. Three different design of functionalized liposome. A) Ligands conjugated directly on phspholipid head group of non-PEGylated liposome. B) Ligands conjugated directly on phspholipid head group of PEGylated liposome. C) Ligands are conjugated on the free terminus of PEGylated chain [12].

In this project, I designed azithromycin decorated liposomes for lung tissue selective delivery of therapeutic agents (Figure B.3). Three phospholipid functionalized azithromycin analogues were synthesized to construct liposome in which targeting ligands are embedded in the PEG layer.

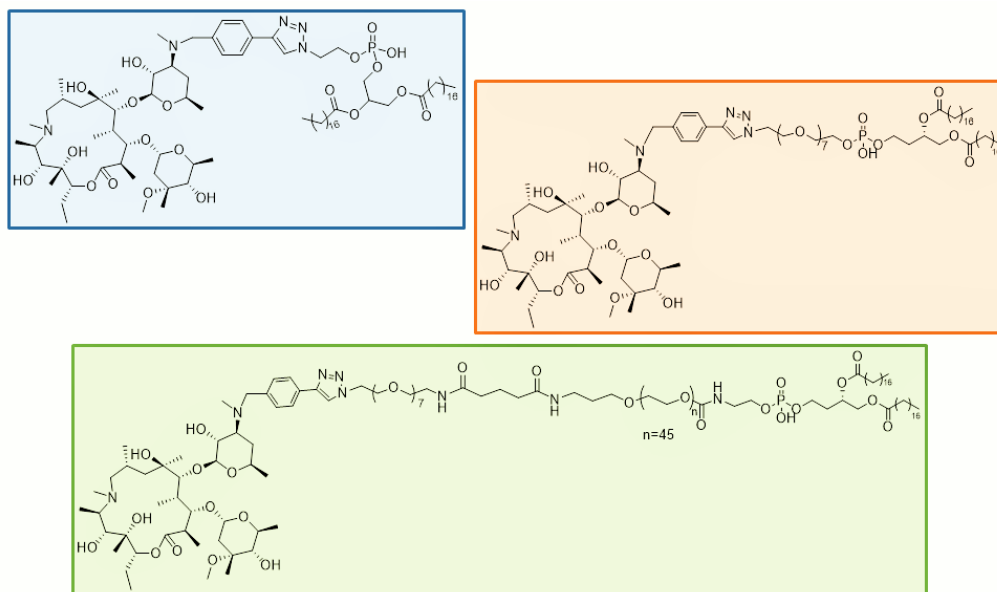


Figure B.3. Three different designs of azithromycin functionalized phospholipid.

Azithromycin is a 15 membered macrolide (Figure B.4). Which has been used widely for respiratory tract infection treatment, middle ear infection, sexually transmitted diseases and trachoma [13], [14], [15]. Compared to the 14 membered ring erythromycin, a macrolide originally isolated from *Streptomyces Species* [16], azithromycin is more chemically stable and better tolerated. Its high accumulation in cells and tissues specifically lung tissue results in 10-100 fold higher concentration compared to plasma. The high intracellular accumulation results in prolonged half-life, and more favorable regimen and shorter dosage schedule. Azithromycin, contains two basic amine groups, and relative to erythromycin, it has greater tissue penetration as well as higher potency against gram negative bacteria [17]. The anti-bacterial property of erythromycin class of macrolides is due to their reversible binding to the 50s subunit of the bacterial ribosome which results in inhibiting translocation and transpeptidation reaction [14], [18].

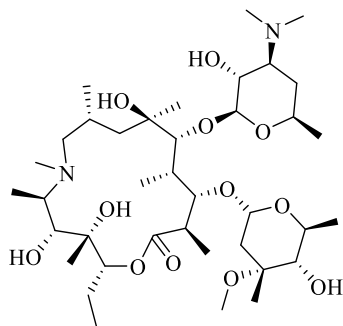
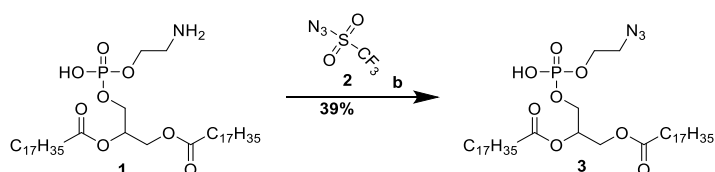


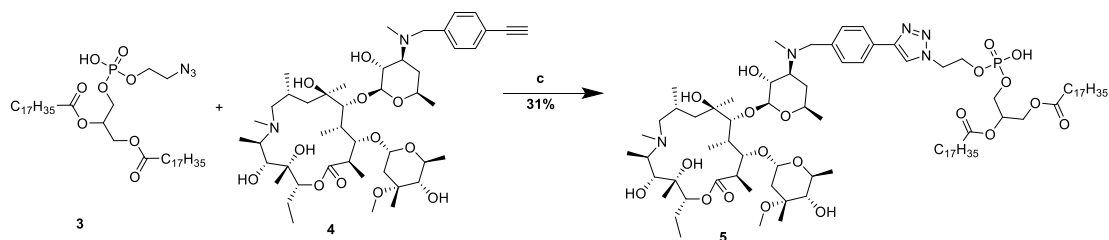
Figure B.4. Azithromycin structure, a FDA approved antibiotic for treating bacterial infection.

Based on its lung tissue accumulation property, azithromycin could serve as ligand for lung targeted delivery of therapeutic agents. It is therefore conceivable that liposomal formulations incorporating liposome-forming macrolides, derived from azithromycin (AZM) will generate a new class of nanocarriers that are selectively accumulated in the lung tissues [19].

B.3. Chemistry and synthesis

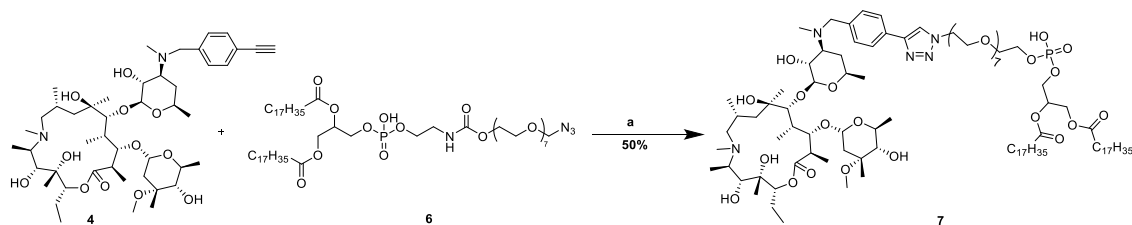
Toward obtaining liposomal formulation for lung tissue selective delivery of therapeutic agents, three different phospholipid functionalized azithromycins were synthesized. The short chain phospholipid functionalized azithromycin **5** was synthesized through conversion of amine group to azide by performing a diazotransfer reaction [13] followed by Cu (I) cycloaddition with *N*-ethynyl benzyl azithromycin **4** [14] (Scheme B.1).





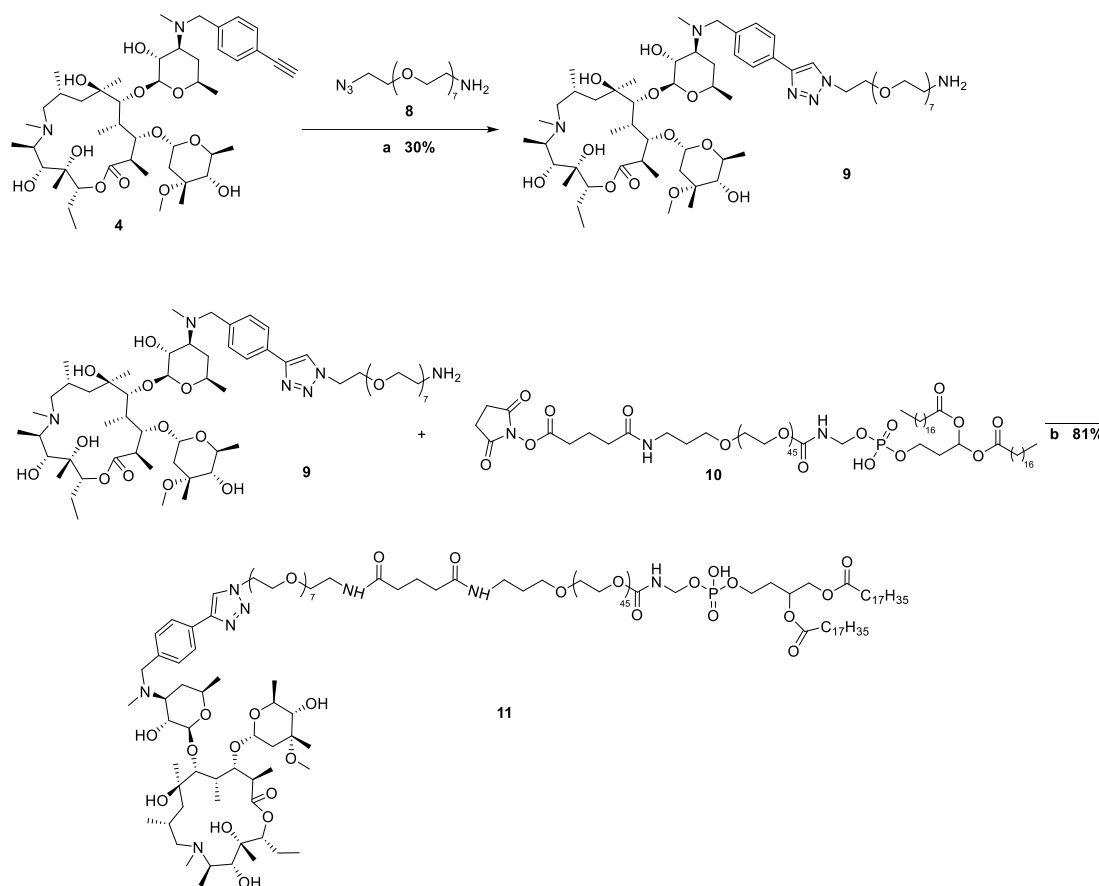
Scheme B.1. (a) TEA, CuSO₄, MeOH: H₂O, rt, overnight, 51%; (c) CuI, Hunig's base, THF, rt, overnight, 39%.

To synthesize the middle length liposome **7**, a click reaction was performed between *N*-ethynyl benzyl azithromycin **4** and PEGylated phospholipid **6** (provided by Idris Raji) (Scheme B.2).



Scheme B.2. CuI, Hunig's base, THF, rt, overnight, 50%.

To synthesize the long chain of azithromycin functionalized liposome, *N*-ethynyl benzyl azithromycin **4** was reacted with amine azide PEG **8** through CuI (I) cyclization reaction followed by nucleophilic reaction with commercially available NHS PEG 2000 derivative **11** (Scheme B.3).



Scheme B.3. (a) CuI, Hunig's base, THF, rt, Overnight, 30% ; (b) CH₃Cl, rt, 24 h, 81%.

B.4. Discussion and future studies

The liposome-forming capability and macrophage uptake potential of these AZM –derived liposome-forming macrolides will be investigated in the future by another lab member.

B.5. Material and Synthesis

Azithromycin was purchased from Greenfield chemical. 4-ethynylbenzyl alcohol was purchased from Sigma-Aldrich. All commercially available starting materials were used without purification. Reaction solvents were high performance liquid chromatography (HPLC) grade or American Chemical Society (ACS) grade and used without purification. Analtech silica gel plates (60 F₂₅₄) were used for analytical TLC,

and Analtech preparative TLC plates (UV 254, 2000 μm) were used for purification. UV light and anisaldehyde/iodine stain were used to visualize the spots. 200-400 Mesh silica gel was used in column chromatography. Nuclear magnetic resonance (NMR) spectra were recorded on a Varian-Gemini 400 MHz or Bruker 500 MHz magnetic resonance spectrometer. ^1H NMR Spectra were recorded in parts per million (ppm) relative to the residual peaks of CHCl_3 (7.24 ppm) in CDCl_3 or CHD_2OD (4.78 ppm) in CD_3OD or $\text{DMSO-}d_5$ (2.49 ppm) in $\text{DMSO-}d_6$. ^{13}C spectra were recorded relative to the central peak of the CDCl_3 triplet (77.0 ppm) or CD_3OD septet (49.3 ppm) or $\text{DMSO-}d_6$ septet (39.7 ppm) and were recorded with complete hetero-decoupling. Original 'fid' files were processed using MestReNova LITE (version 5.2.5-5780) program. High-resolution mass spectra were recorded at the Georgia Institute of Technology mass spectrometry facility in Atlanta.

Compounds **4**, and **8** were synthesized as described before [22], [23], [24], [25].

B.5.1. 3-(((2-azidoethoxy)(hydroxy)phosphoryl)oxy)propane-1,2-diyl distearate (**3**)

Triethyl amine (2 mL, 14.2 mmol) and catalytic amount of $\text{CuSO}_4 \cdot 5\text{H}_2\text{O}$ were added to a suspension of compound **1** (218 mg, 0.3 mmol) in $\text{MeOH}:\text{H}_2\text{O}$ (4:1 mL). Freshly made trifluoromethanesulfonyl azide **2** (152.2 mg, 0.9 mmol) was added. The reaction mixture was allowed to stir overnight. The reaction mixture was concentrated and dissolved in EtOAc (60 mL) and organic layer was washed with 5% KHSO_4 (5 mL) and brine (2 \times 5 mL) brine solution and dried over Na_2SO_4 . Crude product was purified using preparative TLC (Silica gel, 4:1:0.1 $\text{DCM}:\text{MeOH}:\text{NH}_4\text{OH}$) to yield product **3** (114 mg, 51%). ^1H NMR (400 MHz, CDCl_3) δ 3.99 (s, 2H), 3.66 (s, 1H), 3.47 (s, 2H), 2.31 (d, $J = 7.6$ Hz, 2H), 1.59 (s, 2H), 1.25 (s, 64H), 0.87 (t, $J = 6.7$ Hz, 6H). ^{31}P NMR (162 MHz, CDCl_3) δ -4.47.

B.5.2. (Azithromycin-4''-(methylamino)-N(methyl)(4-benzyltriazolyl))-ethoxy(hydroxy)phosphoryl)oxy)propane-1,2-diyl distearate (5)

Compound **4** (113.8 mg, 0.1 mmol) and phospholipid **3** (114 mg, 0.1 mmol) were dissolved in anhydrous THF (10 mL) and stirred under argon at room temperature. Copper (I) iodide (12.8 mg, 0.07 mmol) and Hunig's base (0.05 mL, 0.3 mmol) were added to the mixture and stirring continued for overnight. A solution of 4:1 saturated NH₄Cl/NH₄OH (10 mL) was added to the reaction mixture and extracted with 20% MeOH/ CH₂Cl₂ (3×10 mL). The organic layer was dried over Na₂SO₄ and concentrated *in vacuo*. The crude product was purified by preparative chromatography (Silica gel, 12:2:0.5 CHCl₃: MeOH: NH₄OH) to give the product (84.4 mg, 39%) as white solid. ¹H NMR (400 MHz, CDCl₃) δ 8.55 (s, 1H), 7.91 – 7.68 (m, 2H), 7.30 – 7.08 (m, 2H), 4.45 – 3.83 (m, 6H), 3.86 – 3.57 (m, 3H), 3.49 (dd, *J* = 27.0, 20.3 Hz, 2H), 2.88 (s, 3H), 2.44 – 2.19 (m, 5H), 2.05 – 1.82 (m, 3H), 1.72 (d, *J* = 9.6 Hz, 3H), 1.63 – 1.50 (m, 5H), 1.48 – 1.41 (m, 3H), 1.42 – 1.14 (m, 81H), 1.09 (d, *J* = 5.8 Hz, 6H), 1.06 – 0.95 (m, 5H), 0.97 – 0.80 (m, 16H), 0.72 (dt, *J* = 15.0, 7.6 Hz, 3H). ³¹P NMR (162 MHz, CDCl₃) δ -2.34. HRMS (MALDI) *m/z* Calcd. for C₈₇ H₁₅₆ O₂₀ N₅ P [M]: 12624.1.

B.5.3. (Azithromycin-4''-(methylamino)-N(methyl)(4-benzyltriazolyl))- octa ethylene glycol(hydroxy)phosphoryl)oxy)propane-1,2-diyl distearate (7)

Compound **4** (145.2 mg, 0.2 mmol) and phospholipid **6** (200 mg, 0.2 mmol) were dissolved in anhydrous THF (10 mL) and stirred under argon at room temperature. Copper (I) iodide (16 mg, 0.08 mmol) and Hunig's base (0.06 mL, 0.3 mmol) were added to the mixture and stirring continued for overnight. A solution of 4:1 saturated NH₄Cl/NH₄OH (10 mL) was added to the reaction mixture and extracted with 20% MeOH/ CH₂Cl₂ (3×10 mL). The organic layer was dried over Na₂SO₄ and concentrated *in vacuo*. The crude product was purified by preparative chromatography (Silica gel,

15:2:0.3 DCM: MeOH: NH₄OH) to give the product (142 mg, 50%) as white solid. ¹H NMR (400 MHz, CDCl₃) δ 8.04 (s, 1H), 7.81 (d, *J* = 6.9 Hz, 2H), 7.36 (s, 2H), 5.20 (s, 1H), 4.96 (s, 1H), 4.74 (d, *J* = 6.7 Hz, 1H), 4.59 (t, *J* = 4.7 Hz, 2H), 4.43 – 4.26 (m, 2H), 4.23 – 4.04 (m, 4H), 4.03 – 3.83 (m, 7H), 3.76 (s, 1H), 3.69 – 3.48 (m, 29H), 3.44 (d, *J* = 27.0 Hz, 4H), 3.03 (s, 2H), 2.90 (d, *J* = 30.4 Hz, 6H), 2.65 (s, 2H), 2.24 (ddd, *J* = 33.5, 18.2, 9.2 Hz, 9H), 1.80 (t, *J* = 24.1 Hz, 3H), 1.55 (s, 5H), 1.49 – 1.35 (m, 5H), 1.36 – 1.15 (m, 67H), 1.15 – 1.05 (m, 6H), 0.98 (dd, *J* = 20.3, 7.2 Hz, 8H), 0.91 – 0.76 (m, 9H). ³¹P NMR (162 MHz, MeOH) δ 0.08.

B.5.4. (Azithromycin-4''-(methylamino)-N(methyl)(4-benzyltriazolyl))- octa ethylene glycol amine (9)

Compound **4** (183.945.2 mg, 0.01 mmol) and azido octa ethylene glycol amine **8** (39 mg, 0.01 mmol) were dissolved in anhydrous THF (5 mL) and stirred under argon at room temperature. Copper (I) iodide (9.4 mg, 0.05 mmol) and Hunig's base (0.03 mL, 0.2 mmol) were added to the mixture and stirring continued for overnight. A solution of 4:1 saturated NH₄Cl/NH₄OH (10 mL) was added to the reaction mixture and extracted with 20% MeOH/ CH₂Cl₂ (3×10 mL). The organic layer was dried over Na₂SO₄ and concentrated *in vacuo*. The crude product was purified by preparative chromatography (Silica gel, 20:2:0.5 EtOAc: MeOH: NH₄OH) to give the product (37 mg, 30%) as white solid. ¹H NMR (400 MHz, cd₃od) δ 7.77 (t, *J* = 10.2 Hz, 1H), 7.47 (d, *J* = 6.3 Hz, 2H), 7.39 (s, 2H), 5.03 (d, *J* = 4.7 Hz, 2H), 4.88 (s, 28H), 4.58 – 4.48 (m, 3H), 4.18 (ddd, *J* = 21.5, 13.9, 4.3 Hz, 5H), 3.89 – 3.76 (m, 7H), 3.36 – 3.26 (m, 7H), 3.22 (d, *J* = 5.6 Hz, 5H), 3.01 (t, *J* = 7.9 Hz, 3H), 2.87 – 2.67 (m, 7H), 2.55 (d, *J* = 11.5 Hz, 2H), 2.35 – 2.27 (m, 8H), 2.28 – 2.21 (m, 8H), 2.09 – 1.89 (m, 14H), 1.89 – 1.70 (m, 19H), 1.70 – 1.46 (m, 26H), 1.38 – 1.31 (m, 9H), 1.30 – 1.21 (m, 18H), 1.22 – 1.15 (m, 15H), 1.13 – 1.02

(m, 19H), 0.96 – 0.87 (m, 13H). HRMS (ESI) m/z Calcd. $C_{62}H_{111}O_{19}N_6$ $[M+H]^+$: 1243.7899, found for 1243.7890.

B.5.5. (Azithromycin-4''-(methylamino)-N(methyl)(4-benzyltriazolyl)) PEG 2000 phosphoryl)oxy)butane-1,2-diyl distearate (11)

PEG 2000 **10** (167.1 mg, 0.05 mmol) and compound **9** (76 mg, 0.06 mmol) were dissolved in chloroform (10 mL). The reaction was allowed to stir at rt for 24 h. The reaction mixture was then washed with brine (5 mL) and dried over Na_2SO_4 . The crude product was purified on preparative TLC (10:1.2:0.5 DCM:MeOH: NH_4OH) to yield the product as a white solid (185 mg, 81%). 1H NMR (400 MHz, MeOH) δ 8.42 (s, 1H), 7.83 (d, J = 8.0 Hz, 2H), 7.49 (d, J = 8.0 Hz, 2H), 5.02 (d, J = 4.8 Hz, 1H), 4.64 (t, J = 4.9 Hz, 2H), 4.54 (d, J = 7.1 Hz, 1H), 4.44 (dd, J = 11.9, 3.1 Hz, 1H), 4.20 – 4.08 (m, 4H), 3.96 (dt, J = 7.8, 5.3 Hz, 4H), 3.87 (q, J = 5.4 Hz, 1H), 3.68 – 3.58 (m, 175H), 3.47 (ddd, J = 20.6, 13.8, 8.6 Hz, 7H), 3.33 (ddd, J = 10.0, 6.5, 4.9 Hz, 7H), 3.23 (dd, J = 14.8, 7.9 Hz, 2H), 3.19 (s, 3H), 3.03 (d, J = 9.4 Hz, 2H), 2.72 (s, 3H), 2.34 (dt, J = 15.1, 11.0 Hz, 7H), 2.21 (dd, J = 14.5, 7.0 Hz, 4H), 1.86 (dt, J = 21.2, 10.8 Hz, 4H), 1.81 – 1.70 (m, 2H), 1.57 (dd, J = 21.3, 6.4 Hz, 6H), 1.43 (s, 3H), 1.29 (s, 57H), 1.25 – 1.18 (m, 8H), 1.16 (d, J = 10.8 Hz, 6H), 1.08 (d, J = 7.4 Hz, 2H), 1.02 (d, J = 6.7 Hz, 3H), 0.90 (t, J = 6.8 Hz, 8H).

B.5 References

1. Siegel, R. L.; Miller, K. D.; Jemal, A. Cancer statistics, 2016. *CA: a cancer journal for clinicians* **2016**, 66, 7-30.
2. Lian, T.; Ho, R. J. Trends and developments in liposome drug delivery systems. *Journal of pharmaceutical sciences* **2001**, 90, 667-680.
3. McKinnell, R. G. *The biological basis of cancer*. Cambridge University Press: 1998.
4. Hrkach, J.; Von Hoff, D.; Ali, M. M.; Andrianova, E.; Auer, J.; Campbell, T.; De Witt, D.; Figa, M.; Figueiredo, M.; Horhota, A. Preclinical development and clinical

translation of a PSMA-targeted docetaxel nanoparticle with a differentiated pharmacological profile. *Science translational medicine* **2012**, 4, 128ra39-128ra39.

5. Allen, T. M.; Cullis, P. R. Liposomal drug delivery systems: from concept to clinical applications. *Advanced drug delivery reviews* **2013**, 65, 36-48.

6. Torchilin, V. P. Recent advances with liposomes as pharmaceutical carriers. *Nature reviews Drug discovery* **2005**, 4, 145-160.

7. Biswas, S.; Dodwadkar, N. S.; Sawant, R. R.; Torchilin, V. P. Development of the novel PEG-PE-based polymer for the reversible attachment of specific ligands to liposomes: synthesis and in vitro characterization. *Bioconjugate chemistry* **2011**, 22, 2005-2013.

8. Li, S.; Goins, B.; Zhang, L.; Bao, A. Novel multifunctional theranostic liposome drug delivery system: construction, characterization, and multimodality MR, near-infrared fluorescent, and nuclear imaging. *Bioconjugate chemistry* **2012**, 23, 1322-1332.

9. Béduneau, A.; Saulnier, P.; Hindré, F.; Clavreul, A.; Leroux, J.-C.; Benoit, J.-P. Design of targeted lipid nanocapsules by conjugation of whole antibodies and antibody Fab' fragments. *Biomaterials* **2007**, 28, 4978-4990.

10. Çağdaş, M.; Sezer, A. D.; Bucak, S. Liposomes as potential drug carrier systems for drug delivery. *Application of Nanotechnology in Drug Delivery* **2014**.

11. Alexis, F.; Pridgen, E.; Molnar, L. K.; Farokhzad, O. C. Factors affecting the clearance and biodistribution of polymeric nanoparticles. *Molecular pharmaceutics* **2008**, 5, 505-515.

12. Sawant, R. R.; Torchilin, V. P. Challenges in development of targeted liposomal therapeutics. *The AAPS journal* **2012**, 14, 303-315.

13. Hirsch, R.; Deng, H.; Laohachai, M. Azithromycin in periodontal treatment: more than an antibiotic. *Journal of periodontal research* **2012**, 47, 137-148.

14. Zuckerman, J. M. Macrolides and ketolides: azithromycin, clarithromycin, telithromycin. *Infectious Disease Clinics* **2004**, 18, 621-649.

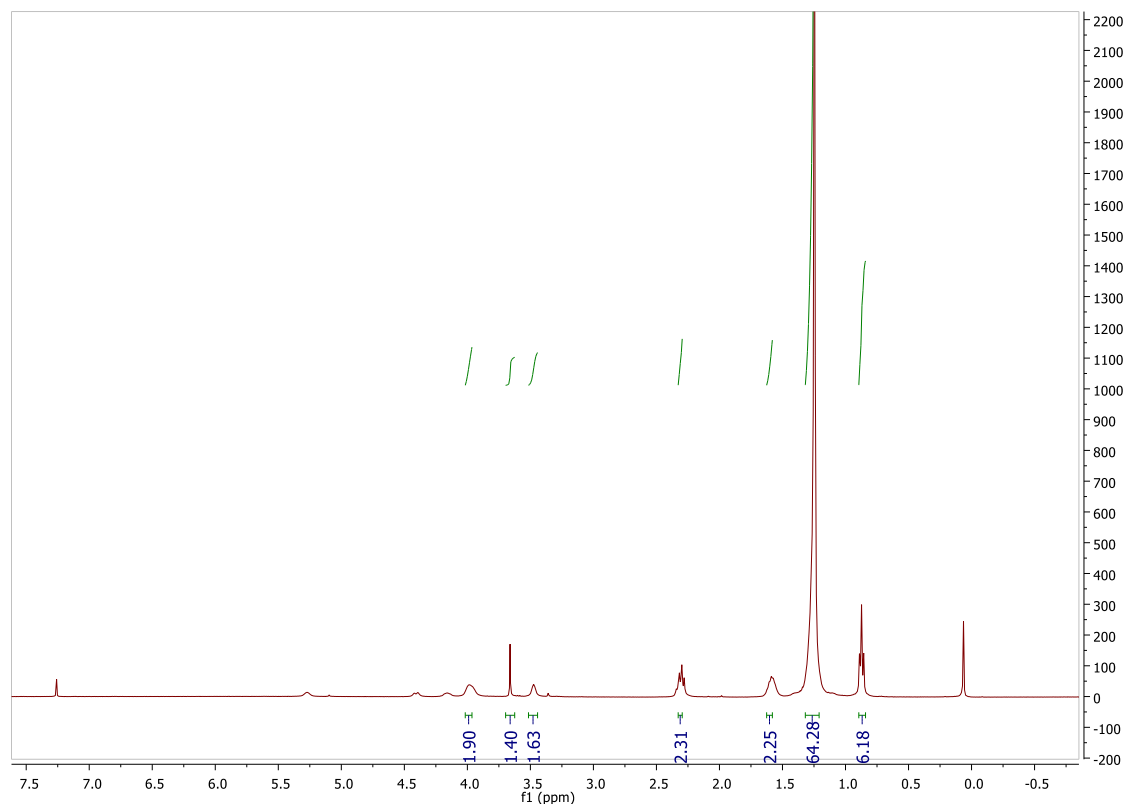
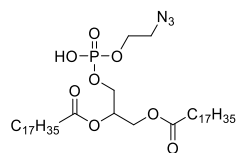
15. Stepanić, V. n.; Koštrun, S.; Malnar, I.; Hlevnjak, M.; Butkovic, K.; Caleta, I.; Dukši, M.; Kragol, G.; Makaruha-Stegic, O.; Mikac, L. Modeling cellular pharmacokinetics of 14- and 15-membered macrolides with physicochemical properties. *Journal of medicinal chemistry* **2011**, 54, 719-733.

16. Vos, R.; Vanaudenaerde, B. M.; Verleden, S. E.; Ruttens, D.; Vaneylen, A.; Van Raemdonck, D. E.; Dupont, L. J.; Verleden, G. M. Anti-inflammatory and immunomodulatory properties of azithromycin involved in treatment and prevention of chronic lung allograft rejection. *Transplantation* **2012**, 94, 101-109.

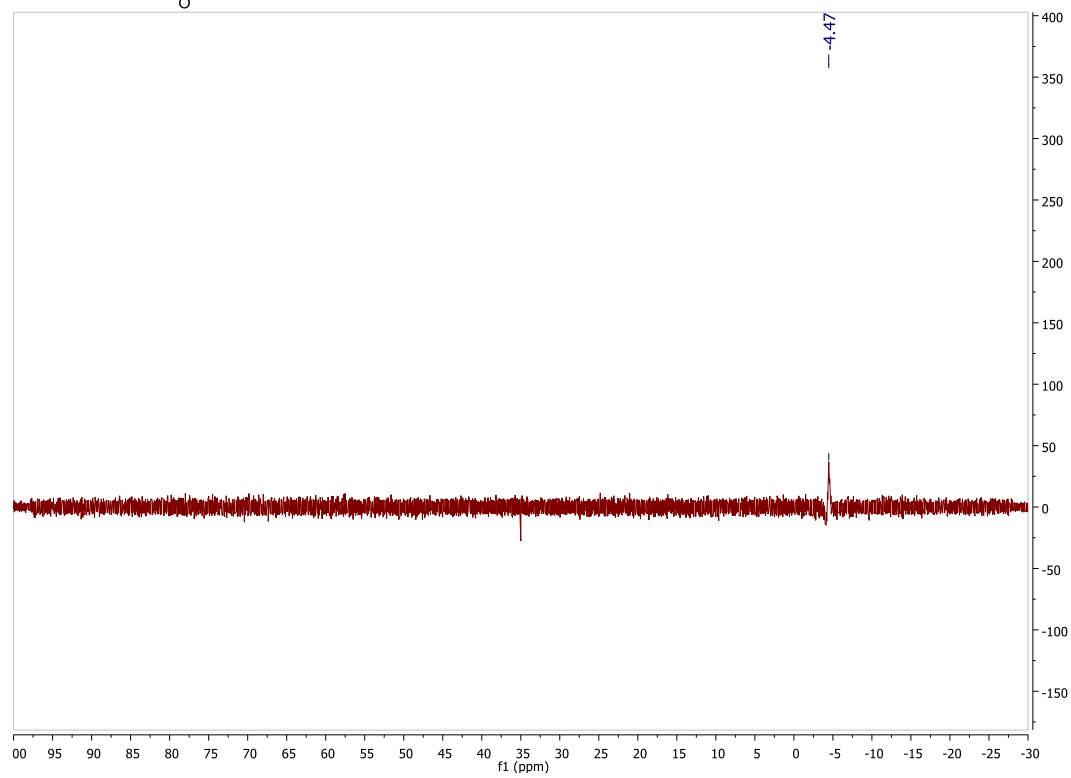
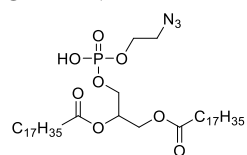
17. Gladue, R.; Bright, G.; Isaacson, R.; Newborg, M. In vitro and in vivo uptake of azithromycin (CP-62,993) by phagocytic cells: possible mechanism of delivery and release at sites of infection. *Antimicrobial Agents and Chemotherapy* **1989**, 33, 277-282.
18. Bieliauskas, A. V.; Pflum, M. K. H. Isoform-selective histone deacetylase inhibitors. *Chemical Society Reviews* **2008**, 37, 1402-1413.
19. Chang, H.-I.; Yeh, M.-K. Clinical development of liposome-based drugs: formulation, characterization, and therapeutic efficacy. *Int J Nanomedicine* **2012**, 7.
20. Alper, P. B.; Hung, S.-C.; Wong, C.-H. Metal catalyzed diazo transfer for the synthesis of azides from amines. *Tetrahedron Letters* **1996**, 37, 6029-6032.
21. Bock, V. D.; Hiemstra, H.; Van Maarseveen, J. H. CuI-Catalyzed Alkyne–Azide “Click” Cycloadditions from a Mechanistic and Synthetic Perspective. *European Journal of Organic Chemistry* **2006**, 2006, 51-68.
22. Tapadar, S.; Fathi, S.; Raji, I.; Omesiete, W.; Kornaki, J. R.; Mwakwari, S. C.; Miyata, M.; Mitsutake, K.; Li, J.-D.; Mrksich, M.; Oyelere, A. K. A structure–Activity Relationship of Non-Peptide Macrocyclic Histone Deacetylase Inhibitors and Their Anti-Proliferative and Anti-Inflammatory Activities. *Bioorganic & Medicinal Chemistry* **2015**, 23, 7543-7564.
23. Oyelere, A.K.; Chen, P. C.; Guerrant, W.; Mwakwari, S.C.; Hood, R.; Zhang, Y.; Fan, Y. Non-Peptide Macrocyclic Histone Deacetylase Inhibitors. *Journal of medicinal chemistry* **2008**, 52, 456-468.
24. Dreaden, E.C.; Mwakwari, S. C.; Sodji, Q. H.; Oyelere, A. K.; El-Sayed, M. A. Tamoxifen– Poly (Ethylene Glycol)– Thiol Gold Nanoparticle Conjugates: Enhanced Potency and Selective Delivery for Breast Cancer Treatment. *Bioconjugate chemistry* **2009**, 20, 2247-2253.
25. Dreaden, E.C.; Raji, I.; Austin, L. A.; Fathi, S.; Mwakwari, S. C.; Humphries IV, W. H.; Kang, B.; Oyelere, A. K.; El-Sayed, M. A. P-Glycoprotein-Dependent Trafficking of Nanoparticle-DrugConjugates, *Small* **2014**, 10, 1719-1723.

B.6. Supplementary data

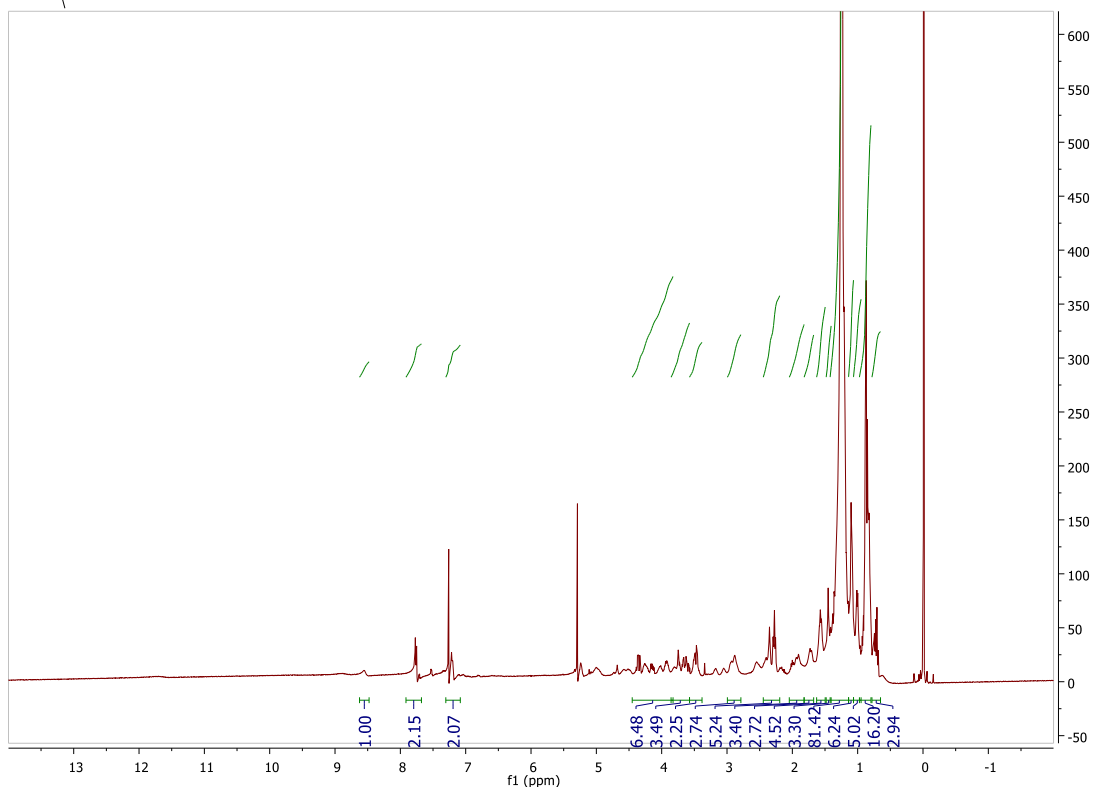
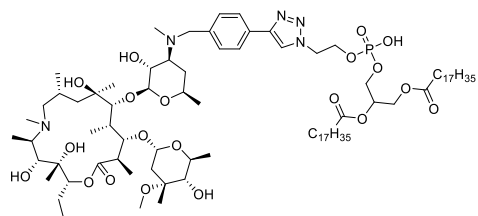
3 ¹HNMR



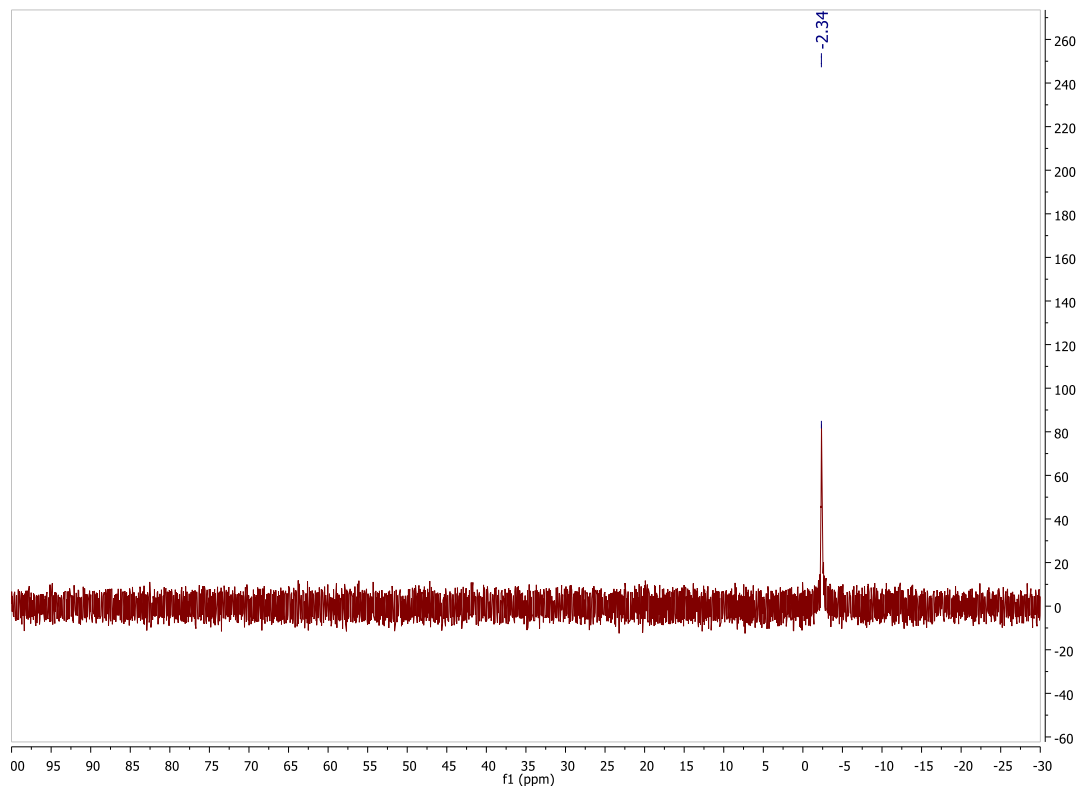
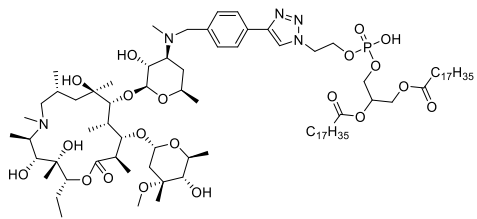
3 ^{31}P NMR



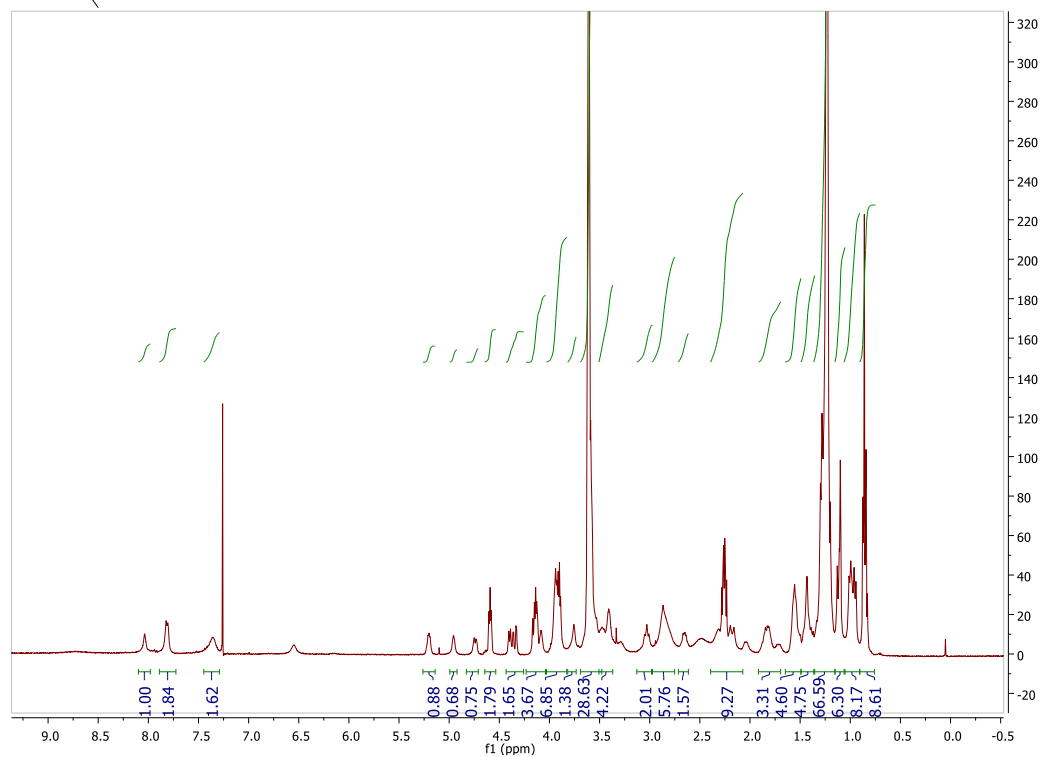
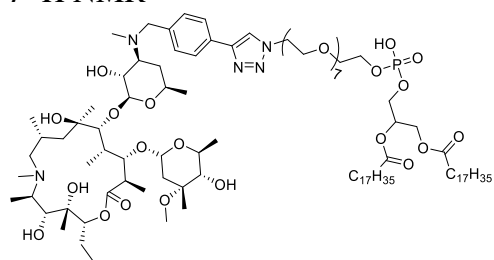
5 ^1H NMR



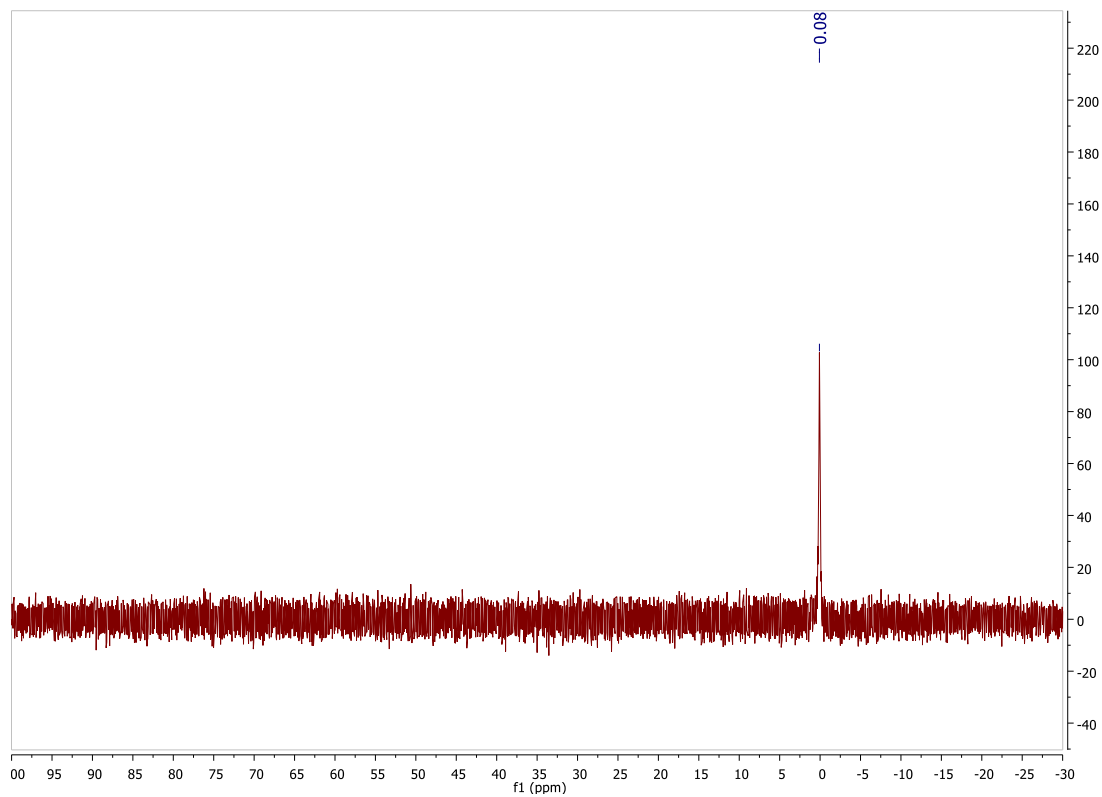
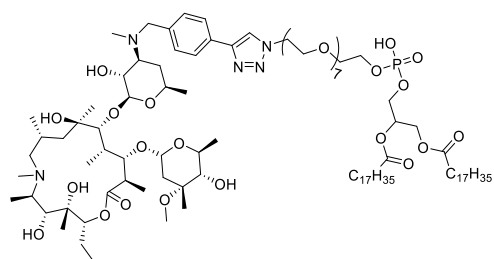
5 ^{31}P NMR



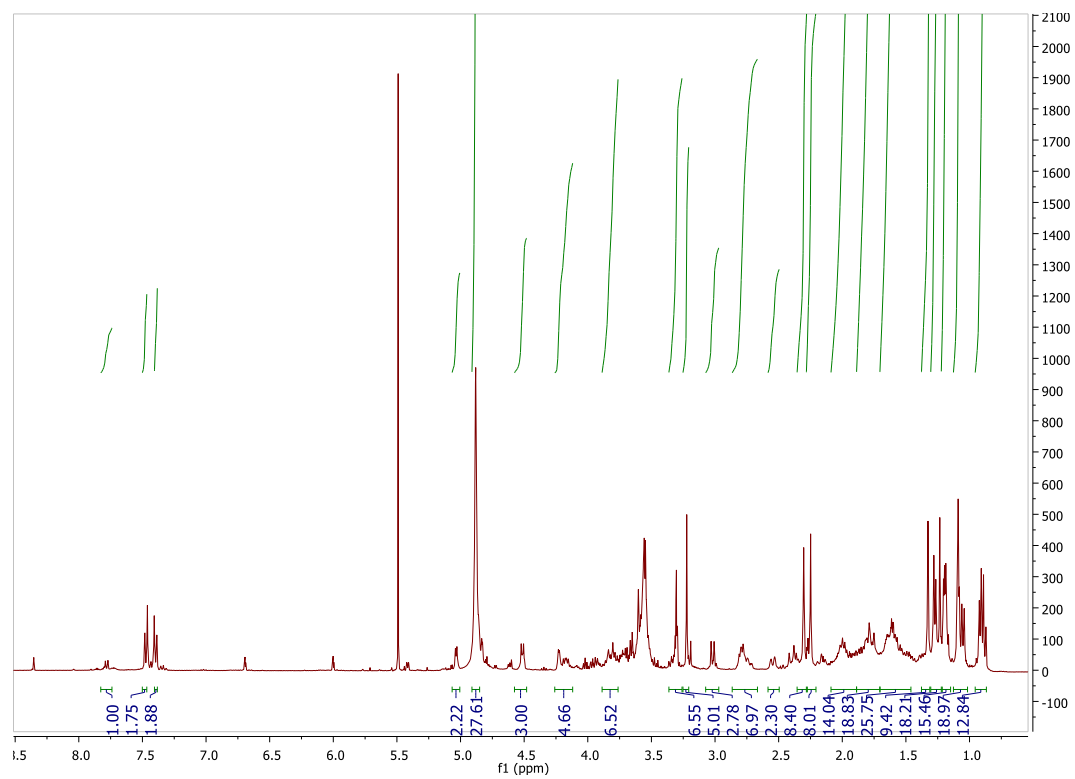
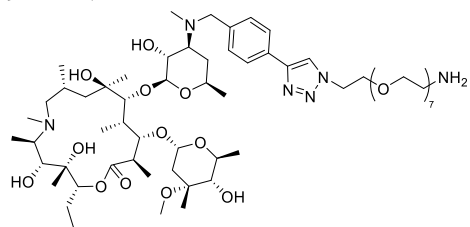
7 ^1H NMR



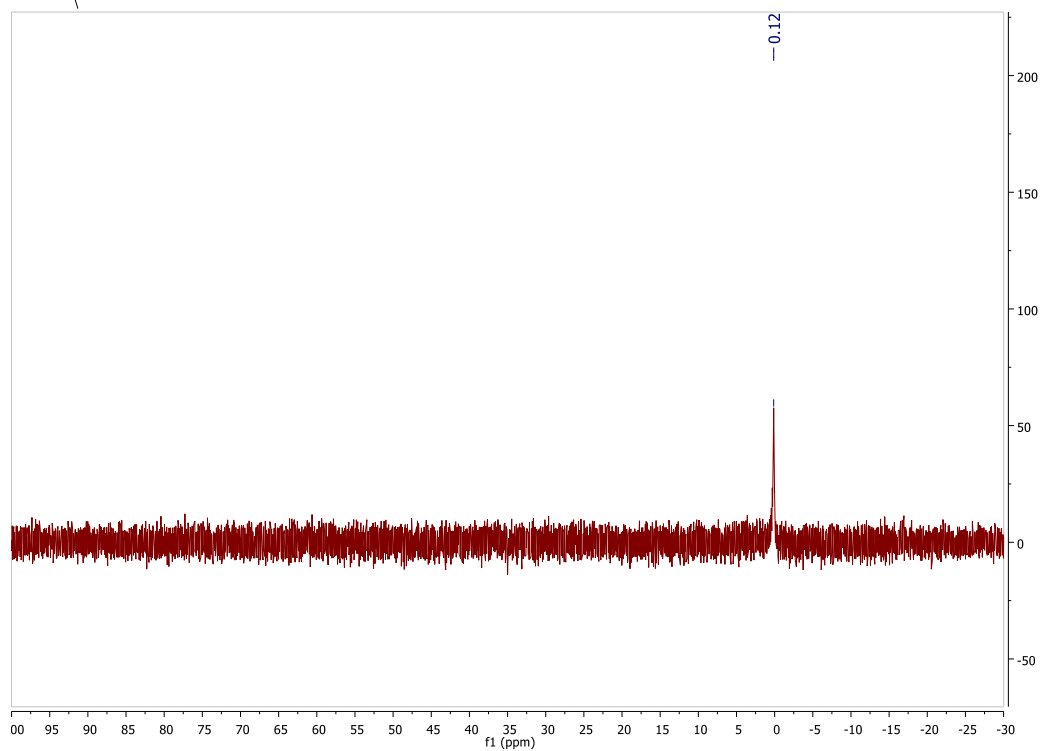
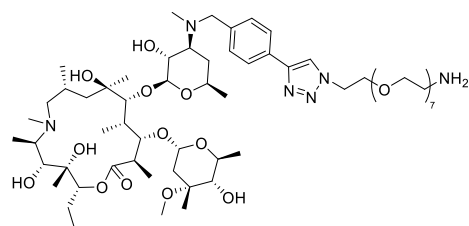
7 ³¹P NMR



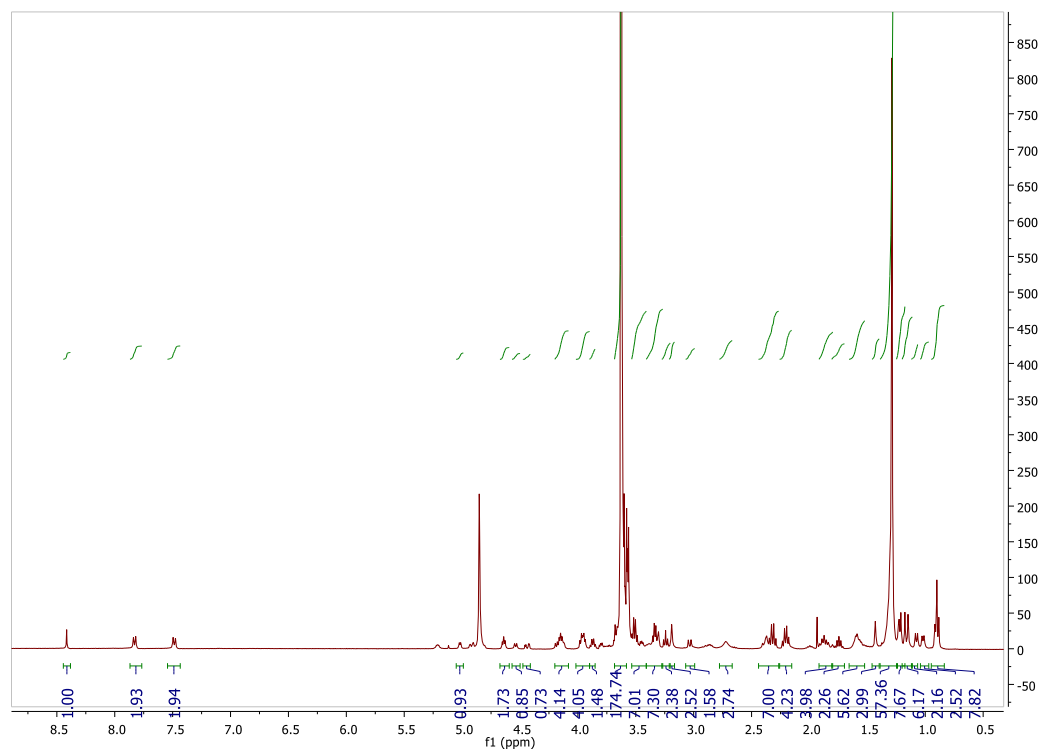
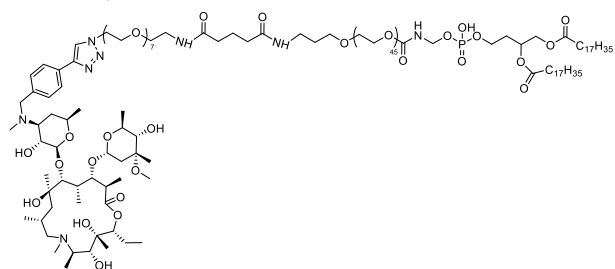
9 ^1H NMR



9 ^{31}P NMR



11 ¹H NMR



VITA

Shaghayegh Fathi

Shaghayegh Fathi was born and raised in Tehran, Iran. After finishing high school in 2005, she attended Sharif University of Technology in Tehran, Iran, where she received both her B.S and M.Sc in chemistry in 2009 and 2011 respectively. She joined the PhD program in the chemistry/biochemistry department at Georgia Institute of Technology in 2011. On her way to earn a PhD degree, she earned a M.Sc degree in chemistry in 2015 from Georgia Tech as well. Shaghayegh Fathi enjoys hanging out with friends when she is not working in the lab.